UNIVERSITY OF SOUTHAMPTON

FACULTY OF NATURAL AND ENVIRONMENTAL SCIENCES

Centre for Biological Sciences

Volume 1 of 1

The impact of systemic immune system activation on the retina: implications for age-related macular degeneration

by

Paul Ibbett

Thesis for the degree of Doctor of Philosophy

September 2017

UNIVERSITY OF SOUTHAMPTON

ABSTRACT

FACULTY OF NATURAL AND ENVIRONMENTAL SCIENCES

Biological Sciences

Thesis for the degree of Doctor of Philosophy

THE IMPACT OF SYSTEMIC IMMUNE SYSTEM ACTIVATION ON THE RETINA: IMPLICATIONS FOR AGE-RELATED MACULAR DEGENERATION

Paul Luke Ibbett

Age-related macular degeneration (AMD) is a neurodegenerative disease of the retina and the leading cause of blindness in the UK. Genetic studies and mouse models demonstrate a clear role for local immune activation in AMD pathology, but it is not clear whether systemic inflammation can contribute to AMD pathology. Systemic inflammation, particularly due to bacterial infection, has been shown to exacerbate neurodegeneration in Alzheimer's and Prion disease. There is also evidence that patients who have been exposed to chronic bacterial infections (i.e. periodontitis, pneumonia) are at increased risk of AMD development. Consequently, this thesis tests the hypothesis that systemic inflammation can contribute to the progression of AMD by exacerbating local inflammation in the retina, leading to earlier development of blindness.

Systemic bacterial (*Salmonella*) infection induced retinal microglial activation, Müller cell activation, T cell recruitment and pro-inflammatory cytokine production in mice. When subsequent peripheral immune stimulation was induced by LPS, retinal inflammation was reduced, indicating a protective mechanism. However, during ongoing local retinal inflammation induced by immune complexes, systemic inflammation exacerbated the recruitment of immune cells to the subretinal space. No retinal degeneration was observed in this model, so a novel laser-induced model of acute outer retinal atrophy was developed showing RPE dysfunction, photoreceptor loss, functional deficits and inflammation mimicking aspects of human geographic atrophy. This model could be used to investigate the interaction of systemic inflammation and degeneration, gaining insights into AMD pathobiology. In AMD patients, increased aqueous humour IL-8 was identified compared to age-matched controls but no differences in serum cytokine levels were observed at baseline or in whole blood cultured with various immune stimuli.

Data from mouse experiments indicate that systemic infections can induce chronic retinal inflammation and, during local inflammation, immune cell recruitment to the subretinal space - the site of AMD pathology. Meanwhile, human data demonstrates that local inflammation in AMD patients does not arise due to an exaggerated systemic inflammatory response to infections.

Table of Contents

Table of Tables

Table of Figures

Academic Thesis: Declaration Of Authorship

I, Paul Ibbett

declare that this thesis and the work presented in it are my own and has been generated by me as the result of my own original research.

The impact of systemic immune system activation on the retina: implications for age-related macular degeneration

I confirm that:

1. This work was done wholly or mainly while in candidature for a research degree at this University;
2. Where any part of this thesis has previously been submitted for a degree or any other qualification at this University or any other institution, this has been clearly stated;
3. Where I have consulted the published work of others, this is always clearly attributed;
4. Where I have quoted from the work of others, the source is always given. With the exception of such quotations, this thesis is entirely my own work;
5. I have acknowledged all main sources of help;
6. Where the thesis is based on work done by myself jointly with others, I have made clear exactly what was done by others and what I have contributed myself;
7. None of this work has been published before submission

Signed: .....

Date: .....

Acknowledgements

Firstly, I would like to thank my supervisory team of Profs. Jessica Teeling, Andrew Lotery and V. Hugh Perry for the advice and support given for this project and personal development. I hope to work with them again in the future! I also want to thank the charities sponsoring this project – Fight for Sight and Gift of Sight – without whom this work would not be possible.

A huge thank you must go to Elena Pipi and Alex Collcutt, who have assisted me with many *in vivo* procedures through my PhD, including tissue harvesting, electroretinography, optical coherence tomography and intravitreal injections and more importantly, provided great company and sanity over the past few years. Ursula Püntener also deserves a special mention for teaching me many of the techniques used in this thesis, many discussions around the project and making sure I was settled in the lab, before leaving me to have two beautiful children. I'd also like to thank all the past and present members of the Teeling lab - Daniel Cohn, James Fuller, Joe Chouhan and Salome Murinello – and the Lotery Lab – Angela Cree, Arjuna Ratnayaka, Jenny Scott, Helen Griffiths, Helena Lee, Savannah Lynn – for their expertise and discussions, both work related and non-work related! Along these lines, I'd also like to acknowledge Joanna Gould, Matt Morton, Renzo Mancuso and Juliane Obst for making the hospital/pub a more pleasant place to be.

I would like to thank the following people for the support they have provided during this project. Richard Jewell for invaluable (and often late-night) FACS support and guidance along with Dave Copland and Jo Boldison at the University of Bristol for training in retinal FACS. Dave Johnston and the Biomedical Imaging Unit for training and much ongoing support for the range of tissue imaging techniques used in this thesis. All the BRF staff, including Leslie Lawes, Mike Broome, Russell Soper and Lorraine House, who do a fantastic job of caring for the mice used in this thesis. I would like to thank all members of the administrative, nursing and surgical teams who enabled the collection of human samples for Chapter 7 of this thesis. In particular, Amanda Smith, Thea Sass and Mercy Jeyeraj for their weekly support in recruiting patients, collecting proforma data, consent and blood samples; Andrew Lotery and Christine Rennie for collecting aqueous samples and Marie Nelson and Angela Cree for ensuring the coordination of this human study. Srini Goverdhan, Maureen Gatherer and Elena Pipi provided great support during the development of laser-induced lesions and generated the histological data shown in Chapter 6.

Finally, thanks to all my family and friends who have supported me, particularly those that have had to deal with me when stressed, annoyed or non-communicative! The people mentioned here have made my time here in Southampton enjoyable and I can't thank them enough.

Definitions and Abbreviations

7-AAD	7-aminoactinomycin D
A2E	Apolipoprotein 2E
AD	Alzheimer's disease
AMD	Age-related macular degeneration
ANOVA	Analysis of variance
APRP	Apical pseudopodial RPE processes
ASC	Apoptosis-associated speck-like protein
Bb	Activated factor B
BCA	Bicinchoninic acid
BLamD	Basal laminar deposits
BLinD	Basal linear deposits
BMI	Body mass index
BRB	Blood-retinal barrier
BrM	Bruch's membrane
BSA	Bovine serum albumin
C. pneumoniae	*Chlamydia pneumoniae* or *Chlamydophila pneumoniae*
C1q	Complement component 1 subcomponent q
C1r	Complement component 1 subcomponent r
C1s	Complement component 1 subcomponent s
C2	Complement component 2
C2a	Complement component 2 cleavage product a
C3	Complement component 3
C3a	Complement component 3 cleavage product a
C3b	Complement component 3 cleavage product b
C4	Complement component 4
C4b	Complement component 4 cleavage product b
C5	Complement component 5
C5a	Complement component 5 cleavage product a
C5b	Complement component 6 cleavage product a
C6	Complement component 6
C7	Complement component 7
C8	Complement component 8
C9	Complement component 9

CCL	CC chemokine ligand
CCR	CC chemokine receptor
CD	Cluster of differentiation
CEP	2-(ω-carboxyethyl)pyrrole
CFB	Complement factor B
CFD	Complement factor D
CFH	Complement factor H
CFI	Complement factor I
cfu	colony forming units
cGMP	Cyclic guanosine monophosphate
Ch/Chor	Choroid
CLP	Common lymphoid progenitor
CML	N(6)-carboxymethyllysine
CMP	Common myeloid progenitor
CMV	*Cytomegalovirus*
CNS	Central nervous system
CNV	Choroidal neovascularisation
COX2	Cyclooxygenase 2
CRP	C-reactive protein
CSF-1R	Colony stimulating factor 1 receptor
CX3CL1	CX3C chemokine ligand 1
CX3CR1	CX3C chemokine receptor 1
CXCL	CXC chemokine ligand
CXCR	CXC chemokine receptor
DAB	3,3'-Diaminobenzidine
DAMPs	Danger associated molecular patterns
DAPI	4',6'-Diamidino-2-Phenylindole
EAU	Experimental autoimmune uveitis
EDTA	Ethylenediaminetetraacetic acid
eGFP	Enhanced green fluorescent protein
EIU	Endotoxin induced uveitis
ELM	External limiting membrane
eNOS	Endothelial nitric oxide synthase
ERG	Electroretinography
Fab	Fragment antigen-binding
FasL	Fas ligand

Fc	Fragment crystallisable region
FCRLS	Fc receptor-like scavenger protein
FcγR	Fcγ receptor
FDA	Food and drug administration
GA	Geographic atrophy
GABA	Gamma-aminobutyric acid
GAPDH	Glyceraldehyde 3-phosphate dehydrogenase
GCL	Ganglion cell layer
GDP	Guanosine diphosphate
GFAP	Glial fibrillary acidic protein
GFP	Green fluorescent protein
GM-CSF	Granulocyte macrophage colony-stimulating factor
GPCR	G protein-coupled receptor
GTP	Guanosine triphosphate
HLA	Human leukocyte antigen
HO-1	Heme oxygenase 1
HSC	Haematopoietic stem cells
HSP70	Heat shock protein 70
IBA-1	Ionised calcium-binding adapter molecule 1
ICs	Immune complexes
iC3b	Inactivated complement component 3 cleavage product b
ICAM-1	Intercellular adhesion molecule 1
IFNγ	Interferon γ
IgA	Immunoglobulin A
IgD	Immunoglobulin D
IgE	Immunoglobulin E
IgG	Immunoglobulin G
IgM	Immunoglobulin M
IL-	Interleukin-
IL-12p40	Interleukin-12 subunit p40
IL-12p70	Interleukin-12 subunit p70
IL-1RA	Interleukin-1 receptor antagonist
ILM	Inner limiting membrane
INL	Inner nuclear layer
iNOS	Inducible nitric oxide synthase
IP-10	Interferon gamma-induced protein 10

IPL	Inner plexiform layer
IS/OS	Inner photoreceptor segments/Outer photoreceptor segments
LFA-1	Lymphocyte function-associated antigen 1
LIX	Limb and CNX expressed 1
LLOQ	Lower limit of quantitation
LPS	Lipopolysaccharide
M1	Classically activated macrophage polarisation
M2	Alternatively activated macrophage polarisation
mAb	Monoclonal antibody
MAC	Membrane attack complex
MASPs	Mannose-associated serine protease 1
MBL	Mannose-binding lectin
MCP-	Monocyte chemoattractant protein-
MDA	Malondialdehyde
MFI	Median fluorescence intensity
MHC	Major histocompatibility class
MHRA	Medicines and healthcare products regulatory agency
Mig	Monokine induced by inferferon-gamma
MIP-2	Macrophage inflammatory protein 2
mKC	Murine keratinocyte chemoattractant
NADPH	Nicotinamide adenine dinucleotide phosphate
NFL	Nerve fibre layer
NF-κB	Nuclear factor kappa light chain enhancer of activated B cells
NK	Natural killer
NLRC4	NLR family CARD-domain containing protein 4
NLRP3	NLR family pyrin-domain containing protein 3
nNOS	Neuronal nitric oxide synthase
NO	Nitric oxide
NOX	NADPH oxidase
OCT	Optical coherence tomography
OD	Optic disc
OLM	Outer limiting membrane
ON	Optic nerve
ONL	Outer nuclear layer
OPL	Outer plexiform layer
ORT	Outer retinal tubulation

OVA	Ovalbumin
P. gingivalis	*Porphyromonas gingivalis*
P2RY12	Purinergic receptor P2Y, G-protein coupled, 12
pAb	Polyclonal antibody
PAMP	Pathogen-associated molecular pathogen
PBMCs	Peripheral blood mononuclear cells
PDL1	Programmed death-ligand 1
PECAM-1	Platelet and endothelial cells adhesion molecule 1
PR	Photoreceptor
PRR	Pathogen recognition receptor
R848	Resiquimod
RAP	Retinal angiomatous proliferation
rd8	Retinal degeneration mutation 8
RM	Repeated measures
RNFL	Retinal nerve fibre layer
ROS	Reactive oxygen species
RPE	Retinal pigment epithelium
RT	Room temperature
Salmonella	*Salmonella enterica* subspecies enterica serovar Typhimurium
SD-OCT	Spectral domain optical coherence tomography
SR	Subretinal space
sTNFRII	Soluble tumour necrosis factor receptor II
T_C	Cytotoxic T cell
TCR	T cell receptor
TGF-	Transforming growth factor-
T_H	Helper T cell
TIMP3	Tissue inhibitor of metalloproteinase 3
TLR	Toll-like receptor
TNFα	Tumour necrosis factor α
T_{REG}	Regulatory T cell
UV	Ultraviolet
VCAM-1	Vascular cell-adhesion protein 1
VEGF	Vascular endothelial growth factor
ZO-	Zonula occludens-

Chapter 1:

General Introduction

1.1 Overview of the systemic immune system

The immune system protects the host from a broad range of pathogens, including bacteria, viruses and parasites. There are diverse tissue-resident immune systems throughout the body, which may be required for local control of infection/disease, but all tissue-resident systems are linked to the systemic immune system. Activation of the systemic immune system leads to a large cascade of inflammatory processes, including activation of immune cells and production of inflammatory mediators and proteins, which are typically critical for the elimination of pathogens. Here, I provide an overview of the systemic immune system, focusing on pathways relevant to this thesis on systemic inflammation and the retina during healthy and diseased conditions.

1.1.1 Immune cells

Leukocytes (white blood cells) are derived from the differentiation of haematopoietic stem cells, which are separated into two key lineages: myeloid and lymphoid cells (Figure 1.1). In general, myeloid cells play a critical role in early-stage innate immunity where non-specific systems control pathogen growth, while lymphoid cells are essential for later-stage adaptive immunity where antigen-specific systems are developed to eliminate a pathogen. However, this is an oversimplification with lymphoid and myeloid cells, and their communication important at all stages of the immune response (Murphy & Weaver, 2017). Myeloid cells can generally be distinguished from lymphoid cells due to high expression of CD11b, a key component of complement receptor 3 (CD11b/CD18), and F4/80 on myeloid cells, which are absent, or in certain cases weakly expressed, on lymphoid cells (Yu et al., 2016)

1.1.1.1 Myeloid cells

Myeloid cells can be further subdivided into monocytes, dendritic cells and granulocytes (i.e. neutrophils, basophils, eosinophils). The overall role of these immune cells is to detect pathogens, reduce pathogen growth, and signal to the adaptive immune system to generate an antigen-specific immune response (Murphy & Weaver, 2017). These innate immune cells can engulf and ingest pathogens via a process called phagocytosis, where the pathogen is digested and its antigens are presented on the cell surface to communicate with antigen-specific lymphoid cells. Innate immune cells express many pattern-recognition receptors (PRRs) to detect generic molecular patterns associated with pathogens (Medzhitov, 2001). For example, toll-like receptor 4 (TLR4) recognises lipopolysaccharide (LPS) in the cell walls of gram-negative bacteria, while TLR7/8 recognise the structure of single stranded RNA typical of many viruses (Figure 1.2). In response to pathogen detection, a range of genes are upregulated that enhance phagocytosis of

pathogens by immune cells and induce the production of a range of inflammatory proteins, in particular cytokines, which communicate with and influence the function of other immune cells (Iwasaki & Medzhitov, 2004). Granulocytes also contain large numbers of toxic granules that can be released to destroy pathogens or infected cells (Murphy & Weaver, 2017).

Monocytes are generated in the bone marrow and are rapidly released into the blood circulation. Monocytes make up 5-10% of leukocytes and remain in the circulation for 1-3 days before entering tissues and differentiating into tissue-resident macrophages and dendritic cells in order to replace dying tissue-resident immune cells (Owen et al., 2013). Dendritic cells are a specialised type of macrophage, which mainly present antigens to stimulate adaptive immunity. Dendritic cells can normally be distinguished from monocytes/macrophages due to high expression of CD11c, a key component of complement receptor 4 (Poltorak & Schraml, 2015). Neutrophils are also generated in the bone marrow and have a short life-span in the blood with reports ranging from 5-90hrs. They make up the majority of leukocytes (50-70%) in the circulation (Owen et al., 2013). Neutrophils can be distinguished from other myeloid cells based on the expression of surface marker Ly6G or internal expression of neutrophil elastase and myeloperoxidase (Daley et al., 2007; Amanzada et al., 2011).

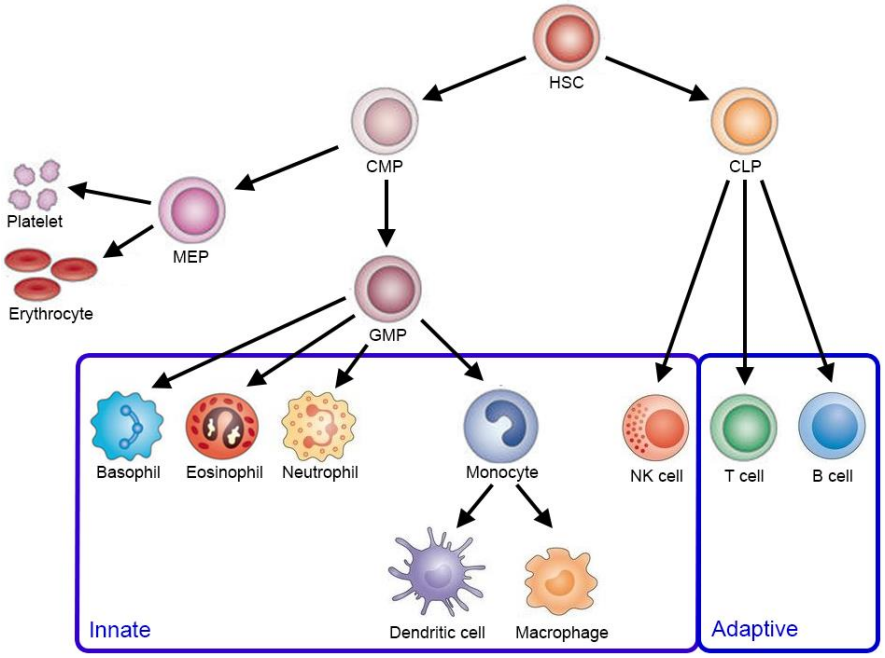

Figure 1.1 – Origins of myeloid and lymphoid cells.

Differentiation pathways of the key cell types responsible for innate and adaptive immunity. HSC, haematopoietic stem cell; CMP, common myeloid progenitor; CLP, common lymphoid progenitor; GMP, granulocyte-macrophage progenitor; MEP, megakaryocyte-erythrocyte progenitor. Cell illustrations taken from Nature Reviews Immunology. Data compiled from Murphy & Weaver, 2017 and Owen et al., 2013.

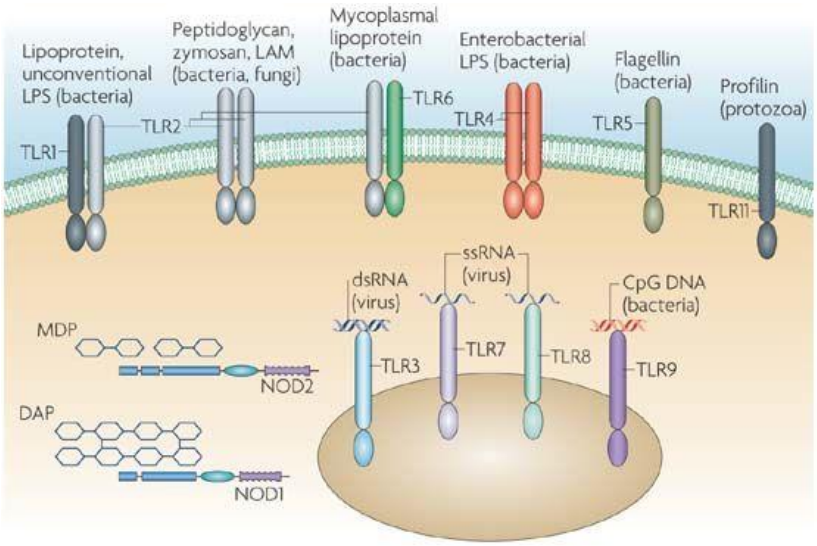

Figure 1.2 – Examples of pattern recognition receptors.

Pathogen-associated molecular patterns (PAMPs) are recognised by a range of pattern recognition receptors (PRRs) expressed by immune cells. These receptors can be intra- or extracellular. The subsequent gene transcription pathways induced by activation of these receptors can shape different immune responses based on the pathogen. Taken from Kaufmann, 2007.

1.1.1.2 Lymphoid cells

Lymphoid cells can be further subdivided into T cells, B cells and NK cells. T and B cells are considered the main cellular components of adaptive immunity.

T cells are typically separated into CD4+ helper T cells (T_H cells), which communicate with other cell types to orchestrate the immune system, and CD8+ cytotoxic T cells (T_C cells), which can kill cells expressing foreign antigens (Owen et al., 2013). In order to activate antigen-specific T cells, major histocompatibility class (MHC) I and II are expressed on the surface of cells and present antigens from within the cell to T cells, which will be activated if the T cell is specific for the antigen and receives further co-stimulation (Figure 1.3) MHCII typically presents antigens to T_H cells, while MHCI presents antigens to T_C cells (Alberts et al., 2015). Almost all human cells express MHCI, whereas MHCII is typically found only on antigen presenting cells. To prevent the immune system attacking host cells, T cells mature in the thymus where they are exposed to host antigens and reactive cells are removed before entering the circulation. Failures in this process to discriminate self and non-self can lead to autoimmunity (Owen et al., 2013).

Activated T_H cells have several known activation patterns, most notably type 1 (T_H1), type 2 (T_H2) and type 17 (T_H17) responses, which shape the immune response by releasing specific combinations of cytokines (Owen et al., 2013). Broadly speaking, T_H1 cells respond to intracellular

pathogens (e.g. intracellular viruses and bacteria), while T_H2 cells respond to extracellular pathogens (e.g parasites). T_H17 cells are important for immune responses at mucosal surfaces, such as the intestine, but are also linked to autoimmune disorders. These cellular responses affect the phenotype of other immune cells, for example cytokines from T_H1 cells polarise monocytes towards an M1 (classically activated) phenotype, while a T_H2 response polarises monocytes towards an M2 (alternatively activated) phenotype. Regulatory T cells (T_{REG}) comprise another important T cell subset that is responsible for reducing inflammation, particularly by suppressing other T cell populations (Murphy & Weaver, 2017).

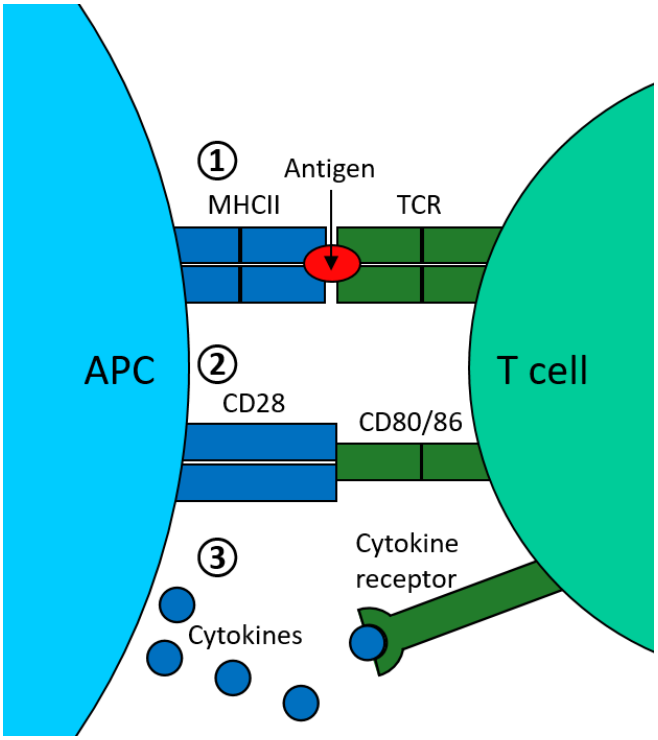

Figure 1.3 – Schematic of antigen-specific T cell activation.

1) MHCII on APCs presents internal antigens on the cell surface. T cells with a TCR specific for the epitope will bind the antigen and MHC molecule to form a complex. 2) Additional co-stimulation between ligands and receptors on T cells and antigen presenting cells (e.g CD28-CD80/86) will result in the activation of T cells. 3) The function of activated T cells will then be modulated by cytokines (e.g IFNγ). In the absence of co-stimulation, the T cell will become anergic, a form of functional inactivation. APC, Antigen presenting cell; MHCII, major histocompatibility complex class II; TCR, T cell receptor; IFNγ, interferon γ.

B cells provide the humoral component of adaptive immunity. In most cases, B cell responses are dependent on T cells (Figure 1.4), although some antigens (e.g. LPS) can stimulate B cells directly in a T cell independent manner (Parker, 1993). During T cell-dependent B cell activation, B cells express immunoglobulins as part of the B cell receptor on the cell surface, which binds and internalises antigens with the complementary structure. Parts of these antigens are then presented on the cell surface via MHCII. T cells specific for this antigen then bind to the MHCII-antigen complex and stimulate the B cell via receptors and cytokines (e.g CD40-CD40L). Stimulated B cells undergo clonal expansion, somatic hypermutation and class switching resulting in plasma cells that typically produces large amounts of immunoglobin G (IgG) with high-affinity for the antigen (Murphy & Weaver, 2017). T_H2 cells are particularly efficacious at stimulating immunoglobulin responses in B cells. The process of T and B cell interactions largely occurs at specialised immune sites, such as the spleen and lymph nodes.

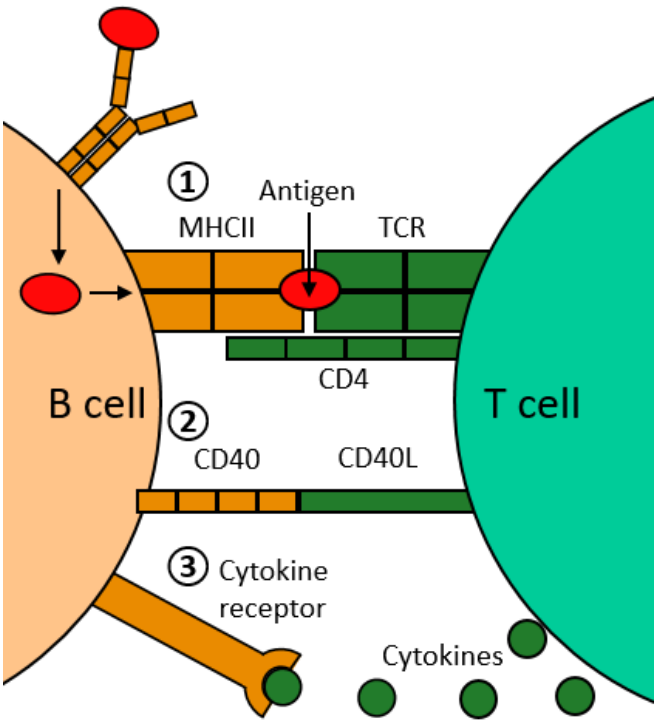

Figure 1.4 – T_H cell dependent activation of B cells.

1) The B cell receptor (BCR) internalises an antigen and presents it via MHCII to the TCR of the T cell, while CD4 binds to MHCII to stabilise the interaction. 2) T cells reactive to the antigen stimulate B cells via costimulatory ligand receptor interactions (e.g. CD40-CD40L). 3) Cytokines (e.g. IL-2/4/5) released from T cells communicate with B cells to eventually drive high affinity immunoglobulin production. MHCII; major histocompatibility complex class II; TCR, T cell receptor; IL-, interleukin-.

In addition to the effector cells described, the adaptive immune system can also generate memory T and B cells, which are long-lasting cells that can quickly generate an antigen-specific immune response when subsequently challenged with the same antigen. There are also lymphoid cells associated with innate immunity, NK (natural killer) cells. NK cells possess activating and inhibitory receptors and will release cytotoxic granules like T_C cells if a cell induces more activation than inhibition, indicating a foreign, viral-infected or diseased cell (Martinet & Smyth, 2015). Activated NK cells also release a range of cytokines that help to shape the innate and adaptive immune responses.

1.1.2 Effector molecules of the immune system

1.1.2.1 Cytokines

Cytokines are molecules responsible for the communication between immune cells and are typically soluble, although membrane-bound forms are found. A complex network of cytokine expression regulates the immune response during health and disease. In response to an infection, a specific pattern of cytokines is released at specific time-points to regulate and communicate between the innate and adaptive immune systems. Table 1.1 summarises the function of the key cytokines discussed in this thesis.

Cytokines can act on a variety of different systems to fight infection. For example, IL-1β, IL-6 and TNFα can communicate with the brain to induce fever and sickness behaviours, such as anorexia and apathy, to reduce pathogen growth (Dantzer et al., 2008). Meanwhile, IL-6 and TNFα also act on the liver to produce a range of acute phase proteins, such as C-reactive protein (CRP), complement pathway components and coagulation factors, each of which have specific functions that can assist the immune system in clearing pathogens (Gabay & Kushner, 1999).

An analysis of cytokines can provide insights into the polarisation of the immune response (Table 1.2). IFNγ, IL-12 and TNFα are all indicative of a type 1 immune response, while IL-4, IL-5 and IL-13 are key cytokines involved in type 2 immune responses (Mills et al., 2000). This T_H1/M1 and T_H2/M2 paradigm of immune responses is a useful tool to categorise immune responses and is very common within the literature, but doesn't properly convey the complexities or subtle nuances of the immune system. Indeed, although intracellular bacterial infections typically induce a skew towards T_H1 cells as the dominant polarisation status, activation of T_H1, T_H2 and T_H17 cells to different extents is required to properly fight infection. In this thesis, shifts towards cytokines of the either the type 1 and type 2 immune response are frequently discussed, but this does not exclude important roles for the less dominant immune response in these studies.

Cytokine	Response*	Secreted by	Functions
IFNγ	Adaptive	T_H1 cells, CD8+ T cells, NK cells	Macrophage activation, increased MHC expression and antigen presentation, suppression of T_H2 cells
IL-1β	Innate	Monocytes, macrophages, endothelial cells, epithelial cells	Activation of macrophages and T cells, fever
IL-2	Adaptive	T cells	Proliferation of all T cell subsets
IL-4	Adaptive	T_H2 cells, mast cells	T_H2 cell polarisation, suppression of T_H1 subsets, B cell activation
IL-5	Adaptive	T_H2 cells, mast cells	Growth and differentiation of eosinophils
IL-6	Innate	Macrophages, endothelial cells, T_H2 cells	Growth and differentiation of T and B cells, fever, production of acute phase proteins
IL-8$^{\Delta}$	Innate	Monocytes, macrophages, endothelial cells	Recruits and activates neutrophils, macrophages and naive T cells to sites of inflammation
IL-10	Adaptive	T cells, macrophages	Strongly suppresses macrophage function
IL-12	Innate	Macrophages, dendritic cells, B cells	NK cell activation, T_H1 cell polarisation
IL-13	Adaptive	T_H2 cells	Suppression of macrophages and T_H1 cells, Growth and differentiation of B cells
IL-18	Innate	Activated macrophages	Stimulates IFNγ production by T and NK cells. Promotes early-stage T_H1 responses and later-stage T_H2 responses
TNFα	Innate	Monocytes, macrophages, neutrophils, activated T cells, NK cells	Supports local inflammation, activation of endothelial cells, production of acute phase proteins

Table 1.1 – Summary of important innate and adaptive cytokines in the immune response.
Information in table was summarised from Owen et al., 2013 and Murphy & Weaver, 2017.
**Cytokines can be broadly characterised into dominant expression by innate or adaptive immune cells, although there is a great deal of overlap in expression, for example IL-10 can be produced by both T-cells and macrophages.* $^{\Delta}$ *IL-8 (CXCL8) is classified as a chemokine – a group of small cytokines that induce immune cell chemotaxis, which is the migration of immune cells along a concentration gradient towards areas of high expression of chemokines. IFNγ, interferon γ; IL-, interleukin; TNFα, tumour necrosis factor α.*

Polarisation	Polarising Cytokines	Effector Cytokines	Functions
T_H1	IFNγ IL-12 IL-18	IFNγ TNFα	Co-ordinates response to intracellular pathogens
T_H2	IL-4	IL-4 IL-5 IL-13	Co-ordinates response to extracellular pathogens
T_H17	IL-6 TGF-β	IL-17 IL-22	Co-ordinates response to some fungal and bacterial infections
T_{REG}	IL-2 TGF-β	IL-10 TGFβ	Suppression of inflammation, particularly other T cell subsets

Table 1.2 – Characterisation of different immune system polarisation states.
IL-, interleukin-; IFN-γ, interferon γ; TGF-β, transforming growth factor β. Information in table was summarised from Owen et al., 2013 and Murphy & Weaver, 2017.

Most cytokines/chemokines are well conserved between mouse and human, but notably the chemokine IL-8 does not have an equivalent protein in mice. Instead the protein mKC (murine keratinocyte-derived chemokine/CXCL1) largely compensates for IL-8 function in mice, although MIP-2 (macrophage interacting protein 2/CXCL2) and LIX (lipopolysaccharide-induced CXC chemokine/CXCL5) can also replicate some IL-8 function in mice (Hol et al., 2010).

1.1.2.2 Inflammasomes

Inflammasomes are a component of the innate immune system formed in response to a range of pathogens. The best characterised inflammasome is the NLRP3 inflammasome, which is a multi-protein complex responsible for the maturation of IL-1β and IL-18 into active cytokines (Latz et al., 2013). NLRP3 protein production is stimulated by PAMPs or DAMPs and further activating signals induce conformational changes in NLRP3 allowing the recruitment of ASC adaptor proteins, which in turn bind multiple inactive pro-caspase 1 molecules leading to autocleavage forming active caspase-1 (Figure 1.5). Caspase-1 then cleaves pro-IL-1β and pro-IL-18 into active IL-1β and IL-18, which can drive activation of macrophages, T cells and NK cells.

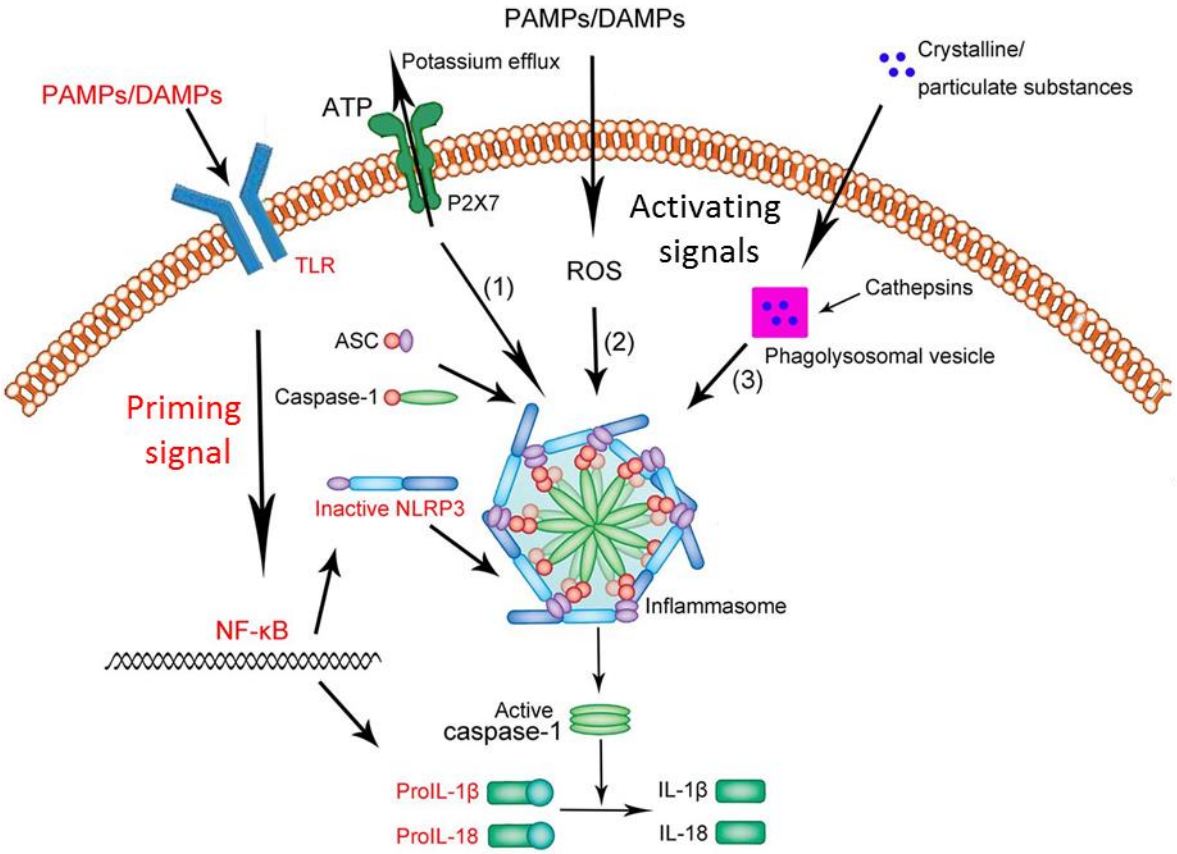

Figure 1.5 – Activation of the NLRP3 inflammasome.

The activation of the NLRP3 inflammation requires a 'priming' and 'activating' signal. A 'priming' signal (signal 1) activates NF-κB, leading to expression of NLRP3, pro-IL-1β and pro-IL-18. An example of this signal is activation of a range of toll-like receptors (TLRs). An 'activating' signal (signal 2) is then required to induce the assembly of the inflammasome components NLRP3, ASC and pro-caspase 1. A variety of signals have been identified that can provide this activation, including low intracellular K^+, presence of ROS or lysosomal disruption by crystalline salts. ASC, apoptosis-associated speck-like protein; ATP, adenosine triphosphate; PAMP, pathogen-associated molecular pattern; DAMP, danger-associated molecular pattern; IL-, interleukin-; NF-κB, nuclear factor kappa-light-chain-enhancer of activated B cells; NLRP3, NLR family pyrin domain-containing protein 3; ROS, reactive oxygen species. Adapted from Shao et al., 2015.

1.1.2.3 Immunoglobins

Immunoglobulins are produced by B cells and have a range of possible downstream functions (Figure 1.6). There are 5 types of immunoglobulin (IgA, IgD, IgE, IgG and IgM), each of which has a different capacity to activate effector functions (Owen et al., 2013). In this thesis, the main circulating form, immunoglobulin G, is discussed. IgG is comprised of a variable antigen binding domain (Fab) and a constant (Fc) region. The diversity of the Fab region enables the generation of

antibodies against virtually any antigen, while the constant region can bind C1q to activate the complement pathway and bind Fc receptors expressed by many immune cells to activate cytotoxic and phagocytic functions (Owen et al., 2013).

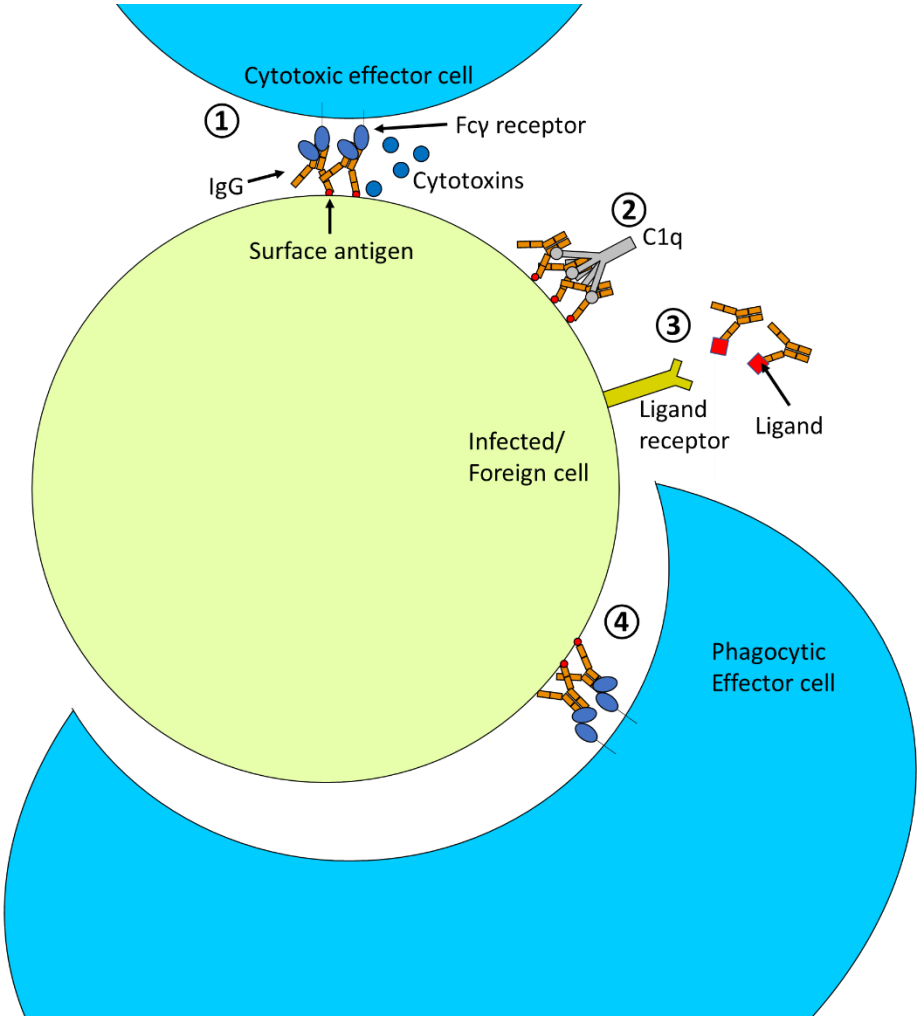

Figure 1.6 – Effector functions of immunoglobulins.

1) Antigen dependent cell cytotoxicity – Antibodies bind antigens expressed on the surface of infected/foreign cells and activate Fc receptor-expressing cytotoxic effector cells (e.g. NK cells via FcγRIII) to release cytotoxic granules that kill the infected/foreign cell or pathogen.

2) Complement dependent cytotoxicity – Antibodies bind to surface antigen to form a complex, which activates the classical complement pathway via C1q to induce inflammation and tissue damage. 3) Blocking - neutralisation of soluble proteins by sequestration (e.g. toxins).

4) Opsonisation and phagocytosis – Antibodies bind to surface antigens and activate Fc receptor expressing-phagocytic effector cells (e.g macrophages, neutrophils). IgG, immunoglobulin G; C1q, Complement component 1, subcomponent q.

In mouse and humans there are 4 major subclasses of IgG termed IgG1, IgG2, IgG3 and IgG4 in humans and IgG1, IgG2a, IgG2b and IgG3 in mouse and these have differential capacity to activate effector functions. Broadly speaking, human IgG1 and mouse IgG2a are most similar as they induce similar levels of complement fixation and mainly bind proteins; human IgG2 and mouse IgG3 are most similar as they mainly bind carbohydrates; human IgG3 and mouse IgG2b are most similar as they induce similar levels of complement fixation and mainly bind proteins; human IgG4 and mouse IgG1 are most similar due to their capacity to activate mast cells (Hussain et al., 1995).

In response to infections, the immune system undergoes IgG subclass switching, where the production of the different IgG subclasses is varied to activate specific effector functions designed to destroy the particular pathogen. For example, in mice cytokines associated with the T_H1 immune response (i.e. IFNγ and IL-12) induce production of IgG2a, IgG2b and IgG3 and inhibits IgG1 production, while the inverse is true during an IL-4 dominant T_H2 immune response (Germann et al., 1995). Compared to mouse IgG1, mouse IgG2a and IgG2b can strongly bind Fc receptors to activate immune cells and IgG3 can strongly activate the complement pathway (Lefeber et al., 2003), meaning that the IgG subtypes during a T_H1 immune response are associated with a more pro-inflammatory response at a cellular and protein level.

1.1.2.4 Complement

The complement system is a collection of over 30 proteins that interact to fight pathogens (Murphy & Weaver, 2017). Most of these proteins are acute phase proteins synthesised by the liver during an immune response. There are three recognised pathways of complement activation, classical, lectin and alternative, which are summarised in Figure 1.7. The classical, lectin and alternative pathways are initiated by crosslinking of C1q, C2 binding to microbial-associated sugars and spontaneous production of C3b respectively. The number of active complement components is amplified at each stage, leading to a strong and rapid effect, which can include recruitment of immune cells via anaphylatoxins (C3a and C5a), enhanced phagocytosis of pathogens via C3b and cell lysis via the membrane attack complex (MAC, C5b-9).

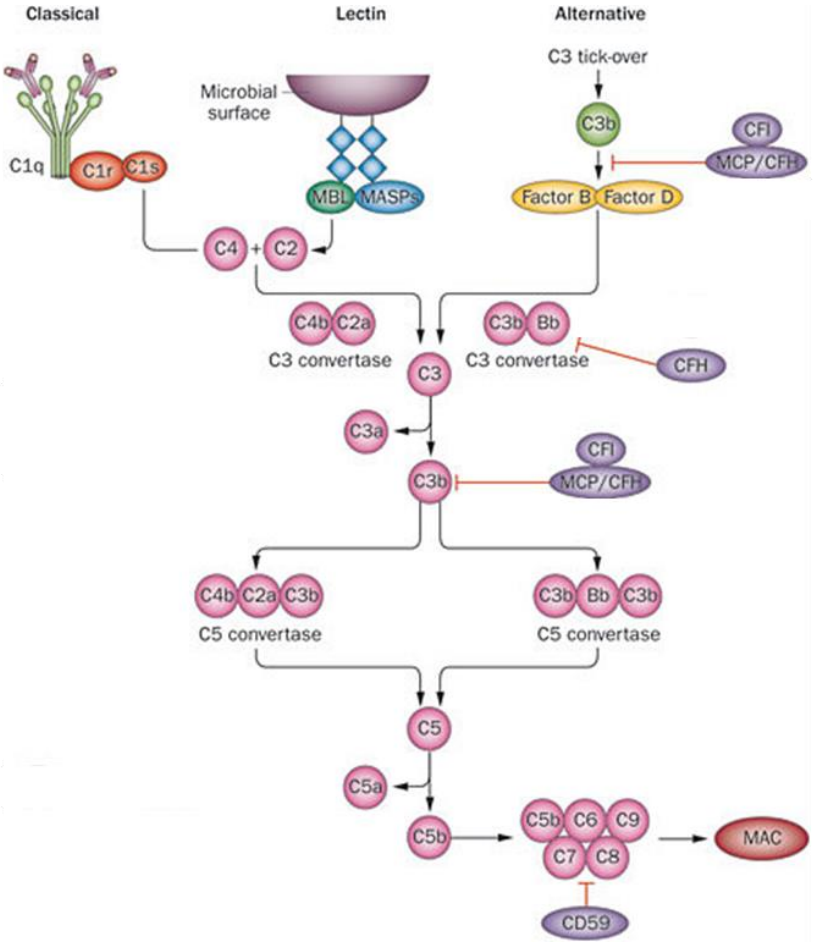

Figure 1.7 – Different pathways of complement activation.

In the classical cascade C1q, C1r and C1s combine to produce C3 convertase, an enzyme which splits C3 into C3a and C3b subunits. The C3b subunit then forms part of C5 convertase, which splits C5 into C5a and C5b subunits. C5b then associates with C6, C7, C8 and C9 to form the membrane attack complex (MAC). The MAC is a complex with a central pore that allows unrestricted diffusion of molecules into and out of the cell, leading to cell death if enough pores are formed. At the same time, release of potent anaphylatoxins C3a and C5a increases local inflammation and often induces immune cell recruitment. In the lectin pathway, mannose binding lectin (MBL) binds to sugar structures expressed by certain bacteria leading to activation of C3 convertase and downstream signalling as seen with the classical pathway. The alternative pathway relies on the spontaneous low-level production of C3b from C3. C3b coats the surface of pathogens and infected/foreign cells and in combination with activated factor B (Bb), which is activated by factor D, forms an alternative C3 convertase that converges on the downstream cascades of the classical and lectin pathways. There are several negative regulators of the complement pathway, notably complement factor I (CFI), which cleaves C3b to form inactive C3b (iC3b), and complement factor H, which acts both as a cofactor for CFI activity and by enhancing degradation of the alternative (C3b-Bb) C3 convertase. There are also receptors that act as negative regulators of the complement system, for example CD46 (membrane cofactor protein/MCP) can bind and sequester

C3b and C4b and act as a cofactor for CFI activity. Bb, activated factor B; C1q, complement component 1 subcomponent q; C1r, complement component 1 subcomponent r; C1s, complement component 1 subcomponent s; C2, complement component 2; C2a, complement component 2 cleavage product a; C3, complement component 3; C3a, complement component 3 cleavage product a; C3b, complement component 3 cleavage product b; iC3b inactivated complement component 3 cleavage product a; C4, complement component 4; C4b, complement component 4 cleavage product b; C5, complement component 5; C5a, complement component 5 cleavage product a; C5b, complement component 5 cleavage product b; C6, complement component 6; C7, complement component 7; C8, complement component 8; C9, complement component 9; MAC, membrane attack complex. Adapted from Noris et al., 2012.

1.1.3 Summary

The immune system is a complex biological arrangement of immune cells that interact to control and eliminate disease or pathogens. In response to a pathogen, an integrated network of non-specific innate immune cells controls pathogen growth and initiates the development of an antigen-specific adaptive immune cell response to eliminate the pathogen. Immune cells use cytokines to communicate and shift immune responses towards a specific polarisation status best suited to respond to the pathogen. These events lead to activation of effector pathways and clearance of infected/foreign cells or pathogens. Such pathways include activation of cytotoxic cells (neutrophils, NK cells, T_C cells), phagocytosis (e.g. monocytes/dendritic cells) and activation of the complement pathway, each of which can be enhanced by immunoglobulin deposition.

1.2 Overview of the retina and the retinal immune system

1.2.1 Retinal structure and function

All vertebrate species possess a retina within the eye (Figure 1.8), which develops from outgrowths of the developing brain and forms part of the central nervous system (CNS) (Randlett et al., 2011). Photons of light enter the eye through the pupil and are focused by the lens onto the retina. The retina is comprised of 5 different neuronal cell types: photoreceptor, horizontal, bipolar, amacrine and ganglion cells (Figure 1.9). Light passes through the inner layers of the retina to reach the photoreceptors, which transduce light into electrical signals. These signals are then passed onto synapsing neurons, most commonly along the photoreceptor > bipolar cell > ganglion cell route (Purves et al., 2011). Ganglion cells, whose long axons meet to form the optic nerve, pass information for visual processing to the brain. Horizontal cells, which can sit between photoreceptors and bipolar cells, and amacrine cells, which can sit between bipolar cells and ganglion cells, are mainly responsible for lateral flows of information with the retina. Overall, the interactions of these neuronal cell types allow light to be converted into electrical signals, which are summated, integrated and sent for visual processing in the brain, largely through projections to the thalamic dorsal lateral geniculate nucleus, which in turn projects to the primary visual cortex (Purves et al., 2011).

The mechanisms surrounding light transduction into electrical stimuli and subsequent processing can be recorded by electroretinography (Figure 1.10). Following light stimulation, there is an initial negative deflection, which corresponds to hyperpolarisation of the photoreceptors (Frishman & Wang, 2011). Photons of light pass through the inner layers of the retina and induce photoisomerisation of retinal molecules causing conformational changes in the associated opsin G-protein coupled receptors (GPCRs) that lead to less frequent opening of photoreceptor cGMP-gated cation channels (Ebrey & Koutalos, 2001). Reduced entry of cations, predominantly Na^+ but also Ca^{2+}, causes photoreceptor membrane hyperpolarization (Schmitz & Witkovsky, 1997). Following this negative deflection, there is a large positive deflection as the reduction of glutamate release from hyperpolarised photoreceptors leads to the activation of the inner retinal neurons, particularly ON bipolar cells, and a subsequent wave of depolarisation (Frishman & Wang, 2011).

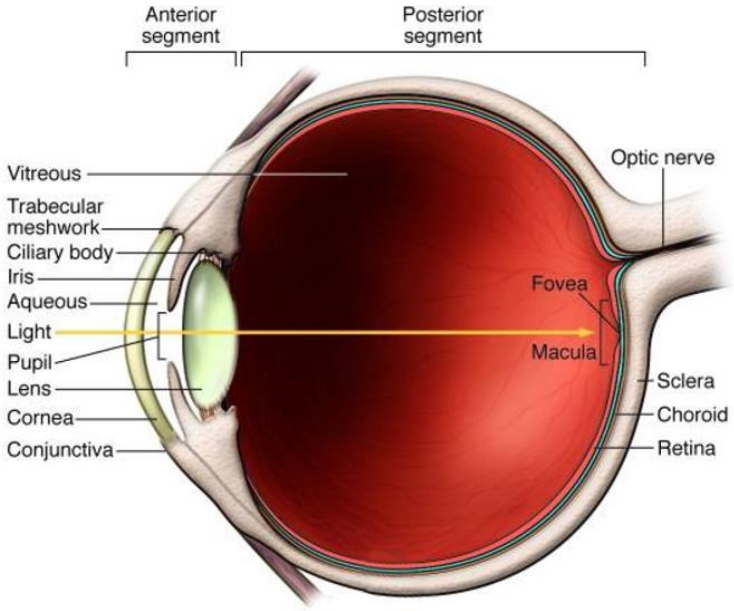

Figure 1.8 – Anatomy of the eye.

Light enters the eye through the pupil and is focused by the lens onto the retina, particularly at the centre of the retina termed the macula. The vitreous humour is a fluid that fills the inside of the posterior segment to maintain the eye's structural integrity and to assist light focusing, while the aqueous humour fills the anterior segment. The neural retina is supported by the retinal pigment epithelium and choroidal blood supply, which is attached to the sclera. Adapted from Caspi, 2010.

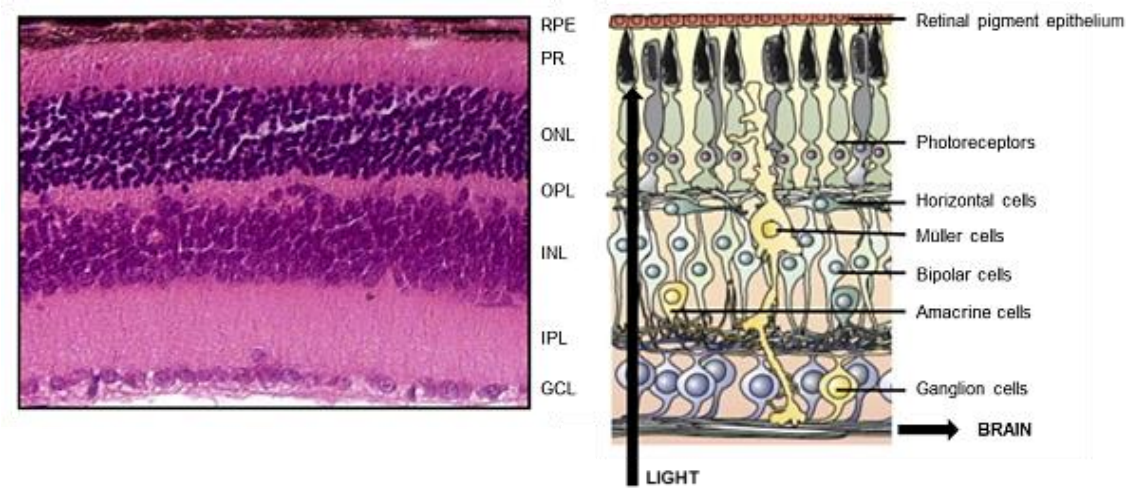

Figure 1.9 – Structure of the retinal layers and the underpinning cell types.

Left – Haematoxylin & eosin stain of the human retina showing the retinal layers (RPE, Retinal pigment epithelium; PR, photoreceptors; ONL, outer nuclear layer; OPL, outer plexiform layer; INL, inner nuclear layer; IPL, inner plexiform layer; GCL, ganglion cell layer). Right – illustration of cell localisation and types forming the retinal layers. The RPE is the outermost layer of the retina and supports the rod and cone photoreceptors. The light sensing compartments of photoreceptors and

are found in the PR layer. The ONL, INL and GCL are comprised of the cell bodies of photoreceptors, bipolar cells and ganglion cells respectively, while the OPL and INL consist mainly of the synapses between photoreceptors and bipolar cells, and bipolar cells and ganglion cells respectively. Adapted from Sanges et al., 2013.

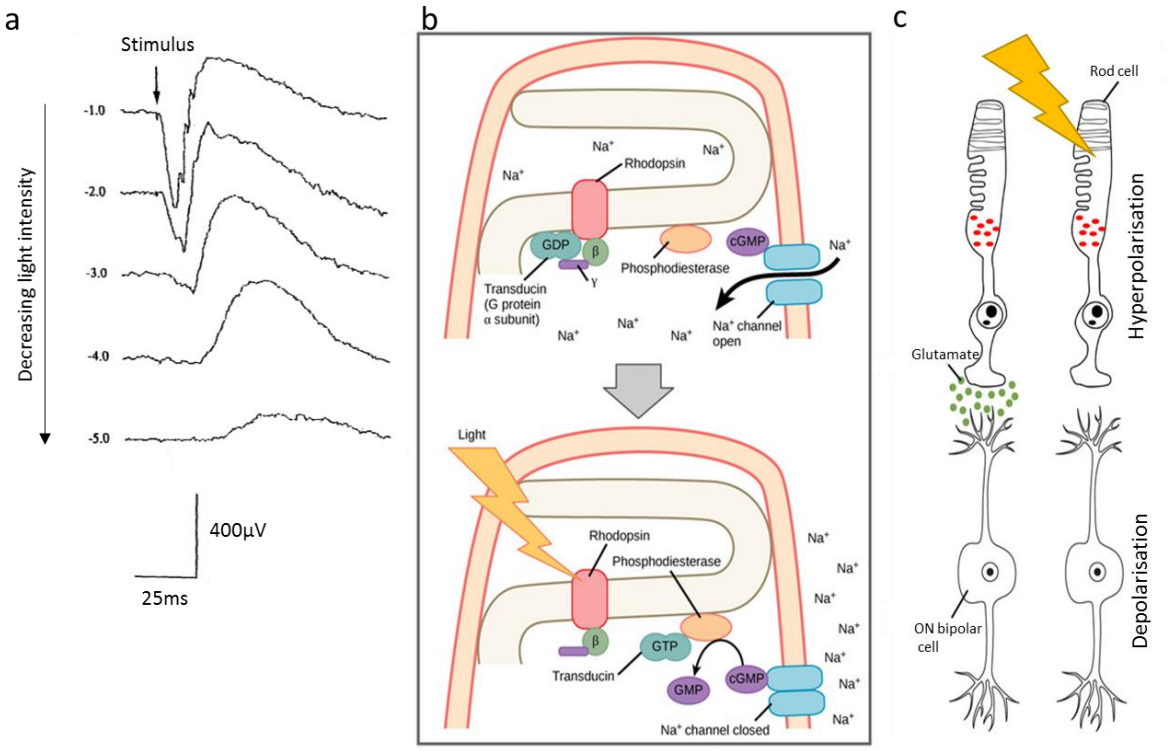

Figure 1.10 – Electrical recordings during phototransduction and retinal processing.
(a) Electroretinogram (ERG) from a healthy human subject showing an initial wave of hyperpolarisation (a-wave) followed by a wave of depolarisation (b-wave) in response to high light intensity (-1.0 log relative intensity), but not low light intensity (-5.0 log relative intensity). (b) The a-wave results from photon-induced conformational changes in rhodopsin leading to the closure of cGMP-gated cation channels and photoreceptor hyperpolarisation. (c) The b-wave results from the depolarisation of most inner retinal neurons in response to reduced glutamate release by hyperpolarised photoreceptors, although there are a minority of cells (i.e OFF bipolar cells) that hyperpolarise in response to reduced glutamate signalling. GDP, guanosine diphosphate; cGMP, cyclic guanosine monophosphate; GTP, guanosine triphosphate. (a) Adapted from Asi & Perlman, 1992, (b, c) Adapted from Boundless Biology, 2016.

Photoreceptors are highly active cells with high metabolic demand and are constantly exposed to light and damaging ultraviolet (UV) radiation (Yu & Cringle, 2005; Xu et al., 2009). To cope with these conditions, the photoreceptors are supported by a specialised epithelial monolayer termed the retinal pigment epithelium (RPE), which is critical for healthy retinal function. The outer layers of the retina (photoreceptors and RPE cells) are not vascularised, and instead the fine choriocapillaris of the choroidal vasculature lie in close apposition to the RPE cells and are separated from the RPE by Bruch's membrane (BrM), a thin membrane composed of collagen and elastin layers (Figure 1.11) (Mettu et al., 2012; Bhutto & Lutty, 2012). RPE cells support photoreceptor survival by selectively allowing the flow of essential nutrients from the choroid to the photoreceptors, including amino acids, oxygen and antioxidants (Erickson et al., 2007). In addition, RPE cells phagocytose shed segments/disks of photoreceptors to prevent accumulation of damage within the photoreceptors (Lueck et al., 2012; Xu et al., 2009). RPE cells also secrete a variety of trophic factors (e.g pigment epithelium-derived factor/PEDF) to promote photoreceptor survival (Tombran-Tink et al., 1995; Bhutto & Lutty, 2012).

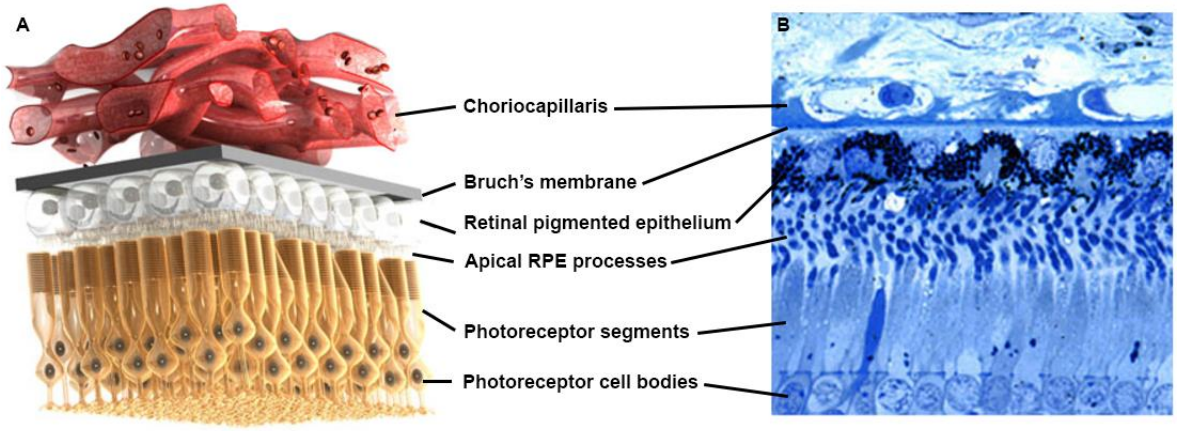

Figure 1.11 – Structure of the outer retinal layers and choroid.

(A) Schematic and (B) toluidine blue histology of the outer retinal layers and choroid. The choriocapillaris lie in close apposition to the retinal pigment epithelium (RPE) and are separated by Bruch's membrane. The photoreceptor segments shed discs of macromolecules (small blue dots) that are phagocytosed by the RPE via apical processes, a key process in retinal homeostasis. RPE, retinal pigment epithelium. (A) Adapted from The Angiogenesis Society, 2012, (B) Adapted from Hageman et al., 2007.

Light entering the eye is maximally detected by a 5.5mm wide structure termed the macula im huamns (Figure 1.12) (Agarwal, 2012). Histologically, the structure can be defined as a specialised area with two or more layers of ganglion cells (Remington, 2012). The macula consists of a central fovea containing a high density of cone cell photoreceptors responsible for high acuity vision in high light conditions (Curcio, 2001; Hildebrand & Fielder, 2011). The parafovea region surrounding the fovea is dominated by densely packed rod cells responsible for monochrome vision in low light conditions (Curcio, 2001; Curcio et al., 1990). At the fovea, the inner retinal layers are displaced outwards, presumably to prevent light scattering through the retina before reaching the fovea, which would reduce visual acuity (Provis et al., 1998). The inner layers of the retina are vascularised with capillaries extending from branches of the central retinal artery, but these capillaries are sparse at the macula, where reduced light scattering due to lack of blood vessels would greatly improve visual acuity (Provis et al., 1998). Although the human macula is only a small part of the retina, the dense levels of photoreceptors and displacement of inner retinal layers provides a high level of visual acuity that is unmatched by the rest of the retina. The macula can be visualised as a dark spot in images of the retinal surface (fundus) mostly due to the high expression of pigments lutein and zeaxanthin, which absorb damaging UV and blue light and scavenge free radicals to protect the retina from oxidative damage (Carpentier et al., 2009; Trieschmann et al., 2008; Snodderly et al., 1984; San Giovanni & Neuringer, 2012). RPE cells have a black/brown appearance due to high levels of pigment, particularly melanin pigment in melanosomes, to absorb any scattered light not used by the photoreceptors and as the fovea is thinner than the surrounding retina, this improved visualisation may also contribute to the dark appearance of the macular in fundoscopy (Agarwal, 2012; Bhutto & Lutty, 2012).

In contrast to humans, rodents do not possess a macula but instead have a consistent retinal structure, which makes their use in modelling macular diseases limited to analysis of more general retinal degeneration (Ramkumar et al., 2010). Overall, rodents have fewer cone cells (≈3%) than humans (≈5%), completely lack cone cells against red light and show little change in ratio of cones:rods throughout the retina, while cones are greatly enriched in the human macula compared to the peripheral retina (Curcio et al., 1990; Jacobs, 1993; Jeon et al., 1998; Carter-Dawson & LaVail, 1979). Mice also have much larger neuronal receptive fields in the retina/visual cortex compared to primates (average 14° in mice and <1° in macaques) providing greater sensitivity to light, but greatly reduced visual acuity (Hübener, 2003). Overall, these parameters enable mice to have better night vision, at the expense of high acuity colour vision during high light conditions.

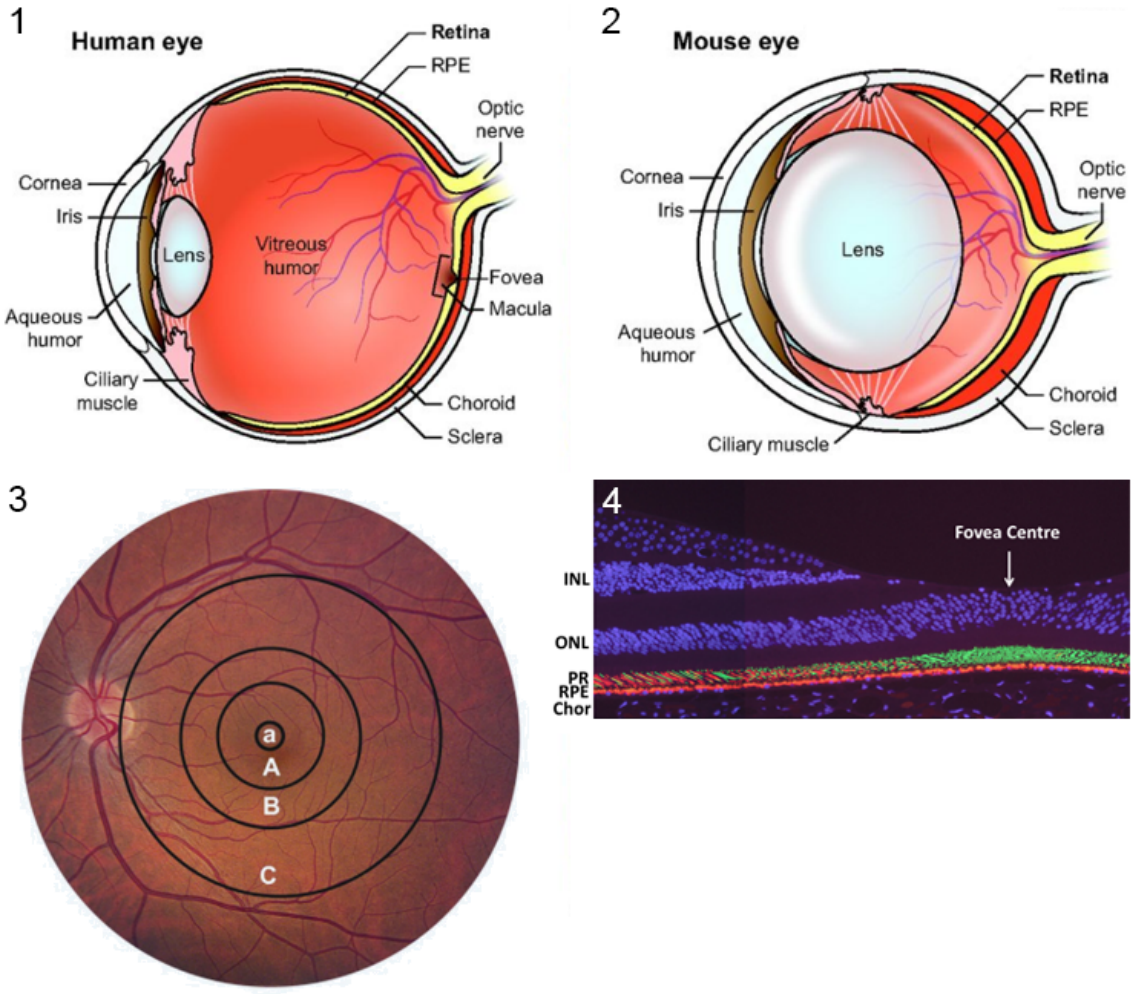

Figure 1.12 – Location and structure of the macula.

(1,2) The human retina has a specialised structure termed the macula, which is not present in the rodent retina. (3) The macular is a 5.5mm structure demarcated into 3 zones: (A) the fovea, which includes the (a) central foveola, (B) the parafovea and (C) the perifovea. (4) At the fovea, the inner retinal layers are displaced outwards and the ganglion cell layer is more than one cell thick. At the fovea, cone cells (green) are the dominant photoreceptors while the outer macula areas and the peripheral retina are dominated by rod cell photoreceptors (red). RPE, retinal pigment epithelium; INL, inner nuclear layer; ONL, outer nuclear layer; PR, photoreceptors; Chor, choroid. (1,2) Taken from Veleri et al., 2015, (3) taken from Agarwal, 2012, (4) adapted from Leung & Snodderly, 2006.

1.2.2 Macroglial cells – Müller cells and astrocytes

There are three types of glial cells in the retina: astrocytes and Müller cells, which are both macroglial cells, and microglial cells. Glial cells are non-neuronal cells responsible for a variety of functions to support neurons, including homeostasis, physical support and immune defence.

Müller cells are specialised radial glial cells and are the dominant glial cell of the retina, representing ≈90% of glia (Reichenbach et al., 1995; Vecino et al., 2016). They span the neurosensory retinal layers, providing structural support, and can detect and respond to mechanical deformation (Macdonald et al., 2015; Jadhav et al., 2009) (Figure 1.13). Müller cells also have many key homeostatic functions. They can provide nutrients (e.g. glucose) and trophic factors (e.g retinoic acid) to support neuronal survival as well as suppressing angiogenesis via PEDF and thrombospondin-1 (Edwards, 1994; Eichler et al., 2004a, 2004b; Poitry et al., 2000; Poitry-Yamate et al., 1995; Bringmann et al., 2009). They are responsible for the clearance of waste products from neurons (e.g. CO_2, amino acids, ammonia) and phagocytosis of larger debris (Reichenbach & Robinson, 1995; Bejarano-Escobar et al., 2017). Müller cells can also uptake extracellular potassium to protect neurons from excessively high potassium levels, which can be damaging and toxic, and also regulate water concentrations and retinal pH (Reichenbach & Robinson, 1995). Finally, Müller cells can release a number of signalling molecules (e.g. glutamate, dopamine, taurine, GABA) to directly alter neural function (Reichenbach & Bringmann, 2013; Ando et al., 2012).

Astrocytes are almost entirely limited to the retinal nerve fibre layer comprised of the long axons of ganglion cells (Figure 1.13). Astrocytes share many roles of Müller cells, including the storage and provision of nutrients (e.g. glucose) for the ganglion cells and support of neuronal function through the uptake and metabolism of neurotransmitters and regulation of extracellular potassium levels (Hollander et al., 1991; Newman, 2003; Tsacopoulos & Magistretti, 1996; Vecino et al., 2016). The processes of astrocytes, along with Müller glia, encompass retinal blood vessels to form a blood-retinal-barrier (BRB) that separates the systemic circulation and the retinal microenvironment, which is discussed further in section 1.2.4.

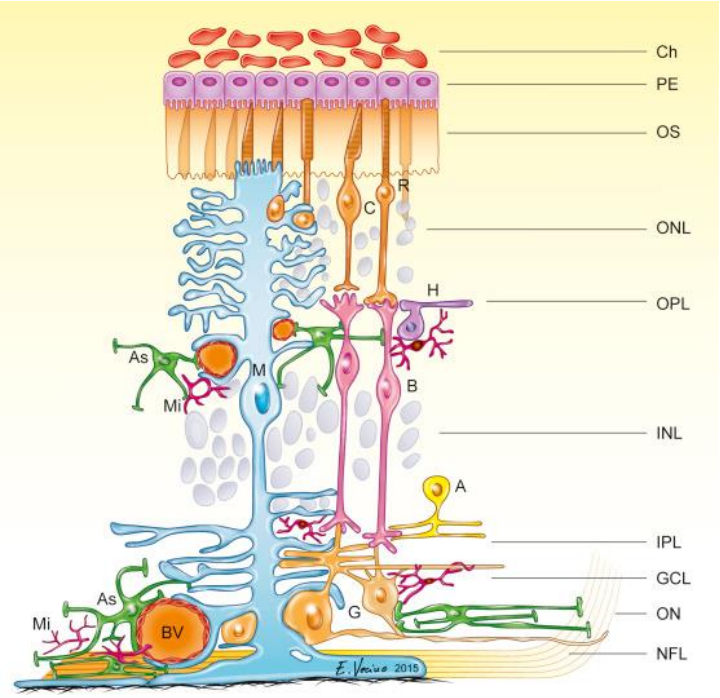

Figure 1.13 –Location of glial cells within the retina.

Müller cells (M) span the entire neurosensory retina, while astrocytes (As) are confined to the nerve fibre layer (NFL) and microglia (Mi) are typically found in the inner and outer plexiform layers (IPL/OPL). BV, blood vessel; G, ganglion cell; A, amacrine cell; B, bipolar cell; H, horizontal cell; C, cone photoreceptor; R, rod photoreceptor; Ch, choroid; PE, retinal pigment epithelium; OS, outer segments; ONL, outer nuclear layer; OPL, outer plexiform layer; INL, inner nuclear layer; IPL, inner plexiform layer; GCL, ganglion cell layer; NFL; nerve fibre layer; ON, optic nerve. Taken from Vecino et al., 2016.

1.2.3 Microglia cells – the resident immune cell of the CNS

The eye is, in some aspects, immune privileged as it lacking many immune cell types found in the systemic immune system (Stein-Streilein, 2013). T and B lymphocytes do not enter the retina under healthy conditions and immunohistochemical staining confirms a lack of T and B cells in the healthy human retina along with few dendritic cells (Yang et al., 2000; Crane & Liversidge, 2008). Microglia, which are the resident immune cells of the CNS, therefore have a critical role in immune defence. Microglia are tissue resident macrophages that are typically located near inner retinal blood vessels in the inner and outer plexiform layers in healthy eyes (Figure 1.13) (Ambati et al., 2013).

Under healthy conditions, microglia typically display a ‘resting’ phenotype characterised by a small cell body with long, highly ramified processes that survey the microenvironment (Saraswathy et al., 2006). This ‘resting’ phenotype is controlled by co-ordinated suppressive

signals from a range of cellular sources, including neuron-microglia interactions (e.g. CD200-CD200R) and suppressive cytokine production by RPE cells and astrocytes (Figure 1.14) (Langmann, 2007; Karlstetter et al., 2015). There is some evidence that microglia are critical for outer retinal homeostasis, as microglia migrate to the subretinal space to clear away debris such as lipofuscin and melanin, particularly during aging in mice (Xu et al., 2008).

In response to pathogenic or damaged cell stimuli, microglia become activated, adopt a round hypertrophic cell morphology and migrate to the stimulus site (Saraswathy et al., 2006). Activated microglia develop macrophage-like effector functions (Figure 1.14), including cytokine production and phagocytosis, to clear pathogens or debris and subsequently return to a resting state once the activating stimulus is removed (Saraswathy et al., 2006), although previous activation may have functional consequences on the response of microglia to subsequent activation (Püntener et al., 2012; Perry & Holmes, 2014). Peripheral macrophages can be divided into classical (M1) macrophages that can secrete IL-1β, IL-6, IL-12 and TNFα, while alternatively-activated (M2) macrophages may secrete immunoregulatory factors, including IL-10, IL-1RA and TGF-β (Mantovani et al., 2013; Mosser & Edwards, 2008). Along these lines, microglial activation has been broadly classified into two categories: classical (M1-like) activation and alternative (M2-like) activation. This paradigm is important because many studies looking at retinal microglia have been characterised in these terms. However, this duality is becoming outdated due to an increasing number of subcategories that simultaneously express traditional M1 and M2 factors and the high plasticity of myeloid cells to alter phenotype in response to changing local and systemic environments *in vivo* that is not identified by *in vitro* studies (Perry & Teeling, 2013; Gleissner, 2012; Kadl et al., 2010).

Microglial cells originate from the yolk-sac and, unlike many other tissue-resident macrophages, are not thought to require the infiltration and differentiation of monocytes from the circulation for renewal of the population (Hoeffel et al., 2015; Ginhoux et al., 2010). Microglial cells also show slower turnover compared to other macrophage populations, and there is evidence for self-renewal of the population under healthy conditions (Prinz & Priller, 2014). However, under stressful conditions (e.g. light-injury, neurodegeneration and irradiation) circulating monocytes can infiltrate and differentiate into macrophages in the retina with characteristic microglial-like morphology (Xu et al., 2007a; O'Koren et al., 2016). Monocytes infiltrating into the retina express higher levels of CD45 and CD11b than microglia, but these may downregulate over time to become similar to microglial levels (O'Koren et al., 2016). Consequently, bone-marrow chimera experiments, where retinal microglia are GFP- and infiltrating monocytes are GFP+, are common to distinguish these cell types (O'Koren et al., 2016; Xu et al., 2007b; Zinkernagel et al., 2013). A recent study has indicated that low levels of CD45, CD11c, F4/80 and MHCII are a consistent

microglial signature across a range of retinal injuries and that increases in these markers observed post injury are due to infiltrating cells instead of microglial activation (O'Koren et al., 2016). Microglia and infiltrating monocytes are thought to be functionally distinct; the infiltration of monocytes into the retina has been suggested to occur following strong or chronic microglial cell activation to reduce local inflammation in an attempt to restore homeostasis (London et al., 2013).

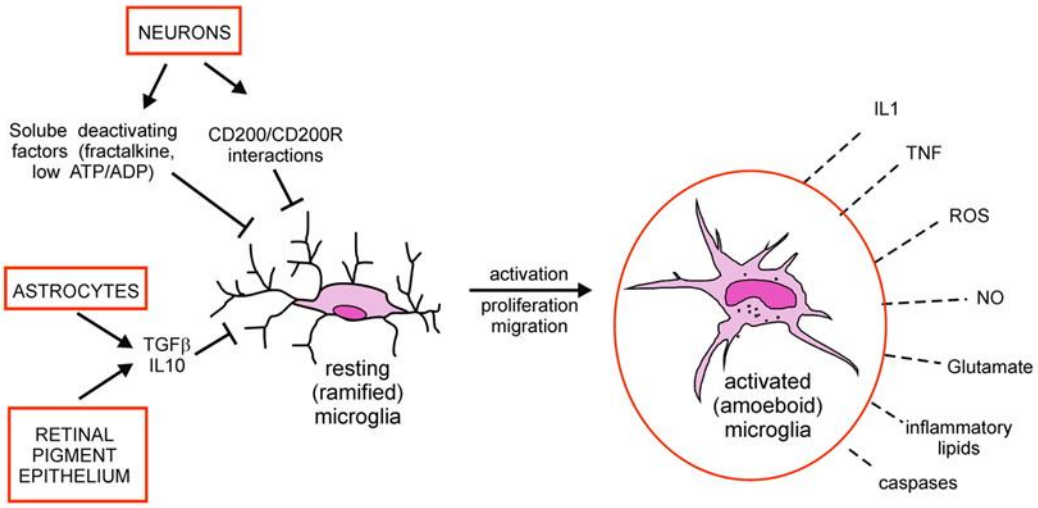

Figure 1.14 – Regulation of microglial activation and microglial effector function.
In the absence of activatory stimuli, microglia adopt a 'resting' morphology characterised by long, thin processes surveying the microenvironment. Microglia are kept in this 'resting' state by a range of suppressive interactions, including neuronal-microglial interactions (e.g. CD200/CD200R and CX3CL1/CX3CR1) and immunosuppressive cytokines (e.g. TGF-β, IL-10) derived from glia and/or RPE cells. Activating stimuli can overcome these suppressive factors, causing microglial activation, proliferation and migration. The classical (M1-like) phenotype of activated microglia is an activated hypertrophic cell body with condensed processes and secretion of inflammatory cytokines (e.g. IL-1β, TNFα) and mediators (e.g. NO, inflammatory lipids). ROS, reactive oxygen species; NO, nitric oxide. Adapted from Langmann, 2007.

1.2.4 The blood-retinal barriers

There are two main blood supplies to the retina: the inner retina is vascularised by capillaries and arterioles from the central retinal artery, while the avascular outer retina is supported by an extensive network of choriocapillaris (Figure 1.15). The barriers between these two blood supplies are both regulate the flow of molecules/cells between the retina and the periphery, but have very distinctive structures.

The outer BRB is characterised by fenestrated choroidal blood vessels separated from a monolayer of RPE cells by BrM (Campbell & Humphries, 2013). The RPE cells are linked by tight junctions comprised of a variety of proteins including occludins and zonula occludens-1 (ZO-1), -2 and -3, which greatly restrict access of circulating factors, including antibodies and immune cells, to the retina (Campbell & Humphries, 2013). The RPE cells regulate the transport of nutrients to the photoreceptors, including ions, amino acids, sugars and oxygen and also modulate the phenotype of immune cells in close contact with the barrier (Shechter et al., 2013). The RPE secretes a variety of immunosuppressive factors, including TGF-β and IL-10, and also skews immune cells towards a T_H2/M2 phenotype by inducing apoptosis of T_H1 via to engagement of FasL and PDL1 on RPE cells (Shechter et al., 2013)

The inner BRB is characterised by non-fenestrated endothelial cells linked by tight junctions and in close association with retinal astrocytic endfeet and pericytes (Figure 1.15). There are an equal number of pericytes and endothelial cells in the inner BRB, with pericytes responsible for a range of functions including structural support, regulation of blood flow and pinocytosis of soluble small molecules (Trost et al., 2016; Bergers & Song, 2005; Stewart & Tuor, 1994). Additionally, perivascular macrophages are dispersed along the inner retinal blood vessels and lie between the astrocytic endfeet and the blood-vessel basement membrane (Mendes-Jorge et al., 2009). These perivascular macrophages express scavenger receptors allowing clearance of retinal debris and removal of blood-borne proteins from the retina (Mendes-Jorge et al., 2009). Unlike the outer BRB, the inner BRB is not known to modulate the phenotype of infiltrating cells, although cells can only infiltrate through the inner BRB under strong inflammatory conditions (Shechter et al., 2013).

Much of our knowledge of cell infiltration through the inner and outer retinal barriers is derived from rodent studies of experimental autoimmune uveitis (EAU). In this model, rodents are immunised against a retinal antigen leading to the development of antigen-specific T cells and B cells, which generate an immunoglobulin response against the antigen (Agarwal et al., 2012). There is variation in EAU disease course due to species, strains and antigen choice, but generally, T_H1/M1 and T_H17 cells enter the retina through the inner retinal blood vessels in the early stages of EAU, in line with a lack of immunoskewing by the inner BRB (Kerr et al., 2008b; Luger et al., 2008; Amadi-Obi et al., 2007; Agarwal et al., 2012; Shechter et al., 2013). The infiltration of these cells is largely dependent on the interaction of LFA-1 on T cells and ICAM-1 on activated endothelial cells, although LFA-1 independent mechanisms have been described along with a role for other adhesion molecules (e.g. VCAM-1, PECAM-1, P-selectin) (Xu et al., 2003; Crane & Liversidge, 2008; Greenwood et al., 1995). Later in the disease course, there is a resolution phase to control retinal inflammation typified by the presence of T_H2/M2 cells in the subretinal space (Kerr et al., 2008a). This is in line with the immunoskewing nature of the outer BRB for an M2

phenotype, although it is not clear if these cells enter through the outer BRB or represent a phenotypic change of immune cells already in the retina (Shechter et al., 2013). Cells can infiltrate into the retina through the outer BRB via ICAM-1 and VCAM-1 dependent mechanisms (Dewispelaere et al., 2015).

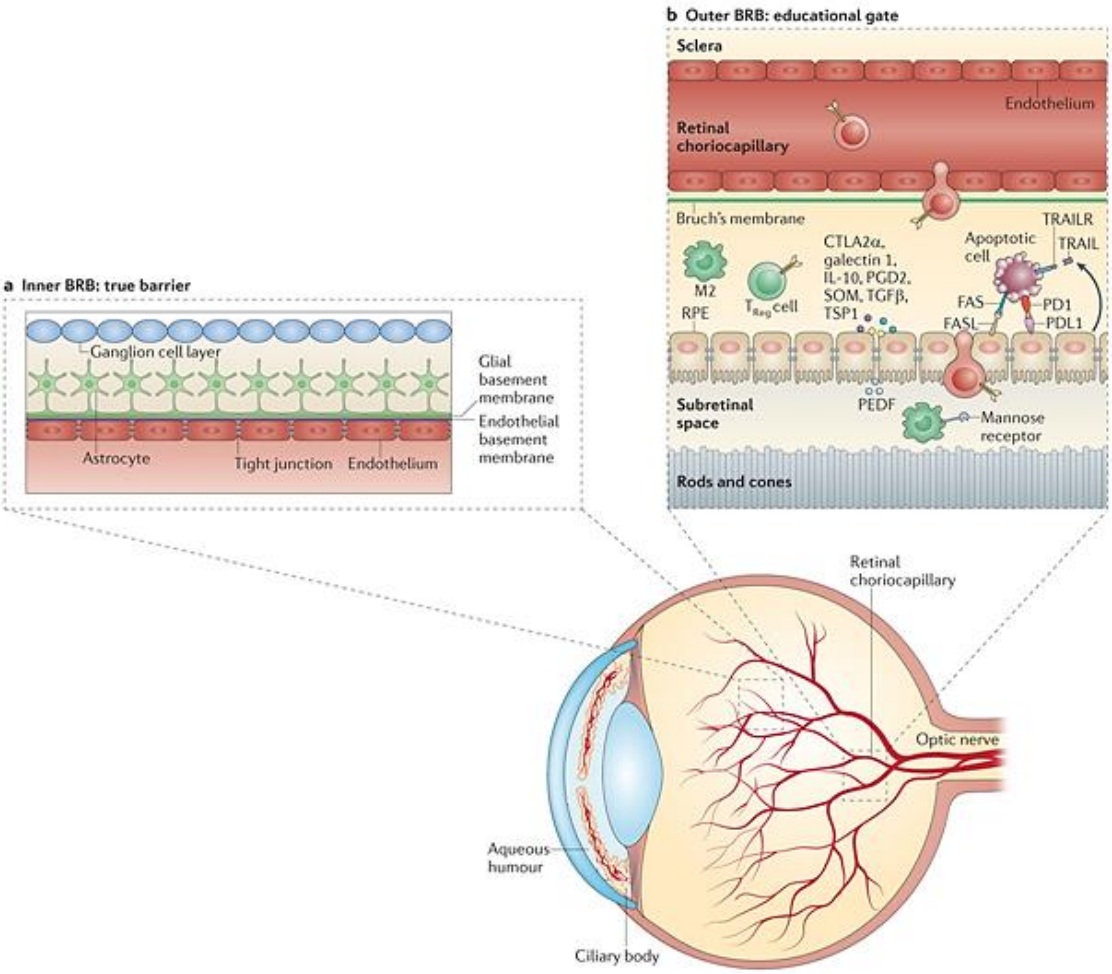

Figure 1.15 – Structure of the inner and outer blood-retinal barriers.

(a) The inner BRB consists of glial cell processes, which completely encompass the endothelial cell layer of retinal blood vessels, to restrict access to the retina. The endothelial cells are connected by tight junctions to further restrict access to the retina. The inner BRB is considered a true barrier as it restricts entry of cells under healthy conditions and does not skew the phenotype of any infiltrating cells. (b) The outer BRB consists of fenestrated capillaries in close apposition to the BrM and the RPE. The RPE cells are linked by tight junctions to restrict access to the retina. The RPE is considered an educational gate as it expresses many factors and receptors to modify the phenotype and function of infiltrating immune cells. Adapted from Shechter et al., 2013.

1.2.4.1 Summary

The retina has a specialised structure that underpins its main function of sensing and transducing light into electrical signals that are summated and sent to the brain for visual processing. The outer layers of the retina, which contain the light-sensing photoreceptors, are not vascularised and are instead dependent on the RPE and the adjacent choroidal blood supply for survival. The RPE cells and choroid also form the outer BRB, preventing access of the systemic immune system and other systemic components to the retina. The inner layers of the retina are vascularised and processes of astrocytes and Müller cells ensheath the inner retinal blood vessels to form the inner BRB, which also restricts access of systemic cells/factors. Glial cells of the retina are essential in supporting retinal function and providing immune defence. As the inner and outer BRBs restrict access of the systemic immune system to the retina, the resident immune cells of the retina, microglia, have a critical role in responding to infection, inflammation and injury within the retina. Overall, the variety and distribution of specialised cells throughout the healthy retina allows the retina to function effectively.

1.3 Age-related macular degeneration

1.3.1 Epidemiology

Age-related macular degeneration (AMD) is a neurodegenerative disease of the macula and the leading cause of blindness in many developed countries (Congdon et al., 2004). Globally in 2014, AMD was estimated to affect 170 million patients, with 9.6 million patients in the advanced stages characterised by severe visual impairment/blindness (Wong et al., 2014). In the UK alone, over 500,000 people were estimated to have late stage AMD in 2009, while a further 1.2 million people were estimated to have early signs of the disease preceding sight loss (Access Economics, 2009; Owen et al., 2012). Degeneration of the macula, which is responsible for high acuity central vision, can lead to devastating central vision loss (Figure 1.16). In general, patients with vision loss have a reduced ability to perform daily tasks, often leading to loss of independence, increased emotional distress and reduced quality of life (Williams et al., 1998). The condition also has a negative impact on family and friends, many of whom will have to care for the patient.

There are two different types of AMD – 'wet' and 'dry' – that are distinguished based on clinical pathology. Dry AMD affects the majority of patients (70-90%) and has no effective treatments (Buschini et al., 2011). At the late stages, dry AMD can progress into atrophic lesions termed geographic atrophy (GA) or develop into wet AMD, with approximately a 1:1 ratio of incidence in 2009 UK population (GA: 276,000 patients; wet AMD: 263,000 patients) (Owen et al., 2012). There are currently treatments available for wet AMD patients to slow, and in many cases improve, vision loss, but no treatments are available for dry AMD. In the UK between 2010 and 2020, the cost of direct medical treatments, such as wet AMD treatments and hospitalisation due to falls is estimated at £2.93bn, while the economic costs arising, such as informal/paid care and lost productivity, are estimated to cost £12.5bn (EpiVision, 2010). Therefore, if effective treatments become available, the AMD sufferer and their relatives may be spared from the negative effects of vision loss and increased health care costs may be outweighed by reduced social costs.

Aging is the main risk factor for AMD development, with each additional decade of life associated with increased risk of AMD; 3.5% of people in the 45-49 age group have AMD, 5.7% for 50-59 years, 10.2% for 60-69 years, 17.6% for 70-79 years and 24.96% for 80-84 years (Wong et al., 2014). As a result of the aging population, globally it is estimated that 288 million people will suffer from AMD by 2040, a 70% increase in AMD incidence compared to 2014. Furthermore, aging has an even great effect on increasing incidence of late-stage AMD; 0.1% of people in the 45-49 age group have AMD, 0.1% for 50-59 years, 0.4% for 60-69 years, 1.4% for 70-79 years and

3.3% for 80-84 years. The number of people with late-stage AMD are estimated to reach 18.6 million by 2040, a 95% increase on late-stage AMD incidence compared to 2014 (Wong et al., 2014). Therefore, effective treatments will be critical to manage the social and economic impacts of increasing AMD incidence amongst the rising elderly population.

Figure 1.16 – Illustrative example of vision loss in AMD.

AMD sufferers can develop an area of complete vision loss termed a scotoma in the centre of the visual field, while most peripheral vision is retained, but may have reduced visual acuity. This vision loss has a profound impact on the ability of AMD patients to carry out routine tasks. Image taken from the National Eye Institute (www.nei.nih.gov).

In addition to aging as a risk factor, numerous other risk factors have been identified in epidemiological studies (Table 1.3). A family history of AMD is a strong risk factor for AMD, demonstrating a role for genetics in AMD. Most genetic polymorphisms altering AMD risk have been found in genes relating to the immune system and these genetic risk factors will be described in more detail when discussing local inflammation in AMD. Overall, the risk factors including aging, environment and genetics, are all thought to contribute to parainflammation, which is a chronic low level inflammatory response that attempts to maintain homeostasis and repair tissue damage, either by increasing oxidative stress/damage or by directly affecting the immune system (Chen & Xu, 2015).

Risk factor	Odds Ratio	References	Comments
History of AMD in sibling	15.1 (All AMD) 19.8 (Late AMD) 10.3 (Wet AMD) 25.2 (All AMD)	Shahid et al., 2012 Klaver, 1998 B. E. K. Klein, 2001 Silvestri et al., 1994	OR 36.4 for parental history OR 4.8 for early AMD
Increasing age	4.2 per decade	Rudnicka et al., 2012*	Advanced AMD
Smoking	2.38 (Current) 1.66 (Former)	Cong et al., 2008*	All AMD
Caucasian Ethnicity	2.22 (vs Blacks) 2.38 (vs Hispanics) 0.56 (vs Chinese)	Klein et al., 2006*	Advanced AMD (0.25 vs Chinese for wet AMD)
Blue light exposure	2.23 (Late AMD) 0.44 (Late AMD) 3.5 (Late AMD) 1.25 (Late AMD) 1.09 (Wet AMD) 1.10 (Wet AMD)	Cruickshanks et al., 1993 Delcourt et al., 2001 Huang et al., 2014 Khan et al., 2006 Fletcher et al., 2008 EDC-CSG, 1992	Years of occupational exposure Annual ambient solar radiation >8hrs sunlight exposure per day Occupational/leisure exposure Occupational exposure Occupational/leisure exposure
Obesity	1.93 (GA) 2.0 (Late AMD) 1.46 (Late AMD) 1.19 (Wet AMD) 1.51 (GA) 2.29 (Late AMD) 2.1 (Late AMD)	AREDSG, 2005 Seddon et al., 2010 Ersoy et al., 2014 Smith et al., 2001 Smith et al., 2001 Delcourt et al., 2001 Seddon et al., 2006	Body mass index >30 vs <25
Alcohol intake	1.67 (Early AMD)	Chong et al., 2008*	Heavy alcohol consumption (>30g/day) vs none/mild The 4 studies of alcohol intake and late AMD have shown 1 significant positive, 1 non-significant positive, 1 null and 1 negative association
Female gender	1.05 (All) 0.69/0.99 (GA) 1.24/1.05 (Wet)	Rudnicka et al., 2012* Smith et al., 2001*	There is not convincing evidence that gender alters AMD incidence at any stage.

Table 1.3 – Summary of several non-genetic AMD risk factors associated with AMD risk.

*References marked with * are extensive meta-analyses of numerous cohorts.*

1.3.2 Clinical features of early/intermediate AMD

The clinical features of AMD are well known and are used to classify disease stage, but the mechanisms underpinning these clinical features are unclear. AMD is termed 'dry' during early and intermediate stages, as there is no leakage of peripheral fluid termed exudate into the retina. Compared to age-matched controls, sufferers with early- or intermediate-stage AMD have an increased level of yellowish subretinal deposits termed drusen in the macula (Figure 1.17a,b). Drusen are extracellular aggregates consisting of proteins, lipids and carbohydrates that develop between the RPE basement membrane and inner collagenous layer of BrM (Buschini et al., 2011). Drusen are classified into different types based on size and structure. Development of hard drusen, which are small (<63µm) in size and have well-defined edges, is typical in normal aging (Bhutto & Lutty, 2012). 2.9% of patients with hard drusen developed late-stage AMD over a 14 year follow-up period, whereas no patients without drusen progressed to late-stage AMD. Soft drusen are medium (63-125µm) or large (>125µm) in size and have poorly-defined edges, which often coalesce to become confluent (Bhutto & Lutty, 2012). 26.7% of patients with soft drusen developed late-stage AMD over a 14 year follow-up period, showing that it is a much stronger risk factor for AMD than hard drusen (Buch et al., 2005). Soft drusen also tend to develop specifically in the macular area, while hard drusen develop throughout the retina (Buschini et al., 2011).

Early/intermediate AMD can be graded by severity using a number of different grading systems. One of the most common is the grading system devised for the Age-Related Eye Disease Study (AREDS), which grades early to intermediate AMD based primarily on the extent of drusen (Categories I-III) or signs of advanced AMD (Category IV) present in fundoscopic images (Figure 1.18). In addition to fundoscopy, optical coherence tomography (OCT) scans of the retinal layers can also detect changes to the retina during early AMD, mainly appearing as deformed or thickened RPE layers due to the presence of underlying drusen (Figure 1.17e,f). Finally, electrophysiological studies show that early AMD patients have deficits in a-wave and b-wave amplitudes, indicating a deficit in neuronal communication preceding sight loss (Walter et al., 1999).

Figure 1.17 – Fundoscopy and OCT images at different AMD stages.

(A-D) Fundoscopy and (E-H) OCT images of (A, D) healthy retina, (B, F) early AMD, (C, G) geography atrophy and (D, H) wet AMD. In early AMD, yellow drusen deposits are present in the macula and the RPE layer is deformed by drusen. During geographic atrophy, choroidal vessels become visible as the outer layers of the retina collapse. During wet AMD, a variety of clinical features may appear, including haemorrhage, subretinal fluid, RPE detachment and fibrosis. (A-D) taken from A. Agarwal, 2012, (E-H) taken from Lumbroso & Rispoli, 2012.

Drusen are comprised of components from photoreceptors, RPE cells, endothelial cells of the choroid and serum constituents, with the majority of lipids coming from the photoreceptors/RPE and proteins coming from the choroid/serum (Booij et al., 2010). The most abundant proteins found in drusen are clusterin, crystallins, serum albumin, tissue inhibitor of metalloproteinase 3 (TIMP3) and vitronectin, while the major lipid components of drusen are esterified cholesterol, phosphocholine, sphingomyelin and fatty acids (Crabb, 2014; Wang et al., 2010). In addition to drusen, two types of sub-RPE deposits have been described that occur between the RPE and Bruch's membrane; Basal linear deposits (BLinD), which are largely comprised of membranous debris (i.e lipids), and basal laminar deposits (BLamD), which are largely comprised of collagen (Bhutto & Lutty, 2012). BLinD development is strongly associated with an risk of AMD incidence (Curcio & Millican, 1999). Several age-related mechanisms have been suggested to contribute drusen/BLinD/BLamD formation (Figure 1.19). Bruch's membrane becomes thicker and less permeable with age preventing clearance of components to the choriocapillaris and there is reduced blood flow through the choriocapillaris. RPE cells show reduced capacity for autophagy with age and a chronic parainflammatory response develops in response to accumulated insults over time (Mettu et al., 2012).

Category 1:	No drusen or nonextensive small drusen only in both eyes
Category 2:	Extensive small drusen, nonextensive intermediate drusen, or pigment abnormalities in at least one eye
Category 3:	Large drusen, extensive intermediate drusen, or noncentral geographic atrophy in at least one eye
Category 4:	Advanced age-related macular degeneration, or visual acuity less than 20/32 attributable to lesions of nonadvanced age-related macular degeneration, such as large drusen in the fovea, in only one eye
Definitions	
Drusen size	Based on largest drusen diameter as follows (relative to the size of an average optic disc, considered by convention to be 1500 mm): small drusen , 63 mm (1/24 disc diameter, standard circle C-0), intermediate drusen $ 63 mm but , 125 mm,and large drusen $ 125 mm (1/12 disc diameter, standard circle C-1).
Drusen extent	Variability in drusen size required that total drusen area, rather than drusen number, be considered when defining extent of drusen. Small drusen were conside red to be extensive when their cumulative area within two disc diameters of the center of the macula was at least that of AREDS standard circle C-1 (with diameter 1/12 that of the average disc). This corresponds to approximately 15 small drusen from stereo photographs and probably 5 to 10 small drusen by ophthalmosc opic examination. Intermediate drusen were considered to be extensive when soft indistinct drusen were present and the total area occupied by the drusen was equivalent to the area that would be occupied by 20 drusen each having a diameter of 100 mm. If no soft indistinct drusen were present, intermediate drusen were considered to be extensive when they occupied an area equivalent to at least 1/5 disc area (approximately 65 100-mm diameter drusen).
Advanced age-related macular degeneration	Defined by the presence of at least one of the following features: geographic atrophy, retinal pigment epithelial detachment in one eye (nondrusenoid retinal pigment epithelial detachment, serous sensory or hemorrhagic retinal detachment), choroidal neovascularization (subretinal hemorrhage, subretinal pigment epithelial hemorrhage, subretinal fibrosis), or scars of confluent photocoagulation for neovascular age-related macular degeneration. Other features of age-related macular degeneration are specified in detail in the fundus photograph grading protocol (AREDS Manual of Operations, The EMMES Corporation, Potomac, MD).

Figure 1.18 – AREDS grading scale for AMD severity.

Taken from AREDSG, 2000.

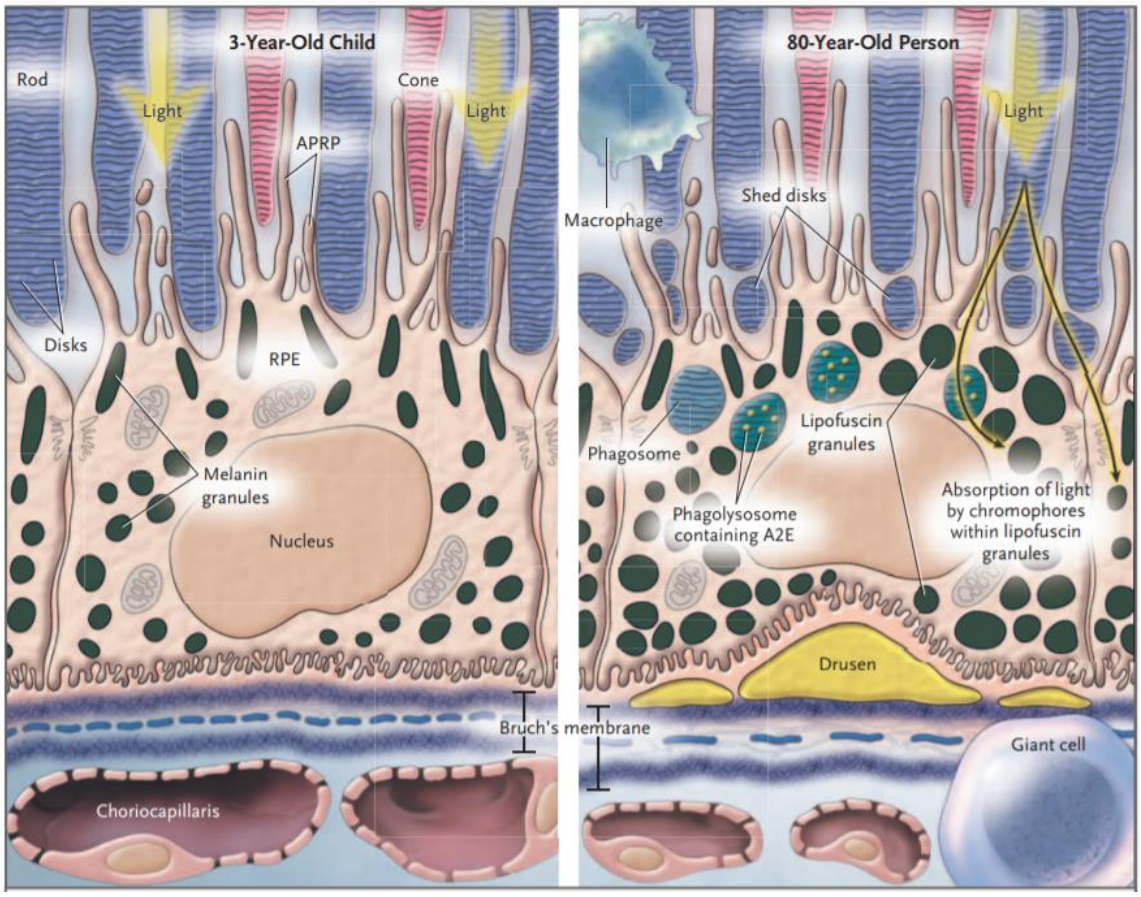

Figure 1.19 – Aging and the process of drusen formation.

(Left) In the young retina with normal homeostasis, light induces damage to the rod/cone photoreceptors and RPE cells, which contain melanin and lipofuscin granules to absorb light. To prevent accumulation of damage in the photoreceptors, the photoreceptors shed disks, which are uptaken by APRP and are cleared by autophagy or transported to the choriocapillaris circulation. (Right) In the aged retina with impaired homeostasis, there is an accumulation of melanin and lipofuscin granules in the RPE cells, Bruch's membrane is thicker and the choroidal blood vessels are atrophied and have reduced blood flow. Consequently, there is a failure to clear the photoreceptor disks along with accumulation of pigment granules and drusen develops between BrM and RPE cells. Failure to clear waste to the choriocapillaris is suggested to be due to the thickening of BrM and reduced blood flow, while failures in autophagy are also suggested to contribute and are, at least in part, due to the build-up of lipofuscin component A2E, which strongly inhibits autophagy in high concentrations. Alongside these changes, microglia/macrophages in the retina migrate towards the site of impaired homeostasis, possibly in an attempt to clear debris, along with giant cells (a cell formed from several fused macrophages) in the choroid. RPE, retinal pigment epithelium; APRP, apical pseudopodial RPE processes; A2E, apolipoprotein 2E. Taken from de Jong, 2006.

1.3.3 Clinical features of geographic atrophy

Geographic atrophy (GA) is the late stage conclusion of dry AMD, where large areas of cellular atrophy are found specifically at the macula. GA lesions can be identified by fundoscopy, where they can be clearly demarcated from non-atrophic tissue as areas of depigmentation and thinning of the outer retinal layers, typically allowing improved visualisation of the choroid (Figure 1.17c). Although some patients have only 1 GA lesion, typically there are several lesions, which are most likely to develop in the parafovea and then spread outwards, eventually coalescing into larger lesions (Schmitz-Valckenberg, 2017). Fundoscopy is not particularly sensitive to retinal changes and lesion area can be monitored more precisely with fundus autofluorescence (FAF) scans, which detects areas of RPE loss based on the lack of autofluorescent lipofuscin (Holz et al., 2007). Lesions can also be tracked by OCT to monitor lesion depth and area over time. OCT scans show that there is loss of the outer retinal layers during GA (Figure 1.17g), whereas the thickness of the inner retinal layers is constant throughout the disease and these findings are corroborated by histological analysis of post-mortem tissue from GA patients (Ebneter et al., 2016; Pilotto et al., 2013; Sarks et al., 1988). Electrophysiological recordings show that GA patients have similar ERG deficits in a-wave and b-wave amplitude compared to early AMD patients (Walter et al., 1999), indicating that despite ongoing neurodegeneration and visual loss, overall electrical activity of the retina is affected mainly in the early stages of the disease and not by progression.

For >65% of patients there is a consistent order in the events leading from early AMD to GA: Drusen development (>6.6 years before GA onset) > RPE hyperpigmentation (5 years before GA onset) > drusen regression & RPE hypopigmentation (2.5 years before GA onset) > Geographic atrophy (Klein et al., 2008). These findings were based on fundoscopy images taken over 13 years from nearly 100 patients with dry AMD that went on to develop GA during the study. Having said that, there is a wide variation in the timings of each stage, and in some patients, multiple stages occur at the same time.

Evidence from several histological and OCT studies of GA lesions indicate that, in most cases, RPE dysfunction is the initial step that leads to subsequent photoreceptor degeneration and progressive central vision loss, which is then finally followed by RPE cell loss (Wolf-Schnurrbusch et al., 2008; Bird et al., 2014; Hogan, 1972; Sarks, 1976; Fleckenstein et al., 2008; Bearelly et al., 2009). The importance of RPE cell function to photoreceptor survival makes RPE dysfunction a highly plausible event upstream of photoreceptor loss. However, the clinical observations are also highly variable between patients, including some evidence of photoreceptor loss in areas of normal RPE (Bird et al., 2014), providing the possibility that further subgroups of the disease will need to be described as our understanding evolves.

1.3.4 Clinical features of wet AMD and successful interventions

At late stages, AMD can diverge towards a 'wet' neovascular AMD instead of GA (Figure 3.4). Wet AMD and GA show similar incidences, despite only 10-30% of AMD cases being classified as 'wet' (Friedman et al., 2004; Owen et al., 2012), reflecting rapid disease progression and vision loss in wet AMD patients. In wet AMD, choroidal neovascularisation (CNV) begins with the growth of small blood vessels derived from the choroid into the sub-RPE space, termed occult CNV, where the RPE/neuroretina are minimally affected (Agarwal, 2012). Exudative fluid can build up in the retina over time causing further neovascularisation and in some cases detachment of the RPE (Arias & Mones, 2010). New blood vessels may grow through the RPE monolayer and affect the subretinal space, termed classic CNV (Agarwal, 2012). Eventually, there is a shift towards anti-angiogenic factors and new blood vessels becomes collagenised to prevent further proliferation and form a fibrotic disciform scar (Agarwal, 2012). Blood vessels and infiltrating exudate allow the peripheral immune system, including immunoglobulins, complement proteins and leukocytes, access to the retina, resulting in a strong immune response which can further drive neovascularisation (Ambati et al., 2013).

In a minority of wet AMD patients, neovascularisation of the inner retinal blood vessels, termed retinal angiomatous proliferation (RAP), is present and these vessels may eventually anastomose with choroidal blood vessels (Ding et al., 2009). Due to the diverse stages and pathologies associated with CNV, there are many possible observable features in fundoscopy/OCT (Figure 1.17d,h), including subretinal fluid, haemorrhage, fibrotic scars and RPE detachment (Agarwal, 2012). Fluorescein angiography can be used to fluorescently identify blood vessels in the retina, enabling visualisation of the location of choroidal neovascularisation within the retina (Arias & Mones, 2010). In a similar manner to GA patients, there do not appear to be progressive deficits in retinal function in CNV patients assessed by ERG compared to early AMD patients (Walter et al., 1999).

VEGFA is the primary factor driving angiogenesis and can be produced by most retinal cell types, including neurons, RPE cells, Müller cells, astrocytes/pericytes, endothelial cells, microglia and infiltrating myeloid cells, under certain conditions (Tolentino, 2011; Ambati et al., 2013). Inhibitors of VEGFA have shown efficacy in slowing disease progression and often improve the visual acuity of patients (Wang et al., 2011). There are three common VEGFA inhibitors used in human wet AMD patients: bevacizumab (Avastin), ranibizumab (Lucentis) and aflibercept (Eylea). Bevacizumab is a humanised anti-VEGF monoclonal antibody, which is often used as an off-label treatment for AMD. In contrast, ranibizumab is an anti-VEGF Fab fragment with the same antigen binding region as bevacizumab, but without the Fc region and is approved for use in AMD by the

MHRA/FDA (Mitchell, 2011). The removal the Fc region of the antibody in ranibizumab was theorised to be better for eye treatments due to lack of ability of the Fc region to induce microglial/complement activation and improved penetrance into the retina due to its smaller size (Ventrice et al., 2013; Magdelaine-Beuzelin et al., 2010). Additionally, bevacizumab requires preparation by pharmacies, is not glycosylated and contains larger particulate matter than ranibizumab (Mitchell, 2011; Magdelaine-Beuzelin et al., 2010). However, bevacizumab is a much cheaper option than ranibizumab, so several studies have compared the safety and efficacy of these drugs and have found similar visual improvement with both drugs, but have identified a possible slight increase in intraocular inflammation and serious systemic adverse events with bevacizumab that is worthy of continued study (CATT research group, 2010; Mitchell, 2011; Maguire et al., 2017). More recently, aflibercept, which is comprised of the two binding domains of VEGF receptors 1 and 2 linked by the human IgG1 Fc region, has been approved by the MHRA/FDA (Balaratnasingam et al., 2015). All three drugs show efficacy in treating wet AMD (Schmid et al., 2015) and further studies comparing the efficacy, side-effect profiles and cost-benefit analysis of aflibercept, bevacizumab and ranibizumab are ongoing. Alongside these studies, the contributions of other angiogenic factors (e.g. IL-8, angiopoietin 2, endothelin 1) need to be further characterised, particularly as there is evidence that these angiogenic factors are upregulated following bevacizumab injection to inhibit VEGF (Cabral et al., 2017).

A laser-induced mouse model of CNV has provided invaluable insights into the pathology of wet AMD. (Tobe et al., 1998). In this model, application of 532nm laser light ruptures BrM leading to the rapid growth of new blood vessels into the retina, which is maximal around 1-week post laser (Lambert et al., 2013). As in humans, VEGF is the key driver of the angiogenesis in this experimental CNV model (Seo et al., 1999; Kwak et al., 2000; Saishin et al., 2003). This highly acute model has offered insights into the disease with other contributing factors identified (e.g. CCL2, TNFα and MAC), which are possible targets for combination therapy (Liu et al., 2011b; Shi et al., 2006). There is also a role for immune cells in experimental CNV; inhibition of neutrophils or macrophages/microglia results in reduced CNV development (Caicedo et al., 2005; Espinosa-Heidmann et al., 2003; Zhou et al., 2005). These insights provide a rationale to investigate the benefits of such inhibitors in wet AMD patients to drive further drug discovery. The lack of effective therapies in GA patients may, in part, be due to the lack of a well characterised mouse model of dry AMD pathology.

1.4 Local inflammation during AMD

1.4.1 The inflammatory basis of drusen

As the hallmark of AMD pathology, many studies have investigated how drusen development in the macula is linked to the development and progression of AMD, especially due to the strong correlation of numbers between drusen and risk of progression to advanced AMD. As with disease associated deposits in other neurodegenerative disease (e.g. amyloid-beta plaques in Alzheimer's disease) it is not clear whether drusen drives progression of the disease or is simply a by-product of the disease process, but many researchers have suggested that drusen can contribute to disease pathology by inducing local inflammation (Ambati et al., 2013). A combination of proteomic and histological studies have revealed that numerous immune system proteins are present within drusen, including immunoglobulins, HLA-DR (an allele of MHCII), complement components: C1q, C3, C5, and C5b-9 (MAC); complement pathway regulators: clusterin, CD46 and complement receptor 1; acute phase proteins: vitronectin, C-reactive protein, amyloid P component, α1-antichymotrypsin and clotting factors: factor X, thrombin and fibrinogen (Crabb et al., 2002; Wang et al., 2010; Anderson et al., 2002; Johnson et al., 2000; Mullins et al., 2000; Ambati et al., 2013). Proteomic analysis of drusen from cynomolgus monkeys revealed that many inflammatory proteins in human drusen (i.e. C5, C5b-9, amyloid P component, vitronectin, CD46 and immunoglobulins) are identifiable in other primate species (Umeda et al., 2005).

Drusen is closely associated with processes of inflammatory cells, indicating a capacity for drusen to induce inflammation (Ambati et al., 2013)(Figure 1.20b). *In vitro* studies using human peripheral blood mononuclear cells (PBMCs) and mouse macrophages indicate that extracts of drusen are inflammatory, as assessed by IL-1β secretion, whereas extracts of the RPE are not inflammatory (Doyle et al., 2012). Additionally, isolated components of drusen (e.g. C1q, Aβ) have been shown to induce activation of RPE cells and macrophages/microglia *in vitro* and *in vivo* (Doyle et al., 2012; Tseng et al., 2013; Liu et al., 2013). These findings of inflammatory components in drusen are further supplemented by proteomic analysis of the BrM/choriocapillaris complex, which may include BLinD and BLamD. 60% of the differentially expressed genes between age-matched controls and AMD patients are immune-related (Yuan et al., 2010). These genes include upregulated expression of C3, C5, C6-9, vitronectin, clusterin and α1-antichymotrypsin, which are all observed in drusen (Yuan et al., 2010; Wang et al., 2010; Crabb et al., 2002).

Many of the protein components of drusen are tagged with oxidative stress epitopes including 2-(ω-carboxyethyl)pyrrole (CEP), N(6)-carboxymethyllysine (CML), oxidised phosphocholine, malondialdehyde (MDA) and pentosidine, most of which result from lipid peroxidation and have been identified in the aging retina (Schutt et al., 2003; Crabb et al., 2002; Weismann et al., 2011; Handa et al., 2016; Suzuki et al., 2007). CEP and CML are further increased in AMD patients compared to age-matched controls along with increased levels of crystallins, a stress response protein family, indicating higher oxidative stress in AMD patients and an attempt to maintain homeostasis. The retina is particularly susceptible to oxidative stress because it has the highest oxygen demand per gram of any body tissue, is frequently exposed to damaging UV/blue light and contains a high proportion of polyunsaturated fatty acids that can be easily oxidised (Wangsa-Wirawan & Linsenmeier, 2003; Ethen et al., 2007). Furthermore, risk factors for AMD, such as aging, smoking, obesity and blue light exposure increase oxidative stress and damage (Chen & Xu, 2015; Cano et al., 2010; Johnson, 2005). Genetic polymorphisms in the SOD2 gene, responsible for production of antioxidants to control oxidative stress as part of homeostasis, have been associated with altered AMD incidence in 3 genetically independent cohorts, although many more studies have failed to find an association (Kimura et al., 2000; Kowalski et al., 2010; Kan et al., 2014). Taken together, these findings present a compelling role for oxidative stress in AMD pathology. Oxidative stress can activate inflammatory pathways, as will be discussed later, providing another route by which drusen can be considered inflammatory.

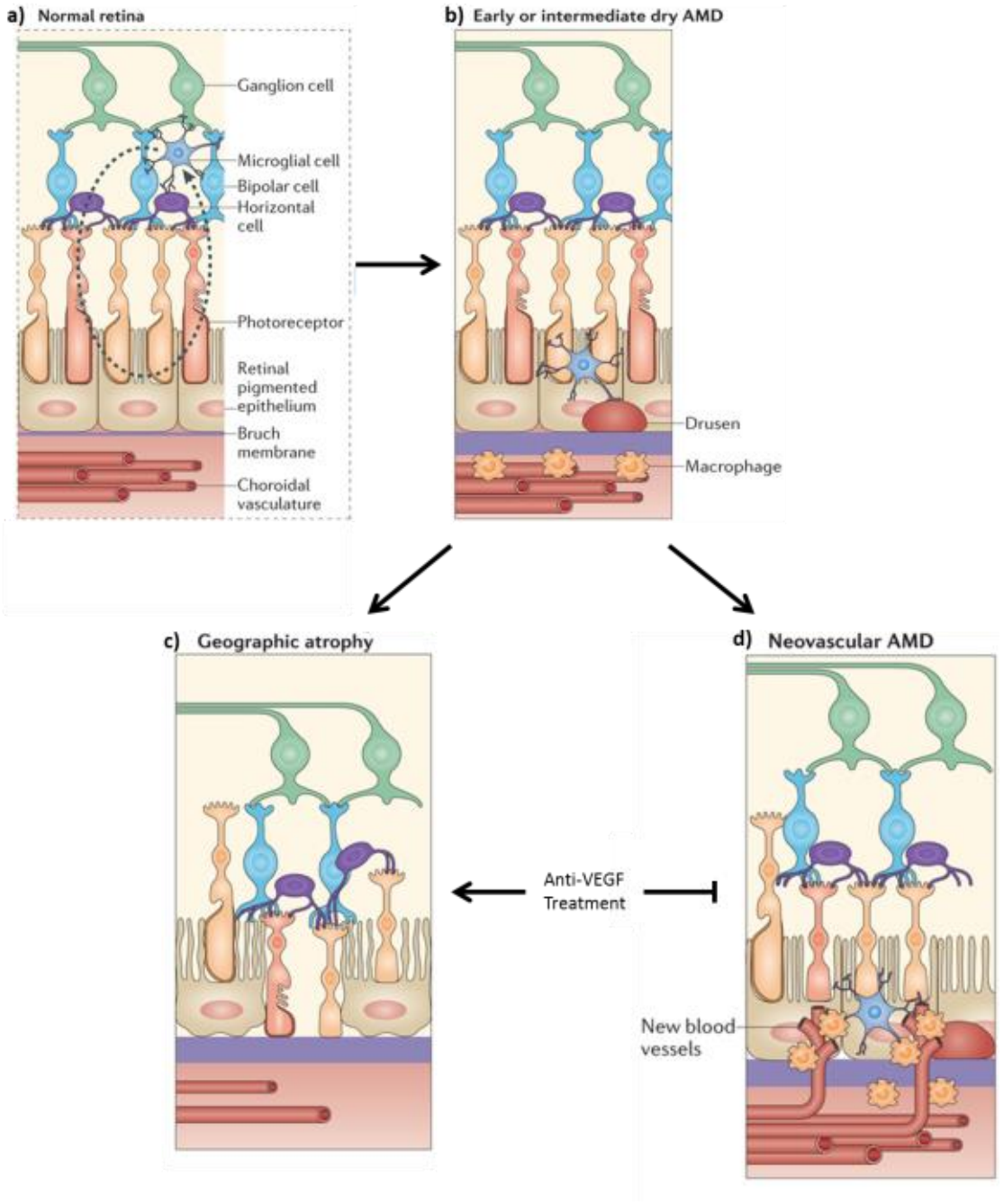

Figure 1.20 – Schematic of AMD progression and myeloid cell migration.

a) Schematic of the healthy retina. b) In early AMD, drusen accumulates next to a thickening Bruch's membrane. Microglial cells migrate towards drusen from inner retinal layers, while choroidal macrophages are also found in close proximity to drusen. Late-stage AMD is classified as either c) geographic atrophy, where RPE cells and photoreceptor cells degenerate or d) wet AMD, where growth of choroidal blood vessels into the retina allows infiltration of exudate fluid and choroidal macrophages. 30% of patients with neovascular AMD who have anti-VEGF treatment develop geographic atrophy. Image adapted from Ambati et al., 2013.

1.4.2 Myeloid cell activation in AMD

Cherepanoff et al., 2010 have completed the most comprehensive study (n=125) of myeloid cell activation in different stages of AMD pathology (Table 1.4). Overall, they find increases in myeloid cell number at BrM during progression of early to intermediate AMD in line with increasing amounts of sub-RPE deposits and drusen (grading I > IV). However, in this study the authors do not comment on whether BrM macrophages represent microglia and/or infiltrating myeloid cells. Increasing numbers and activation of choroidal macrophages were also observed in grades III and IV (Figure 1.20b). These cells may also show functional differences, as in early AMD patients choroidal CD45+ cells show a higher ratio of activatory to inhibitory Fc receptors, indicating a greater capacity for activation (Murinello et al., 2014). In GA, the number of myeloid cells decreases from stage IV and myeloid cells are mainly found in the margins of lesions (Cherepanoff et al., 2010), indicating that myeloid cells within the atrophic lesions gradually die along with the rest of the tissue (Figure 1.20c). Myeloid cells that are still present in atrophic lesions display a highly activated amoeboid morphology seen in a range of retinal degenerative diseases (Combadière et al., 2007; Gupta et al., 2003). In contrast, in CNV, there is a large infiltration of systemic macrophages due to the disruption of the outer BRB, making it impossible to define myeloid cells at BrM (Cherepanoff et al., 2010). Microglia/infiltrating myeloid cells are one of main producers of VEGF in the retina, showing how systemic immune cells can contribute to angiogenesis in wet AMD and accelerate vision loss (Figure 1.20d) (Ambati et al., 2013).

The polarisation and phenotype of myeloid cells during AMD remains an important question. During healthy aging, microglia show increasing expression of M1 (CXCL11) and M2 (CCL22) associated chemokines, but an overall trend towards M2 polarisation (Cao et al., 2011). Based on this chemokine analysis, a pilot study showed dry AMD is more associated with a shift back towards M1 polarisation, while wet AMD is associated with further M2 polarisation. Histological staining for CD68+ (M1-like) and CD163+ (M2-like) cells revealed increased M2 cells in wet AMD compared to GA patients (Cao et al., 2011). Supporting these findings, the number of M2-like CD163+ macrophages is threefold higher than M1-like CD68+ macrophages in neovascular membranes and furthermore both cell types are able to express VEGF (Nakamura et al., 2015). In GA patients, CD68+ cells are found in the margins of atrophic lesions (Cherepanoff et al., 2010), but the presence of CD163+ cells is less clear. A recent qualitative report showed CD163+ sub-RPE cells in the inner layers in aged eyes, which progressively increased in number and activated morphology with AMD severity, but there is ongoing debate over whether these are of phagocytic macrophage or RPE origin as melanin is present in the cells (Lad et al., 2015; Curcio & Ach, 2016; Lad et al., 2016). Additionally, the authors state that the reactivity pattern of the CD163+ antibody varies according to the immunohistochemistry (IHC) protocol, which may explain why CD163+

cells were rarely found during dry AMD and GA in a different study (Lad et al., 2015; Cao et al., 2011). Overall, the phenotype and origin of activated myeloid cells needs to be better understood to intervene with possible therapeutics.

AMD grading	Grading definition	BrM macrophages (mean no. per field ±SEM)
I	No BLamD	0
II	Patchy BLamD	0.03±0.14
III	Thin continuous BLamD	3.14±5.82
IV	Thick continuous BLamD	7.14±5.90
V	GA	2.72±3.03
VI	CNV	BrM Disrupted

Table 1.4 – Number of myeloid cells at Bruch's membrane at different AMD stages.
Information taken from Cherepanoff et al., 2010.

Beyond immunohistochemical studies, polymorphisms in receptors expressed on microglia, which regulate activation (MHCI, MHCII, TLR3, TLR4) and migration (CX3CR1, CCR3) have been associated with altered AMD incidence/progression (Tuo et al., 2012), further supporting a direct role for these cells in AMD pathology.

Aging also contributes to the activation of microglia; in the retina of aged (20 month old) mice expression of receptors on macrophages (i.e. CD11b, FcγRIIb, FcγRIII, TLR2 and TLR4) are increased compared to young (3 month old) mice (Chen et al., 2010). Microglia from aged mice also displayed a more activated phenotype than those from young mice. This activation may result from reduced microglia-neuron suppressive signalling (e.g CD200-CD200R, CX3CR1-CX3CL1) with aging and reduced microglial responsiveness to anti-inflammatory cytokines, which has been shown in the brain (Corona et al., 2012; Norden & Godbout, 2013). Aged retinal microglia in *ex vivo* explants migrate more slowly to sites of laser-injury than young microglia, but persist at the injury site for much longer (Damani et al., 2011), which may cause prolonged and damaging inflammation.

Aging, along with other risk factors for AMD, induces high levels of oxidative stress, which are strongly implicated in AMD pathology. Several oxidative stress epitopes have been suggested to activate retinal microglia to induce inflammation. For example, CEP adducts can be recognised by TLR2 and *in vitro* stimulate an M1 phenotype expressing IL-1β, IL-12, TNFα and iNOS (inducible nitric oxide synthase, which generates nitric oxide) (Cruz-Guilloty et al., 2014; Doyle et al., 2012). Other oxidative stress epitopes, including 4-hydroxynonenal and MDA can activate myeloid cells via the LOX1 scavenger receptor, while oxidised phospholipid and oxidised phosphatidylserine bind the CD36 scavenger receptor on myeloid cells to induce inflammation (Binder et al., 2016).

1.4.3 Macroglial activation in AMD

The activation status and function of macroglia in AMD are very poorly characterised. GFAP is a common marker used to identify macroglial cells in the healthy retina. Under healthy conditions, astrocytes express high levels of GFAP, whereas GFAP expression is largely absent from Müller cells processes, except for weak expression in the inner retinal layers (Mizutani et al., 1998; Ramirez et al., 1994). However, under inflammatory/injury conditions, reactive gliosis of Müller cells can occur and strong GFAP expression is observed throughout Müller cell processes (Nork et al., 1986; Mizutani et al., 1998). The level of GFAP expression in the NFL/GFL layer, which is predominantly astrocytic, is increased in patients with drusen but is not further increased in GA patients (Wu et al., 2003). In contrast, GFAP expression in the outer retina (IPL to OLM), which is representative of Müller cell processes, is not increased by the presence of drusen, but is upregulated during GA (Wu et al., 2003). Overall, this suggests that astrocytic gliosis occurs early in the disease process when drusen is present, while Müller cell activation occurs later when more severe pathology/inflammation is present. The activation status of macroglia in wet AMD is not characterised by immunohistochemistry, but macroglia have been shown to express VEGF during stressful conditions and this should be investigated to determine whether they contribute to neovascularisation during AMD. In aging, there is a significantly increased area of overall retinal GFAP staining, but this was not significant for the inner or outer layers alone, and these changes are minor in comparison to those induced by AMD pathology (Wu et al., 2003).

1.4.4 Role of cytokines/chemokines in AMD

Several studies have investigated the levels of ocular cytokines during wet AMD by analysing cytokine levels in the aqueous humour (Table 1.5). Aqueous humour can be collected during cataract surgery, meaning the control groups in these studies are cataract patients without other ocular pathology. Overall these studies show increased levels of inflammatory proteins in the aqueous humour, but there is considerable discrepancy between results for many of the analytes. Chemokines CCL2, CXCL9 (Mig), CXCL10 (IP-10) and IL-8 represent the most consistently upregulated inflammatory proteins along with cytokine IL-1α. This may highlight the importance of systemic immune cell recruitment in driving wet AMD pathology. Unfortunately, no study has yet looked at levels of aqueous humour cytokines during dry AMD or GA pathology, which would give better insights into possible mechanisms of disease progression.

Molecule	Upregulation	Downregulation	No change
Cytokines			
IL-1α	Jonas et al., 2012; Sakurada et al., 2015		Rezar-Dreindl et al., 2016
IL-2			Rezar-Dreindl et al., 2016; Sakurada et al., 2015
IL-3	Jonas et al., 2012		Rezar-Dreindl et al., 2016
IL-4			Rezar-Dreindl et al., 2016; Sakurada et al., 2015
IL-5			Rezar-Dreindl et al., 2016
IL-6	Chalam et al., 2014; Jonas et al., 2012		Agawa et al., 2014; Fauser et al., 2015; Rezar-Dreindl et al., 2016; Sakurada et al., 2015
IL-10			Rezar-Dreindl et al., 2016; Sakurada et al., 2015
IL-12p40	Jonas et al., 2012		
IL-12p70		Rezar-Dreindl et al., 2016	Jonas et al., 2012; Sakurada et al., 2015
IL-13	Fu et al., 2017; Sakurada et al., 2015		
IL-15	Sakurada et al., 2015		
IL-17			Sakurada et al., 2015
TNFα		Rezar-Dreindl et al., 2016	Jonas et al., 2012
Chemokines			
CCL2	Agawa et al., 2014; Fauser et al., 2015; Jonas et al., 2012; Rezar-Dreindl et al., 2016		Sakurada et al., 2015
CCL4	Agawa et al., 2014		
CCL5			Agawa et al., 2014
CCL7			Jonas et al., 2012
CXCL9	Agawa et al., 2014; Jonas et al., 2012; Rezar-Dreindl et al., 2016		
CXCL10	Agawa et al., 2014; Sakurada et al., 2015		Jonas et al., 2012
IL-8	Agawa et al., 2014; Jonas et al., 2012		Rezar-Dreindl 2016; Sakurada et al. 2015
Other			
CRP	Sakurada et al., 2015		Fauser et al., 2015
Fas ligand	Agawa et al., 2014		
TGF-β2			Jonas et al., 2012; Rezar-Dreindl et al., 2016
VEGF	Agawa et al., 2014; Cha et al., 2013; Chalam et al., 2014		Fauser et al., 2015; Jonas et al. 2012; Rezar-Dreindl et al., 2016; Sakurada et al., 2015

Table 1.5– Studies analysing the levels of aqueous humour proteins in wet AMD patients.

Studies are grouped into those showing upregulated, downregulated or consistent levels of proteins compared to age-matched controls.

In addition to the upregulation of chemokines IL-8 and CCL2 in the retina, genetic polymorphisms also indicate a role for altered chemokine signalling in AMD. IL-8 haplotype variants result in an increased risk of wet AMD in 3 independent studies (Ricci et al., 2013; Goverdhan et al., 2008; Tsai et al., 2008) and IL-8 is known to have angiogenic activity in the eye (Ghasemi et al., 2011). Moreover, a novel CCR3 polymorphism increasing AMD risk has been identified in an Indian cohort and aberrant CCR3 expression is detected on the endothelial cells of neovascular membranes (Takeda et al., 2009; Sharma et al., 2013). CCR3 binds a variety of chemokines, with CCL2, CCL5, CCL7 and eotaxins showing agonistic activity and CXCL9 and CXCL10 showing antagonistic activity (Murphy & Weaver, 2017; Daugherty et al., 1996). CX3CR1 polymorphisms have also been associated with an increased incidence of AMD in 5 of 11 published studies (Ma et al., 2015; Li et al., 2015; Combadière et al., 2007; Gupta et al., 2014; Tuo et al., 2004; Yang et al., 2010; Zhang et al., 2015a; Briõn et al., 2011; Anastasopoulos et al., 2012; Schaumberg et al., 2014; Zerbib et al., 2011). CX3CR1/CX3CL1 signalling is important for the migration of microglia towards sites of injury and also promotes survival of peripheral monocytes, but its effect on microglial survival is not characterised (Landsman et al., 2009; Liang et al., 2009). Transcriptomic analysis of the RPE/Choroid showed that elevations in CCL2, CXCL9, CXCL10 and CXCL11 is common to CNV and GA patients (Newman et al., 2012).

Animal studies also provide evidence of a role for dysfunctional chemokine signalling in retinal degeneration, although variability between labs makes it difficult to draw strong conclusions. CCL2- and CCR2-deficient mice show development of subretinal deposits containing inflammatory drusen-associated components (i.e. IgG, C5a, CD46 and vitronectin) at 6 months, followed by photoreceptor degeneration at 16 months (Ambati et al., 2003). CNV developed in 25% of mice by 20 months, indicating as in humans, the possibility of differential late stage pathology. However, a study by a different lab identified no discernible degeneration at 12-14 months, despite an increase in subretinal microglia (Luhmann et al., 2013b). In CX3CR1 knockout mice, increased subretinal accumulation of microglia, subretinal deposits, and retinal degeneration is observed in 18-month-old mice compared to CX3CR1 heterozygotes (Combadière et al., 2007). However, another study demonstrated increased retinal degeneration in the CX3CR1 knockout retina, but an age-dependent recruitment of subretinal microglia was not altered based on CX3CR1 genotype (Chinnery et al., 2012). Finally, a third study showed no evidence of retinal degeneration or increased microglial accumulation in CX3CR1 knockout mice (Luhmann et al., 2013b). Overall, these studies show that mice with altered chemokine signalling may recapitulate some features of AMD pathology but require extensive aging and lack consistency between groups. For all studies presented, except Ambati et al. 2003, mice were tested to ensure that the confounding retinal

degeneration 8 (rd8) mutation in mice of C57BL/6N background was not present (Luhmann et al., 2013a).

The presence of the rd8 mutation is an important factor because a combined CCL2/CX3CR1 knockout mice was generated, which showed early onset (2-3 months) inflammation, RPE changes and photoreceptor atrophy with greater consistency amongst mice, but this contaminating rd8 mutation was present (Tuo et al., 2007; Popp et al., 2013; Luhmann et al., 2013b). The CCL2/CX3CR1 mice and wild-type C57BL6/N mice with rd8 mutation show different localisation and progression of retinal degeneration (Chu et al., 2013), but the presence of the rd8 mutation makes results difficult to interpret. Furthermore, the CCL2/CX3CR1 strain without the rd8 mutation shows Müller cell gliosis and microglial activation by 9 months, but no early-onset AMD phenotype (Vessey et al., 2012). An independent lab also showed no subretinal microglial accumulation or photoreceptor degeneration in 14 months old CCL2/CX3CR1 knockout mice without the rd8 mutation, whereas an another group found photoreceptor degeneration and retinal inflammation in 18 month-old-mice, showing a phenotype in between the observations from other labs (Chen et al., 2013b; Luhmann et al., 2013b). Consequently, further study is required to identify an early onset model with AMD phenotypes that are consistent between labs and ideally do not require extensive aging before use. Alongside the aqueous humour and genetic polymorphism data, these animal studies argue for further investigation of chemokines and altered immune cell migration in AMD. An analysis of CX3CL1 levels in aqueous humour of AMD patients would be particularly insightful.

While the investigation of inflammatory proteins has been far more extensive in wet AMD patients than dry AMD patients, there has been an interesting line of research linking inflammasome activation with geography atrophy. Increased expression of NLRP3, caspase 1, pro-IL-1β and pro-IL-18 mRNA has been identified in GA-AMD patients compared to controls (Tarallo et al., 2012; Wang et al., 2016). Moreover, immunohistochemical staining shows staining for NLRP3 at sites of GA (Tarallo et al., 2012; Tseng et al., 2013). Human drusen has also been shown to stimulate the NLRP3 inflammasome in macrophages *in vitro* (Doyle et al., 2012) and active IL-18 is toxic to RPE cells in mice, which may represent a mechanism for inflammation to drive AMD pathology towards GA (Tarallo et al., 2012). Microglia/macrophages accumulate near the RPE during AMD, which may allow elevated levels of proinflammatory cytokines to drive RPE cell degeneration and subsequent photoreceptor loss. Cells other than microglia/macrophages may play a role as RPE cells show inflammasome activation and secretion of IL-1β and IL-18 when exposed to oxidative stress epitope 4-hydroxynonenal *in vitro*, indicating that RPE cells may also contribute to retinal inflammation during AMD pathology (Tseng et al., 2013; Brandstetter et al., 2015; Kauppinen et al., 2012).

1.4.5 Complement activation in AMD

Overactivity of the complement pathway is the strongest genetic risk factor for AMD. In particular polymorphisms in CFH, a negative regulator of the alternative complement pathway, account for over 50% of AMD heritability with 10 specific CFH polymorphisms associated with increased AMD incidence (Ambati et al., 2013). Additionally, 9 other complement pathway genes altering AMD incidence/progression have been identified: CFI, factor B, C2, C3, C4, C5, C9, CFH related protein (CFHR)-1, CFHR-3 and vitronectin (Geerlings et al., 2017; Tuo et al., 2012). These polymorphisms indicate that overactivity of the complement pathway, particularly the alternative pathway, increase risk of AMD incidence and/or progression. Administration of an intravitreal complement factor D inhibitor has also shown some success in Phase II clinical trials; after 18 months of intravitreal lampalizumab, GA lesion size is reduced by 20% compared to control, with patients with CFI mutations appearing to benefit further with a 44% reduction in GA lesion size (Yaspan et al., 2017). A study of C5 inhibition in the retina didn't show any success in GA patients (Zamiri, 2016), despite being common to all complement pathways and directly upstream of the tissue damaging MAC. As the complement pathway is a large amplification cascade, intervening at the early steps may greatly reduce inflammation compared to intervention at the level of C5.

Complement pathway overactivity also occurs because of aging, the greatest risk factor for AMD. Aged 20 month old mice show increased expression (>2-fold) of many genes encoding complement pathway components (e.g. C1q, C3, C4b) (Chen et al., 2010). Aged mouse retinas also have increased C3d deposition, particularly in the subretinal region, and 12.5-fold elevations in C1q protein levels (Chen et al., 2010; Stephan et al., 2013). In humans, the presence of numerous complement pathway components in drusen argues for a local role of complement in the disease. Complement is an interesting candidate for the conversion of retinal inflammation into neurodegeneration via MAC formation. Several complement pathway components can activate microglia via complement receptors (CD11b, CD11c) to induce inflammation (Mevorach et al., 1998). In peripheral macrophages, activation by the complement pathway can lead to production of more C1q leading to an inflammatory feedback loop driving inflammation and tissue damage and this process may also occur in the microglia of the retina (Karsten & Köhl, 2012). However, in early stage AMD, C1q staining is observed mainly at the choriocapillaris as opposed to the retina, while increased levels of MAC staining is also observed in the choriocapillaris and drusen (Murinello et al., 2014). This suggests that complement components, particularly at the early stages, may originate from the periphery.

Complement factors may also provide a link between oxidative stress and retinal inflammation/degeneration. The CFH (Y402H) polymorphism is one of the highest risk factors for AMD, with homozygous patients 7 times more likely to develop AMD (Seddon et al., 2006). 24 month old CFH knockout mice develop visual dysfunction, retinal C3 deposition, autofluorescent subretinal deposits, reduced BrM thickness and photoreceptor disorganisation, but no evidence of photoreceptor loss (Coffey et al., 2007). Moreover, a transgenic mouse expressing human CFH (Y402H) variant under the murine ApoE promoter develop basal laminar deposits, retinal C3 deposition, BrM thickening, accumulation of lipofuscin in RPE and subretinal macrophage accumulation, but again no evidence of photoreceptor loss (Ufret-Vincenty et al., 2010). These studies indicate that defects in CFH alone only lead to an early AMD phenotype. One proposed mechanism for the role of CFH in AMD is based on the fact that CFH normally binds and hides oxidative stress induced malonaldehyde (MDA) epitopes to prevent MDA-mediated complement activation (Wang et al., 2015). It has been shown that certain CFH polymorphisms encode CFH with a reduced ability to bind and hide MDA epitopes, resulting in increased complement activation and possibly microglial activation (Weismann et al., 2011). Additionally, the CFH Y402H polymorphism has been associated with increased GM-CSF in the vitreous of healthy patients and increased numbers of choroidal macrophages (Wang et al., 2015), indicating that this polymorphism may link oxidative stress, complement activation and myeloid cell activation in AMD patients.

1.4.6 Antibody deposition and a role for autoimmunity in AMD

Several immunoglobulin components have been identified in drusen by proteomic and immunohistochemical analyses (Anderson et al., 2002; Crabb et al., 2002; Johnson et al., 2000; Mullins et al., 2000). In 1990, elevated levels of autoantibodies against retinal antigen GFAP were identified in AMD patient sera compared to controls and since then high titres of autoantibodies against more than 30 antigens expressed in the retina have been found in AMD patients (Morohoshi et al., 2012b; Penfold et al., 1990). Strikingly, 9% of controls have a high serum titre of anti-retinal antibodies, compared to 94% of early AMD patients (Patel et al., 2005). High IgG and/or IgM levels against host antigens associated with inflammation (e.g. GFAP, MHC subunit B2-microglobulin), stress responses (e.g. αβ-crystallin, α-enolase, HSP70 family members), structural components of Bruch's membrane (e.g. elastin, collagen III, collagen IV) and oxidative stress epitopes (e.g. CEP) have been found in AMD patients (Morohoshi et al., 2012b; Gu et al., 2003; Penfold et al., 1990). High IgG:IgM ratios, a typical measure of autoimmunity, against several retinal antigens confer a 7- to 44-fold increase in AMD risk (Morohoshi et al., 2012a). Control patient sera shows little binding to retinal sections, whereas AMD patient sera binds strongly to

the choroid, Bruch's membrane and RPE (Patel et al., 2005), demonstrating that anti-retinal antibodies can deposit at the site of AMD pathology.

During healthy aging, IgG deposition is observed in the choriocapillaris and inner retinal blood vessels, but in AMD patients, IgG deposition in the choriocapillaris is co-localised strongly with C1q and MAC deposition (Murinello et al., 2014). There is also an increase in FcγR-expressing CD45+ immune cells in the choriocapillaris along with a shift to a higher ratio of activatory to inhibitory Fc receptors (Murinello et al., 2014). As IgG is the ligand for Fc receptors and activates the classical complement cascade, antibodies may lie upstream of both complement and myeloid cell activation in the choriocapillaris to drive a local inflammatory response in AMD.

A possible role of antibodies in AMD has been identified in two mouse studies. Immunisation against a foreign protein (ovalbumin) followed by intravitreal injection of the antigen leads to the deposition of immune complexes of antigen and antibody in the retina. These deposits induce strong myeloid cell activation and migration of immune cells into the subretinal space in a FcγR, but not C1q, dependent manner (Murinello et al., 2014). This study demonstrates that antibody deposition in the retina can directly activate immune cells. Another study immunised against oxidative stress epitope CEP, an antigen that increases in an age-dependent manner in the retina. Unlike traditional EAU, which immunises against an abundant retinal protein and induces strong and rapid retinal inflammation, by immunising against an age dependent epitope the autoimmune process occurs more gradually. In this model, autoantibodies against CEP, which are observed in AMD patients, accumulate in the retina and, along with antigen-specific T cells, activate myeloid cells (microglia and/or macrophage) to drive tissue damage and retinal degeneration over a 6 month follow-up period (Hollyfield et al., 2010; Cruz-Guilloty et al., 2014).

The role of T cells in local inflammation in AMD patients is poorly understood. Although T cells are not generally present in the healthy retina, whether they infiltrate or contribute to AMD pathology is not characterised. In healthy aging, there is an increase in T_H17 cells and a reciprocal reduction in suppressive T_{REGS} (Schmitt et al., 2013). T_H17 responses are associated with immunosenescence, systemic autoimmunity and neurodegenerative diseases with an autoimmune component (e.g. Multiple Sclerosis) (Murphy & Weaver, 2017). A role for IL-17A, the main cytokine of the T_H17 response, has been implicated in AMD, as polymorphisms in the IL-17A gene increase the likelihood of developing AMD (Zhang et al., 2015b; Popp et al., 2016). Moreover, AMD patients have reduced methylation of the IL-17 receptor C (IL-17RC) promoter resulting in increased peripheral and retinal expression of IL-17RC (Wei et al., 2012). RNA levels of IL-17A and IL-23, a cytokine driving T_H17 differentiation, are increased in the macula of AMD patients compared to age-matched controls (Chan & Ardeljan, 2014). Recombinant IL-17A is toxic

to human RPE cells *in vitro*, indicating damage could result from local production of IL-17 (Chan & Ardeljan, 2014). IL-17+ cells, mainly CD3+ T cells but also some myeloid IBA-1+ cells, have been identified in the choroid of GA patients, but not age matched controls, so IL-17A production may occur in the choroid (Camelo et al., 2016). In mouse models and multiple sclerosis, T cell activation is a critical component in driving the disease pathology, but infiltrating myeloid cells are thought to mediate late-stage neurodegeneration (Cruz-Guilloty et al., 2014; Sriram & Rodriguez, 1997; Najafi & Mirshafiey, 2015). Consequently, further work needs to be performed to determine whether there is an autoimmune component to AMD in terms of immunoglobulin based activation of myeloid cells and complement and the role of T_H17 cells.

1.4.7 Summary

AMD is a chronic neurodegenerative disease of the retina responsible for the majority of blindness in developed countries. In the early stages, drusen deposits at the back of the retina and is thought to promote local inflammation. Two inflammatory proteins capable of activating microglia, immunoglobulins and complement, are found within drusen. These immune pathways can all interact to drive a feedback loop of increasing inflammation (Figure 1.21). There are two distinct late-stage pathologies associated with AMD: GA and wet AMD. In GA, the RPE cells become dysfunctional leading to photoreceptor loss due to lack of support. Inflammasome activation and M1-like microglial polarisation have been implicated in GA pathology. During wet AMD, production of VEGF leads to the growth of new blood vessels into the outer retina, allowing access of the systemic immune system to the retina and rapid vision loss. M2-like microglial polarisation and presence of many cytokines/chemokines in the eye are particularly associated with wet AMD pathology.

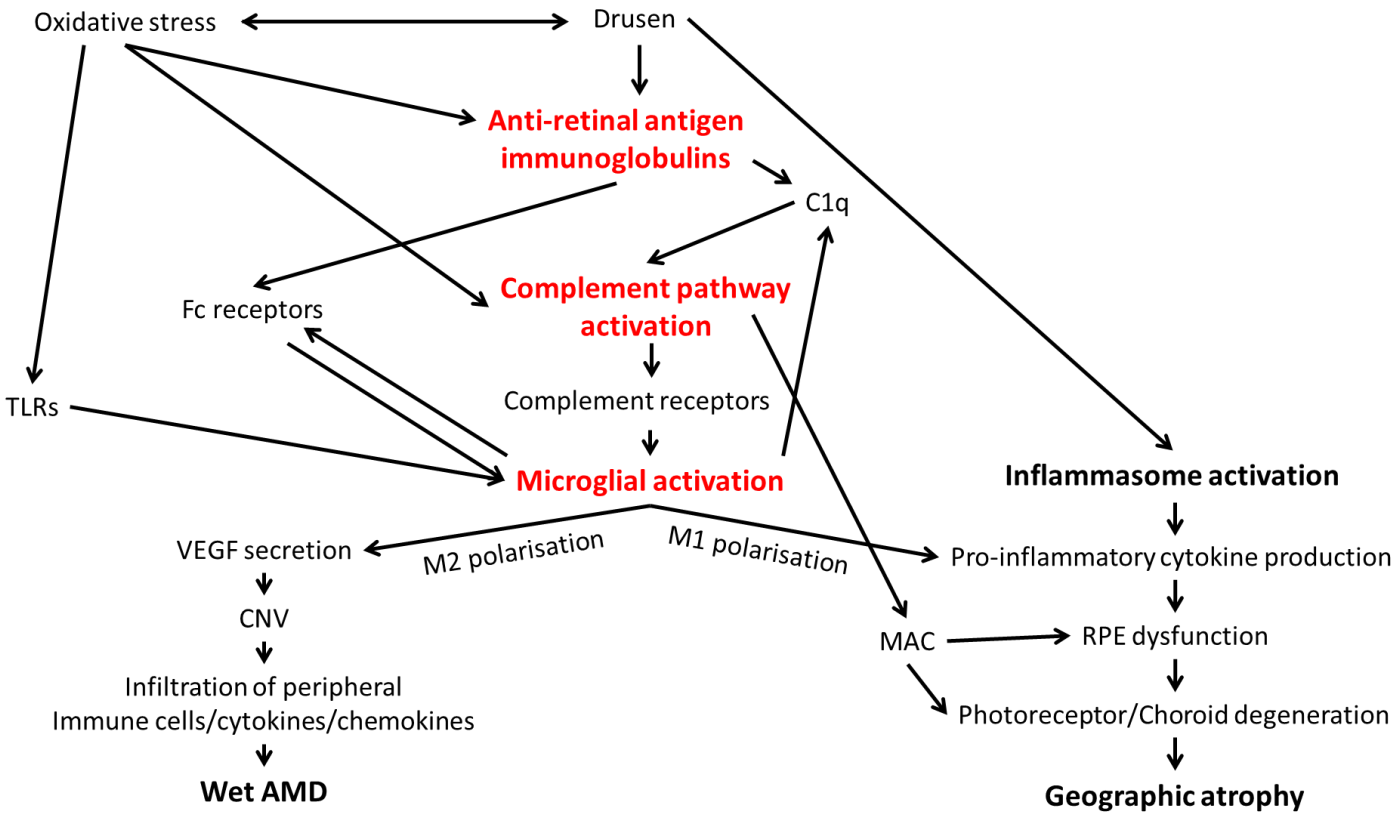

Figure 1.21 – Proposed inflammatory mechanisms leading from early to late-stage AMD pathology.

Deposition of immunoglobulins in drusen could activate the complement pathway and microglia, driving disease progression towards GA or wet AMD. TLRs, toll-like receptors; CNV, choroidal neovascularisation; RPE, retinal pigment epithelium; MAC, membrane attack complex.

1.5 Systemic inflammation and age-related macular degeneration

The role of systemic inflammation in age-related macular degeneration is not clearly defined, but there are several pieces of indirect evidence that together strongly implicate a contribution of systemic inflammation in the pathogenesis and progression of AMD. I have already discussed how AMD patients show increased autoimmunity to retinal antigens, leading to generation of autoantibodies in the periphery that enter the retina and may contribute to local inflammation. Further support for this comes from the fact that patients suffering from the autoimmune disease rheumatoid arthritis who are given strong systemic immunosuppressants are around ten times less likely to develop AMD (McGeer & Sibley, 2005). These findings suggest that the systemic immune system may be a contributor to AMD pathology and a possible target for future therapies. Here, I summarise the key differences in the systemic immune system identified between AMD patients and age-matched controls.

1.5.1 Alterations in systemic inflammatory protein levels in AMD patients

1.5.1.1 Complement

Genetic polymorphisms in complement pathway components account for the majority of AMD heritability, demonstrating a key role for complement activation in the pathobiology of AMD. While much research has focused on the local role of complement activation, there is clear systemic complement activation in AMD patients. Alternative pathway components CFB and CFD and downstream C3a, C3d, C5a and soluble C5b-9 (MAC) are all elevated in AMD patient plasma (Scholl et al., 2008; Guymer et al., 2015; Liu et al., 2011a). In addition, high systemic C3d/C3 ratios, indicative of complement activation, are a risk factor for the development of all forms of AMD (Paun et al., 2015; Ristau et al., 2014; Smailhodzic et al., 2012). Plasma C3d levels are higher in early and GA patients, compared to wet AMD patients (Scholl et al., 2008), possibly indicating a less important role for systemic complement activation in neovascularisation. Furthermore, low systemic levels of CFH and CFI, which are negative regulators of the complement pathway, are a risk factor for AMD (Ansari et al., 2013; Kavanagh et al., 2015). Overall, overactivity of the systemic complement pathway, particularly the alternative pathway, is associated with all types of AMD. As many complement factors are produced by the liver during inflammation/infection, there may be a role for systemic complement in AMD (Murphy & Weaver, 2017). Interestingly, the choroid has been identified as a site of extrahepatic complement production and there is strong immunoreactivity against complement components in early AMD, indicating that choroidal synthesis may be possible during AMD (Murinello et al., 2014; Anderson et al., 2010). AMD risk

factors are likely to contribute to overactivity of the systemic complement pathway. Genetic risk factors in complement pathway components/regulators are likely to affect both systemic and retinal immune systems, while systemic complement activation can also result from non-genetic risk factors such as systemic infections, aging and obesity (Reynolds et al., 2009; Stanton et al., 2011; Murphy & Weaver, 2017; Ristau et al., 2014; Hakobyan et al., 2008; Hecker et al., 2009).

1.5.1.2 Cytokine/chemokines

Dysregulation of cytokine and chemokine axes have also been identified in AMD with most studies focusing on wet AMD patients. Increased serum levels of IL-1α, IL-1β, IL-4, IL-5, IL-10 and IL-13, but not IL-6, have been reported in wet AMD patients (Nassar et al., 2015). However, increased IL-6 in serum of wet AMD patients has been reported in other studies (Ambreen et al., 2015; Yildirim et al., 2012; Haas et al., 2015). Higher levels of soluble TNF receptor II (sTNFRII), which is generated upon TNFα stimulation, are found in wet AMD patients compared to controls, although TNFα levels are unchanged (Faber et al., 2015). High levels of serum TNFα have, however, been associated with increased responsiveness to anti-VEGF treatment (Nassar et al., 2015). Finally, altered chemokine levels are also identified in wet AMD patients, who have reduced levels of lymphocyte recruiting CXCL12 and higher levels of neutrophil/monocyte recruiting CCL2 and IL-8 compared to controls (Anand et al., 2012; Machalińska et al., 2011; Ambreen et al., 2015). This may reflect a shift towards innate immunity and away from adaptive immunity in AMD patients, which is a shift that has been previously associated with aging. However, there also appears to be increased expression of classical pro-inflammatory cytokines (IL-1 and IL-6), T_H2 associated cytokines (IL-4, IL-5, IL-13) and anti-inflammatory cytokines (IL-10), which may indicate general inflammation as opposed to specific pathways of activation.

Proinflammatory cytokines are also increased in dry AMD patients, but have been less studied than wet AMD patients. High IL-6 levels are a risk factor for the development and progression of early AMD (Klein et al., 2014; Seddon et al., 2005). Serum IL-6, along with IL-8, is further increased in dry AMD patients compared to wet AMD patients (Ambreen et al., 2015). High sTNFRII, but not TNFα, is associated with increased risk of developing early AMD (Faber et al., 2015). In addition to innate cytokines, patients with high levels of T cell proliferation/differentiation cytokine IL-2 have increased risk of early AMD (Klein et al., 2014). These data indicate increased innate and adaptive immunity may play a role in the pathogenesis of dry AMD. Additionally, several cytokines, including IL-1β, IL-6 and IL-18, are increased in patients with genetic complement polymorphisms raising AMD risk, indicating an association between genetic risk factors and cytokine levels in AMD patients (Cao et al., 2013).

1.5.1.3 C-reactive protein (CRP)

Pentraxins, a class of pattern recognition receptor, are acute-phase proteins that are increased in AMD patients. Most notably, high systemic CRP levels are associated with increased risk of early AMD and progression of AMD to late stages, and systemic CRP levels are found upregulated in patients with dry and wet AMD (Ambreen et al., 2015; Klein et al., 2014; Seddon et al., 2005). CRP levels are further increased in wet AMD patients compared to dry AMD patients (Ambreen et al., 2015). CRP is a common marker in haematology to assess general levels of inflammation (Heidari, 2012), which indicates that there are higher levels of systemic inflammation in AMD patients compared to controls. Moreover, increased plasma levels of pentraxin-3 have been identified in wet AMD patients, although another study failed to show the same association (Min et al., 2014; Juel et al., 2015). Pentraxins can increase systemic inflammation in a similar manner to C1q, by activation of the complement pathway or activation of Fc receptor-expressing immune cells (Lu et al., 2012).

1.5.2 Altered systemic immune cell phenotypes in AMD

In addition to systemic cytokines, there is also evidence for the altered phenotype of certain immune cell populations in AMD patients. Flow cytometric immunophenotyping of leukocytes in disease is common in areas such as cancer, but in recent years several studies have investigated in detail immune cell populations and receptor expression changes on PBMCs from AMD patients.

1.5.2.1 Neutrophil: lymphocyte cell ratio

Wet AMD patients have a decreased lymphocyte population compared to age matched controls and an increased neutrophil population is observed dry and wet AMD patients (Ilhan et al., 2015; Lechner et al., 2015). Overall, a high neutrophil:lymphocyte ratio indicative of higher levels of systemic inflammation is present in dry and wet AMD patients and is positively correlated with disease severity (Ilhan et al., 2015). This again reflects a shift towards innate immunity and away from adaptive immunity in AMD patients, indicating an increased rate of immunosenescence compared to age-matched controls. Furthermore, increased neutrophil populations correlate with development of retinal angiomatous proliferation, while a reduced CD4+ T-cell population is associated with subretinal fibrosis during CNV (Lechner et al., 2015), demonstrating that some features of wet AMD may be systemic in origin.

1.5.2.2 T cell phenotype

Changes in receptor expression on T cells have been identified in PBMCs from AMD patients. AMD patients have an increased population of CD56+ CD28- T cells, particularly among T_C cells , and this positively correlates with AMD susceptibility (Faber et al., 2013). CD56 upregulation and CD28 downregulation are associated with previous activation and expansion of the population, while CD56 expression has been previously associated with immunosenescence and is increased in autoimmune diseases (i.e. rheumatoid arthritis) (Vallejo et al., 2011; Faber et al., 2013). These findings again support a role for accelerated immunosenescence in AMD patients compared to controls.

Wet AMD patients have decreased populations of CD8+CXCR3+ cells, which are mostly associated with T_H1 responses, providing further support for a shift from T_H1 to T_H2 responses in wet AMD patients (Falk et al., 2014b; Qin et al., 1998). CXCL10 signalling via CXCR3 is associated with reduced fibrosis and angiogenesis in wet AMD patients, which may explain why reduced CXCR3 expression can increase risk for CNV (Fujimura et al., 2012).

Wet AMD patients also have reduced population of CD8+CX3CR1+ cells, which represent a population of cytotoxic memory T cells (Böttcher et al., 2015; Falk et al., 2014a). While CX3CR1-CX3CR1 signalling has been previously implicated in AMD, most research into CX3CR1 has focused on macrophages/microglia instead of T cells and this is worthy of further investigation. Finally, wet AMD patients have increased expression of CD35 (Complement receptor 1) on T cells (Haas et al., 2011), again indicating a role for complement pathway overactivity in AMD patients.

1.5.2.3 Monocyte phenotype

CD14+ monocytes from wet AMD patients express higher levels of CD35, as seen with T cells, but additionally show downregulation of negative regulators of complement CD46 and CD59 (Haas et al., 2011; Singh et al., 2012). Low CD46 expression is associated with development of subretinal fibrosis during CNV, indicating the role of complement in CNV pathology (Singh et al., 2012).

Wet AMD patients have an increased number of CD200+ monocytes and CD200R+ granulocytes (Singh et al., 2013). Upregulation of immunosuppressive CD200:CD200R interactions in AMD patients may be a compensatory mechanism attempting to reduce systemic inflammation seen in AMD patients. Proinflammatory CD14+CD16+ monocytes have increased expression of CCR1 and CCR2 in wet AMD patients (Grunin et al., 2012). This again implicates a role for chemokine signalling in wet AMD patients and identifies possible overactivity of the CCL2-CCR2 axis in the periphery of wet AMD patients. It will be important to determine whether these changes are specific to peripheral myeloid cells or whether microglia also show a similar phenotype.

Finally, stratification of monocytes based on production of inflammatory cytokines shows that patients with monocytes producing high levels of TNFα mRNA have a 5-fold greater risk of developing CNV than those with monocytes producing low levels of TNFα mRNA (Cousins et al., 2004). This may indicate a role for TNFα in wet AMD patients, which has been suggested based on higher serum levels of sTNFRII, or may instead demonstrate that wet AMD patients generally have more active monocytes. For all the changes observed, it is unclear whether the altered immune cell populations in AMD patients result in the altered levels of cytokines/chemokines in the systemic immune system of AMD patients, or alternatively the differences in systemic cytokines/chemokine levels may impact on immune cell phenotype. The true situation is probably somewhere in between, with genetic and environmental risk factors contributing by inducing low level chronic inflammation.

1.5.2.4 Capacity of immune cells to respond to stimulation

Although serum cytokine levels provide a general measure of systemic inflammation, one of the main problems with this analysis is the variation in baseline cytokine levels between patients, which can be caused by factors other than AMD status (e.g. infections, co-morbidities, smoking). In order to avoid this, Zhu et al., 2013 assessed the inflammatory potential of immune cells from AMD patients to produce cytokines in response to activating stimuli. PBMCs from wet AMD patients produce more IL-6 and IL-8 in response to *ex vivo* stimulation with bacterial peptidoglycans and more IL-6 in response to viral mimetic poly(I:C). This demonstrates that immune cells from wet AMD patients may respond in an exaggerated manner *in vivo* when activated, causing greater systemic inflammation in response to insults. *In vitro* stimulation and analysis of immune cells from AMD patients may identify pathways that are upregulated during activation and eventually an activation signature unique to AMD patients, or subgroups of AMD patients, that could identify patients at risk before disease onset.

1.5.3 AMD risk factors and systemic inflammation

The majority of genetic AMD risk factors are associated with inflammatory pathways and are likely to affect levels of inflammation in the systemic immune system, as well as the retina. Moreover, the majority of non-genetic AMD risk factors can all contribute to parainflammation (Chen & Xu, 2015). This elevated inflammation represents an adaptive response to attempt to maintain homeostasis. It is clear that AMD risk factors can induce oxidative stress and consequently systemic inflammation, but there is also evidence that environmental risk factors can act directly on the systemic immune system, which may explain some of the elevations in cytokines and alterations in immune cell phenotypes observed in AMD patients.

Aging, which is the strongest risk factor for AMD, is associated with numerous changes in the systemic immune system that result from 'inflammaging' (Franceschi et al., 2007). Some of these principles (i.e. immunosenescence, autoimmunity) have already been discussed, but there are several other important functional changes. The number of innate immune cells (monocytes, neutrophils and NK cells) increases with age, but they display altered function compared to younger cells (Corona et al., 2012; Beerman et al., 2010). For monocytes, there is an overall shift from M1 to M2 polarisation with age and when aged monocytes are stimulated with bacterial mimetic LPS, they show reduced expression of M1-associated cytokines IL-1β, IL-6 and IL-12 and increased expression of M2-associated cytokine IL-10, indicating a state of hyporesponsiveness or 'tolerance' to stimulation (Chelvarajan et al., 2006). In response to skin burn injury, aged neutrophils showed reduced cytotoxic activity and this reduced function results in prolonged inflammation and increased bystander damage in aged mice compared to young mice (Nomellini et al., 2008). These changes to myeloid cell function may therefore have reduced ability to control growth of pathogens until the adaptive immune response is generated, leading to more prolonged and damaging inflammation.

In terms of adaptive immunity, both T and B cells are decreased with age and have impaired functions; T cells show reduced proliferative ability, while B cells show reduced production of antibodies in response to vaccination (Aw et al., 2007; Sansoni et al., 1993; Jiang et al., 2007; Grubeck-Loebenstein et al., 2009). There is an increase in memory T cells during aging along with a propensity for these cells to mount a stronger immune response to restimulation by a previously encountered antigen, which may again contribute to prolonged and damaging inflammation the elderly (Jiang et al., 2007; Corona et al., 2012).

Many of the genes associated with the immune system are increased in the periphery with aging. These genes include complement components C1q, C3 and C4 and MHC class II antigens A and E (Ferrucci et al., 2005; Singh & Newman, 2011; Petersen & Pedersen, 2005). Older people with no detectable infection have slight to moderate elevations in TNFα, IL-6, IL-1RA, IL-18 and CRP levels compared to young controls and these elevations are in the range of low-grade chronic inflammation as defined as 2-3 times normal levels (Singh & Newman, 2011; Petersen & Pedersen, 2005). Several mechanisms for increased cytokine levels with age have been suggested: cytokine secretion from increasing amounts of visceral adipose tissue with age; loss of regulation of cytokine secretion due to reduction in sex hormone levels with age and oxidative damage inducing a low-level inflammatory response (Godbout et al., 2005).

Smoking is also a strong risk factor for AMD that can directly impact the immune system. Cigarette smoke contains over 4,500 chemicals, many of which are toxic and carcinogenic and

have diverse effects on the immune system in isolation. On balance, cigarette smoke appears to exert immunosuppressive effects on a range of immune cells including lung-resident macrophages, NK cells, T cells and B cells (Sopori, 2002). Macrophages and NK cells from patients who smoke chronically have an impaired ability to clear bacterial pathogens and respond to immune stimulation (King et al., 1988; Martin & Warr, 1977), which like aging may contribute to prolonged and damaging inflammation in smokers. T cells and B cells are elevated in chronic smokers, but the function of these cells are greatly suppressed (Holt & Keast, 1977; Holt, 1987). Impaired T cell proliferation and reduced antibody responses result from chronic smoking, although total levels of autoantibodies against host antigens are increased due to smoking (Mathews et al., 1973; Sopori, 2002; Masdottir et al., 2000).

Furthermore, obesity is associated with AMD and components of diet have been shown to alter immune cell phenotype. Following a high cholesterol diet, which is associated with obesity, there is a threefold increase in bone marrow production of monocytes/macrophages and splenic myeloid cells show an activated morphology compared to control diet in mice (van Kampen et al., 2014). This study demonstrates that poor diet and obesity can alter myeloid cell populations. Furthermore, saturated fatty acids typical of an unhealthy diet increase lymphocyte proliferation and pro-inflammatory cytokine production in mice, while fatty acids associated with healthier diets (e.g polyunsaturated fatty acids from fish oil) inhibit lymphocyte proliferation and demonstrate a skew towards T_H2 polarisation when cells are stimulated (Wallace et al., 2001). This demonstrates how elements of an unhealthy diet can lead to increased pro-inflammatory cytokines and a state of parainflammation, as is observed with aging.

1.5.4 Systemic infections and AMD

Certain systemic infections have also been identified as a risk factor for AMD and can act to induce chronic systemic inflammation. Interestingly, these bacterial and viral infections have remarkable similarities: they are mostly asymptomatic; highly prevalent; induce acute, and often reoccurring, infections and develop into chronic persistent infections in a minority of patients (Carmichael, 2012; Miyashita et al., 2003).

Seropositivity or high antibody titres against bacterial infection *Chlamydophila pneumoniae (C. pneumoniae)* is associated with increased incidence and/or progression of AMD in 6 of 12 published studies (Baird et al., 2008; Ishida et al., 2003; Kalayoglu et al., 2003; Robman et al., 2005; Shen et al., 2009; Haas et al., 2009; Khandhadia et al., 2012; Klein et al., 2005; Miller et al., 2004; Robman et al., 2007; Turgut et al., 2010; Nakata et al., 2015), although a recent meta-analysis found no association (Chen et al., 2014). However, the authors suggest that vast

geographical variation in the proportion of the population infected with *C. pneumoniae* may contribute to disparities between studies. One of the largest studies reports that patients with the highest antibody titres against C. pneumoniae have a threefold higher risk of AMD progression (Robman et al., 2005). In addition to AMD, *C. pneumoniae* infection has been associated with a range of other neurodegenerative conditions, including Alzheimer's disease and multiple sclerosis (Sriram et al., 1999; Ide et al., 2016). C*. pneumoniae* is an intracellular pathogen that commonly infects monocytes/macrophages, resulting in cytokine production (Gaydos, 2000), which may contribute to parainflammation during chronic *C. pneumoniae* infection.

Some evidence has pointed towards possible mechanisms through which *C. pneumoniae* could contribute to wet AMD progression. *C. pneumoniae* has been detected in the membranes of neovascularized vessels from 'wet' AMD patients in 2 of 3 studies, indicating the probable presence of the pathogen at the site of angiogenesis (Kalayoglu et al., 2005; Kessler et al., 2006; Wolf-Schnurrbusch et al., 2013). Human RPE cell lines produce chemokines CCL2 and IL-8 in response to *C. pneumoniae* antigens, which could recruit VEGF-expressing immune cells (Kalayoglu et al., 2005). Moreover, while VEGF is not upregulated in response to *C. pneumoniae* antigens, IL-8 also has angiogenic properties (Kalayoglu et al., 2005). Intraocular injection of *C. pneumoniae* antigens into the retina exacerbates murine laser-induced CNV, a well-respected model of wet AMD, which again indicates increased angiogenesis with bacterial infection, although systemic administration of these antigens would be more representative of route of infection (Fujimoto et al., 2010). It would be interesting to examine whether systemic bacterial infection in mice can also exacerbate AMD mouse models.

Periodontitis, a chronic inflammatory gum disease caused by a range of bacterial infections, is also associated with ≈1.8-fold risk of AMD incidence in patients less than 60 years in two independent cohorts, although this association is lost in older age (Han & Park, 2017; Wagley et al., 2015). In an Alzheimer's disease cohort, previous exposure to the periodontitis-causing bacteria *Porphyromonas gingivalis (P. gingivalis)* is associated with a sixfold rate of cognitive decline, indicating that systemic infections are capable of exacerbating neurodegeneration (Holmes et al., 2009). A large-scale study investigating whether systemic infections increase the rate of vision loss in AMD has never been carried out, but would be interesting given these findings.

Finally, high IgG titres against *Cytomegalovirus* (CMV) have been indicated as a risk factor for the development of wet AMD, indicating low-grade viral infection may accelerate AMD pathology (Miller et al., 2004). Unlike *C. pneumoniae*, this association has not been examined in independent cohorts. Laser-induced CNV is exacerbated in mice given systemic murine CMV three months prior, indicating a role of the virus in the pathogenesis of wet AMD (Cousins et al., 2012). It would

be interesting to investigate whether administration of the virus after laser-induced CNV can also exacerbate progression of CMV.

The mechanism by which systemic infections exacerbate CNV is unclear, although mouse studies indicate that systemic infections can induce retinal inflammation. Chronic CMV infection results in systemic IFNγ production that drives the recruitment of myeloid cells to the subretinal space (Zinkernagel et al., 2013). Therefore, systemic infection could have a role in recruiting microglia/infiltrating monocytes to the site of AMD pathology and also increasing their activation, leading to increased inflammation in AMD. In addition, the total myeloid cell population is increased and there is a subset expressing MHCII, indicating an inflammatory phenotype (Zinkernagel et al., 2013). Many of the effects seen with viral infection are also seen following systemic fungal *Candida albicans* infection: recruitment of myeloid cells to the subretinal space; increased myeloid cells numbers and an MHCII+ subset (Maneu et al., 2014). This shows that aspects of retinal inflammation after infection may be applicable to a wide range of pathogens.

Having said that, the effect of systemic bacterial infection on the retina has been most implicated in AMD risk and has not been characterised. Systemic administration of the bacterial mimetic LPS induces retinal inflammation and is an established inflammatory rodent model termed endotoxin-induced uveitis (EIU). However, the exact nature of inflammation is highly variable based on the strain of mouse or rat used as well as the strain and administration route/dose of LPS (Shen et al., 2000a). In C3H/HeN mice, which are highly susceptible, LPS results in biphasic inflammation peaking at 1 and 5 days post injection, characterised by increased numbers of inflammatory cells in the eye as well as higher levels of pro-inflammatory cytokines (Shen et al., 2000b). In contrast in C57BL/6, inflammation is monophasic, with a peak at 18 hours post injection and resolution by 1 week post injection. At 18 hours post injection, there are a large number of infiltrating neutrophils in the retina, which are the principal effector cell in EIU, along with particularly high expression of CCL2 and CXCL10 (Chu et al., 2016). However, using LPS as a bacterial mimetic fails to recapitulate the inflammatory effects of a real infection, which activates a wide variety of immune pathways and shows much greater chronicity. Consequently, the effect of systemic bacterial infection on the retina still requires characterisation. Treatments that alter the way the systemic immune system and retina interact during infection may be interesting therapeutics in AMD, although many of these drugs could risk compromising the ability to fight infection in the elderly.

1.5.5 Summary

Several systemic immune alterations are observed in AMD patients compared to age-matched controls (Figure 1.22). A shift towards innate immunity and away from adaptive immunity is associated with aging, but AMD patients appear to show a stronger effect along with increased autoimmunity. Higher levels of systemic cytokines, complement components and CRP indicate a state of chronic low-grade inflammation in AMD patients. However, it is unclear whether these system immune changes contribute to AMD pathology, or are purely symptomatic. Choroidal complement synthesis, retinal autoantibody deposition in drusen, choroidal macrophages in close association with drusen and reduced risk of AMD in rheumatoid arthritis patients given systemic immunosuppressants argue for a role of the systemic immune system in AMD pathology. Moreover, AMD risk factors (e.g. aging, smoking, obesity) are capable of modifying the systemic immune system directly and via oxidative stress, leading to parainflammation which may impact on the retina. Finally, chronic bacterial and viral systemic infections have been associated with an increased risk of AMD incidence. These infections are thought to be limited to the periphery, indicating that activation of the systemic immune system can contribute to AMD pathology, although in the case of wet AMD, it is possible that bacteria may penetrate the neovascular membrane. Ultimately, the contribution of systemic inflammation/infections to retinal inflammation and neurodegeneration requires further investigation. Neutralising systemic immune pathways that contribute to AMD pathology represents an attractive therapy to slow AMD progression.

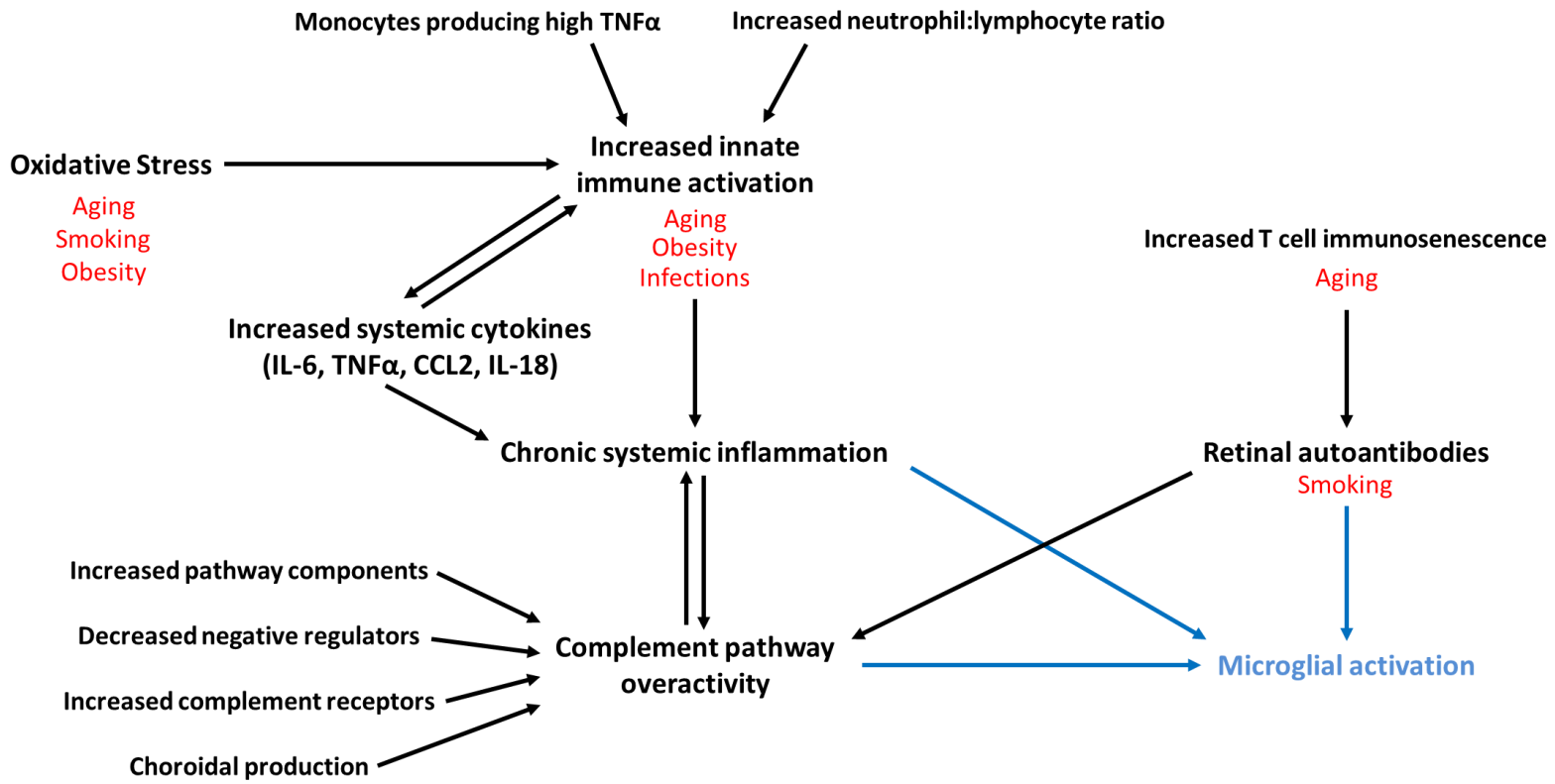

Figure 1.22 – Summary of systemic inflammatory changes in AMD patients.

Systemic inflammatory changes in AMD patients are shown in black, while contributing AMD risk factors are shown in red. Proposed mechanisms by which systemic inflammation contribute to microglial activation are shown in blue.

1.6 Summary

Age-related macular degeneration is the commonest cause of blindness in developed countries and there are no effective therapies for the vast majority of patients. While, wet AMD pathology can be reduced by anti-VEGF treatments, no underpinning mechanisms have been well characterised for GA, although complement inhibition is showing some success in trials. The lack of well-respected mouse models of early AMD and GA make it difficult to find possible mechanisms and test possible therapies.

The immune system appears to play an important role in AMD pathology, with the presence of many inflammatory components deposited in drusen along with activation of microglial and macroglial cells. Furthermore, there is evidence for increased levels of cytokines/chemokines in the aqueous humour of wet AMD patients, but the levels in dry AMD patients are not characterised. AMD patients also show systemic chronic low-grade inflammation, increased autoimmunity and choroidal complement synthesis, indicating a role for systemic inflammation in AMD. There is also evidence that patients with monocytes that have the capacity to produce high levels of inflammatory cytokines have a 5-fold increase in AMD risk. Consequently, there is substantial evidence for systemic inflammation in AMD, although it is unclear whether it directly impacts disease pathobiology or is purely symptomatic.

Mouse studies have shown that systemic viral and fungal infections can induce retinal inflammation, and that viral infection can exacerbate wet AMD pathology in a mouse model, which is in line with observations for increased wet AMD risk with viral infections. AMD risk has also been linked to systemic bacterial infection, but the effect of systemic bacterial infection on the healthy retina or AMD mouse models has never been characterised. If systemic bacterial infection can cause retinal inflammation, the underpinning mechanisms may represent an attractive target to block the effect of systemic inflammation on retinal diseases with an inflammatory component (e.g. AMD).

1.7 Aims and Objectives

I hypothesise that systemic bacterial infection, which is a risk factor for AMD, can induce retinal inflammation in terms of microglial activation and pro-inflammatory cytokine production, as observed during sickness behaviour responses in the brain. Moreover, that such infections induce long-lasting functional changes to the microglial cells, and possibly peripheral monocytes, meaning that they respond in an exaggerated 'primed' manner to subsequent local or peripheral inflammation. This could have consequences for AMD, where local inflammation may be exacerbated by systemic infections leading to accelerated AMD pathology and vision loss. Testing the effects of systemic bacterial infection on mouse models recapitulating key features of early and atrophic AMD would enable us to test parts of this hypothesis. Finally, I hypothesise that the systemic immune system of AMD patients may be primed to respond to systemic infections in an exaggerated manner compared to age-matched controls, making the effects of systemic infection on the retina stronger in AMD patients.

Aim 1. To characterise the effect of systemic bacterial infection on the healthy mouse retina in terms of glial cell activation, blood vessel activation and cytokine responses.

Aim 2. To determine the functional consequences of systemic bacterial infection on the mouse retina in terms of responsiveness to subsequent systemic immune cell activation.

Aim 3. To investigate the effect of systemic bacterial infection in a mouse model of retinal inflammatory processes observed in early AMD, including immunoglobulin deposition and myeloid cell activation in the retina.

Aim 4. To describe the relationship between systemic and local cytokines in a cohort of wet and dry AMD patients and investigate the capacity of systemic immune cells from AMD patients and age-matched controls to respond to *ex vivo* immune stimulation.

Aim 5. To develop a novel mouse model of late-stage geographic atrophy, which can be used in the future to gain insights into systemic infection and retinal neurodegeneration.

Chapter 2:

Materials and methods

2.1 In vivo experiments

2.1.1 Experimental Animals

Female mice were housed in groups of 2-10 in plastic cages under a 12h:12h light-dark at 19-24°C. Mice had water and standard Chow diet (RM1, SDS, UK) *ad libitum*. All procedures had local ethical approval and were carried out under the authority of a UK Home Office License. The following mouse strains were used in the experiments detailed in this thesis:

- BALB/c - standard inbred strain
- C57BL/6J - standard inbred strain
- MacGreen ($Csf1r^{eGFP/eGFP}$) mice that express functional colony stimulating factor 1 receptor (CSF1R) and eGFP under the promoter for CSF1R, which results in macrophages and microglia strongly expressing eGFP. These mice were backcrossed 10x onto C57BL/6J background.

All mice were obtained from Charles River (Margate, UK) and bred at the Biomedical Research Facility, Southampton General Hospital, UK.

2.1.2 Injection of mice with immune stimuli

High density stocks of a strain of *Salmonella enterica* subsp. *enterica* Serovar Typhimurium (Salmonella) were kindly provided by Ursula Püntener and were stored at -80°C until use. This live vaccine strain - SL3261 (*his* G46 (del) *aro*A 554) – is attenuated due to mutations preventing the synthesis of *p*-amino-benzoic acid and 2,3-dihydroxybenzoate from folate, which are essential for *Salmonella* replication (Hoiseth et al, 1981). C57BL/6, BALB/c and MacGreen mice were infected with 10^6 colony forming units (cfu) of *S.* Typhimurium by intraperitoneal (i.p.) injection, which is a sublethal dose in healthy mice (Püntener et al., 2012). This dose induced typical weight loss of 8-12% at 1 day post injection and mice were culled if they showed signs of distress or suffered >20% body weight loss. In chapter 4, mice were injected with 0.5mg/kg lipopolysaccharide (LPS) derived from *Salmonella abortus equi* (L5886, Sigma-Aldrich, UK) in 0.9% sterile saline. The solution was vortexed for 10 minutes before injection to increase homogeneity of the solution.

Mouse body weight and appearance were monitored daily for the first week and daily or weekly thereafter until tissue was harvested. Experiments were performed in a Containment Level 2 facility in accordance with Health and Safety Executive regulations.

2.1.3 Formation of retinal immune complexes

BALB/c mice received an i.p. injection of 50µg OVA (Sigma-Aldrich, UK) dissolved in a 1:1 mixture of alum (Imject Alum Adjuvant; Thermo Scientific, UK) and sterile saline (NaCl 0.9% w/v; Fannin, UK). Mice were boosted by i.p. injection of 100µg OVA dissolved in sterile saline at two and four weeks after initial immunisation to boost levels of anti-OVA IgG. Six weeks after initial immunisation, general anaesthesia was induced by i.p. injection of 10% Ketamine (Fort Dodge Pharma, UK) and 5% Xylazine (Bayer, UK) in sterile saline at 10µl/g of mouse weight. Lignocaine 5% m/m ointment (TEVA Pharmaceutical Industries, UK) was applied to the ears and mice were restrained in a stereotaxic frame. Pupils were dilated to observe the injection using 2.5% phenylephrine eye drops (Centaur Services, UK) for >1min followed by 1% tropicamide eye drops (Centaur Services, UK) for >1min. Intravitreal injections of 10µg endotoxin-free OVA (EndoGrade OVA; Hyglos, Germany) in 1µl sterile saline (10mg/ml OVA) were performed using a Hamilton Neuros Syringe with a 33G-needle 12° bevel (Esslab, UK). As a negative control for immune complexes, age-matched non-immunised mice received a 1µl intravitreal injection of 10mg/ml endotoxin-free OVA. Lacrilube (Allergan, UK) was applied to eyes after injection and mice were left to recover at 30°C.

2.1.4 *In vivo* assessment of retinal structure and function

All drugs required for *in vivo* assessment of the retina were supplied by Centaur Services, UK. BALB/c and C57BL/6 mice were given reversible anaesthesia comprised of 6% ketamine, 10% Dexdomitor in sterile saline at 10µl/g of mouse weight. Anaesthesia was reversed at the end of the procedure with 10% Antisedan in sterile saline at 10µl/g of mouse weight. Mouse eyes were maximally dilated using 2.5% phenylephrine eye drops for >1min followed by 1% tropicamide eye drops for >1min. Eyes were prevented from drying out by applying 0.2% Carbomer gel (Clinitas, Altacor). As part of the imaging procedure, mice underwent electroretinography (ERG), followed by fundoscopy and then optical coherence tomography (OCT) unless otherwise stated.

2.1.4.1 Electroretinography

ERGs were obtained using a Micron III retinal imaging system with a focal ERG attachment (Phoenix Research Laboratories, CA, USA). Mice were dark-adapted overnight to ensure maximum sensitivity of rods and cones to light. Dark adaptation was maintained by conducting the procedure under low-level red light. Following pupil dilation, mice were orientated on a stage so that the limbus was aligned in parallel to the ERG attachment to provide maximum illumination to the retina. Three electrodes were attached to the mouse to obtain readings: the corneal electrode was placed in close apposition to the cornea and was immersed in 0.2% Carbomer gel for

improved conductivity; the reference electrode was placed subcutaneously to the skull; the ground electrode was placed subcutaneously just above the base of the tail. Mice were exposed to three flashes of white light at 6.8 log(cd/m^2) intensity for 1ms, with each flash separated by 120s to restore dark adaptation (Herrmann et al., 2010). Recordings were obtained for 50ms prior to and 250ms post light exposure using LabScribeERG v3 software (iWorx, NH, USA) with a bandpass filter at 2-1000Hz, sampling frequency of 5kHZ and 50Hz noise reduction. Recordings of the unlasered control eyes for each mouse were taken to allow variation in ERG recordings between different sessions to be taken into account. Variation between sessions is caused by many variables, notably room temperature, duration of anaesthesia and positioning of electrodes (Brandli & Stone, 2015). ERG plots were generated by exporting the data into Microsoft Excel, shifting each curve so that the amplitude is 0µV when stimulus is applied at 50ms and then averaging the data from each experimental group. The A-wave amplitude, B-wave amplitude and B-wave implicit time for each retina was calculated to assess photoreceptor and retinal function (Figure 2.1).

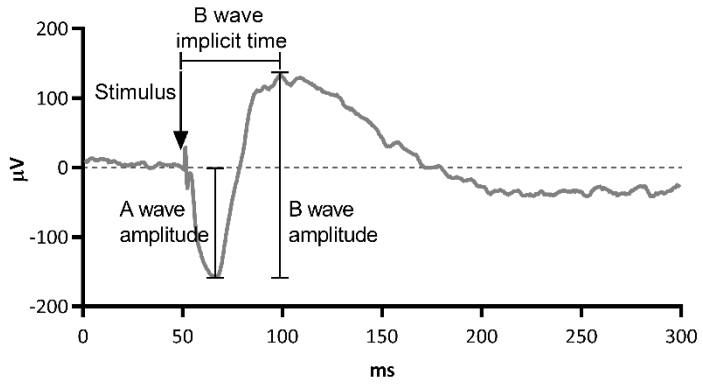

Figure 2.1 - Representative ERG trace highlighting the different components of the waveform. *At 50ms, a light stimulus is applied to the mouse retina (arrow) causing the hyperpolarisation of photoreceptor cells in response to light followed by a wave of depolarisation as the electrical signals are propagated through the bipolar and ganglion cells towards the optic nerve. A-wave amplitude is calculated from baseline to the maximum amplitude of hyperpolarisation and is a measure of photoreceptor function. The B-wave is calculated from the maximum amplitude of hyperpolarisation to the maximum amplitude of depolarisation, and is therefore affected by both photoreceptors and the function of the inner retinal layers. B-wave implicit time is calculated as the duration from the application of the stimulus to reaching the maximum B-wave amplitude.*

2.1.4.2 Fundoscopy

Following ERG, unless otherwise stated, fundoscopy was performed using a Micron III retinal imaging system with a camera imaging attachment (Phoenix Research Laboratories). Mice were placed on a rotatable stage and orientated so that the optic nerve was visible in each image (Figure 2.2). 0.2% Carbomer Gel was used to prevent light refraction by air between the camera and eye. Brightfield fundoscopy images were captured using Phoenix Micron IV Retinal Imaging Microscope Software and were assessed for abnormalities.

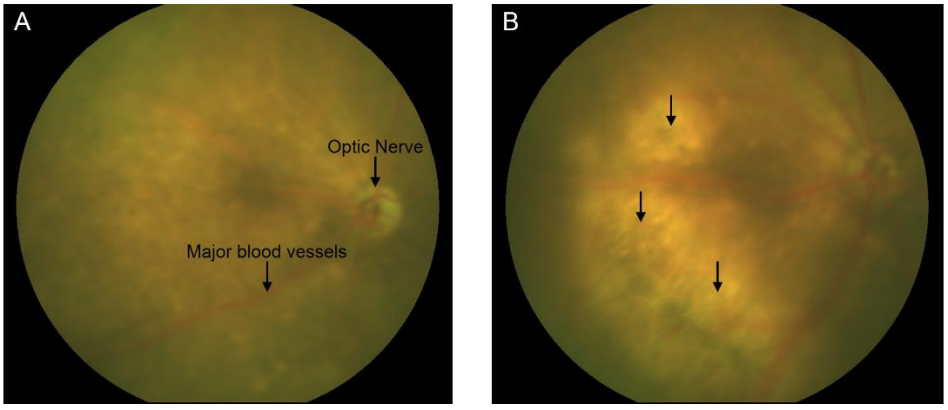

Figure 2.2 – Example healthy and pathological fundoscopy images.
(A) The optic nerve and blood vessels in the healthy mouse retina and (B) a retina with pathological areas marked with black arrows.

2.1.4.3 Optical Coherence Tomography

Following fundoscopy, unless otherwise stated, spectral domain OCT scans (SD-OCT) were taken of the experimental eye using a Bioptigen Envisu R machine (Leica Microsystems, USA). SD-OCT provides an accurate assessment of the location and thickness of each layer, based upon the different reflective properties of each layer (Figure 2.3). 0.2% Carbomer gel was removed from each eye and replaced with Systane Lubricant Eye Drops (Alcon) to prevent light impedance. Mice were orientated on a stage so that the optic nerve was visible in each image and if the mice were tracked over time, the optic nerve was imaged in the same place to previous scans to allow consistent follow-up. 100 B-scans (each of which was the average of 25 individual B scans comprising 1000 A scans) were captured using InVivoVue v2.3 (Leica Microsystems, USA) to provide an image of the retinal layers across a 1.4mm^2 area of retina.

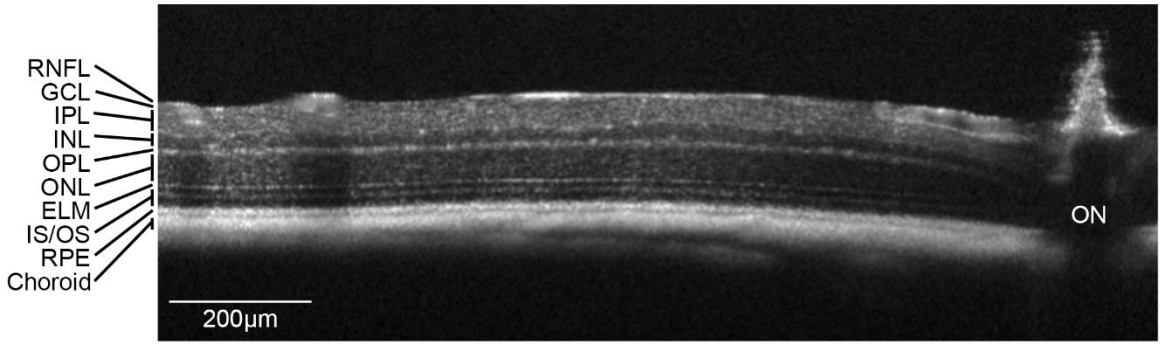

Figure 2.3 – OCT B-scan from a healthy mouse retina showing the retinal layers and optic nerve. *OCT, optical coherence tomography; RNFL, retinal nerve fibre layer; GCL, ganglion cell layer; IPL, inner plexiform layer; INL, inner nuclear layer; OPL, outer plexiform layer; ONL, outer nuclear layers; ELM, external limiting membrane; IS/OS inner/outer photoreceptor segments; RPE, retinal pigment epithelium; ON, optic nerve.*

2.1.5 Laser-induced retinal atrophic lesions

C57BL/6 mice were given anaesthesia and eyes were dilated as for *in vivo* imaging (Section 2.1.4). Atrophic retinal lesions were induced using an 810nm constant wave diode laser coupled with a multi-mode optical fibre (Changchun New Industries Optoelectronics Technology Co., China) to the laser injector attachment (diameter 400µm) of a Micron III platform (Phoenix Labs, USA). The laser injector also has an imaging camera for fundoscopy to enable to orientation and visualisation of the lasered area. Mice were orientated on a stage so that the optic nerve was on the right in each image and the eye and laser injector were coated in 0.2% carbomer gel to reduce light refraction. The retina was targeted with a focused laser beam at a fixed power (32mW for ≈60s unless otherwise stated) until discolouration of the retina was apparent. The duration of laser was approximate and laser duration was judged by eye until discolouration of each lasered area was consistent. Duration of laser was different for each spot and is likely due to subtle differences in angle, distance and size of each spot as the laser was oriented to a new site. Mice received multiple (average 7) laser spots until the field of view of the camera was lesioned, except near the optic nerve, which was spared. The areas were lasered in close apposition to allow the possibility of reaching confluence. Mice were imaged before and after laser and then recovered at 30°C.

2.1.6 Perfusion

Experimental mice were terminally anaesthetised with rat Avertin – 2,2,2'-tribromoethanol (3% w/v, Sigma-Aldrich, UK), 7.2% ethanol, 1.8% tertiary amyl alcohol (Sigma-Aldrich, UK) diluted in 0.9% NaCl (ThermoFisher Scientific, UK). The left atrium was punctured and blood collected. Mice were transcardially perfused with 0.9% NaCl containing 5 units/ml heparin sodium (CP Pharmaceuticals, UK). Blood was centrifuged at 1500g for 10 mins and serum was taken and stored at -20°C until use. Unless otherwise stated, the spleens of mice infected with Salmonella and their controls were snap-frozen on dry ice and were subsequently weighed to assess level of immune response to *S.* Typhimurium and, by extension, level of infection.

2.1.6.1 Tissue collection for immunohistochemistry

Following perfusion, eyes were enucleated, embedded in optimal cutting temperature medium (VWR, UK) and frozen on isopentane (ThermoFisher Scientific, UK) stored on dry ice. Samples were stored at -20°C until use.

2.1.6.2 Tissue collection for FACS

Following perfusion, eyes were enucleated and the retina was immediately dissected out of the eye cup and kept in ice-cold HBSS (Ca-/Mg-) (Sigma-Aldrich, UK) until further processing.

2.1.6.3 Tissue collection for qPCR and ELISA/multiplex analysis

Following perfusion, eyes were enucleated and the retina was immediately dissected out of the eye cup, placed into an RNase free sterile eppendorf and snap-frozen in liquid nitrogen. Samples were stored at -80°C until use.

2.2 Immunohistochemical analysis of mouse eye sections

2.2.1 Sectioning

20µm thick eye sections were cut from eyes embedded in optimal cutting temperature medium using a cryostat at -20°C (chamber temperature) and -16°C (object temperature). Sections were transferred onto 3'-aminopropyltriethoxysilane (Sigma-Aldrich, UK) coated glass microscope slides (VWR, UK), which were air dried for 1 hr and then stored at -20°C until use.

2.2.2 DAB immunohistochemistry

Slides were dried at 37°C for 40mins, fixed in 100% ethanol (ThermoFisher Scientific, UK) at 4°C for 15 mins, washed in 1X PBS containing 0.01% Triton X-100 (Sigma-Aldrich, UK) (PBS-T, pH 7.2-7.4) for 15 mins and sections were separated using a wax pen (Vector Labs, UK). Sections were quenched with 1% H_2O_2 (ThermoFisher Scientific, UK) in PBS-T for 10 mins and then washed in PBS-T for 15 mins. Sections were blocked with 5% bovine serum albumin (ThermoFisher Scientific, UK) and 10% appropriate normal animal serum (Sigma-Aldrich, UK) in PBS-T for 30mins. Sections were then incubated with primary antibodies (Table 2.1) in PBS-T (or PBS-T only for controls) at 4°C for 40-48 hrs. Slides were washed 3x5mins in PBS-T and then incubated for 1hr at RT with appropriate biotinylated secondary antibodies in PBS-T (Table 2.2). Sections were washed 3x5 mins in PBS-T and then incubated with avidin-biotin complex (Vectastain ABC Kit; Vector Labs, UK) as per the manufacturer's protocol for 30 mins. Sections were washed 3x10mins in PBS-T. Slides were placed in 0.1M phosphate buffer containing 0.05% 3,3'-Diaminobenzidine (DAB, Sigma-Aldrich, UK) and 0.015% H_2O_2. Sections were counterstained in haematoxylin (BDH Laboratory supplies, UK) and destained in acid alcohol (70% ethanol and 1% HCl). Slides were dehydrated by placing them in increasing ethanol concentrations and xylene (ThermoFisher Scientific, UK) and then coverslipped (VWR, UK) using DPX mounting medium (ThermoFisher Scientific, UK).

2.2.3 DAB Imaging and Quantification

Overlapping 20x maximal projected images were taken of each retinal section and stitched together into a composite .tif image using the dotSlide or VS110 Virtual Slide Microscopy Systems (Olympus). Sections stained with the same marker were blinded prior to quantification. For percentage area stained quantification, the whole retina was selected, excluding areas of major damage, in ImageJ and the colour deconvolution plugin (FIJI) was used to produce an image of DAB staining without haematoxylin or background colouring. The DAB image was then converted into a black/white binary image where any level of staining above a defined threshold was

converted into black, while anything below the threshold was converted into white. The threshold for each stain was manually defined based on stain intensity and background while blinded and was kept constant for each marker. The percentage area in black within the selected retinal area was then calculated to determine percentage area stained. For cell counts, the number of positive cells in the retina or specific retinal layers were manually counted and normalised to the total retinal area or length.

2.2.4 Immunofluorescence

Slides were dried at 37°C for 40mins, fixed in 100% ethanol at 4°C for 15 mins, washed in 1X PBS-T for 15 mins and sections were separated using a wax pen. Sections were blocked with 5% BSA and 10% normal animal serum (Sigma-Aldrich, UK) in PBS-T for 30mins. Sections were then incubated with primary antibodies (Table 2.1) in PBS-T (or PBS-T only for controls) at 4°C for 40-48 hours. Slides were washed 3x5 mins in PBS-T and then incubated for 1 hr at RT with fluorescent secondary antibodies in PBS-T (Table 2.2). Slides were placed in DAPI solution (1µg/ml in PBS-T, Sigma-Aldrich, UK) for 10 mins and were then washed for 3x10 mins in PBS-T and coverslipped with Mowiol mounting medium (Cold Spring Harbour Protocols). 10x maximal projection images of fluorescent staining were taken using the VS110 Virtual Slide Microscopy System (Olympus). Settings for the blue, green and red channels were optimised for each stain and kept constant throughout imaging.

2.2.5 Confocal imaging

For OVA and IgG staining (Chapter 5) and immune cell activation in laser lesions (Chapter 6), confocal images were taken for representative images. Sections were imaged with a confocal laser scanning microscope (Leica TCS SP8, Leica Microsystems, UK). DAPI was excited with a 405nm laser, AF488 was excited with the 488 line of an argon laser and AF568 was excited with a 561nm solid state laser. Detection bandwidths were placed under peaks of the emission spectrum for each dye. Sequential imaging of DAPI and AF568 followed by AF488 was performed to avoid spectral bleed-through of DAPI into the AF488 channel. Secondary antibody only controls were used to set the maximum sensitivity of each detector, thereby controlling for autofluorescence and non-specific binding. A Z-stack through the whole section was taken and a maximum intensity projection of each stack was generated in FIJI (Schindelin et al., 2012).

Target	Antibody type	Distributor	Product ID (Clone)	Concentration (Dilution)
CD11b	Rat anti-mouse mAb	AbD Serotec, UK	MCA711 (5C6)	2µg/ml (1:500)
CD11c	Hamster anti-mouse mAb	Cancer Sciences, SGH, UK#	N/A (N418)	2µg/ml (1:500)
CD3 (Chapter 4)	Rabbit anti-mouse mAb	Abcam, UK#	ab16669 (SP7)	(1:500)
CD3 (Chapter 6)	Rat anti-mouse mAb	Cancer Sciences, SGH, UK#	KT3	1µg/ml (1:5000)
CD31	Rat anti-mouse mAb	eBioScience, UK	11-0311 (390)	(1:500)
CD68	Rat anti-mouse mAb	AbD Serotec, UK	MCA1957 (FA-11)	0.1µg/ml (1:500)
Collagen IV	Rabbit anti-mouse pAb	Abcam, UK	ab6586	2µg/ml (1:500)
FcγRI	Rat anti-mouse mAb	Cancer Sciences, SGH, UK#	N/A (AT152-9)	2µg/ml (1:500)
FcγRIV	Rat anti-mouse mAb	Cancer Sciences, SGH, UK#	N/A	2µg/ml (1:500)
FCRLS	Rat anti-mouse mAb	Harvard Medical School, USA*	N/A	(1:500)
GFAP	Rabbit anti-mouse pAb	Aligent, UK	Z0334	(1:1000)
ICAM-1	Rat anti-mouse mAb	Abcam, UK	ab25375 (YN1/1.7.4)	1µg/ml (1:500)
IgG	Sheep anti-mouse pAb-FITC	Sigma-Aldrich, UK	F2266	n/a (1:500)
MHCII	Rat anti-mouse mAb	Abcam, UK	ab64528 (M5/114.15.2)	0.4µg/ml (1:500)
P2ry12	Rabbit anti-mouse mAb	Harvard Medical School, USA*	N/A	(1:500)
VCAM-1	Rat anti-mouse mAb	AbD Serotec, UK	MCA2297 (MVCAM A (429))	2µg/ml (1:500)

Table 2.1 – Primary antibody information for mouse immunohistochemistry.

*Antibodies were kindly provided by *Dr. Oleg Butovsky, Harvard Medical School, Boston and # Prof. Mark Cragg, Cancer Sciences, University of Southampton.*

Target (Conjugate)	Antibody type	Dilution	Product ID	Distributor
Rabbit IgG (Biotin)	Goat anti-rabbit pAb	1:200	BA-1000	Vector Labs, UK
Rabbit IgG (Alexa Fluor 568)	Goat anti-rabbit mAb	1:500	A-11011	ThermoFisher Scientific, UK
Rat IgG (Biotin)	Rabbit anti-rat pAb	1:200	BA-4001	Vector Labs, UK
Rat IgG (Alexa Fluor 488)	Donkey anti-rat mAb	1:500	A-21208	ThermoFisher Scientific, UK

Table 2.2 – Secondary antibody information for mouse immunohistochemistry

2.3 Murine Flow Cytometry

2.3.1 Sample Preparation

All reagents for flow cytometry were purchased from Sigma-Aldrich, UK, unless otherwise stated. FACS buffer comprising 1% FCS, 0.01M EDTA (ethylenediaminetetraacetic acid), in 1x PBS was prepared, filter sterilised and cooled to 4°C. All steps were performed at 4°C until sample acquisition. MacGreen retinas stored in 5ml ice-cold HBSS (Ca-/Mg-) in 15ml falcon tubes were centrifuged at 400g for 5 mins and supernatant was poured off. Retinal cells were dissociated in residual liquid using mechanical dissociation by running the falcon tube along a 1.5ml microcentrifuge tube rack ten times. Cells were resuspended in 20ml HBSS (Ca-/Mg-) and passed through a 70µm cell strainer (ThermoFisher Scientific, UK) on a 50ml falcon tube. Samples were centrifuged at 400g for 8 mins, supernatant was poured off and cells were resuspended in 550µl HBSS (Ca-/Mg-) per retina. 250µl of sample were moved in duplicate to a V bottom 96 well plate (Nunc, ThermoFisher Scientific, UK) for staining. Plate was centrifuged at 400g for 3 mins, supernatant was poured off and cells were resuspended in 100µl CD16/32 block (1:500 in FACS buffer; BD Biosciences) for 10 mins. Cells were stained for 20 mins in the dark with 100µl of staining antibody or isotype control antibody mastermixes in FACS buffer (Table 2.3). Plate was centrifuged at 400g for 3 mins, supernatant was poured off and cells were washed by resuspending in 250µl FACS buffer. Plate was centrifuged at 400g for 3 mins, supernatant was poured off and cells were resuspended in 300µl FACS buffer containing 7-AAD viability solution (1:100, eBioscience). Samples were transferred into FACS tubes and acquired using a FACSAria II Flow Cytometer (BD Biosciences, UK).

Antibody Target (Fluorochrome)	Antibody type	Antibody code (Distributor)	Isotype code (Distributor)	Dilution in FACS buffer
CD11b (BV421)	Rat anti-mouse IgG2b mAb	562605 BD Biosciences	562603 BD Biosciences	1:40
CD11c (PE)	Armenian hamster anti-mouse mAb	117307 BioLegend	400907 BioLegend	1:50
CD45 (PE-Cy7)	Rat anti-mouse mAb	561868 BD Biosciences	552849 BD Biosciences	1:50
MHCII (APC)	Rat anti-mouse IgG2b mAb	17-5321-81 eBioscience	17-4031-81 eBioscience	1:250

Table 2.3 – Antibody information for murine flow cytometry staining/isotype mastermixes.

2.3.2 Compensation

To set compensation controls for eGFP expression, C57BL/6 and MacGreen retinal samples were prepared as above without antibody or 7-AAD staining. To set compensation controls for 7-AAD staining, C57BL/6 retinal samples with and without 7-AAD staining were prepared as above without antibody staining. To set compensation controls for the staining antibodies, individual antibodies were bound to compensation beads (UltraComp eBeads, eBioscience) during a 10-minute incubation as per the manufacturer's protocol. Automatic compensation was performed by FACSDiva software (BD Biosciences, UK).

2.3.3 Sample acquisition and analysis

Samples were analysed with a 3-laser FACSAria II flow cytometer (BD Biosciences) with a neutral density 1.5 filter and the following laser and bandpass filter configuration:
405nm laser - 450/40 (BV421)
488nm laser - 488/10 (SSC), 530/30 (FITC), 576/26 (PE), 695/40 (7-AAD), 780/60 (PE-Cy7)
633nm laser - 660/20 (APC)
Lasers were fired sequentially to greatly reduce interlaser compensation. Samples were run under constant low flow rate until tubes were nearly empty (≈300,000 events per tube). Debris and doublet cells were excluded from analysis via FSC/SSC analysis and dead/dying cells were excluded based on uptake of 7-AAD. The median fluorescence intensity (MFI) and percentage of positive cells for each marker were analysed for the eGFP+ macrophage/microglia cell population in FlowJo v10 (OR, USA).

2.4 Quantitative Real Time PCR analysis of mouse retinas

2.4.1 RNA isolation

Retinas were homogenised in 800µl Trizol (ThermoFisher Scientific, UK) using a handheld electric homogeniser with disposable pestles (Sigma-Aldrich, UK). Samples were incubated in Trizol for 1hr and then 80µl of 1-bromo-3-chloropropane (Sigma-Aldrich, UK) was added. Tubes were shaken vigorously for 15s and incubated for 3mins. Tubes were centrifuged at 12,000g for 15mins at 4°C. 300µl of the upper aqueous phase was moved into a new tube to which 300µl of 70% molecular biology grade ethanol (Sigma-Aldrich, UK) in molecular biology grade water (ThermoFisher Scientific, UK) was added and vortexed to mix well. RNA was purified from this solution using a PureLink RNA Mini Kit (ThermoFisher Scientific, UK) as per the manufacturer's instructions. Briefly, samples were added to a spin cartridge and spun at 12,000g for 15s to capture RNA on the column. The columns were washed sequentially with wash buffers I, II and II and spun at 12,000g for 15s, the cartridge was dried by centrifugation at 16,100g for 3mins and then RNA was eluted by incubation of 30µl RNase free water on the column for 2mins followed by centrifugation at 16,100g for 2mins. RNA concentration and quality was assessed by a nanodrop spectrophotometer. A 260/280 ratio of 1.8-2.1 indicates RNA is not contaminated with proteins and/or phenol, while a 260/230 ratio below 1.6 indicates high contamination with guanethidium, phenol and/or carbohydrates. Samples with high contamination were repurified by adding 170µl RNAse free water, 200µl 70% ethanol and 200µl Lysis Buffer containing 1% 2-mercaptoethanol (Sigma-Aldrich, UK) to the RNA sample, transferring this mixture to a spin column and purifying with the PureLink RNA Mini kit as described above. RNA samples were stored at -80°C until use.

2.4.2 RNA to cDNA conversion

250ng RNA was transcribed into cDNA using the TaqMan Reverse Transcription Reagents Kit (ThermoFisher Scientific, UK) as per the manufacturer's protocol for a 20µl reaction. Briefly, 250ng RNA in 7.7µl of molecular biology grade water was added to 12.3µl of a mastermix of reaction buffer, 25mM $MgCl_2$, RNAse inhibitor, random hexamers, DNTPs and Multiscribe Reverse Transcriptase. The 20µl solutions were placed in a PTC240 tetrad 2 peltier thermal cycler (MJ research, Canada) at 25°C for 10mins, 48°C for 30mins, 95°C for 5mins and then kept at 4°C until cDNA was diluted 1:5 in RNAse free water and stored at -20°C.

2.4.3 Quantitative real-time PCR

Lyophilised primers purified by desalting were purchased from Sigma-Aldrich, UK and reconstituted to a 100µM stock solution in RNase free water and stored at -20°C until use. Primers were designed according to the specification in Table 2.4.

	Minimum	Optimum	Maximum
Product length (bp)	70	-	300
Melting temperatures (°C)	57	60	63
Primer size (bp)	15	20	25
Max self complementarity	0	0	7
Max 3' self complementarity	0	0	3
Primer GC content%	35	50	65

Table 2.4 – Criteria used during primer design using Primer-BLAST (NCBI).
One primer of each pair recognised an exon-exon boundary to prevent the amplification of genomic DNA.

15µl of a mastermix of 0.4µM forward and reverse primers (Sigma-Aldrich, UK) (Table 2.5) and 1.33X SYBR green (Bio-Rad, UK) in RNAse free water was added to wells of a 96 well non-skirted low profile plates (Starlab, UK). 5µl of 1:5 diluted cDNA was added to each well in duplicate. As a negative control, RNAse free water without cDNA was added to mastermix. Plates were covered with optical caps (Starlab, UK) and placed in a C1000 Thermal Cycler with a CFX96 detection module (Bio-Rad, UK). qPCR was carried out using the following protocol: 95°C 10mins; 95°C 15s, 60°C 1min x 50; 72°C 10mins; 95°C 10mins; 4°C forever. MJ Opticon Monitor Software (Bio-Rad, UK) was used to plot fluorescence intensity over time and C(t) values were calculated for each marker at the autocalculated threshold. Melting curves in 0.2°C intervals between 55°C to 90°C were compiled to ensure that the template was amplified specifically.

C(t) values for glyceraldehyde-3-phosphate dehydrogenase (GADPH) levels were measured for each cDNA sample as a reference C(t) value. C(t) values for other genes were obtained and relative gene of interest (GOI) expression levels were calculated by normalising the GOI C(t) values to the GADPH C(t) values using the $2^{-\Delta\Delta C(t)}$ method such that relative expression = $2^{(C(t)\ GADPH\ -\ C(t)\ GOI)}$

Gene name	NCBI Gene ID	Common protein names	Strand	Primer Sequence (5'-3')
Arg1	11846	Arginase 1	Forward Reverse	ACAAGACAGGGCTCCTTTCAG CTTGGGAGGAGAAGGCGTTT
C3	12266	Complement component 3	Forward Reverse	CAACAACCAACACGGCATCT AACTGGGCAGCACGTATTCC
Casp1	12362	Caspase 1	Forward Reverse	AGGCACGGGACCTATGTGAT AGCTGATGGAGCTGATTGAAG
Casp8	12370	Caspase 8	Forward Reverse	AGCACAGAGAGAAGAATGAGCC TTGGCGAGTCACACAGTTCC
Ccl2	20296	CCL2/MCP-1	Forward Reverse	AGCATCCACGTGTTGGCTC CCAGCCTACTCATTGGGATCAT
Cyba	13057	p22phox, Cytochrome B α-subunit	Forward Reverse	TGGCCTGATTCTCATCACTGG TAGAGTAGGCGCCGAAATACC
Cybb	13058	NADPH oxidase 2 (NOX2), Cytochrome B β-subunit	Forward Reverse	GCTGGAAACCCTCCTATGACTT GCCAAAACCGAACCAACCTC
Dicer1	192119	DICER1	Forward Reverse	ACATGACGAGGAGGAGACCA ACTCTGGAATTGCTTTGGGGT
Fcgr1	14129	FcγRI, CD64	Forward Reverse	TACTTTGGGTTCCAGTCGGT CCTGTATTCGCCACTGTCCT
Gapdh	14433	GAPDH	Forward Reverse	TGAACGGGAAGCTCACTGG TCCACCACCCTGTTGCTGTA
Gfap	14580	Glial fibrillary acidic protein	Forward Reverse	AGTGGTATCGGTCTAAGTTTGC GACTCCAGATCGCAGGTCAA
Hmox1	15368	Heme oxygenase 1 (HO-1)	Forward Reverse	GCTAGCCTGGTGCAAGATAC TGGGGGCCAGTATTGCATTT
Il1b	16176	Interleukin 1β	Forward Reverse	CAAAAGATGAAGGGCTGCTTCC ATGTGCTGCTGCGAGATTTG
Il18	16173	Interleukin 18	Forward Reverse	TCAAAGTGCCAGTGAACCC GTCACAGCCAGTCCTCTTACT
Nfe2l2	18024	NRF2, Nuclear factor erythroid derived 2 like 2	Forward Reverse	GGTTGCCCACATTCCCAAAC GCAAGCGACTCATGGTCATC
Nlrp3	216799	NLRP3	Forward Reverse	CCCGAGAAAGGCTGTATCCC CGTGTCATTCCACTCTGGCT
Nos1	18125	Neuronal nitric oxide synthase (nNOS)	Forward Reverse	AGAGGAAGAGCTACAAGGTCC GGCCGAAGACTGAGAACCTC
Nos2	18126	Inducible nitric oxide synthase (iNOS)	Forward Reverse	ATGCCACCAACAATGGCAAC TAGGTCGATGCACAACTGGG
Nos3	18127	Endothelial nitric oxide synthase (eNOS)	Forward Reverse	CCGGAGAATGGAGAGAGCTT CAGAAGTGGGGGTATGCTCG
Ptgs2	19225	Cyclooxygenase 2 (COX2), PTGS2	Forward Reverse	GGGTGTCCCTTCACTTCTTTCA TGGGAGGCACTTGCATTGA
Sod2	20656	Superoxide dismutase 2 (MnSOD)	Forward Reverse	GAACAATCTCAACGCCACCG CCAGCAACTCTCCTTTGGGTT
Tnf	21926	TNFα	Forward Reverse	CGAGGACAGCAAGGGACTAG GCCACAAGCAGGAATGAGAA
Vegfa	22339	Vascular Endothelial Growth Factor A	Forward Reverse	GATCCGCAGACGTGTAAATGTT TCACCGCCTCGGCTTGTCACAT

Table 2.5 – List of primer sequences used for qPCR.

2.5 Binding assays and multiplex ELISA (Mesoscale)

2.5.1 Protein extraction from retina

Lysis buffer was prepared as 150mM NaCl (Sigma-Aldrich, UK), 25mM TRIS (Sigma-Aldrich, UK), 1% Triton X-100 (ThermoFisher Scientific, UK) in dH_2O and filter sterilised. One tablet each of protease inhibitors (Complete protease inhibitors; Roche, UK) and phosphatase inhibitors (PhosStop; Sigma-Aldrich, UK) were dissolved in 10ml lysis buffer, which was then cooled to 4°C. All subsequent steps were performed at 0-4°C. Retinas were homogenised in 70µl of lysis buffer using a handheld electric homogeniser with disposable pestles (Sigma-Aldrich, UK). Retinal homogenates were centrifuged at 20,000g for 30 mins to pellet insoluble material. The protein-containing supernatants were taken and stored at -80°C until use.

2.5.2 Total protein level quantification

Levels of protein were assayed using a bicinchoninic acid (BCA) protein kit (Pierce, USA) as per the manufacturer's instructions. Briefly, retinal homogenate was diluted 1:5 in lysis buffer and 5µl of sample was added to a 96 well plate in triplicate. 5µl of different BSA solutions at known concentrations was pipetted in duplicate on each plate to generate a standard curve. 200µl of working reagent (Reagent B diluted 1:50 in reagent A) was added to each well and the plate was incubated at 37°C for 30 mins. The absorbance of each well was measured at 450nm and values were interpolated using the standard curve to determine the total protein levels of each sample.

2.5.3 Mesoscale (Multiplex ELISA assays)

The mouse 7- and 10-plex proinflammatory panel I plates (Mesoscale Discovery, MD, USA) were used to assay the levels of IFNγ, IL-1β, IL-2, IL-4, IL-5, IL-6, mKC (IL-8 homolog), IL-10, IL12p70 and TNFα in retinal homogenates or serum samples. Assay was performed as per the manufacturer's protocol. Briefly, samples were diluted 1:1 with provided diluent and 50µl of sample or calibrators for standard curve were incubated for two hours on an orbital shaker. Plates was washed three times with PBS containing 0.05% tween, pH7.2, and then incubated for two hours with a cocktail of secondary detection antibodies. The plates were washed three times and 150µl of read buffer was added to each well. Plates were read and analysed using a Sector PR400 reader with Discovery Workbench v4 software (Mesoscale Discovery, MD, USA). Concentration values for each cytokine per well were calculated based on the standard curve and values for retinal homogenates were normalised to total protein level as measured by BCA.

2.5.4 Binding assay for OVA-specific IgG levels

All reagents for assaying OVA-specific IgG levels were purchased from Sigma-Aldrich, UK, unless otherwise stated. 96 well Nunc Maxisorp plates (ThermoFisher Scientific, UK) were coated overnight at 4°C with 100µl of 10µg/ml OVA in carbonate buffer (3g Na_2CO_3, 6g $NaHCO_3$ in 1L water, pH9.6). Wells were washed 5 times with 200µl wash buffer: 1xPBS+0.05% Tween-20, pH7.2. Wells were blocked for 30mins with blocking buffer: 100µl 1% BSA (ThermoFisher Scientific, UK) in 1X PBS. Serum samples were added to blocking buffer and serial diluted across the plate (10^3-10^{10}). Plates were incubated for 1hr on an orbital shaker at 600rpm. Wells were washed 5 times with wash buffer followed by incubation with 100µl of biotinylated horse anti-mouse IgG (1:500 dilution in blocking buffer; Vector Labs, USA) for 1hr on an orbital shaker at 600rpm. Wells were washed 5 times with 200µl wash buffer followed by incubation with 100µl of streptavidin poly-HRP (1:10,000 dilution in blocking buffer; Sanquin, Netherlands) for 30 mins. Plates were washed 5 times with 200µl wash buffer. 100µl of Ultra-TMB detection solution (ThermoFisher Scientific, UK) was added to each well and colour change reaction was stopped using 100µl 1M H_2SO_4. Absorbance of each well at 450nm was measured with a FLUOstar OPTIMA plate reader (BMG Labtech, UK).

2.6 Graphs and Statistics for mouse experiments

GraphPad Prism (v7; La Jolla, CA) was used to perform statistical analyses and create graphs. Data was tested for normality and similar variances between groups using Shapiro-Wilk and Bartlett's test respectively. Data that passed these tests were analysed by parametric T-test (for tests between 2 groups), 1-way ANOVA (for 3 or more groups with one independent variable) or 2-way ANOVA (for two independent variables) followed by Holm-Šídák multiple comparison testing. All data that failed Shapiro-Wilk and/or Bartlett's test were log or square root transformed as appropriate and analysed using the parametric tests described above. Repeated measured testing was performed when the same mice were tracked over time or when the control and experiment eye of the same mouse were analysed. All graphs were produced in GraphPad Prism v7.0 and display mean±SEM for each experimental group.

2.7 Human sample collection and analysis

2.7.1 Study design

39 patients undergoing cataract surgery with or without concomitant AMD were recruited to the study titled 'A study of the Molecular and Cellular Pathophysiology of Retinal Disease' between July 2015 to November 2016. This study was approved by NHS Research Ethics Committee South Central – Hampshire B (ID: 09/H0504/67) and sponsored by Southampton University Hospitals NHS Trust (ID: RHM OPH0142). Aqueous humour and blood samples were collected from patients to compare the levels of inflammation in the eye and periphery of patients with or without concomitant AMD. All patients were given a patient information leaflet at least 24 hours before their appointment and recruitment. The study and its procedures were explained to each patient by authorised research nurses and written consent was obtained for each patient both for this specific study and for their use in further studies if appropriate. A proforma for the collection of anonymised data was completed for each patient to take into account possible confounding factors, notably age, gender, past ophthalmic history, past medical history, drug history, smoking status and blood pressure. A breakdown of patient numbers for each technique used is provided in Table 2.6.

AMD status	Serum cytokine levels	Aqueous humour cytokine levels	Stimulated cell supernatant cytokines	Stimulated cell FACS analysis
None	**16**	**15**	**16**	**8**
Any	**17**	**19**	**15**	**8**
Dry	8	8	8	5
Wet	8	11	6	3
Dry & Wet	1	0	1	0

Table 2.6 – Overview of patient numbers and disease status for each study technique.

2.7.2 Aqueous collection

As part of standard cataract surgery, a main incision and paracentesis incision are made into the anterior chamber at the limbus and aqueous humour is removed and simultaneously replaced with a viscoelastic substance. Cataract surgeries were performed by qualified ophthalmic surgeons based in the Eye Unit, Southampton General Hospital, Southampton University Hospitals NHS Trust. In this study, some undiluted aqueous humour was collected via a cannula in the paracentesis incision prior to injection of viscoelastic. The amount of aqueous humour taken from each patient was highly variable (average: 60µl, range: 5µl-150µl). Aqueous humour was collected and immediately stored on ice in theatre. Aqueous humour was stored at -80°C within 2 hours of collection for long term storage.

2.7.3 Blood collection

Following patient consent, authorised research nurses collected 10mls of blood in each of the following BD Vacutainer tubes: Plasma tubes containing sodium heparin (green top), serum tubes (red top) and tubes containing K_2EDTA (lavender top). Serum tubes were left to clot at RT for 1-2hrs followed by centrifugation at 490g for 15mins at 4°C and aspiration of serum, which was stored at -80°C until use. Tubes containing K_2EDTA were frozen at -20°C within 1hr of collection for DNA genotyping and are stored for possible future analysis. 6mls of blood stored in the sodium heparin tubes was used for plasma and PBMC isolation, which are stored for possible future analysis.

2.7.4 Whole blood stimulation with immune system activators

400µl of blood collected in tubes containing sodium heparin were incubated alone or with either 10µg/ml LPS (from *E. coli* O127:B8 purified by ion-exchange chromatography, Sigma, UK), 5µg/ml resiquimod (R848, Sigma, UK) or 10µg/ml mouse anti-human CD3 mAb (Functional Grade Purified from clone OKT3, eBioscience, UK) for FACS and mesoscale analysis. Samples were incubated at 37°C with 5% CO_2 for 19 hours. Samples for FACS analysis were treated with 2µl of protein transport inhibitor (GolgiStop containing monensin, BD Biosciences, UK) 4 hours into the incubation step to trap cytokines within the cell. After the 19hr incubation, samples for mesoscale analysis were centrifuged at 490g for 15 mins at 4°C and supernatant was stored at -80°C until analysis.

2.7.5 FACS analysis of stimulated blood cells

After the 19hr incubation, whole blood samples for FACS analysis were incubated for 25mins with extracellular staining antibodies against CD3, CD4, CD14 (Table 2.7). Samples were diluted 1:10 with 1X FACS lysing buffer (BD Biosciences, UK) and left at RT for 15 mins to lyse red blood cells. Samples were centrifuged (all centrifugation steps in this protocol are 400g for 5 mins with maximum acceleration and braking), inverted to remove supernatant and washed with 4ml FACS buffer (1% FCS in 1X PBS). Samples were centrifuged, inverted to remove supernatant and vortexed gently to resuspend in residual liquid. Cells were permeabilised for intracellular cytokine staining by addition of 200µl 1X Perm2 permeabilising solution (BD Biosciences). After a 10 minute incubation at RT, samples were washed with 4ml FACS buffer, centrifuged, and vortexed gently to resuspend in residual liquid. Samples were incubated for 25mins with intracellular staining antibodies against IFNγ, IL-6, IL-8, IL-17 and TNFα (Table 2.7). Samples were washed with 4ml FACS buffer, centrifuged and resuspended in 400µl FACS buffer.

Samples were analysed with a 3-laser FACSAria II flow cytometer (BD Biosciences) with a neutral density 1.5 filter and the following laser and bandpass filter configuration:
405nm laser - 450/40 (V450), 525/50 (V500)
488nm laser - 488/10 (SSC), 530/30 (FITC), 576/26 (PE), 695/40 (PerCP), 780/60 (PE-Cy7)
633nm laser - 660/20 (APC), 780/60 (APC-Cy7)

Automatic compensation was performed using compensation beads stained with individual antibodies as per the manufacturer's protocol (UltraComp Beads, eBioscience, UK). Samples were analysed with a 3-laser FACSAria II flow cytometer (BD Biosciences) with a neutral density 1.5 filter and the following laser and bandpass filter configuration:
405nm laser - 450/40 (V450), 530/30 (V500)
488nm laser - 488/10 (SSC), 530/30 (FITC), 576/26 (PE), 695/40 (PerCP), 780/60 (PE-Cy7)
633nm laser - 660/20 (APC), 780/60 (APC-Cy7)

Lasers were fired sequentially to greatly reduce interlaser compensation. Samples were run under constant low flow rate until tubes were nearly empty (≈350,000 cells per tube). Data was analysed using FlowJo v10 (OR, USA). Debris and doublet cells were excluded from analysis via FSC/SSC and monocytes and lymphocytes were gated based on different FSC/SSC characteristics (see Appendix F). For each cytokine, the size of the positive cell population was multiplied by its median fluorescence intensity (MFI) to achieve an overall expression index.

Antibody Target (Fluorochrome)	Antibody type (Clone)	Antibody code (Distributor)	Staining mastermix	Amount per test
CD3e (V500)	Mouse anti-human (UCHT1)	561416 (BD Biosciences)	Extracellular	5µl
CD4 (APC-Cy7)	Mouse anti-human (RPA-T4)	557871 (BD Biosciences)	Extracellular	5µl
CD14 (V450)	Mouse anti-human (MφP9)	560349 (BD Biosciences)	Extracellular	5µl
IFNγ (PE-Cy7)	Mouse anti-human (B27)	557643 (BD Biosciences)	Intracellular	5µl
IL-6 (APC)	Rat anti-human (MQ2-13A5)	501112 (BioLegend)	Intracellular	5µl
IL-8 (PerCP)	Mouse anti-human (BH0814)	514606 (BioLegend)	Intracellular	5µl
IL-17 (FITC)	Mouse anti-human (eBio64DEC17)	11-7179-42 (eBioscience)	Intracellular	5µl
TNFα (PE)	Mouse anti human (MAb11)	559321 (BD Biosciences)	Intracellular	20µl

Table 2.7 – Antibody information for human flow cytometry staining/isotype mastermixes.

2.7.6 Mesoscale analysis of human samples

Human V-PLEX proinflammatory panel I plates (Mesoscale Discovery, USA) were used to assay the levels of IFNγ, IL-1β, IL-2, IL-4, IL-6, IL-8, IL-10, IL12p70, IL-13, TNFα in human samples as per the manufacturer's protocol. Samples were diluted in provided diluent as follows: Serum samples (1:1); aqueous samples (1:4); control and CD3 stimulated cell supernatants (1:6); R848-stimulated cell supernatants (1:200) and LPS-stimulated cell supernatants (1:400). All other steps were performed as previously described for the mouse mesoscale panel (Section 2.5.3).

Chapter 3:

The inflammatory effect of systemic bacterial infection on the mouse retina

3.1 Introduction

For many years it was believed that the CNS was segregated from the immune system. However, this view is now outdated as several pathways of immune-to-brain communication between the systemic immune system and the CNS have been described (McCusker & Kelley, 2013). For example, systemic infections activate the systemic immune system leading to body changes controlled by the brain termed 'sickness behaviours', which include fever and lack of appetite. These sickness behaviours are shared across species, showing that mouse studies could be used to dissect the underpinning mechanisms. Sickness behaviours are driven by local cytokine production in the brain and coincide with activation of microglia, the immune cells of the CNS (Dantzer et al., 2008).

Far less is known about the impact of systemic infections on the retina. Systemic infections can lead to severe retinal inflammation and blindness in cases where the infectious agent enters the retina and replicates locally (e.g Ebola, ocular toxoplasmosis). However, there is also some evidence that underlying systemic diseases (e.g Behçet's Disease and sarcoidosis) and systemic infections without retinal infiltration (tuberculosis, syphilis, herpes viruses and systemic toxoplasmosis) can cause retinal inflammation (Durrani et al., 2004). Furthermore, bacterial (*Chlamydia pneumoniae*) and viral (*Cytomegalovirus*) infections have been associated with an increased risk/progression of the retinal neurodegenerative disease age-related macular degeneration (see introduction section 1.5.4). Before we can understand how these infections can interplay with neurodegeneration, it is critical to characterise their effect on the healthy retina.

Mouse studies can be used to gain knowledge about how systemic infections affect the retina, as inbred strains have far less variation in comparison to humans, who have a huge range of confounding factors. Furthermore, infection dosage and tissue collection can be kept constant to further reduce variation, allowing fundamental changes to be observed. Only two studies have investigated the effect of live systemic infections on the mouse retina. The studies used viral (murine *Cytomegalovirus*) and fungal (*Candida albicans*) infections to confirm microglial activation in the retina following systemic infection (Maneu et al., 2014; Zinkernagel et al., 2013). However, these studies don't characterise other retinal cell types which are critical for normal function of the retina, nor do these examine locally activated inflammatory pathways. In addition, the effect of a live systemic bacterial infection has not been characterised in the retina, which is what this chapter aims to address.

Research from our lab has shown that systemic infection with a live attenuated strain of Salmonella leads to activation of cerebral blood vessels and microglia of the brain, along with elevated levels of IL-1β and IL-12 (Püntener et al., 2012). This chapter will investigate whether the

inflammatory findings in the brain after Salmonella infection are also present in the retina. These effects are characterised in detail at different time points in terms of the production of inflammatory proteins and the response of a range of cell types in the retina. Finally, the impact of aging on retinal inflammation following Salmonella infection is considered.

3.2 Methods

3.2.1 Effect of Salmonella at 1 and 4 weeks post injection

C57BL/6 mice (2-3 months old) were injected i.p. with 10^6 cfu Salmonella or saline as a control (see section 2.1.2). Daily body weight was recorded and mice showing >20% body weight loss were culled according to home office regulations (PPL 30/3057). In this chapter, mice were infected by Alexander Collcutt. At 1 and 4 weeks post injection, mice were transcardially perfused (see section 2.1.6) and spleens were weighed to assess levels of peripheral immune activation. Blood was collected before transcardial perfusion and serum was isolated (see section 2.1.6) and frozen at -80°C until cytokine levels were assessed by multiplex ELISA (see section 2.5.3). For retinal cytokine analysis, a whole retina was frozen at -80°C and then homogenised in TRIS buffer before cytokine levels were assessed by multiplex ELISA (see sections 2.1.6.3, 2.5.1 and 2.5.3). Cytokine levels were normalised to total protein levels in each homogenate using a BCA assay (see section 2.5.2). For retinal qPCR analysis, both retinas from each mouse were pooled and frozen at -80°C (see sections 2.1.6.3). RNA was isolated, converted to cDNA and analysed by qPCR (see sections 2.4). For immunohistochemistry, a whole eye was snap-frozen in optimal cutting temperature medium (see section 2.1.6.1), cryosectioned and stored at -20°C until DAB immunohistochemistry and analysis (see section 2.2).

For flow cytometry, MacGreen mice with eGFP+ myeloid cells (see section 2.1.1 for detailed description) were injected i.p. with 10^6 cfu Salmonella or were uninjected controls (naïve). Retinas were harvested following transcardial perfusion at 1 and 4 weeks post injection (see section 2.1.6.2) and injections were staggered so that all mouse tissue was harvested on the same day. Flow cytometric analysis was performed as described in section 2.3 and Dr. Elena Pipi assisted in the processing of samples.

3.2.2 Effect of Salmonella at 8 and 24 weeks post injection in C57BL/6 mice

C57BL/6 mice (2-3 months old) were injected i.p. with 10^6 cfu Salmonella or saline. Body weight was periodically assessed over 24 weeks. Tissue was harvested at 8 and 24 weeks post injection.

Serum and retinal cytokine measurements and immunohistochemistry were performed as detailed in section 3.2.1.

3.2.3 Effect of Salmonella at 4 weeks post injection in young and middle-aged mice

C57BL/6 mice at 3 months old (young) and 12 months old (middle-aged) were injected i.p. with 10^6 cfu Salmonella or saline. Body weight was periodically assessed over 4 weeks, at which point tissue was harvested. Serum and retinal cytokine measurements were performed as detailed in section 3.2.1.

3.2.4 Statistics

For each figure, the statistical test used is stated in the figure legend. Data that failed homogeneity of variance tests or normalisation tests were transformed before analysis (see section 2.6). Due to the large number of statistics performed, the key results of each test are provided in the figures and the full results of each statistical test are provided in Appendix A.

3.3 Results

3.3.1 Physiological changes following Salmonella infection

Physiological responses to infection, including weight loss and splenomegaly, were characterised to provide insight into the chronicity of the Salmonella disease course. At 24 hours post injection, strong weight loss (≈13%, $p<0.0001$) is observed in infected mice (Figure 3.1a). The infected mice then proceed to gain weight over the next four weeks ($p<0.0001$), as is observed for the control mice. However, the Salmonella infected mice do not regain the lost weight when compared to saline controls ($p<0.0001$).

In comparison to saline controls, the Salmonella infected mice exhibit biphasic weight loss, with 13-14% weight loss observed between 1 and 4 days post injection compared to pre-injection weight ($p<0.0001$ for each comparison) (Figure 3.1b). Weight loss is strongest at day 2 and there is significant weight gain from day 2 to days 6-9 (Day 2 vs 6, $p=0.0408$; Day 2 vs 7, $p=0.0004$; Day 2 vs 8, $p<0.0001$; Day 2 vs 9, $p=0.0213$). This is followed by a period of weight loss (Day 8 vs Day 16, $p=0.0495$). As the body weight loss is calculated with respect to starting weight, the starting weights of each group were equal to ensure that this factor didn't confound the analysis (Figure 3.1c).

Salmonella induces splenomegaly at 1 and 4 weeks post infection, with an increase (fold change ≈6, $p<0.0001$) in spleen weight observed at both timepoints. Taken together, absence of body weight loss and spleen weight gain can be used to exclude mice injected with Salmonella that show no signs of infection (≈1 in 15 mice). The reasons for this are unclear, but may be due to an incorrect injection site.

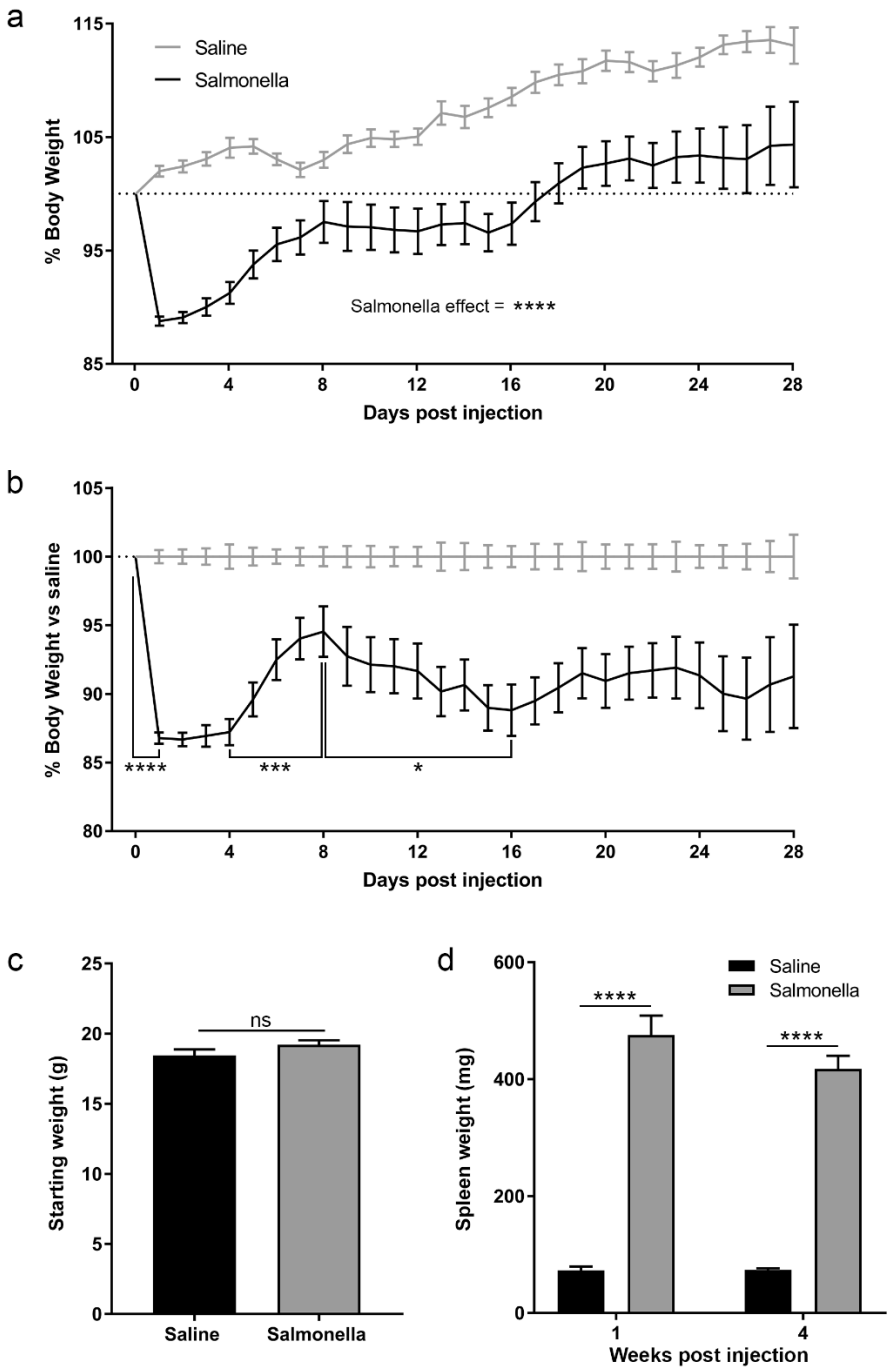

Figure 3.1 – Body weight and spleen weight changes during Salmonella infection.

*Graphs shows (a) daily body weight as a percentage of starting weight for each mouse, (b) Salmonella-induced weight loss normalised to saline controls over 4 weeks post saline or Salmonella injection (n=9-10 mice per group). (c) Pre-injection body weight of saline and Salmonella injected groups (n=9-10 mice per group). (d) Spleen weight at 1 and 4 weeks post saline or Salmonella injection (n=9-12 mice per group). Graphs are as presented as mean±SEM. Weight changes over time were analysed using repeated measures two-way ANOVA with Holm-Sidak post-hoc testing. Starting weight changes were analysed by unpaired two-tailed T-test. Spleen weight changes were analysed by two-way ANOVA with Holm-Sidak post-hoc testing. Stars denote significance as follows: *p<0.05, ***p<0.001, ****p<0.0001, ns = not significant.*

3.3.2 Peripheral cytokine production following Salmonella infection

The timecourse of the peripheral immune response was investigated at a molecular level by assaying circulating cytokine levels. At 1 week post injection, Salmonella induces increased levels of all 10 cytokines assayed compared to saline controls ($p<0.0001$ in each case) (Figure 3.2). These changes are described in detail as follows: IFNγ (Saline: 1.99pg/ml, Salmonella: 7990pg/ml, fold change ≈4000); IL-1β (Saline: 2.04pg/ml, Salmonella: 46.5pg/ml, fold change ≈20); IL-2 (Saline: 2.74pg/ml, Salmonella: 54.1pg/ml, fold change ≈20); IL-4 (Saline: 1.20pg/ml, Salmonella: 33.6pg/ml, fold change ≈30); IL-5 (Saline: 4.98pg/ml, Salmonella: 27.4pg/ml, fold change ≈6); IL-6 (Saline: 16.7pg/ml, Salmonella: 17,500pg/ml, fold change ≈1000); IL-10 (Saline: 28.3pg/ml, Salmonella: 497pg/ml, fold change ≈20), IL-12 (Saline: 49.5pg/ml, Salmonella: 1110pg/ml, fold change ≈20); mKC (Saline: 85.0pg/ml, Salmonella: 405pg/ml, fold change ≈5); TNFα (Saline: 13.0pg/ml, Salmonella: 1160pg/ml, fold change ≈90).

At 4 weeks post injection, 6 of 10 cytokines assayed remain elevated compared to saline controls: IFNγ (82.3pg/ml, fold change ≈80, $p<0.0001$); IL-1β (3.43pg/ml, fold change ≈2, $p=0.0306$); IL-5 (9.04pg/ml, fold change ≈2, $p=0.0007$); IL-6 (131pg/ml, fold change ≈9, $p<0.0001$); IL-10 (107pg/ml, fold change ≈4, $p<0.0001$); TNFα (120pg/ml; fold change ≈10, $p<0.0001$). Levels of IL-2, IL4, IL-12 and mKC return to saline control levels at 4 weeks post injection ($p<0.0001$ for each).

Although some cytokines are elevated at both 1 and 4 weeks post infection compared to saline controls, in these cases there is a large decrease in cytokine levels from 1 week to 4 weeks post infection ($p<0.0001$ in each case): IFNγ (fold change ≈50); IL-1β (fold change ≈ 10); IL-5 (fold increase ≈3); IL-6 (fold change ≈12); IL-10 (fold change ≈5); TNFα (fold change ≈10).

Overall, serum cytokine levels are strongly elevated at 1 week post Salmonella infection, and inflammation is still detected at 4 weeks post infection, although at much lower levels. It is interesting to note that IFNγ is the most upregulated cytokine at both timepoints by a large margin.

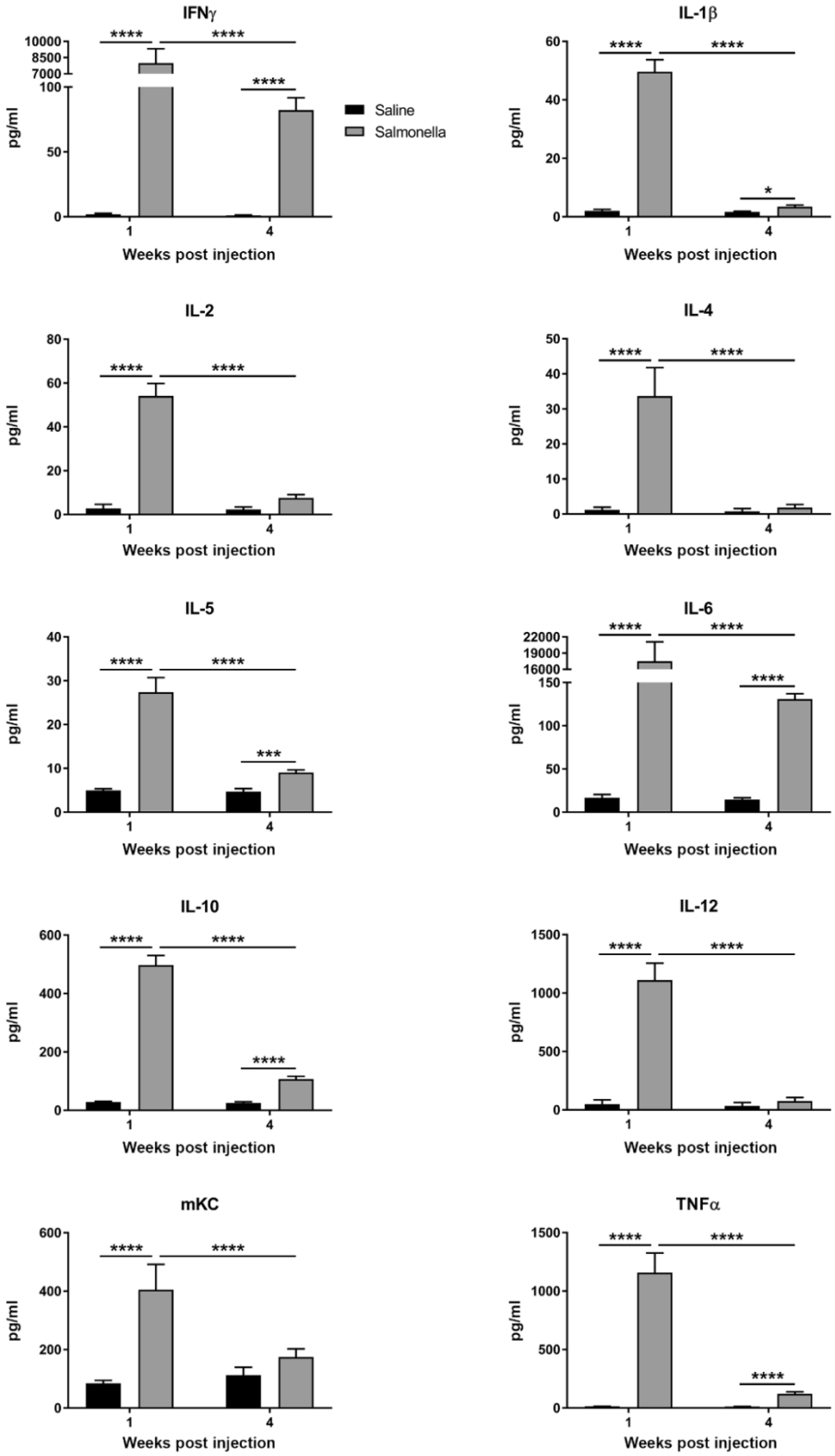

Figure 3.2 – Serum cytokine levels at 1 and 4 weeks post saline or Salmonella injection.

*Serum cytokine levels of IFNγ, IL-1ɓ, IL-2, IL-4, IL-5, IL-6, IL-10, IL-12, mKC and TNFα were quantified in pg/ml by multiplex ELISA (Mesoscale Discovery). Graphs are presented as mean±SEM (n=5-6 mice per group). Data was analysed using two-way ANOVA with Holm-Sidak post-hoc testing. Stars denote significance as follows: *p<0.05, ***p<0.001, ****p<0.0001.*

3.3.3 Retinal cytokine levels following Salmonella infection

Retinal cytokine levels during Salmonella infection were assayed to identify whether there is a local immune signature following systemic infection. At 1 week post injection, Salmonella induces increased retinal levels of 5 of the 10 cytokines assayed compared to saline controls (Figure 3.3): IFNγ (Saline: 0.056pg/mg, Salmonella: 1.79pg/mg, fold change ≈30, $p<0.0001$); IL-1β (Saline: 0.036pg/mg, Salmonella: 0.139pg/mg, fold change ≈3.9, $p=0.0061$); IL-6 (Saline: 1.86pg/mg, Salmonella: 6.99pg/mg, fold change ≈3.8, $p<0.0001$); mKC (Saline: 1.53pg/mg, Salmonella: 4.75pg/mg, fold change ≈3.1, $p<0.0001$) and TNFα (Saline: 0.59pg/mg, Salmonella: 1.23pg/mg, fold change ≈2.1, $p=0.0033$).

At 4 weeks post infection, 2 of 5 cytokines assayed remain upregulated in comparison to saline controls: IFNγ (0.199pg/mg, fold change ≈7, $p<0.0001$) and mKC (1.72pg/mg, fold change ≈2.4, $p=0.0022$), whereas IL-1β ($p=0.0140$), IL-6 ($p<0.0001$) and TNFα ($p=0.0457$) return to saline control levels. However, for the cytokines that are upregulated by Salmonella at both 1 and 4 weeks, there is a substantial decrease in levels of cytokines from 1 to 4 weeks post infection: IFNγ (fold change: ≈9, $p<0.0001$) and mKC (fold change: ≈2.8, $p=0.0002$).

IL-2 is also increased by Salmonella overall when the 1 and 4 week timepoints are considered together ($p=0.0302$), but at individual timepoints does not reach significance with post-hoc testing.

Overall, these data show that several retinal cytokines are elevated following Salmonella infection at 1 week, and upregulation of some of these cytokines is still apparent at 4 weeks post infection, albeit at lower levels.

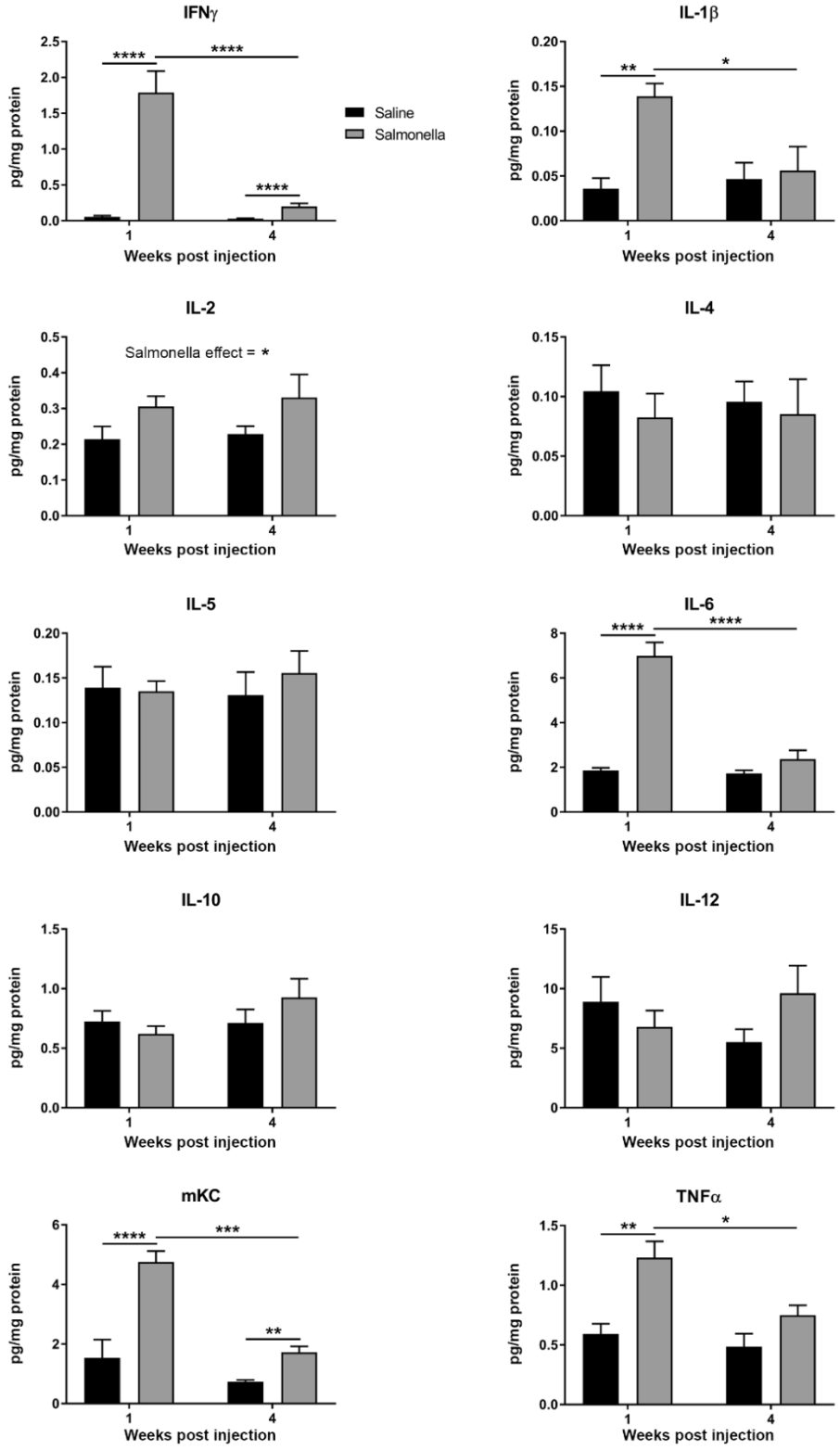

Figure 3.3 – Retinal cytokine levels at 1 and 4 weeks post saline or Salmonella injection.

*Retinal cytokine levels of IFNγ, IL-1β, IL-2, IL-4, IL-5, IL-6, IL-10, IL-12, mKC and TNFα were quantified in pg/ml by multiplex ELISA (Mesoscale Discovery) and normalised to mg total protein as measured by BCA assay. Graphs are presented as mean±SEM (n=5-6 mice per group). Data was analysed using two-way ANOVA with Holm-Sidak post-hoc testing. Stars denote significance as follows: *p<0.05, **p<0.01, ***p<0.001, ****p<0.0001.*

3.3.4 Upregulation of inflammatory pathways in the retina following Salmonella infection

As retinal cytokine levels are increased after Salmonella, the effect of systemic infection on a broader range of inflammatory pathways was investigated using qPCR (Figure 3.4). Following Salmonella infection, there is increased mRNA expression of microglial activation marker FcγRI at 1 week (fold increase ≈3.8, $p<0.0001$) and 4 weeks (fold change ≈2.4, $p<0.0001$) post infection compared to saline controls. There is a significant decrease in FcγRI from 1 to 4 weeks post infection (fold change ≈1.5, $p=0.0030$). There is also an increase in astrocyte/Müller cell marker GFAP at 1 week post Salmonella (fold change ≈1.8, $p=0.0350$), which returns to saline control levels by 4 weeks post infection.

At 1 week post infection, there are increased levels of chemokines/cytokines CCL2 (fold change ≈9, $p=0.014$), TNFα (fold change ≈6, $p=0.0455$) and IL-1β (fold change ≈2.3, $p=0.0149$), which return to saline control levels at 4 weeks post infection. In contrast, there are no changes in retinal levels of IL-18 mRNA following Salmonella infection. Despite a lack of upregulation of IL-18 following Salmonella, overall expression of IL-18 appeared substantially higher than for most genes, indicating constitutive expression in the retina is possible (data not shown).

Both IL-1β and IL-18 mRNA are translated into an inactive precursor protein requiring cleavage by the inflammasome to derive mature IL-1β and IL-18. There is an upregulation of genes encoding proteins associated with the inflammasome: NLRP3 (fold change ≈2.6, $p=0.0034$) and caspase-1 (fold change ≈5, $p<0.0001$) at 1 week post Salmonella infection compared to saline controls. NLRP3 returns to saline control levels at 4 weeks post infection, while caspase-1 remains elevated compared to saline (fold change ≈3.2, $p=0.0006$), but decreased compared to 1 week post infection (fold change ≈1.6, $p=0.0146$).

Changes in retinal mRNA expression are also observed in some additional oxidative stress and inflammatory pathways (Figure 3.5). There are no significant increases in nitric oxide synthase genes (nNOS, iNOS, eNOS), but in contrast at 1 week post infection there is robust upregulation of NADPH oxidase subunit 2 (NOX2) gene Cybb (fold change ≈5, $p=0.008$), which is expressed by phagocytes such as microglia and is responsible for the generation of superoxides, a reactive oxygen species (ROS) that greatly contributes to oxidative stress. Cybb expression returns to saline control levels at 4 weeks post Salmonella infection.

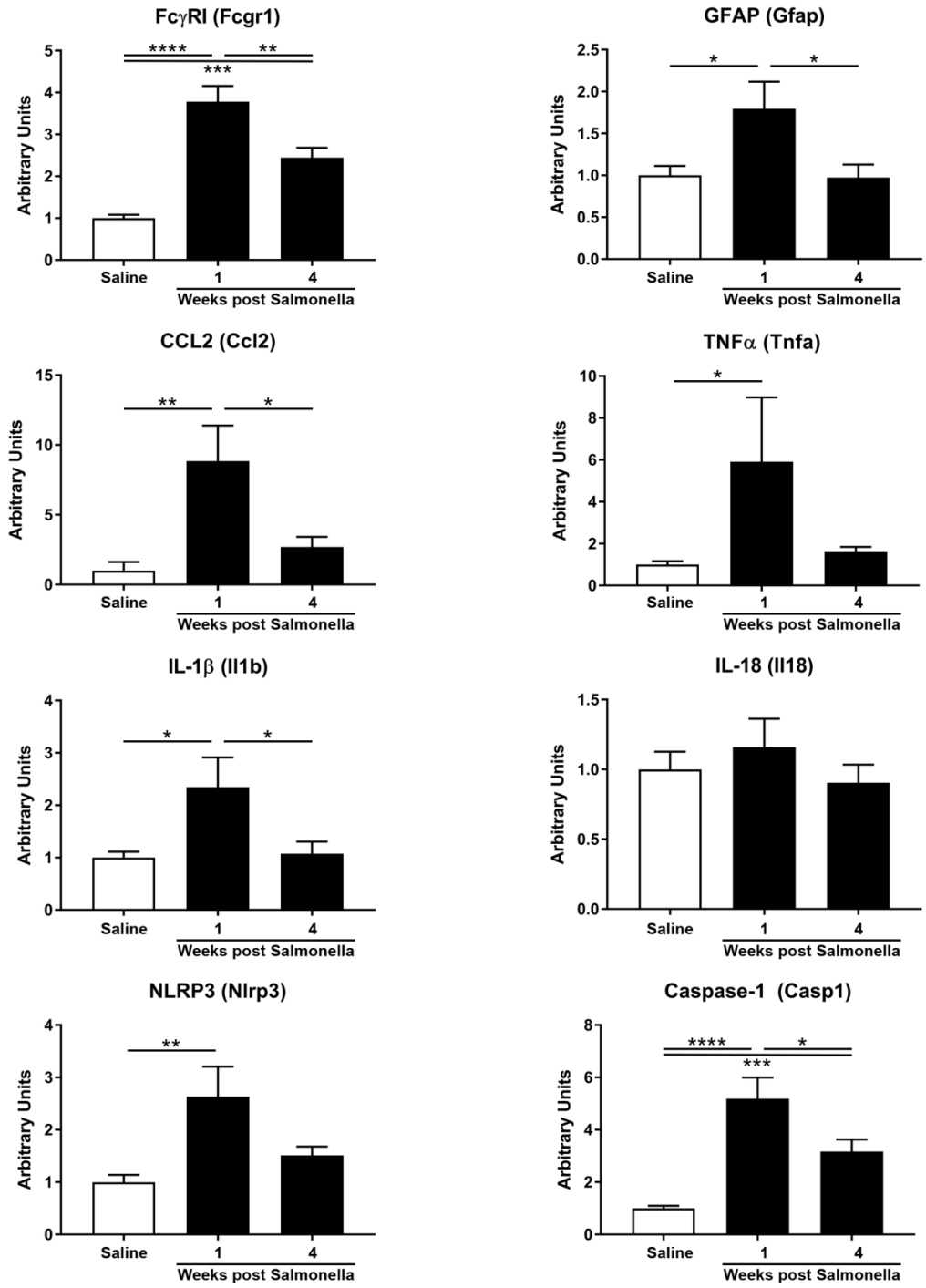

Figure 3.4 – Retinal gene expression of proinflammatory pathways at 1 and 4 weeks post saline or Salmonella injection.

*Retinal mRNA expression of genes encoding FcγRI, GFAP, CCL2, TNFα, IL-1β, IL-18, NLRP3 and caspase-1 was assayed by SYBR green qPCR. Gene expression was normalised to housekeeping gene GAPDH using the $2^{-\Delta\Delta Ct}$ method and is shown as fold change from saline control. Graphs are presented as mean±SEM (Saline group: n=3 mice at 1 week post injection, n=4 mice at 4 weeks post injection, Salmonella groups: n=5 mice per timepoint). Data was analysed by one-way ANOVA with Holm-Sidak post-hoc testing. Stars denote significance as follows: *p<0.05, **p<0.01, ***<p<0.001, ****p<0.0001.*

Levels of the gene Hmox-1 encoding the oxidative stress response protein heme oxygenase 1 (HO-1) is not increased at 1 or 4 weeks post Salmonella infection compared to saline controls. COX2, a key enzyme in the production of a range of prostaglandins, is the most upregulated gene assayed at 1 week post Salmonella (fold change ≈11, $p<0.0001$). COX2 levels are also increased compared to saline controls at 4 weeks post infection (fold change ≈3, $p=0.0085$), but decreased compared to 1 week post infection (fold change ≈3.4, $p<0.0001$). Levels of complement component 3 (C3), a critical component of the classical and alternative complement pathway, is increased at 1 week post infection (fold change ≈5, $p=0.0082$) and returns to saline control levels at 4 weeks post infection. mRNA levels of vascular endothelial growth factor (VEGFα), responsible for angiogenesis, is not altered by Salmonella infection at 1 or 4 weeks post infection compared to saline controls.

Overall, the mRNA changes following Salmonella infection show a range of activated retinal cell types (microglia and astrocytes/Müller cells) and a range of activated inflammatory pathways (cytokines/chemokines, inflammasome, NADPH oxidase, prostaglandins and complement).

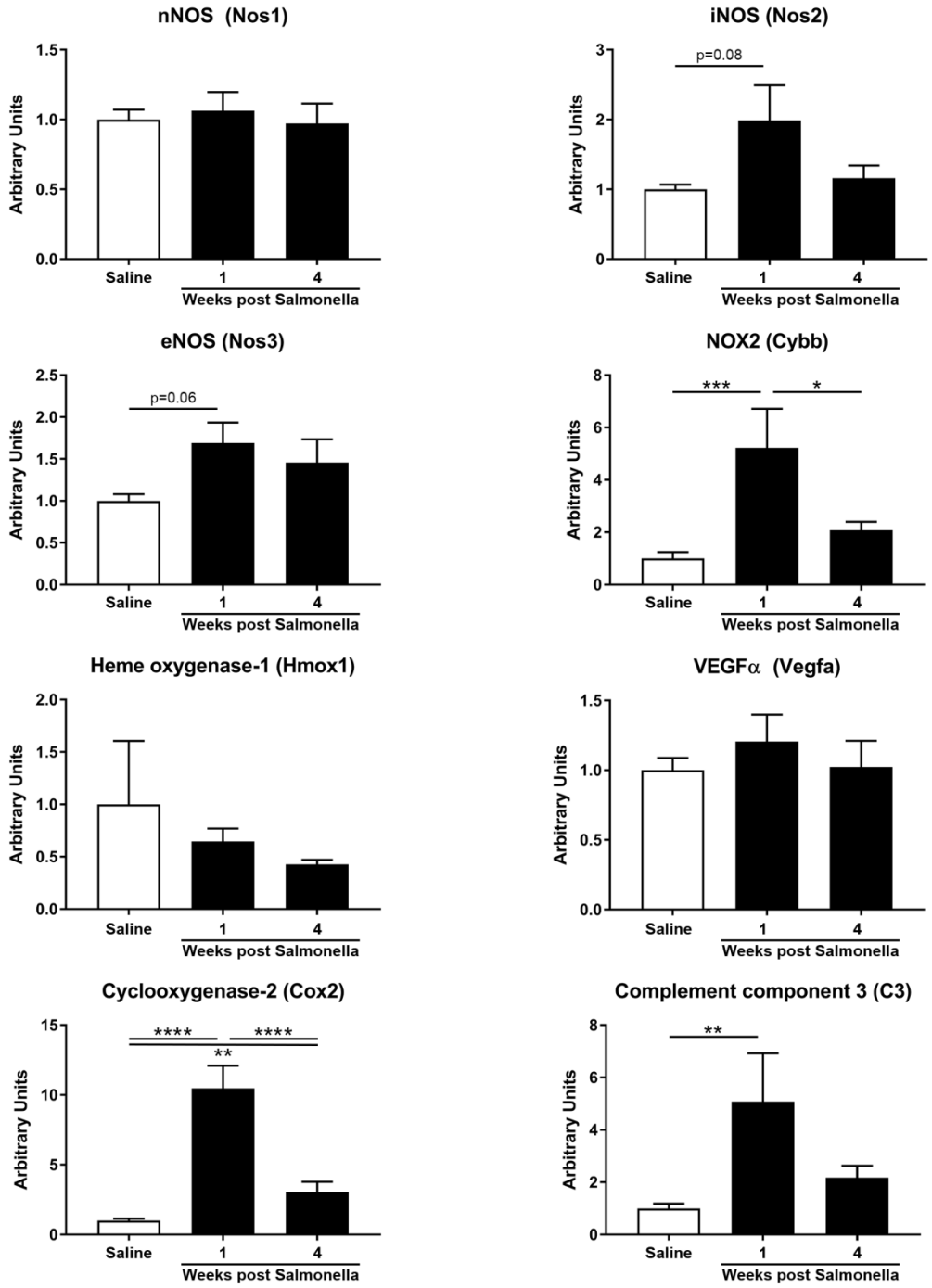

Figure 3.5 – Retinal gene expression of oxidative and inflammatory pathways at 1 and 4 weeks post Saline or Salmonella injection.

*Retinal mRNA expression of genes encoding nNOS, iNOS, eNOS, NOX2, HO-1, COX2, C3 and VEGF was assayed by SYBR green qPCR. Gene expression was normalised to housekeeping gene GAPDH using the $2^{-\Delta\Delta Ct}$ method and is shown as fold change from saline control. Graphs are presented as mean±SEM (Saline group: n=3 mice at 1 week post injection, n=4 mice at 4 weeks post injection, Salmonella groups: n=5 mice per timepoint). Data was analysed by one-way ANOVA with Holm-Sidak post-hoc testing. Stars denote significance as follows: *p<0.05, **p<0.01, ***<p<0.001, ****p<0.0001.*

3.3.5 Retinal myeloid cell activation following Salmonella infection

Upregulation of FcγRI mRNA at 1 and 4 weeks post Salmonella infection provides evidence for sustained activation and/or increased numbers of myeloid cells in the retina in response to systemic bacterial infection. Here, the localisation, phenotype and number of these cells is studied in more detail.

Immunohistochemistry images show that the expression pattern of CD11b and FcγRI appear localised to the inner layers of the retina (Figure 3.6a). This is in line with the typical localisation of microglia in the retina. In addition, these cells have the ramified morphology generally associated with quiescent or 'resting' microglia. To quantify marker expression by DAB immunohistochemistry, a set threshold of brown staining was defined as positive staining and then area of positive staining as a percentage of total retina area was calculated. This method demonstrates a sustained increase in CD11b+ (fold change ≈1.5, $p=0.0006$) and FcγRI+ (fold change ≈1.9, $p<0.0001$) area following Salmonella infection compared to saline controls, with no differences between expression at 1 and 4 weeks post infection (Figure 3.6b, c).

Increased area of positive staining may be due to increased receptor expression on each cell, changes in microglial morphology or increased number of positive cells. However, these changes are very difficult to confirm with immunohistochemistry as with thin sections as it isn't always clear which staining belongs to which cell. As a result, flow cytometry was employed to give a more quantitative assessment of microglial number and phenotype before and after Salmonella infection.

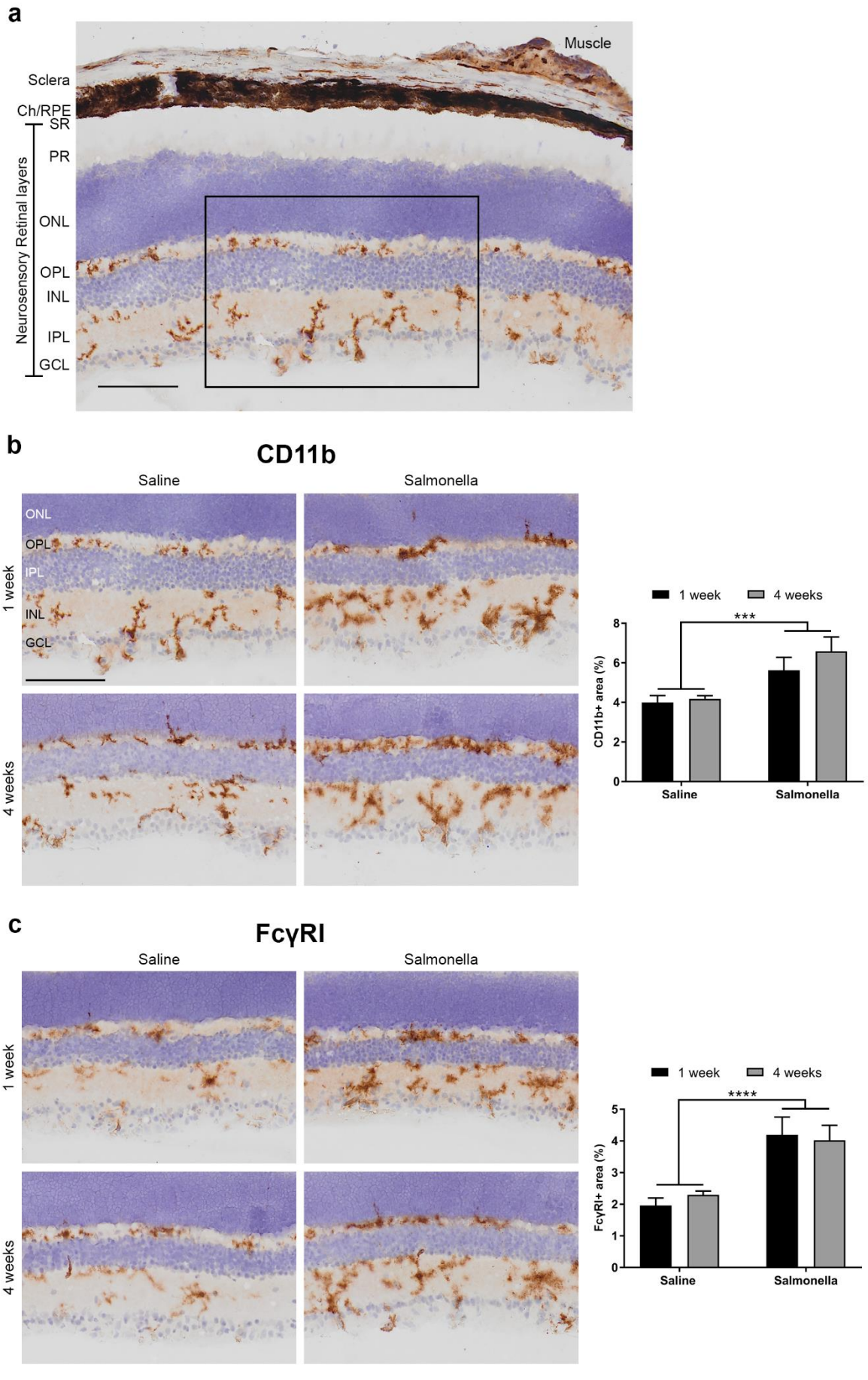
a
Muscle
Sclera
Ch/RPE
SR
PR
ONL
OPL
INL
IPL
GCL
Neurosensory Retinal layers
b
CD11b
Saline
Salmonella
1 week
4 weeks
1 week
4 weeks
***
CD11b+ area (%)
Saline
Salmonella
c
FcγRI
Saline
Salmonella
1 week
4 weeks
1 week
4 weeks
****
FcγRI+ area (%)
Saline
Salmonella

Figure 3.6 – Expression of microglial activation markers in the retina at 1 and 4 weeks post saline or Salmonella injection.

*(a) Representative DAB immunohistochemistry image showing the layers of the posterior eye; CD11b+ microglial cells are found almost exclusively in the inner layers of the retina. Representative DAB immunohistochemistry images of (b) CD11b and (c) FcγRI expression in the inner retina (taken from region denoted by black box) and quantification of each marker as positively stained (brown) area as a percentage of total retinal area. Graphs are presented as mean±SEM (n=6-8 mice per group). Data was analysed using two-way ANOVA. Stars denote significance as follows: ***<p<0.001, ****p<0.0001. Images were taken with a 20x objective and scale bars represent 100µm. Ch/RPE, Choroid/RPE; SR, subretinal space; PR, photoreceptor segments, ONL, outer nuclear layer; OPL, outer plexiform layer; INL, inner nuclear layer; IPL, inner plexiform layer; GCL, ganglion cell layer.*

Flow cytometry of individual mouse retinas is very challenging, due to the low proportion of microglial cells (0.5-1% of total retinal cells), low sample volume and reasonably low expression of CD11b and CD45, the markers typically used to define a myeloid population under resting conditions. To overcome these challenges, MacGreen mice (with eGFP+ expression in CSF-1R expressing cells) were used in flow cytometry to accurately distinguish the myeloid cell population (Figure 3.7a). Myeloid cells of the retina are mostly microglia, but may include infiltrating myeloid cells including monocytes, neutrophils and dendritic cells under inflammatory conditions. The expression of CSF-1R on positive cells is not altered following Salmonella infection (Figure 3.7b), making it an ideal marker to define the population. The percentage of eGFP+ cells is not altered during Salmonella infection, indicating that Salmonella does not cause the proliferation of microglia or infiltration of peripheral immune cells at 1 or 4 weeks post infection. 98.6% of eGFP+ events were also CD11b+, showing good agreement between the two myeloid cell markers (Figure 3.7c). At 1 week post Salmonella infection, there is increased expression of CD11b (fold change ≈1.1, p=0.0401) and CD45 (fold change ≈1.2, p=0.0107) on eGFP+ cells compared to naive mice (Figure 3.7c, d). At 4 weeks post Salmonella infection, there is also increased expression of CD11b (fold change ≈1.2, p=0.0004) and CD45 (fold change≈1.3, p=0.0003) on eGFP+ cells compared to naive mice. There is a significant increase in CD11b (fold change ≈1.1, p=0.0401) and CD45 (fold change ≈1.1, p=0.0479) expression from 1 week to 4 weeks post infection. Median fluorescence intensity of MHCII was similar to isotype control levels, indicating no/low expression of MHCII on these cells, although there is a trend to increased expression at 1 week post infection (p=0.07) compared to naive controls.

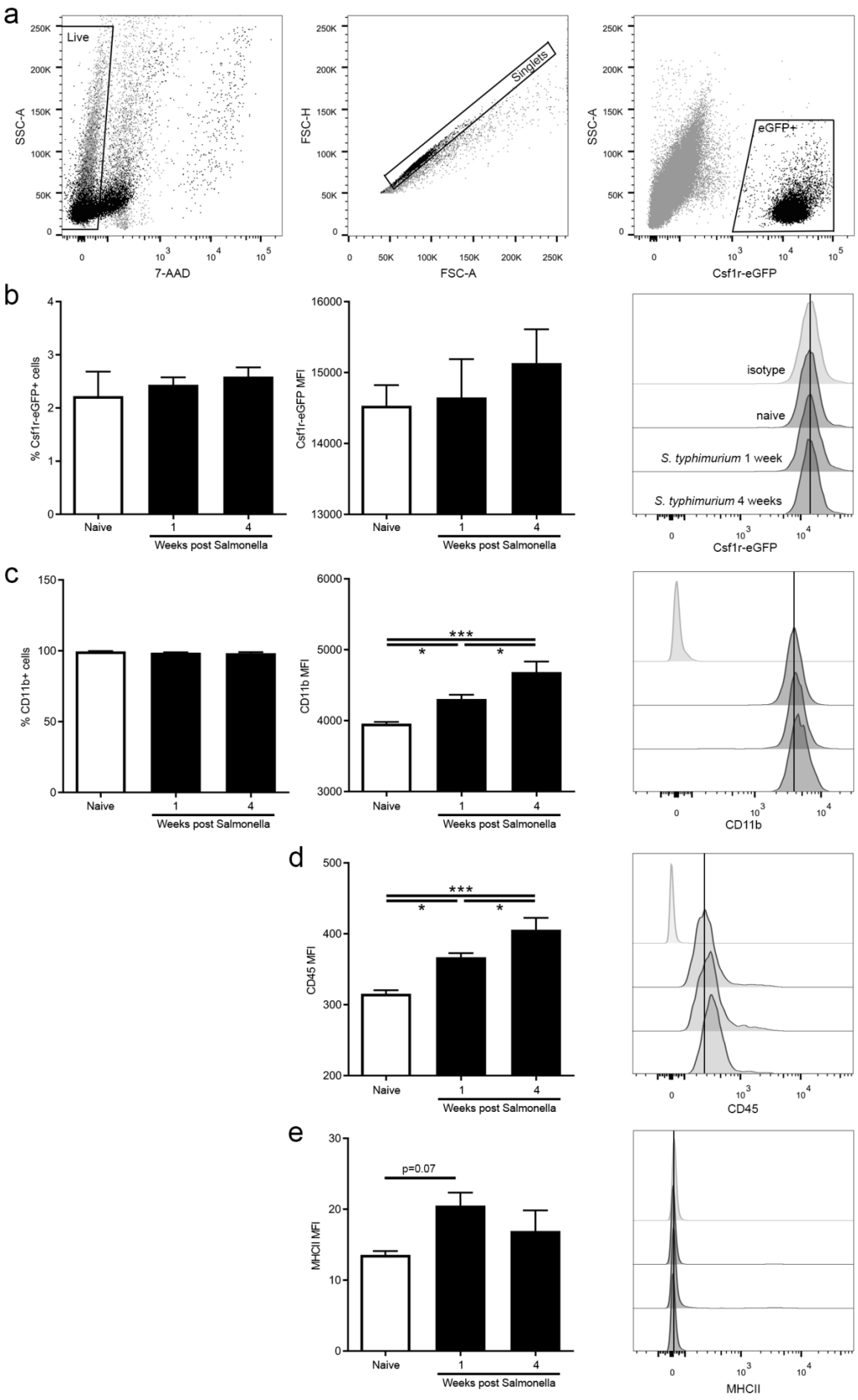
a
Live
SSC-A
7-AAD
Singlets
FSC-H
FSC-A
eGFP+
SSC-A
Csf1r-eGFP
b
% Csf1r-eGFP+ cells
Csf1r-eGFP MFI
Naive
1
4
Weeks post Salmonella
isotype
naive
S. typhimurium 1 week
S. typhimurium 4 weeks
Csf1r-eGFP
c
% CD11b+ cells
CD11b MFI
***
*
*
CD11b
d
CD45 MFI
CD45
e
MHCII MFI
p=0.07
MHCII

Figure 3.7 – Effect of Salmonella on myeloid cell number and surface marker expression.
*(a) Flow cytometry gating strategy for retinal live singlet cells of myeloid lineage (defined as CSF1R+ cells in MacGreen mice). (b) Quantification of CSF1R+ cells as a percentage of positive live singlet cells and expression of CSF1R by median fluorescence intensity (MFI) shown graphically and by histogram. (c) Quantification of CD11b+ cells as a percentage of CSF-1R+ live singlet cells and expression of CD11b by MFI. Quantification of (d) CD45 and (e) MHCII by expression of each marker by MFI. Graphs are presented as mean±SEM (n=4-5 mice per group). Data was analysed using one-way ANOVA with Holm-Sidak post-hoc testing. Stars denote significance as follows: *p<0.05, ***p<0.001. 7-AAD, 7-aminoactinomycin D; FSC, forward scatter; SSC, side scatter; eGFP, enhanced green fluorescent protein.*

The greatest Salmonella-induced changes in myeloid cell phenotype were observed for expression of CD11c (Figure 3.8b). There is an increased number of CD11c+ cells in the retina at 1 week post Salmonella infection (fold change ≈1.4, p=0.0072) compared to naïve mice. There is also an increased number of CD11c+ cells in the retina at 4 weeks post infection when compared to naïve mice (fold change ≈2.1, p<0.0001) and 1 week post Salmonella (fold change ≈1.5, p<0.0072). Alongside this increase in the CD11c+ population, there is also an increase in the level of expression of CD11c on these cells. At 1 week post Salmonella infection, there is increased expression of CD11c (fold change ≈1.3, p=0.0087) on eGFP+ cells compared to naive mice. At 4 weeks post Salmonella infection, there is also increased expression of CD11c (fold change ≈2, p<0.0001) on eGFP+ cells compared to naïve mice, and there is a significant increase in CD11c (fold change ≈1.5, p<0.0001) expression from 1 week to 4 weeks post infection.

There appears to be three distinct CD11c+ cell populations in the retina underpinning the changes in cell number/expression:

- $CD11b^{high}/CD11c^{low}/CD45^{low}/MHCII^{-/low}$ population (82.3% of CD11c+ cells)
- $CD11b^{high}/CD11c^{int}/CD45^{int}/MHCII^{int}$ (11.8% of CD11c+ cells)
- $CD11b^{-low}/CD11c^{high}/CD45^{high}/MHCII^{high}$ populations (5.7% of CD11c+ cells)

Overall, immunohistochemistry and flow cytometry show good agreement indicating microglial activation following Salmonella infection. Immunohistochemistry shows that microglia following Salmonella infection are mainly confined to the inner retinal layers, while flow cytometry indicates that microglia show a more activated phenotype at 4 weeks post infection than 1 week post infection.

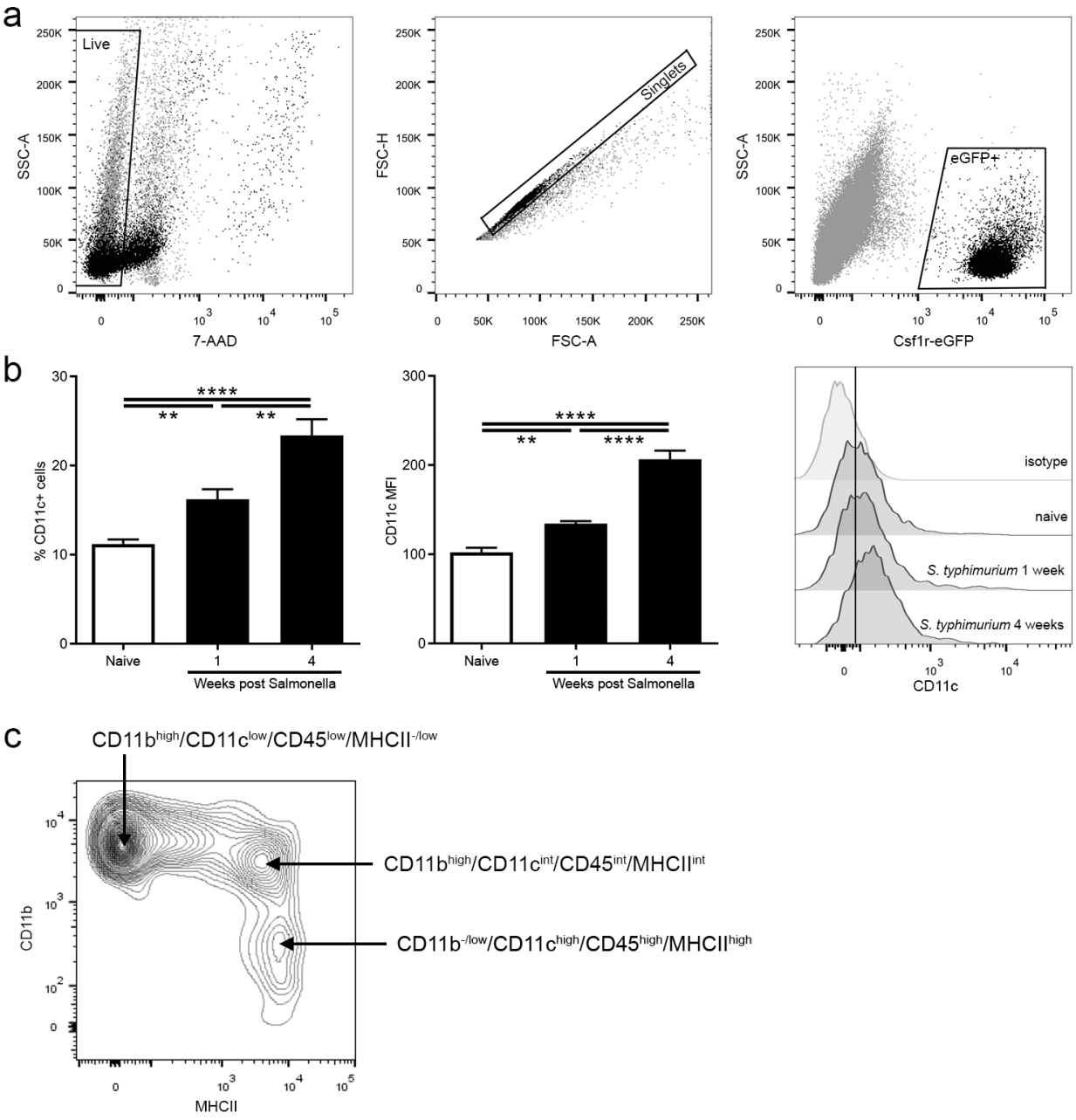

Figure 3.8 – Effect of Salmonella on CD11c+ cell number and surface expression.

*(a) Flow cytometry gating strategy for retinal live singlet cells of myeloid lineage (defined as Csf1r+ cells in MacGreen mice). Quantification of (b) CD11c+ cells as a percentage of CSF1R+ live singlet cells and expression by median fluorescence intensity (MFI) shown graphically and by fluorescence intensity histogram. (c) CD11c+ cells can be separated into three distinct populations based on surface marker expression. Graphs are presented as mean±SEM (n=4-5 mice per group). Data was analysed using one-way ANOVA with Holm-Sidak post-hoc testing. Stars denote significance as follows: **p<0.01, ****p<0.0001. 7-AAD, 7-aminoactinomycin D; FSC, forward scatter; SSC, side scatter; eGFP, enhanced green fluorescent protein; ^{int}, intermediate expression.*

3.3.6 Retinal blood vessel activation following Salmonella infection

As my data indicates that systemic bacterial infection can drive microglial activation in the inner retina, I investigated whether the inner retinal blood vessels could be a route of activation.

There is strong upregulation of MHCII at 1 and 4 weeks post Salmonella infection (fold change ≈50, $p<0.0001$) compared to saline controls (Figure 3.9a). MHCII staining is rarely observed in the retina in saline control animals, with very occasional staining of small cells in the GCL, whereas sustained MHCII staining of the inner retinal blood vessels (arterioles and capillaries) is observed during Salmonella infection.

At 1 week post Salmonella injection, ICAM-1 shows higher expression (fold change ≈7, $p<0.0001$) compared to saline controls (Figure 3.9b). There is also increased expression of ICAM-1 at 4 weeks post infection (fold change ≈2.7, $p=0.0014$) compared to saline controls, although this expression is decreased compared to 1 week post infection (fold change ≈2.7, $p=0.0305$). In saline control animals, ICAM-1 expression is found on inner retinal arterioles, but very rarely on the inner retinal capillaries. Following Salmonella infection, ICAM-1 expression is found both on the inner retinal arterioles and capillaries.

Overall, these results show strong activation of the inner retinal blood vessels following 1 and 4 weeks of Salmonella infection.

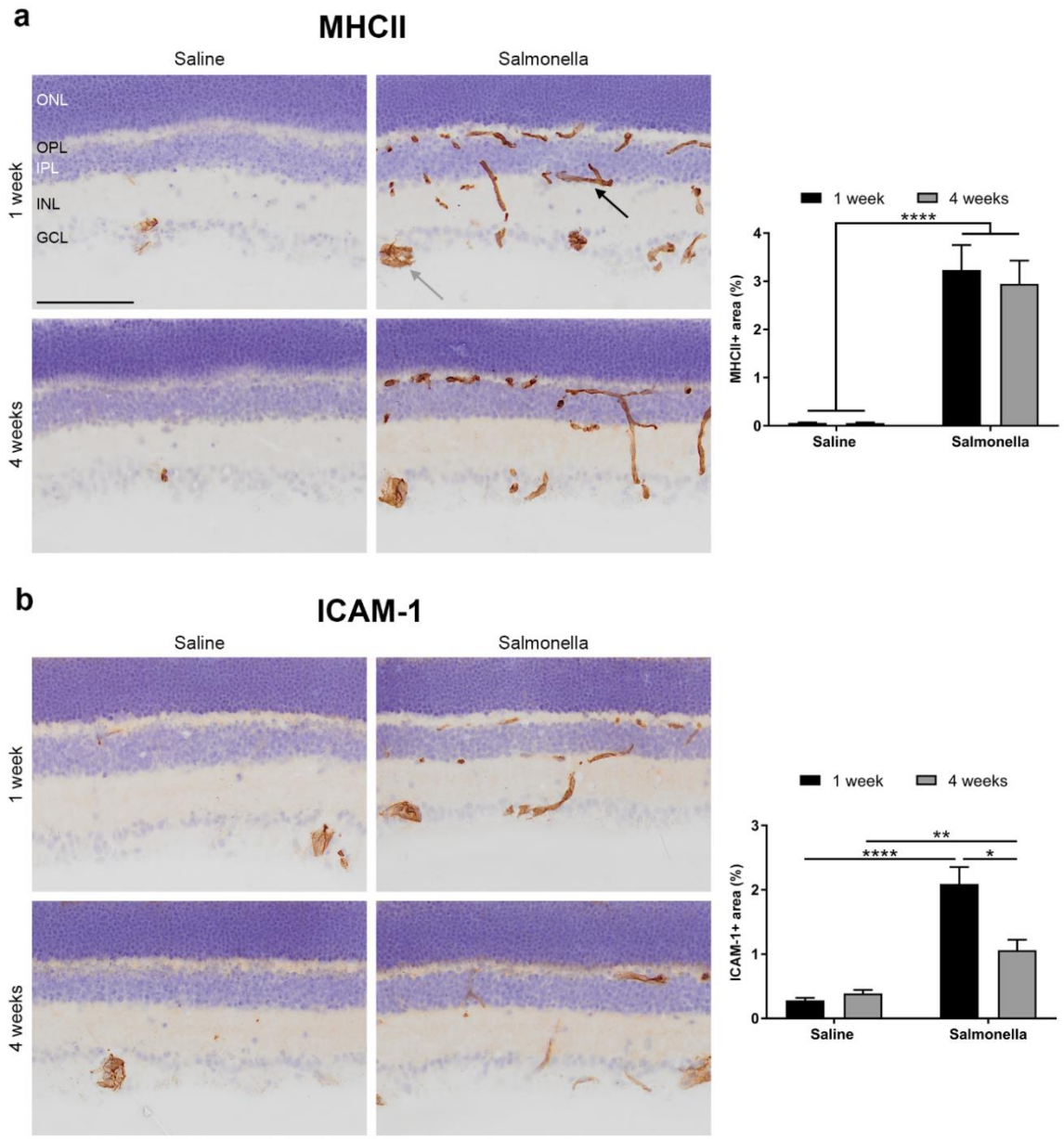

Figure 3.9 – Expression of blood vessel activation markers in the retina at 1 and 4 weeks post saline or Salmonella injection.

*Representative DAB immunohistochemistry images of (a) MHCII and (b) ICAM-1 expression in the inner retina. MHCII expression is quantified as positively stained (brown) area as a percentage of total retinal area. Due to confounding ICAM-1 expression in the photoreceptor layer, ICAM-1 expression was quantified as positive area as a percentage of inner retinal area. Graphs are presented as mean±SEM (n=6-8 mice per group). Data was analysed using two-way ANOVA with Holm-Sidak post-hoc testing. Stars denote significance as follows: *p<0.05, **<p<0.01, ****p<0.0001. Images were taken with a 20x objective and scale bars represent 100µm. Grey arrow denotes inner retinal arteriole. Black arrow denotes inner retinal capillaries. ONL, outer nuclear layer; OPL, outer plexiform layer; INL, inner nuclear layer; IPL, inner plexiform layer; GCL, ganglion cell layer.*

3.3.7 Long-term effects of Salmonella infection on the retina

Many of the changes observed following Salmonella are sustained for at least one month post infection, including increased cytokine levels and blood vessel/microglial cell activation. As a result, later timepoints of two and six months were investigated to determine for how long these changes are sustained.

There is significant weight loss at 1 day post Salmonella infection (≈10%, p=0.0253) compared to saline controls (Figure 3.10). From 1 day post infection, both saline and Salmonella groups gain 65% of initial starting weight over 24 weeks, but Salmonella infected mice do not regain the initial weight lost with respect to saline controls (p=0.0139).

At 2 months post injection, only 2 of 10 cytokines assayed are elevated in the serum (Figure 3.11). Levels of IFNγ (Saline: 1.18pg/ml, Salmonella: 9.75pg/ml, fold change ≈8, p=0.0004) and IL-10 (Saline: 25.5pg/ml, Salmonella: 39.5pg/ml, fold change ≈1.5, p=0.0212) remain elevated at 2 months post Salmonella infection. Overall, this indicates that there is still peripheral inflammation at 2 months post infection, albeit at lower levels than observed at 1 and 4 weeks.

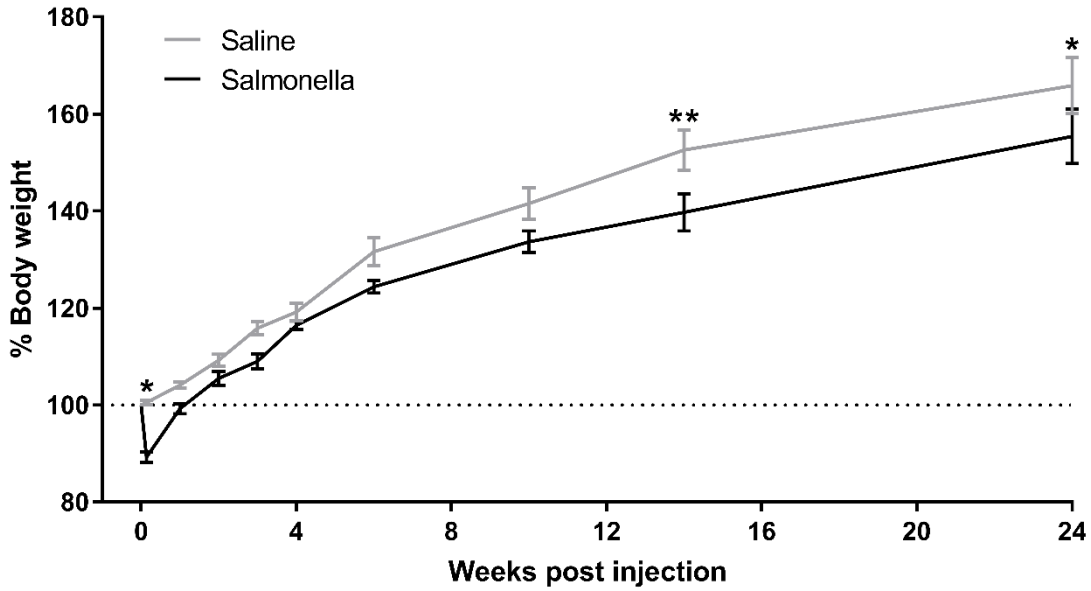

Figure 3.10 – Body weight changes induced by saline or Salmonella over 6 months post injection.

*Body weight is shown as a percentage of starting weight for each mouse (n=8 mice per group). Graphs are presented as mean±SEM. Data was analysed by repeated measures two-way ANOVA with Holm-Sidak post-hoc testing. Stars denote significance as follows: *p<0.05, **p<0.01.*

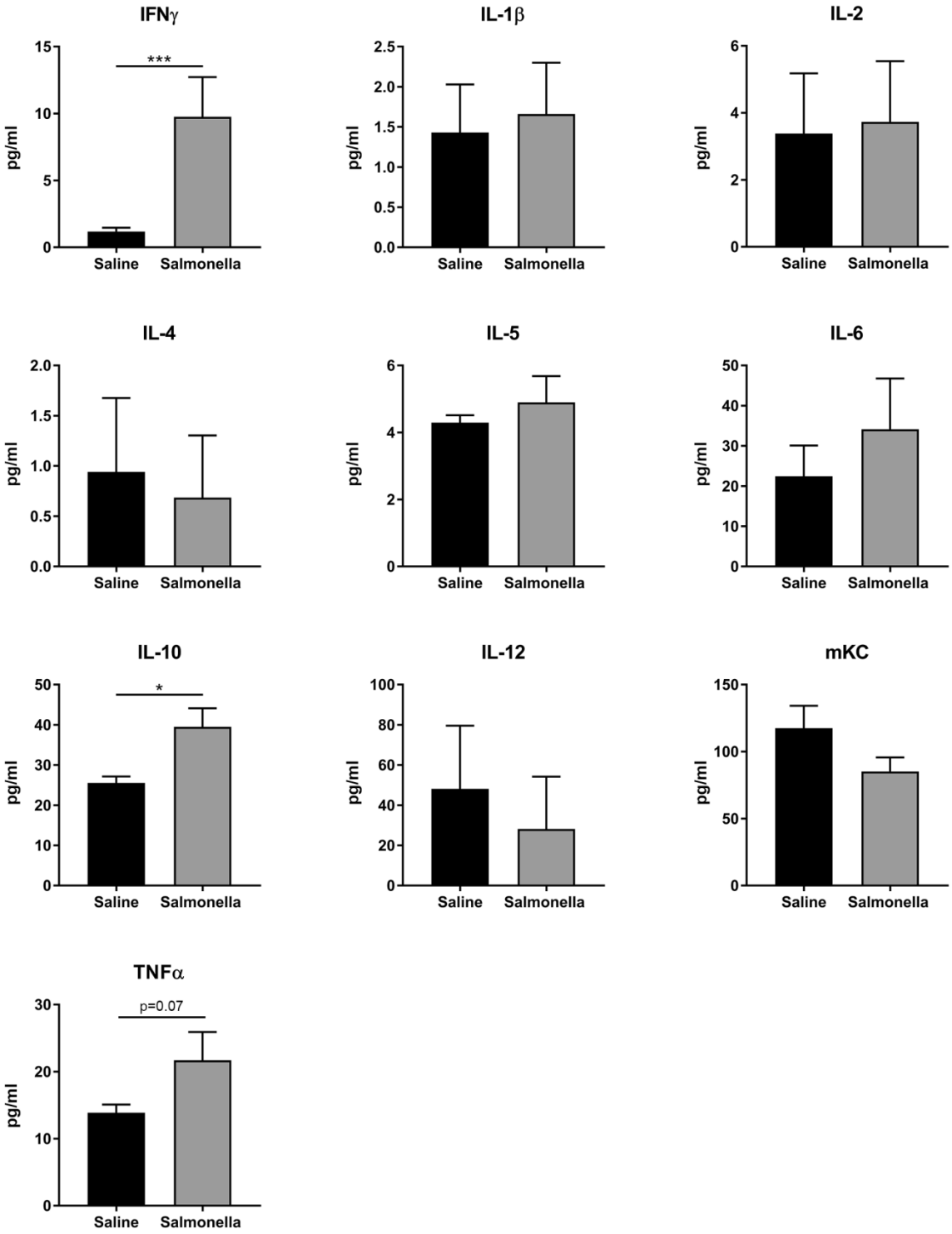

Figure 3.11 – Serum cytokine levels at 8 weeks post saline or Salmonella injection.

*Serum cytokine levels of IFNγ, IL-1β, IL-2, IL-4, IL-5, IL-6, IL-10, IL-12, mKC and TNFα were quantified in pg/ml by multiplex ELISA (Mesoscale Discovery). Graphs are presented as mean±SEM (n=5 mice per group). Data was analysed using unpaired two-tailed T-test. Stars denote significance as follows: *p<0.05, ***p<0.001.*

For all 10 cytokines assayed, no significant differences in the level of retinal cytokines were observed between saline and Salmonella at 2 months post injection (Figure 3.12). This provides evidence that peripheral inflammation is no longer causing retinal inflammation by this timepoint.

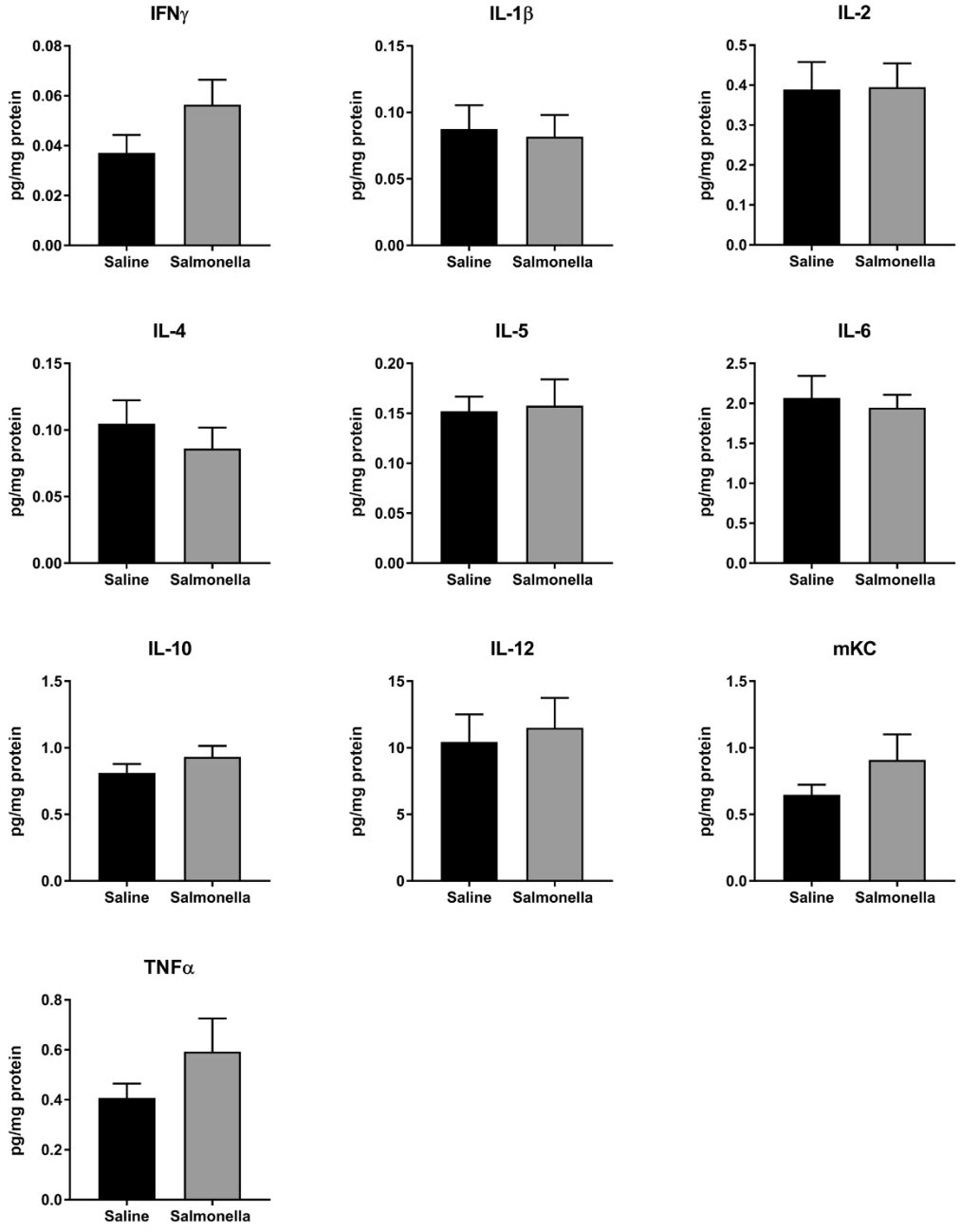

Figure 3.12 – Retinal cytokine levels at 8 weeks post saline or Salmonella injection.
Retinal cytokine levels of IFNγ, IL-1β, IL-2, IL-4, IL-5, IL-6, IL-10, IL-12, mKC and TNFα were quantified in pg/ml by multiplex ELISA (Mesoscale Discovery) and normalised to mg total protein measured by BCA assay. Graphs are presented as mean±SEM (n=6-7 mice per group). Data was analysed using unpaired two-tailed T-test.

Alongside these cytokine findings, there was no evidence that Salmonella caused sustained microglial activation at 8 or 24 weeks post infection in terms of CD11b (Figure 3.13a) or FcγRI expression (Figure 3.13b). Interestingly, it was observed that microglial markers appear to increase as part of aging, with higher expression of CD11b (fold change ≈1.1, p=0.0384) and FcγRI (fold change ≈1.3, p=0.0191) in 9-month-old mice (harvested at 24 weeks post injection) compared to 5-month-old mice (harvested at 8 weeks post injection).

There is evidence for sustained activation of the inner retinal blood vessels following Salmonella infection (Figure 3.14). MHCII is still upregulated at 8 weeks (fold change ≈19, p<0.0001) and 24 weeks (fold change ≈11, p<0.0001) post Salmonella infection compared to saline controls, although the expression is reduced at 24 weeks compared to 8 weeks post infection (fold change ≈1.7, p=0.0467). MHCII expression is still observed on both the retinal blood arterioles and capillaries. Unlike with microglial staining, there was no difference in MHCII levels with aging. ICAM-1 is also increased at 8 and 24 weeks post infection (fold change ≈1.8, p=0.0010) but does not reach significance at individual timepoints with post-hoc testing. The staining pattern of ICAM-1 shows that the changes observed are mainly due to differences in expression on retinal blood arterioles, as staining of the inner retinal blood capillaries is rarely observed at 8 and 24 weeks post infection. There is also an aging effect with ICAM-1, which is increased in 9-month old mice compared to 5-month-old mice (fold change ≈1.7, p=0.0087).

Overall, these data indicate that inner retina blood vessel activation persists at least 6 months after Salmonella infection, while microglial activation and cytokine production is back to baseline levels at 2 months post infection.

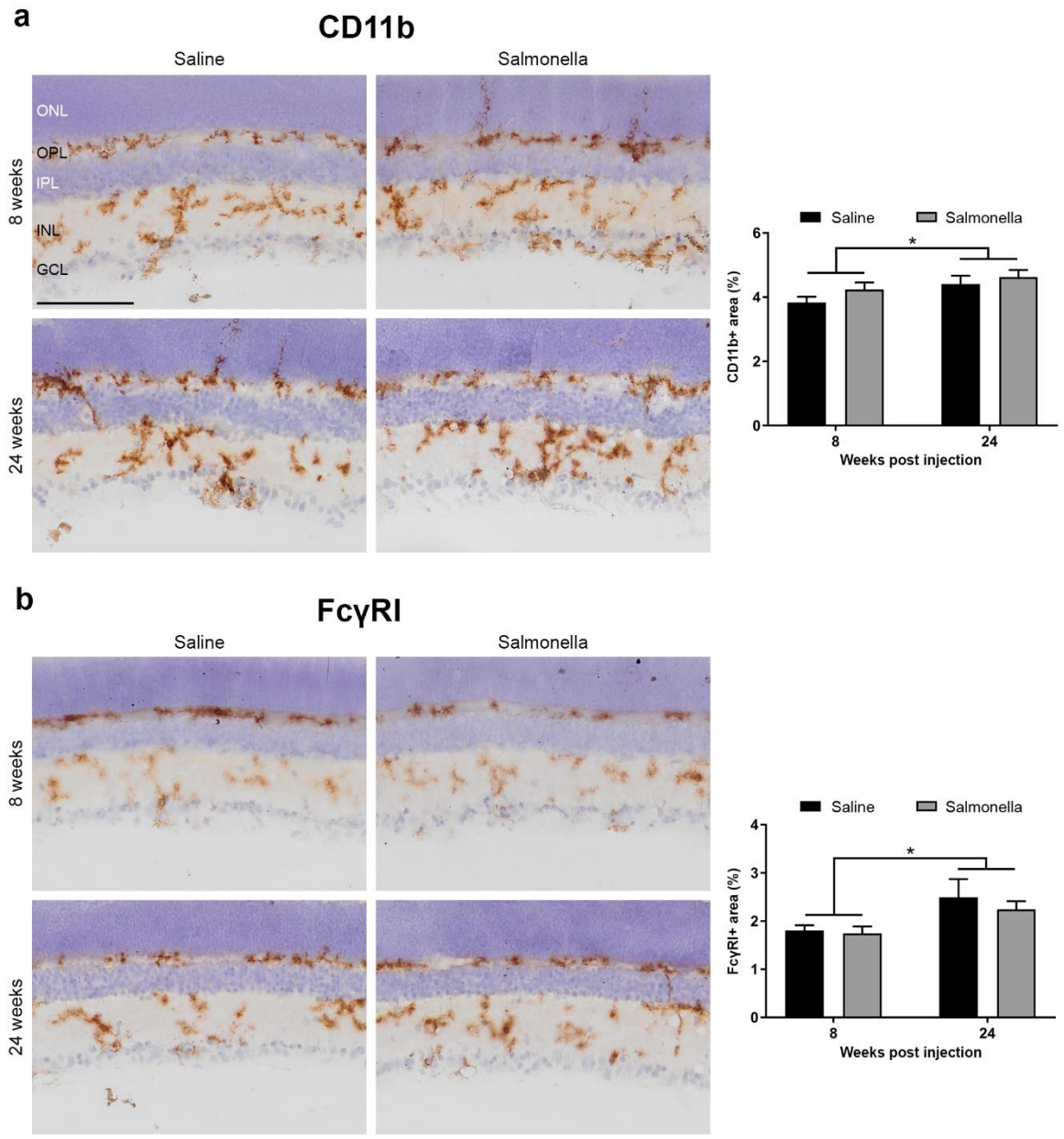

Figure 3.13 – Expression of microglial activation markers in the retina at 8 and 24 weeks post saline or Salmonella injection.

*Representative DAB immunohistochemistry images of (a) CD11b and (b) FcγRI expression in the inner retina and quantification as positively stained (brown) area of each marker as a percentage of total retinal area. Graphs are presented as mean±SEM (n=7-8 mice per group). Data was analysed using two-way ANOVA. Stars denote significance as follows: *p<0.05. Images were taken with a 20x objective and scale bars represent 100µm. ONL, outer nuclear layer; OPL, outer plexiform layer; INL, inner nuclear layer; IPL, inner plexiform layer; GCL, ganglion cell layer.*

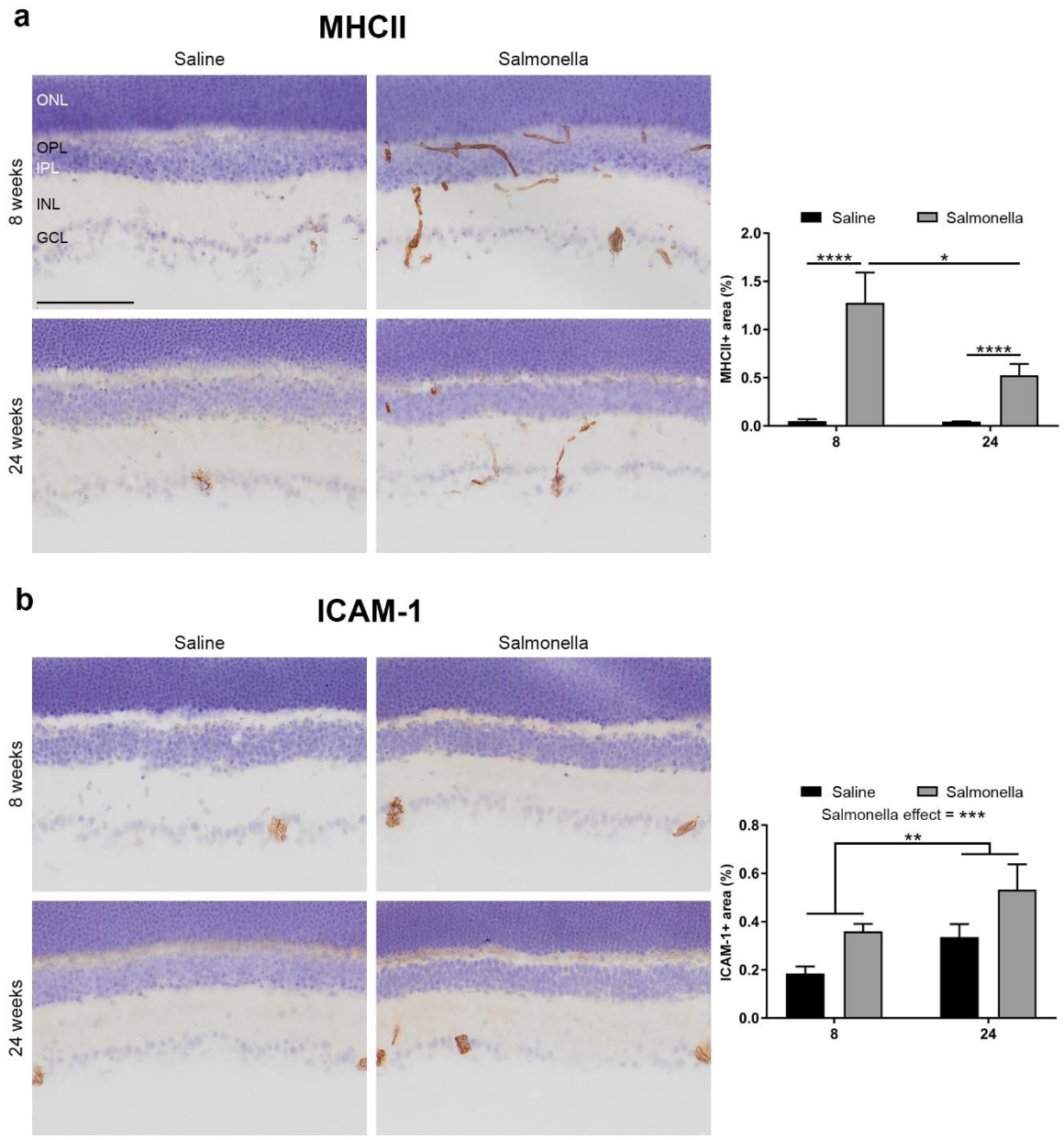

Figure 3.14 – Expression of blood vessel activation markers in the retina at 8 and 24 weeks post saline or Salmonella injection.

*Representative DAB immunohistochemistry images of (a) MHCII and (b) ICAM-1 expression in the inner retina. MHCII expression is quantified as positively stained (brown) area as a percentage of total retinal area. Due to confounding ICAM-1 expression in the photoreceptor layer, ICAM-1 expression was quantified as positive area as a percentage of inner retinal area. Graphs are presented as mean±SEM (n=7-8 mice per group). Data was analysed using two-way ANOVA. Stars denote significance as follows: *p<0.05, **p<0.01, ***p<0.001, ****p<0.0001. Images were taken with a 20x objective and scale bars represent 100µm. ONL, outer nuclear layer; OPL, outer plexiform layer; INL, inner nuclear layer; IPL, inner plexiform layer; GCL, ganglion cell layer.*

3.3.8 Effects of aging on peripheral and retinal inflammation following Salmonella infection

Salmonella induces weight loss in young mice at 24hrs post infection (11.9%, p<0.0001, Figure 3.15a). This is followed by weight gain over the following 4 weeks, as seen for saline controls (p<0.0001). In middle-aged mice, Salmonella also induces weight loss at 24hrs post infection (5.2%, p=0.0012 Figure 3.15b), but this is not followed by weight gain over the following 4 weeks, again in accordance with saline controls. A comparison of the Salmonella groups for young and middle-aged mice found a non-significant trend to higher weight loss in the young mice (p=0.12, Figure 3.15c). This is interesting as young mice have a lower starting weight than middle aged mice (p=0.0001) so it would be expected that they would have proportionally less weight to lose, not more. Regardless of this, it is clear for both groups that mice do not regain the initial weight lost with respect to saline controls (young, p=0.0003; middle-aged, p=0.0004).

None of the elevations in cytokines following Salmonella are significantly different between young and middle-aged mice. However, Salmonella infection alone causes an increase in 9 of 10 cytokines at 4 weeks post infection (Figure 3.16): IFNγ (Saline: 0.65pg/ml, Salmonella: 201pg/ml, fold change ≈300, p<0.0001); IL-1β (Saline: 0.67pg/ml, Salmonella: 3.44pg/ml fold change ≈5, p=0.0031); IL-2 (Saline:1.19pg/ml, Salmonella: 5.57pg/ml, fold change ≈5.5, p<0.0001); IL-5 (Saline: 7.07pg/ml, Salmonella: 12.0pg/ml, fold change ≈1.7, p=0.0055); IL-6 (Saline: 15.7pg/ml, Salmonella: 300pg/ml, fold change ≈19, p<0.0001); IL-10 (Saline: 1.40pg/ml, Salmonella: 2.00pg/ml, fold change ≈1.4, p<0.0001); IL-12 (Saline: 2.46pg/ml, Salmonella: 53.5pg/ml, fold change ≈22, p<0.0001); mKC (Saline: 101pg/ml, Salmonella: 132pg/ml, fold change ≈1.3, p=0.0090); TNFα (Saline: 8.82pg/ml, Salmonella: 97.4pg/ml, fold change ≈11, p<0.0001). IL-4 is not significantly increased, although this appears to be elevated when compared to saline controls (Saline: 0.42pg/ml, Salmonella: 3.52pg/ml, fold change ≈8, p=0.1115) but is substantially more variable than other cytokines after Salmonella infection. In addition, a general increase in serum cytokines with aging was observed for IL-10 (fold change: ≈1.8, p=0.0306) and mKC (fold change ≈1.2, p=0.0482).

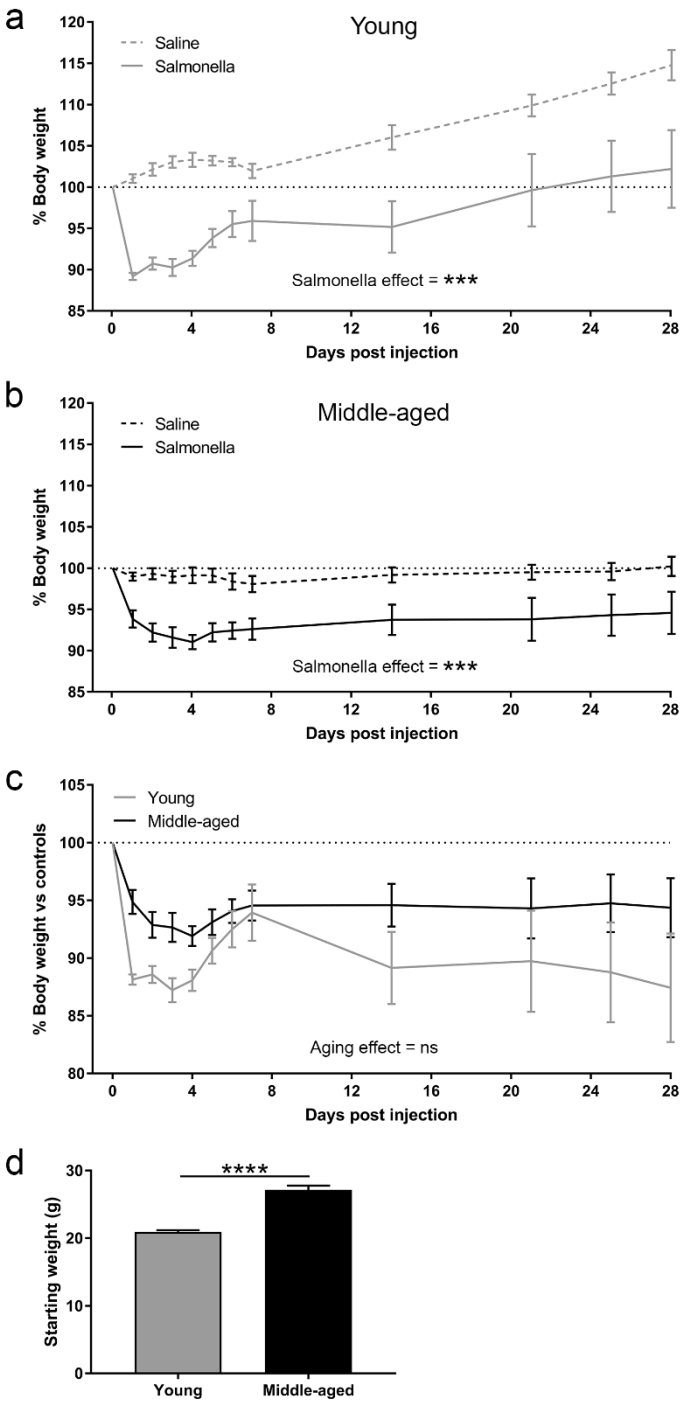

Figure 3.15 - Body weight changes following Salmonella infection in young and middle-aged mice.

*Body weight changes over time following saline or Salmonella injection as a percentage of starting weight in (a) young 3-month-old mice and (b) middle-aged 12-month-old mice. (c) Salmonella-induced weight loss normalised to saline controls for young and middle-aged mice. (d) Pre-injection weight of young and middle-aged mouse groups. Graphs are presented as mean±SEM (n=6-8 mice per group). Data was analysed by repeated measures two-way ANOVA with Holm-Sidak post-hoc testing, except starting weight which was analysed by unpaired two-tailed T-test. Stars denote significance as follows: ***p<0.01, ****p<0.0001, ns = not significant.*

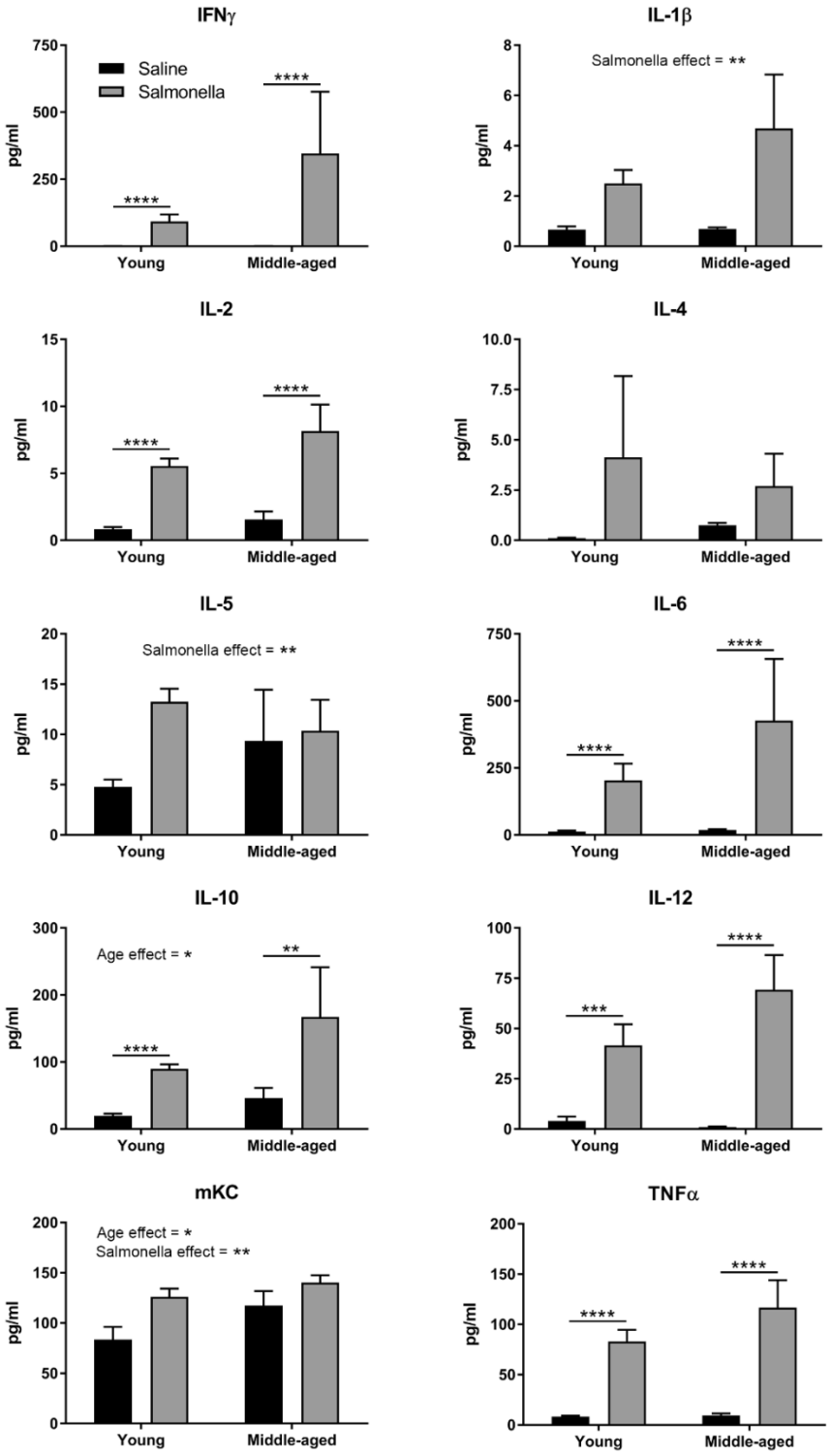

Figure 3.16 - Serum cytokine levels at 4 weeks post saline or Salmonella injection in young and middle-aged mice.

*Serum cytokine levels of IFNγ, IL-1β, IL-2, IL-4, IL-5, IL-6, IL-10, IL-12, mKC and TNFα were quantified in pg/ml by multiplex ELISA (Mesoscale Discovery). Graphs are presented as mean±SEM (n=6-8 mice per group). Data was analysed using two-way ANOVA with Holm-Sidak post-hoc testing. Stars denote significance as follows: *p<0.05, **p<0.01, ***p<0.001, ****p<0.001.*

No differences are observed in retinal levels of any cytokine assayed between Salmonella groups in young and middle-aged mice, although 5 of 10 cytokines assayed are increased due to Salmonella overall (Figure 3.17): IFNγ (Saline: 0.036pg/mg, Salmonella: 0.28pg/mg, fold change ≈8, $p<0.0001$) IL-1β (Saline: 0.054pg/mg, Salmonella: 0.102pg/mg, fold change ≈1.9, $p=0.0036$), IL-6 (Saline: 3.33pg/ml, Salmonella: 5.54pg/ml, fold change ≈1.7, $p=0.0015$), mKC (Saline: 1.33pg/ml, Salmonella: 2.18pg/ml, fold change: ≈1.9, $p=0.0014$), TNFα (Saline: 0.55pg/ml, Salmonella: 1.00pg/ml, fold change: ≈1.8, $p=0.0064$). Notably, an increase in retinal IL-1β with aging is observed from 3-month-old mice to 12-month-old mice (fold change ≈1.5, $p=0.0492$).

Overall, these data show that there is no difference between young and middle-aged mice in terms of weight loss and peripheral/retinal cytokine levels at 1 month post Salmonella infection. This reaffirms that there is substantial inflammation at 1 month post infection, which does not seem to be affected by the addition of aging as a cofactor.

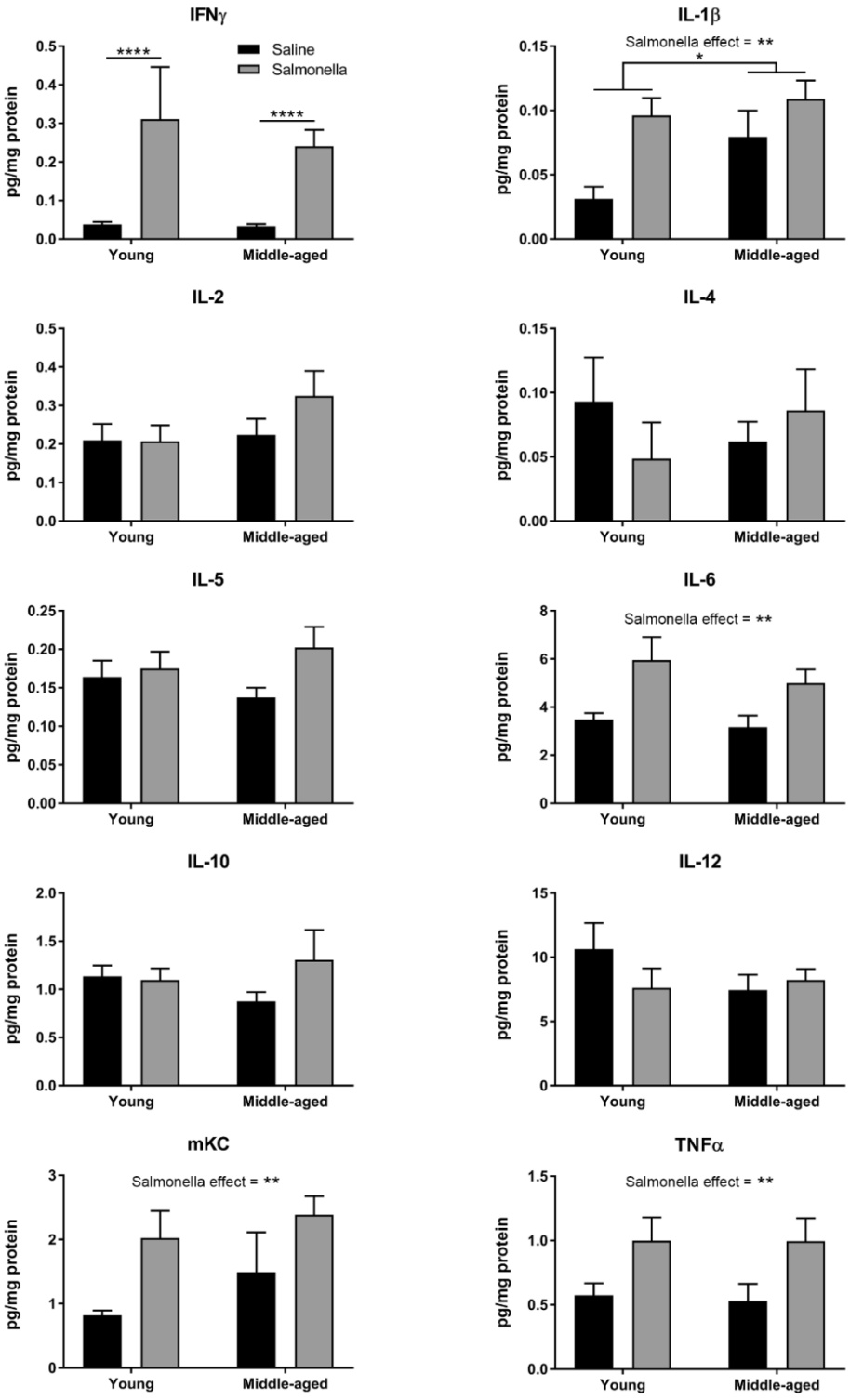

Figure 3.17 – Retinal cytokine levels at 4 weeks post saline or Salmonella injection in young and middle-aged mice.

*Retinal cytokine levels of IFNγ, IL-1β, IL-2, IL-4, IL-5, IL-6, IL-10, IL-12, mKC and TNFα were quantified in pg/ml by multiplex ELISA (Mesoscale Discovery) and normalised to mg total protein measured by BCA assay. Graphs are presented as mean±SEM (n=6-8 mice per group). Data was analysed using two-way ANOVA with Holm-Sidak post-hoc testing. Stars denote significance as follows: *p<0.05, **p<0.01, ****p<0.001.*

3.4 Discussion

3.4.1 Peripheral kinetics of Salmonella infection

Weight loss is strongest at day 2 post infection, after which mice regain weight peaking at day 8. This typical sickness behaviour, anorexia, is thought to attempt to starve the pathogen of critical nutrients essential for its replication and demonstrates the strong effect that systemic infections exert on the CNS (Hart, 1988). Interestingly, there is then a second wave of weight loss which is strongest at day 16 post infection. Such biphasic weight loss has been shown for certain viral infections (Srivastava et al., 2009; Harker et al., 2010) and may represent the metabolic demand for energy needed by the adaptive immune response. Noteworthily, even by 6 months post Salmonella infection, mice have not reached the same weight has saline controls, showing long-lasting weight deficits that may have long-term consequences for metabolism and general health.

Alongside these changes, there is splenomegaly at 1 and 4 weeks post infection, indicating that live Salmonella infection drives a chronic systemic immune response. This is supported by serum cytokine measurements showing increased levels of cytokines at 1, 4 and 8 weeks post infection, although levels are greatly reduced at each subsequent timepoint. From these data, 1 and 4 week timepoints are investigated further in Chapters 4 and 5 of this thesis. At the 1 week timepoint, there are high levels of systemic inflammation, while at 4 weeks post infection, there are lower levels of systemic inflammation, but a much longer duration of exposure. Furthermore, a strong innate immune response is able to contain Salmonella infection in mice for several weeks until a strong adaptive immune system is generated to clear the pathogen (Mittrücker & Kaufmann, 2000). These distinctions may allow different aspects of systemic inflammation on the retina to be investigated at 1 and 4 week timepoints.

3.4.2 Changes in retinal myeloid cell populations following infections

Previous studies have suggested an increased number and activation state of myeloid cells in the retina following systemic fungal and viral infection (Maneu et al., 2014; Zinkernagel et al., 2013). In this study, an increased activation state was clearly observed in terms of CD11b and CD45 upregulation, but there is not convincing evidence of increased numbers of myeloid cells in the retina following systemic Salmonella infection at 1 or 4 weeks post infection, using two independent methods (flow cytometry and immunohistochemistry). The expression of CD11c has not been investigated by these other studies, and showed the strongest effect of all the markers investigated. Interestingly, when the CD11c population was analysed by flow cytometry a large $CD11b^{high}/CD11c^{low}/CD45^{low}/MHCII^{-/low}$ population, which would be characteristic of microglia, was

identified along with two smaller CD11b^{high}/CD11c^{int}/CD45^{int}/MHCII^{int} and CD11b^{-low}/CD11c^{high}/CD45^{high}/MHCII^{high} populations. It is unclear what cell populations these latter two populations represent, although an interesting candidate would be dendritic cells, which are traditionally CD11c^{high} in comparison to macrophages/microglia and CD11b- (plasmacytoid) and CD11b+ (central) subsets have been described systemically (Chistiakov et al., 2015). Small dendritic cell populations have been described in the retina (Xu et al., 2007b), but require far more phenotypic and functional characterisation. Another possible cell type would be retinal perivascular macrophages, which are also MHCII+ and CD11c+ (Liyanage et al., 2016; O'Koren et al., 2016). During Alzheimer's disease, many microglia surrounding plaques have a specific disease associated phenotype and are often CD11c+, which is considered a marker of primed microglia in the brain (Hart et al., 2012; Keren-Shaul et al., 2017; Perry & Holmes, 2014; Perry & Teeling, 2013; Püntener et al., 2012) and this may also be true in the retina.

This study shows a marked increase in microglial activation at 4 weeks post Salmonella infection compared to 1 week. Expression of FcγRI and CD11b on myeloid cells is also increased at 1 and 4 weeks post Salmonella infection compared to saline controls according to immunohistochemistry, but a further increase in expression from 1 to 4 weeks post infection, as is characterised by flow cytometry, could not be identified. DAB immunohistochemistry is used to analyse binary (positive and negative) staining of samples and is only sensitive to dramatic changes in expression levels or changes in cell morphology, because the deposition of DAB does not follow a linear relationship with marker expression (van der Loos, 2008). Flow cytometry is therefore a more sensitive staining method using fluorescence for accurate quantification of marker expression levels on individual cells, while immunohistochemistry provides more general overview for presence or absence of microglial activation. For example, immunohistochemistry provides clear evidence that CD11b and FcγRI expression returns to saline control levels at 8 and 24 weeks post Salmonella infection.

3.4.3 Changes in other retinal cell populations following Salmonella infection

One of the most striking observations in the brain following Salmonella is the dramatic upregulation of MHCII on the cerebral vasculature (Püntener et al., 2012). As a result, I investigated whether this phenomenon of blood vessel activation is also present in the retina. The activation of inner retinal vasculature may be a key step in the transduction of systemic inflammation into retinal inflammation, as has been described in immune-to-brain communication (Khandaker & Dantzer, 2016).

Strong MHCII staining is observed at 1-8 weeks post infection and is clearly present even at 6 months after infection. Indeed, there is a clear correlation between lack of weight loss/splenomegaly following Salmonella, indicating failed infection, and lack of MHCII on the retinal blood vessels. ICAM-1 is also strongly expressed on retinal capillaries at 1 week post infection, although expression drops at 4 weeks post expression, unlike with MHCII. Despite this ICAM-1 levels still do not return to control levels even after 6 months post infection. Overall, these findings show that blood vessel activation is the most chronic Salmonella-induced change observed in this study.

mRNA expression of GFAP is also increased at both 1 and 4 weeks post Salmonella infection, indicating increased astrocytosis and/or activation of Müller cells (Verderber et al., 1995). Both astrocytes and Müller cells can respond to inflammation and have the ability to release cytokines (e.g TNFα, CCL2) (de Hoz et al., 2016). Considering this, the effect of infections, or even mimetics such as LPS, on these populations have been poorly considered. Immunohistochemical staining for GFAP at 1, 4, 8 and 24 weeks post infection would provide the kinetics of activation of these cells, as well as being able to distinguish between activation of astrocytes and Müller cells.

Overall, these data show that it is important to investigate a range of retinal cells and not solely microglia following systemic infection to gain a better overview of ongoing changes.

3.4.4 Retinal molecular changes following Salmonella infection

Although it is known that systemic LPS administration leads to cytokine production in the retina (Chu et al., 2016) to my knowledge, no study has investigated cytokine levels in the retina following a live systemic infection. Mice showed increased retinal protein levels of IFNγ, IL-1β, IL-2, IL-6, mKC and TNFα at 1 week post Salmonella infection, with IFNγ and mKC still upregulated at 4 weeks, albeit at greatly reduced levels compared to 1 week. These cytokines are considered pro-inflammatory cytokines/chemokines typical of a T_H1 response to bacterial infection (Mills et al., 2000). The T_H2 cytokines IL-4, IL-5 and IL-10 (Mills et al., 2000) were not elevated at 1 week post infection in the retina. Levels of pro-inflammatory cytokines return to baseline by 1 week post LPS injection (Chu et al., 2016), exemplifying the acute nature of the LPS model in comparison to live bacterial infection.

Data from young and middle-aged mice confirm significant increases in IFNγ and mKC levels at 4 weeks post Salmonella infection that was found in the initial analysis of retinal cytokine levels at 1 and 4 weeks post infection. However, it also identifies IL-1β, IL-6 and TNFα as significantly increased at 4 weeks post infection, whereas these were non-significant trends in the initial analysis. This discrepancy can be explained by much greater statistical power focused on the 4

week timepoint in young/middle aged analysis. Overall, these data indicate that most proinflammatory cytokines are still present in the retina at 4 weeks post infection, although at greatly reduced levels compared to 1 week.

Whether circulating cytokines diffuse into the CNS is debated within the literature. It is generally thought that local production of cytokines is responsible for CNS effects (e.g. sickness behaviours) (Dantzer et al., 2008). Consequently, an mRNA analysis was performed to determine whether cytokine changes observed are locally produced and to investigate a broader range of inflammatory pathways. In line with protein levels, pro-IL-1β and TNFα were increased at 1 week post infection. mRNA levels of pro-IL-1β and TNFα return to baseline level by 4 weeks post infection, while the protein levels are greatly reduced, but have not yet returned to baseline. These results neatly show a decrease in RNA expression preceding a reduction in protein expression, showing the benefits of investigating genes at an RNA level.

Neither pro-IL-1β mRNA or IL-1β measurements by mesoscale distinguish between pro- and mature IL-1β, a maturation process which is typically inflammasome dependent (Latz et al., 2013). Therefore, I investigated levels of inflammasome components and found upregulation of the Nlrp3 inflammasome gene, along with the co-component caspase-1 at 1 week post infection. Caspase-1 was one of the most upregulated and sustained genes of the 16 investigated, with expression still found after 4 weeks post infection. IL-18 maturation from pro-IL-18 is also inflammasome dependent, but no change was observed in mRNA levels of pro-IL-18. However, this gene showed one of the lowest C(t) values of the 16 genes investigated, which is not surprising as constitutive expression of pro-IL-18 has been observed in most animal cells, where its activity is minimised by IL-18 binding protein (Dinarello et al., 2013). If constitutively expressed, active IL-18 may be produced due to inflammasome activation despite an apparent lack of upregulation of pro-IL-18 at an mRNA level and this could be tested by western blot.

mRNA levels of the chemokine CCL2 (MCP-1) were also investigated due to its key role in mediating retinal inflammation after systemic LPS administration (Tuaillon et al., 2002). CCL2 showed a similar pattern to IL-1β and TNFα, with expression upregulated at 1 week and returned to baseline at 4 weeks post infection.

Cyclooxgenase 2 (COX2) was also upregulated at an mRNA level at 1 and 4 weeks post infection. Overall, it was the most upregulated and sustained gene of the 16 investigated. COX2 is responsible for the production of prostaglandins, lipid-based inflammatory mediators that have been previously described as critical for the cross-talk of inflammation between the systemic immune system and the brain (Teeling et al., 2007; Ek et al., 2001). Based on these data, it would

appear that COX2 is also a key component in converting systemic inflammation into local retinal inflammation.

The effect of Salmonella on oxidative stress was also considered. There were no significant changes in nNOS (neurons), iNOS (phagocytes) and eNOS (endothelium), although iNOS and eNOS were close to significance at 1 week post infection ($p=0.08$ and $p=0.06$ respectively). In contrast, at 1 week post infection there was a much stronger increase in NOX2, an NADPH oxidase pathway component responsible for generation of superoxides, a reactive oxygen species (ROS) that greatly contributes to oxidative stress in phagocytes (Panday et al., 2015). This indicates a role for oxidative stress in the retina following infection and is particularly interesting if nitric oxide (NO) is also generated by iNOS and eNOS, as NO and superoxides react to form peroxynitrite, one of the most toxic ROS family members (Li et al., 2005). In contrast, heme oxygenase-1, an oxidative stress response protein with antioxidant properties (Lundvig et al., 2012), was not found upregulated following Salmonella infection, indicating a balance towards oxidative stress.

Finally, two genes strongly related to AMD were analysed - VEGF and complement component C3. VEGF is the critical factor driving development of wet AMD in humans, while overactivity of the complement pathway is the strongest genetic risk factor for AMD development (Ferrara, 2010). There was no evidence that VEGF levels were increased by Salmonella infection, but C3 expression in the retina was elevated, representing a mechanism by which systemic infections could exacerbate retinal inflammation and possibly drive AMD progression.

3.4.5 Interplay between Salmonella infection and aging

Aging affects the systemic immune system with an increase in innate immunity and a decline in adaptive immunity that can contribute to prolonged and potentially damaging inflammation (Aw et al., 2007). Aging also affects the retinal immune system, with increased expression of microglial markers (e.g. CD11b, CD11b), cytokines/chemokines (e.g. TNFα, CCL2) and vascular markers (ICAM-1) reported in 20-month-old mouse retinas (Chen et al., 2010). Functionally, these age-related changes can have effects on the response to systemic inflammation; in aged (20-24 month old) mice, peripheral LPS injection results in higher expression of IL-1β and IL-6 in the brain as well as prolonged expression of IL-6 compared to young (3-month-old) controls (Godbout et al., 2005). As a result, I looked at whether aging could exacerbate the effect of a live bacterial infection on the retina, as observed for LPS and the brain.

No clear difference in weight changes following Salmonella infection were observed in young and middle-aged mice. Similarly, no significant changes in cytokine expression were observed in the serum of young and middle-aged mice infected with Salmonella, although there was a trend for

increased expression at 12 months. Regardless of whether aging primes the peripheral response to Salmonella or not, the retina showed no such trend; there is upregulation of IFNγ, IL-1β, IL-6, mKC and TNFα in the retina at 4 weeks following Salmonella, but this was not altered by aging. This indicates that aging, or at least being middle-aged, does not result in exacerbated retinal inflammation following systemic infection that could accelerate or drive neurodegeneration. Immunohistochemistry in these mice should be performed to check that this is also the case at the cellular level.

Despite no clear differences following Salmonella infection in young and middle-aged mice, several general aging effects were observed across experiments. Increased serum levels of IL-10 and mKC and increased retinal levels of IL-1β were observed due to aging in 12 month old mice compared to 3 month old mice. Increased levels of FcγRI, CD11b and ICAM-1 were observed between 5 and 9 month old mice and these findings could be supplemented by immunohistochemistry from the 3 and 12 month old mice. It would be interesting to look in older mice (20-24 months) to see if more extreme aging can exacerbate the response to systemic infections, as was seen in the brain for LPS (Godbout et al., 2005). A rationale for this comes from an AD patient study, where bacterial infection *P. gingivalis* accelerates cognitive decline in AD patients in a cohort with a mean age of 78 (Ide et al., 2016).

3.4.6 Summary

Systemic bacterial infection induces robust systemic innate and adaptive immune activation characterised by sustained peripheral cytokine production, most notably for IFNγ, and retinal inflammation characterised by BRB activation, microglial activation and production of pro-inflammatory cytokines. RNA analysis showed a broad range of upregulated inflammatory pathways in the retina following systemic infection (i.e. inflammasome, prostaglandins, complement and NADPH oxidase pathways) that may be interesting therapeutic targets to reduce the effect of systemic inflammation on the retina. In general, live bacterial infection with Salmonella provides reproducible systemic and retinal inflammation, which could be investigated for mechanistic insights into communication between the periphery and retina, along with functional consequences for retinal immune cell activation.

Chapter 4:

Retinal responsiveness to a secondary immune stimulus following systemic bacterial infection

4.1 Introduction

During life animals including humans and mice often experience inflammatory events, both local and systemic, due to a range of stimuli including intrinsic factors (e.g. neurodegeneration) and extrinsic factors (e.g. infection). Given that Salmonella infection can induce sustained inflammatory responses in the retina for at least one month post infection, I was interested in whether there are long-term functional consequences of such infection. These consequences could be hyper-responsiveness ("priming") and hypo-responsiveness ("tolerance") of the immune system to a subsequent immune stimulus, which have been observed previously in the periphery and brain (Locati et al., 2013). For example, mouse studies show that systemic Salmonella infection primes microglia in the mouse brain to respond in an exaggerated or 'primed' manner to local CNS inflammation (Püntener et al., 2012). This is interesting as local microglial changes have been identified in numerous neurodegenerative diseases, including Alzheimer's disease, Parkinson's disease, Huntingdon's disease, prion disease and AMD (Gomez-Nicola & Perry, 2015).

Previously in our lab, in order to assess responsiveness of microglia following Salmonella infection to subsequent local inflammation, intracerebral injections of low doses of LPS were performed (Püntener et al., 2012). LPS can be used as a bioassay to assess microglial priming to a secondary inflammatory stimulus, as it induces robust microglial activation by direct stimulation of TLR4 (and for some LPS strains TLR2) (Tapping et al., 2000). However, the previous study of microglial priming following Salmonella doesn't consider the functional response of microglia activated by Salmonella infection to respond to subsequent systemic inflammatory stimuli (Püntener et al., 2012). This paradigm is common in humans, particularly the elderly, many of whom suffer from chronic inflammatory diseases (e.g. autoimmune diseases) and show increased susceptibility, as well as a more chronic immune response, to infections (Aw et al., 2007; Nasa et al., 2012). Furthermore, this previous study of microglial priming following Salmonella doesn't consider whether the 'priming' effect is a specific CNS response or also occurs within the periphery.

In this chapter, I investigate whether Salmonella infection primes microglia to respond to further systemic immune activation. Here, LPS is used as secondary stimulus to test if the threshold for activation by a secondary challenge is altered by Salmonella infection. Additionally, because priming and tolerance can be influenced by many factors, both environmental and genetic, I chose to test these responses in two different mouse strains, C57BL/6 and BALB/c, to test for consistent effects of Salmonella, LPS, and their interaction amongst strains.

4.2 Methods

For this chapter, C57BL/6 and BALB/c mice were injected i.p. with saline or 10^6 cfu Salmonella (see section 2.1.2). Daily body weight was recorded and mice showing >20% body weight loss were culled. 4 weeks post injection, mice were given a subsequent i.p. injection of saline or 0.5mg/kg LPS (see section 2.1.2). 24hrs after this second injection, mice were transcardially perfused and tissue was harvested for analysis (see section 2.1.6). Serum samples were taken and analysed for cytokine levels by multiplex ELISA (Mesoscale Discovery, see section 2.5.3). Retinas were dissected, snap-frozen, homogenised in TRIS buffer and analysed for cytokine levels by multiplex ELISA (Mesoscale Discovery, see sections 2.5.1 and 2.5.3). Levels of retinal cytokines were normalised to total protein levels in the homogenate as assessed by BCA assay (see section 2.5.2). DAB immunohistochemistry using antibodies against CD3, CD11b, CD11c, FcγRI, ICAM-1, MHCI, MHCII, VCAM-1 was performed on 20µm fresh-frozen eye sections and quantified as percentage area of DAB staining (see section 2.2). Statistical tests used are described in each figure legend with full details and results of tests provided in Appendix B.

4.3 Results

4.3.1 Body weight changes following Salmonella infection and/or LPS injection

Physiological changes to live Salmonella infection and bacterial mimetic LPS (derived from Salmonella) were studied in two mouse strains to provide insight into their interaction and comparative chronicity. At 24 hours post infection, Salmonella induces weight loss of 8.3% in BALB/c mice ($p<0.0001$, Figure 4.1a) and 12.1% in C57BL/6 mice ($p<0.0001$, Figure 4.1b). Weight loss is significantly stronger in C57BL/6 mice compared to BALB/c mice ($p<0.0001$, Figure 4.1c). BALB/c mice demonstrate monophasic weight loss followed by complete recovery of weight by day 14 post infection. In contrast, C57BL/6 mice exhibit biphasic weight loss following Salmonella infection with weight gain after the initial weight loss (Day 2 vs Day 7, $p<0.0001$) followed by another period of weight loss (Day 7 vs Day 21, $p<0.0001$, Day 7 vs Day 28, $p=0.0044$). At no timepoint is there evidence that C57BL/6 mice fully recover their body weight compared to saline controls ($p<0.0001$). Overall, BALB/c mice have a lower starting weight (5.6%, $p<0.0001$) compared to C57BL/6 mice, despite being matched for age and gender (Figure 4.1d).

At 1 week post Salmonella infection, splenomegaly is observed in C57BL/6 mice (fold change ≈5.7, $p<0.0001$) and BALB/c mice (fold change ≈5.0, $p<0.0001$) compared to saline controls (Figure 4.2a). At 4 weeks post injection, splenomegaly is observed in C57BL/6 mice (fold change ≈5.5, $p<0.0001$) and BALB/c mice (fold change ≈3.4, $p<0.0001$), which is significantly larger in C57BL/6 mice (fold change ≈1.5, $p<0.0001$) compared to BALB/c mice.

In C57BL/6 mice, there is similar body weight loss at 24 hours post LPS injection (Figure 4.3a) in mice treated 4 weeks previously with Salmonella (8.4%, $p<0.0001$) or saline (9.6%, $p<0.0001$). BALB/c mice also show weight loss at 24 hrs post LPS injection (Figure 4.3b) in Salmonella (7.7%, $p<0.0001$) and saline injected (10.9%, $p<0.0001$) mice. LPS induced weight loss is significantly reduced in BALB/c mice previously infected with Salmonella compared to saline controls ($p<0.0001$).

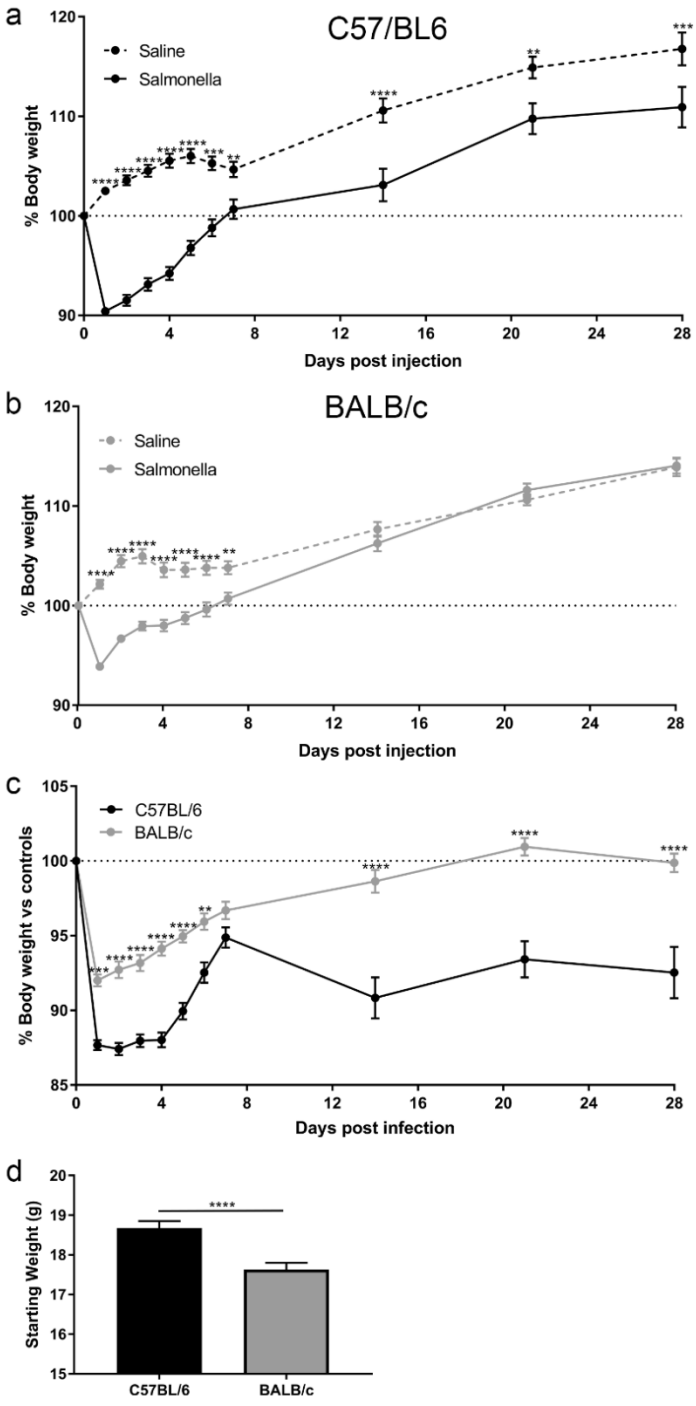

Figure 4.1 – Body and spleen weight changes following Salmonella infection in BALB/c and C57BL/6 mice.

*Body weight as a percentage of starting weight for (a) C57BL/6 and (b) BALB/c mice over 4 weeks following saline or Salmonella injection. (c) % Body weight following Salmonella injection over 4 weeks in C57BL/6 and BALB/c normalised to their respective saline controls. (d) Starting weight of C57BL/6 and BALB/c groups. Graphs are presented as mean±SEM (n=18-25 mice per group). Data was analysed using two-way ANOVA with Holm-Sidak post-hoc testing, except for starting weight, which was analysed by unpaired two-tailed T-test. Stars denote significance as follows: **p<0.01 ***p<0.001, ****p<0.0001.*

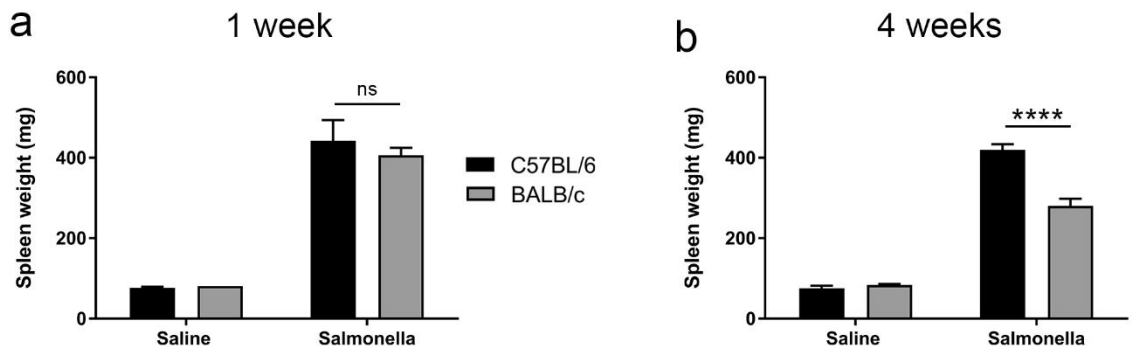

Figure 4.2 – Spleen weight following Salmonella infection in C57BL/6 and BALB/c mice.

*Spleen weight at (a) 1 week and (b) 4 weeks post saline or Salmonella injection. Graphs are presented as mean±SEM (n=4-8 mice per group). Data was analysed using two-way ANOVA with Holm-Sidak post-hoc testing. Stars denote significance as follows: ****p<0.0001, ns = not significant.*

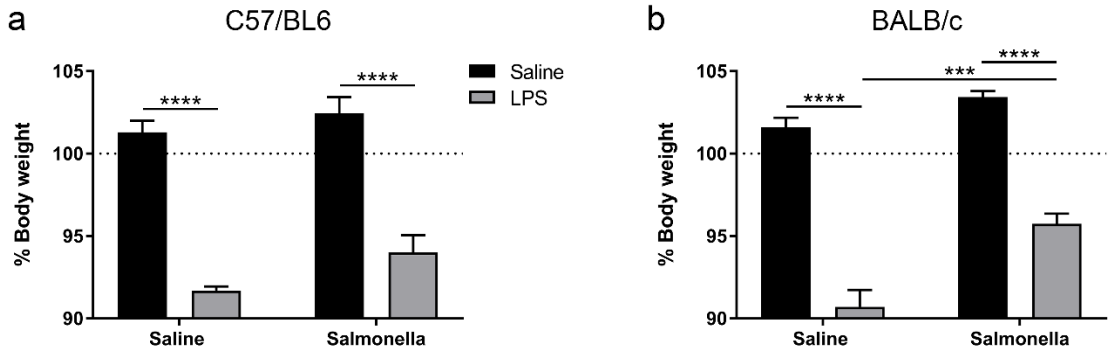

Figure 4.3 – Weight loss at 24hrs after peripheral saline or LPS injection in mice injected 4 weeks prior with saline or Salmonella.

*Percentage body weight change 24hrs post injection of 0.5mg/kg LPS or saline in (a) C57BL/6 and (b) BALB/c mice that have received an injection of saline or Salmonella 4 weeks before LPS injection. Graphs are presented as mean±SEM (n=4-5 mice per group). Data was analysed using two-way ANOVA with Holm-Sidak post-hoc testing. Stars denote significance as follows: ***p<0.001, ****p<0.0001.*

4.3.2 Peripheral cytokine changes following Salmonella infection and/or LPS injection

The peripheral inflammatory effect that Salmonella infection has alone and in conjunction with a subsequent LPS challenge was investigated to test for priming and tolerance effects (Figure 4.4).

4.3.2.1 IFNγ

Both C57BL/6 and BALB/c strains show increased serum levels of IFNγ following Salmonella infection, albeit at different levels (C57BL/6: fold change ≈500, $p<0.0001$, BALB/c: fold change ≈8, $p<0.0001$). The serum levels of IFNγ are further increased following LPS injection (C57BL/6: fold change ≈30, $p<0.0001$, BALB/c: fold change ≈2.5, $p=0.0112$). Salmonella infection and LPS injection show an additive effect when combined, although it appears the fold changes for IFNγ in BALB/c are much smaller than in C57BL/6.

4.3.2.2 IL-1β, IL-6, IL-12 and mKC

In C57BL/6 mice, this additive inflammatory effect of Salmonella infection and LPS injection is also observed for IL-1β (Salmonella: fold change ≈6, $p<0.0001$, LPS: fold change ≈7, $p<0.0001$), IL-6 (Salmonella: fold change ≈2.3, $p=0.0471$, LPS: fold change ≈12, $p<0.0001$) and IL-12 (Salmonella: fold change ≈3, $p=0.0087$, LPS: fold change ≈5, $p=0.0011$), whereas a dominant LPS response is observed for mKC (LPS: fold change ≈8, $p<0.0001$). Notably, IL-12 also shows an interaction effect ($p=0.0239$) indicating that there is a super-additive or 'priming' effect of Salmonella infection on the subsequent response to LPS.

In BALB/c mice, LPS induces increased serum levels of IL-1β (fold change ≈2.2, $p<0.0001$), IL-6 (fold change ≈5, $p<0.0014$), IL-12 (fold change ≈5, $p=0.0192$) and mKC (fold change ≈3.2, $p<0.0001$), as seen in C57BL/6 mice. However unlike in C57BL/6 mice, there are reduced levels of serum cytokines following Salmonella infection for IL-1β (fold change ≈1.8, $p=0.0008$), IL-12 (fold change ≈7, $p=0.0033$), mKC (fold change ≈3.2, $p<0.0001$) and a trend for IL-6 (fold change ≈3.1, $p=0.0512$). There is an interaction factor for IL-6 ($p=0.0164$) and mKC ($p=0.0002$), showing an inhibitory or 'tolerance' effect of Salmonella infection on the subsequent response to LPS.

4.3.2.3 TNFα

C57BL/6 mice exhibit increased TNFα levels at 4 weeks post Salmonella infection ($p=0.0099$), and a trend to increased levels after LPS ($p=0.0916$) However, there is substantial variation in the combined Salmonella and LPS injected group. BALB/c mice show an increase due to both Salmonella infection ($p<0.0001$) and LPS injection ($p<0.0001$) along with a tolerance response where the effect of LPS, in terms of TNFα production, is diminished in Salmonella infected mice when compared to saline controls ($p=0.0177$).

Overall, these results show that several cytokines are increased in an additive or super-additive manner due to Salmonella infection and LPS injection in C57BL/6 mice, which is indicative of Salmonella-induced priming. In contrast, BALB/c mice show increased inflammation due to LPS, which is decreased for several cytokines when the mice are previously infected with Salmonella, which is indicative of Salmonella-induced tolerance.

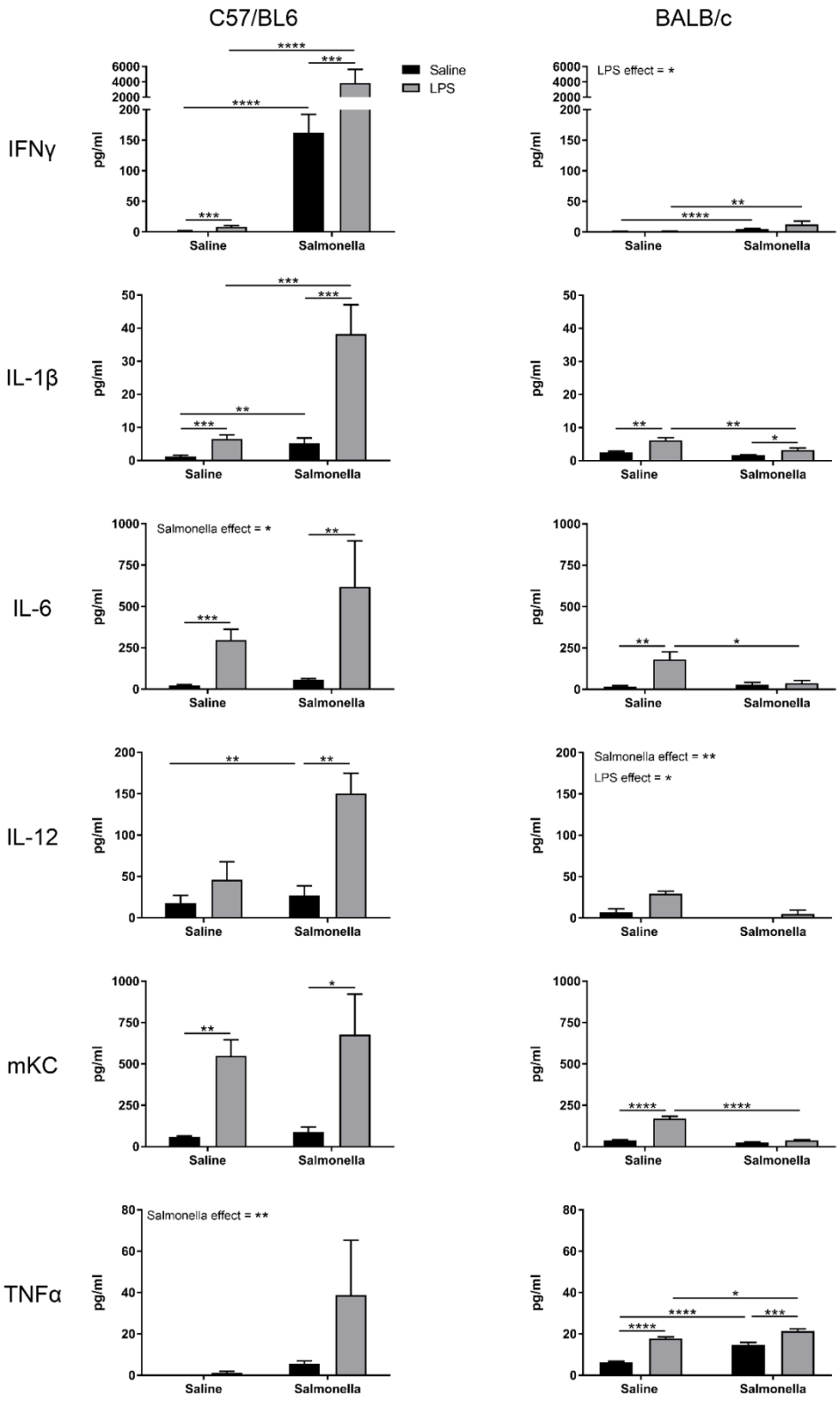

Figure 4.4 – Serum cytokine levels at 24hrs post peripheral saline or LPS injection in mice injected 4 weeks prior with saline or Salmonella.

*Serum cytokine levels of IFNγ, IL-1β, IL-6, IL-12, mKC and TNFα were quantified using multiplex ELISA (Mesoscale Discovery). Graphs are presented as mean±SEM (n=4-5 mice per group). Data was analysed using two-way ANOVA with Holm-Sidak post-hoc testing. Stars denote significance as follows: *p<0.05, **p<0.01, ***p<0.001, ****p<0.0001.*

4.3.3 Retinal cytokine levels following Salmonella and LPS injection

Retinal cytokine levels following Salmonella infection and/or LPS injection were assayed next. IL-12, mKC and TNFα show the same trends between C57BL/6 and BALB/c mice (Figure 4.5). IL-12 is not significantly changed by Salmonella infection or LPS injection, while TNFα levels are increased by LPS only (C57BL/6 fold change ≈1.3, p=0.0050; BALB/c fold change ≈1.5, p=0.0040). mKC levels in the retina are increased by LPS following previous saline treatment (C57BL/6 fold change ≈8, p<0.0001; BALB/c fold change ≈9, p<0.0001) and Salmonella infection (C57BL/6 fold change ≈2.2, p=0.0366; BALB/c fold change ≈4, p=0.0224). However, the increases in mKC caused by LPS are reduced in the Salmonella infected groups (C57BL/6 fold change ≈1.8, p=0.0476; BALB/c fold change ≈1.8, p=0.0224) compared to the saline controls, indicating that Salmonella infection induces retinal tolerance to LPS.

Both C57BL/6 and BALB/c mice show an increase in retinal IL-1β in response to LPS (C57BL/6: fold change ≈1.5, p=0.0022, BALB/c: fold change ≈1.9, p=0.0003) which is not observed in mice previously infected with Salmonella (C57BL/6: fold change ≈1.3, p=0.0375, BALB/c: fold change ≈1.7, p=0.0035). However, in BALB/c mice there is a significant interaction factor (p=0.0051), indicating that Salmonella infection induces retinal tolerance to LPS in this strain, which is not seen in C57BL/6 mice. LPS increases retinal IL-6 levels in C57BL/6 mice (fold change ≈1.3, p=0.0057), but not in BALB/c mice. IFNγ levels are increased by Salmonella infection in C57BL/6 mice (fold change ≈3.4, p<0.0001), but by LPS in BALB/c mice (fold change ≈1.3, p=0.0164).

Overall, the retinal cytokines show substantially different expression patterns due to Salmonella infection, systemic LPS injection and their interaction. These trends are the same between C57BL/6 and BALB/c mice for IL-12, mKC and TNFα with Salmonella-induced tolerance to LPS challenge particularly clear for mKC. Retinal tolerance is consistent between these strains despite differences in the responsiveness of the systemic immune system.

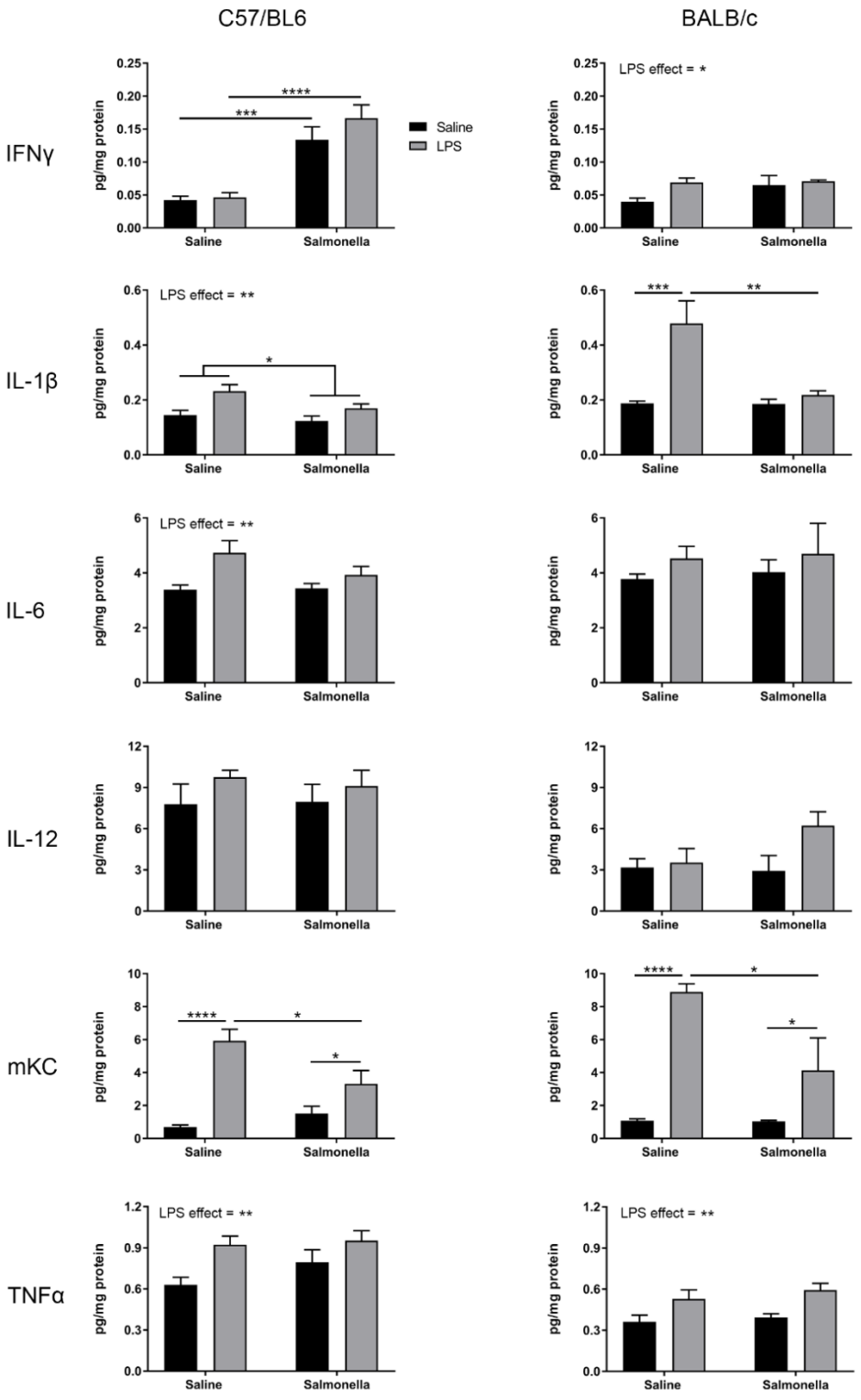

Figure 4.5 – Retinal cytokine levels at 24hrs after peripheral saline or LPS injection in mice injected 4 weeks prior with saline or Salmonella.

*Retinal cytokine levels of IFNγ, IL-1β, IL-6, IL-12, mKC and TNFα were quantified using multiplex ELISA (Mesoscale Discovery) and normalised to total protein levels quantified by BCA assay. Graphs are presented as mean±SEM (n=4-6 mice per group). Data was analysed using two-way ANOVA with Holm-Sidak post-hoc testing. Stars denote significance as follows: *p<0.05, **p<0.01, ***p<0.001, ****p<0.0001.*

4.3.4 Retinal cellular changes following Salmonella infection and/or LPS injection

As activation of retinal blood vessels and microglia are key features of Salmonella infection in C57BL/6 mice, I investigated the effect of LPS alone or in combination with Salmonella infection on these parameters in both strains.

4.3.4.1 Blood vessel changes

MHCII is highly expressed at 4 weeks post Salmonella infection in both C57BL/6 (fold change ≈50, $p<0.0001$) and BALB/c (fold change ≈10, $p<0.0001$) mice (Figure 4.6a). LPS causes decreased MHCII expression in C57BL/6 mice (fold change ≈1.5, $p=0.0223$) and, by contrast, increased expression of MHCII in BALB/c mice (fold change ≈1.6, $p=0.0310$). MHCI is also upregulated at 4 weeks post Salmonella infection (fold change ≈20, $p<0.0001$) in C57BL/6 mice (Figure 4.6b), but this was not tested in BALB/c mice. Both MHCI and MHCII are expressed solely on the inner retinal blood vessels.

ICAM-1 is upregulated by Salmonella infection in C57BL/6 mice (fold change ≈7, $p<0.0001$), but contrastingly LPS induces upregulation of ICAM-1 in BALB/c mice (fold change ≈5, $p<0.0001$) (Figure 4.7a). Interestingly, LPS-induced ICAM-1 expression is abolished in BALB/c mice infected with Salmonella ($p=0.0021$). VCAM-1 is upregulated by Salmonella infection in C57BL/6 mice (fold change ≈2.5, $p=0.0017$), but by LPS in BALB/c (fold change ≈2.2, $p=0.0128$) mice (Figure 4.7b). ICAM-1 and VCAM-1 expression is localised to inner retinal blood vessels with arteriole staining similar between all groups, whereas inner retinal capillaries express both markers following Salmonella infection in C57BL/6 mice and LPS in BALB/c mice.

4.3.4.2 Microglial changes

FcγRI expression is increased on myeloid cells following Salmonella infection in C57BL/6 (fold change ≈4.3, $p=0.0013$) mice, but by LPS in BALB/c (fold change ≈1.6, $p=0.0456$) mice (Figure 4.8a). CD11b is also increased by Salmonella infection in C57BL/6 (fold change ≈2, $p=0.0264$) mice, but not significantly by LPS in BALB/c mice ($p=0.1390$), although there is a similar trend to FcγRI (Figure 4.8b). CD11c expression is increased by Salmonella infection (fold change ≈5, $p=0.0032$), but decreased by LPS (fold change ≈2, $p=0.0490$) in C57BL/6 mice (Figure 4.9). CD11c staining was performed in BALB/c mice, but no staining of any cells was observed, including in the choroid or muscle, which contain peripheral immune cells (data not shown).

4.3.4.3 T cell changes

The number of CD3+ cells is increased in the retina following Salmonella infection in C57BL/6 mice (fold change ≈20, $p<0.0001$), but not BALB/c mice (Figure 4.10). In C57BL/6 mice, there is also a trend to reduced T cell numbers in the retina following Salmonella infection when LPS was given compared to saline ($p=0.0680$).

Overall, these data indicate that MHCII expression on blood vessels following Salmonella infection is the only similarity between these two strains, with a strong inflammatory response to Salmonella infection in C57BL/6 mice and LPS injection in BALB/c mice. There no evidence for interaction between these stimuli except for ICAM-1 expression in BALB/c mice.

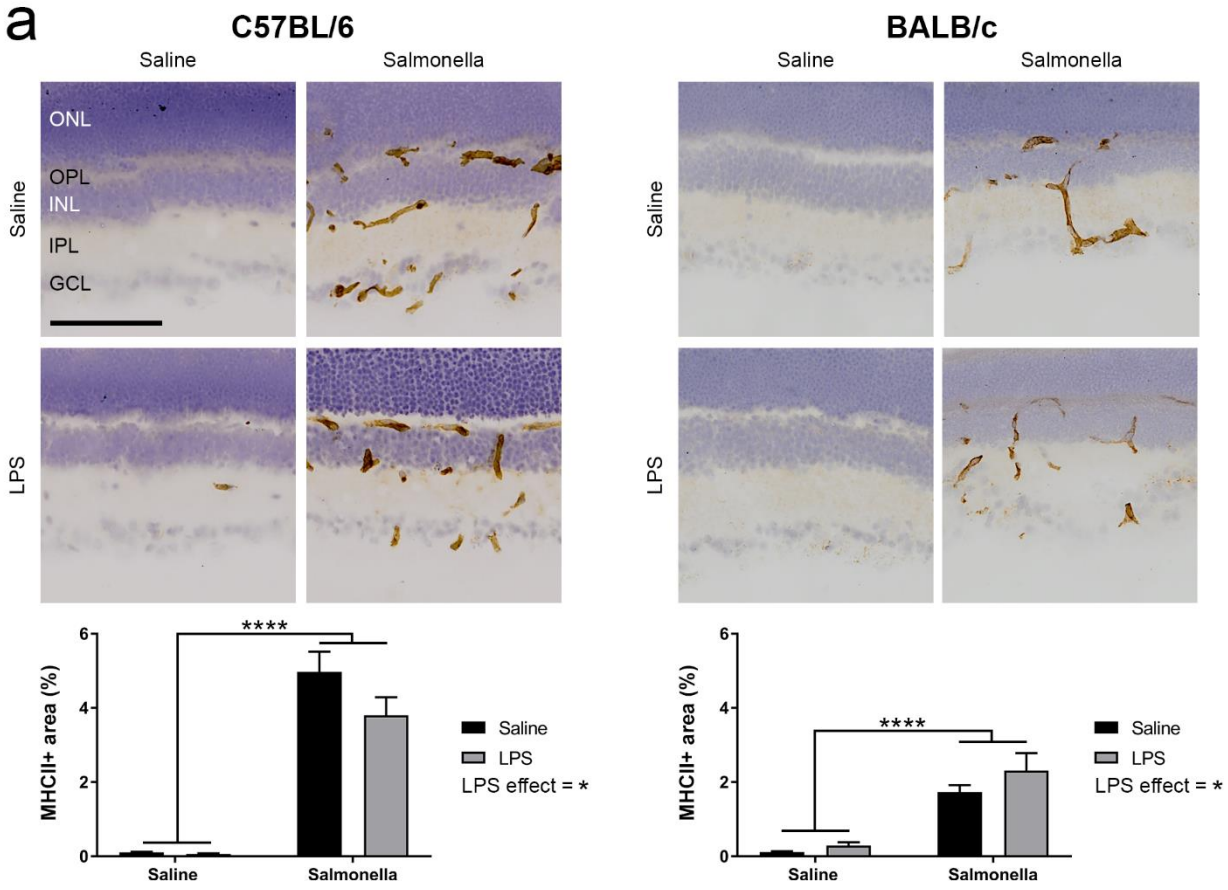
a
C57BL/6
Saline
Salmonella
ONL
OPL
INL
IPL
GCL
Saline
LPS
MHCII+ area (%)
****
Saline
LPS
LPS effect = *
BALB/c
b
C57BL/6
MHCI+ area (%)

Figure 4.6 – Expression of MHCI and MHCII at 24hrs after peripheral saline or LPS injection in mice injected 4 weeks prior with saline or Salmonella.

*Representative images and quantification of percentage area of DAB immunoreactivity against (a) MHCII in C57BL/6 and BALB/c mice and (b) MHCI in C57BL/6 mice. Graphs are presented as mean±SEM (n=4-5 mice per group). Data was analysed using two-way ANOVA. Stars denote significance as follows: *p<0.05, ****p<0.0001. Images were taken with a 20x objective and scale bars represent 100µm. ONL, outer nuclear layer; OPL, outer plexiform layer; INL, inner nuclear layer; IPL, inner plexiform layer; GCL, ganglion cell layer.*

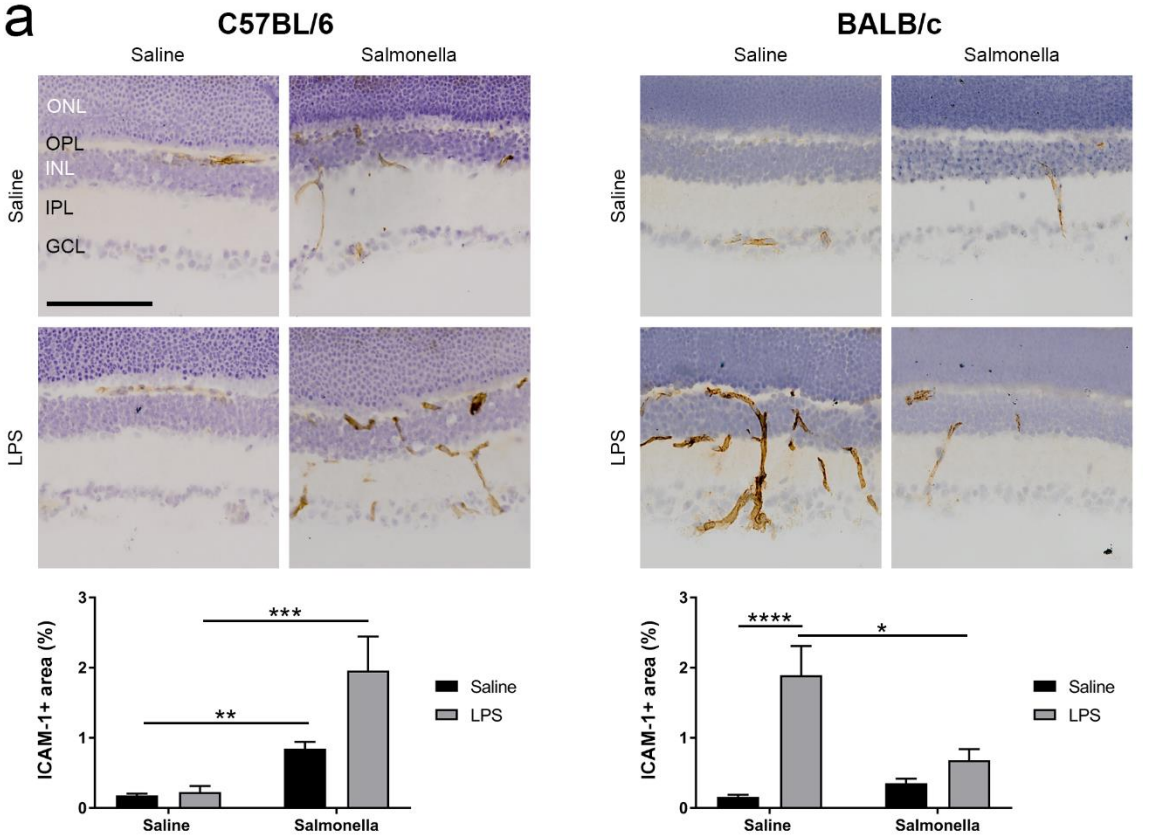
a
C57BL/6
BALB/c
Saline
Salmonella
ONL
OPL
INL
IPL
GCL
Saline
LPS
ICAM-1+ area (%)
***
**
****
*
Saline
LPS

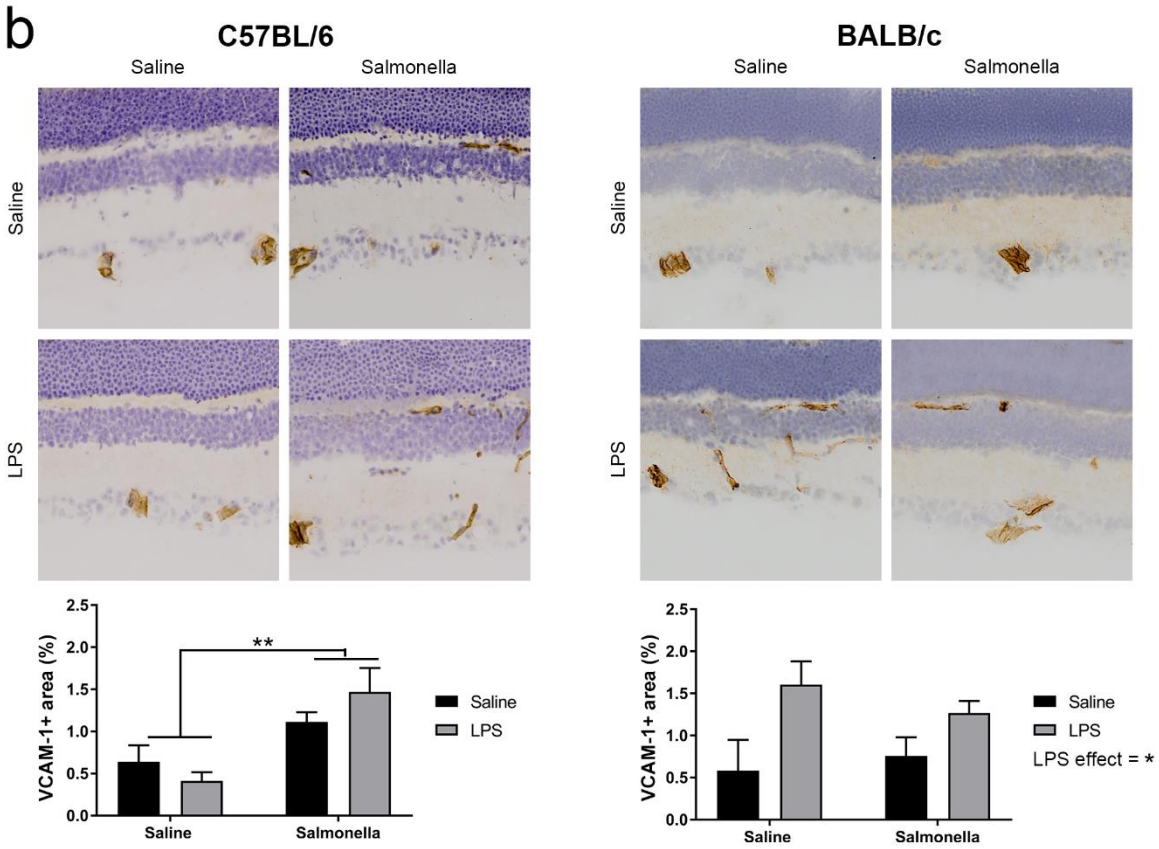
b
C57BL/6
BALB/c
Saline
Salmonella
Saline
LPS
VCAM-1+ area (%)
**
Saline
LPS
LPS effect = *

Figure 4.7 – Expression of ICAM-1 and VCAM-1 at 24hrs after peripheral saline or LPS injection in mice injected 4 weeks prior with saline or Salmonella.

*Representative images and quantification of percentage area of DAB immunoreactivity against (a) ICAM-1 and (b) VCAM-1 in C57BL/6 and BALB/c mice are provided. VCAM-1 percentage area is calculated as stained area as a percentage of total retinal area. ICAM-1 percentage area is calculated as stained area as a percentage of inner retinal area due to confounding ICAM-1 staining in the photoreceptor layer. Graphs are presented as mean±SEM (n=4-5 mice per group). Data was analysed using two-way ANOVA with Holm-Sidak post-hoc testing. Stars denote significance as follows: *p<0.05, **p<0.01, ***p<0.001, ****p<0.0001. Images were taken with a 20x objective and scale bars represent 100µm. ONL, outer nuclear layer; OPL, outer plexiform layer; INL, inner nuclear layer; IPL, inner plexiform layer; GCL, ganglion cell layer.*

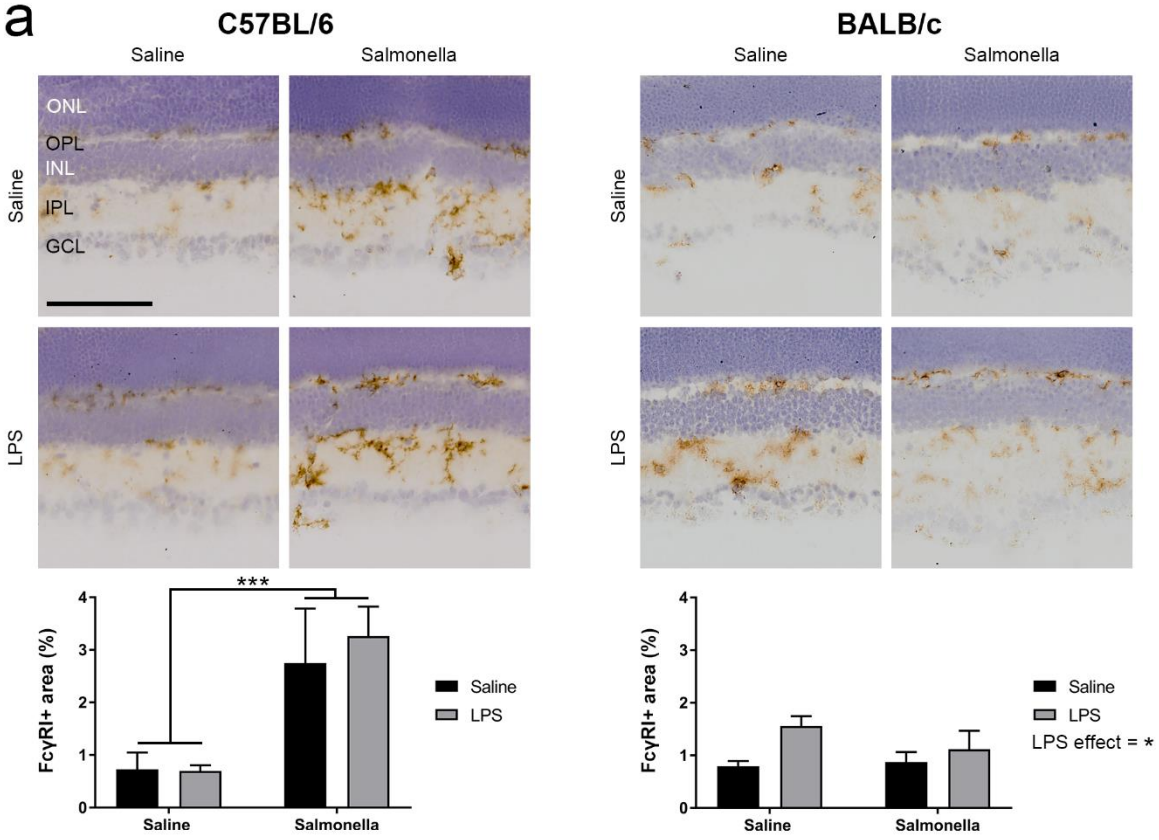
a
C57BL/6
BALB/c
Saline
Salmonella
ONL
OPL
INL
IPL
GCL
Saline
LPS
FcγRI+ area (%)
***
Saline
LPS
LPS effect = *

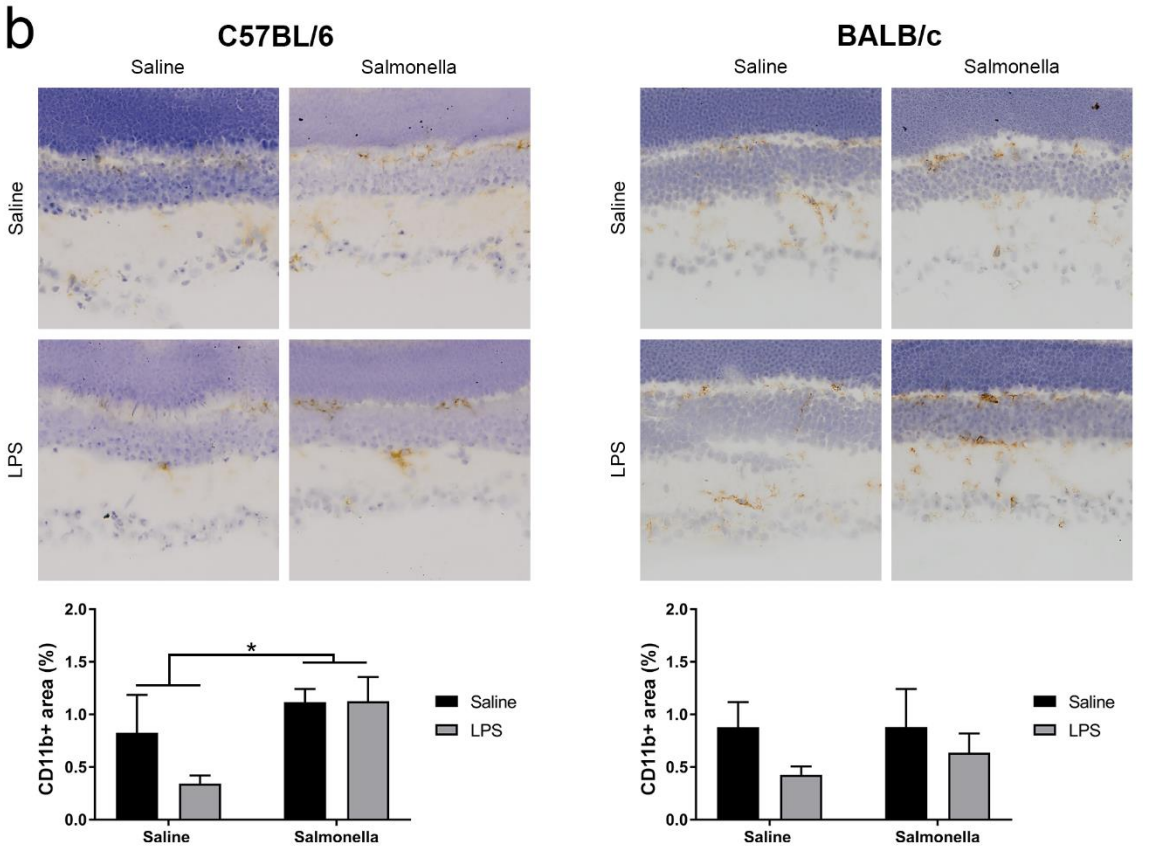
b
C57BL/6
BALB/c
Saline
Salmonella
Saline
LPS
CD11b+ area (%)
*
Saline
LPS

Figure 4.8 – Expression of FcγRI and CD11b at 24hrs after peripheral saline or LPS injection in mice injected 4 weeks prior with saline or Salmonella.

*Representative images and quantification of percentage area of DAB immunoreactivity against (a) FcγRI and (b) CD11b in C57BL/6 and BALB/c mice are provided. FcγRI and CD11b staining appears localised to microglia in the inner retinal layers. Graphs are presented as mean±SEM (n=4-5 mice per group). Data was analysed using two-way ANOVA. Stars denote significance as follows: *p<0.05, ***p<0.001. Images were taken with a 20x objective and scale bars represent 100µm. ONL, outer nuclear layer; OPL, outer plexiform layer; INL, inner nuclear layer; IPL, inner plexiform layer; GCL, ganglion cell layer.*

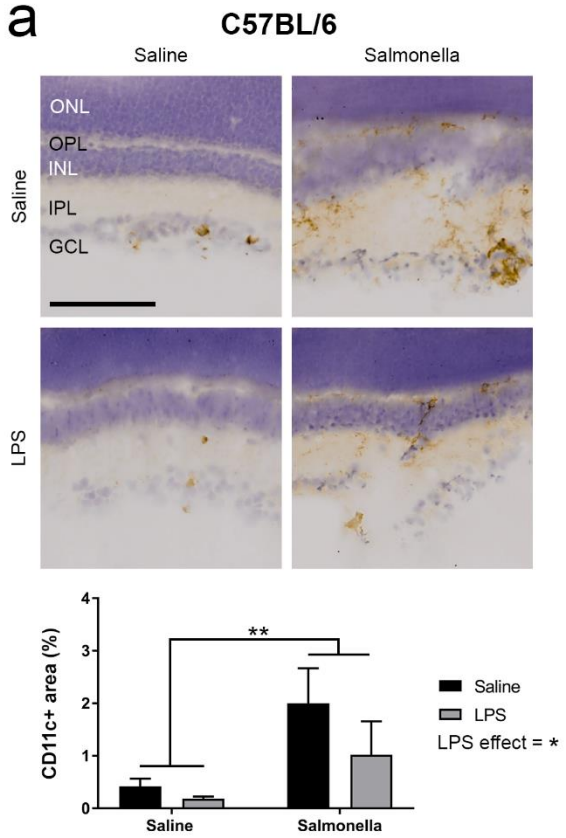

Figure 4.9 – Expression of CD11c at 24hrs after peripheral saline or LPS injection in mice injected 4 weeks prior with saline or Salmonella.

*Representative images and quantification of percentage area of DAB immunoreactivity against (a) CD11c in C57BL/6 mice are provided (n=3-5 mice per group). CD11c staining in the retina appears to be localised to microglia in the inner retinal layers. Graphs are presented as mean±SEM. Data was analysed using two-way ANOVA. Stars denote significance as follows: *p<0.05. **p<0.01. Images were taken with a 20x objective and scale bars represent 100µm. ONL, outer nuclear layer; OPL, outer plexiform layer; INL, inner nuclear layer; IPL, inner plexiform layer; GCL, ganglion cell layer.*

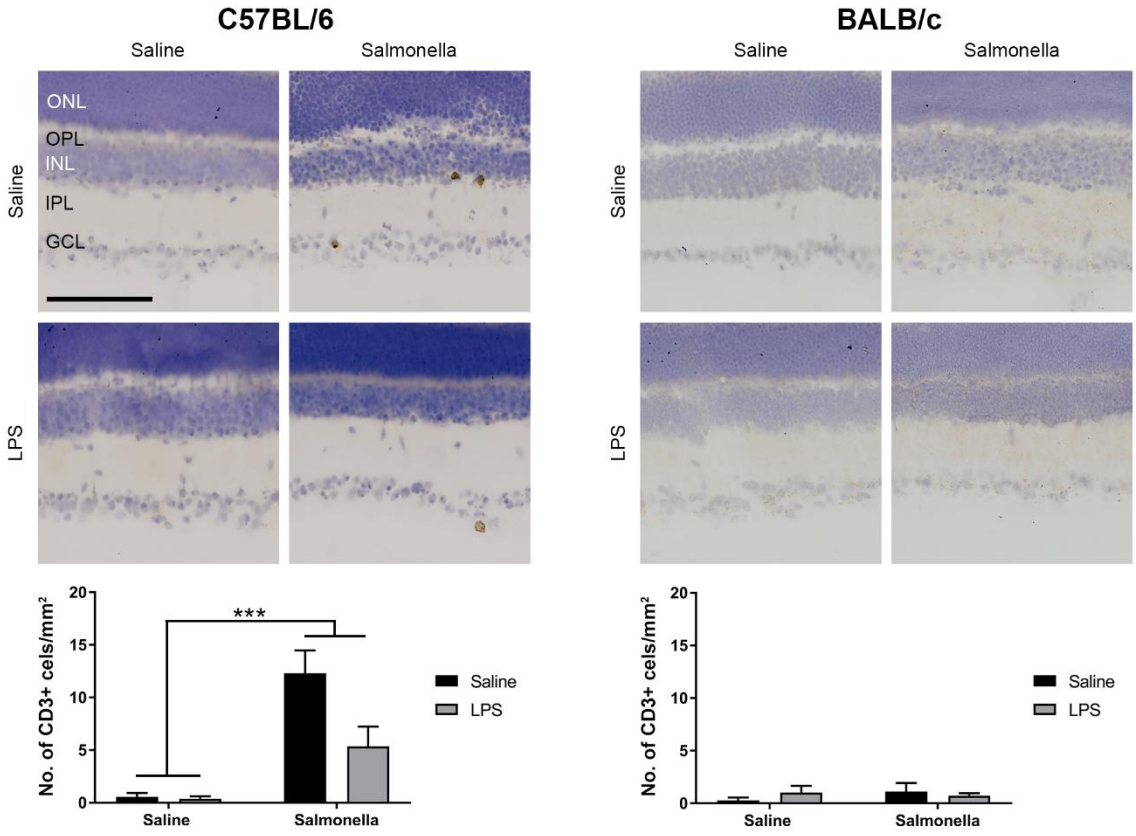

Figure 4.10 – Enumeration of CD3+ T cells at 24hrs after peripheral saline or LPS injection in mice injected 4 weeks prior with saline or Salmonella.

*Representative images and quantification of number of CD3+ cells per mm^2 of retina in C57BL/6 and BALB/c mice (n=4-5 mice per group). T cells are mainly localised in the inner retinal layers, although occasionally T cells are seen in the outer layers. Graphs are presented as mean±SEM. Data was analysed using two-way ANOVA. Stars denote significance as follows: ***p<0.001. Images were taken with a 20x objective and scale bars represent 100µm. ONL, outer nuclear layer; OPL, outer plexiform layer; INL, inner nuclear layer; IPL, inner plexiform layer; GCL, ganglion cell layer.*

4.4 Discussion

4.4.1 Inflammation induced weight loss in C57BL/6 and BALB/c mice

Weight loss induced by infections varies greatly depending on the specific pathogen and the mouse strain used. For example, BALB/c mice lose more weight in response to avian influenza virus H7N9 compared to C57BL/6 mice, but the opposite is true for Neuraodapted Sindbis virus (Thach et al., 2000; Zhu et al., 2013b). Both C57BL/6 and BALB/c mice are known to be susceptible to Salmonella infection (Roy & Malo, 2002), but to my knowledge, no study has compared weight loss in C57BL/6 and BALB/c mice specifically for Salmonella infection. C57BL/6 mice exhibit biphasic weight loss comprised of initial weight loss driven by sickness behaviours followed by a second period of weight loss, which is strongest at 2 weeks post infection. It is unclear what drives this second phase of weight loss, but it may represent the energy demands of the adaptive immune response. In contrast, BALB/c mice show monophasic weight loss with an initial weight loss that gradually recovers by 2 weeks post infection. C57BL/6 mice lose approximately 50% more weight than BALB/c mice at 1 day post infection, which likely reflects reduced anorexia in BALB/c mice compared to C57BL/6 mice (Hart, 1988).

Interestingly, C57BL/6 mice never recover the initial weight lost after Salmonella infection compared to saline controls, but by two weeks post infection BALB/c mice have returned to the normal control weight. In diet studies, BALB/c mice on normal diet gain more weight than C57BL/6 mice by 32 weeks of age, however, when fed with high fat diet (HFD) for 24 weeks, C57BL/6 mice gain more weight than BALB/c mice, showing that these strains have metabolic differences, which can be influenced by environmental factors (Jovicic et al., 2015). This gives an indication that differential immune responses in these strains could result in altered metabolic responses to stressful conditions such as Salmonella infection.

In contrast to Salmonella infection, C57BL/6 and BALB/c mice show similar weight loss at 24hrs after LPS injection. Again, this exemplifies some differences observed between live Salmonella infection and mimetic LPS. It is unclear what difference between these stimuli is responsible for this absence or presence of differential weight loss between BALB/c and C57BL/6 mice. Sickness behaviours are generally thought to be driven by the innate immune system, however LPS also strongly stimulates B cells to produce cytokines, which may drive consistent weight loss between strains (Vaure & Liu, 2014; Dantzer, 2004).

When BALB/c mice are pre-treated with Salmonella, the body weight loss induced by LPS is reduced compared to non-infected mice, but this effect is not observed in C57BL/6 mice. Consequently, there is either a metabolic difference between the C57BL/6 and BALB/c mice or

there is a tolerance effect in BALB/c mice. BALB/c mice have a T_H2-dominant immune response, which is associated with inhibition of macrophages due to IL-10 and arginase production (Mills et al., 2000). This inhibitory environment for macrophages following Salmonella infection in BALB/c mice may well underpin reduced sickness behaviour in response to a secondary immune challenge with LPS. Another reason may be that LPS contained within the Salmonella tolerises the immune system to a subsequent LPS challenge, although if this were the case, there isn't a clear reason why C57BL/6 mice would be unaffected.

4.4.2 Cytokine induction in C57BL/6 and BALB/c mice

At 4 weeks post Salmonella infection, serum IFNγ and TNFα are upregulated in C57BL/6 and BALB/c mice, but the total levels of IFNγ are hugely different (C57BL/6: 160pg/ml, BALB/c: 5pg/ml). IFNγ is a critical cytokine for development of T_H1 cells and suppresses the expansion of T_H2 cells (Scott, 1991; Mills et al., 2000). In line with this, higher IFNγ production in C57BL/6 drives a more T_H1 dominant immune response than BALB/c mice, which produce much less IFNγ. Pro-inflammatory cytokines IL-1β, IL-6 and IL-12 are also upregulated at 4 weeks post infection in C57BL/6 mice, whereas IL-1β, IL-12 and mKC are downregulated at 4 weeks post infection in BALB/c mice, further highlighting these peripheral differences. IL-12 is also a key factor driving T_H0 cell (naïve undifferentiated T cells) differentiation towards a T_H1 dominant immune response (Lapaque et al., 2009) so the differential expression of this cytokine in C57BL/6 and BALB/c mice is not surprising.

In response to LPS, both C57BL/6 and BALB/c mice show increased serum IFNγ, IL-1β, IL-6, IL-12, mKC and TNFα at 24 hours post injection, with the sole exception of TNFα in C57BL/6 mice, which showed the same trend (p=0.09). Consequently, the results for LPS amongst strains show greater consistency than for Salmonella infection. Typically, serum cytokines and chemokines are increased at 2-4 hours following LPS, but have returned to low/baseline levels by 24-28 hours post injection (Biesmans et al., 2013; Erickson & Banks, 2011). However, in this study there is upregulation of a range of cytokines at 24 hours post LPS injection, which may be because a particularly high dose (0.5mg/kg) was used. The dose, species and strain of LPS derivation, endotoxin units per batch and supplier all contribute to lack of reproducibility of these results between labs.

The most interesting serum cytokine changes are observed when these two immune stimuli are combined. In C57BL/6 mice, the combination of Salmonella infection and LPS results in additive inflammation for serum IFNγ, IL-1β, IL-6 and super-additive or 'primed' inflammation for IL-12. TNFα shows a similar non-significant trend, while LPS, but not Salmonella infection, seems to

cause dominant increases in mKC. This is similar to observations from brain microglia in C57BL/6 mice, which are primed to respond in an exaggerated manner to local inflammation induced by LPS (Püntener et al., 2012). In contrast, BALB/c mice show a similar additive trend for only IFNγ, although the total levels following both immune stimuli are hugely reduced in BALB/c mice compared to C57BL/6 mice (C57BL/6: 3860pg/ml, BALB/c: 12.5pg/ml). LPS induction of serum IL-1β, IL-6, mKC and TNFα are reduced in BALB/c mice previously injected with Salmonella compared to saline. This gives further indications of tolerance in the BALB/c mice, which are not observed in C57BL/6 mice and fits with the reduction in LPS-induced weight loss observed in BALB/c mice compared to C57BL/6 mice. It would be very interesting to look at the serum levels of T_H2 associated cytokines (IL-4, IL-5, IL-10) (Pashine et al., 1999) to see whether these are preferentially increased in BALB/c mice over C57BL/6 mice. Transcriptomic analysis has shown stronger differences in T cell gene expression between different mouse strains compared to other factors such as gender (Bearoff et al., 2016), although to my knowledge C57BL/6 and BALB/c mice have not been directly compared.

Although serum cytokines in C57BL/6 and BALB/c mice show different patterns, the retinal cytokines are more similar. In both strains, LPS increases retinal levels of IL-1β, mKC, TNFα, but not IL-12. IFNγ shows clear differential expression in the retina, with Salmonella infection inducing increased IFNγ in C57BL/6 mice, but LPS inducing increased IFNγ in BALB/c mice. Both C57BL/6 and BALB/c mice show remarkable similarity in mKC levels, where expression following LPS is reduced when mice are previously infected with Salmonella. BALB/c mice also show this effect for IL-1β and the same trend is observed for IL-1β in C57BL/6 mice ($p=0.29$). Overall these data indicate that despite completely different systemic immune responses in terms of priming and tolerance effects, the retina appears to show tolerance to subsequent inflammation in both C57BL/6 and BALB/c mice. The exception to this is IFNγ, which shows additive increases in both the serum and retina due to Salmonella infection and LPS. Priming and tolerance of the CNS has been mainly assessed via microglial activation in immunohistochemistry (Püntener et al., 2012), and these cytokines provide more insights into the type of activation.

4.4.3 Blood vessel activation in C57BL/6 and BALB/c retinas

A dramatic change found after Salmonella infection is the expression of MHCII on the retinal blood vessels in C57BL/6 and BALB/c mice. Staining appears stronger in C57BL/6 mice than BALB/c mice and IFNγ is a key regulator of MHCII expression on endothelial cells (Collins et al., 1984), so increased expression of MHCII on retinal blood vessels in C57BL/6 mice compared with BALB/c mice would be in line with the peripheral levels of IFNγ in these strains. However, it must be considered that these strains possess different MHC haplotypes (Baumgart et al., 1998). The

antibody used is known to work for both the H-2b (C57BL/6) and H-2d (BALB/c) haplotypes of MHCII, however, it is not clear if these structural differences may alter the affinity of the antibody for MHCII in the different strains, making it hard to prove differences in expression between strains via immunohistochemistry.

LPS further increases MHCII expression in BALB/c mice, but not in C57BL/6 mice, although these changes were small in comparison to the effect of Salmonella infection on MHCII expression. Another antigen-presenting molecule MHCI is also greatly increased on blood vessels in C57BL/6 mice. Staining was not performed in BALB/c mice and this should be tested to check MHCI is also upregulated following Salmonella infection in BALB/c mice.

Salmonella infection also induces the expression of ICAM-1 and VCAM-1 on retinal blood capillaries in C57BL/6 mice, but not in BALB/c mice. In contrast, LPS induces the expression of ICAM-1 and VCAM-1 on retinal blood capillaries in BALB/c mice, but not C57BL/6 mice. Most notably, following Salmonella infection, LPS does not induce ICAM-1 expression in BALB/c mice, again indicating a role of tolerance. Both ICAM-1 and VCAM-1 are cell adhesion molecules responsible for the recruitment of peripheral immune cells to inflamed tissues and are mainly upregulated by cytokines IL-1β and TNFα (Dustin et al., 1986; Cook-Mills et al., 2011; Myers et al., 1992). Peripheral IL-1β looks like a likely candidate responsible for inducing ICAM-1 and VCAM-1, as the patterns of serum IL-1β and retinal ICAM-1/VCAM-1 expression are remarkably similar in this study.

4.4.4 Myeloid cells in C57BL/6 and BALB/c retinas

Microglial activation following Salmonella infection, as assessed by FcγRI and CD11b expression, is observed in C57BL/6 mice, but not BALB/c mice. There is also a substantial increase in CD11c in C57BL/6 mice, as further evidence of microglial activation, but the antibody didn't stain any retinal cells in BALB/c mice. It is unclear whether this is due to lack of expression of CD11c or whether there may be some strain differences in CD11c structure. However, previous immunohistochemistry studies have shown CD11c expression on BALB/c mice splenocytes and liver using this antibody (Witmer-Pack et al., 1993; De Smedt et al., 1997), arguing for a lack of expression in this strain.

A lack of microglial activation in BALB/c mice could be due to differences in peripheral immune response, for example IFNγ is responsible for the migration of microglia to the subretinal space following viral infection (Zinkernagel et al., 2013) and is much higher in C57BL/6 mice than BALB/c mice. Alternatively, differences may be due to distinct activation patterns of retinal blood vessels between strains. Both strains express MHCII after Salmonella, but C57BL/6 also expresses ICAM-1

and VCAM-1. There may be functional consequences for the blood vessels (e.g. prostaglandin synthesis, tight junction permeability) of these distinct phenotypes, which are important in immune-to-brain communication and microglial activation (Ek et al., 2001; Khandaker & Dantzer, 2016).

C57BL/6 mice show activation of microglia following Salmonella infection in terms of FcγRI, CD11b and CD11c expression. In contrast, there is no evidence for microglial activation in BALB/c mice following Salmonella infection, but there is increased expression of FcγRI after LPS. However, complement receptors CD11b and CD11c show the opposite trends in expression to FcγRI, with both CD11b and CD11c appearing lower after LPS in BALB/c mice, although this is not significant for CD11b ($p=0.11$). These data may show that there is a differential regulation of FcγRI, CD11b and CD11c on retinal microglia depending on immune stimuli. Consistent with this, LPS has been shown to increase FcγRI expression in the brain, but not CD11c in young or aged mice (Hart et al., 2012).

4.4.5 Lymphoid cells in C57BL/6 and BALB/c retinas

Salmonella infection causes T cell infiltration (defined as CD3+) into the retina in C57BL/6 mice, but not in BALB/c mice. A lack of ICAM-1/VCAM-1 expression on the retinal blood capillaries may prevent T-cell infiltration in BALB/c mice. However, the T_H2 cells in BALB/c mice may also have different capacities to infiltrate into the retina compared to T_H1 cells in C57BL/6 mice and it is known that different chemokine expression is required for the chemotaxis of T_H1 and T_H2 cells (Aloisi et al., 2000). Alongside these changes in T cell infiltration, there is reduced splenomegaly at 4 weeks post infection in BALB/c mice, but not C57BL/6 mice. In contrast, at 1 week post infection the levels of splenomegaly are the same for BALB/c and C57BL/6 mice, indicating that this 4 week difference is not due to different maximal sizes of inflamed spleens in these two mouse strains. The reduction in splenomegaly in BALB/c mice may indicate faster clearance of the pathogen in BALB/c mice compared to C57BL/6 mice. It would be interesting to assess Salmonella load at different timepoints in these strains to see if there are different levels of infection or rates of clearance. Another possible mechanism is that a T_H2 response with higher levels of anti-inflammatory mediators (e.g. IL-10, arginase) compared to T_H1 (Mills et al., 2000) may result in earlier resolution of inflammation in BALB/c mice.

Following LPS injection, CD3+ T cells do not infiltrate into the retinas of C57BL/6 or BALB/c mice. This is not surprising due to the acute nature of LPS injection and its classical activation of the innate immune system and B cells, but not T cells (Vaure & Liu, 2014). Indeed, LPS is described as a T-cell independent B-cell stimulus (Donahue & Fruman, 2003). Intriguingly, C57BL/6 shows a

trend (p=0.06) to reduced levels of infiltrating T cells when Salmonella infection is combined with LPS administration. This is very possible given the high levels of serum cytokines observed when Salmonella infection and LPS are combined in C57BL/6 mice. Many immune cells undergo chemotaxis towards sites showing the highest inflammation and therefore T cells may leave the retina and return to the periphery, which has a high gradient of chemokines following LPS. In particular, CCL2 (MCP-1) and MIP-1α are both potent attractors of T cells to the CNS and both are elevated in the periphery following LPS injection (Erickson & Banks, 2011; Aloisi et al., 2000). However, evidence from the brain suggests that antigen-specific T cells are unable to leave the parenchyma and instead are removed through apoptosis (Bauer et al., 1998). The mechanisms of such apoptosis are not clear, but may be the end result of a lack of costimulation and subsequent anergy, overactivity leading to T cell exhaustion, Fas-Fas Ligand interactions or functional suppression by TGF-β (Barron et al., 2008; Yi et al., 2010). It is possible that systemic LPS induced retinal inflammation may accelerate the process of retinal T cell apoptosis, leading to the observed decrease in T cells following Salmonella and LPS.

4.4.6 Summary

The differences in this chapter show the immune responses in C57BL/6 and BALB/c mice are black and white. In C57BL/6 mice, the periphery is primed by Salmonella to subsequent LPS-induced inflammation, as has been observed with brain microglia, indicating similar effects in the periphery and CNS. However, in BALB/c mice, Salmonella results in tolerance of the peripheral immune system to subsequent LPS-induced inflammation. In C57BL/6 mice, Salmonella, but not LPS, induced microglial activation, T cell recruitment and ICAM-1/VCAM-1 expression. BALB/c mice also showed no evidence of microglial activation, T cell recruitment and ICAM-1/VCAM-1 expression in response to Salmonella, while LPS induced activation of microglia and ICAM-1/VCAM-1 expression. These findings demonstrate the strong effects that genetics can play in the function of the immune system. Despite this, the retinal cytokines showed good agreement between C57BL/6 and BALB/c, showing a general pattern of tolerance to subsequent LPS-induced inflammation. This tolerance to subsequent peripheral inflammation may be a conserved protective mechanism during chronic inflammation/infections commonly seen in elderly people and AMD patients.

Chapter 5:

The inflammatory effect of systemic bacterial infection on immune complex mediated retinal inflammation

5.1 Introduction

Salmonella does not appear to prime the retinal immune response to subsequent systemic inflammation, but how systemic inflammation interacts with local inflammation has not been considered. There is evidence in mice and humans that systemic inflammation can exacerbate ongoing neuropathology (Holmes et al., 2009; Cunningham et al., 2005). For example, patients with Alzheimer's disease and acute systemic inflammatory events show double the rate of cognitive decline compared to patients without acute systemic inflammation (Holmes, et al. 2009). More specifically, exposure to the bacterial infection *P. gingivalis*, which causes periodontitis, is associated with a sixfold increase in the rate of cognitive decline in Alzheimer's disease (Ide et al., 2016). There is evidence that bacterial infections can also affect retinal neurodegeneration; in two independent cohorts, periodontitis is also associated with a 1.6 and 2-fold risk of developing AMD in patients less than 60 years old, but this association is lost in older age (Han & Park, 2017; Wagley et al., 2015). Furthermore, pneumonia caused by *C. pneumoniae* has been associated with increased risk and progression of AMD in some studies (see introduction section 1.5.4).

Animal studies allow us to investigate the interaction of neurodegeneration and systemic inflammation in more detail. For example, when mice with chronic neurodegeneration (prion disease) are given a peripheral LPS injection, the combination results in greatly exaggerated expression of hippocampal iNOS, IL-1β, IL-6 and TNFα (Cunningham et al., 2005). Furthermore, CNS cell apoptosis in mice with chronic neurodegeneration is greatly increased following peripheral LPS injection, linking inflammation and degeneration (Cunningham et al., 2009). Systemic inflammation can also precede local inflammation and prime the CNS to respond in an exaggerated manner to subsequent local inflammation. Notably, 4 weeks of systemic Salmonella infection leads an exaggerated microglial response to intracerebral LPS administration. (Püntener et al., 2012). This demonstrates that systemic infection can prime microglia to respond to local inflammatory challenges, but these studies use LPS as a tool to assess priming, which has different characteristics to a real-life infection.

In a more disease-relevant context, CMV infection has been associated with increased progression of wet AMD in humans (Miller et al., 2004). Similarly, a murine model of wet AMD, laser-induced CNV, is exacerbated following murine CMV infection (Cousins et al., 2012). While these studies provide evidence for the interaction of inflammation and wet AMD, only systemic inflammation and retinal neovascularisation following CMV infection have been characterised, meaning the critical understanding of retinal inflammatory changes is missing. Furthermore, these findings are not relevant to the majority (70-90%) of AMD patients, who have dry AMD. Consequently, in this

chapter I investigated whether systemic infection alters ongoing local inflammation in a published mouse model recapitulating several inflammatory aspects of early-stage dry AMD (Murinello et al., 2014).

5.2 Methods

5.2.1 Immune complexes

BALB/c mice were immunised against OVA or injected with saline as unimmunised controls. All mice then received an intravitreal injection of OVA under anaesthesia (see section 2.1.3). Mice were investigated with *in vivo* OCT and ERG analysis at 1 and 4 weeks post intravitreal OVA injection to assess retinal structure and function (see sections 2.1.4). Dr. Elena Pipi assisted with *in vivo* imaging and intravitreal injections by preparing mice for these procedures (i.e. anaesthesia, tropicamide, phenylephrine) and recovering mice after the procedure. Dr. Elena Pipi dispensed the OVA solution during intravitreal injections once I confirmed that I had successfully placed the Hamilton needle in the vitreous. Serum samples were taken and a binding assay against OVA was performed to confirm production of OVA-specific IgG following immunisation (see sections 2.1.6 and 2.8).

5.2.2 Immune complexes + Salmonella

BALB/c mice were immunised against OVA or injected with saline as unimmunised controls. All mice then received an intravitreal injection of OVA under anaesthesia. Mice were transcardially perfused and tissue was harvested for analysis at 1 and 4 weeks post injection (see section 2.1.6). DAB immunohistochemistry using antibodies against CD3, CD11b, FcγRI, ICAM-1 and VCAM-1 was performed on 20µm fresh-frozen eye sections (see section 2.2). Immunofluorescence staining was performed for GFAP, FCRLS, P2YR12 and CD11b (see section 2.2). Statistical tests and key results are described in each figure legend with the full results of tests provided in Appendix C. For cell counts of positive amoeboid immune cells, the number of cells between the SR and GCL was quantified and vitreal cells in very close (<30µm) proximity to the nuclei of the retinal GCL were included in the quantification in line with previous quantification of the model (Salome Murinello, Personal communication).

5.3 Results

5.3.1 Immune complex deposition in the retina

Mice immunised against OVA and subsequently challenged intravitreally with OVA form immune complexes of IgG and OVA in the retina, mainly in the subretinal space/photoreceptor layers, although some complexes are found in other layers (Figure 5.1a). Levels of immune complexes were scored while blinded and there is a significant reduction in immune complex levels from 1 to 4 weeks post OVA injection ($p=0.0036$, Figure 5.1b). No immune complexes were observed in control mice that were unimmunised against OVA and then challenged intravitreally with OVA. This is expected as anti-OVA antibodies are generated in immunised mice, but not in unimmunised mice (Figure 5.1c). Immune complexes show colocalisation of OVA and IgG as co-staining is observed in all 3 axes simultaneously (Figure 5.1d).

Overall, these data demonstrate that immune complexes are formed and retained mostly in the subretinal space/photoreceptor layer in OVA immunised mice. Immune complexes can be detected up to 4 weeks post OVA challenge, including at the choroid/RPE interphase, although total levels of immune complexes have decreased by this time point.

5.3.2 Immune complexes induce sustained inflammation in the retina

Retinal immune complex formation induces myeloid cell activation in the retina, which can be quantified by counting the number of immune cells in the retina with a highly activated amoeboid morphology (Murinello et al., 2014). Here, this is studied in more detail and the effects of immune complexes on other cell types (Müller cells and T cells) are characterised.

Intravitreal OVA challenge induces inflammation in the retina irrespective of immunisation status. For example, MHCII expression on microglia and the presence of amoeboid immune cells can be observed in unimmunised mice following intravitreal OVA challenge. OVA injection in immunised mice results in immune complex deposition, which induces further inflammation compared to OVA injection in unimmunised mice. This can be shown by the increased presence of cells with an amoeboid morphology that are FcγRI+ (fold change ≈2.0, $p=0.0196$), CD11b+ (fold change ≈2.6, $p=0.0034$) and MHCII+ (fold change ≈3.9, $p<0.0001$) in immunised mice compared to unimmunised mice (Figure 5.2). The number of amoeboid cells expressing FcγRI (fold change ≈1.5, $p=0.0497$) and MHCII (fold change ≈2.8, $p=0.0017$) is reduced at 4 weeks post OVA injection compared to 1 week post OVA injection, indicating that myeloid cell activation is transient.

Immune complexes also increase the area of GFAP expression in the retina (fold change ≈1.4, p=0.0435) compared to unimmunised mice injected intravitreally with OVA (Figure 5.3). Increased GFAP expression appears to be similar at 1 and 4 weeks post injection. The GFAP staining pattern shows that astrocytes express GFAP in all conditions, whereas Müller cell staining is stronger in mice with immune complexes compared to unimmunised mice.

Immune complexes also induce the recruitment of CD3+ cells to the retina (fold change ≈11, p=0.0028) compared to unimmunised mice injected intravitreally with OVA (Figure 5.4). Levels of T cells in immunised mice appear to be similar at 1 and 4 weeks post intravitreal OVA challenge. These T cells appear to be mainly localised to the inner layers of the retina, although some can be found in the subretinal space/photoreceptor layer.

Overall, immune complex formation in the retina induces myeloid and Müller cell activation alongside T cell infiltration. Microglial cell activation appears reduced at 4 weeks post immune complex formation compared to 1 week, while Müller cell activation and T cell infiltration appear equal at 1 and 4 weeks post immune complex formation.

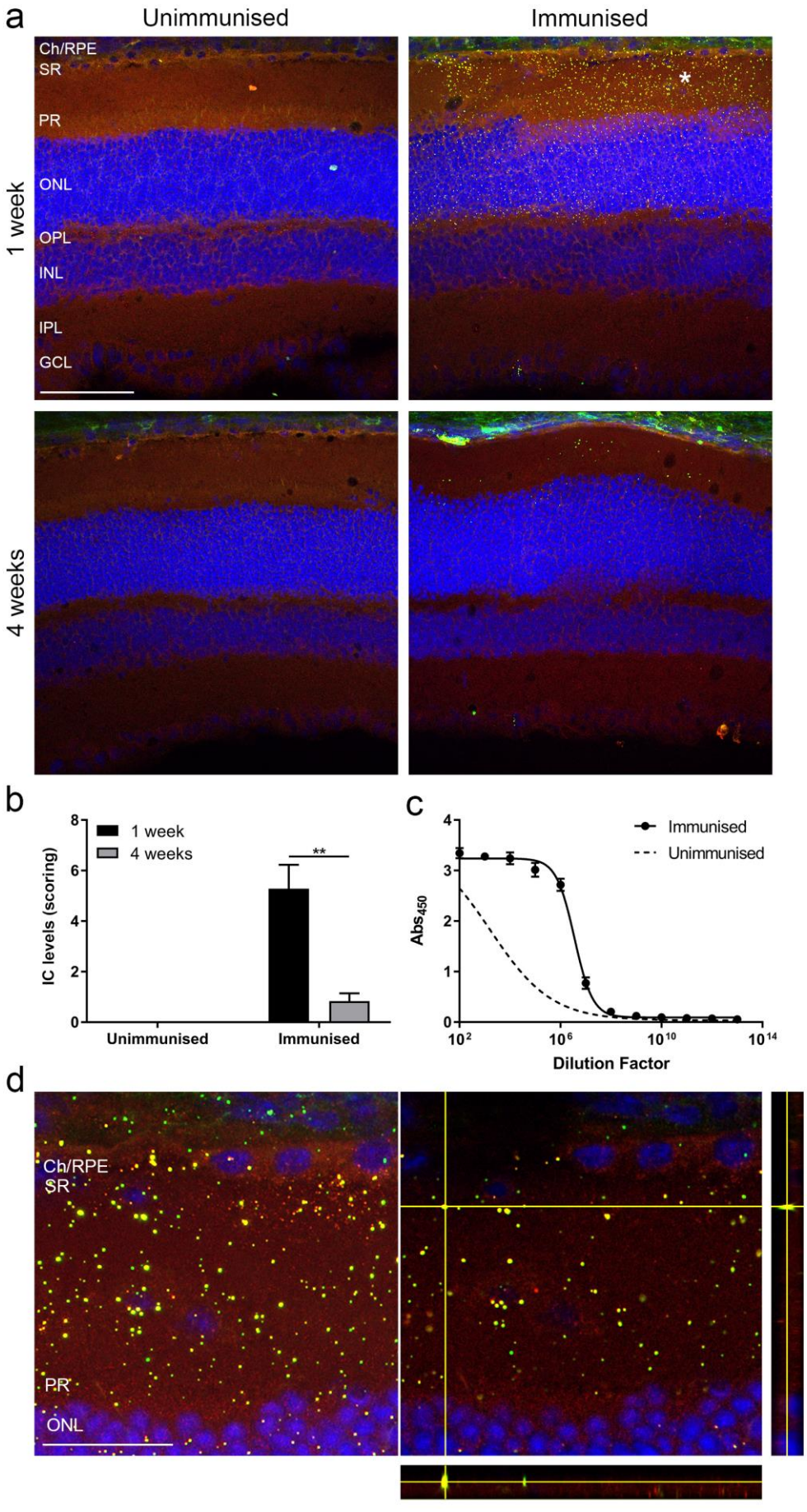
a
Unimmunised
Immunised
1 week
4 weeks
Ch/RPE
SR
PR
ONL
OPL
INL
IPL
GCL
b
1 week
4 weeks
IC levels (scoring)
**
Unimmunised
Immunised
c
Immunised
Unimmunised
Abs450
Dilution Factor
d
Ch/RPE
SR
PR
ONL

Figure 5.1 – Immune complex formation at 1 and 4 weeks post OVA injection in OVA-immunised mice.

*Half of the mice were immunised against OVA and the other half remained unimmunised. All mice received an intravitreal injection of OVA (n=6-8 mice per group). (a) Representative immunohistochemistry showing OVA (red) and IgG (green) staining with DAPI (blue) counterstaining at 1 and 4 weeks post intravitreal OVA challenge in unimmunised and immunised mice. (b) Quantification of the level of immune complexes using a scoring system, where 0 represents no complexes and 10 represents many deposits across the entire retina. (c) OVA binding assay showing the levels of anti-OVA IgG in the serum in immunised mice. (d) High-magnification images of immune complexes in the outer retina (white asterisk shows area the magnified image was taken from). A maximum projection (left) and single Z-slice with orthogonal views (right) are provided. Images were taken by confocal microscopy with (a) x40 objective and (d) x100 objective. Graphs are presented as mean±SEM. Scale bars represent (a) 100µm and (d) 25µm. Immune complex levels in immunised mice were analysed using unpaired two-tailed T-test, as all unimmunised mice scores were 0. Stars denote significance as follows: **p<0.01. Ch/RPE: Choroid/retinal pigment epithelium; SR, subretinal space; PR, photoreceptors; ONL, outer nuclear layer; OPL, outer plexiform layer; INL, inner nuclear layer; IPL, inner plexiform layer; GCL, ganglion cell layer.*

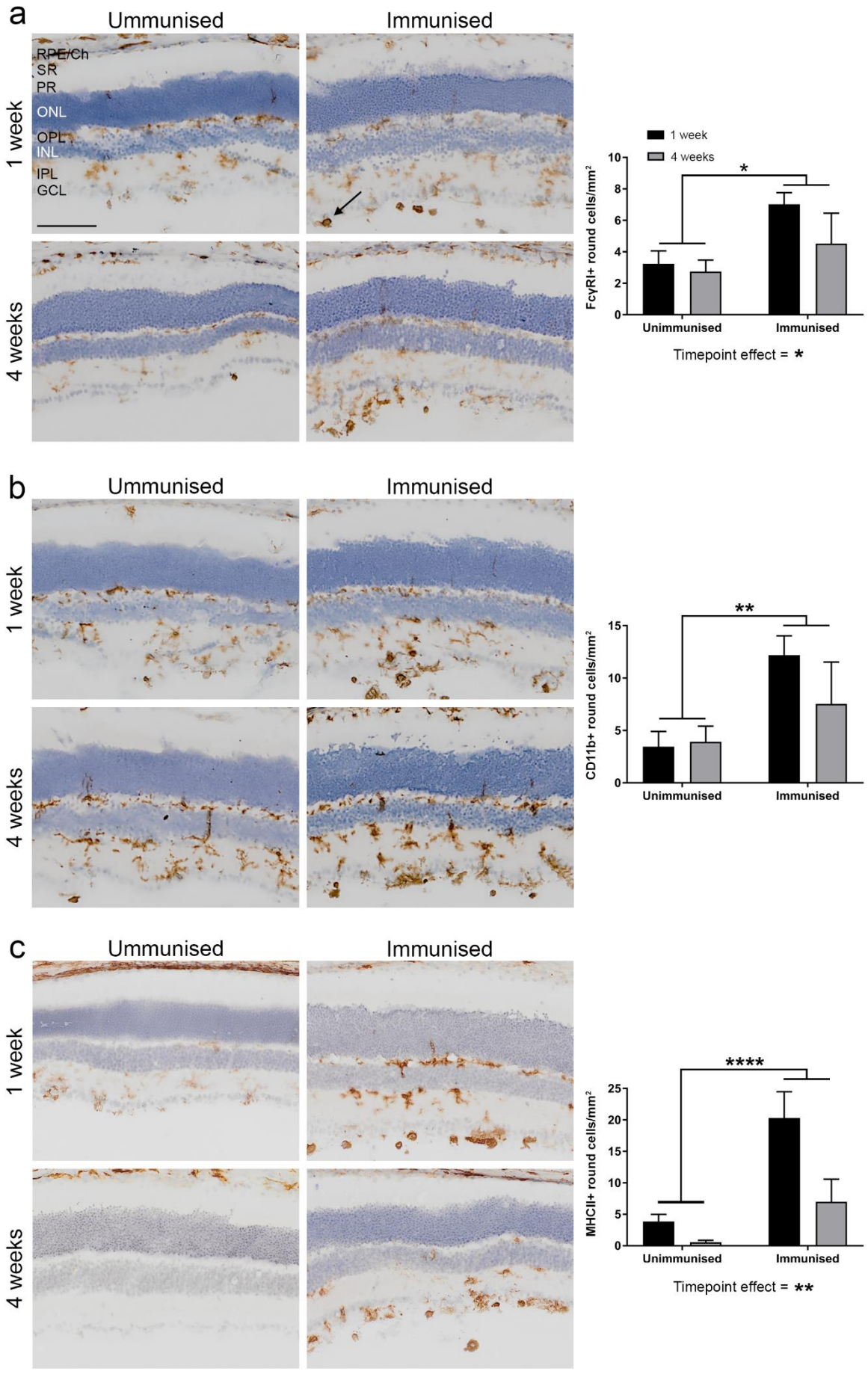
a
Ummunised
Immunised
1 week
4 weeks
RPE/Ch
SR
PR
ONL
OPL
INL
IPL
GCL
1 week
4 weeks
FcγRI+ round cells/mm²
*
Unimmunised
Immunised
Timepoint effect = *
b
Ummunised
Immunised
1 week
4 weeks
CD11b+ round cells/mm²
**
Unimmunised
Immunised
c
Ummunised
Immunised
1 week
4 weeks
MHCII+ round cells/mm²
****
Unimmunised
Immunised
Timepoint effect = **

Figure 5.2 – Increased numbers of highly activated amoeboid immune cells are present in the retina after immune complex formation.

*Half of the mice were immunised against OVA and the other half remained unimmunised. All mice received an intravitreal injection of OVA (n=6-8 mice per group). Representative DAB immunohistochemistry images and corresponding quantification of amoeboid cells per mm^2 of total retinal area at 1 and 4 weeks post intravitreal OVA challenge for (a) FcγRI, (b) CD11b and (c) MHCII. Black arrow indicates a highly activated amoeboid immune cell. Graphs are presented as mean±SEM. Data was analysed by two-way ANOVA. Stars denote significance as follows: *p<0.05, **p<0.01, ****p<0.0001. RPE/Ch, Retinal pigment epithelium/Choroid; SR; subretinal space; PR, photoreceptor segments; ONL, outer nuclear layer; OPL, outer plexiform layer; INL, inner nuclear layer; IPL, inner plexiform layer; GCL, ganglion cell layer. Scale bar represents 100µm.*

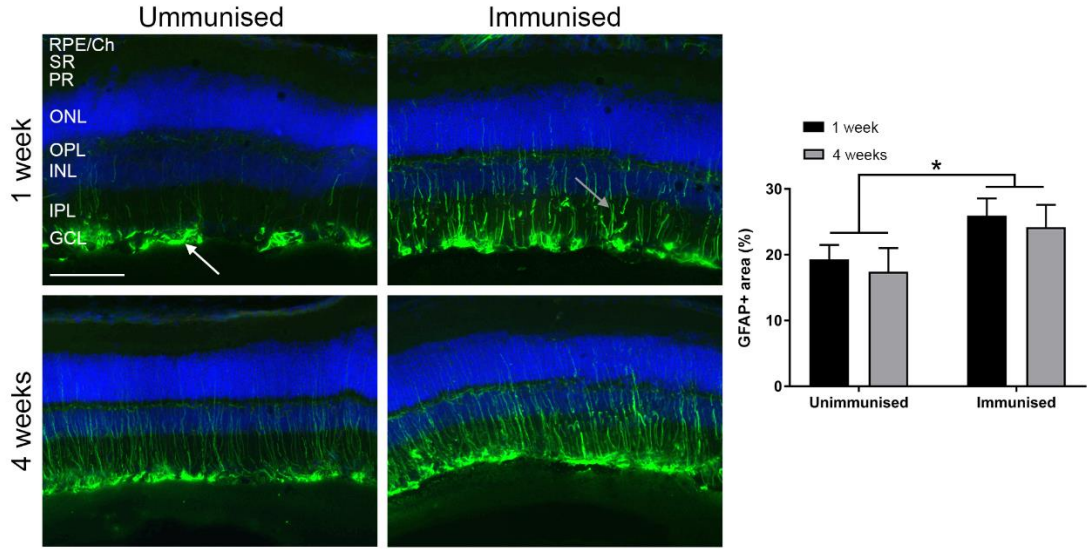

Figure 5.3 – Increased GFAP expression in the retina after immune complex formation.

*Half of the mice were immunised against OVA and the other half remained unimmunised. All mice received an intravitreal injection of OVA (n=6-8 mice per group). Representative images of immunofluorescence staining for GFAP (green) with DAPI (blue) counterstaining at 1 and 4 weeks post intravitreal OVA challenge and corresponding quantification of area of GFAP staining as a percentage of total retinal area. Grey arrow shows GFAP staining of the long and thin Müller cell processes in the inner retinal layers, while the white arrow shows GFAP staining at the GCL characteristic of either astrocytes or Müller cells. Graphs are presented as mean±SEM. Data was analysed using two-way ANOVA. Stars denote significance as follows: *p<0.05. RPE/Ch, Retinal pigment epithelium/Choroid; SR, subretinal space; PR, photoreceptor segments; ONL, outer nuclear layer; OPL, outer plexiform layer; INL, inner nuclear layer; IPL, inner plexiform layer; GCL, ganglion cell layer. Scale bar represents 100µm.*

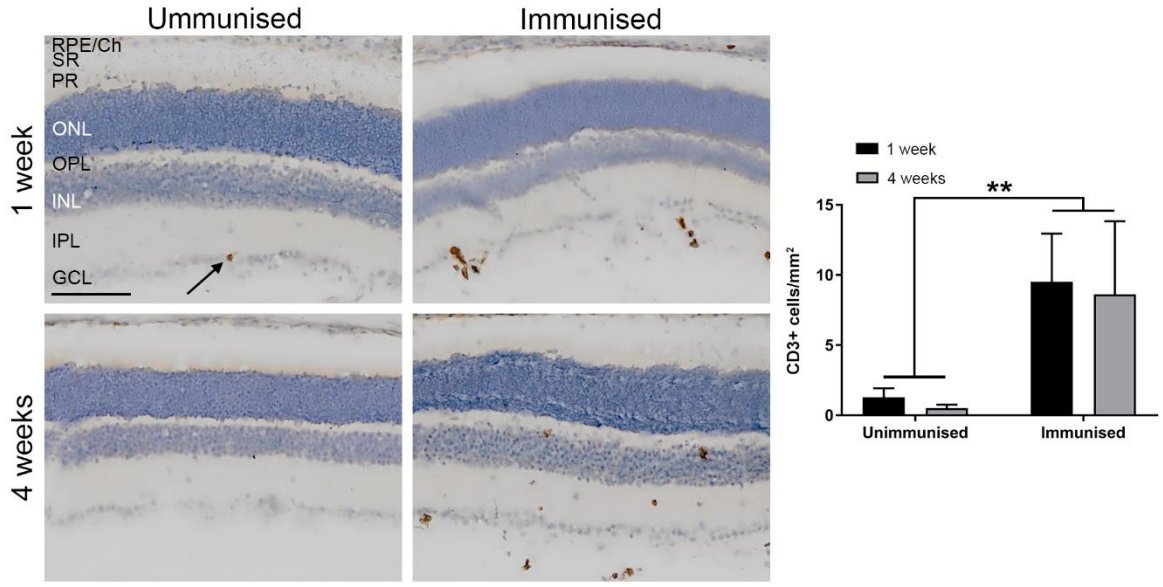

Figure 5.4 – Increased T cell numbers in the retina after immune complex formation.

*Half of the mice were immunised against OVA and the other half remained unimmunised. All mice received an intravitreal injection of OVA (n=6-8 mice per group). Representative images showing DAB immunohistochemical staining for CD3 with haematoxylin counterstain at 1 and 4 weeks post OVA injection and corresponding quantification of number of CD3+ cells/mm^2 of total retinal area. Black arrow shows a CD3+ cell. Graphs are presented as mean±SEM. Data was analysed using two-way ANOVA. Stars denote significance as follows: **p<0.01. RPE/Ch, Retinal pigment epithelium/Choroid; SR, subretinal space; PR, photoreceptor segments; ONL, outer nuclear layer; OPL, outer plexiform layer; INL, inner nuclear layer; IPL, inner plexiform layer; GCL, ganglion cell layer. Scale bar represents 100µm.*

5.3.3 *In vivo* effects of immune complexes on retinal structure and function

One of the benefits of studying the retina in comparison to the brain is the ability to perform non-invasive imaging of the retina. Accordingly, the effect of immune complexes on retinal structure and function was assessed *in vivo*.

OCT scans of the retinal layers were performed to identify areas of pathology following immune complex formation (Figure 5.5). Pathological features observed by OCT were only identified in immunised mice at 1 week post intravitreal OVA challenge. While these areas of pathology are small and sporadic, no pathological feature was observed in unimmunised mice or in immunised mice at 4 weeks post intravitreal OVA challenge.

Electroretinography (ERG) was performed to assess scotopic (rod cell-induced) electrical activity of the retina in response to light stimulation (Figure 5.6). ERG analysis shows that retinal function, as assessed by b-wave amplitude, is reduced at 1 week post injection in immunised mice (change ≈34%, $p=0.0068$) compared to unimmunised mice. These ERG deficits in immunised mice recover by 4 weeks post injection, compared to 1 week post injection (change ≈32%, $p=0.0367$) to return to the levels of unimmunised controls. No deficits were observed in the a-wave amplitude as a result of immunisation status or timepoint.

Overall, these findings show abnormalities in retinal structure and function at 1 week post immune complex formation, which are resolved by 4 weeks post immune complex formation.

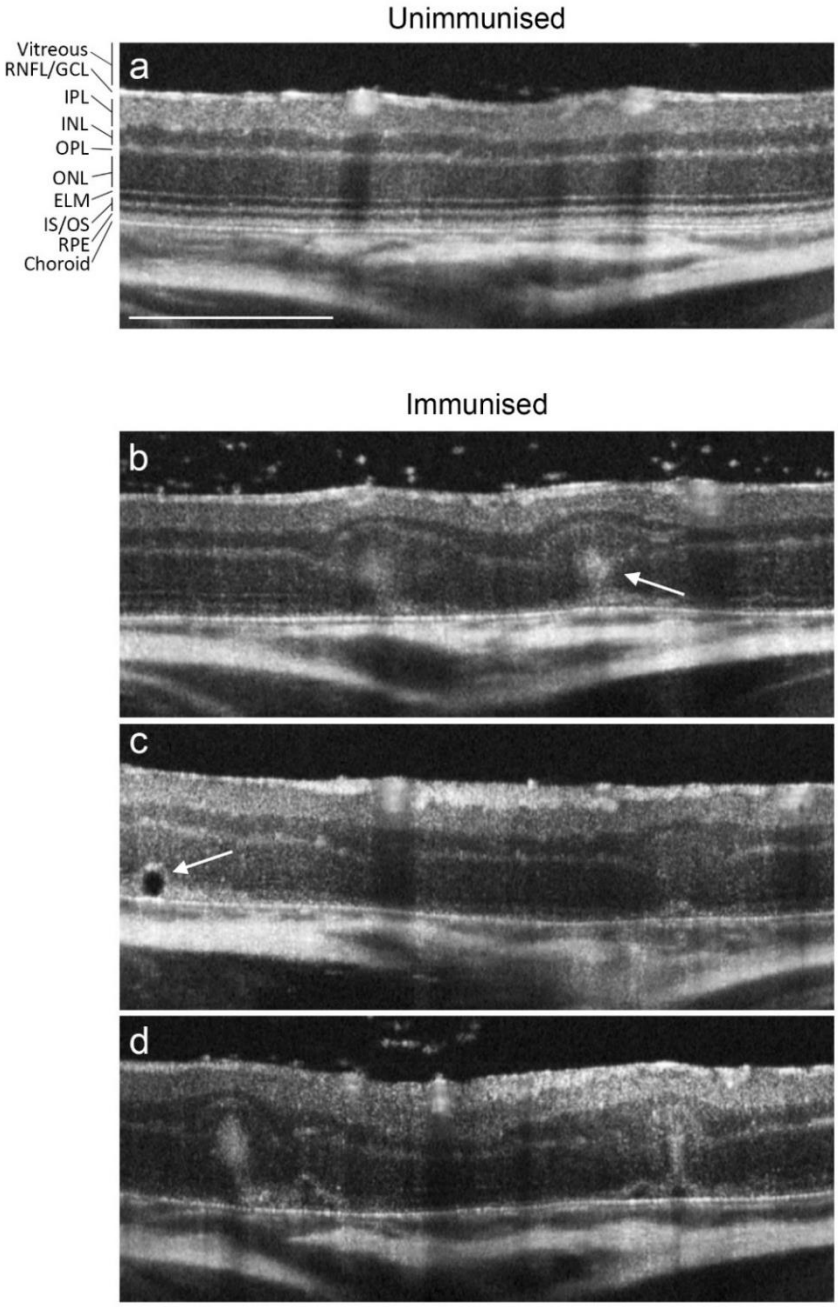

Figure 5.5 – Altered retinal structures are observed *in vivo* at 1 week post immune complex formation.

Representative retinal OCT scans taken at 1 week post intravitreal OVA challenge in (a) unimmunised and (b-d) OVA-immunised mice. Examples of pathology are as follows: (b) cells are present in the vitreous and hyper-reflective areas are seen in the outer retinal layers (white arrow) distorting the retinal structure; (c) a hyper-reflective bubble with a hypo-reflective core (white arrow) is observed in the outer retina; (d) both hypo- and hyper-reflective pathology is observed. Scale bar represents 400µm. RNFL, Retinal nerve fibre layer; GCL, ganglion cell layer; IPL, inner plexiform layer; INL, inner nuclear layer; OPL, outer plexiform layer; ONL, outer nuclear layer; ELM, external limiting membrane; IS/OS, photoreceptor inner segments/outer segments; RPE, retinal pigment epithelium.

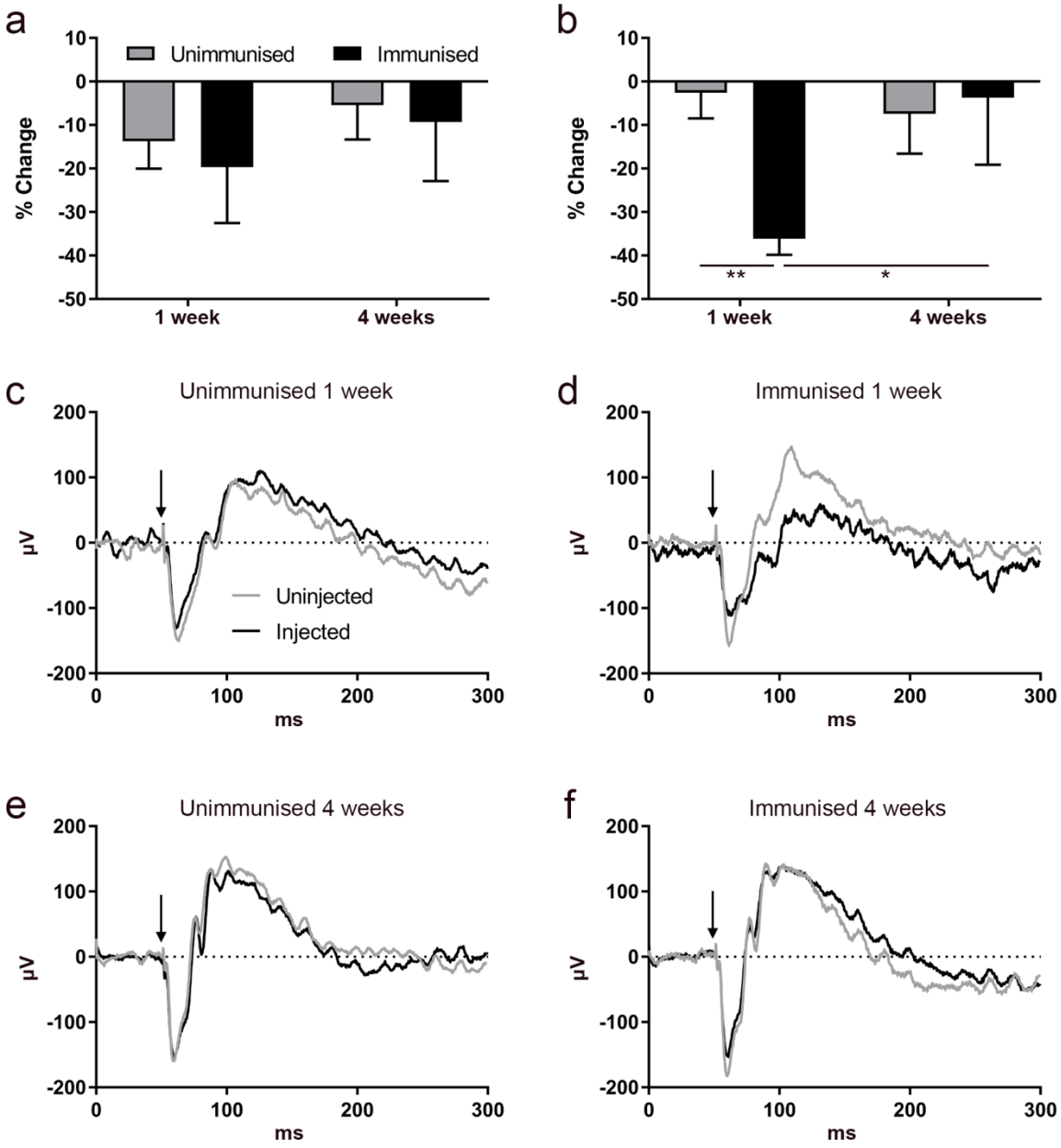

Figure 5.6 – Electrophysiological deficits in the retina are observed at 1 week post immune complex formation.

*Half of the mice were immunised against OVA and the other half remained unimmunised. All mice received an intravitreal injection of OVA (n=6-8 mice per group). Percentage change in (a) a-wave and (b) b-wave amplitude for the unimmunised and immunised groups at 1 and 4 weeks post intravitreal OVA challenge. Percentage change was calculated for each mouse as the amplitude of the injected eye compared to the uninjected eye. Averaged group ERG traces for the uninjected and injected eye of (c, e) unimmunised mice and (d, f) immunised mice at (c, d) 1 week and (e, f) 4 weeks post intravitreal OVA challenge. Light stimulus (black arrow) was applied after a 50ms baseline reading. Graphs are presented as mean±SEM. Data was analysed using two-way ANOVA with Holm-Sidak post-hoc testing. Stars denote significance as follows: *p<0.05, **p<0.01.*

5.3.4 Microglial cell responses to immune complexes and Salmonella infection

Immune complexes activate microglia at 1 and 4 weeks post intravitreal OVA challenge with higher activation at 1 week than 4 weeks post challenge. Salmonella infection can also induce microglial activation, which is higher at 4 weeks than 1 week post infection. These models of local and systemic inflammation were combined to investigate microglial responses when both inflammatory stimuli interact with each other. Microglial phenotype changes induced by Salmonella have been analysed in the brain by percentage area of DAB staining (Püntener et al., 2012). Immune complex-induced microglial activation has been analysed in terms of the number of highly activated amoeboid immune cells (Murinello et al., 2014). Finally, the effect of systemic viral infection on the retina has been assessed by the number of myeloid cells present in the subretinal space (Zinkernagel et al., 2013). These three parameters were investigated to identify any interaction between immune complexes and Salmonella.

There is no change in FcγRI+ area due to immunisation status or Salmonella infection at 1 or 4 weeks post intravitreal OVA challenge (Figure 5.7b, f). At 1 week post intravitreal OVA challenge, there is a significant increase in the number of FcγRI+ amoeboid cells in the retina of immunised mice (fold change ≈2.9, $p<0.0001$), which is not altered by Salmonella infection, and this effect is absent by 4 weeks post intravitreal OVA challenge (Figure 5.7c, g). At 1 week post intravitreal OVA challenge, immunisation status (fold change ≈2.2, $p=0.0038$) and Salmonella (fold change ≈2.1, $p=0.0022$) both result in an increase in the number of FcγRI+ subretinal cells and these effects are additive (Figure 5.7d). This pattern is maintained at 4 weeks post intravitreal OVA challenge, where immunisation status (fold change ≈1.7, $p=0.0458$) and Salmonella (fold change ≈1.7, $p=0.0043$) increase the number of FcγRI+ subretinal cells in an additive manner (Figure 5.7h).

There is no change in CD11b+ area due to immunisation status or Salmonella infection at 1 or 4 weeks post intravitreal OVA challenge (Figure 5.8b, f). At 1 week post intravitreal OVA challenge, there is a significant increase in the number of CD11b+ cells in the retina of immunised mice (fold change ≈3.5, $p<0.0001$), which is not altered by Salmonella infection, and this effect is absent by 4 weeks post intravitreal OVA challenge (Figure 5.8c, g). At 1 week post intravitreal OVA challenge, immunisation status (fold change ≈1.7, $p=0.0152$) and Salmonella (fold change ≈2.0, $p=0.0145$) both result in an increase in the number of CD11b+ subretinal cells in an additive manner (Figure 5.7d). At 4 weeks post intravitreal OVA challenge, Salmonella (fold change ≈2.2, $p=0.0133$) increases the number of CD11b+ subretinal cells (Figure 5.7h), but immunisation status no longer has a significant inflammatory effect, though there is a trend (fold change ≈1.7, $p=0.0986$).

Overall, CD11b and FcγRI expression is remarkably similar and indicates that systemic and local inflammation additively recruit myeloid cells, either microglia or peripheral cells, to the subretinal space. The staining of the choroid/RPE interphase is intense after Salmonella infection and is a relevant region for more detailed investigation as this is the site of AMD pathology and immune complex deposition.

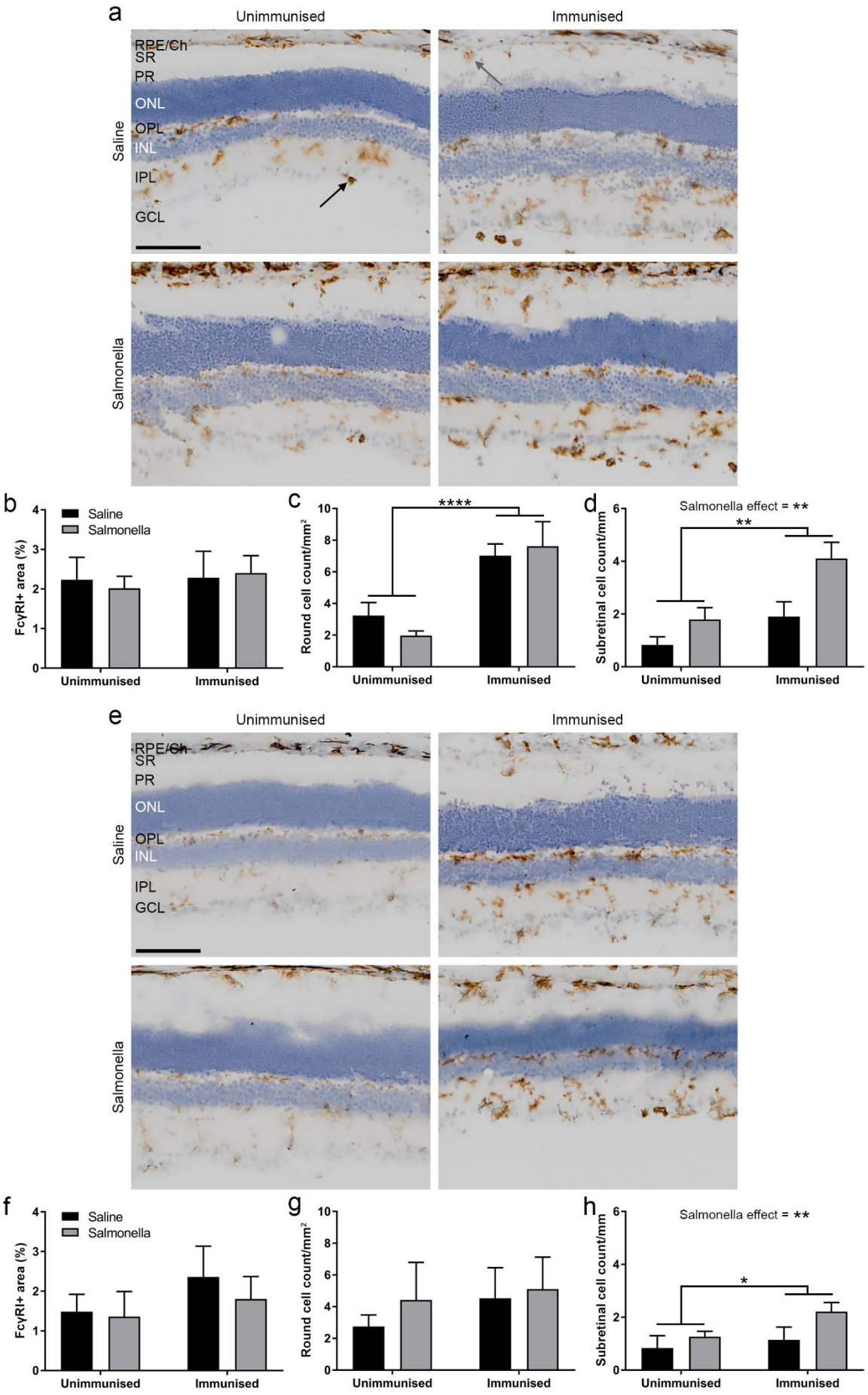
a
Unimmunised
Immunised
RPE/Ch
SR
PR
ONL
OPL
INL
IPL
GCL
Saline
Salmonella
b
Saline
Salmonella
FcγRI+ area (%)
Unimmunised
Immunised
c
****
Round cell count/mm²
Unimmunised
Immunised
d
Salmonella effect = **
**
Subretinal cell count/mm
Unimmunised
Immunised
e
Unimmunised
Immunised
RPE/Ch
SR
PR
ONL
OPL
INL
IPL
GCL
Saline
Salmonella
f
Saline
Salmonella
FcγRI+ area (%)
Unimmunised
Immunised
g
Round cell count/mm²
Unimmunised
Immunised
h
Salmonella effect = **
*
Subretinal cell count/mm
Unimmunised
Immunised

Figure 5.7 – The effect of immune complexes and Salmonella on FcγRI expression in the retina. *Half of the mice were immunised against OVA and the other half remained unimmunised. All the mice received an intravitreal injection of OVA (n=6-8 mice per group). At 24hrs post intravitreal OVA challenge, mice were injected i.p. with saline or Salmonella and tissue was harvested at 1 and 4 weeks post intravitreal OVA challenge. Expression of FcγRI was analysed at (a-d) 1 and (e-h) 4 weeks post intravitreal OVA challenge. (a, e) Representative DAB immunohistochemistry for FcγRI with haematoxylin counterstaining. Quantification of FcγRI expression is based on (b, f) area of DAB staining as a percentage of total retinal area, (c, g) number of positive amoeboid cells per mm^2 of total retinal area and (d, h) number of positive subretinal cells per mm of subretinal space. Black arrow represents a positive amoeboid cell. Grey arrow represents a positive subretinal cell. Graphs are presented as mean±SEM. Data was analysed using two-way ANOVA. Stars denote significance as follows: *p<0.05, **p<0.01, ****p<0.0001. RPE/Ch, Retinal pigment epithelium/Choroid; SR, subretinal space; PR, photoreceptor segments; ONL, outer nuclear layer; OPL, outer plexiform layer; INL, inner nuclear layer; IPL, inner plexiform layer; GCL, ganglion cell layer. Scale bar represents 100µm.*

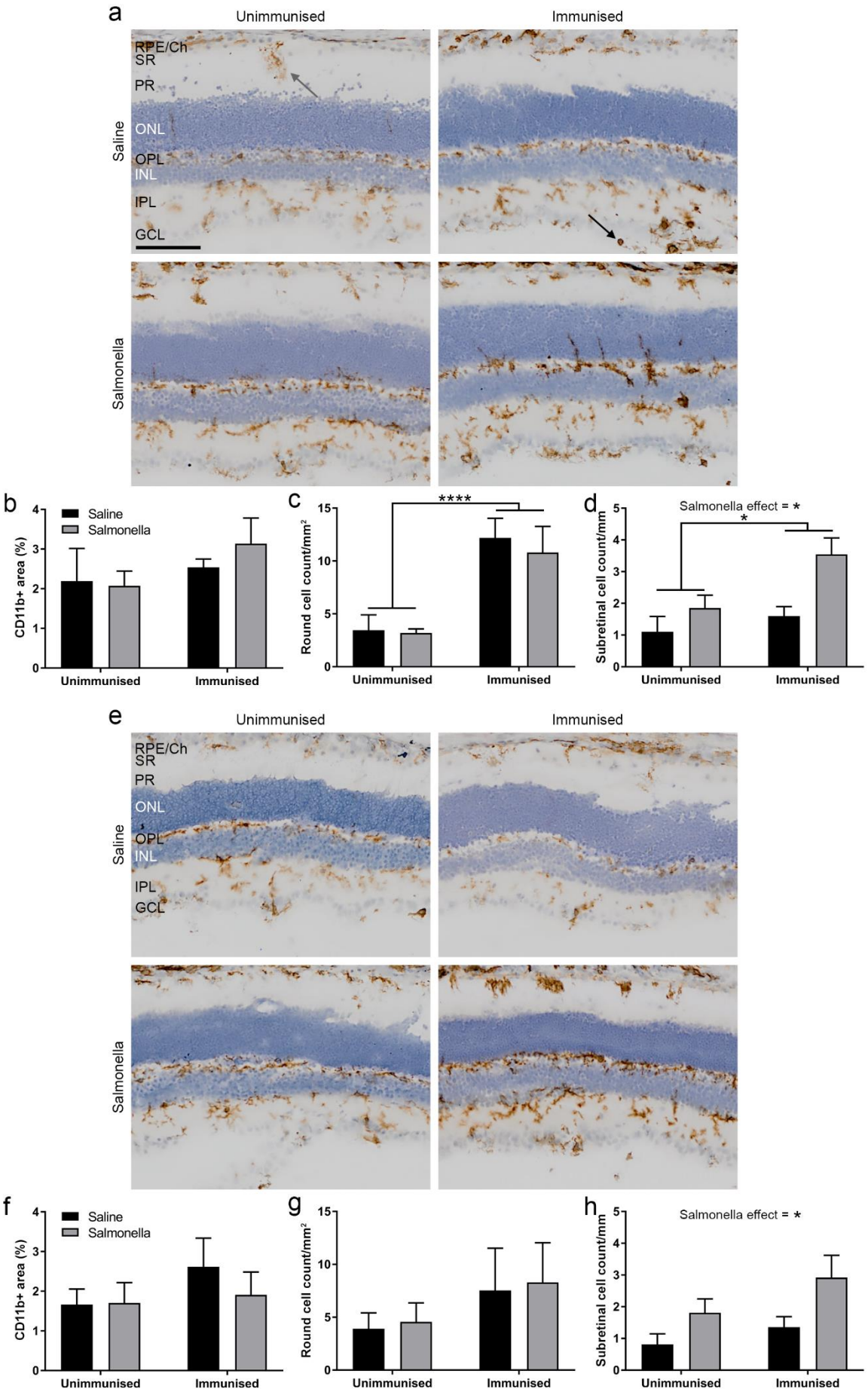
a
Unimmunised
Immunised
RPE/Ch
SR
PR
ONL
OPL
INL
IPL
GCL
Saline
Salmonella
b
Saline
Salmonella
CD11b+ area (%)
Unimmunised
Immunised
c
****
Round cell count/mm²
Unimmunised
Immunised
d
Salmonella effect = *
*
Subretinal cell count/mm
Unimmunised
Immunised
e
Unimmunised
Immunised
RPE/Ch
SR
PR
ONL
OPL
INL
IPL
GCL
Saline
Salmonella
f
Saline
Salmonella
CD11b+ area (%)
Unimmunised
Immunised
g
Round cell count/mm²
Unimmunised
Immunised
h
Salmonella effect = *
Subretinal cell count/mm
Unimmunised
Immunised

Figure 5.8 – The effect of immune complexes and Salmonella on CD11b expression in the retina. *Half of the mice were immunised against OVA and the other half remained unimmunised. All the mice then received an intravitreal injection of OVA (n=6-8 mice per group). At 24hrs post intravitreal OVA challenge, mice were injected i.p. with saline or Salmonella and tissue was harvested at 1 and 4 weeks post intravitreal OVA challenge. Expression of CD11b was analysed at (a-d) 1 and (e-h) 4 weeks post intravitreal OVA challenge. (a, e) Representative DAB immunohistochemistry for CD11b with haematoxylin counterstaining. Quantification of CD11b expression is based on (b, f) area of DAB staining as a percentage of total retinal area, (c, g) number of positive amoeboid cells per mm^2 of total retinal area and (d, h) number of positive subretinal cells per mm of subretinal space. Black arrow represents a positive amoeboid cell. Grey arrow represents a positive subretinal cell. Graphs are presented as mean±SEM. Data was analysed using two-way ANOVA. Stars denote significance as follows: *p<0.05, ****p<0.0001. RPE/Ch, Retinal pigment epithelium/Choroid; SR, subretinal space; PR, photoreceptor segments; ONL, outer nuclear layer; OPL, outer plexiform layer; INL, inner nuclear layer; IPL, inner plexiform layer; GCL, ganglion cell layer. Scale bar represents 100µm.*

5.3.5 Other cellular changes following immune complexes and Salmonella infection

Retinal immune complexes increase expression of GFAP in the retina and result in T cell recruitment. Salmonella infection results in strong expression of MHCII on activated retinal blood vessels. Based on these findings, the interaction of immune complexes and Salmonella on these inflammatory parameters was investigated.

At 1 week post intravitreal OVA challenge, the number of T cells in the retina is increased by the presence of immune complexes (fold change ≈3.3, p=0.0261), but not by Salmonella (Figure 5.9a). In contrast, at 4 weeks post intravitreal OVA challenge, the number of T cells in the retina is increased by both the presence of immune complexes (fold change ≈3.3, p=0.0100) and Salmonella (fold change ≈1.6, p=0.0373), but not in an additive manner (Figure 5.9b). T cells were mainly found in the inner retinal layers, with occasional T cells in the subretinal/photoreceptor layers. Several T cells were also identified in the choroid, but these were not quantified as part of the retina.

GFAP expression in the retina was assessed by immunofluorescence staining. Percentage area of GFAP expression was quantified similarly to DAB images, where a threshold of green staining was set, above which was considered positive. Mean fluorescence intensity of pixels was also calculated to identify shifts in overall fluorescence levels. At 1 week post intravitreal OVA challenge, both GFAP+ percentage area (fold change ≈1.7, p=0.0003) and mean fluorescence intensity (fold change ≈1.4, p<0.0001) are increased by the presence of immune complexes, but not Salmonella (Figure 5.10b, c). At 4 weeks post intravitreal OVA challenge, GFAP+ percentage area and mean fluorescence intensity are not affected by presence of immune complexes or Salmonella infection (Figure 5.10e, f). There appears to be a greater change in Müller cell staining of the inner retinal layers between groups compared to astrocytic staining adjacent to the GCL.

At 1 week post intravitreal OVA challenge, the presence of immune complexes results in increased ICAM-1+ area (fold change, ≈2.0, p=0.0306), which is not affected by Salmonella infection (Figure 5.11a). The converse is true at 4 weeks post intravitreal OVA challenge, where Salmonella infection increases ICAM-1+ area (fold change ≈1.7, p=0.0418), while the presence of immune complexes has no effect (Figure 5.11b). Increased expression of ICAM-1 appears to be confined to the inner retinal capillaries, with staining of the inner retinal arterioles consistent between groups. ICAM-1 staining as a percentage of the inner retinal area was quantified, so that ICAM-1 expression in the photoreceptor layer didn't confound the analysis.

MHCII can be expressed on both microglia and blood vessels following immune complex formation and Salmonella infection (Figure 5.12). At 1 week post intravitreal OVA challenge, MHCII+ area is increased by the presence of immune complexes (fold change ≈2.3, $p=0.0102$). In contrast, at 4 weeks post intravitreal OVA challenge, while presence of immune complexes still has an inflammatory effect (fold change ≈1.6, $p=0.0120$) there is a stronger Salmonella effect (fold change ≈3.5, $p<0.0001$).

At 1 week post intravitreal OVA challenge, MHCII is expressed on cells with ramified microglial morphology and amoeboid cells in all groups, and this is more pronounced in immunised mice compared to unimmunised mice. Salmonella infection induces MHCII staining on retinal blood vessels, regardless of immunization status. MHCII expression on microglia appears to be the main contributor to MHCII+ area at this timepoint. At 4 weeks post OVA injection, there is clear microglial activation in immunised mice without Salmonella infection and clear inner retinal capillary staining in unimmunised mice given Salmonella. Interestingly, both staining patterns are not observed simultaneously in mice given immune complexes and Salmonella, with 5 of 8 mice in this group showing only blood vessel staining and 3 of 8 mice showing only microglial staining.

Overall, MHCII is expressed on blood vessels due to Salmonella and microglia due to immune complexes. At 1 week post OVA challenge, the microglial and blood vessel patterns overlap whereas at 4 weeks post OVA challenge, either microglia or blood vessel staining is observed, but not both.

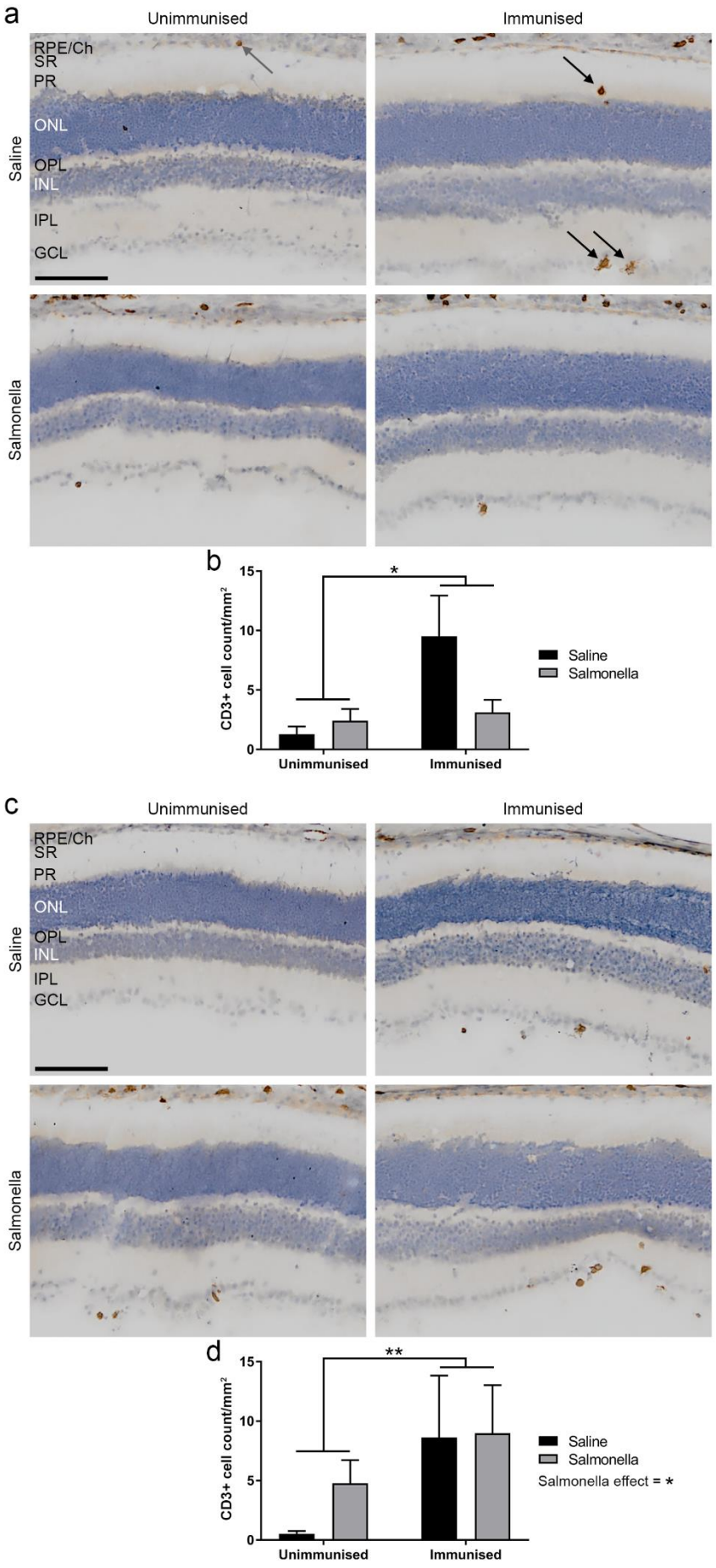
a
Unimmunised
Immunised
RPE/Ch
SR
PR
ONL
OPL
INL
IPL
GCL
Saline
Salmonella
b
CD3+ cell count/mm²
15
10
5
0
*
Unimmunised
Immunised
Saline
Salmonella
c
Unimmunised
Immunised
RPE/Ch
SR
PR
ONL
OPL
INL
IPL
GCL
Saline
Salmonella
d
CD3+ cell count/mm²
15
10
5
0
**
Unimmunised
Immunised
Saline
Salmonella
Salmonella effect = *

Figure 5.9 – The effect of immune complexes and Salmonella on CD3+ cell number in the retina. *Half of the mice were immunised against OVA and the other half remained unimmunised. All the mice then received an intravitreal injection of OVA (n=6-8 mice per group). At 24hrs post intravitreal OVA challenge, mice were injected i.p. with saline or Salmonella. Expression of CD3 was analysed at (a, b) 1 and (c, d) 4 weeks post intravitreal OVA challenge. (a, c) Representative DAB immunohistochemistry for CD3 with haematoxylin counterstaining. (b, d) Quantification of number of CD3+ cells per mm^2 of total retinal area. Grey arrow represents a CD3+ cell in the choroid (not quantified as part of the retina). Black arrows represent CD3+ cells in the retina. Graphs are presented as mean±SEM. Data was analysed using two-way ANOVA. Stars denote significance as follows: **p<0.01. RPE/Ch, Retinal pigment epithelium/Choroid; SR, subretinal space; PR, photoreceptor segments; ONL, outer nuclear layer; OPL, outer plexiform layer; INL, inner nuclear layer; IPL, inner plexiform layer; GCL, ganglion cell layer. Scale bar represents 100µm.*

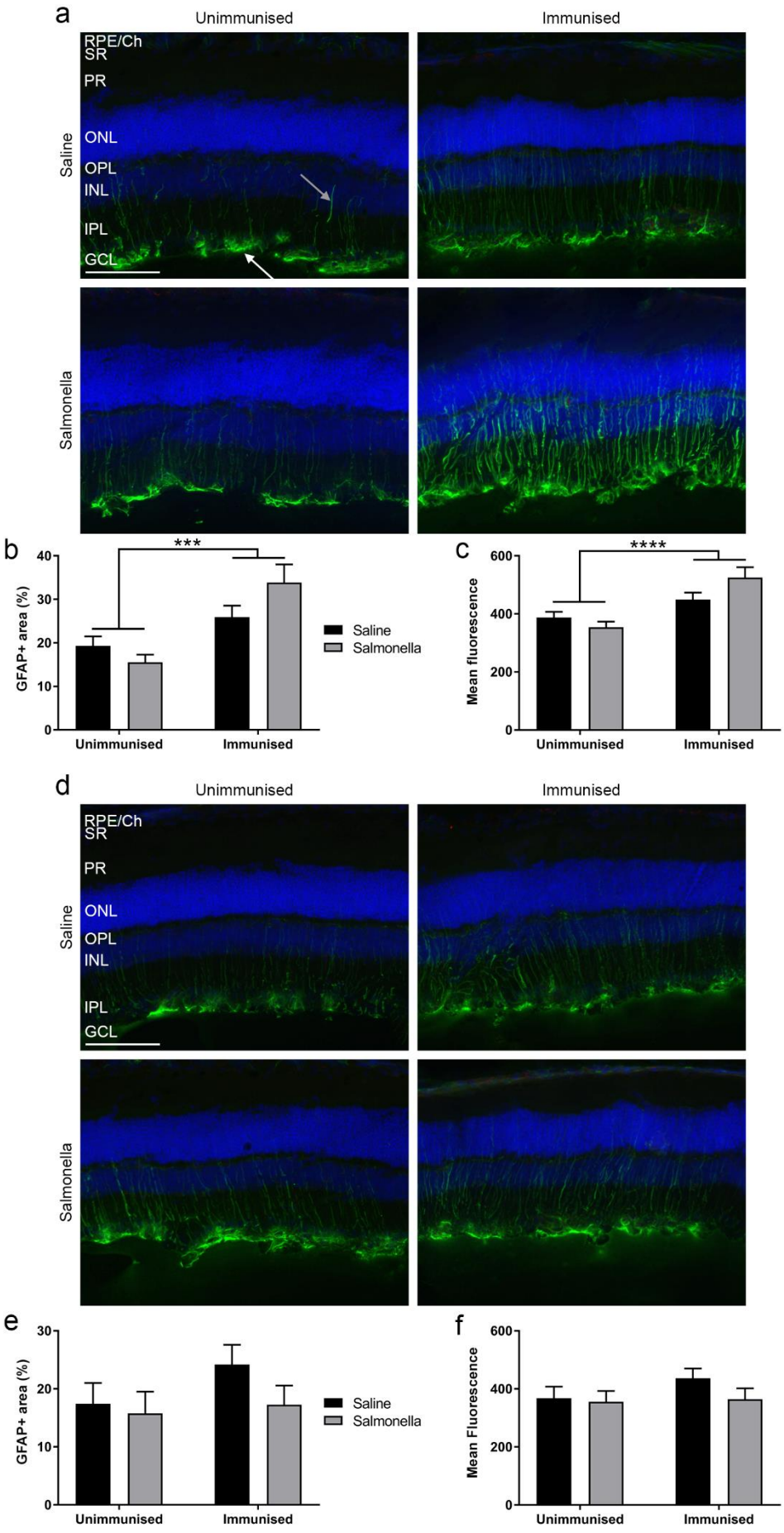
a
Unimmunised
Immunised
RPE/Ch
SR
PR
ONL
OPL
INL
IPL
GCL
Saline
Salmonella
b
***
GFAP+ area (%)
40
30
20
10
0
Unimmunised
Immunised
Saline
Salmonella
c
****
Mean fluorescence
600
400
200
0
Unimmunised
Immunised
d
Unimmunised
Immunised
RPE/Ch
SR
PR
ONL
OPL
INL
IPL
GCL
Saline
Salmonella
e
GFAP+ area (%)
30
20
10
0
Unimmunised
Immunised
Saline
Salmonella
f
Mean Fluorescence
600
400
200
0
Unimmunised
Immunised

Figure 5.10 – The effect of immune complexes and Salmonella on GFAP expression in the retina. *Half of the mice were immunised against OVA and the other half remained unimmunised. All the mice then received an intravitreal injection of OVA (n=6-8 mice per group). At 24hrs post intravitreal OVA challenge, mice were injected i.p. with saline or Salmonella. Expression of GFAP was analysed at (a-c) 1 and (d-f) 4 weeks post intravitreal OVA challenge. (a, d) Representative immunofluorescence images of GFAP (green) with DAPI (blue) counterstaining. Quantification of GFAP by (b, e) stained area as a percentage of total retina area and (c, f) mean fluorescence intensity. White arrow shows astrocytic GFAP staining at the GCL and the grey arrow shows GFAP staining of the long, thin Müller cell processes in the inner retinal layers. Graphs are presented as mean±SEM. Data was analysed using two-way ANOVA. Stars denote significance as follows: ***p<0.001, ****p<0.0001. RPE/Ch, Retinal pigment epithelium/Choroid; SR, subretinal space; PR, photoreceptor segments; ONL, outer nuclear layer; OPL, outer plexiform layer; INL, inner nuclear layer; IPL, inner plexiform layer; GCL, ganglion cell layer. Scale bar represents 100µm.*

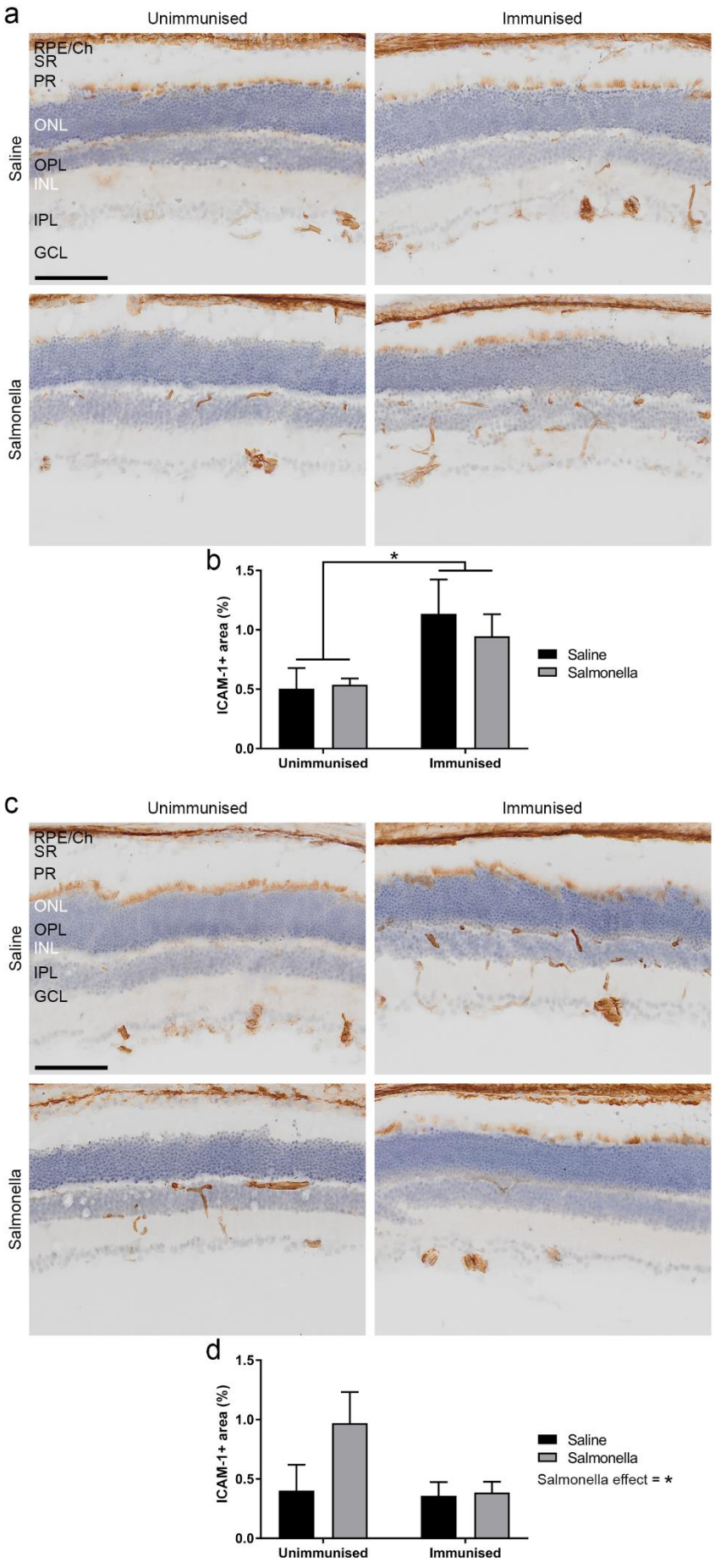
a
Unimmunised
Immunised
RPE/Ch
SR
PR
ONL
OPL
INL
IPL
GCL
Saline
Salmonella
b
ICAM-1+ area (%)
1.5
1.0
0.5
0.0
*
Saline
Salmonella
Unimmunised
Immunised
c
Unimmunised
Immunised
RPE/Ch
SR
PR
ONL
OPL
INL
IPL
GCL
Saline
Salmonella
d
ICAM-1+ area (%)
1.5
1.0
0.5
0.0
Saline
Salmonella
Salmonella effect = *
Unimmunised
Immunised

Figure 5.11 – The effect of immune complexes and Salmonella on ICAM-1 expression in the retina.

*Half of the mice were immunised against OVA and the other half remained unimmunised. All the mice then received an intravitreal injection of OVA (n=6-8 mice per group). At 24hrs post intravitreal OVA challenge, mice were injected i.p. with saline or Salmonella. Expression of ICAM-1 was analysed at (a, b) 1 and (c, d) 4 weeks post intravitreal OVA challenge. (a, c) Representative DAB immunohistochemistry for ICAM-1 with haematoxylin counterstaining. (b, d) Quantification of positive area as a percentage of inner retinal area. Graphs are presented as mean±SEM. Data was analysed using two-way ANOVA. Stars denote significance as follows: *p<0.05. RPE/Ch, Retinal pigment epithelium/Choroid; SR, subretinal space; PR, photoreceptor segments; ONL, outer nuclear layer; OPL, outer plexiform layer; INL, inner nuclear layer; IPL, inner plexiform layer; GCL, ganglion cell layer. Scale bar represents 100µm.*

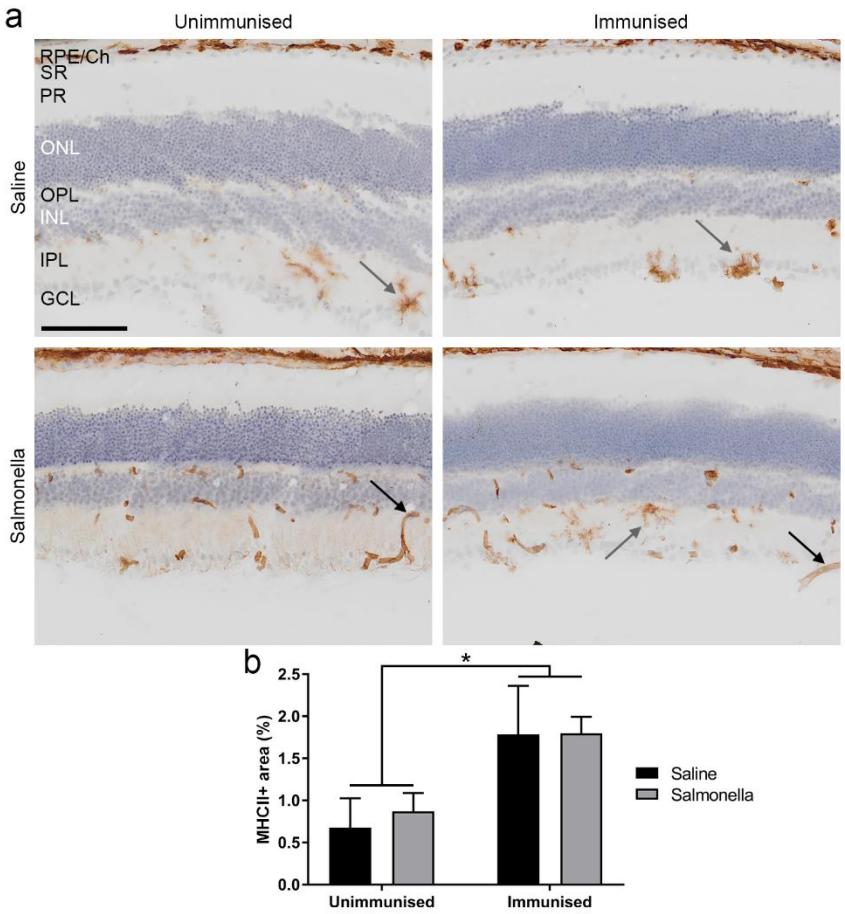
a
Unimmunised
Immunised
RPE/Ch
SR
PR
ONL
OPL
INL
IPL
GCL
Saline
Salmonella
b
*
MHCII+ area (%)
2.5
2.0
1.5
1.0
0.5
0.0
Unimmunised
Immunised
Saline
Salmonella

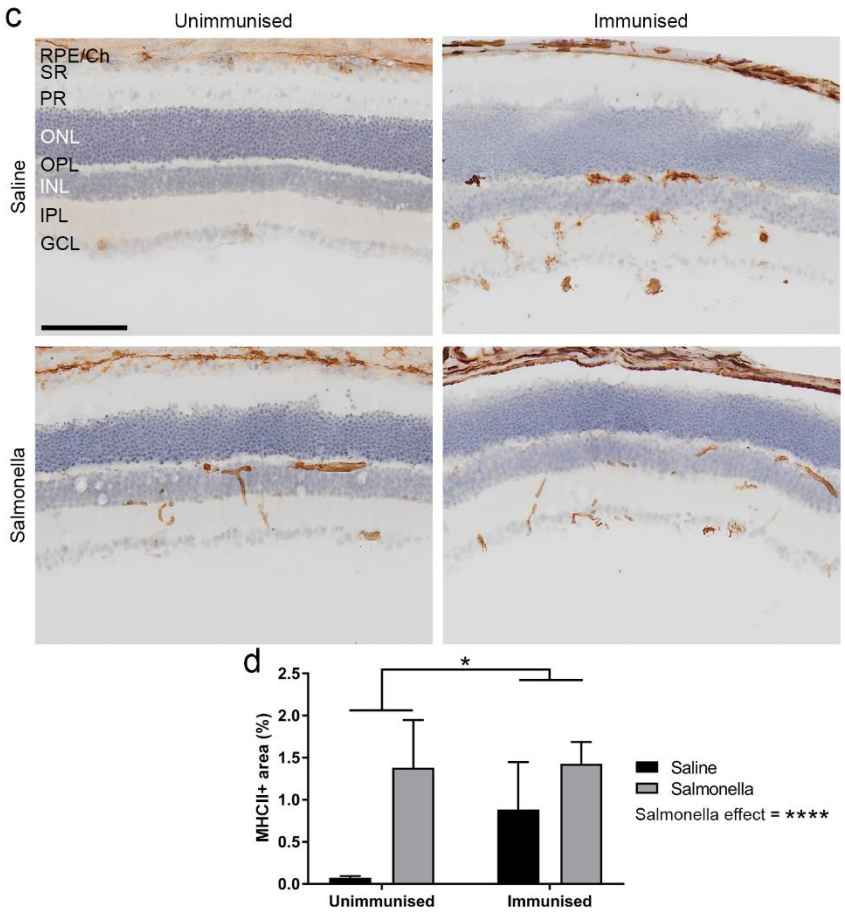
c
Unimmunised
Immunised
RPE/Ch
SR
PR
ONL
OPL
INL
IPL
GCL
Saline
Salmonella
d
*
MHCII+ area (%)
2.5
2.0
1.5
1.0
0.5
0.0
Unimmunised
Immunised
Saline
Salmonella
Salmonella effect = ****

Figure 5.12 – The effect of immune complexes and Salmonella on MHCII expression in the retina.

*Half of the mice were immunised against OVA and the other half remained unimmunised. All the mice then received an intravitreal injection of OVA (n=6-8 mice per group). At 24hrs post intravitreal OVA challenge, mice were injected i.p. with saline or Salmonella. Expression of MHCII was analysed at (a, b) 1 and (c, d) 4 weeks post intravitreal OVA challenge. (a, c) Representative DAB immunohistochemistry for MHCII with haematoxylin counterstaining. (b, d) Quantification of positive area as a percentage of total retinal area. Grey arrows indicate MHCII expression on microglia, while black arrows indicate MHCII expression on inner retinal capillaries. Graphs are presented as mean±SEM. Data was analysed using two-way ANOVA. Stars denote significance as follows: *p<0.05, ****p<0.0001. RPE/Ch, Retinal pigment epithelium/Choroid; SR, subretinal space; PR, photoreceptor segments; ONL, outer nuclear layer; OPL, outer plexiform layer; INL, inner nuclear layer; IPL, inner plexiform layer; GCL, ganglion cell layer. Scale bar represents 100µm.*

5.3.6 Immune complex levels following Salmonella infection

Immune complex clearance is likely to depend on phagocytosis by either the RPE and/or microglia. Salmonella can induce functional changes in the retina, notably microglial activation, and as a result I tested whether systemic infection could affect the rate of clearance of immune complexes in the retina.

Immunofluorescence staining shows that immune complexes are only generated in immunised mice (Figure 5.13). Salmonella infection has no significant effect on the levels of immune complexes in immunised mice at 1 or 4 weeks post intravitreal OVA challenge when compared to unimmunised controls. Additionally, the number of immune complexes appears substantially reduced at 4 weeks compared to 1 week post intravitreal OVA challenge for both the saline and Salmonella treated groups ($p<0.0001$). Overall, Salmonella has no effect on the rate of clearance of immune complexes.

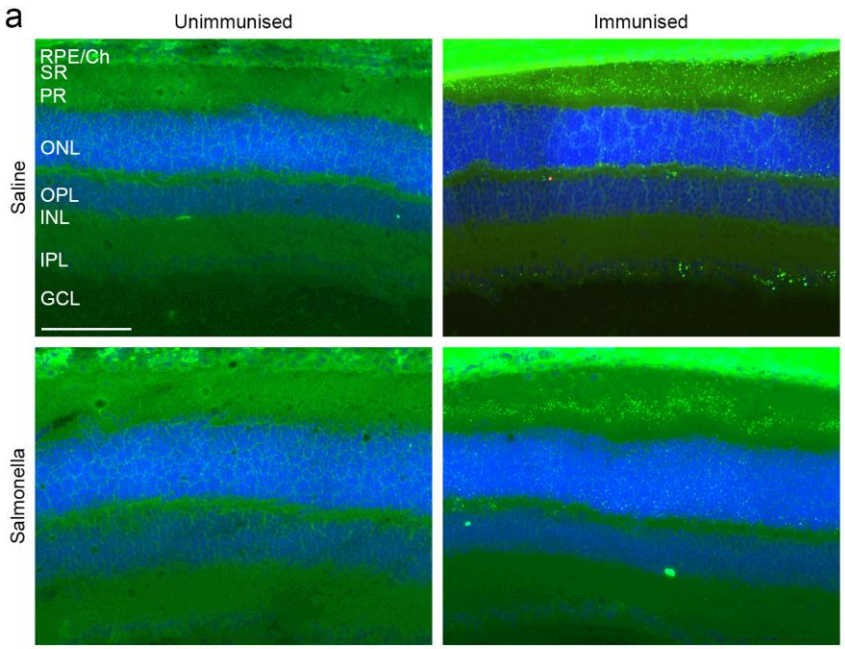
a
Unimmunised
Immunised
RPE/Ch
SR
PR
ONL
OPL
INL
IPL
GCL
Saline
Salmonella

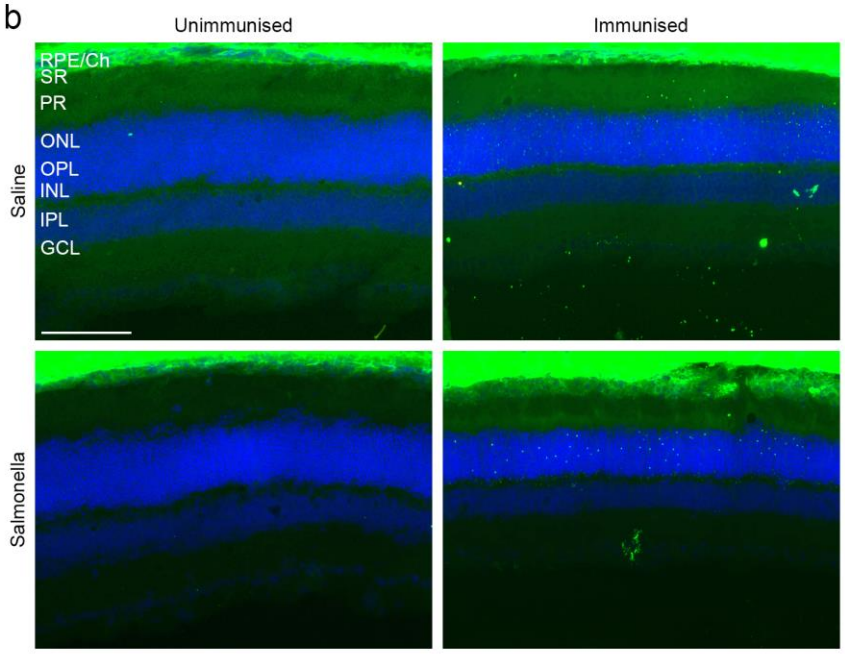
b
Unimmunised
Immunised
RPE/Ch
SR
PR
ONL
OPL
INL
IPL
GCL
Saline
Salmonella

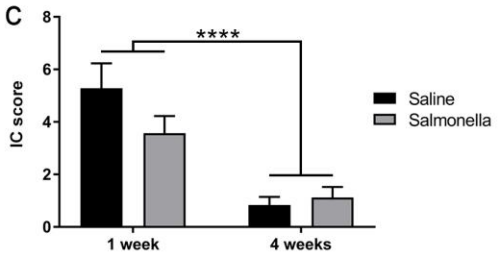
c
IC score
8
6
4
2
0
****
Saline
Salmonella
1 week
4 weeks

Figure 5.13 – The effect of Salmonella on number of immune complex in the retina.
*Half of the mice were immunised against OVA and the other half remained unimmunised. All the mice received an intravitreal injection of OVA (n=6-8 mice per group). At 24hrs post intravitreal OVA challenge, mice were injected i.p. with saline or Salmonella. Immune complex levels were analysed at (a) 1 and (b) 4 weeks post intravitreal OVA challenge. (a, b) Representative immunofluorescence showing OVA (red) and IgG (green) staining with DAPI (blue) counterstaining. (c) Quantification of immune complex levels using a scoring system, where 0 represents no complexes and 10 represents many deposits across the entire retina. Graphs are presented as mean±SEM. Data was analysed using two-way ANOVA for immunised mice only, as all scores for unimmunised mice were 0. Stars denote significance as follows: ****p<0.0001. RPE/Ch, Retinal pigment epithelium/Choroid; SR, subretinal space; PR, photoreceptor segments; ONL, outer nuclear layer; OPL, outer plexiform layer; INL, inner nuclear layer; IPL, inner plexiform layer; GCL, ganglion cell layer. Scale bar represents 100µm.*

5.3.7 Origin of activated amoeboid cells in the retina recruited by immune complexes

The FcγRI, CD11b and MHCII+ amoeboid immune cells that are present after OVA injection could be either activated microglia or cells recruited from the periphery (e.g. monocytes, neutrophils). It is difficult to distinguish microglia from macrophages by immunohistochemistry due to a lack of commercially available antibodies that are selective for microglia over macrophages. To determine the origin of these cells, I obtained two antibodies targeting FCRLS and P2RY12 (kindly donated by Dr. Oleg Butovsky, Harvard), which are highly expressed in microglia compared to other tissue-resident macrophage subpopulations (e.g. lung, liver, muscle) and also other immune cells (e.g. neutrophils, dendritic cells). These antibodies have previously been used to distinguish microglia in the brain from myeloid cells infiltrating into the brain (Butovsky et al., 2013). The FCRLS antibody showed clear staining of retinal microglia, but also cells in the choroid, sclera, muscle tissue, iris and cornea (Figure 5.14a-c). In contrast, P2RY12 staining was only found on a small number of cells, with faint staining on a couple of CD11b+ microglia and staining of CD11b+ cells in the choroid/sclera (Figure 5.14d-f). Overall, these antibodies appear unsuitable for addressing the question of cellular origins using the current immunohistochemistry protocol as microglial specificity with these antibodies is not observed.

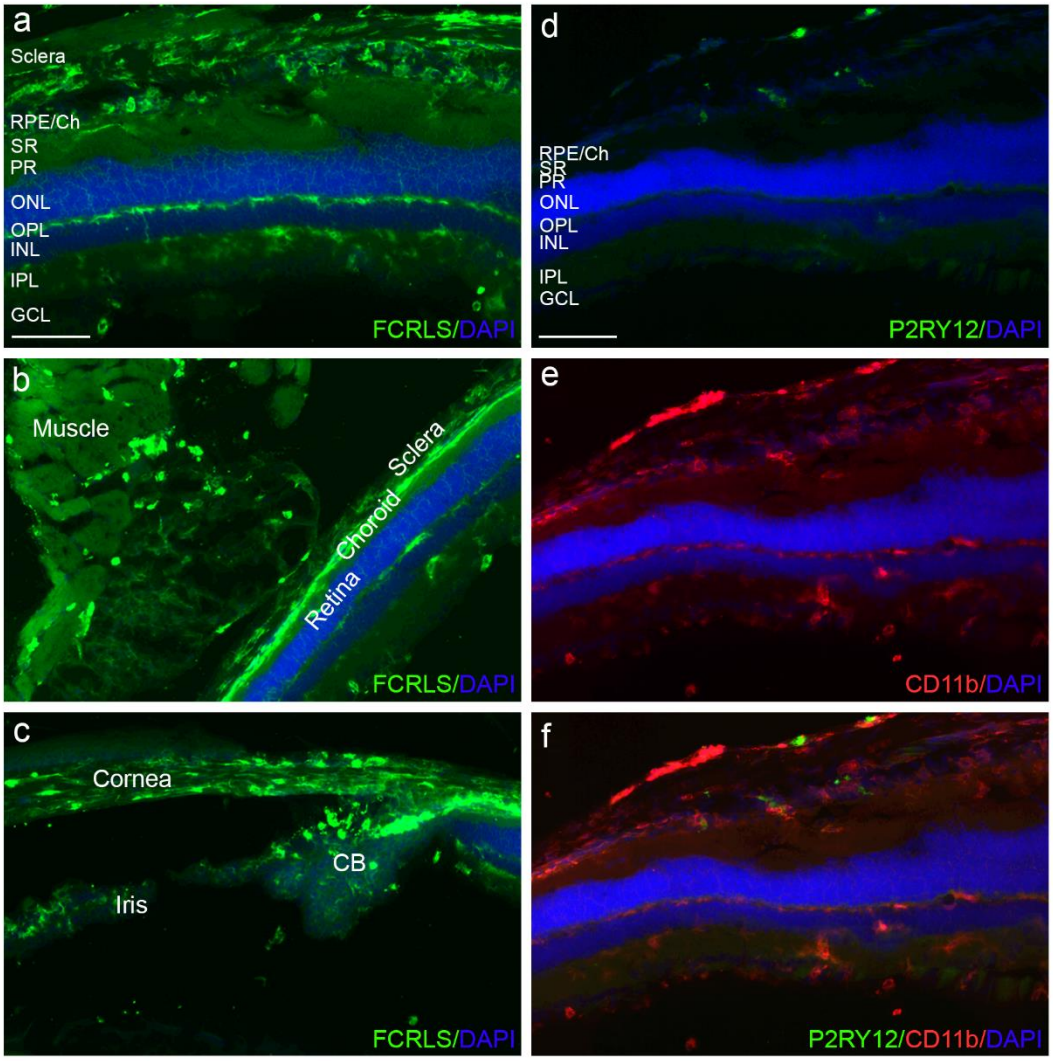

Figure 5.14 – Immunoreactivity of FCRLS and P2RY12 antibodies.

Representative immunofluorescent images of FCRLS (green) and DAPI (blue) counterstaining show that FCRLS is observed on (a) microglia and choroidal/scleral cells, (b) muscle tissue and (c) corneal and iris stromal tissue. Representative immunofluorescent images of P2RY12 (green), CD11b (red) and DAPI (blue) counterstaining shows (d) weak expression of P2RY12 on a few microglial cells, with staining also observed in choroidal cells. (e) CD11b staining reveals the full range of microglial/choroidal myeloid cells. (f) In the few cases of positive P2RY12 staining, they appear to colocalise with CD11b+ cells. RPE/Ch, Retinal pigment epithelium/Choroid; SR, subretinal space; PR, photoreceptor segments; ONL, outer nuclear layer; OPL, outer plexiform layer; INL, inner nuclear layer; IPL, inner plexiform layer; GCL, ganglion cell layer. Scale bar represents 100µm.

5.4 Discussion

5.4.1 Immune complex deposition and chronicity

There are 4 types of hypersensitivity reaction, which are characterised by overactivity of the immune system when responding to an antigen to which it is pre-sensitised. The type III hypersensitivity reaction occurs when immune complexes of antigen and antibodies are formed, leading to activation of many inflammatory pathways. Many human autoimmune conditions are driven by the formation of immune complexes, including rheumatoid arthritis and systemic lupus erythematosus. These have been modelled previously in mice using the Arthus reaction, where animals are immunised against an antigen and then injected intradermally to model a type III hypersensitivity reaction in the skin (Eggleton, 2001).

More recently, our lab has applied the Arthus reaction to the eye to generate immune complex mediated inflammation in the retina (Murinello et al. 2014). Immunisation against OVA, followed by intravitreal OVA challenge results in the development of retinal immune complexes, which are highly prevalent at 1 day post injection, moderately prevalent at 1 week post injection and absent at 2 weeks post injection (Murinello et al. 2014). In this study, immune complexes were clearly present in large numbers at 1 week post injection and there were also a small number of complexes remaining at 4 weeks post injection, demonstrating that this study showed greater chronicity of immune complex deposition than the previous study. Confocal analysis was undertaken to demonstrate that OVA and IgG are co-localised in immune complexes and are not just closely associated. In this study, immune complexes also appeared to deposit mostly in the subretinal/photoreceptor layers and less frequently in the ganglion cell layer in comparison to the previous study. There was one substantial change from the protocol used in the previous study, which was the use of a Hamilton syringe instead of pulled glass capillaries. The use of the syringe allows for more reproducible injections, both in terms of injection site and accurate administration of 1µl of solution. Another contributing factor may also have been the fresh preparation of OVA solution for each series of injections, preventing issues with freeze-thaw cycles or degradation over long term storage. These changes in terms of greater outer retinal deposition and chronicity are critical when trying to mimic some of the inflammatory changes which occur during AMD, a neurodegenerative mainly occurring at the back of the retina, which develops over many years.

5.4.2 Immune complex mediated inflammation

Drusen is the hallmark of AMD pathology and contains many inflammatory proteins, including IgG and complement components, as identified by immunohistochemistry and proteomics (Crabb et al., 2002; Johnson et al., 2000; Anderson et al., 2002). In this mouse model, immune complexes of antigen and antibody mostly deposit in the subretinal/photoreceptor layer, transiently recapitulating the deposition and inflammatory basis of human drusen. Immune complexes induce inflammation via two main pathways, which are activation of the complement pathway and activation of microglia, both of which are observed in AMD patients (Cherepanoff et al., 2010; Penfold et al., 1997; Combadière et al., 2007; Gupta et al., 2003; Karsten & Köhl, 2012).

A previous study of retinal immune complex mediated inflammation showed strong myeloid cell activation peaking at 3-7 days and returning to baseline by 2 weeks post injection (Murinello et al., 2014). Many of these cells show a highly activated amoeboid morphology, which may represent activated microglia or infiltrating immune cells. In this study, high levels of myeloid cell activation were identified in terms of the number of FcγRI, CD11b and MHCII+ amoeboid immune cells at 1 week post immune complex formation followed by reduced, but not absent, inflammation at 4 weeks post immune complex formation. Therefore, increased chronicity of microglial activation in this study correlates with the longer presence of immune complexes when compared to the previous study (Murinello et al., 2014).

The effect of immune complexes on other retinal cell types was also investigated. Activation of GFAP+ cells is also observed at 1 and 4 weeks post immune complex formation and is not different at each timepoint, indicating sustained activation. It appears that Müller cells are activated following immune complexes based on GFAP expression on Müller cell processes (Verderber et al., 1995). Oxidative stress has been shown to induce GFAP expression on Müller cells and oxidative stress may arise during inflammation due to production of ROS species by microglia (McVicar et al., 2015; Block et al., 2007). GFAP expression on astrocytes occurs strongly under healthy conditions, therefore assessing astrocytosis in this model is far more challenging. GFAP expression in the retina is increased in AMD patients (Wu et al., 2003), indicating another key feature of AMD that this model recapitulates.

There are also infiltrating T cells at 1 and 4 weeks post immune complex formation. This could be due to expression of chemokines in the retina causing chemotaxis of non-specific T cells. Alternatively, it could be more a specific process of recruiting OVA-specific T cells, which have been previously shown to migrate into the retina in response to intraocular OVA (Hu et al., 2000). Whether T cells are involved in AMD is far less clear than for myeloid cells and GFAP+ cells; there is certainly some indirect evidence for an autoimmune component in AMD (see introduction

section 1.4.6). This model provides a platform to investigate T cell responses in the retina in more detail that may be relevant to our understanding of AMD pathology.

5.4.3 *In vivo* changes following immune complex formation

At 1 week post immune complex formation in the retina, occasional areas of hyper- and hypo-reflective pathology were identified by OCT. A hyporeflective core surrounded by a hyperreflective border was observed in 2 of 8 mice following immune complex formation. This pathology shows remarkable similarity to human OCT scans of outer retinal tubulation (ORT), an abnormal structure observed in many retinal diseases including advanced AMD (Schaal et al., 2015). ORT is an area of neurodegeneration and gliosis where degenerating photoreceptors are enveloped by Müller cells (Dolz-Marco et al., 2016). Hyperreflective pathology was also observed as large, roughly circular, structures that displaced the inner retinal layers in 4 of 8 mice. The origins of this pathology are unclear, but similar structures are observed in OCT scans of murine EAU (Chen et al., 2013a). The high levels of inflammation in EAU and infiltration of neutrophils, T cells and monocytes may result in these abnormalities (Zhao et al., 2014). Alternatively, the area may be due to the formation of a giant immune complex in the inner retina. It is unlikely to be due to oedema, as intraretinal fluid is typically hyporeflective (Al-Mujaini et al., 2013).

Alongside these OCT abnormalities at 1 week post immune complex formation, there are ERG deficits in b-wave amplitude, indicating a deficit in retinal function. There were no significant deficits in a-wave amplitude, which means that b-wave deficits are likely due to dysfunction of signal processing throughout the retina as opposed to a specific deficit occurring at the photoreceptors (Pinto et al., 2007). At 4 weeks post immune complex formation, these b-wave deficits have resolved and retinal function returns to the level of unimmunised mice. This indicates a transient inflammation-induced deficit in neuronal communication at 1 week after immune complex formation. In AMD patients, both a- and b-wave deficits are observed in early AMD, but these deficits remain stable throughout further disease progression (Walter et al., 1999). Immune complexes induce transient b-wave deficits but do not recapitulate the a-wave deficits indicative of photoreceptor dysfunction in AMD patients, despite immune complexes forming mainly in the subretinal space/photoreceptor.

Overall, these *in vivo* imaging techniques reveal transient structural alterations to the retina that have not been previously detected using immunohistochemistry and have functional consequences for retinal excitability.

5.4.4 The effect of Salmonella infection on immune complex mediated myeloid cell activation

The immune complex model provides a tool to investigate the impact of systemic infection on a variety of inflammatory processes associated with early stage AMD pathology. Although the inflammatory effect of Salmonella appears to be stronger in C57BL/6, this strain is also less capable of generating immune complexes under our current protocol (Salome Murinello, PhD thesis). Consequently, it was necessary to use BALB/c mice to test the effects of Salmonella on immune-complex mediated retinal inflammation. Other advantages to using this strain are the ability to observe immune cells at the back of the retina with immunochemistry due to lack of pigmentation and also if effects are seen in a strain with a weaker response to Salmonella, they are likely applicable to strains with stronger inflammation.

To model the interaction of local and systemic inflammation, mice were given Salmonella 24 hours post intravitreal OVA injection. At the 1 week timepoint, there are high levels of inflammation in the retina following immune complexes and high levels of systemic inflammation following Salmonella infection. At the 4 week timepoint, both immune-complex mediated inflammation in the retina and systemic inflammation due to Salmonella are much lower, but both types of inflammation have persisted for much longer, giving a more chronic model.

At 1 and 4 week post immune complex formation, neither Salmonella or immune complexes increased the percentage area of CD11b or FcγRI staining. However, because OVA injection alone increases CD11b and FcγRI expression and percentage area quantification is binary (i.e. stained or unstained), this quantification method may not be particularly sensitive to changes when applied to this model. Furthermore, highly activated microglia lose ramifications and become hypertrophic, which could reduce the total staining area. At 1 week post immune complex formation, there is an increase in FcγRI+ and CD11b+ amoeboid immune cells, which is not affected by Salmonella infection. The number of amoeboid cells in the retina is a previously published measure of immune complex inflammation (Murinello et al., 2014) and the data suggests that Salmonella infection does not contribute much to the levels of myeloid cell activation/recruitment when immune complexes are present.

The amoeboid cells recruited by immune complexes are mainly found in the inner retinal layers/vitreous and may be infiltrating immune cells or highly activated microglia. Detailed FACS analysis, as performed in other studies, would provide a more comprehensive overview of immune cell phenotype and may identify whether the cells are of retinal or systemic origin (O'Koren et al., 2016; Kerr et al., 2008a). If these amoeboid immune cells have a systemic origin, based on their localisation they may infiltrate from the inner BRB as the vitreous itself is not

vascularised (Streilein, 2003). Alternatively, damage caused by the intravitreal injection may disrupt ocular immune privilege and enable the infiltration of immune cells.

Following viral infection, myeloid cells are recruited to the subretinal space (Zinkernagel et al., 2013). Consequently, I investigated whether this was also the case following Salmonella infection. Interestingly, immune complexes and Salmonella infection could cause recruitment of myeloid cells to the subretinal space individually and these effects were additive when combined for FcγRI+ cells at 1 and 4 weeks post immune complex injection. CD11b+ showed the same additive effect at 1 week post immune complex formation and non-significant synergy at 4 weeks (Salmonella effect: p=0.01, Immunisation effect: p=0.10). Overall, these data indicate that immune complexes induce strong myeloid cell activation and their migration/recruitment to the back of the retina, which lasts beyond 4 weeks post formation. The recruitment/migration of myeloid cells to the back of the retina can be exacerbated by systemic infection. This may have consequences for photoreceptor function, and in the context of AMD accelerate neurodegeneration, as immune cells could be recruited to the site of pathology by infections and then be activated by the inflammatory microenvironment during ongoing local pathology.

Based on bone marrow chimera experiments, subretinal immune cells following systemic viral infection appear to come from the microglial population and are not infiltrating myeloid cells (Zinkernagel et al., 2013). This method used wholemount imaging across the plane of the subretinal space. In contrast, the cryosections in this thesis are taken at 90° to this plane, which allows us to also characterise the inner retinal cells but only provides a snapshot of the subretinal space. I attempted to identify the local or peripheral origin of the subretinal cells in the immune complex and Salmonella models using FCRLS and P2RY12 antibodies, which have been described as highly expressed in microglia compared to other monocyte/macrophage populations (Butovsky et al., 2013). However, neither antibody showed microglial specificity in this study, meaning the origins of these cells in this model remains uncharacterised. There are a large number of immune cells in the choroid following Salmonella infection and these may be able to enter through the outer BRB, particularly in the presence of immune complex mediated inflammation. Future experiments could use bone-marrow chimeras or detailed FACS analysis to distinguish microglia and peripheral monocytes/macrophages. Alternatively, these experiments could be performed in CCR2 knockout mice, where monocytes are mostly depleted from the blood due to sequestration in the bone marrow (Fujimura et al., 2015), but retinal microglial recruitment may also be altered in this strain (see introduction section 1.4.4), which would confound the results.

Under resting conditions, microglia show very low phagocytic/endocytic activity when compared to other macrophage populations, but this activity is greatly increased in highly activated

microglia (Aloisi, 2001). Immune complexes can be phagocytosed by retinal myeloid cells for subsequent degradation as one route of immune complex clearance (Elena Pipi, unpublished observation). Consequently, I investigated whether systemic inflammation during immune complex mediated retinal inflammation could alter the phagocytic function of microglia by assessing immune complex clearance. At 1 and 4 weeks post immune complex formation, no differences in phagocytic activity of microglia were observed, indicating systemic inflammation does not alter phagocytic activity of locally activated immune cells.

5.4.5 Effect of immune complexes and Salmonella on Müller cells and T cells

Immune complexes have been previously shown to recruit T cells to the retina at 1 week post immune complex formation (Salome Murinello, PhD thesis), but a 4 week timepoint was not investigated. As a live bacterial infection, Salmonella activates the adaptive immune system and T cell activation/proliferation and the consequences of this on immune complex-mediated T cell recruitment was investigated. At 1 week post immune complex formation, there is an increased number of T cells in the retina. However, there is a trend to reduced T cells when immune complexes are combined with Salmonella compared to immune complexes alone ($p=0.10$). If this is a true effect then this would suggest that T cell recruitment is impaired by Salmonella. This could be because inflammation is higher in the periphery following Salmonella causing chemotaxis to favour the periphery instead of the retina. Alternatively, infiltration of T cells into the brain parenchyma has been shown to eventually lead to apoptosis (Bauer et al., 1998) and increased retinal inflammation may accelerate this process leading to retinal T cell depletion.

At 4 weeks post immune complex formation, there is a Salmonella effect in addition to an immune complex effect, although the two don't appear to be synergistic. This would be in line with a strong adaptive immune system following 4 weeks of Salmonella infection and reduced peripheral cytokines, meaning the retina may be favoured for chemotaxis. The majority of T cells are located in the inner retinal layers, including that the inner BRB may be responsible for their recruitment. However, in some mice a number of T cells were identified in the choroid, which may be a route of entry into the retina via the outer BRB. T cells are also found as approximately 40% of CD45+ cells found in the aged human choroid (Ezzat et al., 2008). As the outer BRB, but not the inner BRB, skews the phenotype of infiltrating T cells, this may lead to differential function of these cells. The presence of numerous T cells in choroid may also effect outer BRB function (e.g. permeability or induce inflammation). It appears that T cell infiltration can be both beneficial and damaging under different circumstances (Schwartz & Shechter, 2010; Cruz-Guilloty et al., 2014; Boldison et al., 2014; Mcpherson et al., 2014), so a clear picture of the function of infiltrating T cells is important.

In this chapter, it is shown that Müller cells are activated by immune complexes, recapitulating the Müller cell activation that is observed in AMD patients (Wu et al., 2003). I investigated whether this activation could be exacerbated by systemic inflammation. At 1 week post immune complex formation, GFAP expression in the retina was increased, but this was not exacerbated by Salmonella. Furthermore, GFAP expression returned to unimmunised control levels by 4 weeks post immune complex formation, indicating Müller cell/astrocyte activation is not as sustained as microglial activation or T cell recruitment.

5.4.6 Effect of immune complexes and Salmonella on blood vessels

Salmonella activates the inner retinal blood vessels and consequently I investigated whether this activation could be modified by local inflammation. At 1 week post immune complex formation, there is increased ICAM-1 expression on retinal blood vessels. In contrast, at 4 weeks post immune complex formation, Salmonella increases ICAM-1 expression and there is a strong trend for a reduction in ICAM-1 expression back to control levels when Salmonella and immune complexes are combined ($p=0.054$). In this manner, the retina appears to be tolerant to Salmonella-induced ICAM-1 expression when there is ongoing local inflammation. This may be a protective mechanism to reduce recruitment of immune cells to the retina during chronic inflammation. This has been observed in a mouse model of type 2 diabetes, where chronic hyperglycaemia eventually leads to ICAM-1 reduction, although infiltrating cells could still access the retina in an ICAM-1 independent manner (Noda et al., 2014). This tolerance effect may be another explanation for why T cell recruitment to the retina is impaired when Salmonella and immune complexes are combined, as a protective mechanism to prevent excessive inflammation.

Salmonella induces expression of MHCII on blood vessels while immune complexes induce expression of MHCII on microglia at 1 and 4 weeks post challenge. At 1 week post intravitreal injection, immune complexes and Salmonella combine to give both blood vessel and microglial expression in the same retinas. There may be consequences of this combined expression for the function of both cells beyond simple co-expression. Flow cytometric analysis of microglial cell and endothelial cell phenotype or cell sorting for transcriptomic analysis would provide a better overview of the functional characteristics of these cells. In contrast at 4 weeks post intravitreal injection, the combination of immune complexes leads to expression of MHCII either on blood vessels or microglia. Overall these data indicate an active process of MHCII downregulation on either microglia or blood vessels. The reasons for this divergent effect are unclear, but may differ based on the balance of local and systemic inflammation in these mice.

5.4.7 Summary

Retinal immune complexes induce local inflammation characterised by microglial and Müller cell activation, T cell recruitment and transient abnormalities in retinal structure and function. When immune complex formation was combined with Salmonella infection, myeloid cells, which may be microglia or infiltrating cells, were recruited to the subretinal space. Salmonella did not alter the number of highly activated microglia, indicating Salmonella is responsible for recruitment, but not activation, of cells in the subretinal space. In the context of AMD, this means that systemic bacterial infection may recruit myeloid cells to the subretinal space, where there is chronic local inflammation and degeneration, which could activate these recruited cells and accelerate disease pathology.

Chapter 6:

A mouse model of atrophic lesions targeted to the outer retina: insights into human geographic atrophy

6.1 Introduction

The immune complex model developed by our lab and characterised in Chapter 5 allows for the examination of antibody and complement-mediated inflammatory changes in the retina. In this model, there is a clear role for activation of FcγR-expressing immune cells, which can be exacerbated by systemic inflammation, and these insights may be highly relevant to the early stages of AMD. However, the inflammatory changes following immune complex formation do not appear to lead to degeneration in our model of early inflammatory aspects of AMD, preventing its use in understanding later stages of the disease and how inflammation and degeneration are related. Developing a mouse model with features of inflammation and progressive degeneration is critical to understanding GA pathobiology and would represent a model for testing possible therapies.

The importance of such a model is highlighted by successful advances in wet AMD treatment that were supported by findings from a mouse model. The laser-induced mouse model of CNV has become by far the most used and accepted model of late stage wet AMD. In this model, application of 532nm laser light ruptures Bruch's Membrane, leading to the rapid growth of new blood vessels into the retina (Lambert et al., 2013). As seen in humans, VEGF is the key driver of angiogenesis in this experimental CNV model and neutralisation of VEGF leads to reduced disease severity (Seo et al., 1999; Kwak et al., 2000; Saishin et al., 2003). This acute experimental model has also offered many insights into the disease itself with other contributing factors identified (including CCL2, TNFα and MAC), which are possible targets for combination therapy (Liu et al., 2011b; Shi et al., 2006).

In contrast, there is currently is no disease modifying therapy available for GA patients and the main reasons for this are an incomplete understanding of the pathobiology and a lack of mouse models showing enough similarities to the human condition to test therapies. The key features of GA include:

- RPE dysfunction followed by loss of photoreceptors due to lack of trophic support (Bird et al., 2014)
- Abnormalities in retinal structure and function as measured by OCT and ERG (Walter et al., 1999; Litts et al., 2017; Panorgias et al., 2013)
- Microglial cell activation (Cao et al., 2011; Gupta et al., 2003; Cherepanoff et al., 2010; Penfold et al., 1997; Combadière et al., 2007)
- Inflammasome activation leading to mature IL-1β and IL-18 (Tarallo et al., 2012)
- Müller cell activation (Wu et al., 2003)

In this chapter, I characterise a laser-induced model of GA that develops many of these features and may provide an acute and reproducible model of outer retinal atrophy. This model may deliver insights into GA pathobiology and enable screening of possible therapeutic interventions. Photocoagulation of the retina using an 810nm diode laser has been used in humans to cause severe damage to the RPE cells leading to cell death, while greatly minimising damage to the inner layers of the retina. This is possible because the laser passes through the neurosensory retina with minimal absorption and is then strongly absorbed by the melanin in RPE causing thermal damage and the subsequent death of the RPE cells (Yu et al., 2013). As RPE cell dysfunction/death is thought to lead to photoreceptor loss in AMD due to loss of trophic support, this laser application may allow for the geographic loss of RPE cells leading to photoreceptor loss. A limited number of mouse and rabbit studies using 810nm diode laser photocoagulation have observed loss of RPE cells and some have also seen loss of photoreceptor layer (Qiao et al., 2009; Desmettre et al., 2003; Tackenberg et al., 2009; Morimura et al., 2004). These studies have focused on immune privilege, Müller cell activation and heat shock protein expression, which means that the inflammatory and degenerative aspects of these lesions are poorly described. Here, I characterise the progression of lesions in terms of structure and function and examine the expression of inflammatory, oxidative stress and atrophic markers, many of which are highly implicated in GA pathobiology.

6.2 Methods

6.2.1 Laser Power Optimisation

3 month old C57BL/6 mice were given recovery anaesthesia, and pupils were dilated and imaged by fundoscopy (see section 2.1.4.2). A laser injector (diameter 400µm) was used to apply a focused 810nm wavelength diode laser to the retina at fixed power (see section 2.1.5). Multiple adjacent areas of each retina were targeted with either low (22mW for ≈60s), medium (32mW for ≈60s) and high (42mW for ≈60s) power laser (n=5 mice per group). Lesions were investigated by fundoscopy and OCT (see section 2.1.4.3) at 4 weeks after laser treatment to study lesion severity, size and confluence at the different laser powers. Mice were transcardially perfused and eyes were enucleated and snap-frozen in OCT for immunohistochemistry (see section 2.1.6). Dr. Elena Pipi sectioned and stained the lesions after medium power laser treatment to investigate inflammation at the lesion site (see section 2.2).

6.2.2 Lesion Progression Study

Atrophic lesions were induced in 5-month-old C57BL/6 mice (n=14) by medium dose (32mW for ≈60s) laser treatment. During laser treatment, multiple adjacent areas of each retina were targeted and fundoscopy images were taken before and immediately post laser treatment. The mice were tracked over time to follow the progression of laser-induced atrophic lesions. Mice were imaged by ERG (see section 2.1.4.1), OCT and fundoscopy one week before and one, two, four and eight weeks after laser treatment. OCT and fundoscopy images from each mouse over time were compared to study lesion progression. A-wave amplitude, B-wave amplitude and B-wave implicit time were determined from ERG traces (see section 2.1.4.1) and tested for significant differences by two-way ANOVA repeated by both measures (Variable 1: Time; Variable 2: Control versus laser-treated eye) with Holm- Šídák post hoc testing. Mice were excluded from analysis if no/low pathology was observed by these methods or baseline ERG readings showed functional abnormalities. Dr. Elena Pipi assisted with *in vivo* imaging by preparing mice for these procedures (i.e. anaesthesia, tropicamide, phenylephrine) and recovering mice after the procedure.

6.2.3 Laser treatment for RNA and toluidine blue staining

Young (5 months, n=9) and middle-aged (11-13 months, n=4) C57BL/6 mice were laser-treated using an 810nm laser at 32mW by Dr. Srini Goverdhan for RNA analysis of oxidative stress and inflammation. RNA analysis was performed on these mice as described in Section 2.4. 18 paired one-tailed T-tests were conducted on each gene comparing the control and laser-treated eye, followed by Holm-Šídák multiple comparisons correction. All genes were tested for increased expression, except Dicer1 which was tested for decreased expression. For toluidine blue staining, Dr. Srini Goverdan and Maureen Gatherer performed laser treatment on middle-aged mice and tissue was harvested at 12 weeks post laser treatment. Toluidine blue histology was performed by the Histochemistry Research and Biomedical Imaging Units at the University of Southampton.

6.3 Results

6.3.1.1 Laser dosage optimisation study

Three different laser powers were tested to determine the optimum settings to give reproducible lesions for follow-up studies. The doses tested are henceforth described as low (22mW power for approximately 60s), medium (32mW power for approximately 60s) and high (42mW power for approximately 60s). The duration values given for each spot are a guide only because laser duration for each spot was modified to give consistent discolouration to each spot making up the retinal lesion based on visualisation of the lesioned area during fundoscopy.

Fundoscopy images (Figure 6.1a, b) show that low-dose laser treatment did not cause atrophic lesions at one month post laser treatment in most cases. A few small areas of pathology developed from the most severe laser-treated spots, but these were not consistent or reproducible. Both medium and high-dose laser treatment resulted in visible atrophic lesions at one month post laser (Figure 6.1c-f). These lesions were characterised by a central hyperpigmented area surrounded by brighter hazy areas at the margins of the lesion. Medium-dose laser treatment induced many local areas of atrophy, some of which became confluent, while high-dose laser treatment induced large scale confluent atrophy of the laser-treated area. Human GA patients often show separate local areas of atrophy which eventually merge and become confluent (Figure 6.1g), similar to what was observed in a dose-dependent manner with this model (Schmitz-Valckenberg, 2017).

At one month post low-dose laser treatment, OCT scans showed minimal disruption of retinal layers (Figure 6.2b), although it was hard to find the laser-treated sites in these mice as there was not much pathology. At one month post medium-dose laser treatment, the atrophic lesion showed a hyperreflective damaged area at the back of the retina (Figure 6.2c). The reasons for this hyperreflective pathology are unclear but may represent inflammation, atrophy or fibrosis as described in more detail in the discussion. The laser-treated area also shows the disappearance of the photoreceptor segments and nuclei, with the INL now in close apposition to the hyperreflective part of the lesion. Some of the laser-treated areas became confluent while some spots were still distinguishable from each other (Appendix D1), in line with observations from fundoscopy. In contrast, the atrophic areas at one month post high-dose laser treatment showed almost all of the atrophic lesions were confluent (Figure 6.2d). Additionally, the hyperreflective part of the lesion appears wider and thicker in mice receiving high-dose laser treatment compared to medium-dose laser treatment, indicating greater pathology after high-dose laser treatment.

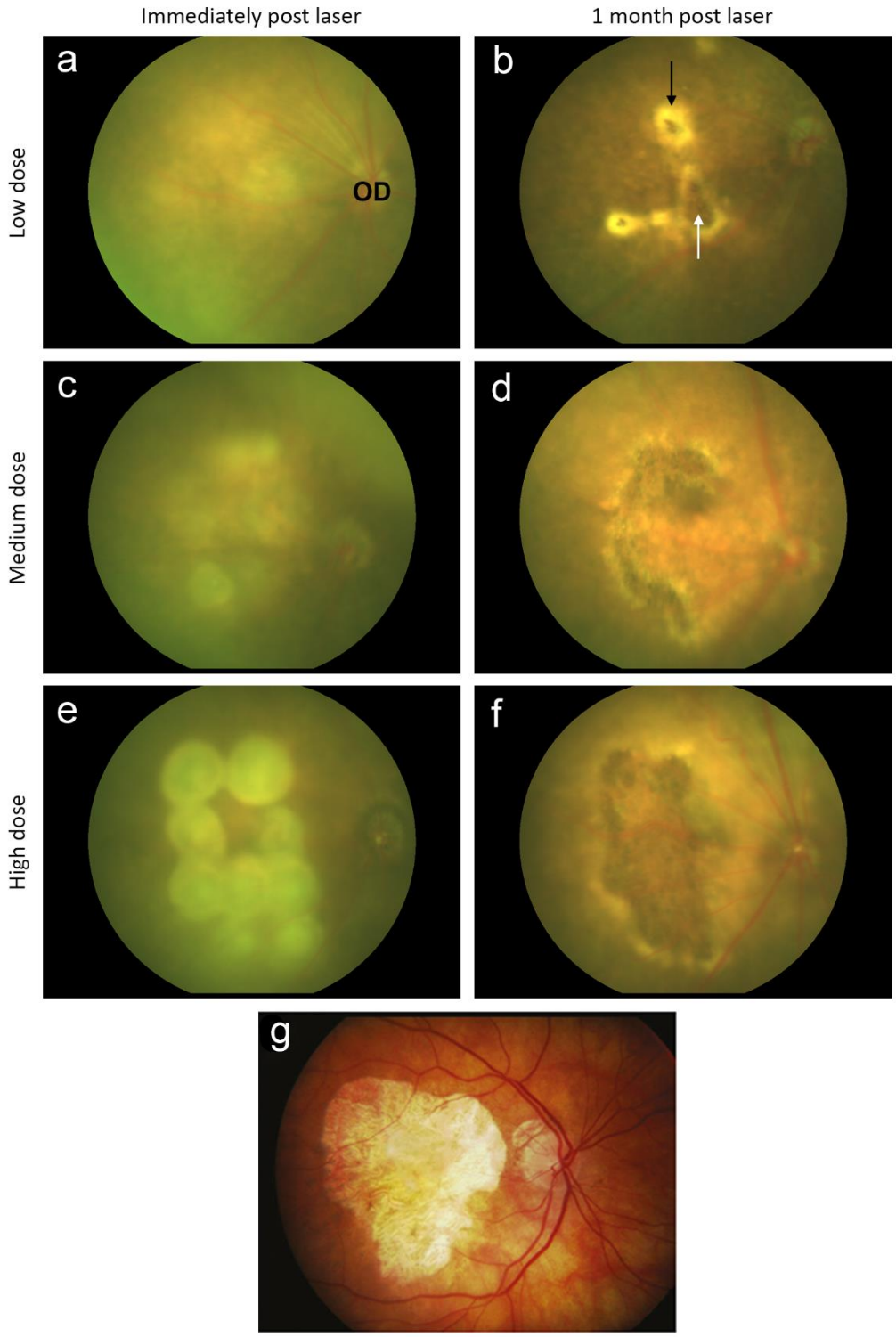

Figure 6.1 – Fundoscopy of laser-induced lesions at different laser powers.

Representative retinal fundoscopy images of (a, b) low, (c, d) medium and (e, f) high-dose laser treatment taken (a, c, e) immediately and (b, d, f) one month post laser treatment (n=4 mice per group, 5 months). (g) Fundoscopy image of human GA (taken from Black & Clark, 2016). Black arrow denotes hypopigmented margins of the atrophic lesions and white arrow denotes hyperpigmented centre of the atrophic lesions. OD, optic disc.

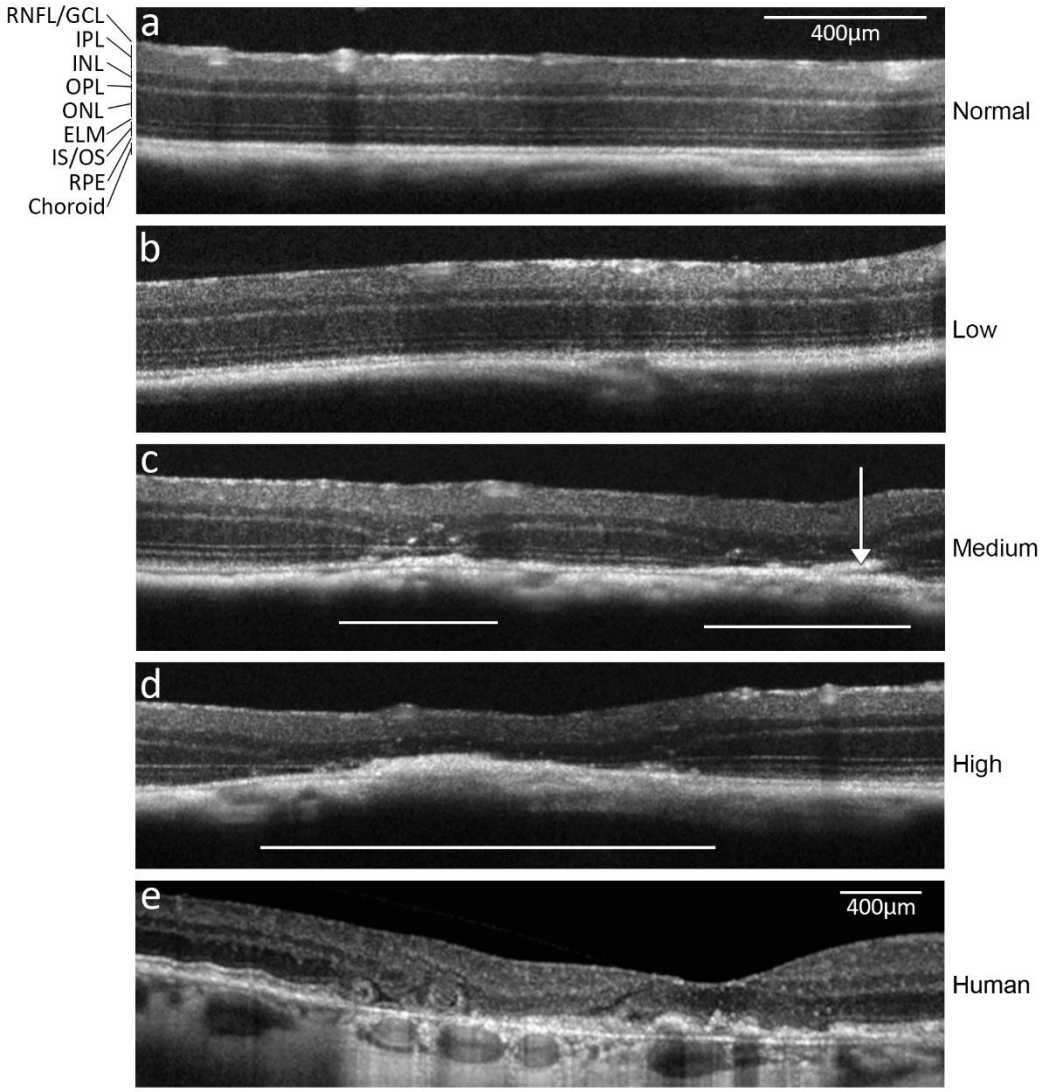

Figure 6.2 – OCT scans of laser-induced lesions at different laser powers.

Representative retinal OCT scans taken from (a) non laser-treated, (b) low-dose laser-treated, (c) medium-dose laser-treated and (d) high-dose laser-treated mice at one-month post laser treatment (n=4 mice per group, 5 months). (e) OCT scan of human GA (taken from Litts et al., 2016. Areas of laser-induced damage are underlined and the white arrow shows an example of a hyperreflective area. RNFL, Retinal nerve fibre layer; GCL, ganglion cell layer; IPL, inner plexiform layer; INL, inner nuclear layer; OPL, outer plexiform layer; ONL, outer nuclear layer; ELM, external limiting membrane; IS/OS, photoreceptor inner segments/outer segments; RPE, retinal pigment epithelium.

Furthermore, it seems that the INL is more disrupted in mice receiving high-dose laser treatment compared to medium dose laser treatment, although it is unclear whether it is due to the enhanced confluence of the lesions or more severe damage to the inner retina, or a combination of both. OCT scans of human GA also show hyperreflective areas of pathology at the outer retina that resemble those seen in this model, as well as a collapse of the outer retina, such that the INL lies close to the choroid (Figure 6.2e).

6.3.1.2 Laser-induced atrophic lesion progression over time

Next, the lesions were investigated to examine the progression of retinal collapse and function over time. Medium-dose laser treatment was used in these experiments as this dose gave reproducible lesions in fundoscopy and OCT scans and showed a lower amount of initial damage in comparison to the mice given high-dose laser treatment. The high-dose laser-treated group is less likely to show progression as the starting level of retinal damage and collapse is greater. The size and severity of medium dose laser-induced retinal lesions over time were tracked using fundoscopy and OCT to investigate retinal structure and focal ERG to investigate retinal function. Overall, 4 of 14 mice showed little evidence of pathology in fundoscopy, OCT and ERG and were excluded from analysis. 2 further mice were excluded from analysis due to severe ERG deficits in one or both eyes during baseline measurements, suggesting prior dysfunction that would prevent an accurate assessment of retinal structure/function post laser treatment.

Fundoscopy images of 8 mice with pathology show that there an evolution of the lesion over time (Figure 6.3). At one week post laser treatment, much of the lesion has a hazy bright appearance, possibly indicating inflammation. Over successive weeks the centre of the lesion becomes more hyperpigmented, while the hazy bright area becomes confined to the margins of the lesion. The margins of the lesion also seem to become more defined over time. The fundoscopy images show that there is not a clear progression in the size of the retinal lesion between one and eight weeks post laser treatment. However, fundoscopy is not a sensitive method to judge lesion area as it is not possible to orientate the mice in an identical manner at every imaging session, which introduces confounding factors in the appearance of each lesion.

OCT scans show evidence of changes to the structure of the atrophic lesions over time (Figure 6.4). At one and two weeks post laser treatment, the hyperreflective pathology at the outer retina is thick and very pronounced, but mean retinal thickness progressively reduces at four and eight weeks. This reduction could indicate clearance of the damaged retinal components or reduced inflammation. At the same time, there appears to be a progressive collapse of the retina over time from 1 week to 2 weeks post laser ($p=0.0207$) and then from 2 weeks post laser to 4 weeks ($p=0.006$) and 8 weeks post laser ($p=0.0207$), although it is unclear whether this is because of the

progressive degeneration of retinal layers or because the layers are already damaged and shift backwards as debris is cleared from the retina. There are also some indications that the width of INL pathology increases over time, indicating progression of the lesion outwards, but quantification of these changes has proven difficult and will be addressed in discussion. Overall, OCT scans provide better tracking of the retinal lesion than fundoscopy, as the orientation of the mouse in the scan is more reproducible between sessions.

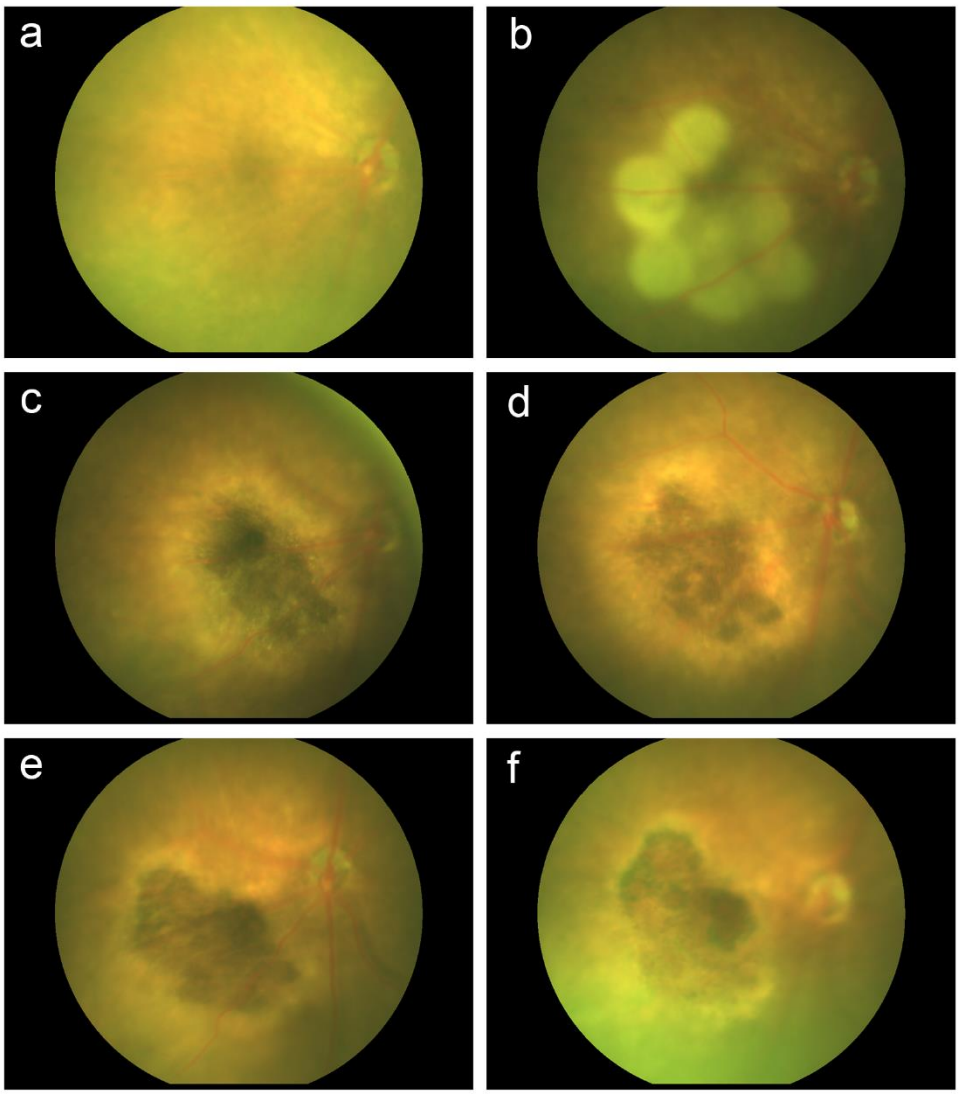

Figure 6.3 – Fundoscopy images showing progression of laser-induced lesions over time. *Representative retinal fundoscopy images of (a) immediately before, (b) immediately post and (c) one, (d) two, (e) four and (f) eight weeks post laser treatment. Eight mice (5 months old) were tracked over time and fundoscopy images of the other mice over time are presented in Appendix D1.*

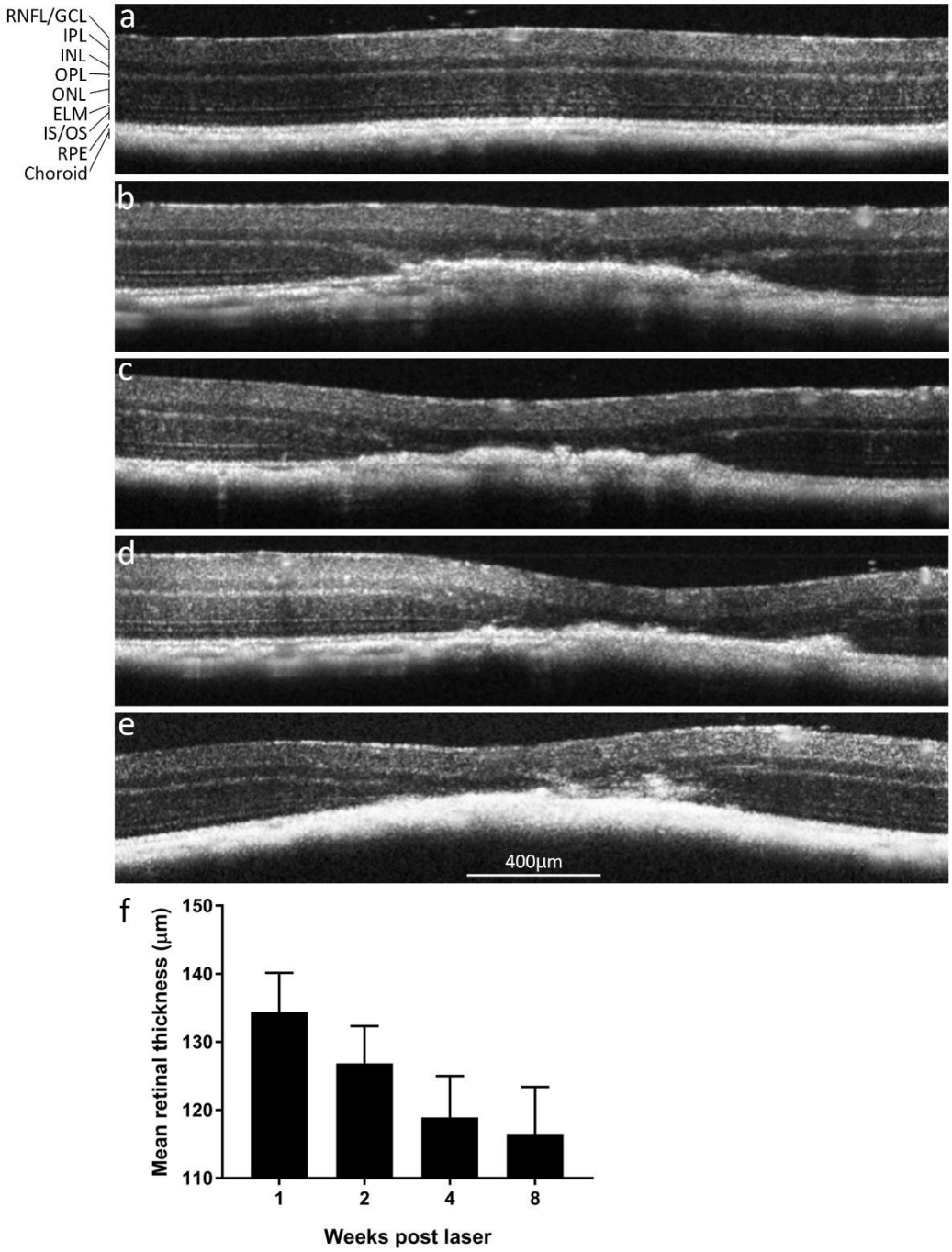

Figure 6.4 – OCT images showing progression of laser-induced lesions over time.

*Representative retinal OCT scans taken from (a) non-laser treated mice and at (b) one, (c) two, (d) four and (e) eight weeks post laser treatment. Eight mice (5 months old) were tracked over time and OCT scans of the other mice over time are provided in Appendix D2. (f) Quantification of mean retinal thickness(RNFL to RPE) across 560µm of retina centred on the lesion. RNFL, Retinal nerve fibre layer; GCL, ganglion cell layer; IPL, inner plexiform layer; INL, inner nuclear layer; OPL, outer plexiform layer; ONL, outer nuclear layer; ELM, external limiting membrane; IS/OS, photoreceptor inner segments/outer segments; RPE, retinal pigment epithelium. Data was analysed using two-way ANOVA with Holm-Sidak post-hoc testing. Stars denote significance as follows: *p<0.05, **p<0.01, ****p<0.0001.*

ERG traces show an overall reduction of 23.4% in A-wave amplitude between the laser-treated and control eye across all timepoints ($F_{1,7}$ = 39.31, p=0.0004). Post-hoc testing demonstrated a significant decrease in A-wave amplitude of 20.2%, 24.4%, 27.1% and 21.8% at one, two, four and eight weeks post laser treatment respectively, showing that ERG deficits are present at one week and persist for at least eight weeks post laser treatment (Figure 6.5a). A-wave deficits indicate impairment of photoreceptor function after laser treatment throughout the experiment. There is an overall reduction of 22.8% in B-wave amplitude between the laser-treated and control eye across all timepoints ($F_{1,7}$ = 64, p=<0.0001). Post-hoc testing showed there is a significant reduction in B-wave amplitude of 19.5%, 24.5%, 26.7% and 20.4% at one, two, four and eight weeks respectively (Figure 6.5b). The degree of A-wave and B-wave deficits are remarkably similar, indicating that the photoreceptor deficits also result in reduced signalling to the bipolar cells/ganglion cell layers. B-wave implicit time is also increased in laser-treated eye compared to control eye ($F_{1,7}$ = 9.646, p=0.0172). These changes didn't reach significance at any timepoint in multiple comparison testing, although there is a trend for increased implicit time in the laser-treated eyes at 1, 2 and 4 weeks post laser treatment, but not at 8 weeks post laser treatment possibly indicating some recovery of ERG deficits by this timepoint.

Overall, medium dose laser treatment induces atrophic lesions with sustained pathology between one and eight weeks post laser treatment. Fundoscopy shows the lesions are geographic and evolve over time to become hyperpigmented, although there is not clear evidence for outward progression of the lesion. OCT scans show hyperreflective pathology at the outer retina at 1 week post laser treatment, which resolves over time. Meanwhile, the outer retinal layers collapse to leave the intact inner retinal layers in apposition with the choroid. Focal ERGs show the lesion results in long-term functional deficits in the photoreceptor layer and subsequent signalling, which are not progressive.

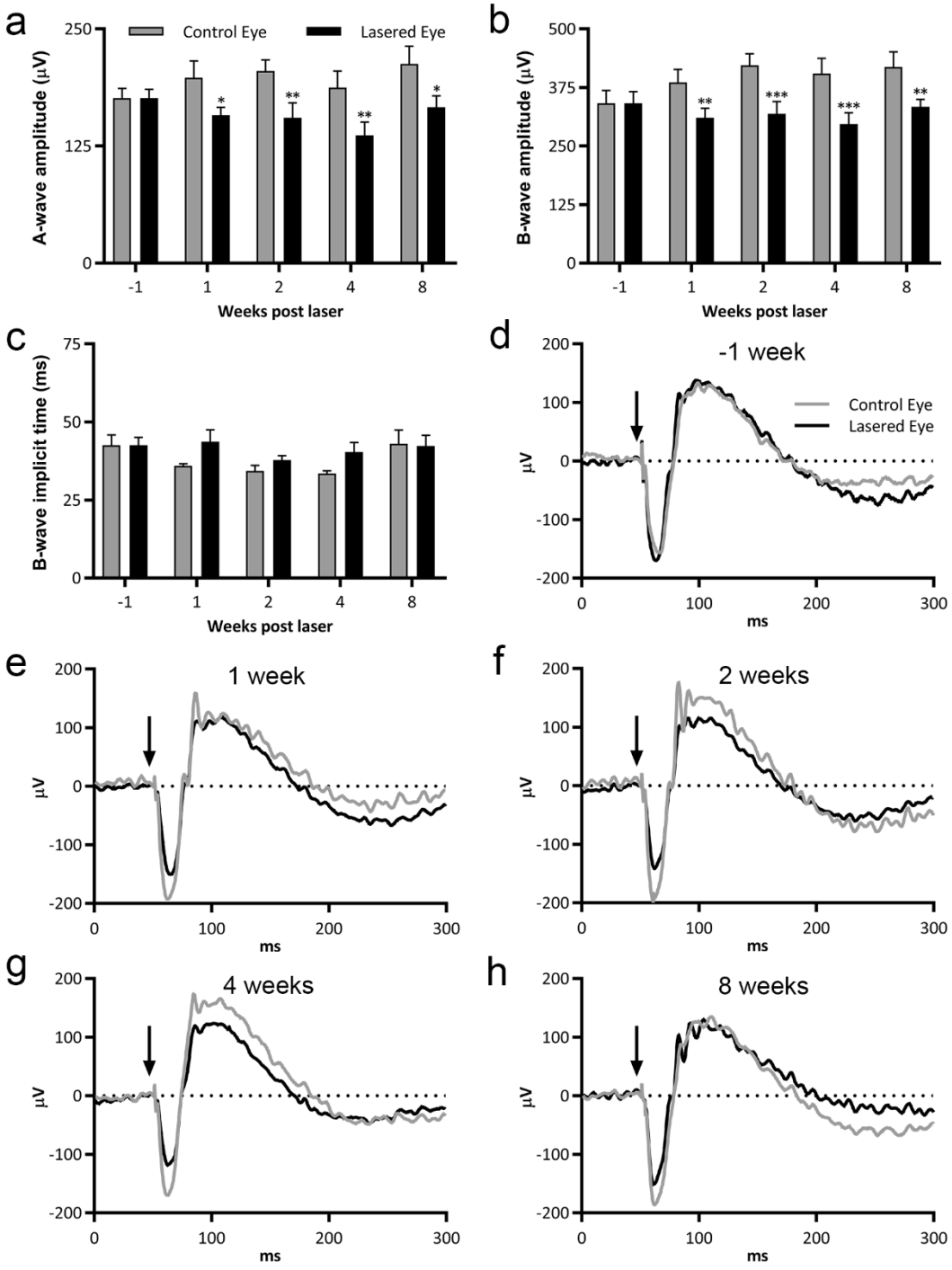

Figure 6.5 – ERG analysis of retinas containing laser-induced lesions over time.

*Quantification of (a) A-wave amplitude, (b) B-wave amplitude and (c) B-wave implicit time from the laser-treated and non-laser treated eyes at baseline and one, two, four and eight weeks post laser treatment (n=8 mice, 5 months). Average ERG traces for each group are shown for (d) one week before and (e) one, (f) two, (g) four and (h) eight weeks post laser treatment. Arrows indicate the application of the light stimulus. Data was analysed using two-way ANOVA (repeated measures by both factors, factor 1: control vs laser-treated eye, factor 2: time) with Holm-Sidak post-hoc testing. Stars denote significance as follows: *p<0.05, **p<0.01, ***p<0.001. Graphs are presented as mean±SEM.*

6.3.1.3 Characterisation of laser-induced atrophic lesions by gene expression and histology

The model was characterised at one timepoint to gain insights into structural and immunological changes occurring post laser treatment. The one month timepoint was chosen for this investigation as it showed the strongest ERG deficits and some hyperreflective pathology is still clearly visible. This study was conducted in young and middle aged mice to see whether the addition of aging as an additional cofactor has an effect on the response to laser-induced atrophic lesions. For gene expression analysis, eight out of nine young mice (5 months) and three out of four middle-aged mice (11-13 months) showed evidence of large areas of atrophic lesions, while two mice showed little pathology and were excluded from analysis. No significant differences in mRNA expression of all genes tested was observed between young and middle-aged mice and consequently the data was pooled for analysis (Figure 6.6), but the separated data is provided in Appendix D3. Complement component 3 (C3) was the most upregulated gene investigated with an increase of 341% (t_{10}=4.637, p=0.0009), indicating a central role of complement in mediating laser-induced atrophy. mRNA analysis also revealed upregulation of astrocytic/Müller cell marker GFAP by 193% (t_{10}=3.957, p=0.0027) and microglial marker FcγRI by 75% (t_9=3.737, p=0.0046). In addition, genes encoding proteins associated with the inflammasome, inflammation and apoptosis were upregulated at one month post laser treatment: Caspase 1 by 162% (t_{10}=5.464, p=0.0003), IL-1β by 73% (t_{10}=4.91, p=0.0006), Caspase 8 by 40% (t_{10}=5.647, p=0.0002) and IL-18 by 14% (t_{10}=3.268, p=0.0085).

Investigation of genes encoding proteins associated with oxidative stress revealed that mRNA levels of NADPH oxidase pathway subunits Cybb and Cyba were increased by 274% (t_{10}=4.2, p=0.0018) and 28% (t_{10}=5.232, p=0.0004) respectively. Cybb encodes a protein known as NADPH oxidase 2 (NOX2) or cytochrome b subunit, while Cyba encodes a protein known as p22phox or cytochrome a subunit. In phagocytes, these NADPH oxidase pathway genes are involved with the generation of superoxides, a reactive oxygen species (ROS) that greatly contributes to oxidative stress (Panday et al., 2015). In contrast, no significant changes were found in the mRNA levels of nitric oxide synthesis enzymes at one month post laser treatment: Nos1 (t_{10}=1.267, p=0.2340), Nos2 (t_{10}=0.7965, p=0.4442) and Nos3 (t_{10}=1.366, p=0.2018). mRNA levels of oxidative stress response genes Hmox1 (t_{10}=1.947, p=0.0802), Nfe2l2 (t_{10}=1.25, p=0.2397) and Sod2 (t_{10}=0.0652, p=0.9493) were not changed at one month post laser treatment, and this was also true for wound healing response gene Arg1 (t_{10}=1.01, p=0.3361). No changes in mRNA expression of Vegfa (t_{10}=0.284, p=0.7822) or Dicer1 (t_{10}=0.6079, p=0.5568), which are associated with wet AMD and GA respectively were observed (Tarallo et al., 2012; Ferrara, 2010). Overall, these data indicate that several distinct inflammatory pathways are activated at one month post laser treatment.

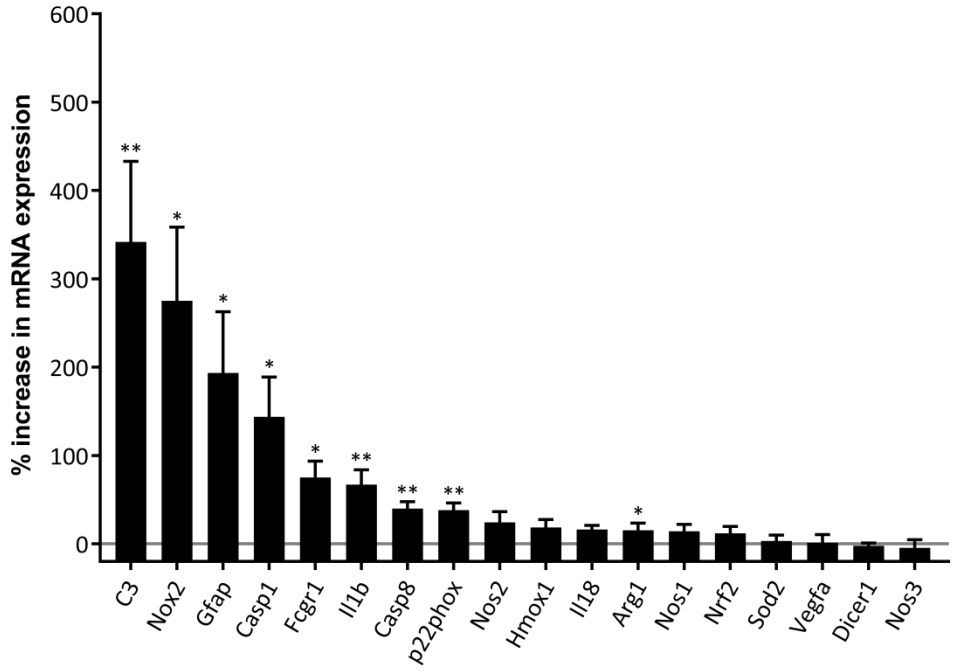

Figure 6.6 – Gene expression in the retina at one month post laser treatment.

*Values are displayed as the average increase in gene expression in the laser-treated retina compared to the control retina for each mouse. Gene expression of eight young mice (5 months old) and three middle-aged mice (11-13 months old) was measured using SYBR Green qPCR (see Appendix D3 for separate graphs of young and middle-aged mice). Data was analysed using multiple paired one-tailed t-tests followed by Holm-Sidak multiple comparisons correction. Stars denote significance as follows: *p<0.05, **p<0.01. Graphs are presented as mean±SEM.*

Next, the immunological changes in the retina were investigated by immunohistochemistry. DAPI counterstaining reveals that there are few remaining photoreceptor cell nuclei in the laser-induced atrophic lesion, as the ONL is mostly destroyed at one month post laser treatment (Figure 6.7a-b). The areas surrounding the lesion appear to have remarkably normal nuclei staining, showing the effects of laser treatment are highly localised. At the laser-treated site, there is an increased expression of GFAP, indicating activation of astrocytes and Müller cells. GFAP staining of astrocytes and Müller cells is spatially distinct, allowing the effect of the laser treatment on both cell types to be determined. Astrocytic GFAP expression was confined to GCL (particularly the vitreal side of the GCL) and this pattern is increased at the laser-induced site, indicating astrocytosis. Müller cells express GFAP on long, fine processes extending from the GCL to the outer retinal layers in the retina at one month post laser treatment, while this staining pattern was not observed in control mice. GFAP expression is very robust at the laser-induced site but is also present in adjacent, non-laser treated areas, indicating that the inflammation at one month post laser treatment is not localised solely to the laser-induced site. FcγRI expression on microglia

appears upregulated in the laser-treated area suggesting microglial activation. There is also an increased number of microglial cells in and around the lesioned area indicating microglial cell recruitment. Some FcγRI+ cells are localised to the back of the retina at the laser-induced site and this was not seen in control mice. It is unclear whether these FcγRI+ cells are recruited microglia or infiltrate the lesion from the choroidal circulation.

The Brightfield channel from the fluorescent images was separated from the other channels and is shown in Figure 6.7c-d. These channels highlight the changes to retinal/choroidal pigment following laser treatment. At one month post laser treatment, the layer of pigment at the back of the retina is thicker and this effect is seen away from the laser-induced site as well, indicating a wider area of disruption at the RPE/choroid interface when compared to the area of ONL loss. Clusters of pigment also appear to separate from the main pigmented area in several places in the laser-treated mice compared to the control, which could indicate RPE damage. However, this may also be due to difficulties during sectioning as the laser-treated areas are prone to cutting artefacts. Overall, these images show that after laser treatment, there is loss of the outer retinal layers, while the inner retinal layers remain remarkably preserved, but are highly inflamed.

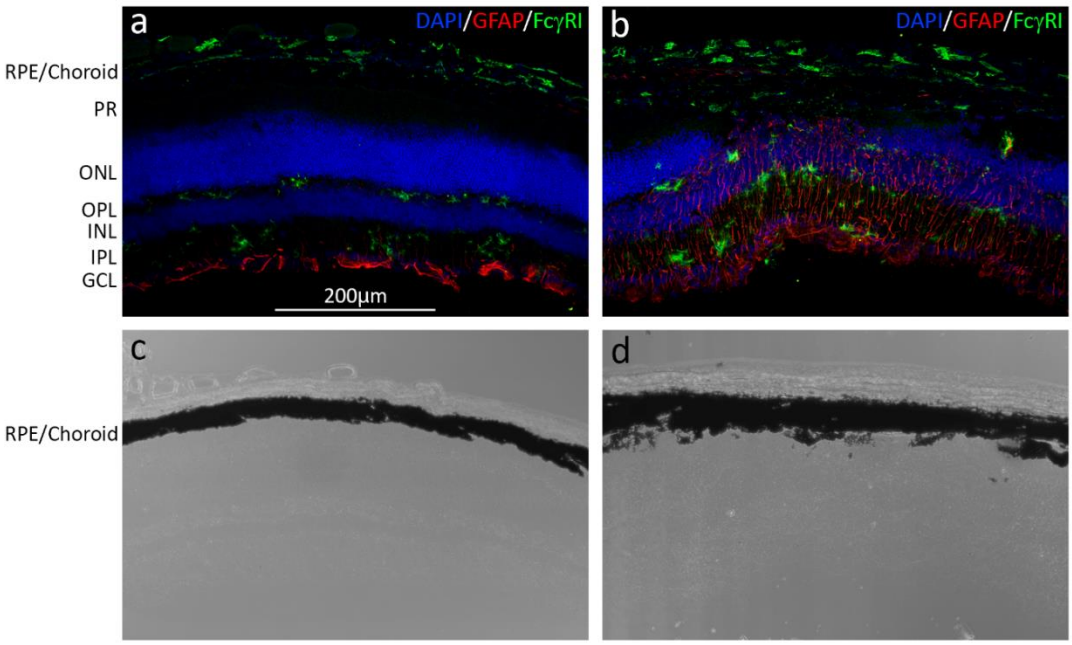

Figure 6.7 – Retinal FcγRI and GFAP expression at one month post laser treatment.
Representative immunohistochemistry images at one month post laser treatment taken (a, c) away from and (b, d) focused on the laser-treated site. (a, b) Immunohistochemical staining of the retina with FcγRI (green), GFAP (red) and DAPI (blue). (c, d) Brightfield images showing the changes in pigmentation of the RPE/Choroid as a separated channel from (a, b). RPE, retinal pigment epithelium; PR, photoreceptor segments; ONL, outer nuclear layer; OPL, outer plexiform layer; INL, inner nuclear layer; IPL, inner plexiform layer; GCL, ganglion cell layer.

Representative histology of a retinal lesion at three months post laser treatment in middle-aged mice was performed by Dr. Srini Goverdhan, Maureen Gatherer, the Histochemistry Research Unit and the Biomedical Imaging Unit (Figure 6.8). Although 3 months post laser treatment is a later timepoint than has been investigated in the other studies in this thesis, the level of pathology appears to be sustained, but not markedly progressed, between 1 and 2 months post laser treatment, meaning insights at this timepoint are likely to be relevant to earlier timepoints. Toluidine blue histology confirms the loss of RPE and photoreceptors in the lesioned area, while the INL was distorted and now lies in apposition to the choroid with the IPL and GCL layers intact. The choroid, which also contains melanin pigment sensitive to 810nm laser absorption, appears severely swollen, either as a result of direct damage or due to clearance of large amounts of debris from the outer retina.

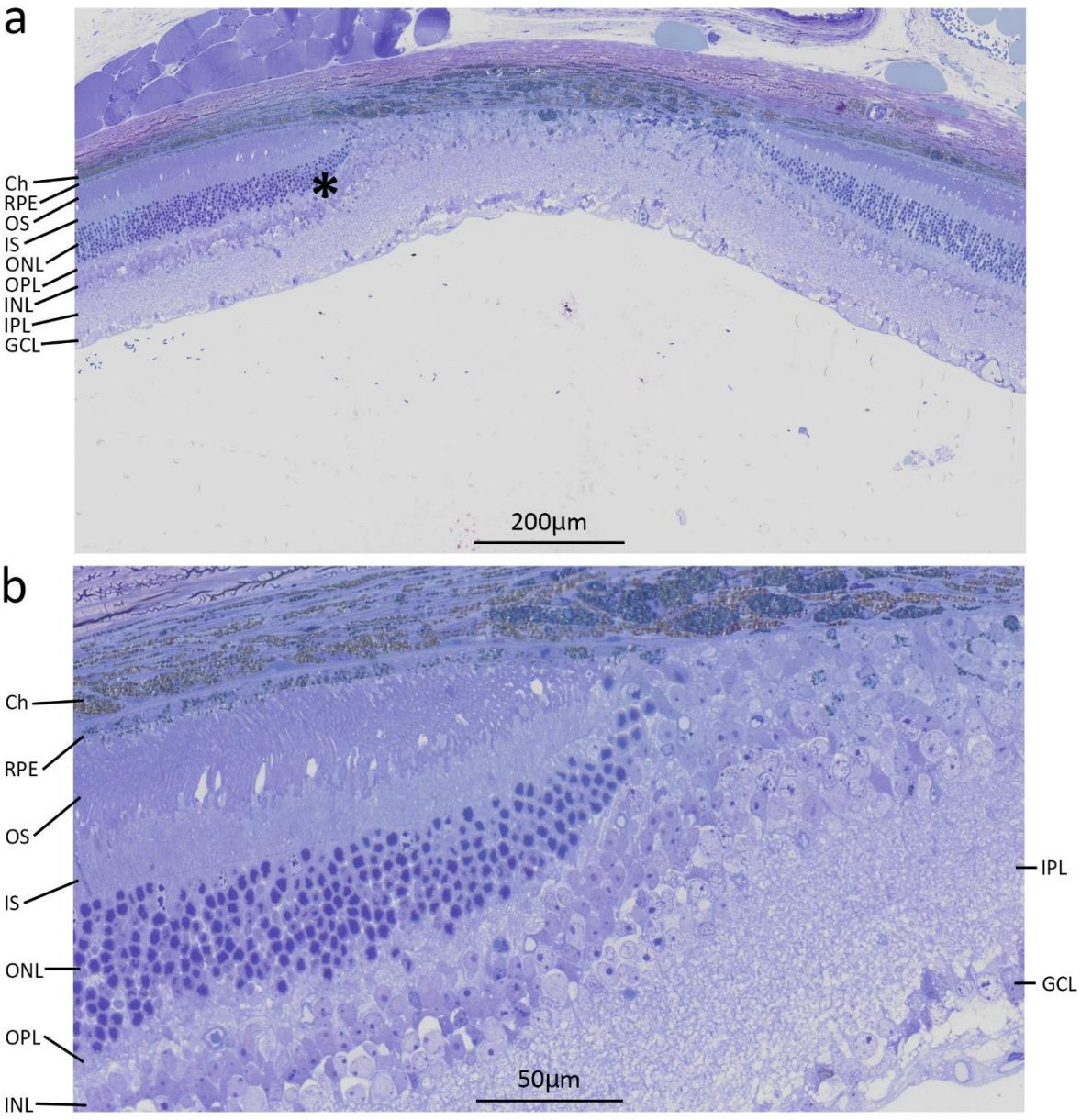

Figure 6.8 – Histology images of laser-induced lesions

Representative toluidine blue histology of a laser-induced atrophic lesion taken at (a) 40x magnification and (b) 160x magnification of the area indicated by an asterisk. Lesions were examined at 12 weeks post laser treatment in three mice (11-13 months). Ch, Choroid; RPE, retinal pigment epithelium; OS, photoreceptor outer segment; IS, photoreceptor inner segment; ONL, outer nuclear layer; OPL, outer plexiform layer; INL, inner nuclear layer; IPL, inner plexiform layer; GCL, ganglion cell layer.

6.4 Discussion

Geographic atrophy, the late stage of dry AMD, is thought to begin with the progressive dysfunction of RPE cells in the macula followed by the loss of photoreceptors due to a lack of support from the RPE. The mechanisms by which this process occurs, however, are poorly understood and this hinders the development of effective therapeutics. Therefore, there is a real need for a mouse model recapitulating aspects of human GA to provide mechanistic insights and test interventions, as seen with the laser-induced CNV model. Here, I discuss the advantages and disadvantages of this laser-induced GA model and highlight how it compares with known features of GA pathobiology.

6.4.1 Laser-induced atrophic lesions: dose dependency and reproducibility

The development of lesions is largely dependent on laser power. There is a dose-dependent effect, where 22mW power induced minimal damage and 42mW power resulted in huge atrophic confluent lesions. At 32mW laser power, faint subthreshold laser burns immediately post laser treatment were observed. This led to collapse of the RPE/outer retinal layer at one month post laser treatment. This intermediate dose provides the best opportunity to look for progression of the lesion over time. However, the dose chosen can be varied based on a specific research question.

Reasonably consistent lesions were induced in mice using 32mW laser power for an average of 60 seconds per laser spot. The exact time that each spot requires is variable and is particularly affected by how central the spot is in the field of view during laser treatment. Some mice required a greater duration of exposure than others to develop subthreshold laser burns. The most likely reason for this is that there are differences in the orientation of each mouse during the procedure, although other factors may also be involved. Despite these limitations, I have managed to develop a procedure yielding reasonably reproducible outer retinal lesions, which are heavily reliant upon the experience of the person using the laser to identify exactly when a burn is at the right dose. Thus, the experiment should always be performed by an experienced user. In these conditions, the laser-induced lesions show good intra- and inter-experiment reproducibility within the same lab. The best way to ensure inter-lab consistency would be for a lab to perform an initial dose-dependency study to identify the optimum laser power for their setup.

Overall, I believe that the model can become consistent between labs, where the key requirements are optimisation of laser power and detailed training of the person performing laser treatment to create reproducible subthreshold burns.

6.4.2 Fundoscopic changes to the retina in GA

Klein et al. 2008 present fundoscopy images taken over 13 years from nearly 100 patients with dry AMD that went on to develop GA during their study. They show that for >65% of patients, the sequence of events leading to GA was:

1. Development of drusen (>6.6 years before GA onset)
2. Hyperpigmentation (5 years before GA onset)
3. Drusen regression & hypopigmentation (2.5 years before GA onset)
4. Geographic atrophy

The authors point out the wide variability amongst the sequence and timings of each stage as well as multiple stages occurring simultaneously, but despite these differences this sequence provides a schematic to which animal models can be compared.

Fundoscopy at 1, 2, 4 and 8 weeks post laser treatment shows the presence of several patches of retinal lesions, some of which because became confluent. These lesions are clearly observable and can be followed up over time as performed in patients. GA is typically comprised multiple sites of focal degeneration that grow to confluence over time (Schmitz-Valckenberg, 2017), so the mix of patchy and confluent degeneration in the laser-induced model represents this aspect well. The laser-induced lesions don't appear to progress outwards over the 2 month follow-up period. In human GA, the size of lesions does increase over time (Schmitz-Valckenberg, 2017), but this is a process that occurs over years so it would be interesting to re-examine these lesions when the mice are much older to see if the area of lesion increases over time.

The main problem, however, is that fundoscopy is not sensitive enough to detect minor changes in lesion appearance. I am currently investigating whether it is possible to use the OCT scans to provide an accurate quantification of the surface area of these lesions. In patients, a combination of OCT and fundus autofluorescence (FAF) scans are recommended to visualise GA lesions. OCT provides fantastic vertical resolution of lesions and retinal layers, while FAF provides better discrimination of lesion boundaries and lateral resolution (Schmitz-Valckenberg, 2017). FAF imaging shows that atrophic lesions have reduced autofluoresence due to lipofuscin loss with RPE cell degeneration. However at the margins of the lesion, different patterns of hyper- and hypofluorescence are observed in patients and these are associated with different rates of GA progression (Holz et al., 2007). It would be interesting to perform FAF on these laser induced lesions, to better track lesion progression and classify these lesions based on subgroups seen in GA patients.

Following laser treatment, the lesioned area becomes hyperpigmented over time, which may be reflective of the RPE/choroid interface being more visible over time as the retina degenerates. Alternatively, it could represent a build-up of pigment in the outer retina due to overwhelmed clearance mechanisms as a result of laser-induced damage. Areas of hyperpigmentation and hypopigmentation are observed in 96% and 82% of dry AMD patients respectively (Klein et al., 2008). However, areas of hyperpigmentation are common in early/intermediate AMD and these then develop into areas of hypopigmentation before the development of GA. This hypopigmented appearance is then retained throughout GA. Although this laser-induced model displays hyperpigmentation and not the hypopigmentation typical of GA, it would be interesting to see whether the hyperpigmented lesions become hypopigmented at later timepoints like in GA patients.

Finally, the laser-induced lesions can be clearly demarcated by a bright hazy border that becomes less apparent over time. Clear demarcation is a key feature of human GA (Schmitz-Valckenberg, 2017), although the borders do not appear to be hazy. However, due to the much larger size of the human retina when compared to the mouse retina, fundoscopy images are far more zoomed out so it may not be possible to observe the edges of these lesions in the same detail.

6.4.3 Structural changes to the retina in GA

SD-OCT scans show that as intermediate AMD progresses towards GA, large confluent drusen, which are typically hyperreflective, regress leaving some hyperreflective abnormalities at the back of the retina, which persist as the outer retinal layers collapse leaving the OPL in close apposition to the back of the retina (Wu et al., 2014). The loss of the outer retinal layers progresses over many years (by an average of 5µm/year), while the inner retinal layer stays at the same size, or even increases slightly in some studies (by an average of 1.5µm/year) (Ebneter et al., 2016; Pilotto et al., 2013). Histopathological studies of retinas with GA show the progressive degeneration of outer retinal layers, starting with the RPE and followed by photoreceptor IS/OS and ONL, such that a thin OPL rests directly on the basal laminar deposits in association with the choroid (Sarks et al., 1988; Sarks, 1976). Meanwhile, the inner nuclear layer is not particularly affected by the loss of the outer retina (Sarks et al., 1988; Sarks, 1976).

At one-week post laser treatment, lesions are characterised by hyperreflective areas of outer retinal damage in the OCT, as seen in patients preceding GA. Over the course of eight weeks these hyperreflective areas regressed to the back of the retina, although some hyperreflective pathology was still apparent. Alongside these changes, the RPE, photoreceptor segments and ONL collapsed at the centre of lesions, leaving the ONL/IPL in apposition with the outer retina as seen

in GA patients. The causes of hyperreflectivity in GA patients and the GA model are not clear and could arise from any combination of the following factors:

1. Drusen is typically hyperreflective, although not always as it depends on the composition of the drusen (Fleckenstein et al., 2008)
2. Regressed drusen, which form sub-RPE deposits, are increasingly calcified (Klein et al., 2008)
3. The RPE layer is naturally hyperreflective and could thicken due to dysfunction (Michalewski et al., 2014)
4. High levels of inflammation, causing deformation of the retina, as has been seen in EAU (Chen et al., 2013a)
5. Fibrosis (Augustin et al., 2016)
6. Rapid cell death (Secondi et al., 2012)

Therefore, although the pattern of hyperreflective damage regression and OPL/INL depression at the lesion site is similar, the underpinning processes could be due to different factors especially given the acute nature of the laser model (e.g. regressed drusen in GA patients, but rapid cell death in the laser-induced model). This model shows progressive collapse of the retina from 1 to 4 weeks post laser treatment, but it is not clear whether there is progressive loss of the outer retina or the INL depression is solely due to the regression of hyperreflective pathology at the back of the retina. The OCT scans also demonstrate that the inner layers of the retina seem to be intact in the lasered area, as observed in GA patients. Histology performed at 4 and 12 weeks post laser treatment agrees strongly with these findings, showing loss of the outer layers at the laser-induced site while the inner layers seem remarkably intact.

The effect of laser on the choroid is also unclear. In GA patients, the choriocapillaris appear atrophied at the site of GA (Schmitz-Valckenberg, 2017). Whereas, the choroid after laser appears to be enlarged overall, although the effect on individual capillaries is unclear. This enlargement may be due to the large volume of material to be cleared away following acute damage caused by the laser and is still observed at 3 months post laser. However, as the choroid contains melanin it is also possible that the laser has induced some direct damage to the choroid.

6.4.4 Functional changes to the retina in GA

Initially with ERG recordings, I tried to focus the light stimulus of the ERG specifically to the lesioned area and identified the lasered area under red light to greatly reduce photobleaching of the rods before recording and then applied the light stimulus. However, the results of focused ERGs were meaningless as strong photobleaching was observed. Consequently, I opted to use the

focal ERG system at the largest aperture to have the best chance of fully encompassing the laser site. This adds some variability to the ERG measurements based on the assumed inclusion of the laser site. Despite this, the ERG data was significant between control and laser-treated eyes at all timepoints for both the a- and b-wave, indicating a clear and reproducible effect of the laser lesion on the retina. The effect sizes were similar across one to eight weeks for both the a- and b-waves, indicating that there were not progressive ERG deficits over time. This fits well with data from human AMD patients, where there are substantial scotopic ERG deficits in AMD patients, but these deficits are reasonably constant at the different stages of AMD (Walter et al., 1999). The laser-treated eyes also have an increased B wave implicit time compared to control eyes, which is also observed in AMD patients (Walter et al., 1999). Overall, the model recapitulates the 3 key electrophysiological changes observed in human AMD patients compared to age-matched controls.

6.4.5 Inflammation in laser-induced atrophic lesions and GA

The role of local inflammation in AMD is well established, although it is unclear whether it drives degeneration or is a by-product of degeneration. GA lesions in human post-mortem eyes have been analysed by immunohistochemistry and qPCR analysis following microdissection. Although the understanding of inflammation in AMD is incomplete, largely due to the limited number of good quality post-mortem eyes available, these studies have given some key findings on the role of inflammatory cells and factors during GA.

At the laser site, GFAP expression is increased in the inner layers of the retina and this is supported by a 2-fold increase in GFAP mRNA. However, as the laser model is geographic and RNA is isolated from the whole retina, it is likely that mRNA levels of GFAP at the laser site is much higher, and this is supported by immunohistochemical staining for GFAP. GFAP is expressed by astrocytes under resting and activated conditions, and by Müller cells only when activated (Verderber et al., 1995). Immunohistochemistry staining for GFAP showed that the Müller cells within the laser-site and around the margins of the laser site are strongly activated, while there is little activation far away from the laser site. The staining pattern of astrocytes is also stronger at the laser site, suggesting some astrogliosis in this model. In human AMD patients, astrogliosis is observed around areas containing drusen, but this does not become worse during GA (Wu et al., 2003). In contrast, drusen does not significantly increase Müller cell activation, but strong Müller cell activation is seen in GA patients. Overall, the laser model recapitulates the GFAP expression pattern seen in GA patients well, with stronger changes in GFAP expression by Müller cells than astrocytes (Wu et al., 2003).

Microglial cell activation is also observed in the laser model as seen by increased mRNA and protein levels of FcγRI. As seen for GFAP, most changes in FcγRI expression are confined to the centre and periphery of the laser site. In healthy young and aged subjects, very few macrophages can be found within Bruch's membrane. In early to intermediate AMD, many macrophages are recruited to Bruch's membrane, although it is unclear whether these are recruited microglia and/or choroidal macrophages. Many of these cells express CX3CR1, MHCII and CD68, but not iNOS (Penfold et al., 1997; Cherepanoff et al., 2010; Combadière et al., 2007). In GA, the number of microglia is reduced 2.5-fold compared to intermediate AMD, with CD68+ macrophages found around the edges of atrophic lesions and a few hypertrophic microglia in the centre of the lesion (Cherepanoff et al., 2010; Gupta et al., 2003). Giant cells from the choroid are also found in atrophic lesions, which are thought to form due to the fusion of multiple mononuclear phagocytic cells (Penfold et al., 1986). In the laser model, activated microglia with a hypertrophic appearance are found in the lesion and its margins and there are also a number of large subretinal cells reminiscent of giant cells at the sites of outer retinal collapse. Consequently, the model recapitulates many features of myeloid cell activation in GA patients. Tracing the origins of the cells in this model may give an indication of the relative contribution of microglia and peripheral macrophages in AMD. It would be interesting to investigate other markers expressed by these microglia, such as MHCII and CD68 to see how their profile compares to GA patients.

The complement system is the immune pathway most commonly associated with AMD (see introduction section 1.4.5). Complement inhibition has been trialled in GA patients with lampalizumab (anti-CFD) reducing progression of atrophy by 20% per year in the MAHALO Phase II trial (Yaspan et al., 2017). In the laser model, C3 is the most upregulated gene of the 18 tested with a 3.5-fold increase, indicating an important role of local complement production in this GA model. It would be interesting to investigate additional complement genes/inhibitors of the classical (i.e. C1q) and alternative pathways (i.e. CFB/CFD) to see whether one arm plays a more important role in driving inflammation/cell lysis during atrophy.

GA patients have increased mRNA levels of IL-18 and Nlrp3, with a trend for elevated IL-1β, and increased protein levels of pro- and mature caspase 1 (Tarallo et al., 2012). In the laser model, there is are increased mRNA levels of IL-18 and IL-1β, and caspase 1, but not the NLRP3 inflammasome. However, upregulation of the NLRP3 gene doesn't necessarily correlate with inflammasome activity, so the NLRP3 inflammasome may become active but not upregulated. In GA patients, loss of Dicer1 is thought to cause a build-up of *Alu* RNA, which can act as a signal for inflammasome activation (Kaneko et al., 2011). In the laser model, levels of Dicer1 were not altered, indicating a different mechanism of inflammasome activation. Increased protein levels of caspase 8 are also found in GA lesions and may be responsible for driving apoptosis following IL-

18 activation by the inflammasome (Kim et al., 2014). In the laser model, caspase 8 is upregulated at an mRNA level and may drive apoptotic cell death at the laser site.

There was also no evidence of VEGF expression in this model at one month post laser. This indicates that the phenotype favours GA over neovascularisation. However, 810nm laser application to the retina has previous shown VEGF expression at 12h post laser in rabbits, so there may be an initial transient expression of VEGF (Yu et al., 2013). Analysis of the laser model at earlier timepoints may show whether there is earlier expression of VEGF.

6.4.6 Oxidative stress and GA

Oxidative stress is highly implicated in AMD patients by risk factors and observations that most of the protein and lipid components in drusen are strongly oxidised (Crabb et al., 2002; Schutt et al., 2003). Furthermore, genetic polymorphisms in the oxidative stress response gene SOD2 are associated with an altered risk of AMD (Kimura et al., 2000). However, the specific oxidative stress pathways active in GA are not well understood. In the laser model, the only oxidative pathway tested that showed activation is the NOX2 pathway involved with the formation of ROS superoxides (Panday et al., 2015). Superoxides can then react with other molecules to generate more toxic ROS species (i.e. peroxynitrate) (Li et al., 2005). Levels of NOX pathway components have not been quantified for GA patients and these data indicate that it may be a pathway for further investigation. The NOX pathway has recently become an interesting area of investigation in many neurodegenerative diseases, most notably Alzheimer's disease, and is also upregulated in the retina of transgenic mice, where it is thought to contribute to rod photoreceptor degeneration (Song et al., 2016; Ma et al., 2017)

None of the nitric oxide synthase genes (nNOS, eNOS, iNOS) were found upregulated preventing the conversion of superoxides into the highly toxic peroxynitrate in the laser model. These findings are in line with AMD patients showing little change in protein levels of nitric oxide synthase in the retina (Bhutto et al., 2010). Levels of oxidative stress response genes (Hmox-1, Nfe2l2, Sod2) controlling antioxidant gene batteries are not altered at one month post laser, indicating that the balance of oxidative stress vs antioxidants is shifted towards oxidative stress. Although it is also possible that these genes were upregulated at early time points in an attempt to maintain homeostasis. It is also unclear whether acute oxidative stress in the laser model is proportionate to the levels of oxidative stress observed during AMD.

6.4.7 Summary

The laser-induced model of CNV is a widely used model for investigating mechanisms and possible therapies for human wet AMD. Here, I present a laser-induced model of outer retinal atrophic lesions that recapitulates many key features of human GA. In detail, this model is characterised by progressive outer retinal collapse from 1 to 4 weeks post laser treatment along with non-progressive ERG deficits. This model also finds evidence for activation of microglial and Müller cells, complement and the inflammasome, which have been previously shown dry AMD patients. As many of the upregulated genes in this model have been found in GA patients, this model could be used to gain insights into atrophic AMD pathology. For example, based on data from lasered mice, NAPDH oxidases may play a key role in driving oxidative stress during atrophy and represents and interesting target for investigation in human AMD. Furthermore, the relative importance of different pathways in driving atrophy, such as complement and inflammasome activation, could be investigated in this model using knockout mice or drug interventions. The laser-induced outer retinal atrophic lesions are therefore useful for both mechanistic and pharmacological studies.

Chapter 7:

The role of systemic and local cytokine production in patients with age-related macular degeneration

7.1 Introduction

Mouse studies are a valuable tool to investigate many biological phenomena, but they can never fully recapitulate processes in humans. Differences in retinal structure (e.g lack of macula), immunology and lifelong exposure to environmental factors between mice and humans are some key reasons why AMD cannot be understood by mouse models alone. Therefore, although data presented in chapter 5 indicates that systemic bacterial infection and retinal inflammation are associated in mouse models, it is important to assess how these are related in a human population.

There is indirect evidence to suggest a role for systemic inflammation in AMD incidence and/or progression. Firstly, the risk factors for AMD are associated with increased peripheral inflammation. For example, environmental factors related to AMD (i.e. smoking and obesity) are associated with higher CRP and IL-6 levels in the serum. Moreover, genetic risk factors, including the high AMD-risk CFH genotype, have been associated with increased IL-8, IL-18 and TNFα serum levels (Cao et al., 2013; Seddon et al., 2005). Secondly, differences in systemic immune cell populations between AMD patients and control patients have been identified (see introduction section 1.5.2). Thirdly, systemic bacterial/viral infections have been associated with increased AMD incidence and/or progression (see introduction section 1.5.4). Notably, presence of periodontitis, which is caused by bacterial infection, is associated with an increased risk of developing AMD in two independent cohorts (Han & Park, 2017; Wagley et al., 2015). Finally, systemic immunosuppressants seem to reduce the risk of developing AMD; RA patients given long-term systemic immunosuppressants are 10 times less likely to develop AMD (McGeer & Sibley, 2005). These findings are not unique to AMD, and systemic immunosuppression, particularly targeting TNFα, is being investigated in Alzheimer's disease (Butchart et al., 2015).

Cytokine measurements provide a reasonable snapshot of inflammatory status. They give an indication of general inflammation, but differential expression patterns can identify specifically activated immune responses (e.g. Type 1: IFNγ, IL-6, IL-8, TNFα; Type 2: IL-4, IL-10, IL-13; Type 17: IL-17, IL-23). In addition to baseline levels of cytokines, it is important to characterise the phenotype/responses of immune cells to determine their activation status. One such study found that people with monocytes producing naturally high levels of TNFα are 5 times more likely to develop AMD (Cousins et al., 2004). These studies can be combined with *ex vivo* cell activation assays using known stimuli, such as LPS, to determine the capacity of immune cells to respond to insults. This has been pioneered in the field of autoimmune diseases, with both early and late RA patients showing increased IL-6, but decreased IL-8, in response to PBMC stimulation with viral stimuli (Davis III et al., 2010). Furthermore, during RA there is reduced production of many

cytokines in response to general T cell stimulation of PBMCs, but increased cytokine production when IL-17 specific T cells responses were investigated (Davis III et al., 2010). This study shows the power of stimulation to dissect the role of different inflammatory cells and pathways during disease. Such techniques may identify inflammatory pathways specifically altered in AMD patients, or could enable AMD patients to be stratified based on different systemic immune profiles.

In this chapter, I describe the local (i.e. aqueous humour) and peripheral cytokine levels in a mixed cohort of dry and wet AMD patients and age-matched controls along with their correlation. In addition, I perform immunophenotyping to characterise the immune signature of the cohort and their inflammatory potential to respond to a range of inflammatory stimuli.

7.2 Methods

39 cataract surgery patients with or without concomitant AMD were recruited to an observational clinical study to investigate the role of local and systemic inflammation in AMD (see section 2.7.1 for further study details). Serum and aqueous humour was collected from patients for quantification of inflammatory cytokine levels by multiplex ELISA (Mesoscale Discovery, see section). Blood was collected by the ophthalmic research nursing team (Amanda Smith, Thea Sass and Mercy Jeyeraj), while aqueous humour was collected by ophthalmic surgeons (Andrew Lotery, Christine Rennie). Whole blood containing sodium lithium anti-coagulant was stimulated with immune stimuli mimicking bacterial (LPS), viral (R848) and T cell activation (stimulatory anti-CD3 mAb OKT3). Supernatant and immune cells were collected 19 hrs after stimulation and assayed for levels of cytokines by mesoscale and intracellular flow cytometry (see sections 2.7.4 and 2.7.5). Not all types of samples were collected for all patients, consequently differences in demographics were analysed for each technique, but age, gender and smoking status was not significantly different between groups for any technique analysed (see appendix E). Gating strategy for flow cytometric analysis is provided in appendix F. Statistics performed are specified in the figure legends. Parametric or non-parametric statistics were performed depending on the normality of each group and most data was non-parametric. For graphs of ranked values, ranking was performed where the lowest result was given a value 1, the next lowest 2 etc. In the event of a tie, both results were given the same value.

7.3 Results

7.3.1 Serum and aqueous humour cytokines in AMD patients versus controls

There is conflicting data on cytokine levels in serum and aqueous humour of AMD patients compared to age-matched controls. Additionally, these studies rarely assess both the serum and aqueous humour cytokines from the same patients. Here, I examine the levels of 10 cytokines in the serum and aqueous humour for this cohort of AMD patients and controls and assess the correlation of local and peripheral inflammation.

No significant differences in serum cytokines were observed between AMD patients and controls (Figure 7.1a). For the combined cohort, levels of IFNγ (9.85pg/ml) and IL-8 (12.5pg/ml) were highest, followed by IL-13 (3.05pg/ml) and TNFα (3.26pg/ml) and then IL-6 (1.36pg/ml, Figure 7.1b). Levels of 5 of the 10 cytokines assayed (IL-1β, IL-2, IL-4, IL-10, IL-12 p70) were below the quantitation limit of the mesoscale assay and were therefore not analysed.

In terms of local cytokine levels, there is a significant increase in levels of IL-8 in aqueous humour of AMD patients compared to controls, but no difference for IL-6 or IL-13 (Figure 7.1c). For the combined cohort, levels of IL-6 (12.6pg/ml), IL-8 (8.57pg/ml) and IL-13 (6.00pg/ml) were not significantly different from each other (Figure 7.1d). Levels of 7 of the 10 cytokines assayed (IFNγ, IL-1β, IL-2, IL-4, IL-10, IL-12 p70, TNFα) were below the quantitation limit of the mesoscale assay and were therefore not analysed. Stratification of patients showed no significant differences in wet or dry AMD patients, although an interesting trend for increased IL-13 in the aqueous humour of dry AMD patients was observed (Figure 7.2). However, this analysis demonstrated that when stratified the data has greatly reduced statistical power.

In terms of correlation between aqueous and serum cytokines, there is a weak but significant positive relationship ($\rho=0.3589$, $p=0.0237$) between aqueous and serum levels of IL-6 (Figure 7.3b). Similarly, there is a weak positive relationship ($\rho=0.3113$, $p=0.0441$) between aqueous and serum levels of IL-8 (Figure 7.3b). In contrast, there is no correlation between aqueous and serum IL-13 (Figure 7.3c). Levels of IL-6 and IL-13 are higher in the aqueous compared to the serum, while IL-8 levels are higher in the serum than the aqueous.

Overall, these data indicate increased IL-8 levels in the aqueous of AMD patients compared to controls, but no differences in serum levels of any cytokine assayed. For the whole cohort, IL-6 and IL-8 levels in the periphery and aqueous humour correlated, indicating a form of crosstalk between the blood and the eye.

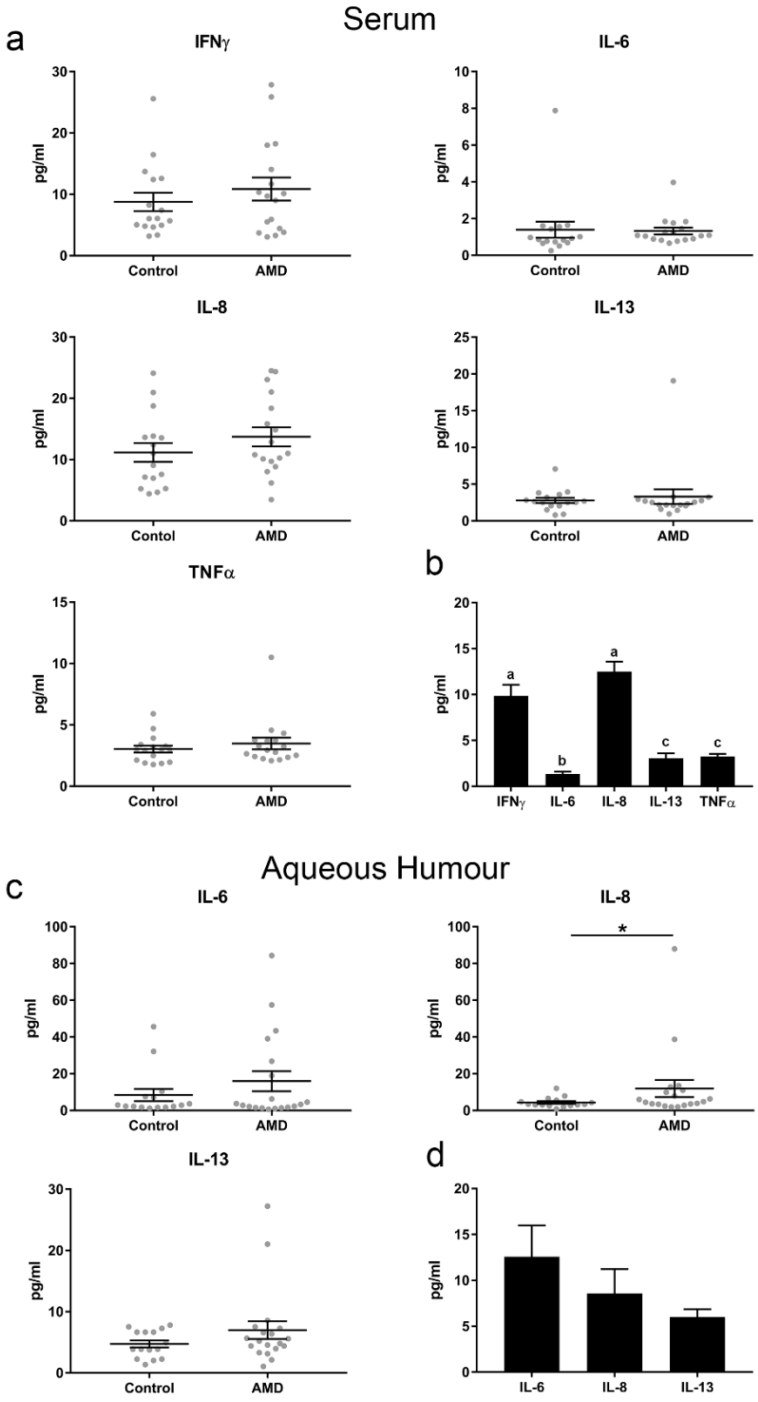

Figure 7.1 – Aqueous and serum cytokine levels in AMD patients and controls.

*Levels of (a) serum IFNγ, IL-6, IL-8, IL-13 and TNFα (n=16-17 per group) and (c) aqueous humour IL-6, IL-8 and IL-13 (n=15-19 per group) were quantified by multiplex ELISA (Mesoscale Discovery). Levels of cytokines in (b) serum and (d) aqueous humour for the whole cohort. Graphs are presented as mean±SEM. (a, c) Data was analysed by non-parametric one-tailed Mann-Whitney U-test, except for IL-8 serum, which was parametric and analysed by unpaired one-tailed T-test. Stars denote significance as follows: *p=0.05. (b, d) Data was analysed by non-parametric repeated measures Friedman test with Dunn post-hoc testing. Different letters denote statistically different means.*

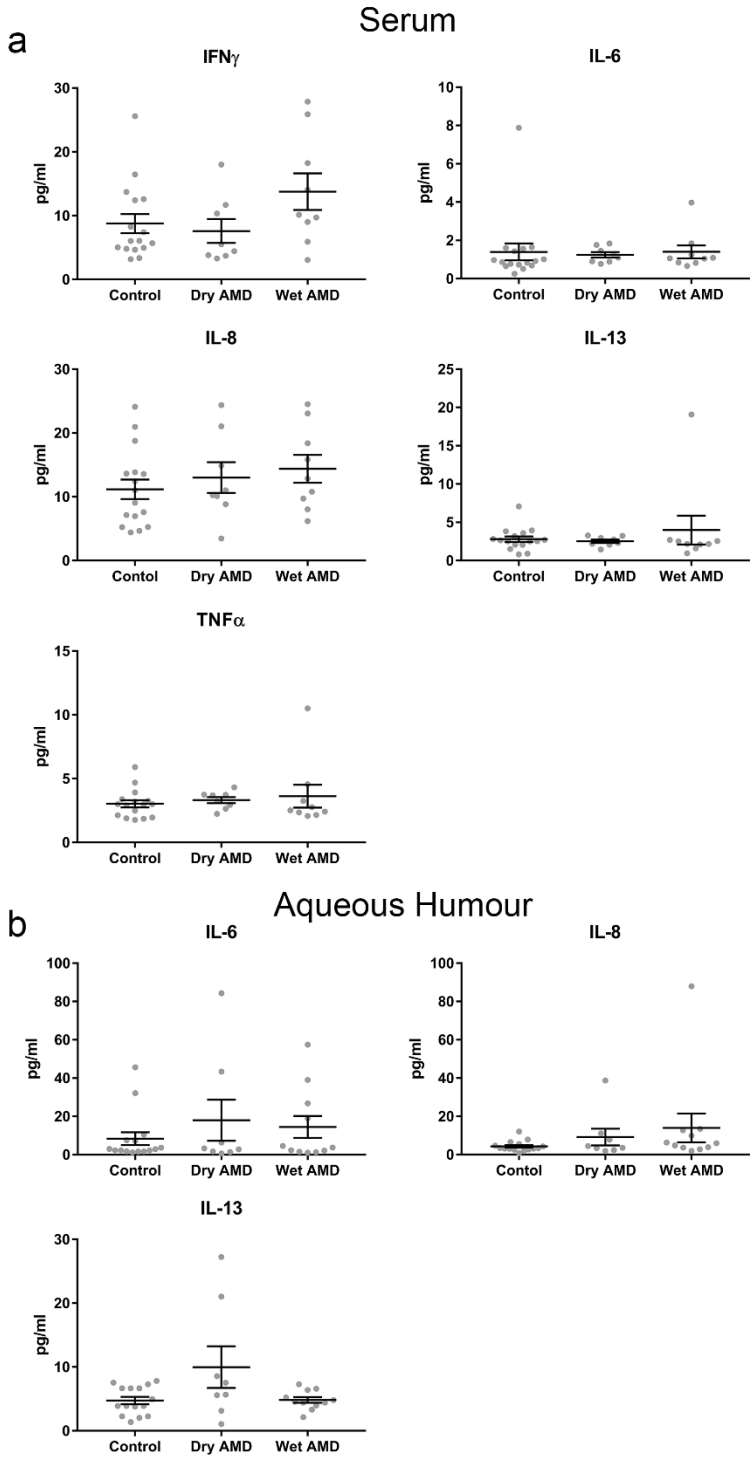

Figure 7.2 – Aqueous and serum cytokine levels stratified by AMD subtype.

Levels of (a) serum IFNγ, IL-6, IL-8, IL-13 and TNFα (control group: n=16, dry AMD group: n=8, wet AMD group: n=9) and (b) aqueous humour IL-6, IL-8 and IL-13 (control group: n=15, dry AMD group: n=8, wet AMD group: n=11) were quantified by multiplex ELISA (Mesoscale Discovery). Graphs are presented as mean±SEM. Data was analysed by non-parametric one-tailed Mann-Whitney U-test, except for IL-8 serum, which was parametric and analysed by unpaired one-tailed T-test.

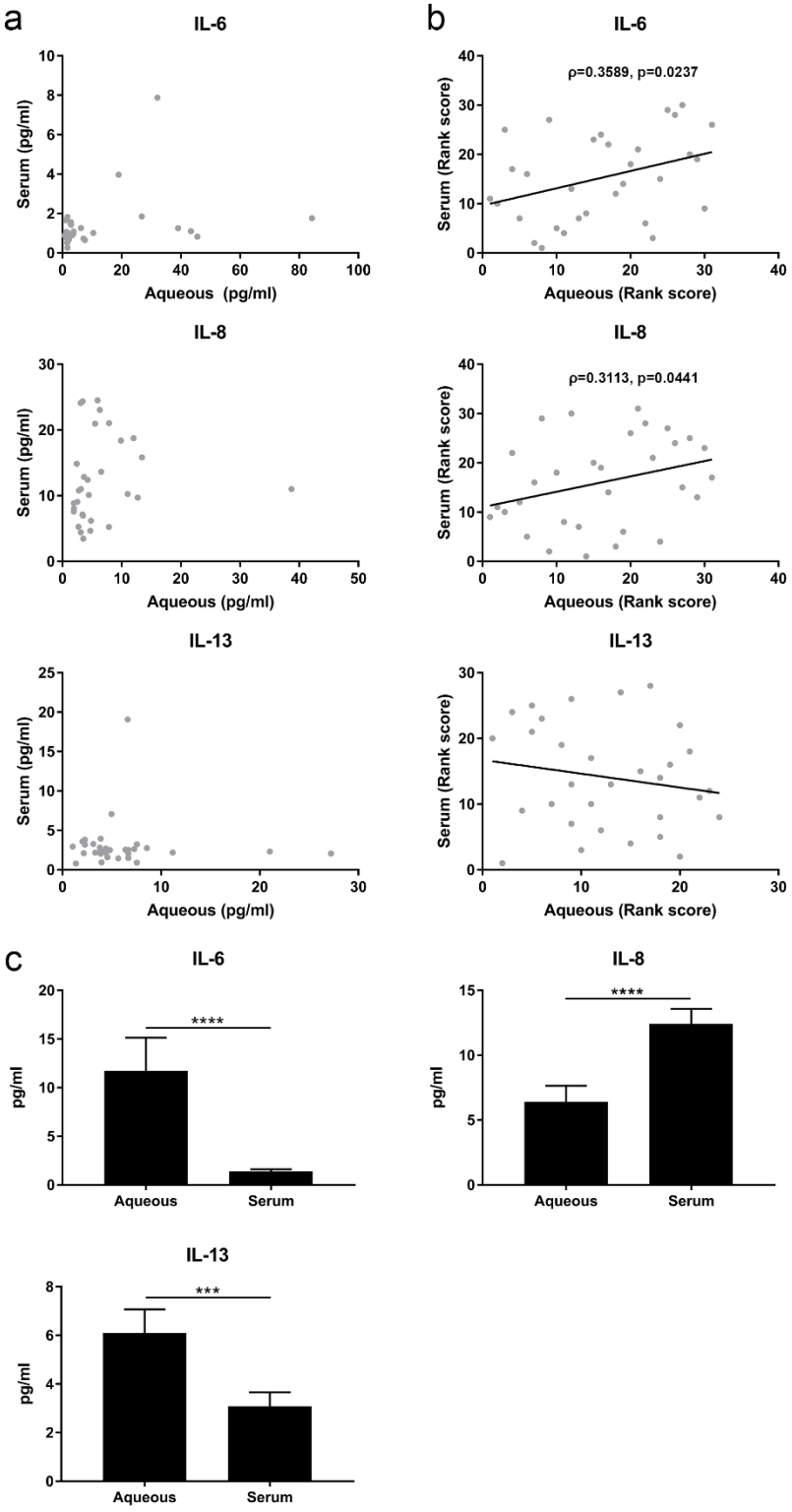

Figure 7.3 – Comparison of serum and aqueous cytokine levels.

Correlation of serum and aqueous IL-6, IL-8 and IL-13 in (a) raw values and (b) ranked values (n=31). As data was non-parametric, correlation was assessed with Spearman rank testing and (b) corresponding lines of best fit are shown on scatter graphs of ranked data. (c) Levels of IL-6, IL-8 and IL-13 in the serum and aqueous presented as mean±SEM and analysed by non-parametric Wilcoxon matched-pairs signed rank test (n=31).

7.3.2 Response of AMD patients and controls to whole blood immune stimulation

The levels of serum cytokines are highly variable between people and can be heavily influenced by confounding factors, such as infections, diseases (e.g autoimmunity, cancer) and environmental stimuli (e.g. BMI, smoking, alcohol intake). To reduce the baseline variation in serum cytokines, some studies have assayed the capacity of peripheral immune cells to respond to immune stimuli (Davis III et al., 2010; Kwok et al., 2012; Kowalski et al., 2008; Liou, 2003). Here, the bacterial mimetic LPS, viral mimetic R848, and T cell stimulatory antibody against CD3 are used to investigate whether AMD patients have a differential capacity to respond to immune stimuli compared to aged matched control subjects.

There was no difference between AMD patients and controls in terms of increases in IFNγ, IL-6, IL-8, IL-13 and TNFα levels following any immune stimulus used (Figure 7.4). However, across the whole cohort, each stimulus induced clear immune activation. IFNγ and TNFα levels were increased in response to LPS ($p<0.0001$), R848 ($p<0.0001$) and CD3 (IFNγ: $p=0.0137$; TNFα: $p=0.0353$), although IFNγ and TNFα levels induced by CD3 are much lower than for LPS ($p<0.0001$) and R848 ($p<0.0001$, Figure 7.5a). IL-6 and IL-8 levels are increased in response to LPS ($p<0.0001$) and R848 ($p<0.0001$), although LPS induces stronger expression of IL-6 and IL-8 compared to R848 (IL-6: $p=0.0260$, IL-8: $p=0.0049$). IL-13 is increased by LPS ($p=0.0059$) but not R848 or CD3. Overall, the pattern of activation in terms of order of cytokine upregulation for LPS (IL-6>IFNγ/TNFα>>IL-8/IL-13) and R848 (IL-6/IFNγ/TNFα>>IL-8/IL-13) are remarkably similar, whereas CD3 only induces strong upregulation of IFNγ (IFNγ>>IL-6/IL-8/IL-13/TNFα) (Figure 7.5b).

In accordance with the supernatant cytokine values, flow cytometric analysis found no differences in cellular cytokine responses following immune stimulation between AMD patients and controls (Figure 7.6). More specifically, neither lymphocytes or monocytes show an increased fold change in expression index for IFNγ, IL-6, IL-8 or TNFα following immune stimulation between AMD patients and controls. The expression index of cytokine production is calculated as the product of the size of the positive population and its median fluorescence intensity. This index gives an overview of total cytokine production by accounting for increased expression of cytokines by positive cells and increased size of a positive cell population.

For the combined cohort, LPS and R848, but not CD3, increased IFNγ expression in lymphocytes (LPS: $p=0.0242$, R848: $p<0.0001$), but not monocytes, compared to their respective unstimulated controls (Figure 7.7). LPS, but not R848 or CD3, induced increased expression of IL-6 ($p=0.0001$) and IL-8 ($p=0.0013$) in monocytes, but not lymphocytes. Finally, both LPS and R848 increased TNFα expression in monocytes ($p<0.0001$) and lymphocytes ($p<0.0001$).

Overall, there was no differences in the capacity of AMD patients to respond to immune stimuli compared to controls in terms of total cytokine levels or lymphocyte- and monocyte- specific cytokine signatures. There are, however, robust inflammatory changes following stimulation with some interesting cytokine pattern differences between stimuli that could be used to guide future studies.

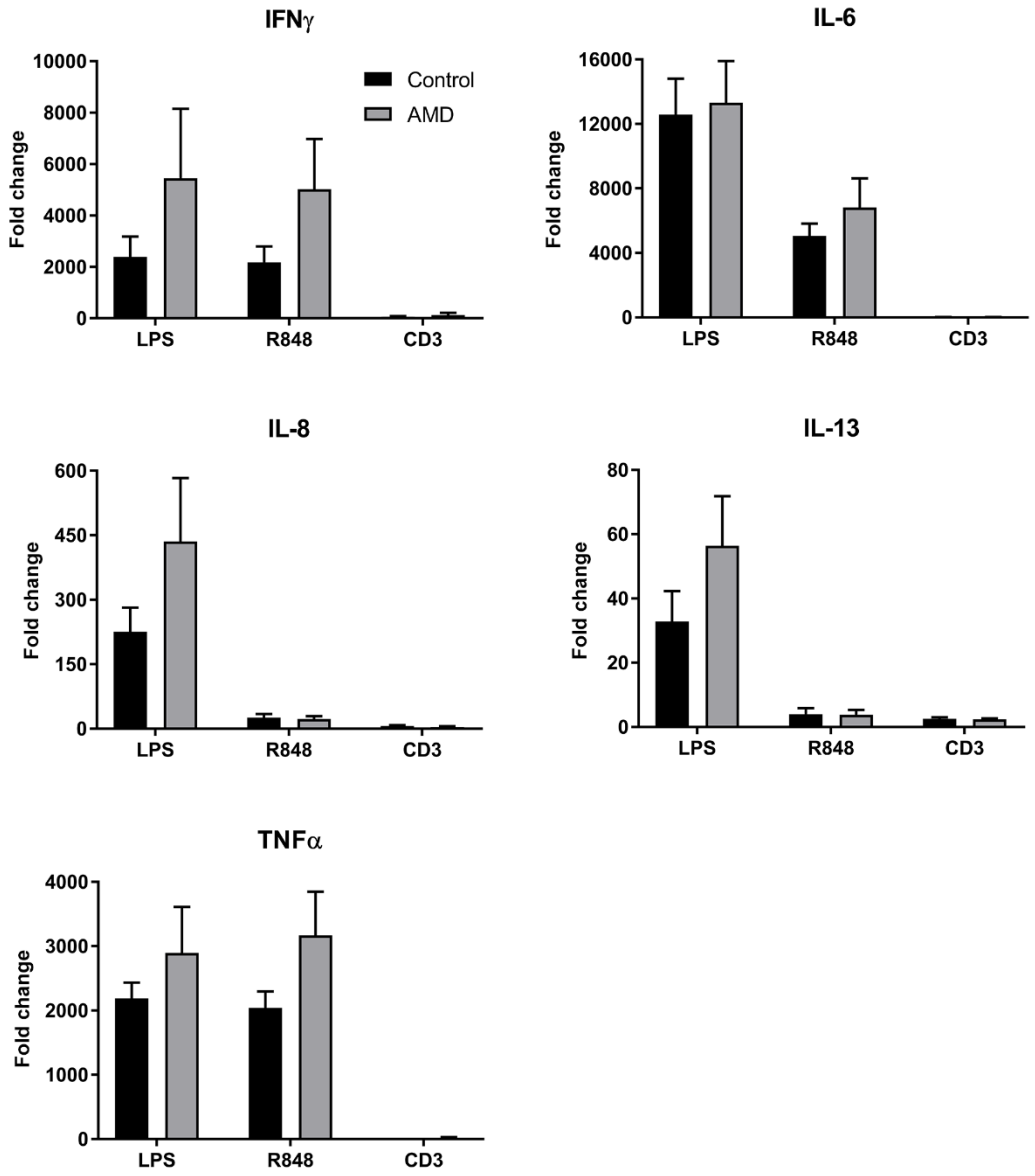

Figure 7.4 – Cytokine production following immune stimulation in whole blood of AMD patients and controls.

Levels of IFNγ, IL-6, IL-8, IL-13 and TNFα in the supernatant of whole blood stimulated for 19 hours with LPS, R848 and CD3 expressed as fold change from unstimulated supernatant for each patient. Cytokines were measured by multiplex ELISA (Mesoscale Discovery). Graphs are presented as mean±SEM (n=15-16 per group). Data was analysed by non-parametric Mann-Whitney U test between AMD and control patients for each cytokine and stimulus combination.

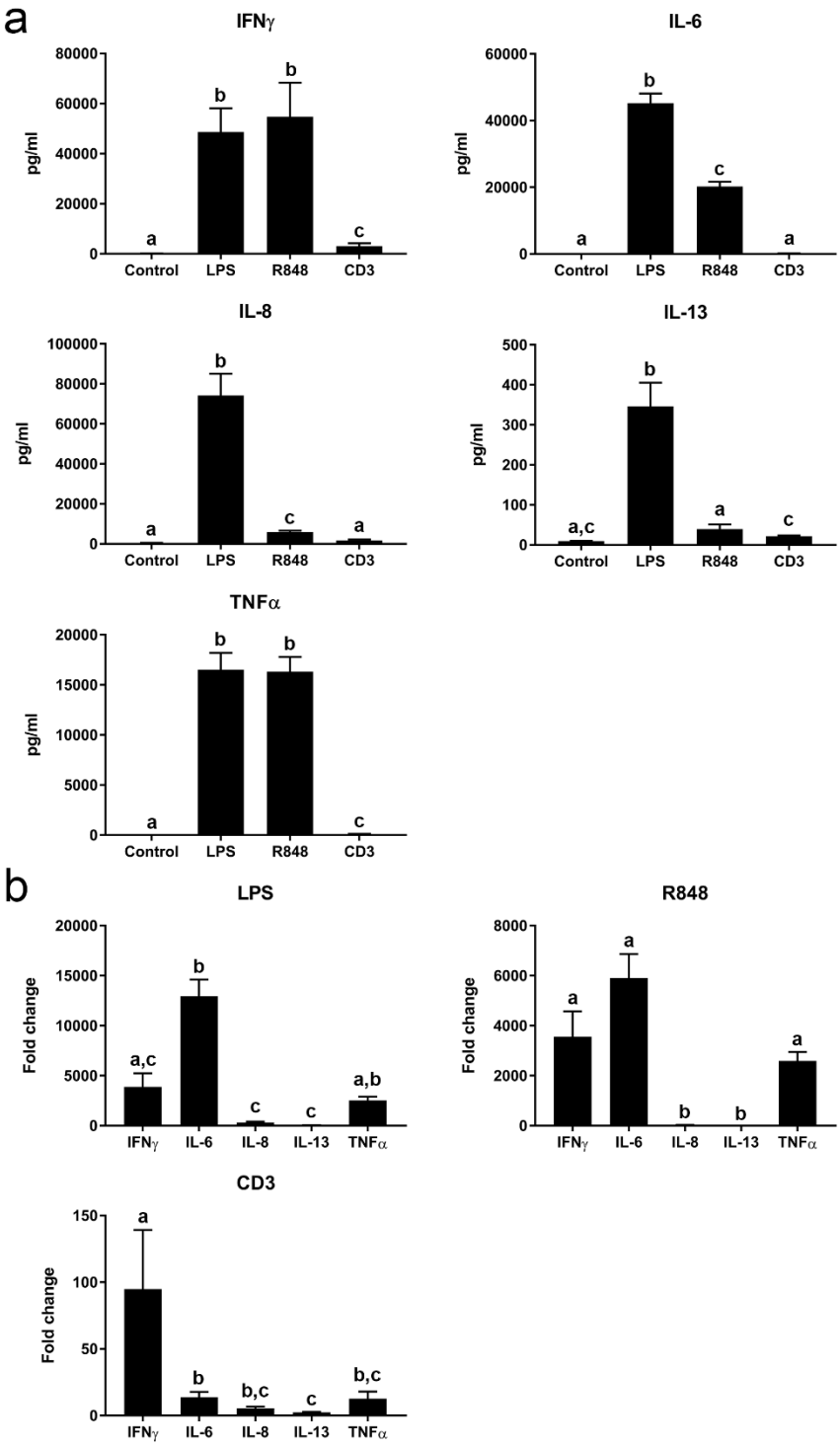

Figure 7.5 – Different immune stimuli increase specific patterns of cytokine increases.

(a) Levels of IFNγ, IL-6, IL-8, IL-13 and TNFα for unstimulated whole blood supernatant and supernatant stimulated with LPS, R848 and CD3. (b) LPS, R848 and CD3-induced cytokine patterns expressed as fold change in cytokine levels from unstimulated to stimulated whole blood supernatant. Cytokine levels were measured by multiplex ELISA (Mesoscale Discovery). Graphs are presented as mean±SEM (n=31). Data was analysed by non-parametric repeated measures Friedman test with Dunn post-hoc testing. Different letters denote statistically different means.

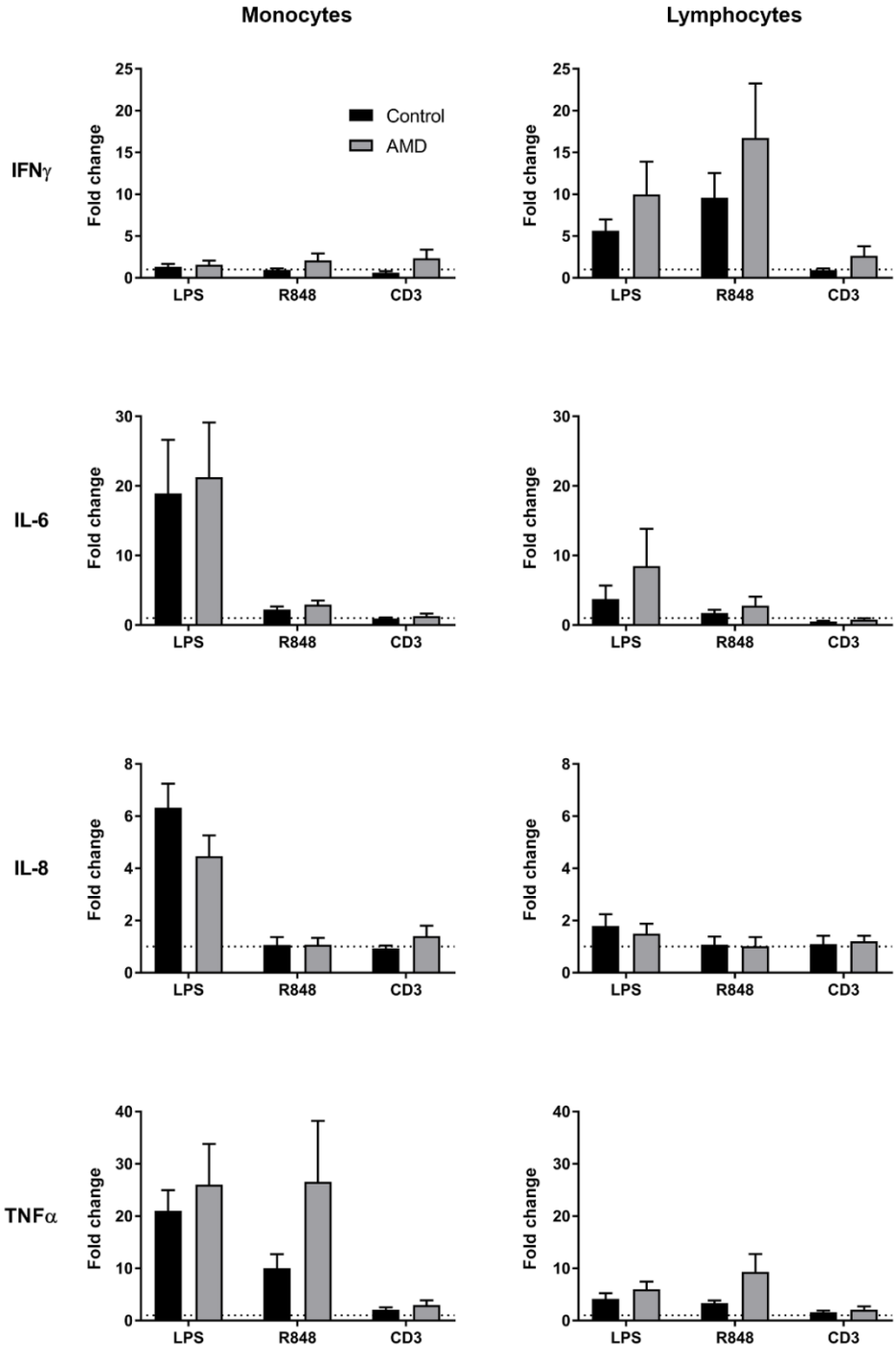

Figure 7.6 – Cytokine expression by monocytes and lymphocytes following whole blood stimulation in AMD patients and controls.

Production of IFNγ, IL-6, IL-8, and TNFα by monocytes and lymphocytes at 4 hours post whole blood stimulation with LPS, R848 and CD3 expressed as fold change in expression index from unstimulated whole blood for each patient. Expression index for each cytokine was calculated as the product of size of the positive population and its median fluorescence intensity as assessed by flow cytometry. Graphs are presented as mean±SEM (n=15-16 per group). Data was analysed by non-parametric Mann-Whitney U test or parametric t-test between AMD and control patients for each cytokine and stimulus combination.

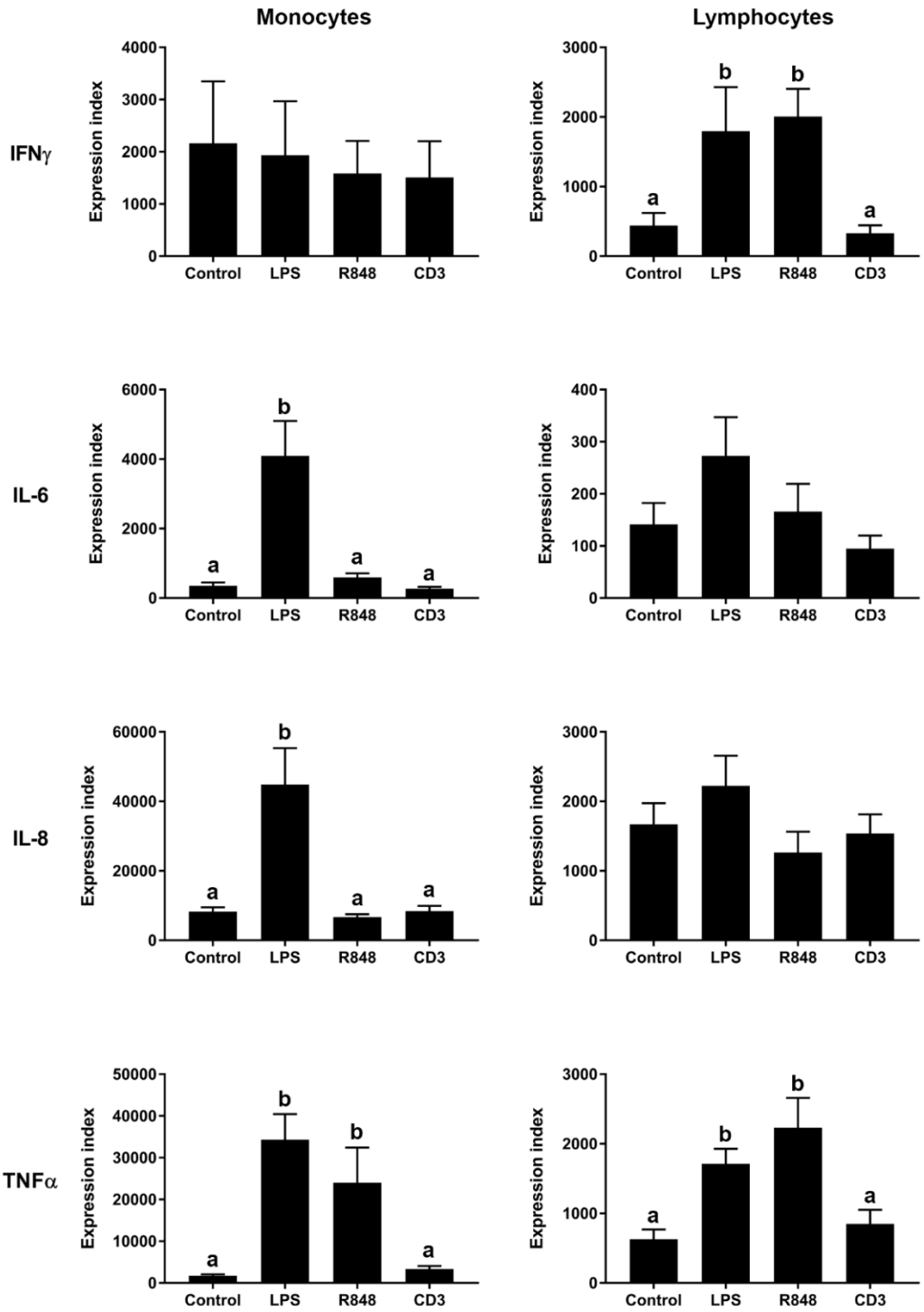

Figure 7.7 – Cytokine expression by monocytes and lymphocytes following whole blood stimulation.

Production of IFNγ, IL-6, IL-8, and TNFα by monocytes and lymphocytes at 4 hours post whole blood stimulation with LPS, R848 and CD3 or unstimulated whole blood quantified as expression index. Expression index for each cytokine was calculated as the product of size of the positive population and its median fluorescence intensity as assessed by flow cytometry. Graphs are presented as mean±SEM (n=31). Data was analysed by non-parametric repeated measures Friedman test with Dunn post-hoc testing. Different letters denote statistically different means.

7.3.3 Aqueous and serum cytokines across aging

Aging is the biggest risk factor for AMD and is also associated with many changes in the peripheral immune response (Aw et al., 2007; Friedman et al., 2004). Consequently, I examined whether aging has an effect on peripheral or local inflammation for the cytokines investigated.

In this cohort, there was a weak positive correlation between age and increased serum IFNγ (ρ=0.2991, p=0.0454) and IL-6 (ρ=0.3217, p=0.0339), but no correlation between age and serum IL-8, IL-13 or TNFα levels (Figure 7.8). There was also no correlation between age and aqueous cytokines in terms of IL-6, IL-8 or IL-13 levels (Figure 7.9).

Overall, there is evidence that increased levels of some systemic cytokines is observed during aging, but no effects were found in the eye.

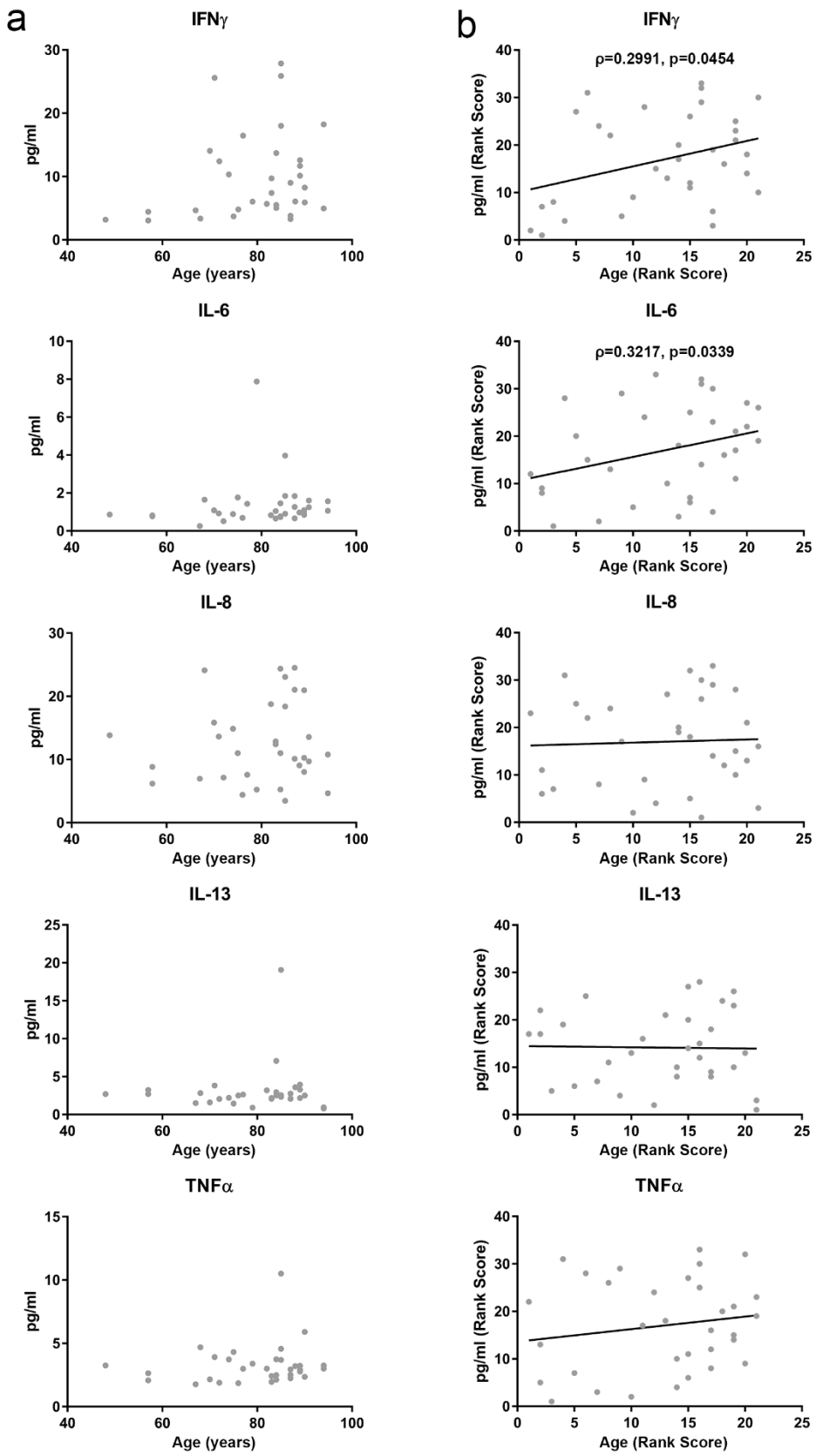

Figure 7.8 – Correlation of serum cytokines with age.

Correlation of age and serum IFNγ, IL-6, IL-8, IL-13 and TNFα in (a) raw values and (b) ranked values. As data was non-parametric, correlation was assessed with spearman rank testing and corresponding lines of best fit are shown on graphs of ranked data.

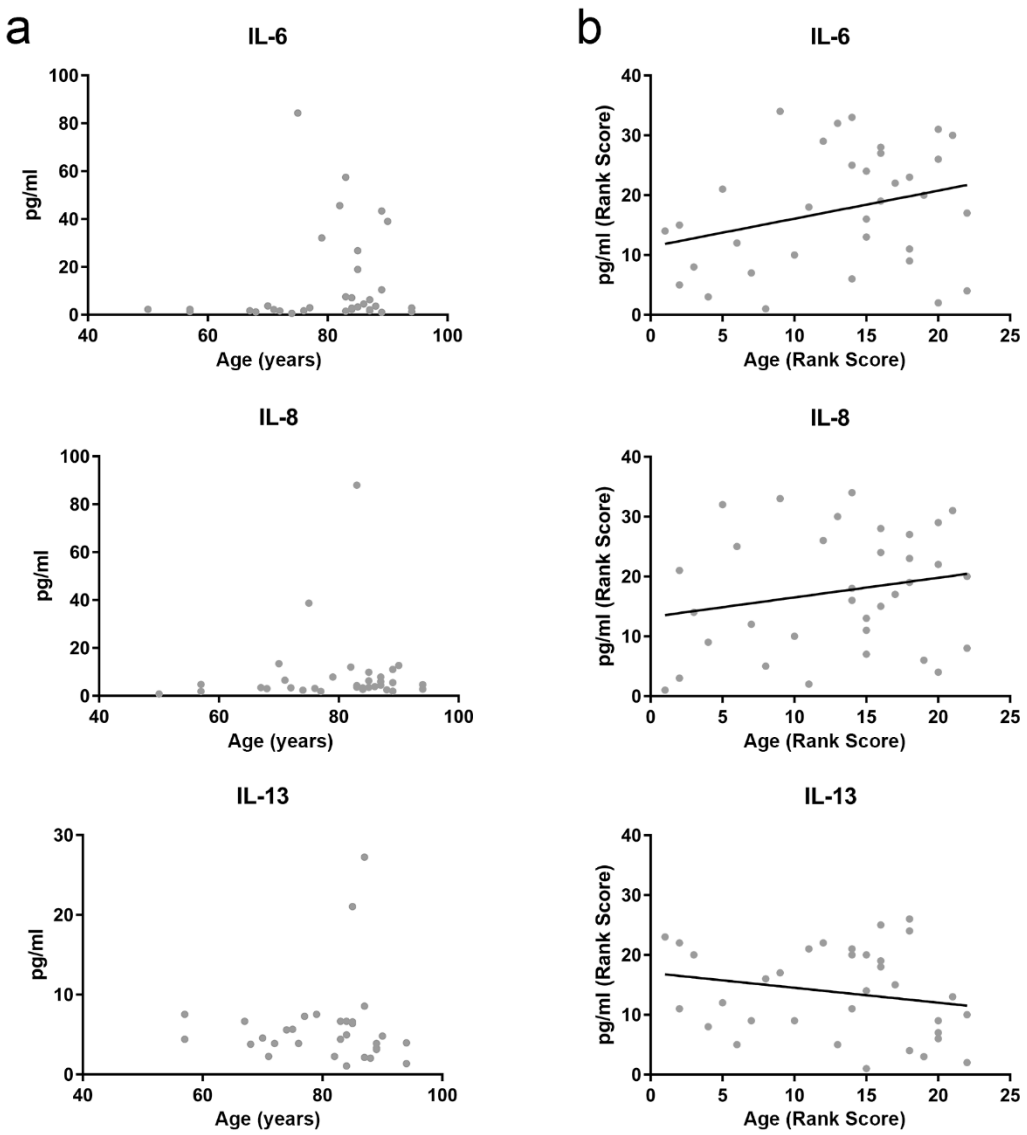

Figure 7.9 – Correlation of aqueous cytokines with age.

Correlation of age and aqueous IL-6, IL-8 and IL-13 in (a) raw values and (b) ranked values. As data was non-parametric, correlation was assessed with spearman rank testing and corresponding lines of best fit are shown on graphs of ranked data.

7.4 Discussion

7.4.1 Peripheral cytokines levels during AMD

In this mixed dry and wet AMD cohort, there was not a significant difference in any cytokine assayed, although there were trends to increased systemic IL-6 (p=0.0784) and IL-8 (p=0.1253) in AMD patients. One previous study has stratified wet and dry AMD patients and identified increased serum IL-6 and IL-8 levels in AMD patients compared to age-matched controls with further elevations in dry AMD patients (n=31) compared to wet AMD patients (n=59) (Ambreen et al. 2015). This is the only study to investigate cytokine levels in the serum of dry AMD patients and used a Pakistani cohort. Most other studies have focused exclusively on wet AMD patients in a Caucasian cohort. Increased IL-6 in the serum of wet AMD patients has been reported in several other studies making this finding more compelling (Ambreen et al. 2015, Haas et al. 2015, Yildrim et al. 2012). IL-8 is also increased in wet AMD patients in a Pakastani cohort and there is also a reported trend (p=0.09) to increased IL-8 serum in wet AMD patients (n=161) compared to control patients (n=43) in a Caucasian cohort (Ambreen et al., 2015; Lechner et al., 2017). However, Nassar et al. 2015 report increased serum levels of IL-1α, IL-1β, IL-4, IL-5, IL-10 and IL-13, but not IL-6 or IL-8, in wet AMD patients (n=30) compared to age-matched controls (n=15). Result described in this chapter reveals only trends of increased serum levels of IL-6 and IL-8 in AMD patients, and increasing the number of patients is required to conclusively determine whether IL-6 and IL-8 is raised in a stratified wet and dry AMD Caucasian cohort.

In this study, solid-phase multiplex ELISA (Mesoscale) was used to assay cytokines, while most other studies have used a bead-based assay (Luminex). In a direct comparison, Mesoscale shows better sensitivity than Luminex in normal sera for IFNγ, IL-2, IL-10, IL-12, and TNFα, the two systems are comparable for IL-6 and Luminex is more sensitive for IL-8 (Fu et al., 2010). In this comparative study, IL-1β was not detectable in normal sera by either method, in line with my observations. Nassar et al. 2015 have published results for more elevations in cytokines than any other study (IL-1α, IL-1β, IL-4, IL-5, IL-10 and IL-13) but stated that ‘adequate signals were detected for all cytokines’, but it is not clear whether these values are above or below the lower limit of quantitation (LLOQ), as other studies, including in this chapter, exclude these from analysis if most values are below the LLOQ.

7.4.2 Ocular cytokine levels during AMD

In this study, I investigated the levels of cytokines in the aqueous humour to measure local intraocular inflammation. Although retinal or vitreal samples would be closer to the site of inflammation than aqueous humour, these samples can only be obtained post-mortem or through vitrectomy, which is rarely performed in AMD patients. However, it has been shown previously in diabetic edema patients that there is strong correlation in levels of IL-6 (ρ=0.737, p=<0.0001) and VEGF (ρ=0.793, p<0.0001) between the aqueous and vitreous humour. Furthermore, aqueous humour has been used previously to show increased intraocular inflammation during other retinal diseases, including diabetic retinopathy and retinal vein occlusion (Cheung et al., 2012; Feng et al., 2013; Jung et al., 2014; Dong et al., 2015), indicating this approach is also valid for AMD patients.

In this study, only levels of IL-6, IL-8 and IL-13 in aqueous humour were above the lower limit of quantitation (LLOQ) in most samples. IL-8 is elevated in the aqueous humour of AMD patients compared to age-matched controls. IL-8 has previously been identified as significantly elevated in 2 of 3 studies of wet AMD patients (Agawa et al., 2014; Jonas et al., 2012; Rezar-Dreindl et al., 2016) and the data presented in this chapter supports this association in a mixed cohort of dry and wet AMD patients. However, when stratified neither cohort reaches significance as the statistical power is much lower, showing more patients are needed to investigate whether there are significant differences between the dry and wet AMD groups. There is little evidence presented in this chapter of elevated IL-6 in the aqueous humour of AMD patients. There is a large conflict in the literature; IL-6 is shown to be upregulated in 2 of 5 studies of wet AMD patients (Agawa et al., 2014; Fauser et al., 2015; Chalam et al., 2014; Jonas et al., 2012; Rezar-Dreindl et al., 2016). IL-13 levels have only been previously reported in one study, which found nearly 8-fold upregulation in wet AMD patients (Fu et al., 2017). The data in this chapter is just the second study of IL-13 in AMD patients and although there is a trend to increased IL-13 in AMD patients, especially dry AMD patients, this effect size is very modest in comparison to the previous report. More studies with larger cohorts investigating the presence of aqueous humour cytokines, notably IL-13, followed by a meta-analysis of results from published studies would be beneficial in clarifying the conflicting data within the literature.

Additionally, there were two patients with remarkably high IL-8 and IL-13 aqueous cytokine levels compared to the rest of the cohort. Based on clinical data, there is nothing remarkable about the past medical and drug history in these patients. In a larger cohort, it would be interesting to see whether these patients represent a subgroup and attempt to identify the basis for these elevations. Different IL-8 haplotypes have been previously associated increased risk of wet AMD (Goverdhan et al., 2008; Ricci et al., 2013; Tsai et al., 2008), so there may be a genetic basis.

Haplotyping/genotyping of DNA from these patients for IL-8 and IL-13 should be able to confirm or disprove this.

7.4.3 Correlation of aqueous and serum cytokines

In this cohort of patients and controls, there was a significant positive correlation between aqueous humour and serum levels of certain cytokines. This may be representative of how changes in peripheral inflammation can affect local inflammation in the eye. However, this may also be due to a genetic, or possibly environmental, predisposition for both local and peripheral cells from AMD patients to produce higher levels of cytokines than controls. No association between levels of the T_H2-associated cytokine IL-13 in the serum and aqueous humour was identified. Previous studies of aqueous and peripheral cytokines in a diabetic retinopathy cohort did not find a correlation between plasma and aqueous humour IL-6 or VEGF levels (Funatsu et al., 2001). However, my findings suggest that correlations between serum and aqueous IL-6 and IL-8 may be present in controls and AMD patients. Overall, the correlations between IL-6 and IL-8 in the aqueous and serum are interesting, but require further investigation to determine the cause of this association.

7.4.4 Comparison of cytokine levels in the aqueous and serum

IL-6 and IL-13 levels are higher in the aqueous than serum, while IL-8 is higher in the serum than the aqueous, revealing a substantial difference in the composition of these local and peripheral fluids. These findings argue against diffusion of IL-6/IL-13 from the serum to raise intraocular levels. A previous study of endotoxin-induced uveitis in mice showed strong upregulation of IL-6 in the aqueous humour, but not IL-1β or TNFα, and the authors argue that these cytokines should correlate if macrophages/microglia are the cellular source and suggest instead ocular parenchymal cells or endothelial cells as the source (Ohta et al., 2000). However, microglia can have many different phenotypes so specific IL-6 production may be a particular activation state. IL-8 can be produced by many cells, notably macrophages, neutrophils and endothelial cells in the periphery and *in vitro* activated RPE cells and Müller cells may also produce IL-8 (Mahieux et al., 2001; Liu et al., 2014; Goczalik et al., 2008). IL-13 has been previously shown to be secreted mainly by T_H2 cells, which may be a source of IL-13 in the aqueous humour. The aqueous microenvironment suppresses inflammatory cells, including monocytes, neutrophils, T_H1 and T_H17 cells entering from the blood, but whether it suppresses T_H2 cells is unclear (Streilein, 2003; Shechter et al., 2013). This cytokine has been rarely studied in the eye and it may otherwise be locally produced by ocular cells or high levels could result from active transport from the serum.

Determining the source of the cytokines in aqueous humour will be an interesting area of research, which may lead to mechanisms to alter its composition.

7.4.5 Immune cell cytokines and phenotype following immune stimulation

PBMC restimulation has been able to provide insights into several diseases. For example, TLR4 (LPS) and TLR7 (imiquimod – a close derivative of R848) stimulation of PBMCs results in increased levels of IL-1β in chronic pain patients compared to controls (Kwok et al., 2012). Furthermore, by assessing levels of 17 cytokines following PBMC stimulation by 8 different immune stimuli, a systemic immune signature of 10 cytokine and stimuli combinations could distinguish RA patients from controls (Davis III et al., 2010). In this study, whole blood restimulation showed no significant differences between AMD patients and controls in terms of cytokine production following stimulation with LPS (bacterial mimetic), R848 (viral mimetic) or anti-CD3 IgG (T cell stimulation). There a general trend to increased cytokine production in AMD patients by all immune stimuli, but no comparison reaches statistical significance. A previous study has found significantly increased IL-8 and CCL2 from wet AMD patient PBMCs stimulated by LPS compared to controls (Lechner et al., 2017), but had a much larger cohort (n=43 controls, n=161 AMD patients). Overall these findings argue for further investigation in both dry and wet AMD patients.

In this study, whole blood restimulation was performed, whereas PBMC restimulation is performed for previous studies in wet AMD, rheumatoid arthritis and chronic pain studies (Kwok et al., 2012; Davis III et al., 2010; Lechner et al., 2017). Whole blood restimulation was chosen over PBMC stimulation as it is more representative of *in vivo* conditions due to the presence of many important factors within the blood and inclusion of more immune cells populations, such as neutrophils (Silva et al., 2013; De Groote et al., 1992). Furthermore, whole blood restimulation does not require the timely, costly and potentially damaging isolation of PBMCs, which is likely to contribute to variation, along with the fact that many studies also freeze and thaw PBMCs before stimulation, reducing cell viability and altering phenotype (Silva et al., 2013; Weinberg et al., 2009).

In addition to multiplex ELISA based cytokine measurements, I also performed flow cytometric analysis of intracellular cytokine production by different immune cell populations. This type of analysis provides a snapshot of which cells are producing specific cytokines at 4 hours post stimulation. There is broad agreement with the total cytokine levels in the supernatant and there are no significant differences between AMD patients are controls in terms of cytokine levels produced by lymphocytes and monocytes in response to LPS, R848 or CD3. However, our study identified the cellular sources of several cytokines found after stimulation, with IFNγ produced by

T cells, IL-6 and IL-8 produced by monocytes and TNFα produced by both. This study did not investigate the contributions of other cell types in whole blood (e.g. granulocytes), which may also produce cytokines when stimulated. Increased IL-8 expression by CD11b+ monocytes from wet AMD patients was identified in a previous study following PMA/ionomycin stimulation, but LPS stimulation wasn't investigated in this context (Lechner et al., 2017). Overall, the data in this chapter do not provide evidence that AMD patients have a greater capacity to respond to innate or adaptive immune stimuli than controls, although there are some trends to increases that are worthy of greater investigation. In autoimmune diseases, these studies have provided insight into disease mechanisms (i.e. increased type 17 immune response in RA), the development of a systemic immune signature that could be used to aid diagnosis, identification of RA patients likely respond to TNFα therapy, and subgroup identification of lupus patients based on differential responsive to LPS and immune complexes (Kayakabe et al., 2012; Liou, 2003; Davis III et al., 2010).

7.4.6 Effect of aging on local and peripheral cytokines

Aging is the main risk factor for age-related macular degeneration (Congdon et al., 2004). Accordingly, I investigated how aging may affect local and systemic inflammation and thereby contribute to AMD. No changes in levels of IL-6, IL-8 or IL-13 were identified in the aqueous humour due to aging. However, aging increased serum levels of IFNγ and IL-6, but not IL-8, IL-13 or TNFα. Therefore, peripheral inflammation is associated with aging, but doesn't seem to impact levels of cytokines within the aqueous humour. The cause of increased peripheral inflammation could be due to increased baseline expression of cytokines or increased susceptibility with aging to inflammatory events e.g. infection and chronic diseases (e.g. autoimmune diseases, cancer). Increased serum/plasma levels of IL-6 with aging has been previously demonstrated by several studies (Wei et al., 1992; Kim et al., 2012; Harris et al., 1999; Bermudez et al., 2002), showing the data from this study is in line with other published observations.

7.4.7 Summary of results and cohort

This study has provided further evidence of IL-8 increases in the aqueous of AMD patients, along with the first evidence of a correlation of IL-6 and IL-8 levels in the aqueous humour and serum of AMD patients and controls. There are several trends in these data that are worthy of further investigation due to the low number of AMD patients and controls in this study. These trends include increased IL-6 and IL-8 in the serum, increased IL-13 in the aqueous humour (especially in dry AMD patients) and possible hyperresponsiveness of immune cells to stimulation. Although these sample sizes have been used previously in many similar studies, larger cohorts will always lead to more reliable results. Furthermore, a larger number of patients allows for stratification of patients. This stratification could be performed for several factors, for example AMD type (i.e. wet and dry AMD patients) or inflammation status (i.e. high and low systemic inflammation). The main reason for a low patient number in this study is that samples from eligible and consenting cataract patients with concomitant AMD were available on average once every 3-4 weeks. The sample size for whole-blood stimulation could be improved by amending the ethics to allow blood collection from AMD patients and controls without the requirement of cataract surgery, which greatly limits the number of eligible patients. Additionally, while groups were matched for age, gender and smoking status, obesity was not considered or measured by BMI, unlike many other studies in AMD patients, meaning the effects of this variable cannot be excluded. Two of the patients within the AMD group also had other ocular pathology, which could confound the results, although neither of these patients showed particularly high expression of cytokines. Overall, this study makes some interesting observations that should be followed-up in a larger cohort.

Chapter 8:

General Discussion

8.1 Salmonella and LPS as models of systemic inflammation

S*almonella enterica* subspecies *enterica* serovar Typhimurium mimics many of the features of human typhoid fever and is used as a well characterised murine model for human systemic Salmonella infection (Ruby et al., 2012). Salmonella infections persist for several weeks as the innate immune system of macrophages, neutrophils and natural killer (NK) cells control bacterial load, while strong adaptive T_H and B cell responses develop to clear the pathogen (Fillatreau, 2011). Macrophages and dendritic cells detect the pathogen and in response secrete pro-inflammatory cytokines that polarise T_H cells and activate NK cells (Godinez et al., 2008; Lapaque, et al., 2009). In C57BL/6 mice, T_H1 and NK cells secrete IFNγ, which act on macrophages to promote their differentiation into M1 macrophages. M1 macrophages support T_H1 polarisation, leading to a feedback loop of differentiating M1 and T_H1 cells (van de Vosse & Ottenhoff, 2006). In BALB/c mice, reduced systemic production of IFNγ and IL-12 compared to C57BL/6 mice leads to a shift away from T_H1 polarisation (Pashine et al., 1999). My results are strongly in line with these previous findings, with C57BL/6 mice showing over 60-fold greater expression of IFNγ at 4 weeks post infection than BALB/c mice (Chapter 4). Interestingly, humans show a T_H1 dominant immune response during typhoidal Salmonella infections and polymorphisms in IFNγ and IL-12 are associated with increased susceptibility to typhoid fever (van de Vosse & Ottenhoff, 2006; Gal-Mor et al., 2014), indicating that systemic immune activation by Salmonella in T_H1-dominant C57BL/6 mice is likely more similar to humans than BALB/c mice.

LPS recognition is a critical component in the immune response to Salmonella as TLR4 knockout mice are unable to control Salmonella infection during the early stages of infection and show low levels of pro-inflammatory cytokine secretion (Talbot et al., 2009). Many studies investigating the effect of systemic inflammation have used LPS derived from bacteria to stimulate immune cells via TLR4 (and sometimes TLR2) to produce proinflammatory cytokines. However, there are many differences between the inflammatory responses that limit the value of using LPS to model a systemic infection. In addition to TLR2/4, other PRRs have been identified that detect Salmonella - TLR1/5/6/9, NOD1/2, NLRP3 and NLRC4 inflammasomes - and subsequently activate innate immune cells, which then present bacterial antigens on their surface to generate antigen-specific T and B cells (Keestra-Gounder et al., 2015; Broz et al., 2012). Additionally, high dose LPS typically used in these studies induces peripheral tolerance to subsequent immune activation by promoting expression of proteins that block TLR4 signalling, whereas Salmonella infection doesn't induce tolerance to further TLR4 stimulation in C57BL/6 mice (Maitra et al., 2012; Püntener et al., 2012). Indeed, I identified that Salmonella primes the systemic immune systemic to produce exaggerated levels of T_H1 polarising cytokine IL-12 in response to subsequent activation by LPS in C57BL/6 mice (Chapter 4). However, tolerance effects were observed in BALB/c mice, showing

that the balance of T_H1 and T_H2 immune responses is also an important consideration in tolerance and priming effects (Chapter 4).

LPS injection induces acute systemic inflammation characterised by high levels of CCL2, IL-1β, IL-6, IFNγ and TNFα in the serum peaking at 2 hours post injection and gradually decreasing over time so that by 24 hours post injection only CCL2 and IL-6 are still slightly elevated (Biesmans et al., 2013). In contrast, systemic Salmonella infection persists for around 35 days in mice (Broz et al., 2012) and I found evidence for increased IFNγ and a strong trend for increased TNFα (p=0.07) at 2 months post Salmonella infection (Chapter 3). Therefore, a single-dose of LPS does not provide insights into chronic inflammation. Furthermore at 24 hours post LPS injection, C57BL/6 mice show higher levels of IL-6 and IL-8 than 4 weeks of Salmonella infection, but the levels of IFNγ are 30-fold lower, indicating a different pattern of proinflammatory cytokine production (Chapter 4). This may be due to the activation of different cell types, with LPS activating TLR4-expressing cells (i.e. monocytes and B cells), while Salmonella activates the full range of innate and adaptive cells (Tapping et al., 2000; Kawai et al., 1999). Overall, the Salmonella model induces chronic systemic inflammation characterised by a diverse range of innate and adaptive processes (Figure 8.1) that will provide greater insight into the effect of systemic infections on the retina than LPS.

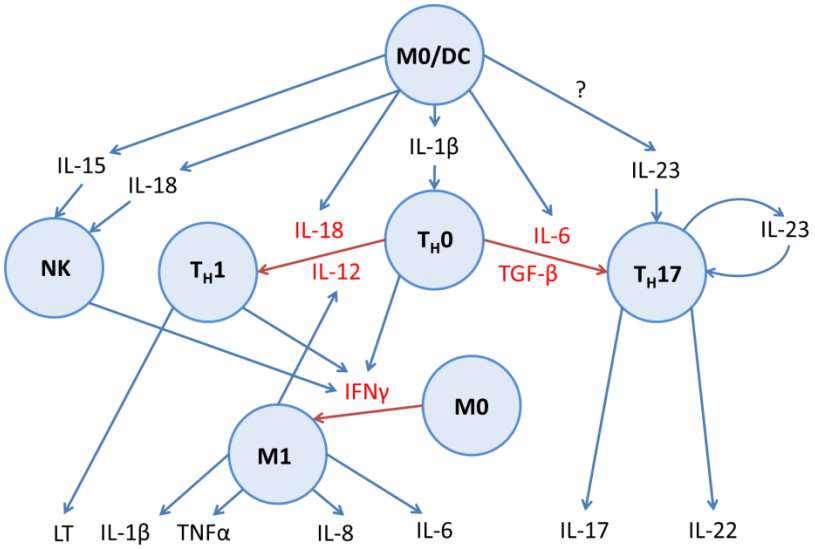

Figure 8.1 – Salmonella infection leads to the activation of diverse immune pathways
In C57BL/6 mice, detection of Salmonella by PRRs results in cytokine release from unpolarised macrophages (M0) and dendritic cells (DC). These cytokines act on a variety of immune cells to drive their activation, polarisation and production of additional cytokines, which result in robust innate and adaptive immune responses. Cytokines shown in red drive polarisation of specific cell types. NK cell, natural killer cell; T_H0 cell, unpolarised T helper cell; T_H1 and T_H17 cell, T helper cell polarised to T_H1 and T_H17 responses respectively; M1 cell; classically activated macrophage; TNFα, tumour necrosis factor α; IL-, interleukin-; LT, lymphotoxin; TGF-β, transforming growth factor β.

8.2 Systemic infections and retinal myeloid cells

Previous exposure to chronic infections (i.e. *Cytomegalovirus, P. gingivalis, C. pneumoniae*) is a known risk factor for neurodegenerative diseases, including AMD and Alzheimer's disease (see introduction section 1.5.4). This is thought to be because systemic infections can activate the local primed immune system, causing accelerated neurodegeneration. Evidence for this comes from human studies where previous exposure to periodontitis-causing bacterial strain *P. gingivalis* increases sixfold the cognitive decline seen in Alzheimer's disease patients (Ide et al., 2016). Furthermore, murine prion disease induces chronic neurodegeneration and neuroinflammation, both of which are exacerbated by LPS-induced systemic inflammation, showing a link between systemic inflammation and neurodegeneration (Cunningham et al., 2009, 2005). These studies provide a rationale for investigating the role that systemic infections may play in inflammation and degeneration during AMD, but in order to better understand these processes, it is important to firstly characterise how systemic infections can affect the healthy retina.

Salmonella infection resulted in retinal myeloid cell activation, in line with previous observations from systemic viral and fungal infections on the retina (Maneu et al., 2014; Zinkernagel et al., 2013), but I did not observe the increased total number of myeloid cells seen in these studies (Chapter 3). These differences in myeloid cell number may show a differential response of the retina to bacterial infections compared to viral and fungal infections. However, the different methods of FACS analysis may also contribute this difference. In Chapter 3, I examine the CSF-1R$^+$ cell population, with high levels of eGFP expressed in myeloid cells. In contrast, the viral study identified myeloid cells as CD45$^+$ CD11b$^+$ F4/80$^+$ cells and the fungal study used CD45$^+$ CD11b$^+$. CD45 and CD11b are expressed at low levels on microglia (Liyanage et al., 2016), so it is possible that a shift in their expression leads to better discrimination from the negative population, which would present as increased numbers of cells. The use of CSF-1R$^+$ cells from MacGreen mice in this study enables the clear discrimination of myeloid cells from other retinal cells, which is particularly important in the retina as they represent such a small population (≈2,600 cells per retina), and are commonly used in brain microglia studies (Getts et al., 2008; Grabert et al., 2016; Gottfried-Blackmore et al., 2008; Liyanage et al., 2016).

MHCII expression on myeloid cells is also identified following fungal and viral infection (Maneu et al., 2014; Zinkernagel et al., 2013). With Salmonella infection, there was a trend to increased MHCII expression on CSF-1R$^+$ cells ($p=0.07$) at 1 week post infection, but much larger and sustained changes were observed with CD45, CD11c and CD11b in comparison. The expression of CD11c has not been considered in other studies, and identifies some interesting population subsets in the retina following infection. Furthermore, this study looks at an early and late

timepoint of infection and identifies increased microglial activation over time. The other studies both use early timepoints (day 4 for fungal infection and day 10 for viral infection) so it would be interesting to know the kinetics of activation in these models.

Taken together, these studies demonstrate that retinal myeloid cell activation is a feature of a diverse range of systemic pathogens. Myeloid cell activation is also one of the major inflammatory features of AMD pathology, where there is evidence for the activation of retinal microglia and choroidal macrophages found in close association to drusen (Cherepanoff et al., 2010; Ambati et al., 2013). It is therefore reasonable to hypothesise that systemic inflammation could exacerbate the inflammatory microenvironment in AMD, leading to further microglial activation or a phenotypic skewing of previously activated cells. This could explain why chronic systemic infections are associated with increased incidence/progression of AMD.

In AMD patients, myeloid cells are recruited to BrM, from the retina and/or choroid, and progressively increase during the transition from early to intermediate AMD (Cherepanoff et al., 2010). In this thesis, I provide further characterisation of a previously published murine model using immune complexes to model inflammatory deposits that activate myeloid cells and induce their recruitment to the subretinal space, in line with observations from AMD patients (Murinello et al., 2014). In addition, drusen has been previously shown to contain immunoglobulins and complement pathway proteins (see introduction section 1.4.1), so this model also transiently recapitulates these inflammatory aspects of AMD. Although this model is acute and transient, it provides a platform to test whether systemic inflammation can influence ongoing local retinal inflammation. The model uses BALB/c mice as far fewer immune complexes form in C57BL/6 mice using our current protocol (Salome Murinello, PhD thesis). This may be because the use of Alum adjuvant promotes stronger antibody responses in BALB/c mice, so other immunisation procedures may be necessary for C57BL/6 mice. Alternatively, the fact that C57BL/6 and BALB/c mice have different dominant IgG subclasses in the periphery may underpin these differences. IgG1 is the predominant subclass in BALB/c mice, while they also express IgG2a (Bruhns, 2012). In contrast, IgG2b is the predominant subclass in C57BL/6 mice, and they don't express IgG2a (Morgado et al., 1989). Human IgG1, which is the predominant subclass in human sera, is similar to murine IgG2a in terms of ability to activate C1q and myeloid cells via FcγRI (Hussain et al., 1995). Consequently, BALB/c mice are likely to show a more similar immune complex response to humans than C57BL/6 mice (Petrushina et al., 2003).

Following Salmonella infection in the healthy retina, microglial cells still display a ramified morphology but have clearly increased levels of activation markers. The majority of inflamed cells in the retina therefore appear to be microglia and this is supported by the fact that FACS analysis

does not reveal an increased number of immune cells in the retina (Chapter 3). In contrast, following immune complex formation there are numerous highly activated CD11b and FcγRI+ amoeboid cells in the vitreous, retina and choroid. These amoeboid myeloid cells are not positive for neutrophil markers (Salome Murinello, PhD thesis), indicating that they are likely either highly activated microglia or infiltrating monocytes. When immune complexes and Salmonella infection are combined, there is a synergistic recruitment of cells to the back of the retina (Chapter 5). This is the site of drusen in AMD pathology and these data indicate that systemic infections can recruit cells to the outer retina, where they could then be activated by the local inflammatory microenvironment to exacerbate AMD. Neutralisation of pathways responsible for microglial migration may therefore be an interesting therapeutic avenue for reducing the effect of systemic infections on AMD development.

The recruitment of myeloid cells to the subretinal space has been previously reported following viral infection in BALB/c mice (Zinkernagel et al., 2013). This is in line with my observations of Salmonella inducing recruitment of myeloid cells to the back of the retina in the absence of immune complexes (Chapter 5). However, in this study the control mice received intravitreal OVA injections, which induce retinal inflammation before Salmonella infection, so this cannot be directly compared to the viral study, which investigates the effect on the uninflamed retina. At 4 weeks post Salmonella infection in BALB/c mice not receiving intravitreal injections, there was not a clear recruitment of myeloid cells to the subretinal space (Chapter 4), but this is a later timepoint compared to the viral infection study, which showed the number of subretinal microglia peaked at day 10 post infection and was greatly reduced, but not at control levels, by day 25 post infection. Bone marrow chimera experiments indicated that subretinal immune cells following viral infection are of microglial origin (Zinkernagel et al., 2013). Based on these findings, it would be interesting to perform this experiment following systemic bacterial infection to see if these findings are generic or specific to viral infection. I attempted to identify the origin of myeloid cells in the combined Salmonella and immune complex model using microglial-specific antibodies, but this approach was not successful (Chapter 5).

Recruitment of microglia to the back of the retina following viral infection is abrogated in IFNγ knockout mice. However, IFNγ is critical to drive T_H1 immune responses in viral and bacterial infections, so the inhibition of this pathway is likely to impact the entire immune response, meaning that the specific pathway responsible for recruitment may not have been identified. Indeed in BALB/c mice, IFNγ was the most upregulated cytokine (8-fold) following Salmonella infection, despite being considered T_H2 dominant in comparison to C57BL/6 mice (500-fold) (Chapter 4). Unfortunately, due to the pigmented RPE/Choroid in C57BL/6 mice it is much more difficult to detect subretinal microglia, despite the strain showing far greater production of IFNγ.

The recruitment of microglia to the outer retina doesn't appear to induce any structural changes, indicating that this transient microglial activation doesn't lead to degeneration. This is supported by ERG data following immune complex formation, where transient functional deficits are identified that are resolved by 4 weeks post injection (Chapter 5).

In order to assess the interrelationship between inflammation and neurodegeneration, an acute onset retinal neurodegenerative model of GA lesions was developed, which could be used in the future to study the impact of systemic infections on retinal degeneration. This laser-induced model of outer retinal atrophic lesions showed activated microglia within areas of atrophy and at the margins of the lesions, in line with observations with GA patients (Cherepanoff et al., 2010). Furthermore, there are large subretinal FcγRI+ cells in the model, which are reminiscent of giant cells and CD163+ macrophages/RPE observed in GA patients (Lad et al., 2015; Penfold et al., 1986). Although several other models exhibiting aspects of GA pathology have been described, few features are recapitulated in a single model in comparison to the laser-induced model described in this thesis (Appendix G). Such features include pathological observations in OCT and ERG reminiscent of GA patients, photoreceptor loss and progressive reduction in retinal thickness, glial cell activation, inflammasome and complement activation and oxidative stress (Chapter 6). The main benefit of this laser-induced model is the development of a single converging lesion that can be clearly demarcated for easily tracking *in vivo* over time, whereas other models use systemic administration of substances or transgenic mice, which cause global retinal effects making progression of individual lesions difficult to track (Hollyfield et al., 2008; Machalińska et al., 2010; Kaneko et al., 2011; Lyzogubov et al., 2016). Finally, most GA models also require extensive aging for phenotypes to manifest, whereas the laser-induced model is an acute onset model capable of rapidly inducing pathology, in line with the well-respected and widely-used laser-induced model of CNV pathology (Lambert et al., 2013). This laser-induced GA model therefore represents a cost-effective platform for intervention studies and functional insights, such as how systemic infections may affect ongoing local inflammatory pathways, microglial activation and progression of degeneration.

8.3 LPS-induced inflammation, priming and tolerance

At 4 weeks post Salmonella infection, brain microglia are primed to respond in an exaggerated manner to subsequent inflammation induced by LPS (Püntener et al., 2012). Based on this finding, I chose to investigate whether microglia are also primed to respond to subsequent systemic inflammation. Elderly people frequently suffer from chronic/recurrent infections and inflammatory diseases and therefore I hypothesised that infections may prime microglia to respond to further systemic inflammatory events in an exaggerated manner, driving inflammation in AMD. My results instead demonstrated that LPS does not enhance retinal microglial activation in mice treated 4 weeks previously with Salmonella and, moreover, there was suppression of IL-1β and mKC expression when Salmonella and LPS were combined, indicating functional tolerance of the retina to subsequent systemic inflammation (Chapter 4). Strikingly, this was one of the few consistent observations in C57BL/6 and BALB/c mice, underscoring its potential as a conserved pathway to protect the retina from chronic inflammation induced by systemic infection. This protective pathway has been suggested in several animal models of stroke, where pretreatment of mice with LPS alters microglial function and protects against ischaemic damage, demonstrating that tolerance may be a neuroprotective response (Marsh et al., 2010).

Many factors could regulate the differential priming and tolerance effects observed by microglia of the brain in response to local LPS and by microglia of the retina in response to systemic LPS respectively. The most likely explanation is that while microglia are primed to respond to local insults via direct stimulation of TLR4, they become tolerant to inflammation arising in a different tissue compartment. This is supported by the similar findings of Salmonella-induced microglial priming observed in the brain of C57BL/6 mice in response to local LPS and data in this thesis showing the systemic immune system is primed to produce IL-12 in response to local LPS, meaning this priming effect is likely not a CNS specific effect (Chapter 4, Püntener et al., 2012)

However, there may also be functional immunological differences between the retina and brain that contribute to tolerance and priming effects. The brain and eye both have aspects of immune privilege and microglia are the primary immune cell responsible for immune defence. However, in the brain, microglia range from 5% of brain cells in the cortex to 12% in the substantia nigra (Lawson et al., 1990), while the proportion of microglia is much lower (0.5-2%) in the retina compared to the brain (Dick et al., 1995; Kezic et al., 2008; Lückoff et al., 2017). However, the presence of Müller cells may compensate for some microglial function in the retina compared to the brain, which lacks radial glia in adulthood (Rakic, 2009; Reichenbach & Bringmann, 2013). During healthy conditions, T cells and dendritic cells are found in the brain, but these are rarely observed in the retina (Yang et al., 2000; D'Agostino et al., 2012; Ransohoff et al., 2003).

Consequently, these differences may allow priming and tolerance effects in different compartments of the CNS.

The LPS dose and route of administration are also substantially different between the two studies. In this study, high dose peripheral LPS was administered i.p. to induce strong systemic inflammation, while in the CNS low dose LPS (50pg) was injected directly into the brain parenchyma (Püntener et al., 2012). The dose of LPS has previously been identified as critical in causing priming or tolerance, as high dose LPS induces tolerance in myeloid cells and ultra-low dose LPS induces priming to subsequent stimulation (Maitra et al., 2012). However, as a secondary stimulus the consequences of different LPS doses on priming and tolerance effects are not characterised. Additionally, intracerebral injection is likely to result in increased CNS pressure, inflammation independent of LPS administration and possibly damage the blood-brain barrier, while with systemic administration the retina remains undamaged.

Finally, the timing between the two immune stimuli is very important to tolerance and priming effects. This has been shown particularly for stroke models, where TLR4 activation following ischaemia exacerbates damage, while TLR4 activation before ischaemia protects against damage (Marsh et al., 2010). For a comparison of this study and the previous study of Salmonella-induced microglial priming the timings of these Salmonella and LPS challenges were kept constant. Having said that, the microglial response to Salmonella appears similar between the retina and hippocampus at 1 weeks post injection, but in the hippocampus microglial activation appears to return to baseline by 4 weeks post injection (Püntener et al., 2012; James Fuller, PhD thesis), whereas strong activation/phenotype changes are still observed at 4 weeks post infection in the retina (Chapter 3). This may again indicate a functional difference in the responses to systemic infection between the retina and brain. It may also indicate that the activation status of the microglia may be responsible for differences between priming and tolerance; where a previously activated microglial cell that has returned to 'resting' state may be functionally primed, while an activated microglial cell may be tolerant to further inflammation.

Overall, this study has highlighted that the retina is tolerant to repeated systemic inflammatory events, which may be a mechanism to protect the retina from excess inflammation. However, in the context of AMD it is unclear whether this retinal tolerance to repeated systemic inflammation could modulate ongoing local immune activation in the retina and, moreover, whether this effect would be protective or detrimental to disease pathology. Many more studies are required to understand the mechanisms of spatial, temporal and dose-dependent regulation of priming and tolerance. Manipulating these biological mechanisms of hypo- and hyperresponsiveness of the immune system may a novel therapeutic strategy for modulating the interaction of systemic and

retinal inflammation to protect the retina from excessive inflammation under inflammatory/diseased conditions.

I also investigated whether there is a role for priming of the systemic immune systemic in AMD patients. Systemic infection causes priming of the systemic immune response to subsequent immune activation and I hypothesised that AMD patients may have differences in the responsiveness of their immune cells to stimulation that underpins the increased systemic inflammation observed in AMD patients. More specifically, that they possessed systemic immune cells that are primed to respond to stimulation. Consequently, when patients develop acute systemic inflammatory events, the immune responses would be stronger and more prolonged leading to greater bystander damage. This study did not provide evidence for increased cytokine expression in response to viral, bacterial or adaptive immune stimuli (Chapter 7). Looking at specific cell types, these data suggested that neither monocytes or lymphocytes are primed to respond to stimulation in AMD patients. However, previous studies have identified increased expression of IL-8 from PBMCs of wet AMD patients following stimulation with bacterial mimetics compared to controls (Zhu et al., 2013a; Lechner et al., 2017). This general trend for increased IL-8, along with IFNγ, was observed in a mixed cohort of AMD patients following whole blood stimulation (Chapter 7), but a larger cohort is needed to investigate this trend and stratify patients based on subgroups.

8.4 Retinal blood vessel activation and T cell recruitment following systemic infection

Following Salmonella infection, strong upregulation of MHCII is observed on the cerebral vasculature (Püntener et al., 2012). Based on these observations, I hypothesised that the inner retinal blood vessels may also be activated following systemic infections. The retinal vasculature expresses MHCI, MHCII, ICAM-1 and VCAM-1 after Salmonella in C57BL/6 mice and these changes are the most chronic of all those examined in this thesis, with MHCII and ICAM-1 still upregulated at 6 months post infection (Chapter 3). MHCII staining was also observed on retinal blood vessels following systemic fungal infection although the authors describe this as non-specific staining (Maneu et al., 2014), but based on the representative images, I believe that this staining may actually be specific.

MHCII upregulation has been previously shown to be critically regulated by IFNγ in human endothelial cell lines (Collins et al., 1984). My data would support this finding *in vivo* as IFNγ is the

most upregulated systemic cytokine observed in both C57BL/6 and BALB/c mice (Chapter 4). Furthermore, BALB/c mice show reduced MHCII compared to C57BL/6 mice and also have lower systemic IFNγ in response to Salmonella, which would support a dose-dependent effect of IFNγ on MHCII expression. In contrast, ICAM-1 and VCAM-1 levels track with systemic IL-1β expression in both C57BL/6 mice and BALB/c mice (Chapter 4). This is supported by previous findings showing that IL-1β and TNFα are the cytokines mostly responsible for expression of ICAM-1 and VCAM-1 on endothelial cells (Dustin et al., 1986; Cook-Mills et al., 2011; Myers et al., 1992). The presence of antigen presenting molecules and cell adhesion molecules on the inner retinal blood vessels in C57BL/6 mice indicates that antigen-specific immune cells may be able to enter through the inner BRB during Salmonella infection.

T cell recruitment to the retina is observed at 4 weeks post Salmonella infection when ICAM-1 and VCAM-1 are expressed in C57BL/6 mice, whereas in BALB/c mice, a lack of ICAM-1 and VCAM-1 is accompanied by a lack of T cell recruitment (Chapter 4). It is unclear whether these cells are antigen-specific, but recruitment of antigen-specific cells may be a form of immunosurveillance to detect whether Salmonella antigens are in the retina and respond accordingly. This process may be critical to fight systemic infections that migrate to the retina (i.e. toxoplasmosis, ebola) by initiating a local immune response (Durrani et al., 2004). However, Salmonella is widely accepted as a non-neurotropic bacterium that is only present systemically (Püntener et al., 2012), therefore these T cells are unlikely to encounter their target antigen in the retina and should theoretically become anergic.

When the retina is stimulated with LPS following Salmonella infection in C57BL/6 mice, there is a trend to reduced T cells in the retina compared to Salmonella alone (Chapter 4). T cell infiltration into the retina is thought to lead to eventual apoptosis of cells within the parenchyma due to anergy, exhaustion or interactions with FasL and TGF-β (Barron et al., 2008; Yi et al., 2010). It is possible that systemic LPS induced retinal inflammation may accelerate the process of retinal T cell apoptosis, leading to the observed decrease in T cells following Salmonella and LPS. Alternatively, these cells may migrate from the retina towards the periphery due to high levels of systemic chemokines following LPS.

Despite BALB/c mice lacking T cell recruitment into the retina at 4 weeks post Salmonella under healthy conditions, there are increased numbers in the retina following OVA injection in unimmunised BALB/c mice (Chapter 5). While these mice do not possess immune complexes, the addition of inflammation induced by OVA injection alone appears to enable the expression of ICAM-1 on retinal capillaries. These findings may have relevance to AMD, where ongoing local

inflammation may allow T cell recruitment to the retina during acute systemic inflammatory events.

Immune complexes recruit immune cells to the retina at 1 and 4 weeks post intravitreal OVA injection. Immunisation of these mice against OVA leads to the generation of OVA specific T cells, in addition to antibodies. T cells from an immunised mouse injected into an unimmunised mouse are recruited to the retina in response to intravitreal OVA challenge, but this does not occur in unimmunised mice alone, demonstrating that recruited T cells are specific for OVA (Hu et al., 2000). Salmonella alone doesn't appear to lead to infiltrating cells at this point, but these mice have only been infected for 6 days so the adaptive component of generating Salmonella-specific T cells is probably still ongoing. Intriguingly, when immune complexes and Salmonella are combined, there is a trend for reduced T cells in the retina compared to immune complexes alone. ICAM-1 and MHCII levels are constant between these immune complex groups, indicating that this effect is not due to differential capacity of the inner BRB to allow entry of immune cells. Instead, T cell chemotaxis into the retina may be prevented due to the strong production of chemokines in the periphery following Salmonella infection.

At the 4 week timepoint, Salmonella does not reduce immune complex-induced T cell recruitment, but also does not increase T cells numbers unlike in unimmunised mice. This coincides with a reduction in ICAM-1 in the retina at 4 weeks post infection and immune complexes, which may be responsible for the prevention of T cell migration to the retina as a protective mechanism to reduce inflammation. Alternatively, both OVA- and Salmonella-specific antibodies may enter the retina but T cell apoptosis may be accelerated by increased retinal inflammation. In this case, this mechanism would be similar to the suggestion of LPS-induced T cell apoptosis of Salmonella-specific T cells.

These interactions are worthy of further investigation, as they highlight the complexity of T cell recruitment and responses in the retina, which are not well understood. The models presented here can be combined to provide numerous insights into the biology and function of retinal T cells. A characterisation of the T cell subsets involved, functional state (i.e. anergy, exhaustion, apoptotic), absence or presence of costimulation from retinal cells and the importance of antigen-specificity are all aspects of T cell biology that can be further defined in these models.

8.5 Activation of inflammatory pathways following systemic infection and AMD

8.5.1 Glial cells

In addition to the activation of microglia, Müller cell activation during geographic atrophy and astrocytosis at sites of drusen have been described in AMD patients (Wu et al., 2003). Increased levels of microglial marker FcγRI and macroglial cell marker GFAP have been demonstrated at an mRNA level following Salmonella infection and in a model of laser-induced outer retinal atrophic lesions recapitulating aspects of geographic atrophy. These findings suggest that systemic infections could exacerbate ongoing gliosis in the retina to accelerate AMD pathology.

8.5.2 Complement

An important role for complement is also well established at all stages of AMD, with genetic studies and promising results from CFD inhibition studies in GA patients particularly implicating the alternative pathway (Yaspan et al., 2017; Tuo et al., 2012). Bacterial infections activate alternative complement pathways in the periphery, which opsonise bacteria via C3b to signal for removal of bacteria (Tosi, 2005), but how complement activity in the retina is altered by live infection has not been described. In the retina, there was evidence for upregulation of C3 in models of systemic infection and geographic atrophy (Chapters 3, 6). These findings suggest that systemic inflammation may exacerbate ongoing complement activation in the retinas of AMD patients. Complement activation can drive both general retinal inflammation via chemoattractive anaphylatoxins (C3a and C5a) and the engagement of complement receptors (e.g iC3b signalling through CD11b/c on microglia) as well as tissue damage via C5b-9 (MAC) (Noris & Remuzzi, 2013). Further investigation of these models of systemic infection and geographic atrophy alone and in combination should focus on determining the relative contribution of complement pathways (i.e. classical and alternative) to C3 production. It would be interesting to perform immunostaining for complement pathway components, including C3 activation states and MAC, to see if there is evidence for inflammation and/or tissue damage at a protein level.

8.5.3 VEGF

VEGF is the major angiogenic growth factor driving wet AMD and anti-VEGF agents are effective at reducing progression of wet AMD (Ferrara, 2010). In CNV membranes, both M1 and M2 myeloid cells have been shown to produce VEGF (Nakamura et al., 2015). Interestingly, cytomegalovirus infection is associated with increased progression of wet AMD in humans and mouse studies show

that murine cytomegalovirus can exacerbate laser-induced CNV (Miller et al., 2004; Cousins et al., 2012). The authors suggest that virally infected peripheral monocytes/macrophages are responsible for systemic VEGF production driving increased CNV. In this study, there was no evidence for increased levels of VEGF expression following Salmonella infection in the healthy retina (Chapter 3). However, it would be interesting to characterise the effects of bacterial infection on the laser-induced CNV model and investigate whether macrophages/microglia infected with intracellular bacteria also express VEGF that could contribute to wet AMD pathology. In the laser-induced GA model, there was no evidence of VEGF upregulation in the retina or evidence of neovascularisation in histology (Chapter 6), indicating that this mouse model largely recapitulates a dry AMD phenotype.

8.5.4 Chemokines/Cytokines

Increased levels of ocular chemokines (i.e. IL-8, CCL2, CXCL9 and CXCL10) are also a feature of wet AMD pathology (see introduction section 1.4.4). Increased levels of aqueous humour IL-8 is also observed in the mixed cohort of dry and wet AMD patients presented in this thesis, with a trend to higher increases in wet AMD patients compared to dry AMD patients (Chapter 7). IL-8 polymorphisms have been associated with increased risk of wet AMD in 3 independent studies (Goverdhan et al., 2008; Ricci et al., 2013; Tsai et al., 2008). In addition to increased levels in the aqueous humour of wet AMD patients, CCL2 has also been identified as an important factor influencing angiogenesis in the laser-induced CNV mouse model (Yamada et al., 2007; Liu et al., 2011b; Tomida et al., 2011). These changes in chemokines may lead to increased numbers of VEGF expressing myeloid cells, although IL-8 can directly act on endothelial cells to enhance survival and proliferation, contributing to angiogenesis independently of VEGF.

Increased retinal expression of mKC (IL-8 homolog) and CCL2 are observed following Salmonella infection in mice (Chapter 3), indicating that systemic infection may contribute to increased chemokine expression in the retina during wet AMD pathology and contribute to accelerated neovascularisation. Furthermore, clear upregulation of cytokines IFNγ, IL-1β and TNFα were observed in the retina following Salmonella infection, which could contribute to higher levels of retinal inflammation and skew immune cell activation in the retina. Both M1- and M2-like myeloid cells in human CNV membranes have been shown to produce VEGF, so the polarisation state of myeloid cells may not be a critical factor in neovascularisation, despite a tendency towards M2 activation (Nakamura et al., 2015; Cao et al., 2011). Although systemic viral infection in mice was shown to exacerbate CNV and increased systemic VEGF expression (Cousins et al., 2012), its effect on retinal inflammation and polarisation would be interesting to characterise.

8.5.5 Inflammasome

While many upregulated pathways have been identified in wet AMD, inflammasome activation is the only clearly described inflammatory pathway that is upregulated in GA patients, who have increased IL-1β, IL-18, NLRP3, caspase 1 and caspase 8 in the retina (Kaneko et al., 2011; Kim et al., 2014; Tarallo et al., 2012). The laser-induced GA model recapitulated increases in IL-1β, IL-18, caspase 1 and caspase 8, while NLRP3 should be tested in the future (Chapter 6). Consequently, this model shows strong evidence for inflammasome activation, but this activation does not arise due to lack of DICER-1 dependent degradation of *Alu* RNA, which is the mechanism suggested in GA patients (Kaneko et al., 2011). This indicates that the model leads to inflammasome activation in a different manner to GA pathology, but this is perhaps unsurprising given the acute onset nature of the model. Salmonella infection increases levels of IL-1β, NLRP3 and Caspase 1, but not IL-18, in the retina suggesting retinal inflammasome activation following infection (Chapter 3). However, IL-18 is constitutively expressed in most animal cell types (Dinarello et al., 2013), so inflammasome activation may lead to mature IL-18 production even in the absence of mRNA upregulation. The combination of systemic inflammation and geographic atrophy may therefore cause increased inflammasome activation, leading to retinal inflammation and cell death via caspase mediated apoptosis/pyroptosis. Beyond inflammasome activation, this study has implicated that IL-13 may be upregulated in the retina during GA (Chapter 7) and it would be interesting to analyse this finding in a larger GA cohort to prove or disprove this trend and measure the levels of this gene in the laser-induced atrophic model for comparison.

8.5.6 Cyclooxygenase

Sickness behaviours following infections are driven by local cytokine changes in the brain, but it has been shown that peripheral blockade of individual cytokines has little effect on LPS-induced sickness behaviour, suggesting systemic cytokines don't directly affect levels of local cytokines (Teeling et al., 2010). However, blockade of the cyclooxygenase pathways COX1 and COX2 have been shown to dramatically reduce LPS-induced sickness behaviours in the brain, implicating prostaglandins as key immune-to-brain communicators (Teeling et al., 2010, 2007). Consequently, I looked at whether COX2 is also implicated in immune-to-retina communication and identified COX2 as the most upregulated gene in the retina following Salmonella of the 16 tested (Chapter 3). This indicates that prostaglandins may play an important role in immune-to-retina communication driving local retinal cytokine production following Salmonella infection. Further research could look at using COX inhibitors to attempt to reduce the effect of systemic infection on the retina, without impacting on the ability of the systemic immune system to fight infection. Moreover, the fenamate class of COX inhibitors also inhibit the inflammasome, meaning that the

effects of neutralising both inflammatory pathways on systemic bacterial infection could be assessed using pharmacological studies (Daniels et al., 2016). Due to common gastrointestinal side-effects in humans, long term use of fenamate NSAIDs in AMD patients to prevent inflammatory cross-talk between the systemic and retinal immune systems is probably not advisable, but these mouse studies would improve our knowledge of pathways to target with other drugs.

8.5.7 Oxidative stress

Finally, the levels of oxidative stress and antioxidant genes in models of systemic infection and geographic atrophy were examined. During infections, phagocytes initiate oxidative burst, where toxic reactive oxygen species are rapidly released into phagolysosomes to destroy intracellular pathogens (Panday et al., 2015). Meanwhile, oxidative stress is highly implicated in AMD because of the oxidative damage induced by AMD risk factors, presence of many oxidised proteins in drusen and polymorphisms in the antioxidant Sod2 gene conferring a risk for increased AMD incidence (see introduction section 1.4.1). There was evidence for increased activation of the NOX2 pathway in the retina, which drives the production of superoxide radicals, following laser-induced atrophy and following systemic bacterial infection (Chapters 3, 6). This indicates a possible role for this oxidative stress pathway in GA pathology that is worthy of investigation in patients, particularly as levels of nitric oxide synthase (NOS) enzymes are not changed in AMD patients or the laser-induced atrophy model (Bhutto et al., 2010). The NOX pathways are also implicated in other neurodegenerative diseases, including Alzheimer's disease and other rodent models of retinal degeneration (Ma et al., 2017; Song et al., 2016). The fact that retinal NOX pathways can be upregulated by systemic infection indicates that systemic infections could contribute to ongoing oxidative stress in the retina during AMD pathology. Furthermore, there is a strong trend to upregulation of eNOS and iNOS in the retina following systemic infection, which produce nitric oxide radicals that can react with superoxide radicals from the NOX pathway to generate peroxynitrate, a potent oxidant that could induce retinal damage (Li et al., 2005). Alongside these changes, no antioxidant response gene tested (Hmox-1 for Salmonella infection and Hmox-1, Sod2 and Nfe2l2 for laser-induced lesions) was upregulated to compensate for oxidative stress. These data indicate that systemic infections may contribute to increased oxidative stress in the retina during AMD pathology.

Overall, these studies indicate that there are many shared gene activation pathways during systemic infection and geographic atrophy and identify several ways in which systemic infection could contribute to late-stage AMD pathology. Examining the effects of combining these models and using pharmacological interventions and/or knockout mice would give further insights into

the relative contribution of these inflammatory pathways to retinal degeneration. Additionally, it would be interesting to investigate gene expression in the early AMD model of inflammatory immune complex deposits in order to see how these pathways may overlap with the systemic infection and retinal atrophy models.

8.6 Summary

While a role for local inflammation in AMD is well established, the effect of the systemic immune system on AMD pathology is less clear. In this AMD patient cohort, increased local cytokine levels were identified in AMD patients. There was little evidence to support a role for priming of the systemic immune system in AMD patients leading to an exaggerated response to infections, but this does not preclude priming at a local level. I demonstrated that systemic bacterial infection can induce retinal inflammation, oxidative stress and chronic microglial activation, in line with previous findings in viral and fungal infection. There are functional consequences for such microglial activation, in terms of tolerance to further systemic inflammation and also for recruitment of cells to the outer retina in response to local inflammation. These interactions are particularly relevant in AMD pathology as mechanisms which could be targeted to reduce the effects of systemic infection on retinal inflammation. However, these studies don't reveal how systemic and retinal inflammation contribute to photoreceptor loss and therefore I developed a model of laser-induced outer retinal atrophy that mimics the inflammatory and progressive degenerative aspects of GA pathology. Further characterisation of this model combined with systemic infection will hopefully lead to a greater understanding of how inflammation and degeneration are linked and identify possible targets for therapeutic intervention.

Appendices

Appendix A: Chapter 3 statistics

RM Two-way ANOVA	**Figure 3.1a**	**Figure 3.1b**
Interaction	$F_{28,476}$=3.327, p<0.0001	$F_{28,476}$=3.328, p<0.0001
Time	$F_{28,476}$=33.56, p<0.0001	$F_{28,476}$=3.328, p<0.0001
Saline vs Salmonella	$F_{1,17}$=35.44, p<0.0001	$F_{1,17}$=35.44, p<0.0001
Subjects (matching)	$F_{17,476}$=32.14, p<0.0001	$F_{17,476}$=32.16, p<0.0001

Unpaired 2-tailed T-test	**Figure 3.1c**
Saline vs Salmonella	t_{18}=1.421, p=0.1725

RM Two-way ANOVA	**Figure 3.1d**
Interaction	$F_{1,41}$=1.79, p=0.1882
1 vs 4 weeks	$F_{1,41}$=1.696, p=0.2000
Saline vs Salmonella	$F_{1,41}$=289.7, p<0.0001

Figure 3.2			
Two-way ANOVA	Interaction	1 vs 4 weeks	Saline vs Salmonella
IFNγ	$F_{1,18}$=73.44, p<0.0001	$F_{1,18}$=127.9, p<0.0001	$F_{1,18}$=796.1, p<0.0001
IL-1β	$F_{1,18}$=65.59, p<0.0001	$F_{1,18}$=76.33, p<0.0001	$F_{1,18}$=145.1, p<0.0001
IL-2	$F_{1,18}$=51.14, p<0.0001	$F_{1,18}$=53.52, p<0.0001	$F_{1,18}$=105.3, p<0.0001
IL-4	$F_{1,18}$=32.67, p<0.0001	$F_{1,18}$=36.52, p<0.0001	$F_{1,18}$=42.20, p<0.0001
IL-5	$F_{1,18}$=22.63, p=0.0002	$F_{1,18}$=30.66, p<0.0001	$F_{1,18}$=125.2, p<0.0001
IL-6	$F_{1,18}$=165.2 p<0.0001	$F_{1,18}$=174.9, p<0.0001	$F_{1,18}$=626.3, p<0.0001
IL-10	$F_{1,18}$=43.53, p<0.0001	$F_{1,18}$=62.57, p<0.0001	$F_{1,18}$=416.5, p<0.0001
IL-12	$F_{1,18}$=51.82, p<0.0001	$F_{1,18}$=57.88, p<0.0001	$F_{1,18}$=69.82, p<0.0001
mKC	$F_{1,18}$=6.634, p=0.0190	$F_{1,18}$=2.115, p=0.1631	$F_{1,18}$=25.34, p<0.0001
TNFα	$F_{1,18}$=36.77, p<0.0001	$F_{1,18}$=52.41, p<0.0001	$F_{1,18}$=399.5, p<0.0001

Figure 3.3			
Two-way ANOVA	Interaction	1 vs 4 weeks	Saline vs Salmonella
IFNγ	$F_{1,28}$=15.98, p=0.0004	$F_{1,28}$=46.08, p<0.0001	$F_{1,28}$=172.5, p<0.0001
IL-1β	$F_{1,28}$=6.051, p=0.0203	$F_{1,28}$=4.198, p=0.0499	$F_{1,28}$=7.419, p=0.0110
IL-2	$F_{1,28}$=0.286, p=0.5969	$F_{1,28}$=0.228, p=0.6392	$F_{1,28}$=5.213, p=0.0302
IL-4	$F_{1,28}$=0.067, p=0.7975	$F_{1,28}$=0.017, p=0.8961	$F_{1,28}$=0.518, p=0.4778
IL-5	$F_{1,28}$=0.419, p=0.5229	$F_{1,28}$=0.076, p=0.7843	$F_{1,28}$=0.222, p=0.6412
IL-6	$F_{1,28}$=26.85, p<0.0001	$F_{1,28}$=36.36, p<0.0001	$F_{1,28}$=61.90, p<0.0001
IL-10	$F_{1,28}$=2.004, p=0.1679	$F_{1,28}$=1.754 p=0.1961	$F_{1,28}$=0.252, p=0.6194
IL-12	$F_{1,28}$=3.030, p=0.0927	$F_{1,28}$=0.023, p=0.8795	$F_{1,28}$=0.312, p=0.5811
mKC	$F_{1,28}$=3.714, p=0.0642	$F_{1,28}$=23.68, p<0.0001	$F_{1,28}$=52.99, p<0.0001
TNFα	$F_{1,28}$=1.521, p=0.2278	$F_{1,28}$=6.684, p=0.0152	$F_{1,28}$=17.49, p=0.0003

Figure 3.4	
One-way ANOVA	**Summary**
Fcgr1	$F_{2,14}$=47.95, p<0.0001
Gfap	$F_{2,14}$=5.211, p=0.0203
Ccl2	$F_{2,14}$=10.22, p=0.0018
Tnfa	$F_{2,13}$=4.132, p=0.0408
Il1b	$F_{2,14}$=6.385, p=0.0107
IL18	$F_{2,14}$=0.636, p=0.5438
Nlrp3	$F_{2,14}$=8.313, p=0.0042
Casp1	$F_{2,14}$=31.38, p<0.0001

Figure 3.5	
One-way ANOVA	**Summary**
nNOS	$F_{2,14}$=0.158, p=0.8555
iNOS	$F_{2,14}$=3.217, p=0.0709
eNOS	$F_{2,14}$=3.496, p=0.0587
NOX2	$F_{2,14}$=12.23, p=0.0008
Hmox-1	$F_{2,14}$=0.333, p=0.7223
Cox2	$F_{2,14}$=45.10, p<0.0001
C3	$F_{2,14}$=6.583, p=0.0097
Vegfa	$F_{2,14}$=0.540, p=0.5944

Two-way ANOVA	Figure 3.6b	Figure 3.6c
Interaction	$F_{1,25}$=0.296, p=0.5912	$F_{1,25}$=0.893, p=0.3538
1 vs 4 weeks	$F_{1,25}$=1.508, p=0.2308	$F_{1,25}$=0.645, p=0.4297
Saline vs Salmonella	$F_{1,25}$=15.20, p=0.0006	$F_{1,25}$=28.79, p<0.0001

Two-way ANOVA	Figure 3.7b	Figure 3.7c
Interaction	$F_{1,25}$=0.011, p=0.9183	$F_{1,25}$=8.559, p=0.0072
1 vs 4 weeks	$F_{1,25}$=0.084, p=0.7744	$F_{1,25}$=0.891, p=03543
Saline vs Salmonella	$F_{1,25}$=342.9, p<0.0001	$F_{1,25}$=76.38, p<0.0001

One-way ANOVA	% Positive	MFI
Figure 3.8b	$F_{2,11}$=0.824, p=0.4638	$F_{2,11}$=0.567, p=0.5827
Figure 3.8c	$F_{2,11}$=2.643, p=0.1155	$F_{2,11}$=16.27, p=0.0005
Figure 3.8d	N/A	$F_{2,11}$=18.41, p=0.0003
Figure 3.8e	N/A	$F_{2,11}$=3.416, p=0.0701
Figure 3.9b	$F_{2,11}$=29.63, p<0.0001	$F_{2,11}$=61.67, p<0.0001

RM Two-way ANOVA	Figure 3.10
Interaction	$F_{9,126}$=1.844, p=0.0665
Time	$F_{9,126}$=216.0, p<0.0001
Saline vs Salmonella	$F_{1,14}$=7.902, p=0.0139
Subjects (matching)	$F_{1,14}$=6.577, p<0.0001

Unpaired two-tailed T test	Figure 3.11	Figure 3.12
IFNγ	t_8=5.738, p=0.0004	t_{11}=1.518, p=0.1573
IL-1β	t_8=0.264, p=0.7987	t_{11}=0.242, p=0.8129
IL-2	t_8=0.136, p=0.8954	t_{11}=0.066, p=0.9483
IL-4	t_8=0.267, p=0.7962	t_{11}=0.789, p=0.4471
IL-5	t_8=0.438, p=0.6730	t_{11}=0.174, p=0.8649
IL-6	t_8=0.793, p=0.4506	t_{11}=0.391, p=0.7030
IL-10	t_8=2.857, p=0.0212	t_{11}=1.104, p=0.2933
IL-12	t_8=0.489, p=0.6381	t_{11}=0.343, p=0.7381
mKC	t_8=1.633, p=0.1410	t_{11}=1.061, p=0.3115
TNFα	t_8=2.165, p=0.0623	t_{11}=1.202, p=0.2545

Two-way ANOVA	Figure 3.13a	Figure 3.13b
Interaction	$F_{1,27}$=0.162, p=0.6905	$F_{1,27}$<0.001 p=0.9955
8 vs 24 weeks	$F_{1,27}$=4.738, p=0.0384	$F_{1,27}$=6.216 p=0.0191
Saline vs Salmonella	$F_{1,27}$=1,996 p=0.1692	$F_{1,27}$=0.202 p=0.6566

Appendix A

Two-way ANOVA	Figure 3.14a	Figure 3.14b
Interaction	$F_{1,27}$=5.453 p=0.0272	$F_{1,28}$=0.982 p=0.3302
8 vs 24 weeks	$F_{1,27}$=0.996 p=0.3272	$F_{1,28}$=7.962 p=0.0087
Saline vs Salmonella	$F_{1,27}$=137.8 p<0.0001	$F_{1,28}$=13.57 p=0.0010

RM Two-way ANOVA	Figure 3.15a	Figure 3.15b	Figure 3.15c
Interaction	$F_{11,154}$=3.259, p=0.0005	$F_{11,132}$=2.404, p=0.0094	$F_{11,132}$=0.924, p=0.5194
Time	$F_{11,154}$=17.88, p<0.0001	$F_{11,132}$= 4.333, p<0.0001	$F_{11,132}$=4.971, p<0.0001
Saline vs Salmonella	$F_{1,14}$=22.47, p=0.0003	$F_{1,12}$=23.32, p=0.0004	$F_{1,12}$=2.734, p=0.1242
Subjects (matching)	$F_{14,154}$=12.17, p<0.0001	$F_{12,132}$=9.691, p=0.0003	$F_{12,132}$=11.81, p<0.0001

Figure 3.16			
Two-way ANOVA	Interaction	Young vs middle-aged	Saline vs Salmonella
IFNγ	$F_{1,26}$=0.918, p=0.3467	$F_{1,26}$=2.859, p=0.1028	$F_{1,26}$=260.1, p<0.0001
IL-1β	$F_{1,26}$=1.462, p=0.2375	$F_{1,26}$=1.533, p=0.2268	$F_{1,26}$=10.63, p=0.0031
IL-2	$F_{1,26}$=0.049, p=0.8258	$F_{1,26}$=2.096, p=0.1597	$F_{1,26}$=65.99, p<0.0001
IL-4	$F_{1,26}$<0.001, p=0.9952	$F_{1,26}$=1.509, p=0.2304	$F_{1,26}$=2.713, p=0.1115
IL-5	$F_{1,26}$=2.049, p=0.1642	$F_{1,26}$=0.006, p=0.9392	$F_{1,26}$=9.176, p=0.0055
IL-6	$F_{1,26}$<0.001, p=0.9788	$F_{1,26}$=3.232, p=0.0839	$F_{1,26}$=64.31, p<0.0001
IL-10	$F_{1,26}$=0.663, p=0.4229	$F_{1,26}$=5.226, p=0.0306	$F_{1,26}$=43.22, p<0.0001
IL-12	$F_{1,26}$=4.306, p=0.0480	$F_{1,26}$=1.568, p=0.2217	$F_{1,26}$=78.19, p<0.0001
mKC	$F_{1,26}$=0.734, p=0.3995	$F_{1,26}$=4.297, p=0.0482	$F_{1,26}$=7.963, p=0.0090
TNFα	$F_{1,26}$=0.200, p=0.6585	$F_{1,26}$=0.772, p=0.3876	$F_{1,26}$=139.5, p<0.0001

Figure 3.17			
Two-way ANOVA	Interaction	Young vs middle-aged	Saline vs Salmonella
IFNγ	$F_{1,25}$=0.172, p=0.6818	$F_{1,25}$<0.001, p=0.9881	$F_{1,25}$=59.19, p<0.0001
IL-1β	$F_{1,25}$=1.450, p=0.2397	$F_{1,25}$=4.276, p=0.0492	$F_{1,25}$=10.30, p=0.0036
IL-2	$F_{1,25}$=1.200, p=0.2837	$F_{1,25}$=1.959, p=0.1739	$F_{1,25}$=1.092, p=0.3061
IL-4	$F_{1,25}$=1.107, p=0.3028	$F_{1,25}$=0.187, p=0.6684	$F_{1,25}$=0.251, p=0.6208
IL-5	$F_{1,25}$=1.601, p=0.2174	$F_{1,25}$<0.001, p=0.9873	$F_{1,25}$=3.188, p=0.0863
IL-6	$F_{1,25}$=0.014, p=0.9062	$F_{1,25}$=0.849, p=0.3656	$F_{1,25}$=12.74, p=0.0015
IL-10	$F_{1,25}$=1.915, p=0.1786	$F_{1,25}$=0.303, p=0.5870	$F_{1,25}$=1.200, p=0.2837
IL-12	$F_{1,25}$=1.464, p=0.2376	$F_{1,25}$=0.670, p=0.4209	$F_{1,25}$=0.500, p=0.4860
mKC	$F_{1,25}$=0.002, p=0.9684	$F_{1,25}$=1.942, p=0.1757	$F_{1,25}$=12.82, p=0.0014
TNFα	$F_{1,25}$=0.019, p=0.8905	$F_{1,25}$=0.023, p=0.8799	$F_{1,25}$=8.860, p=0.0064

Appendix B: Chapter 4 statistics

Unpaired two-tailed T-test	Figure 4.1b
1 week vs 4 weeks	t_{11}=2.778, p=0.0180

RM Two-way ANOVA	Figure 4.1a	Figure 4.1b	Figure 4.1c
Interaction	$F_{10,410}$=27.74, p<0.0001	$F_{10,410}$=13.03, p<0.0001	$F_{10,480}$=8.280, p<0.0001
Time	$F_{10,410}$=254.6, p<0.0001	$F_{10,410}$=113.5, p<0.0001	$F_{10,480}$=61.42, p<0.0001
Saline vs Salmonella	$F_{1,41}$=33.31, p<0.0001	$F_{1,41}$=55.43, p<0.0001	$F_{1,48}$=63.48, p<0.0001
Subjects (matching)	$F_{41,410}$=11.63, p<0.0001	$F_{41,410}$=10.17, p<0.0001	$F_{48,480}$=5.801, p<0.0001

Two-way ANOVA	Figure 4.2a	Figure 4.2b
Interaction	$F_{1,19}$=0.313, p=0.5826	$F_{1,20}$=19.50, p=0.0003
Saline vs Salmonella	$F_{1,19}$=90.13, p<0.0001	$F_{1,20}$=262.0, p<0.0001
C57BL/6 vs BALB/c	$F_{1,19}$=0.196, p=0.6633	$F_{1,20}$=15.27, p=0.0009

Two-way ANOVA	Figure 4.3a	Figure 4.3b
Interaction	$F_{1,15}$=0.543, p=0.4724	$F_{1,15}$=4.878, p=0.0432
Saline vs Salmonella	$F_{1,15}$=4.720, p=0.0463	$F_{1,15}$=22.62, p=0.0003
C57BL/6 vs BALB/c	$F_{1,15}$=128.1, p<0.0001	$F_{1,15}$=164.8, p<0.0001

Figure 4.4			
Two-way ANOVA	Interaction	Saline vs Salmonella	Saline vs LPS
C57BL/6 IFNγ	$F_{1,15}$=0.291, p=0.5978	$F_{1,15}$=179.7, p<0.0001	$F_{1,15}$=39.02, p<0.0001
C57BL/6 IL-1β	$F_{1,15}$=0.165, p=0.6906	$F_{1,15}$=36.51, p<0.0001	$F_{1,15}$=50.26, p<0.0001
C57BL/6 IL-6	$F_{1,15}$=1.335, p=0.2660	$F_{1,15}$=4.678, p=0.0471	$F_{1,15}$=48.61, p<0.0001
C57BL/6 IL-12	$F_{1,15}$=6.317, p=0.0239	$F_{1,15}$=9.089, p=0.0087	$F_{1,15}$=16.24, p=0.0011
C57BL/6 mKC	$F_{1,15}$=0.769, p=0.3945	$F_{1,15}$=0.043, p=0.8391	$F_{1,15}$=30.83, p<0.0001
C57BL/6 TNFα	$F_{1,15}$=2.077, p=0.1701	$F_{1,15}$=8.705, p=0.0099	$F_{1,15}$=3.249, p=0.0916
BALB/c IFNγ	$F_{1,12}$=0.176, p=0.6824	$F_{1,12}$=47.63, p<0.0001	$F_{1,12}$=8.971, p=0.0112
BALB/c IL-1β	$F_{1,12}$=1.132, p=0.3083	$F_{1,12}$=20.06, p=0.0008	$F_{1,12}$=37.47, p<0.0001
BALB/c IL-6	$F_{1,12}$=7.774, p=0.0164	$F_{1,12}$=4.688, p=0.0512	$F_{1,12}$=16.93, p=0.0014
BALB/c IL-12	$F_{1,12}$=1.240, p=0.2873	$F_{1,12}$=13.30, p=0.0033	$F_{1,12}$=7.306, p=0.0192
BALB/c mKC	$F_{1,12}$=29.15, p=0.0002	$F_{1,12}$=69.82, p<0.0001	$F_{1,12}$=69.24, p<0.0001
BALB/c TNFα	$F_{1,12}$=7.542, p=0.0177	$F_{1,12}$=45.75, p<0.0001	$F_{1,12}$=101.2, p<0.0001

Figure 4.5			
Two-way ANOVA	Interaction	Saline vs Salmonella	Saline vs LPS
C57BL/6 IFNγ	$F_{1,20}$=0.138, p=0.7142	$F_{1,20}$=57.09, p<0.0001	$F_{1,20}$=1.105, p=0.3057
BALB/c IFNγ	$F_{1,12}$=2.650, p=0.1295	$F_{1,12}$=3.662, p=0.0798	$F_{1,12}$=7.773, p=0.0164
C57BL/6 IL-1β	$F_{1,20}$=1.160, p=0.2943	$F_{1,20}$=4.966, p=0.0375	$F_{1,20}$=12.39, p=0.0022
BALB/c IL-1β	$F_{1,12}$=11.72, p=0.0051	$F_{1,12}$=13.12, p=0.0035	$F_{1,12}$=25.03, p=0.0003
C57BL/6 IL-6	$F_{1,20}$=2.054, p=0.1673	$F_{1,20}$=1.664, p=0.2118	$F_{1,20}$=9.560, p=0.0057
BALB/c IL-6	$F_{1,12}$=0.004, p=0.9520	$F_{1,12}$=0.103, p=0.7540	$F_{1,12}$=1.211, p=0.2928
C57BL/6 IL-12	$F_{1,20}$=0.133, p=0.7194	$F_{1,20}$=0.039, p=0.8464	$F_{1,20}$=1.800, p=0.1948
BALB/c IL-12	$F_{1,12}$=2.310, p=0.1544	$F_{1,12}$=1.611, p=0.2284	$F_{1,12}$=3.560, p=0.0836
C57BL/6 mKC	$F_{1,20}$=11.50, p=0.0029	$F_{1,20}$=0.004, p=0.9517	$F_{1,20}$=52.99, p<0.0001
BALB/c mKC	$F_{1,12}$=5.081, p=0.0437	$F_{1,12}$=5.797, p=0.0331	$F_{1,12}$=49.12, p<0.0001
C57BL/6 TNFα	$F_{1,20}$=0.869, p=0.3623	$F_{1,20}$=1.819, p=0.1925	$F_{1,20}$=9.960, p=0.0050
BALB/c TNFα	$F_{1,12}$=0.006, p=0.9386	$F_{1,12}$=1.123, p=0.3102	$F_{1,12}$=12.61, p=0.0040

Figure 4.6a		
Two-way ANOVA	**C57BL/6**	**BALB/c**
Interaction	$F_{1,14}$=0.310, p=0.5866	$F_{1,15}$=2.040, p=0.1737
Saline vs Salmonella	$F_{1,14}$=682.5, p<0.0001	$F_{1,15}$=119.8, p<0.0001
Saline vs LPS	$F_{1,14}$=6.597, p=0.0223	$F_{1,15}$=5.663, p=0.0310

Two-way ANOVA	**Figure 4.6b**
Interaction	$F_{1,14}$=1.435, p=0.2508
Saline vs Salmonella	$F_{1,14}$=178.6, p<0.0001
Saline vs LPS	$F_{1,14}$=0.131, p=0.7225

Figure 4.7a		
Two-way ANOVA	**C57BL/6**	**BALB/c**
Interaction	$F_{1,13}$=1.789, p=0.2040	$F_{1,15}$=13.82, p=0.0021
Saline vs Salmonella	$F_{1,13}$=37.87, p<0.0001	$F_{1,15}$=0.093, p=0.7641
Saline vs LPS	$F_{1,13}$=1.108, p=0.3117	$F_{1,15}$=36.89, p<0.0001

Figure 4.7b		
Two-way ANOVA	**C57BL/6**	**BALB/c**
Interaction	$F_{1,14}$=2.170, p=0.1629	$F_{1,15}$=0.892, p=0.3600
Saline vs Salmonella	$F_{1,14}$=14.88, p=0.0017	$F_{1,15}$=0.092, p=0.7656
Saline vs LPS	$F_{1,14}$=0.107, p=0.7490	$F_{1,15}$=7.986, p=0.0128

Figure 4.8a		
Two-way ANOVA	**C57BL/6**	**BALB/c**
Interaction	$F_{1,14}$=0.228, p=0.6443	$F_{1,15}$=1.272, p=0.2772
Saline vs Salmonella	$F_{1,14}$=15.94, p=0.0013	$F_{1,15}$=0.580, p=0.4582
Saline vs LPS	$F_{1,14}$=0.177, p=0.6806	$F_{1,15}$=4.754, p=0.0456
Figure 4.8b		
Two-way ANOVA	**C57BL/6**	**BALB/c**
Interaction	$F_{1,14}$=1.293, p=0.2746	$F_{1,15}$=0.222, p=0.6445
Saline vs Salmonella	$F_{1,14}$=6.162, p=0.0264	$F_{1,15}$=0.230, p=0.6381
Saline vs LPS	$F_{1,14}$=1.198, p=0.2922	$F_{1,15}$=2.442, p=0.1390

Two-way ANOVA	**Figure 4.9**
Interaction	$F_{1,12}$=0.305, p=0.5912
Saline vs Salmonella	$F_{1,12}$=13.45, p=0.0032
Saline vs LPS	$F_{1,12}$=4.798, p=0.0490

Figure 4.10		
Two-way ANOVA	**C57BL/6**	**BALB/c**
Interaction	$F_{1,14}$=2.437, p=0.1408	$F_{1,15}$=0.643, p=0.4361
Saline vs Salmonella	$F_{1,14}$=48.03, p<0.0001	$F_{1,15}$=0.383, p=0.5458
Saline vs LPS	$F_{1,14}$=3.906, p=0.0682	$F_{1,15}$=0.059, p=0.8111

Appendix C: Chapter 5 statistics

Unpaired two-tailed T-test	Figure 5.1b
1 week vs 4 weeks	t_{11}=3.688, p=0.0036

Two-way ANOVA	Figure 5.2a	Figure 5.2b
Interaction	$F_{1,24}$=1.071, p=0.3111	$F_{1,24}$=2.749, p=0.1103
Unimmunised vs Immunised	$F_{1,24}$=6.257, p=0.0196	$F_{1,24}$=10.57, p=0.0034
1 vs 4 weeks	$F_{1,24}$=4.273, p=0.0497	$F_{1,24}$=1.519, p=0.2297

Two-way ANOVA	Figure 5.2c
Interaction	$F_{1,22}$=0.374, p=0.5469
Unimmunised vs Immunised	$F_{1,22}$=23.56, p<0.0001
1 vs 4 weeks	$F_{1,22}$=12.71, p=0.0017

Two-way ANOVA	Figure 5.3	Figure 5.4
Interaction	$F_{1,24}$<0.001, p=0.9760	$F_{1,24}$=0.023, p=0.8816
Unimmunised vs Immunised	$F_{1,24}$=4.545, p=0.0435	$F_{1,24}$=11.12, p=0.0028
1 vs 4 weeks	$F_{1,24}$=0.338, p=0.5667	$F_{1,24}$=0.917, p=0.3477

Two-way ANOVA	Figure 5.6a	Figure 5.6b
Interaction	$F_{1,25}$=6.122, p=0.0205	$F_{1,25}$<0.001, p=0.9240
Unimmunised vs Immunised	$F_{1,25}$=6.951, p=0.0142	$F_{1,25}$=0.203, p=0.6559
1 vs 4 weeks	$F_{1,25}$=2.483, p=0.1276	$F_{1,25}$=0.727, p=0.4021

Two-way ANOVA	Figure 5.7b	Figure 5.7c
Interaction	$F_{1,23}$=0.181, p=0.6745	$F_{1,23}$=1.052, p=0.3158
Unimmunised vs Immunised	$F_{1,23}$=0.075, p=0.7868	$F_{1,23}$=30.34, p<0.0001
Saline vs Salmonella	$F_{1,23}$=0.009 p=0.9263	$F_{1,23}$=1.479, p=0.2363

Two-way ANOVA	Figure 5.7d
Interaction	$F_{1,23}$<0.001, p=0.9841
Unimmunised vs Immunised	$F_{1,23}$=10.36, p=0.0038
Saline vs Salmonella	$F_{1,23}$=11.88, p=0.0022

Two-way ANOVA	Figure 5.7f	Figure 5.7g
Interaction	$F_{1,27}$=0.087, p=0.7709	$F_{1,27}$=0.074, p=0.7874
Unimmunised vs Immunised	$F_{1,27}$=1.432, p=0.2418	$F_{1,27}$=0.646, p=0.4285
Saline vs Salmonella	$F_{1,27}$=1.851, p=0.1849	$F_{1,27}$=0.015, p=0.9033

Two-way ANOVA	Figure 5.7h
Interaction	$F_{1,27}$=0.115, p=0.7375
Unimmunised vs Immunised	$F_{1,27}$=4.385, p=0.0458
Saline vs Salmonella	$F_{1,27}$=9.707, p=0.0043

Two-way ANOVA	Figure 5.8b	Figure 5.8c
Interaction	$F_{1,23}$=0.140, p=0.7120	$F_{1,23}$=1.197, p=0.2852
Unimmunised vs Immunised	$F_{1,23}$=2.902, p=0.1019	$F_{1,23}$=27.47, p<0.0001
Saline vs Salmonella	$F_{1,23}$=0.368, p=0.5499	$F_{1,23}$=0.008, p=0.9290

Two-way ANOVA	Figure 5.8d
Interaction	$F_{1,23}$=0.074, p=0.7874
Unimmunised vs Immunised	$F_{1,23}$=6.880, p=0.0152
Saline vs Salmonella	$F_{1,23}$=6.993, p=0.0145

Two-way ANOVA	Figure 5.8f	Figure 5.8g
Interaction	$F_{1,27}$=0.522, p=0.4763	$F_{1,27}$<0.001, p=0.9790
Unimmunised vs Immunised	$F_{1,27}$=0.408, p=0.5285	$F_{1,27}$=2.329, p=0.1386
Saline vs Salmonella	$F_{1,27}$=0.638, p=0.4314	$F_{1,27}$=0.131, p=0.7198

Two-way ANOVA	Figure 5.8h
Interaction	$F_{1,27}$=0.342, p=0.5633
Unimmunised vs Immunised	$F_{1,27}$=2.926, p=0.0986
Saline vs Salmonella	$F_{1,27}$=7.018, p=0.0133

Two-way ANOVA	Figure 5.9b	Figure 5.9d
Interaction	$F_{1,23}$=2.986, p=0.0974	$F_{1,27}$=1.468, p=0.2362
Unimmunised vs Immunised	$F_{1,23}$=5.654, p=0.0261	$F_{1,27}$=7.684, p=0.0100
Saline vs Salmonella	$F_{1,23}$=0.567, p=0.4592	$F_{1,27}$=4.797, p=0.0373

Two-way ANOVA	Figure 5.10b	Figure 5.10c
Interaction	$F_{1,23}$=4.111, p=0.0543	$F_{1,23}$=3.384, p=0.0788
Unimmunised vs Immunised	$F_{1,23}$=18.64, p=0.0003	$F_{1,23}$=22.59, p<0.0001
Saline vs Salmonella	$F_{1,23}$=0.519, p=0.4787	$F_{1,23}$=1.591, p=0.2199

Two-way ANOVA	Figure 5.10e	Figure 5.10f
Interaction	$F_{1,27}$=0.730, p=0.4003	$F_{1,27}$=0.865, p=0.3605
Unimmunised vs Immunised	$F_{1,27}$=1.512, p=0.2295	$F_{1,27}$=0.363, p=0.5517
Saline vs Salmonella	$F_{1,27}$=1.262, p=0.2712	$F_{1,27}$=0.147, p=0.7045

Two-way ANOVA	Figure 5.11b	Figure 5.11d
Interaction	$F_{1,23}$=0.744, p=0.3972	$F_{1,25}$=2.729, p=0.1111
Unimmunised vs Immunised	$F_{1,23}$=5.310, p=0.0306	$F_{1,25}$=0.905, p=0.3506
Saline vs Salmonella	$F_{1,23}$=0.912, p=0.3496	$F_{1,25}$=4.606, p=0.0418

Two-way ANOVA	Figure 5.12b	Figure 5.12d
Interaction	$F_{1,23}$=0.197, p=0.6617	$F_{1,24}$=2.637, p=0.1175
Unimmunised vs Immunised	$F_{1,23}$=7.828, p=0.0102	$F_{1,24}$=7.390, p=0.0120
Saline vs Salmonella	$F_{1,23}$=1.994, p=0.1713	$F_{1,24}$=26.89, p<0.0001

Two-way ANOVA	Figure 5.13b	Figure 5.13d
Interaction	$F_{1,23}$=2.059, p=0.1647	$F_{1,26}$=0.349, p=0.5599
Unimmunised vs Immunised	$F_{1,23}$=54.97, p<0.0001	$F_{1,26}$=15.72, p=0.0005
Saline vs Salmonella	$F_{1,23}$=2.059, p=0.1647	$F_{1,26}$=0.349, p=0.5599

Unpaired two-tailed T test	Figure 5.13b	Figure 5.13d
Immunised: Saline vs Salmonella	t_{12}=1.496, p=0.1605	t_{12}=0.392, p=0.5946

Appendix D: Additional images of laser-induced lesions

D1: Fundoscopy images of 7 mice with laser induced atrophic lesions at 1, 2 and 4 weeks post laser (each row represents the same mouse).

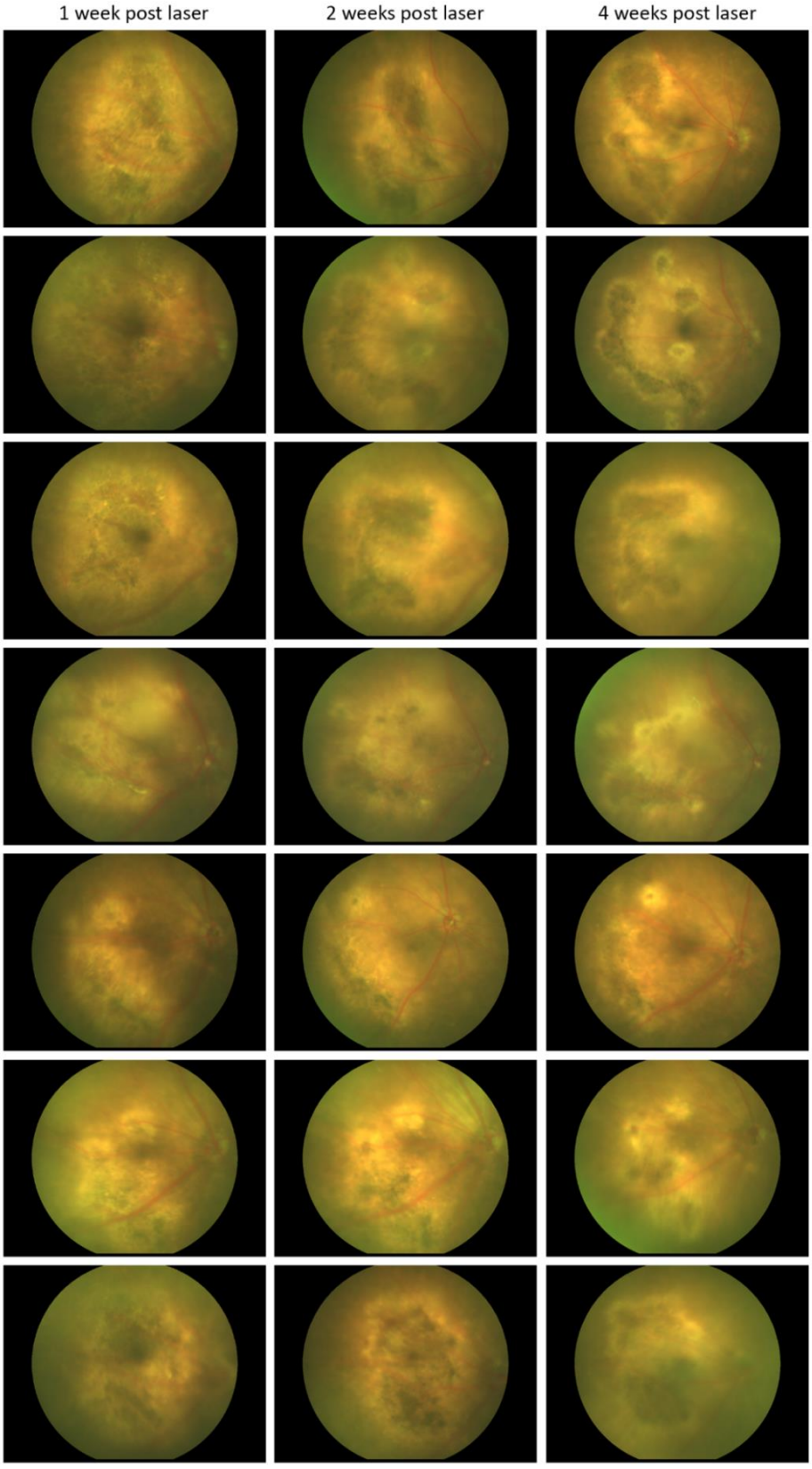

D2: OCT images of 7 mice with laser induced atrophic lesions at 1, 2, 4 and 8 weeks post laser (each row represents the same mouse).

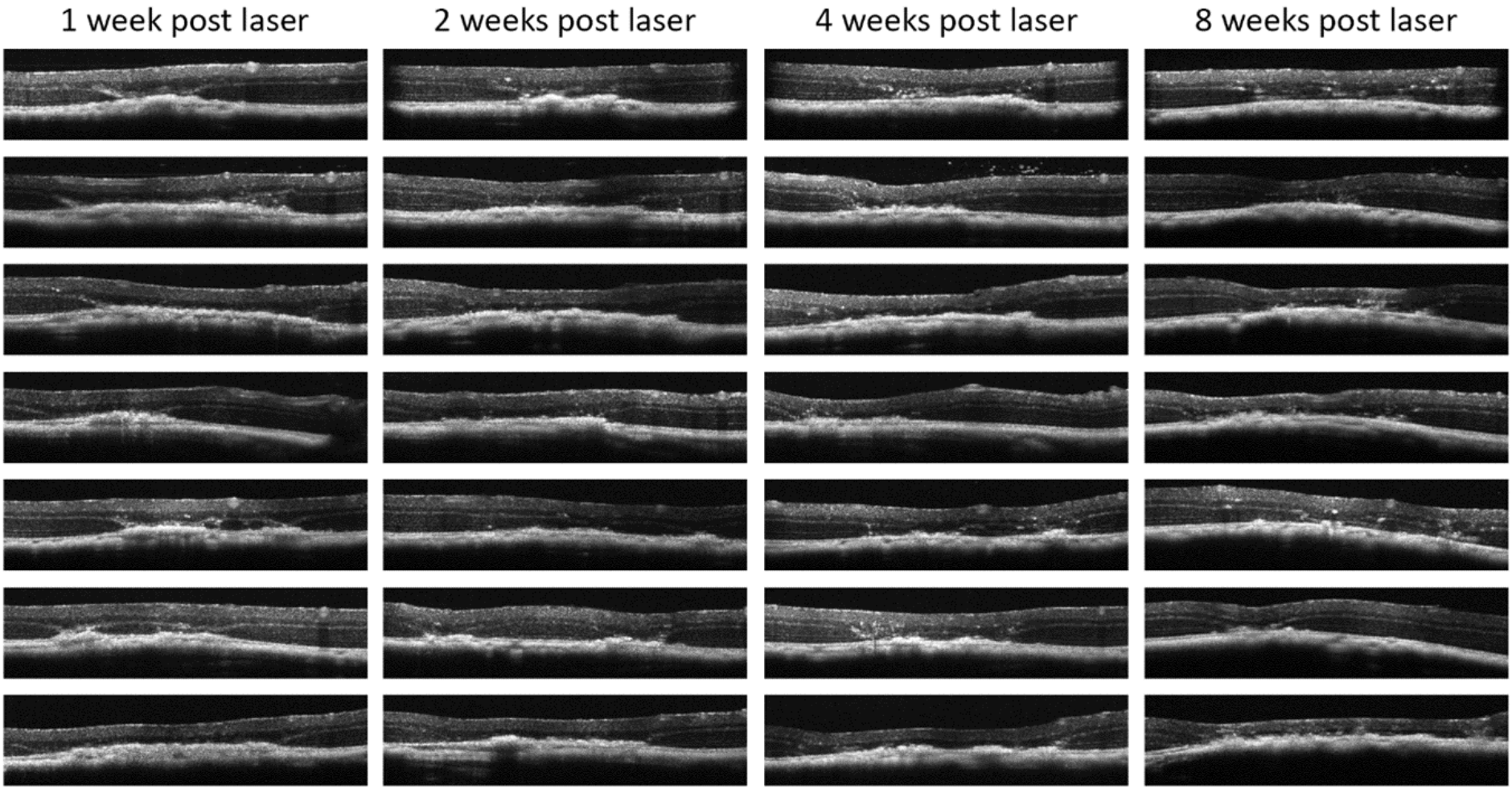

D3: Gene expression in the retina in young and middle-aged mice at 1 month post laser.

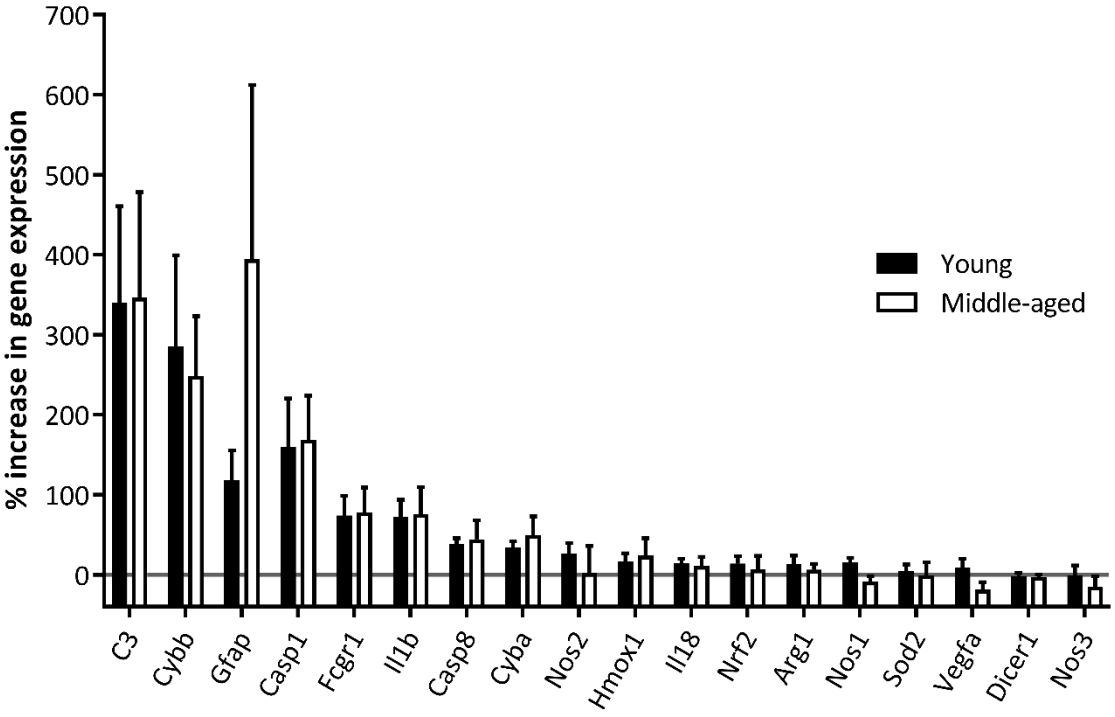

mRNA levels of young (5 months old, n=8) and middle-aged (11-13 months old, n=3) mice were measured using SYBR Green qPCR. Values are displayed as the average increase in gene expression compared to the control eye for each mouse. Data was analysed using multiple paired t-tests followed by Holm-Sidak multiple comparisons correction. GFAP was significantly increased and Nos1 significantly decreased in middle aged mice compared to young mice before multiple comparisons correction, but this significance was lost after correction. Graphs are presented as mean±SEM.

Appendix E: Chapter 7 statistics

Aqueous Cytokines	Control	AMD	p-value	Test
Number of Participants	15	19	-	-
Mean age in years (range)	77.6 (50-94)	81.4 (57-94)	0.1487	Mann-Whitney
Female sex (%)	46.7	63.2	0.4888	Fisher
Former/current smoker (%)	63.2	57.1	>0.9999	Fisher

Serum Cytokines	Control	AMD	p-value	Test
Number of Participants	16	17	-	-
Mean age in years (range)	75.8 (48-94)	81.1 (57-94)	0.1154	Mann-Whitney
Female sex (%)	43.8	64.7	0.3028	Fisher
Former/current smoker (%)	56.3	58.8	>0.9999	Fisher

Restimulated cytokines	Control	AMD	p-value	Test
Number of Participants	16	15	-	-
Mean age in years (range)	78.3 (48-94)	79.6 (57-89)	0.5776	Mann-Whitney
Female sex (%)	37.5	60.0	0.2890	Fisher
Former/current smoker (%)	56.3	60.0	>0.9999	Fisher

Flow cytometry	Control	AMD	p-value	Test
Number of Participants	8	8	-	-
Mean age in years (range)	82.3 (68-94)	84.1 (75-89)	0.4205	Mann-Whitney
Female sex (%)	50.0	62.5	>0.9999	Fisher
Former/current smoker (%)	62.5	62.5	>0.9999	Fisher

Figure 7.1a	**Test Statistics**	**Test Used**
Serum IFNγ	U=121, p=0.3030	One-tailed unpaired Mann-Whitney U test
Serum IL-6	U=96, p=0.0784	One-tailed unpaired Mann-Whitney U test
Serum IL-8	t_{31}=1.171, p=0.1253	One-tailed unpaired T-test
Serum IL-13	U=121, p=0.2998	One-tailed unpaired Mann-Whitney U test
Serum TNFα	U=117, p=0.2551	One-tailed unpaired Mann-Whitney U test

	Test Statistics	**Test Used**
Figure 7.1b	χ^2=99.76, p<0.0001	Friedman test

Figure 7.1c	Test Statistics	Test Used
Aqueous IL-6	U=138, p=0.4456	One-tailed unpaired Mann-Whitney U test
Aqueous IL-8	U=93, p=0.0447	One-tailed unpaired Mann-Whitney U test
Aqueous IL-13	U=119, p=0.2123	One-tailed unpaired Mann-Whitney U test

	Test Statistics	Test Used
Figure 7.1d	χ^2=1.235, p=0.5392	Friedman test

Figure 7.2	Test Statistics	Test Used
Serum IFNγ	χ^2=3.575, p=0.1673	Kruskal-Wallis Test
Serum IL-6	χ^2=2.245, p=0.3255	Kruskal-Wallis Test
Serum IL-8	$F_{2,30}$=0.768, p=0.4728	One-way ANOVA
Serum IL-13	χ^2=0.757, p=0.6849	Kruskal-Wallis Test
Serum TNFα	χ^2=1.484, p=0.4760	Kruskal-Wallis Test
Aqueous IL-6	χ^2=0.057, p=0.9717	Kruskal-Wallis Test
Aqueous IL-8	χ^2=3.565, p=0.1682	Kruskal-Wallis Test
Aqueous IL-13	χ^2=2.328, p=0.3123	Kruskal-Wallis Test

Figure 7.3b	Test Statistics	Test Used
IL-6	r=0.3589, p=0.0237	One-tailed Spearman's rank
IL-8	r=0.3113, p=0.0441	One-tailed Spearman's rank
IL-13	r=-0.1788, p=0.1680	One-tailed Spearman's rank

Figure 7.3c	Test Statistics	Test Used
IL-6	W=476, p<0.0001	Wilcoxon matched-pairs signed rank test
IL-8	W=388, p<0.0001	Wilcoxon matched-pairs signed rank test
IL-13	W=326, p=0.0009	Wilcoxon matched-pairs signed rank test

Figure 7.4	One-tailed unpaired Mann-Whitney U test – AMD vs control		
	LPS	**R848**	**CD3**
IFNγ	U=114, p=0.4512	U=103, p=0.2598	U=94, p=0.1591
IL-6	U=117, p=0.4612	U=118, p=0.4767	U=101, p=0.2350
IL-8	U=107, p=0.3130	U=118, p=0.4767	U=98, p=0.2004
IL-13	U=95.5, p=0.1668	U=116, p=0.4411	U=111, p=0.3702
TNFα	U=112, p=0.3851	U=93, p=0.1497	U=92, p=0.1407

Figure 7.5	Friedman test
IFNγ	χ^2=83.94, p<0.0001
IL-6	χ^2=87.66, p<0.0001
IL-8	χ^2=84.14, p<0.0001
IL-13	χ^2=25.35, p<0.0001
TNFα	χ^2=82.73, p<0.0001
LPS	χ^2=101.1, p<0.0001
R848	χ^2=104.4, p<0.0001
CD3	χ^2=58.63, p<0.0001

Figure 7.6	One-tailed unpaired Mann-Whitney U test – AMD vs control (U=) One-tailed unpaired t-test – AMD vs control (t_{14}=)		
	LPS	**R848**	**CD3**
IFNγ mono	t_{14}=0.396, p=0.6983	U=27, p=0.3227	U=16, p=0.0524
IL-6 mono	U=31, p=0.4796	t_{14}=0.937, p=0.3646	U=29, p=0.3992
IL-8 mono	t_{14}=1.51, p=0.0766	U=28, p=0.3605	U=31, p=0.4796
TNFα mono	t_{14}=0.575, p=0.5746	U=21, p=0.1393	U=25, p=0.2527
IFNγ lympho	U=30, p=0.4392	t_{14}=28, p=0.3605	U=24, p=0.2209
IL-6 lympho	U=27, p=0.3227	U=29, p=0.3992	U=24, p=0.2209
IL-8 lympho	U=25, p=0.2527	U=31, p=0.4796	U=25, p=0.2527
TNFα lympho	t_{14}=0.9942, p=0.3370	U=17, p=0.0652	U=24, p=0.2209

Figure 7.7	Friedman test
IFNγ mono	χ^2=3.225, p=0.3582
IL-6 mono	χ^2=38.78, p<0.0001
IL-8 mono	χ^2=28.13, p<0.0001
TNFα mono	χ^2=37.65, p<0.0001
IFNγ lympho	χ^2=33.08, p<0.0001
IL-6 lympho	χ^2=15.23, p=0.0016
IL-8 lympho	χ^2=6.300, p=0.0979
TNFα lympho	χ^2=33.98, p<0.0001

Figure 7.8	Friedman test
LPS mono	χ^2=38.33, p<0.0001
R848 mono	χ^2=32.93, p<0.0001
CD3 mono	χ^2=8.175, p=0.0425
LPS lympho	χ^2=16.73, p=0.0008
R848 lympho	χ^2=30.08, p<0.0001
CD3 lympho	χ^2=10.88, p=0.0124

Figure 7.9	One-tailed Spearman's rank
IFNγ	r=0.2991, p=0.0454
IL-6	r=0.3217, p=0.0339
IL-8	r=0.0306, p=0.8656
IL-13	r=-0.0379, p=0.4170
TNFα	r=0.1746, p=0.1656

Figure 7.10	One-tailed Spearman's rank
IL-6	r=0.2335, p=0.1837
IL-8	r=0.1777, p=0.3147
IL-13	r=-0.2426, p=0.1668

Appendix F: Human Flow Cytometry Gating Strategy

F1: Gating strategy for human monocyte and lymphocyte populations

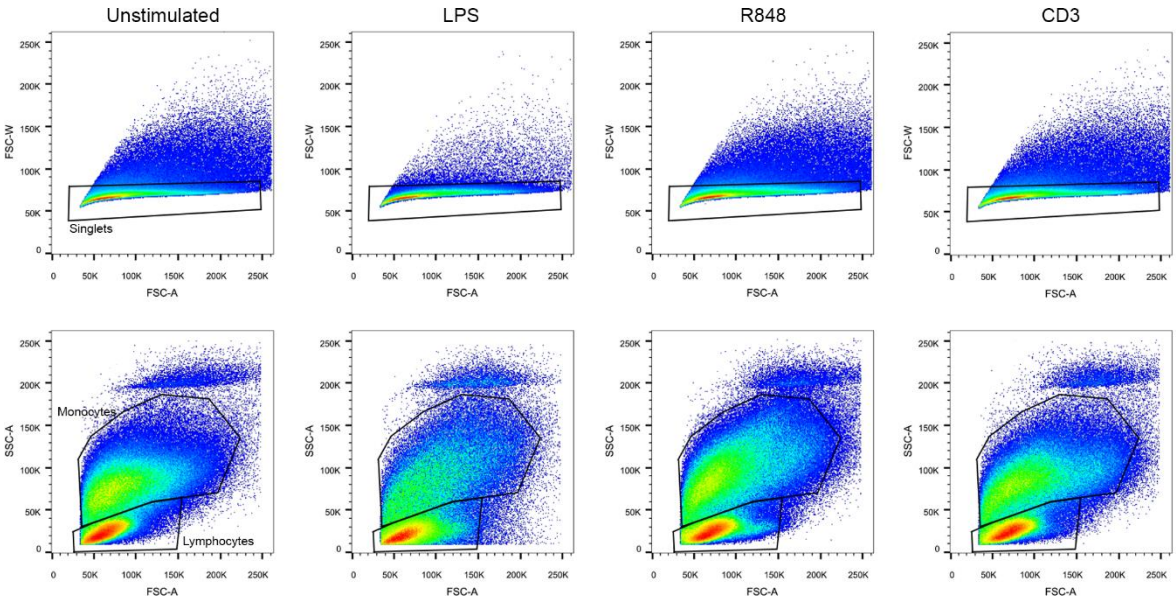

Singlet events were selected based on appearance in a FSC-W vs FSC-A plot. Monocyte and lymphocyte gates of singlet cells were then selected based on differential size/granularity on a SSC-A vs FSC-A plot. Gates were kept constant for each stimulus from the same patient, but were varied for each patient as the location of the populations vary for each patient. The phenotype of lymphocytes and monocytes are provided in Appendix F2 and F3 respectively.

F2: Gating strategy for positive cytokine staining within lymphocytes

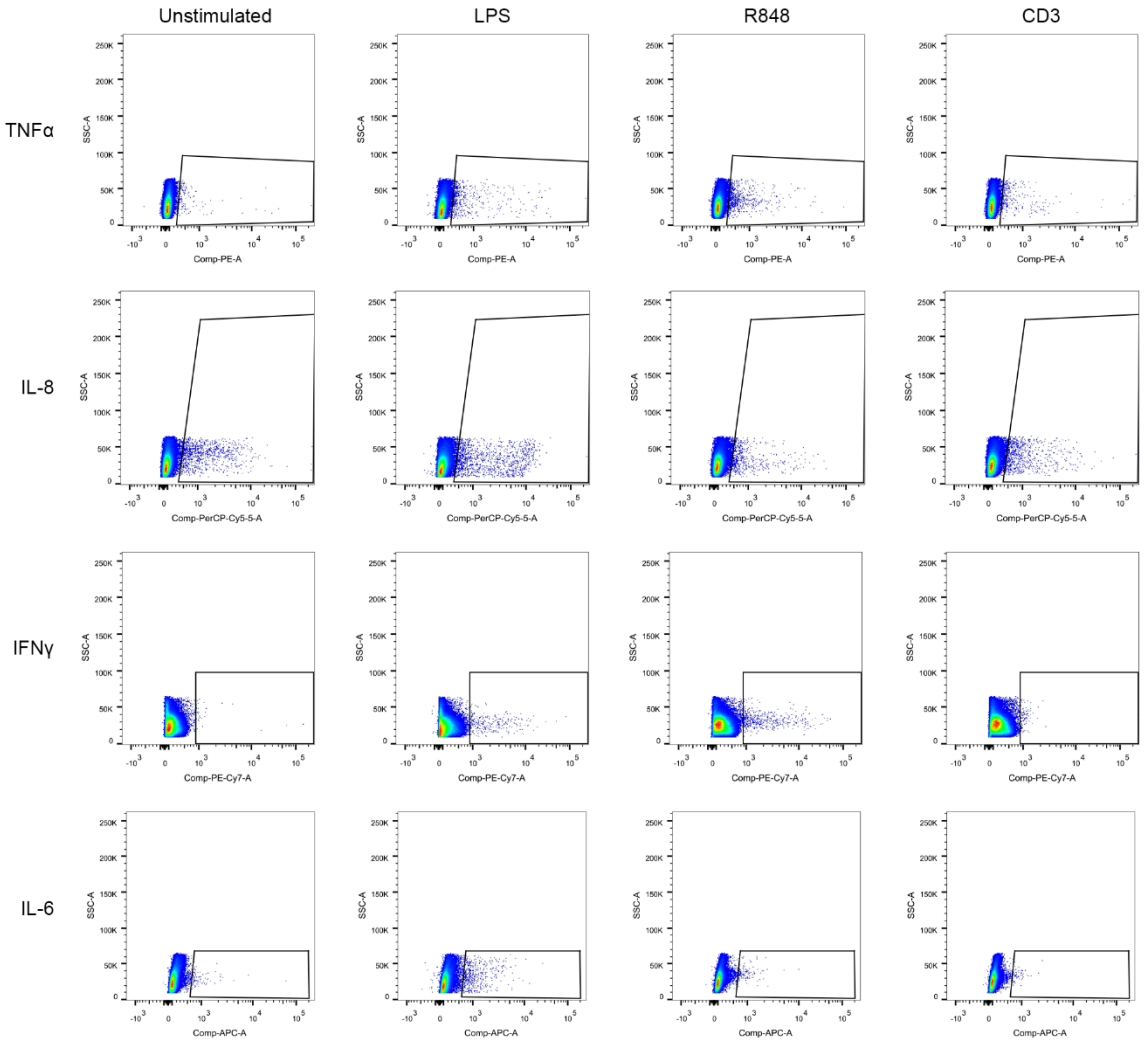

Singlet lympocytes (see appendix F1) were analysed for the MFI and percentage population of lymphocytes expressing cytokines IL-6, IL-8, IFNγ and IL-6. Positive gates were placed to the right of the large negative population in unstimulated controls. Gates were kept constant for each stimulus from the same patient, but were varied for each patient as the location of the populations vary for each patient.

F3: Gating strategy for positive cytokine staining within monocytes

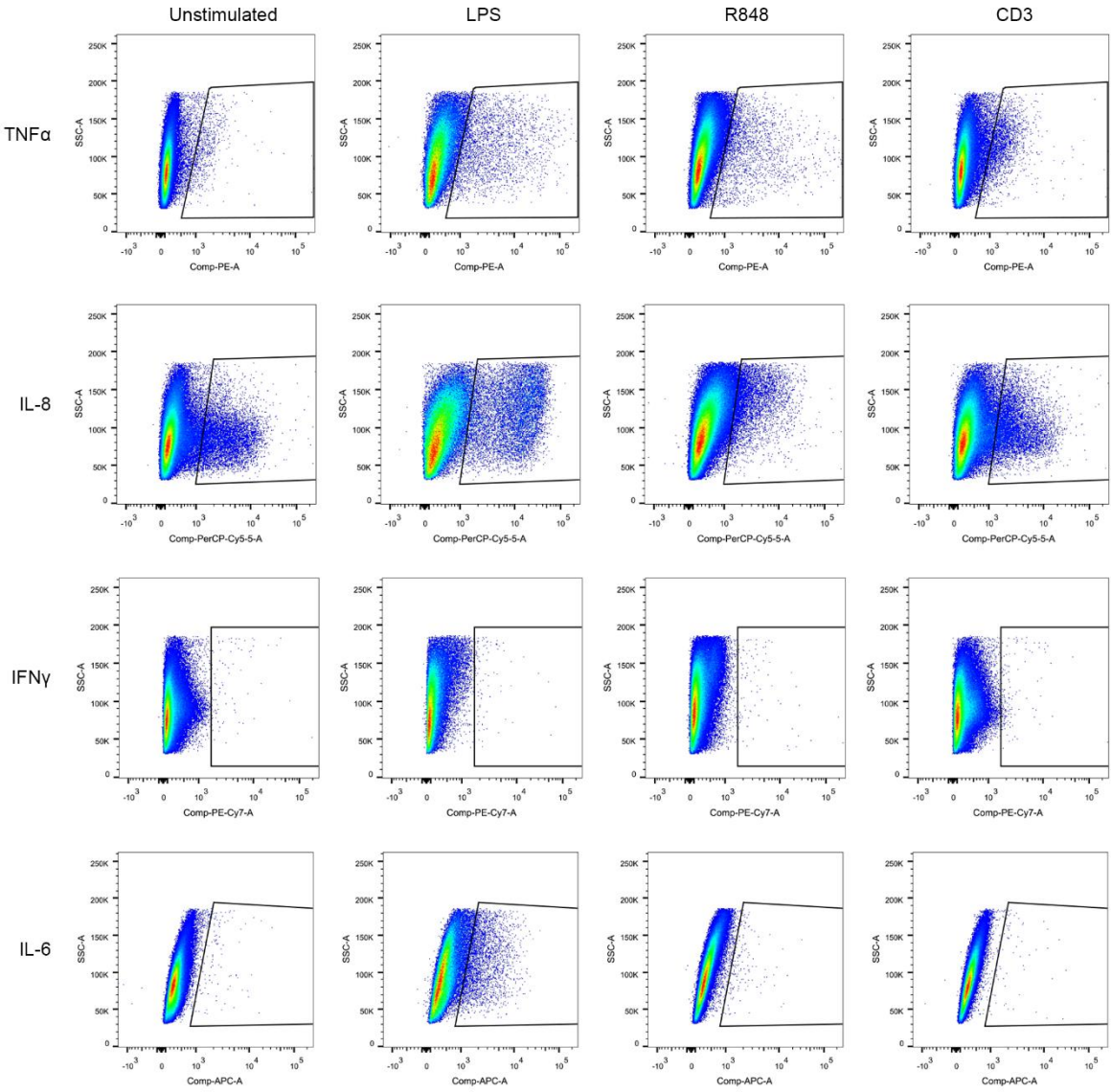

Singlet monocytes (see appendix F1) were analysed for the MFI and percentage population of monocytes expressing cytokines IL-6, IL-8, IFNγ and IL-6. Positive gates were placed to the right of the large negative population in unstimulated controls. Gates were kept constant for each stimulus from the same patient, but were varied for each patient as the location of the populations vary for each patient.

Appendix G: Characteristics of different murine models of geographic AMD features.

	Laser	CEP-MSA		Sodium Iodate		CD46 null		Dicer1-Best-Cre
GM?	No	No		No		Yes		Yes
Geographic or global?	Geographic	Global		Global		Global		Global
Limited to rodents?	No	?		No		Yes		Yes
Aging required?	No	Yes		No		Yes		Not stated
Adjustable dosage?	Yes	?	?	Yes		No	No	No
Conditions	-	2-3 months	12-24 months	15-20mg/kg	30-40mg/kg	2 months	12 months	Not stated
Retinal deposits	?	No	Sub-RPE deposits	?	?	No	Sub-RPE deposits	?
BrM thickening	?	No	Yes	?	?	No	Yes	?
RPE changes?	Atrophy at lesion site	Yes, vesiculation, thickening, some focal atrophy	Further thickening compared to 2-3 month old mice	Patchy RPE loss (Day 3), some recovery over 3 months	Complete RPE loss (Day 3), no recovery over 3 months	No	Thickening, vacuoles, no atrophy	Patchy RPE atrophy
Photoreceptor changes?	Atrophy at lesion site	PR swelling	Complete loss	No loss after 3 months	Complete Loss	≈1.3% loss	≈25% loss	?
Inner retinal changes?	No	?	?	No	No	?	?	?
Fundoscopy appearance	Clearly demarcated lesion for tracking	?	?	Patchy small spots of degeneration (3/14 mice)	Patchy small spots of degeneration	?	?	Patchy RPE loss
OCT appearance	Progressive outer retinal thinning, progressive regression of hyperreflective pathology	?	?	Slight thinning, gradual restoration of disrupted photoreceptor layer	Progressive outer retinal thinning, progressive regression of hyperreflective pathology	?	?	?
ERG deficits?	Yes, no progression	?	?	Yes, no progression	Total loss of response	?	?	?
Inflammasome activation	Yes	?	?	?	?	?	?	Yes
Myeloid cell activation	Yes	Yes in photoreceptor/RPE	Yes in photoreceptor/RPE	?	?	'Macrophage-like' cells in SR increasing with age		?
Müller cell activation	Yes	?	?	?	?	No	?	?
Complement activation	Yes	Yes, C3d at BrM	?	?	?	MAC in retina and choroid		?
Oxidative stress	Yes	Yes	Yes	Yes, toxic levels drive degeneration		?		?
References	*Chapter 6*	Cruz-Guilloty et al., 2013, 2014, Hollyfield et al., 2008, 2010		Machalińska et al., 2010, 2014; Jin Zhao et al., 2017; P. Zhou et al., 2014		Lyzogubov et al., 2014, 2016		Kaneko et al., 2011; Y. Kim et al., 2014; Tarallo et al., 2012

List of References

Access Economics (2009). *Future sight loss UK (1): The economic impact of partial sight and blindness in the UK adult population*. RNIB.

Agarwal, A. (2012). *Gass' atlas of macular diseases*. 5th Ed. Amsterdam: Elsevier Inc.

Agarwal, R.K., Silver, P.B. & Caspi, R.R. (2012). Rodent models of experimental autoimmune uveitis. *Methods Mol Biol.* 900. doi: 10.1007/978-1-60761-720-4_22.

Agawa, T., Usui, Y., Wakabayashi, Y., Okunuki, Y., Juan, M., Umazume, K., Kezuka, T., Takeuchi, M., Yamauchi, Y. & Goto, H. (2014). Profile of intraocular immune mediators in patients with age-related macular degeneration and the effect of intravitreal bevacizumab injection. *Retina*. 34 (9). 1811–8.

Al-Mujaini, A., Wali, U.K. & Azeem, S. (2013). Optical coherence tomography: Clinical applications in medical practice. *Oman Medical Journal*. 28 (2). 86–91.

Alberts, B., Johnson, A., Lewis, J., Morgan, D., Raff, M., Roberts, K. & Walter, P. (2015). *Molecular biology of the cell*. 5th Ed. New York: Garland Science, Taylor & Francis Group.

Aloisi, F. (2001). Immune function of microglia. *Glia*. 36 (2). 165–179.

Aloisi, F., Ria, F. & Adorini, L. (2000). Regulation of T-cell responses by CNS antigen-presenting cells: Different roles for microglia and astrocytes. *Immunology Today*. 21 (3). 141–148.

Amadi-Obi, A., Yu, C.-R., Liu, X., Mahdi, R.M., Clarke, G.L., Nussenblatt, R.B., Gery, I., Lee, Y.S. & Egwuagu, C.E. (2007). TH17 cells contribute to uveitis and scleritis and are expanded by IL-2 and inhibited by IL-27/STAT1. *Nature medicine*. 13 (6). 711–718.

Amanzada, A., Malik, I.A., Nischwitz, M., Sultan, S., Naz, N. & Ramadori, G. (2011). Myeloperoxidase and elastase are only expressed by neutrophils in normal and in inflammed liver. *Histochemistry and Cell Biology*. 135 (3). 305–315.

Ambati, J., Anand, A., Fernandez, S., Sakurai, E., Lynn, B.C., Kuziel, W.A., Rollins, B.J. & Ambati, B.K. (2003). An animal model of age-related macular degeneration in senescent Ccl-2- or Ccr-2-deficient mice. *Nature medicine*. 9 (11). 1390–7.

Ambati, J., Atkinson, J.P. & Gelfand, B.D. (2013). Immunology of age-related macular degeneration. *Nature reviews. Immunology*. 13 (6). 438–51.

Ambreen, F., Ismail, M. & Qureshi, I.Z. (2015). Association of gene polymorphism with serum levels of inflammatory and angiogenic factors in Pakistani patients with age-related macular degeneration. *Molecular Vision*. 21. 985–999.

Anand, A., Sharma, N.K., Gupta, A., Prabhakar, S., Sharma, S.K., Singh, R. & Gupta, P.K. (2012). Single Nucleotide Polymorphisms in MCP-1 and Its Receptor Are Associated with the Risk of Age Related Macular Degeneration. *PLoS ONE*. 7 (11). e49905.

Anastasopoulos, E., Kakoulidou, A., Coleman, A.L., Sinsheimer, J.S., Wilson, M.R., Yu, F., Salonikiou, A., Koskosas, A., Pappas, T., Founti, P., Lambropoulos, A. & Topouzis, F. (2012). Association of sequence variation in the CX3CR1 gene with geographic atrophy age-related macular degeneration in a Greek population. *Current eye research*. 37 (12). 1148–55.

Anderson, D.H., Mullins, R.F., Hageman, G.S. & Johnson, L. V (2002). A role for local inflammation in the formation of drusen in the aging eye. *American Journal of Ophthalmology*. 134 (3). 411–431.

Anderson, D.H., Radeke, M.J., Gallo, N.B., Chapin, E.A., Johnson, P.T., Curletti, C.R., Hancox, L.S., Hu, J., Ebright, J.N., Malek, G., Hauser, M.A., Bowes Rickman, C., Bok, D., Hageman, G.S. & Johnson, L. V (2010). The pivotal role of the complement system in aging and age-related macular degeneration: Hypothesis re-visited. *Progress in Retinal and Eye Research*. 29 (2). 95–112.

Ando, D., Kubo, Y., Akanuma, S., Yoneyama, D., Tachikawa, M. & Hosoya, K. (2012). Function and regulation of taurine transport in Müller cells under osmotic stress. *Neurochemistry International*. 60 (6). 597–604.

Ansari, M., Mckeigue, P.M., Skerka, C., Hayward, C., Rudan, I., Vitart, V., Polasek, O., Armbrecht, A.M., Yates, J.R.W., Vatavuk, Z., Bencic, G., Kolcic, I., Oostra, B.A., Van Duijn, C.M., Campbell,

S., Stanton, C.M., Huffman, J., Shu, X., Khan, J.C., Shahid, H., Harding, S.P., Bishop, P.N., Deary, I.J., Moore, A.T., Dhillon, B., Rudan, P., Zipfel, P.F., Sim, R.B., Hastie, N.D., Campbell, H. & Wright, A.F. (2013). Genetic influences on plasma CFH and CFHR1 concentrations and their role in susceptibility to age-related macular degeneration. *Human Molecular Genetics*. 22 (23). 4857–4869.

AREDSG (2000). Risk factors associated with age-related macular degeneration. A case-control study in the age-related eye disease study: Age-Related Eye Disease Study Report Number 3. *Ophthalmology*. 107 (12). 2224–2232.

AREDSG (2005). Risk factors for the incidence of advanced age-related macular degeneration in the Age-Related Eye Disease Study (AREDS): AREDS report no. 19. *Ophthalmology*. 112 (4). 533–539.

Arias, L. & Mones, J. (2010). Fluorescein Angiography. In: F. M. Bandello (ed.). *Age-related Macular Degeneration*. Loures, Portugal: GER Group, 59–78.

Asi, H. & Perlman, I. (1992). Relationships between the electroretinogram a-wave, b-wave and oscillatory potentials and their application to clinical diagnosis. *Documenta Ophthalmologica*. 79 (2). 125–139.

Augustin, M., Fialova, S., Himmel, T., Gloesmann, M., Lengheimer, T., Harper, D.J., Plasenzotti, R., Pircher, M., Hitzenberger, C.K. & Baumann, B. (2016). Multi-functional OCT enables longitudinal study of retinal changes in a VLDLR knockout mouse model. *PLoS ONE*. 11 (10). e0164419.

Aw, D., Silva, A.B. & Palmer, D.B. (2007). Immunosenescence: emerging challenges for an ageing population. *Immunology*. 120 (4). 435–46.

Baird, P.N., Robman, L.D., Richardson, A.J., Dimitrov, P.N., Tikellis, G., McCarty, C.A. & Guymer, R.H. (2008). Gene-environment interaction in progression of AMD: the CFH gene, smoking and exposure to chronic infection. *Human molecular genetics*. 17 (9). 1299–305.

Balaratnasingam, C., Dhrami-Gavazi, E., McCann, J.T., Ghadiali, Q. & Freund, K.B. (2015). Aflibercept: a review of its use in the treatment of choroidal neovascularization due to age-related macular degeneration. *Clinical ophthalmology*. 9. 2355–71.

Barron, L., Knoechel, B., Lohr, J. & Abbas, A.K. (2008). Cutting edge: contributions of apoptosis and anergy to systemic T cell tolerance. *Journal of immunology*. 180 (5). 2762–2766.

Bauer, J., Bradl, M., Hickley, W.F., Forss-Petter, S., Breitschopf, H., Linington, C., Wekerle, H. & Lassmann, H. (1998). T-cell apoptosis in inflammatory brain lesions: destruction of T cells does not depend on antigen recognition. *American Journal of Pathology*. 153 (3). 715–24.

Baumgart, M., Moos, V., Schuhbauer, D. & Müller, B. (1998). Differential expression of major histocompatibility complex class II genes on murine macrophages associated with T cell cytokine profile and protective/suppressive effects. *Proceedings of the National Academy of Sciences*. 95 (12). 6936–40.

Bearelly, S., Chau, F.Y., Koreishi, A., Stinnett, S.S., Izatt, J.A. & Toth, C.A. (2009). Spectral domain optical coherence tomography imaging of geographic atrophy margins. *Ophthalmology*. 116 (9). 1762–1769.

Bearoff, F., del Rio, R., Case, L.K., Dragon, J.A., Nguyen-Nu, T., Lin, C.-Y., Blackenhorn, E.P., Teuscher, C. & Krementsov, D.N. (2016). Natural genetic variation profoundly regulates gene expression in immune cells and dictates susceptibility to CNS autoimmunity. *Genes and Immunity*. 17 (7). 386–395.

Beerman, I., Bhattacharya, D., Zandi, S., Sigvardsson, M., Weissman, I.L., Bryder, D. & Rossi, D.J. (2010). Functionally distinct hematopoietic stem cells modulate hematopoietic lineage potential during aging by a mechanism of clonal expansion. *Proceedings of the National Academy of Sciences*. 107 (12). 5465–5470.

Bejarano-Escobar, R., Sanchez-Calderon, H., Otero-Arenas, J., Martin-Parido, G. & Francisco-morcillo, J. (2017). Muller glia and phagocytosis of cell debris in retinal tissue. *Journal of anatomy*. doi: 10.1111/joa.12653.

Bergers, G. & Song, S. (2005). The role of pericytes in blood-vessel formation and maintenance. *Neuro-oncology*. 7 (4). 452–464.

Bermudez, E.A., Rifai, N., Buring, J., Manson, J.E. & Ridker, P.M. (2002). Interrelationships among

circulating interleukin-6, C-reactive protein, and traditional cardiovascular risk factors in women. *Arteriosclerosis, Thrombosis, and Vascular Biology*. 22 (10). 1668–1673.

Bhutto, I.A., Baba, T. & Merges, C. (2010). Low Nitric Oxide Synthases (NOS) in Eyes with Age-related Macular Degeneration (AMD). *Experimental eye research*. 90 (1). 155–167.

Bhutto, I.A. & Lutty, G. (2012). Understanding age-related macular degeneration (AMD): Relationships between the photoreceptor/retinal pigment epithelium/Bruch's membrane/choriocapillaris complex. *Molecular aspects of medicine*. 33 (4). 295–317.

Biesmans, S., Meert, T.F., Bouwknecht, J.A., Acton, P.D., Davoodi, N., Haes, P. De, Kuijlaars, J., Langlois, X., Matthews, L.J.R., Donck, L. Ver, Hellings, N. & Nuydens, R. (2013). Systemic Immune Activation Leads to Neuroinflammation and sickness behaviour in mice. *Mediators of Inflammation*. 271359.

Binder, C.J., Papac-Milicevic, N. & Witztum, J.L. (2016). Innate sensing of oxidation-specific epitopes in health and disease. *Nature reviews. Immunology*. 16 (8). 485–497.

Bird, A.C., Phillips, R.L. & Hageman, G.S. (2014). Geographic Atrophy: A histopathological assessment. *JAMA Ophthalmology*. 132 (3). 338–345.

Black, J.R.M. & Clark, S.J. (2016). Age-related macular degeneration: genome-wide association studies to translation. *Genetics in Medicine*. 18 (4). 283–289.

Block, M.L., Zecca, L. & Hong, J.S. (2007). Microglia-mediated neurotoxicity: uncovering the molecular mechanisms. *Nature Reviews. Neuroscience*. 8 (1). 57–69.

Boldison, J., Chu, C.J., Copland, D. a, Lait, P.J.P., Khera, T.K., Dick, A.D. & Nicholson, L.B. (2014). Tissue-Resident Exhausted Effector Memory CD8+ T Cells Accumulate in the Retina during Chronic Experimental Autoimmune Uveoretinitis. *Journal of immunology*. 192 (10). 4541–50.

Booij, J.C., Baas, D.C., Beisekeeva, J., Gorgels, T.G.M.F. & Bergen, A.A.B. (2010). The dynamic nature of Bruch's membrane. *Progress in Retinal and Eye Research*. 29 (1). 1–18.

Böttcher, J.P., Beyer, M., Meissner, F., Abdullah, Z., Sander, J., Höchst, B., Eickhoff, S., Rieckmann, J.C., Russo, C., Bauer, T., Flecken, T., Giesen, D., Engel, D., Jung, S., Busch, D.H., Protzer, U., Thimme, R., Mann, M., Kurts, C., Schultze, J.L., Kastenmüller, W. & Knolle, P.A. (2015). Functional classification of memory CD8(+) T cells by CX3CR1 expression. *Nature communications*. 6:8306.

Boundless Biology (2016). *Transduction of Light*. [Online]. 2016. Boundless Biology. Available from: https://www.boundless.com/biology/textbooks/boundless-biology-textbook/sensory-systems-36/vision-209/transduction-of-light-790-12025/. [Accessed: 1 January 2017].

Brandli, A. & Stone, J. (2015). Using the Electroretinogram to Assess Function in the Rodent Retina and the Protective Effects of Remote Limb Ischemic Preconditioning. *Journal of Visualized Experiments*. (100). e52658.

Brandstetter, C., Mohr, L.K.M., Latz, E., Holz, F.G. & Krohne, T.U. (2015). Light induces NLRP3 inflammasome activation in retinal pigment epithelial cells via lipofuscin-mediated photooxidative damage. *Journal of Molecular Medicine*. 93 (8). 905–916.

Bringmann, A., Iandiev, I., Pannicke, T., Wurm, A., Hollborn, M., Wiedemann, P., Osborne, N.N. & Reichenbach, A. (2009). Cellular signaling and factors involved in Muller cell gliosis: Neuroprotective and detrimental effects. *Progress in Retinal and Eye Research*. [Online]. 28 (6). 423–451. Available from: http://dx.doi.org/10.1016/j.preteyeres.2009.07.001.

Briõn, M., Sanchez-Salorio, M., Cortõn, M., De La Fuente, M., Pazos, B., Othman, M., Swaroop, A., Abecasis, G., Sobrino, B. & Carracedo, A. (2011). Genetic association study of age-related macular degeneration in the Spanish population. *Acta Ophthalmologica*. 89. e12–e22.

Broz, P., Ohlson, M.B. & Monack, D.M. (2012). Innate immune response to Salmonella typhimurium, a model enteric pathogen. *Gut Microbes*. 3 (2). 62–70.

Bruhns, P. (2012). Properties of mouse and human IgG receptors and their contribution to disease models. *Blood*. 119 (24). 5640–5649.

Buch, H., Nielsen, N. V., Vinding, T., Jensen, G.B., Prause, J.U. & La Cour, M. (2005). 14-Year incidence, progression, and visual morbidity of age-related maculopathy: The Copenhagen City Eye Study. *Ophthalmology*. 112 (5). 787–798.

Buschini, E., Piras, A., Nuzzi, R. & Vercelli, A. (2011). Age related macular degeneration and drusen: neuroinflammation in the retina. *Progress in neurobiology*. 95 (1). 14–25.

Butchart, J., Brook, L., Hopkins, V., Teeling, J.L., Puentener, U., Culliford, D., Sharples, R., Sharif, S., McFarlane, B., Raybould, R., Thomas, R., Passmore, P., Perry, V.H. & Holmes, C. (2015). Etanercept in Alzheimer disease. *Neurology*. 84 (21). 2161–2168.

Butovsky, O., Jedrychowski, M.P., Moore, C.S., Cialic, R., Lanser, A.J., Gabriely, G., Koeglsperger, T., Dake, B., Wu, P.M., Doykan, C.E., Fanek, Z., Liu, L., Chen, Z., Rothstein, J.D., Ransohoff, R.M., Gygi, S.P., Antel, J.P. & Weiner, H.L. (2013). Identification of a unique TGF-β–dependent molecular and functional signature in microglia. *Nature Neuroscience*. 17 (1). 131–143.

Cabral, T., Lima, L.H., M. Mello, L.G., Polido, J., P. Correa, É., Oshima, A., Duong, J., Serracarbassa, P., Regatieri, C. V., Mahajan, V.B. & Belfort Jr., R. (2017). Bevacizumab Injection in Patients with Neovascular Age-Related Macular Degeneration Increases Angiogenic Biomarkers. *Ophthalmology Retina*. doi: 10.1016/j.oret.2017.04.004.

Caicedo, A., Espinosa-Heidmann, D.G., Piña, Y., Hernandez, E.P. & Cousins, S.W. (2005). Blood-derived macrophages infiltrate the retina and activate Muller glial cells under experimental choroidal neovascularization. *Experimental Eye Research*. 81 (1). 38–47.

Camelo, S., Lavelette, S., Guillonneau, X., Raoul, W. & Sennlaub, F. (2016). Association of Choroidal Interleukin-17-Producing T Lymphocytes and Macrophages with Geographic Atrophy. *Ophthalmologica*. 236 (1). 53–58.

Campbell, M. & Humphries, P. (2013). The blood-retina barrier: Tight junctions and barrier modulation. In: C. Y. Cheng (ed.). *Biology and Regulation of Blood-Tissue Barriers*. Austin, Texas: Springer Science+Business, 70–84.

Cano, M., Thimmalappula, R., Fujihara, M., Nagai, N., Sporn, M., Wang, A.L., Neufeld, A.H., Biswal, S. & Handa, J.T. (2010). Cigarette smoking, oxidative stress, the anti-oxidant response through Nrf2 signalling and age-related macular degeneration. *Vision research*. 50 (7). 652–664.

Cao, S., Ko, A., Partanen, M., Pakzad-Vaezi, K., Merkur, A.B., Albiani, D.A., Kirker, A.W., Wang, A., Cui, J.Z., Forooghian, F. & Matsubara, J.A. (2013). Relationship between Systemic Cytokines and Complement Factor H Y402H Polymorphism in Patients With Dry Age-Related Macular Degeneration. *American journal of Ophthalmology*. 156 (6). 1176–1183.

Cao, X., Shen, D., Patel, M.M., Tuo, J., Johnson, T.M., Olsen, T. & Chan, C.-C. (2011). Macrophage polarization in the maculae of age-related macular degeneration: A pilot study. *Pathology International*. 61 (9). 528–535.

Carmichael, A. (2012). Cytomegalovirus and the eye. *Eye*. 26 (2). 237–40.

Carpentier, S., Knaus, M. & Suh, M. (2009). Associations between lutein, zeaxanthin, and age-related macular degeneration: an overview. *Crit Rev Food Sci Nutr*. 49 (4). 313–326.

Carter-Dawson, L.D. & LaVail, M.M. (1979). Rods and cones in the mouse retina. I. Structural analysis using light and electron microscopy. *Journal of Comparative Neurology*. 188 (2). 245–62.

Caspi, R.R. (2010). A look at autoimmunity and inflammation in the eye. *Journal of Clinical investigation*. 120 (9). 3073–3083.

CATT research group (2010). Ranibizumab and bevacizumab for neovascular age-related macular degeneration. *New England Journal of Medicine*. 364 (20). 1897–1908.

Cha, D.M., Woo, S.J., Kim, H.-J., Lee, C. & Park, K.H. (2013). Comparative analysis of aqueous humor cytokine levels between patients with exudative age-related macular degeneration and normal controls. *Investigative Ophthalmology and Visual Science*. 54 (10). 7038–44.

Chalam, K. V., Grover, S., Sambhav, K., Balaiya, S. & Murthy, R.K. (2014). Aqueous interleukin-6 levels are superior to vascular endothelial growth factor in predicting therapeutic response to bevacizumab in age-related macular degeneration. *Journal of Ophthalmology*. 502174.

Chan, C. & Ardeljan, D. (2014). Molecular pathology of macrophages and interleukin-17 in age-related macular degeneration. In: J. D. Ash (ed.). *Retinal Degenerative Diseases*. New York: Springer Science+Business.

Chelvarajan, R.L., Liu, Y., Popa, D., Getchell, M.L., Getchell, T. V, Stromberg, A.J. & Bondada, S. (2006). Molecular basis of age-associated cytokine dysregulation in LPS-stimulated macrophages. *Journal of leukocyte biology*. 79 (6). 1314–1327.

Chen, J., Qian, H., Horai, R., Chan, C.-C. & Caspi, R.R. (2013a). Use of Optical Coherence

Tomography and Electroretinography to Evaluate Retinal Pathology in a Mouse Model of Autoimmune Uveitis. *PLoS ONE*. 8 (5). e63904.

Chen, M., Hombrebueno, J.R., Luo, C., Penalva, R., Zhao, J., Colhoun, L., Pandi, S.P.S., Forrester, J. V. & Xu, H. (2013b). Age- and Light-Dependent Development of Localised Retinal Atrophy in CCL2-/-CX3CR1GFP/GFP Mice. *PLoS ONE*. 8 (4). e61381.

Chen, M., Muckersie, E., Forrester, J. V. & Xu, H. (2010). Immune activation in retinal aging: a gene expression study. *Investigative Ophthalmology and Visual Science*. 51 (11). 5888–96.

Chen, M. & Xu, H. (2015). Parainflammation, chronic inflammation, and age-related macular degeneration. *Journal of Leukocyte Biology*. 98 (5). 713–725.

Chen, X., Jhanji, V., Chen, C. & Chen, H. (2014). Serological association of chlamydia pneumoniae infection with age-related macular degeneration: A systematic review and meta-analysis. *PLoS ONE*. 9 (7). e103466.

Cherepanoff, S., McMenamin, P., Gillies, M.C., Kettle, E. & Sarks, S.H. (2010). Bruch's membrane and choroidal macrophages in early and advanced age-related macular degeneration. *British Journal of Ophthalmology*. 94 (7). 918–925.

Cheung, C.M.G., Vania, M., Ang, M., Chee, S.P. & Li, J. (2012). Comparison of aqueous humor cytokine and chemokine levels in diabetic patients with and without retinopathy. *Molecular vision*. 18. 830–7.

Chinnery, H.R., McLenachan, S., Humphries, T., Kezic, J.M., Chen, X., Ruitenberg, M.J. & McMenamin, P.G. (2012). Accumulation of murine subretinal macrophages: Effects of age, pigmentation and CX 3CR1. *Neurobiology of Aging*. 33 (8). 1769–1776.

Chistiakov, D.A., Sobenin, I.A., Orekhov, A.N. & Bobryshev, Y. V. (2015). Myeloid dendritic cells: Development, functions, and role in atherosclerotic inflammation. *Immunobiology*. 220 (6). 833–844.

Chong, E.W., Kreis, A.J., Wong, T.Y., Simpson, J.A. & Guymer, R.H. (2008). Alcohol consumption and the risk of age-related macular degeneration: a systematic review and meta-analysis. *American journal of Ophthalmology*. 145 (4). 707–715.

Chu, C.J., Gardner, P.J., Copland, D.A., Liyanage, S.E., Gonzalez-Cordero, A., kleine Holthaus, S.-M., Luhmann, U.F.O., Smith, A.J., Ali, R.R. & Dick, A.D. (2016). Multimodal analysis of ocular inflammation using the endotoxin-induced uveitis mouse model. *Disease Models and Mechanisms*. 9 (4). 473–481.

Chu, X.K., Wang, Y., Ardeljan, D., Tuo, J. & Chan, C. (2013). Controversial view of a genetically altered mouse model of focal retinal degeneration. *Bioengineered*. 4 (3). 130–135.

Coffey, P.J., Gias, C., McDermott, C.J., Lundh, P., Pickering, M.C., Sethi, C., Bird, A., Fitzke, F.W., Maass, A., Chen, L.L., Holder, G.E., Luthert, P.J., Salt, T.E., Moss, S.E. & Greenwood, J. (2007). Complement factor H deficiency in aged mice causes retinal abnormalities and visual dysfunction. *Proceedings of the National Academy of Sciences*. 104 (42). 16651–16656.

Collins, T., Korman, A.J., Wake, C.T., Boss, J.M., Kappes, D.J., Fiers, W., Ault, K.A., Gimbrone, M.A., Strominger, J.L. & Pober, J.S. (1984). Immune interferon activates multiple class II major histocompatibility complex genes and the associated invariant chain gene in human endothelial cells and dermal fibroblasts. *Proceedings of the National Academy of Sciences*. 81 (15). 4917–4921.

Combadière, C., Feumi, C., Raoul, W., Keller, N., Rodéro, M., Pézard, A., Lavalette, S., Houssier, M., Jonet, L., Picard, E., Debré, P., Sirinyan, M., Deterre, P., Ferroukhi, T., Cohen, S., Chauvaud, D., Jeanny, J., Chemtob, S., Behar-Cohen, F. & Sennlaub, F. (2007). CX3CR1-dependent subretinal microglia cell accumulation is associated with cardinal features of age-related macular degeneration. *Journal of Clinical Investigation*. 117 (10). 2920–8.

Cong, R., Zhou, B., Sun, Q., Gu, H., Tang, N. & Wang, B. (2008). Smoking and the Risk of Age-related Macular Degeneration: A Meta-Analysis. *Annals of Epidemiology*. 18 (8). 647–656.

Congdon, N., O'Colmain, B., Klaver, C.C., Klein, R., Munoz, B., Friedman, D., Kempen, J., Taylor, H., Mitchell, P. & Eye Diseases Prevalence Research Group (2004). Causes and Prevalence of Visual Impairment Among Adults in the United States. *Archives of ophthalmology*. 122 (4). 477–485.

Cook-Mills, J.M., Marchese, M.E. & Abdala-Valencia, H. (2011). Vascular cell adhesion molecule-1

expression and signaling during disease: regulation by reactive oxygen species and antioxidants. *Antioxidants & redox signaling*. 15 (6). 1607–38.

Corona, A.W., Fenn, A.M. & Godbout, J.P. (2012). Cognitive and behavioral consequences of impaired immunoregulation in aging. *Journal of neuroimmune pharmacology*. 7 (1). 7–23.

Cousins, S.W., Espinosa-Heidmann, D.G. & Csaky, K.G. (2004). Monocyte Activation in Patients With Age-Related Macular Degeneration: A Biomarker of Risk for Choroidal Neovascularization? *Archives of ophthalmology*. 122 (7). 1013–1018.

Cousins, S.W., Espinosa-Heidmann, D.G., Miller, D.M., Pereira-Simon, S., Hernandez, E.P., Chien, H., Meier-Jewett, C. & Dix, R.D. (2012). Macrophage activation associated with chronic murine cytomegalovirus infection results in more severe experimental choroidal neovascularization. *PLoS pathogens*. 8 (4). e1002671.

Crabb, J.W. (2014). The proteomics of drusen. *Cold Spring Harbor Perspectives in Medicine*. doi: 10.1101/cshperspect.a017194.

Crabb, J.W., Miyagi, M., Gu, X., Shadrach, K., West, K.A., Sakaguchi, H., Kamei, M., Hasan, A., Yan, L., Rayborn, M.E., Salomon, R.G. & Hollyfield, J.G. (2002). Drusen proteome analysis: an approach to the etiology of age-related macular degeneration. *Proceedings of the National Academy of Sciences*. 99 (23). 14682–7.

Crane, I.J. & Liversidge, J. (2008). Mechanisms of leukocyte migration across the blood-retina barrier. *Seminars in Immunopathology*. 30 (2). 165–177.

Cruickshanks, K.J., Klein, R. & Klein, B.E.K. (1993). Sunlight and age-related macular degeneration. The Beaver Dam Eye Study. *Archives of ophthalmology*. 111 (4). 514–8.

Cruz-Guilloty, F., Saeed, A.M., Duffort, S., Cano, M., Ebrahimi, K.B., Ballmick, A., Tan, Y., Wang, H., Laird, J.M., Salomon, R.G., Handa, J.T. & Perez, V.L. (2014). T cells and macrophages responding to oxidative damage cooperate in pathogenesis of a mouse model of age-related macular degeneration. *PLoS ONE*. 9 (2). e88201.

Cruz-Guilloty, F., Saeed, A.M., Echegaray, J.J., Duffort, S., Ballmick, A., Tan, Y., Betancourt, M., Viteri, E., Ramkhellawan, G.C., Ewald, E., Feuer, W., Huang, D., Wen, R., Hong, L., Wang, H., Laird, J.M., Sene, A., Apte, R.S., Salomon, R.G., Hollyfield, J.G. & Perez, V.L. (2013). Infiltration of Proinflammatory M1 Macrophages into the Outer Retina Precedes Damage in a Mouse Model of Age-Related Macular Degeneration. *International Journal of Inflammation*. 503725.

Cunningham, C., Campion, S., Lunnon, K., Murray, C.L., Woods, J.F.C., Deacon, R.M.J., Rawlins, J.N.P. & Perry, V.H. (2009). Systemic inflammation induces acute behavioral and cognitive changes and accelerates neurodegenerative disease. *Biological psychiatry*. 65 (4). 304–12.

Cunningham, C., Wilcockson, D.C., Campion, S., Lunnon, K. & Perry, V.H. (2005). Central and systemic endotoxin challenges exacerbate the local inflammatory response and increase neuronal death during chronic neurodegeneration. *Journal of Neuroscience*. 25 (40). 9275–84.

Curcio, C.A. (2001). Photoreceptor topography in ageing and age-related maculopathy. *Eye*. 15. 376–383.

Curcio, C.A. & Ach, T. (2016). Macrophages or retinal pigment epithelium expressing macrophage markers in age-related macular degeneration? Comment on Lad et al. 2015. *Graefe's Archive for Clinical and Experimental Ophthalmology*. 254 (6). 1237–1238.

Curcio, C.A. & Millican, C.L. (1999). Basal linear deposit and large drusen are specific for early age-related maculopathy. *Archives of ophthalmology*. 117 (3). 329–339.

Curcio, C.A., Sloan, K.R., Kalina, R.E. & Hendrickson, A.E. (1990). Human Photoreceptor Topography. *Journal of Comparative Neurology*. 292 (4). 497–523.

D'Agostino, P., Gottfried-Blackmore, A., Anandasabapathy, N. & Bulloch, K. (2012). Brain dendritic cells: biology and pathology. *Acta Neuropathologica*. 124 (5). 599–614.

Daley, J.M., Thomay, A.A., Connolly, M.D., Reichner, J.S. & Albina, J.E. (2007). Use of Ly6G-specific monoclonal antibody to deplete neutrophils in mice. *Journal of Leukocyte Biology*. 83 (1). 64–70.

Damani, M.R., Zhao, L., Fontainhas, A.M., Amaral, J., Fariss, R.N. & Wong, W.T. (2011). Age-related Alterations in the Dynamic Behavior of Microglia. *Aging Cell*. 10 (2). 263–276.

Daniels, M.J.D., Rivers-Auty, J., Schilling, T., Spencer, N.G., Watremez, W., Fasolino, V., Booth, S.J., White, C.S., Baldwin, A.G., Freeman, S., Wong, R., Latta, C., Yu, S., Jackson, J., Fischer, N., Koziel, V., Pillot, T., Bagnall, J., Allan, S.M., Paszek, P., Galea, J., Harte, M.K., Eder, C., Lawrence, C.B. & Brough, D. (2016). Fenamate NSAIDs inhibit the NLRP3 inflammasome and protect against Alzheimer's disease in rodent models. *Nature Communications*. 7:12504.

Dantzer, R. (2004). Cytokine-induced sickness behaviour: a neuroimmune response to activation of innate immunity. *European journal of pharmacology*. 500. 399–411.

Dantzer, R., Connor, J.C.O., Freund, G.G., Johnson, R.W. & Kelley, K.W. (2008). From inflammation to sickness and depression: when the immune system subjugates the brain. *Nature reviews. Neuroscience*. 9 (1). 46–56.

Daugherty, B.L., Siciliano, S.J., DeMartino, J.A., Malkowitz, L., Sirotina, A. & Springer, M.S. (1996). Cloning, expression, and characterization of the human eosinophil eotaxin receptor. *Journal of Experimental Medicine*. 183 (5). 2349–54.

Davis III, J.M., Knutson, K.L., Strausbauch, M.A., Crowson, C.S., Therneau, T.M., Wettstein, P.J., Matteson, E.L. & Gabriel, S.E. (2010). Analysis of complex biomarkers for human immune-mediated disorders based on cytokine responsiveness of peripheral blood cells. *Journal of immunology*. 184 (12). 7297–7304.

Delcourt, C., Michel, F., Colvez, A., Lacroux, A., Delage, M. & Vernet, M.H. (2001). Associations of cardiovascular disease and its risk factors with age-related macular degeneration: the POLA study. *Ophthalmic epidemiology*. 8 (4). 237–249.

Desmettre, T., Maurage, C.A. & Mordon, S. (2003). Transpupillary thermotherapy (TTT) with short duration laser exposures induce heat shock protein (HSP) hyperexpression on choroidoretinal layers. *Lasers in Surgery and Medicine*. 33 (2). 102–107.

Dewispelaere, R., Lipski, D., Foucart, V., Bruyns, C., Frère, A., Caspers, L. & Willermain, F. (2015). ICAM-1 and VCAM-1 are differentially expressed on blood-retinal barrier cells during experimental autoimmune uveitis. *Experimental Eye Research*. 137. 94–102.

Dick, A.D., Ford, A.L., Forrester, J. V & Sedgwick, J.D. (1995). Flow cytometric identification of a minority population of MHC class II positive cells in the normal rat retina distinct from CD45lowCD11b/c+CD4low parenchymal microglia. *British Journal of Ophthalmology*. 79 (9). 834–840.

Dinarello, C.A., Novick, D., Kim, S. & Kaplanski, G. (2013). Interleukin-18 and IL-18 binding protein. *Frontiers in Immunology*. 4:289.

Ding, X., Patel, M. & Chan, C.-C. (2009). Molecular pathology of AMD. *Progress in retinal and eye research*. 28 (1). 1–18.

Dolz-Marco, R., Litts, K.M., Tan, A.C.S., Freund, K.B. & Curcio, C.A. (2016). The Evolution of Outer Retinal Tubulation, a Neurodegeneration and Gliosis Prominent in Macular Diseases. *Ophthalmology*. S0161-6420 (16). 31420–8.

Donahue, A.C. & Fruman, D.A. (2003). Proliferation and Survival of Activated B Cells Requires Sustained Antigen Receptor Engagement and Phosphoinositide 3-Kinase Activation. *Journal of immunology*. 170 (12). 5851–5860.

Dong, N., Xu, B., Chu, L. & Tang, X. (2015). Study of 27 aqueous humor cytokines in type 2 diabetic patients with or without macular edema. *PLoS ONE*. 10 (4). e125329.

Doyle, S.L., Campbell, M., Ozaki, E., Salomon, R.G., Mori, A., Kenna, P.F., Farrar, G.J., Kiang, A.-S., Humphries, M.M., Lavelle, E.C., O'Neill, L.A., Hollyfield, J.G. & Humphries, P. (2012). NLRP3 has a protective role in age-related macular degeneration through the induction of IL-18 by drusen components. *Nature medicine*. 18 (5). 791–8.

Durrani, O.M., Meads, C.A. & Murray, P.I. (2004). Uveitis: A potentially blinding disease. *Ophthalmologica*. 218 (4). 223–236.

Dustin, M.L., Rothlein, R., Bhan, A., Dinarello, C.A. & Springer, T. (1986). Induction by IL-1 and interferon-7: tissue distribution, biochemistry, and function of a natural adherence molecule (ICAM-1). *Journal of immunology*. 137. 245–254.

Ebneter, A., Jaggi, D., Abegg, M., Wolf, S. & Zinkernagel, M.S. (2016). Relationship between presumptive inner nuclear layer thickness and geographic atrophy progression in age-related macular degeneration. *Investigative Ophthalmology and Visual Science*. 57 (9). OCT299-

OCT306.
Ebrey, T. & Koutalos, Y. (2001). Vertebrate photoreceptors. *Progress in retinal and eye research*. 20 (1). 49–94.
EDC-CSG (1992). Risk Factors for Neovascular Age-Related Macular Degeneration. *Archives of ophthalmology*. 110 (12). 1701–1708.
Edwards, R.B. (1994). Biosynthesis of Retinoic Acid by Muller Glial Cells : A Model for the Central Nervous System? *Progress in Retinal and Eye Research*. 13 (1). 231–242.
Eggleton, P. (2001). *Hypersensitivity: Immune Complex Mediated (Type III)*. Chicester: John Wiley & Sons.
Eichler, W., Yafai, Y., Keller, T., Wiedemann, P. & Reichenbach, A. (2004a). PEDF derived from glial Muller cells: a possible regulator of retinal angiogenesis. *Experimental cell research*. 299 (1). 68–78.
Eichler, W., Yafai, Y., Wiedemann, P. & Reichenbach, A. (2004b). Angiogenesis-related factors derived from retinal glial (Muller) cells in hypoxia. *Neuroreport*. 15 (10). 1633–7.
Ek, M., Engblom, D., Saha, S., Blomqvist, A., Jakobsson, P.-J.J. & Ericsson-Dahlstrand, A. (2001). Inflammatory response: pathway across the blood-brain barrier. *Nature*. 410 (6827). 430–431.
EpiVision (2010). *Future sight loss UK (2): An epidemiological and economic model for sight loss in the decade 2010-2020.* RNIB.
Erickson, K.K., Sundstrom, J.M. & Antonetti, D.A. (2007). Vascular permeability in ocular disease and the role of tight junctions. *Angiogenesis*. 10. 103–117.
Erickson, M.A. & Banks, W.A. (2011). Cytokine and Chemokine Responses in Serum and Brain After Single and Repeated Injections of Lipopolysaccharide: Multiplex Quantification with Path Analysis. *Brain, behavior, and immunity*. 25 (8). 1637–1648.
Ersoy, L., Ristau, T., Lechanteur, Y.T., Hahn, M., Hoyng, C.B., Kirchhof, B., Hollander, A.I. Den & Fauser, S. (2014). Nutritional Risk Factors for Age-Related Macular Degeneration. *BioMed Research International*. 413150.
Espinosa-Heidmann, D.G., Suner, I.J., Hernandez, E.P., Monroy, D., Csaky, K.G. & Cousins, S.W. (2003). Macrophage depletion diminishes lesion size and severity in experimental choroidal neovascularization. *Investigative Ophthalmology and Visual Science*. 44 (8). 3586–3592.
Ethen, C.M., Reilly, C., Feng, X., Olsen, T.W. & Ferrington, D.A. (2007). Age-related macular degeneration and retinal protein modification by 4-hydroxy-2-nonenal. *Investigative Ophthalmology and Visual Science*. 48 (8). 3469–3479.
Evans, J.R., Smith, W., Assink, J., Klein, R., Mitchell, P., Klaver, C.C., Klein, B.E.K., Hofman, A., Jensen, S., Wang, J.J. & de Jong, P.T.V.M. (2001). Risk factors for age-related macular degeneration. *Progress in Retinal and Eye Research*. 20 (2). 227–253.
Ezzat, M.-K., Hann, C.R., Vuk-Pavlovic, S. & Pulido, J.S. (2008). Immune cells in the human choroid. *British journal of ophthalmology*. 92. 976–980.
Faber, C., Jehs, T., Juel, H.B., Singh, A., Falk, M.K., Sørensen, T.L. & Nissen, M.H. (2015). Early and exudative age-related macular degeneration is associated with increased plasma levels of soluble TNF receptor II. *Acta Ophthalmologica*. 83. 242–247.
Faber, C., Singh, A., Falk, M.K., Juel, H.B., Sørensen, T.L. & Nissen, M.H. (2013). Age-related macular degeneration is associated with increased proportion of CD56+ T cells in peripheral blood. *Ophthalmology*. 120 (11). 2310–2316.
Falk, M.K., Singh, A., Faber, C., Nissen, M.H., Hviid, T. & Sørensen, T.L. (2014a). CX3CL1/CX3CR1 and CCL2/CCR2 chemokine/chemokine receptor complex in patients with AMD. *PLoS ONE*. 9 (12). e0112473.
Falk, M.K., Singh, A., Faber, C., Nissen, M.H., Hviid, T. & Sørensen, T.L. (2014b). Dysregulation of CXCR3 expression on peripheral blood leukocytes in patients with neovascular age-related macular degeneration. *Investigative Ophthalmology and Visual Science*. 55 (7). 4050–6.
Fauser, S., Viebahn, U. & Muether, P.S. (2015). Intraocular and systemic inflammation-related cytokines during one year of ranibizumab treatment for neovascular age-related macular degeneration. *Acta Ophthalmologica*. 93 (8). 734–738.
Feng, J., Zhao, T., Zhang, Y., Ma, Y. & Jiang, Y. (2013). Differences in Aqueous Concentrations of

Cytokines in Macular Edema Secondary to Branch and Central Retinal Vein Occlusion. *PLoS ONE*. 8 (7). e68149.

Ferrara, N. (2010). Vascular endothelial growth factor and age-related macular degeneration: from basic science to therapy. *Nature Medicine*. 16 (10). 1107–1111.

Ferrucci, L., Corsi, A., Lauretani, F., Bandinelli, S., Bartali, B., Taub, D.D., Guralnik, J.M. & Longo, D.L. (2005). The origins of age-related proinflammatory state. *Blood*. 105 (6). 2294–9.

Fillatreau, S. (2011). Novel regulatory functions for Toll-like receptor-activated B cells during intracellular bacterial infection. *Immunological Reviews*. 240 (1). 52–71.

Fleckenstein, M., Issa, P.C., Helb, H.M., Schmitz-Valckenberg, S., Finger, R.P., Scholl, H.P.N., Loeffler, K.U. & Holz, F.G. (2008). High-resolution spectral domain-OCT imaging in geographic atrophy associated with age-related macular degeneration. *Investigative Ophthalmology and Visual Science*. 49 (9). 4137–4144.

Fletcher, A.E., Bentham, G., Agnew, M., Young, I., Augood, C.A., Chakravarthy, U., de Jong, P.T.V.M., Rahu, M., Seland, J., Soubrane, G., Tomazzoli, L., Topouzis, F., Vingerling, J. & Vioque, J. (2008). Sunlight Exposure, Antioxidants, and Age-Related Macular Degeneration. *Archives of Ophthalmology*. 126 (10). 1396–1403.

Franceschi, C., Capri, M., Monti, D., Giunta, S., Olivieri, F., Sevini, F., Panourgia, M.P., Invidia, L., Celani, L., Scurti, M., Cevenini, E., Castellani, G.C. & Salvioli, S. (2007). Inflammaging and anti-inflammaging: A systemic perspective on aging and longevity emerged from studies in humans. *Mechanisms of Ageing and Development*. 128 (1). 92–105.

Friedman, D.S., O'Colmain, B.J., Muñoz, B., Tomany, S.C., McCarty, C., de Jong, P.T.V.M., Nemesure, B., Mitchell, P. & Kempen, J. (2004). Prevalence of age-related macular degeneration in the United States. *Archives of ophthalmology*. 122 (4). 564–72.

Frishman, L.J. & Wang, M.H.W. (2011). Electroretinogram of human, monkey and mouse. In: P. L. Kaufman, F. H. Adler, L. A. Levin, & A. Alm (eds.). *Adler's Physiology of the eye*. Elsevier Inc., 480–501.

Fu, B., Liu, Z., Zhang, H. & Gu, F. (2017). Interleukin-13 and age-related macular degeneration. *International Journal of Ophthalmology*. 10 (4). 535–540.

Fu, Q., Zhu, J. & Van Eyk, J.E. (2010). Comparison of Multiplex Immunoassay Platforms. *Clinical Chemistry*. 56 (2). 314–318.

Fujimoto, T., Sonoda, K.-H., Hijioka, K., Sato, K., Takeda, A., Hasegawa, E., Oshima, Y. & Ishibashi, T. (2010). Choroidal neovascularization enhanced by Chlamydia pneumoniae via Toll-like receptor 2 in the retinal pigment epithelium. *Investigative Ophthalmology and Visual Science*. 51 (9). 4694–702.

Fujimura, N., Xu, B., Dalman, J., Deng, H., Aoyama, K. & Dalman, R.L. (2015). CCR2 inhibition sequesters multiple subsets of leukocytes in the bone marrow. *Scientific Reports*. 5:11664.

Fujimura, S., Takahashi, H., Yuda, K., Ueta, T., Iriyama, A., Inoue, T., Kaburaki, T., Tamaki, Y., Matsushima, K. & Yanagi, Y. (2012). Angiostatic effect of CXCR3 expressed on choroidal neovascularization. *Investigative Ophthalmology and Visual Science*. 53 (4). 1999–2006.

Fuller, J. (2015). *Improving immunotherapy for Alzheimer's Disease- Determining the role of effector function in the clearance of plaques and neuro-inflammatory response*. Centre for Biological Sciences, University of Southampton, UK, PhD Thesis.

Funatsu, H., Yamashita, H., Shimizu, E., Kojima, R. & Hori, S. (2001). Relationship Between Vascular Endothelial Growth Factor and Interleukin-6 in Diabetic Retinopathy. *Retina*. 21 (5). 469–477.

Gabay, C. & Kushner, I. (1999). Acute-Phase Proteins and Other Systemic Responses to Inflammation. *New England Journal of Medicine*. 340 (6). 448–54.

Gal-Mor, O., Boyle, E.C. & Grassl, G.A. (2014). Same species, different diseases: How and why typhoidal and non-typhoidal Salmonella enterica serovars differ. *Frontiers in Microbiology*. 5:391.

Gaydos, C.A. (2000). Growth in Vascular Cells and Cytokine Production by Chlamydia pneumoniae. *Journal of Infectious Diseases*. 181 (s3). S473–S478.

Geerlings, M.J., de Jong, E.K. & den Hollander, A.I. (2017). The complement system in age-related macular degeneration: A review of rare genetic variants and implications for personalized

treatment. *Molecular Immunology*. 84. 65–76.
Germann, T., Bongartz, M., Dlugonska, H., Hess, H., Schmitt, E., Kolbe, L., Koelsch, E., Podlaski, F.J., Gately, M.K. & Ruede, E. (1995). Interleukin-12 profoundly up-regulates the synthesis of antigen-specific complement-fixing IgG2a, IgG2b and IgG3 antibody subclasses in vivo. *European Journal of Immunology*. 25 (3). 823–829.
Getts, D.R., Terry, R.L., Getts, M.T., Müller, M., Rana, S., Shrestha, B., Radford, J., Van Rooijen, N., Campbell, I.L. & King, N.J.C. (2008). Ly6c+ 'inflammatory monocytes' are microglial precursors recruited in a pathogenic manner in West Nile virus encephalitis. *Journal of Experimental Medicine*. 205 (10). 2319–2337.
Ghasemi, H., Ghazanfari, T., Yaraee, R., Faghihzadeh, S. & Hassan, Z.M. (2011). Roles of IL-8 in Ocular Inflammations: A Review. *Ocular Immunology and Inflammation*. 19 (6). 401–412.
Ginhoux, F., Greter, M., Leboeuf, M., Nandi, S., See, P., Gokhan, S., Mehler, M.F., Conway, S.J., Ng, L.G., Stanley, E.R., Samokhvalov, I.M. & Merad, M. (2010). Fate mapping reveals that adult microglia derive from primitive macrophages. *Science*. 330 (6005). 841–845.
Gleissner, C.A. (2012). Macrophage phenotype modulation by CXCL4 in atherosclerosis. *Frontiers in Physiology*. 3:1.
Goczalik, I., Ulbricht, E., Hollborn, M., Raap, M., Uhlmann, S., Weick, M., Pannicke, T., Wiedemann, P., Bringmann, A., Reichenbach, A. & Francke, M. (2008). Expression of CXCL8, CXCR1, and CXCR2 in neurons and glial cells of the human and rabbit retina. *Investigative Ophthalmology and Visual Science*. 49 (10). 4578–89.
Godbout, J.P., Chen, J., Abraham, J., Richwine, A.F., Berg, B.M., Kelley, K.W. & Johnson, R.W. (2005). Exaggerated neuroinflammation and sickness behavior in aged mice after activation of the peripheral innate immune system. *FASEB journal*. 19 (10). 1329–31.
Godinez, I., Haneda, T., Raffatellu, M., George, M.D., Paixão, T.A., Rolán, H.G., Santos, R.L., Dandekar, S., Tsolis, R.M. & Bäumler, A.J. (2008). T cells help to amplify inflammatory responses induced by Salmonella enterica serotype Typhimurium in the intestinal mucosa. *Infection and immunity*. 76 (5). 2008–17.
Gomez-Nicola, D. & Perry, V.H. (2015). Microglial Dynamics and Role in the Healthy and Diseased Brain: A Paradigm of Functional Plasticity. *Neuroscientist*. 21 (2). 169–184.
Gottfried-Blackmore, A., Sierra, A., Jellinck, P.H., McEwen, B.S. & Bulloch, K. (2008). Brain microglia express steroid-converting enzymes in the mouse. *J. Steroid Biochem. Mol. Biol.* 109 (1–2). 96–107.
Goverdhan, S., Ennis, S., Hannan, S.R., Madhusudhana, K.C., Cree, A.J., Luff, A.J. & Lotery, A.J. (2008). Interleukin-8 promoter polymorphism -251A/T is a risk factor for age-related macular degeneration. *British journal of ophthalmology*. 92 (4). 537–40.
Grabert, K., Michoel, T., Karavolos, M.H., Clohisey, S., Baillie, J.K., Stevens, M.P., Freeman, T.C., Summers, K.M. & McColl, B.W. (2016). Microglial brain region−dependent diversity and selective regional sensitivities to aging. *Nature Neuroscience*. 19 (3). 504–516.
Greenwood, J., Wang, Y. & Calder, V.L. (1995). Lymphocyte adhesion and transendothelial migration in the central nervous system: the role of LFA-1, ICAM-1, VLA-4 and VCAM-1. off. *Immunology*. 86 (3). 408–15.
De Groote, D., Zangerle, P.F., Gevaert, Y., Fassotte, M.F., Beguin, Y., Noizat-Pirenne, F., Pirenne, J., Gathy, R., Lopez, M., Dehart, I., Igot, D., Baudrihaye, M., Delacroix, D. & Franchimont, P. (1992). Direct stimulation of cytokines (IL-1β, TNF-α, IL-6, IL-2, IFN-γ and GM-CSF) in whole blood. I. Comparison with isolated PBMC stimulation. *Cytokine*. 4 (3). 239–248.
Grubeck-Loebenstein, B., Della Bella, S., Iorio, A.M., Michel, J.-P., Pawelec, G. & Solana, R. (2009). Immunosenescence and vaccine failure in the elderly. *Aging clinical and experimental research*. 21 (3). 201–9.
Grunin, M., Burstyn-Cohen, T., Hagbi-Levi, S., Peled, A. & Chowers, I. (2012). Chemokine receptor expression in peripheral blood monocytes from patients with neovascular age-related macular degeneration. *Investigative Ophthalmology and Visual Science*. 53 (9). 5292–300.
Gu, X., Meer, S.G., Miyagi, M., Rayborn, M.E., Hollyfield, J.G., Crabb, J.W. & Salomon, R.G. (2003). Carboxyethylpyrrole Protein Adducts and Autoantibodies, Biomarkers for Age-related Macular Degeneration. *Journal of Biological Chemistry*. 278 (43). 42027–42035.

Gupta, D., Gupta, V., Singh, V., Chawla, S., Parveen, F., Agrawal, S. & Phadke, S.R. (2014). Study of polymorphisms in CX3CR1, PLEKHA1 and VEGF genes as risk factors for age-related macular degeneration in indian patients. *Archives of Medical Research*. 45 (6). 489–494.

Gupta, N., Brown, K.E. & Milam, A.H. (2003). Activated microglia in human retinitis pigmentosa, late-onset retinal degeneration, and age-related macular degeneration. *Experimental Eye Research*. 76 (4). 463–471.

Guymer, R.H., Cipriani, T., Rittenhouse, K.D., Lim, L., Robman, L.D., Li, W., Wang, W., Deng, S. & Banerjee, P. (2015). Plasma levels of amyloid beta and other proinflammatory mediators in patients with age-related macular degeneration. *Graefe's Archive for Clinical and Experimental Ophthalmology*. 253 (8). 1347–1354.

Haas, P., Aggermann, T., Nagl, M., Steindl-Kuscher, K., Krugluger, W. & Binder, S. (2011). Implication of CD21, CD35, and CD55 in the pathogenesis of age-related macular degeneration. *American Journal of Ophthalmology*. 152 (3). 396–399.

Haas, P., Kubista, K.E., Krugluger, W., Huber, J. & Binder, S. (2015). Impact of visceral fat and pro-inflammatory factors on the pathogenesis of age-related macular degeneration. *Acta Ophthalmologica*. 93 (6). 533–538.

Haas, P., Steindl, K., Schmid-Kubista, K.E., Aggermann, T., Krugluger, W., Hageman, G.S. & Binder, S. (2009). Complement factor H gene polymorphisms and Chlamydia pneumoniae infection in age-related macular degeneration. *Eye*. 23 (12). 2228–32.

Hageman, G.S., Gaehrs, K., Johnson, L. V & Anderson, D.H. (2007). Age-related macular degeneration (AMD). In: *Webvision: The Organisation of the retina and visual system*. [Online]. Available from: http://webvision.med.utah.edu/book/part-xii-cell-biology-of-retinal-degenerations/age-related-macular-degeneration-amd/.

Hakobyan, S., Harris, C.L., Tortajada, A., Dejorge, E.G., Garcia-Layana, A., Fernandez-Robredo, P., De Cordoba, S.R. & Paul Morgan, B. (2008). Measurement of factor H variants in plasma using variant-specific monoclonal antibodies: Application to assessing risk of age-related macular degeneration. *Investigative Ophthalmology and Visual Science*. 49 (5). 1983–1990.

Han, K. & Park, J.-B. (2017). Association between oral health behavior and periodontal disease among Korean adults: The Korea national health and nutrition examination survey. *Medicine*. 96 (7). e6176.

Handa, J.T., Verzijl, N., Matsunaga, H., Aotaki-Keen, A., Lutty, G.A., Koppele, J.M., Miyata, T. & Hjelmeland, L.M. (2016). Increase in the Advanced Glycation End Product Pentosidine in Bruch's Membrane with Age. *Investigative Ophthalmology and Visual Science*. 40 (3). 775–779.

Harker, J.A., Godlee, A., Wahlsten, J.L., Lee, D.C.P., Thorne, L.G., Sawant, D., Tregoning, J.S., Caspi, R.R., Bukreyev, A., Collins, P.L. & Openshaw, P.J.M. (2010). Interleukin 18 Coexpression during Respiratory Syncytial Virus Infection Results in Enhanced Disease Mediated by Natural Killer Cells. *Journal of Virology*. 84 (8). 4073–4082.

Harris, T.B., Ferrucci, L., Tracy, R.P., Corti, M.C., Wacholder, S., Ettinger, W.H., Heimovitz, H., Cohen, H.J. & Wallace, R. (1999). Associations of elevated interleukin-6 and C-reactive protein levels with mortality in the elderly. *American Journal of Medicine*. 106 (5). 506–512.

Hart, A.D., Wyttenbach, A., Hugh Perry, V. & Teeling, J.L. (2012). Age related changes in microglial phenotype vary between CNS regions: Grey versus white matter differences. *Brain, Behavior, and Immunity*. 26 (5). 754–765.

Hart, B.L. (1988). Biological basis of the behavior of sick animals. *Neuroscience and Biobehavioral Reviews*. 12 (2). 123–137.

Hecker, L.A., Edwards, A.O., Ryu, E., Tosakulwong, N., Baratz, K.H., Brown, W.L., Issa, P.C., Scholl, H.P., Pollok-Kopp, B., Schmid-Kubista, K.E., Bailey, K.R. & Oppermann, M. (2009). Genetic control of the alternative pathway of complement in humans and age-related macular degeneration. *Human Molecular Genetics*. 19 (1). 209–215.

Heidari, B. (2012). The importance of C-reactive protein and other inflammatory markers in patients with chronic obstructive pulmonary disease. *Caspian Journal of Internal Medicine*. 3 (2). 428–435.

Herrmann, R., Lobanova, E.S., Hammond, T., Kessler, C., Burns, M.E., Frishman, L.J. & Arshavsky,

V.Y. (2010). Phosducin regulates transmission at the photoreceptor-to-ON-bipolar cell synapse. *Journal of Neuroscience*. 30 (9). 3239–3253.

Hildebrand, G.D. & Fielder, A.R. (2011). Anatomy and physiology of the retina. In: J. Reynolds & S. Olitsky (eds.). *Pediatric Retina*. Berlin: Springer, 39–65.

Hoeffel, G., Chen, J., Lavin, Y., Low, D., Almeida, F.F., See, P., Beaudin, A.E., Lum, J., Low, I., Forsberg, E.C., Poidinger, M., Zolezzi, F., Larbi, A., Ng, L.G., Chan, J.K.Y., Greter, M., Becher, B., Samokhvalov, I.M., Merad, M. & Ginhoux, F. (2015). C-Myb+ Erythro-Myeloid Progenitor-Derived Fetal Monocytes Give Rise to Adult Tissue-Resident Macrophages. *Immunity*. 42 (4). 665–678.

Hogan, M. (1972). Role of the retinal pigment epithelium in macular disease. *Trans Am Acad Ophthalmol Otolaryngol*. 76 (1). 64–80.

Hol, J., Wilhelmsen, L. & Haraldsen, G. (2010). The murine IL-8 homologues KC, MIP-2, and LIX are found in endothelial cytoplasmic granules but not in Weibel-Palade bodies. *Journal of leukocyte biology*. 87 (3). 501–8.

Hollander, H., Makarov, F., Dreher, Z., Driel, D.V.A.N., Chan-ling, T. & Stone, J. (1991). Structure of the Macroglia of the Retina: Sharing and Division of Labour Between Astrocytes and Muller Cells. *Journal of Comparative Neurology*. 313. 587–603.

Hollyfield, J.G., Bonilha, V.L., Rayborn, M.E., Yang, X., Shadrach, K., Lu, L., Ufret, R.L., Salomon, R.G. & Perez, V.L. (2008). Oxidative damage-induced inflammation initiates age-related macular degeneration. *Nature medicine*. 14 (2). 194–198.

Hollyfield, J.G., Perez, V.L. & Salomon, R.G. (2010). A hapten generated from an oxidation fragment of docosahexaenoic acid is sufficient to initiate age-related macular degeneration. *Molecular Neurobiology*. 41 (2–3). 290–298.

Holmes, C., Cunningham, C., Zotova, E., Woolford, J., Dean, C., Kerr, S., Culliford, D. & Perry, V.H. (2009). Systemic inflammation and disease progression in Alzheimer disease. *Neurology*. 73 (10). 768–74.

Holt, P.G. (1987). Immune and inflammatory function in cigarette smokers. *Thorax*. 42 (4). 241–9.

Holt, P.G. & Keast, D. (1977). Environmentally induced changes in immunological function: acute and chronic effects of inhalation of tobacco smoke and other atmospheric contaminants in man and experimental animals. *Bacteriological reviews*. 41 (1). 205–16.

Holz, F.G., Bindewald-Wittich, A., Fleckenstein, M., Dreyhaupt, J., Scholl, H.P.N. & Schmitz-Valckenberg, S. (2007). Progression of Geographic Atrophy and Impact of Fundus Autofluorescence Patterns in Age-related Macular Degeneration. *American Journal of Ophthalmology*. 143 (3). 463–472.

de Hoz, R., Rojas, B., Ramirez, A.I., Salazar, J.J., Gallego, B.I., Trivino, A. & Ramirez, J.M. (2016). Retinal macroglial responses in health and disease. *BioMed Research International*. 2954721.

Hu, P., Pollard, J.D. & Chan-Ling, T. (2000). Breakdown of the blood-retinal barrier induced by activated T cells of nonneural specificity. *American Journal of Pathology*. 156 (4). 1139–1149.

Huang, E.J.-C., Wu, S.-H., Lai, C.-H., Kuo, C.-N., Wu, P.-L., Chen, C.-L., Chen, C.-Y., King, Y.-C. & Wu, P.-C. (2014). Prevalence and risk factors for age-related macular degeneration in the elderly Chinese population in south-western Taiwan: the Puzih eye study. *Eye*. 28 (6). 705–714.

Hübener, M. (2003). Mouse visual cortex. *Current Opinion in Neurobiology*. 13 (4). 413–420.

Hussain, R., Dawood, G., Abrar, N., Toossi, Z., Minai, A., Dojki, M. & Ellner, J.J. (1995). Selective increases in antibody isotypes and immunoglobulin G subclass responses to secreted antigens in tuberculosis patients and healthy household contacts of the patients. *Clinical and diagnostic laboratory immunology*. 2 (6). 726–32.

Ide, M., Harris, M., Stevens, A., Sussams, R., Hopkins, V., Culliford, D., Fuller, J., Ibbett, P., Raybould, R., Thomas, R., Puentener, U., Teeling, J.L., Perry, V.H. & Holmes, C. (2016). Periodontitis and cognitive decline in Alzheimer's disease. *PLoS ONE*. 11 (3). e0151081.

Ilhan, N., Daglioglu, M.C., Ilhan, O., Coskun, M., Tuzcu, E.A., Kahraman, H. & Keskin, U. (2015). Assessment of Neutrophil/Lymphocyte Ratio in Patients with Age-related Macular Degeneration. *Ocular Immunology and Inflammation*. 23 (4). 287–290.

Ishida, O., Oku, H., Ikeda, T., Nishimura, M., Kawagoe, K. & Nakamura, K. (2003). Is Chlamydia pneumoniae infection a risk factor for age related macular degeneration? *British journal of*

ophthalmology. 87. 523–524.
Iwasaki, A. & Medzhitov, R. (2004). Toll-like receptor control of the adaptive immune responses. *Nature immunology*. 5 (10). 987–95.
Jacobs, G.H. (1993). The distribution and nature of colour vision among the mammals. *Biol Rev Camb Philos Soc*. 68 (3). 413–471.
Jadhav, A.P., Roesch, K. & Cepko, C.L. (2009). Development and neurogenic potential of Muller glial cells in the vertebrate retina. *Progress in Retinal and Eye Research*. 28 (4). 249–262.
Jeon, C.J., Strettoi, E. & Masland, R.H. (1998). The major cell populations of the mouse retina. *Journal of Neuroscience*. 18 (21). 8936–8946.
Jiang, J., Gross, D., Elbaum, P. & Murasko, D.M. (2007). Aging affects initiation and continuation of T cell proliferation. *Mechanisms of ageing and development*. 128 (4). 332–9.
Johnson, E.J. (2005). Obesity, lutein metabolism, and age-related macular degeneration: a web of connections. *Nutrition reviews*. 63 (1). 9–15.
Johnson, L. V, Ozaki, S., Staples, M.K., Erickson, P.A. & Anderson, D.H. (2000). A Potential Role for Immune Complex Pathogenesis in Drusen Formation. *Experimental Eye Research*. 70 (4). 441–449.
Jonas, J.B., Tao, Y., Neumaier, M. & Findeisen, P. (2012). Cytokine concentration in aqueous humour of eyes with exudative age-related macular degeneration. *Acta Ophthalmologica*. 90 (5). 381–388.
de Jong, P.T.V.M. (2006). Age-related macular degeneration. *New England Journal of Medicine*. 355. 1474–85.
Jovicic, N., Jeftic, I., Jovanovic, I., Radosavljevic, G., Arsenijevic, N., Lukic, M.L. & Pejnovic, N. (2015). Differential immunometabolic phenotype in Th1 and Th2 dominant mouse strains in response to high-fat feeding. *PLoS ONE*. 10 (7). e0134089.
Juel, H.B., Faber, C., Munthe-Fog, L., Bastrup-Birk, S., Reese-Petersen, A.L., Falk, M.K., Singh, A., Rørensen, T.L., Garred, P. & Nissen, M.H. (2015). Systemic and ocular long pentraxin 3 in patients with age-related macular degeneration. *PLoS ONE*. 10 (7). e0132800.
Jung, S.H., Kim, K.A., Sohn, S.W. & Yang, S.J. (2014). Association of aqueous humor cytokines with the development of retinal ischemia and recurrent macular edema in retinal vein occlusion. *Investigative Ophthalmology and Visual Science*. 55 (4). 2290–2296.
Kadl, A., Meher, A.K., Sharma, P.R., Lee, M.Y., Doran, A.C., Johnstone, S.R., Elliott, M.R., Gruber, F., Han, J., Chen, W., Kensler, T., Ravichandran, K.S., Isakson, B.E., Wamhoff, B.R. & Leitinger, N. (2010). Identification of a novel macrophage phenotype that develops in response to atherogenic phospholipids via Nrf2. *Circulation Research*. 107 (6). 737–746.
Kalayoglu, M. V, Bula, D., Arroyo, J.G., Gragoudas, E.S., D'Amico, D. & Miller, J.W. (2005). Identification of Chlamydia pneumoniae within human choroidal neovascular membranes secondary to age-related macular degeneration. *Graefe's archive for clinical and experimental ophthalmology*. 243 (11). 1080–90.
Kalayoglu, M. V, Galvan, C., Mahdi, O.S., Byrne, G.I., Mansour, S. & Sciences, C. (2003). Serological Association Between Chlamydia pneumoniae infection and age-related macular degeneration. *Archives of ophthalmology*. 121. 478–482.
van Kampen, E., Jaminon, A., van Berkel, T.J.C. & Van Eck, M. (2014). Diet-induced (epigenetic) changes in bone marrow augment atherosclerosis. *Journal of leukocyte biology*. 96. 833–841.
Kan, M., Liu, F., Weng, X., Ye, J., Wang, T., Xu, M., He, L. & Liu, Y. (2014). Association study of newly identified age-related macular degeneration susceptible loci SOD2, MBP, and C8orf42 in Han Chinese population. *Diagnostic pathology*. 9:73.
Kaneko, H., Dridi, S., Tarallo, V., Gelfand, B.D., Fowler, B.J., Karikó, K., Yoo, J.W., Lee, D., Hadziahmetovic, M. & Ambati, J. (2011). DICER1 deficit induces Alu RNA toxicity in age-related macular degeneration. *Nature*. 471 (7338). 325–330.
Karlstetter, M., Scholz, R., Rutar, M., Wong, W.T., Provis, J.M. & Langmann, T. (2015). Retinal microglia: Just bystander or target for therapy? *Progress in Retinal and Eye Research*. 45. 30–57.
Karsten, C.M. & Köhl, J. (2012). The immunoglobulin, IgG Fc receptor and complement triangle in

autoimmune diseases. *Immunobiology*. 217 (11). 1067–79.
Kaufmann, S.H.E. (2007). The contribution of immunology to the rational design of novel antibacterial vaccines. *Nature Reviews. Microbiology*. 5. 491–504.
Kauppinen, A., Niskanen, H., Suuronen, T., Kinnunen, K., Salminen, A. & Kaarniranta, K. (2012). Oxidative stress activates NLRP3 inflammasomes in ARPE-19 cells--implications for age-related macular degeneration (AMD). *Immunology letters*. 147 (1–2). 29–33.
Kavanagh, D., Yu, Y., Schramm, E.C., Triebwasser, M., Wagner, E.K., Raychaudhuri, S., Daly, M.J., Atkinson, J.P. & Seddon, J.M. (2015). Rare genetic variants in the CFI gene are associated with advanced age-related macular degeneration and commonly result in reduced serum factor I levels. *Human Molecular Genetics*. 24 (13). 3861–3870.
Kawai, T., Adachi, O., Ogawa, T., Takeda, K. & Akira, S. (1999). Unresponsiveness of MyD88-deficient mice to endotoxin. *Immunity*. 11 (1). 115–122.
Kayakabe, K., Kuroiwa, T., Sakurai, N., Ikeuchi, H., Kadiombo, A.T., Sakairi, T., Kaneko, Y., Maeshima, A., Hiromura, K. & Nojima, Y. (2012). Interleukin-1β measurement in stimulated whole blood cultures is useful to predict response to anti-TNF therapies in rheumatoid arthritis. *Rheumatology*. 51 (9). 1639–1643.
Keestra-Gounder, A.M., Tsolis, R.M. & Bäumler, A.J. (2015). Now you see me, now you don't: the interaction of Salmonella with innate immune receptors. *Nature Reviews. Microbiology*. 13 (4). 206–216.
Keren-Shaul, H., Spinrad, A., Weiner, A., Matcovitch-Natan, O., Dvir-Szternfeld, R., Ulland, T.K., David, E., Baruch, K., Lara-Astaiso, D., Toth, B., Itzkovitz, S., Colonna, M., Schwartz, M. & Amit, I. (2017). A Unique Microglia Type Associated with Restricting Development of Alzheimer's Disease. *Cell*. 169 (7). 1276–1290.
Kerr, E.C., Copland, D.A., Dick, A.D. & Nicholson, L.B. (2008a). The dynamics of leukocyte infiltration in experimental autoimmune uveoretinitis. *Progress in Retinal and Eye Research*. 27 (5). 527–535.
Kerr, E.C., Raveney, B.J.E., Copland, D.A., Dick, A.D. & Nicholson, L.B. (2008b). Analysis of retinal cellular infiltrate in experimental autoimmune uveoretinitis reveals multiple regulatory cell populations. *Journal of Autoimmunity*. 31 (4). 354–361.
Kessler, W., Jantos, C.A., Dreier, J. & Pavlovic, S. (2006). Chlamydia pneumoniae is not detectable in subretinal neovascular membranes in the exudative stage of age-related macular degeneration. *Acta Ophthalmologica Scandinavica*. 84 (3). 333–7.
Kezic, J., Xu, H., Chinnery, H.R., Murphy, C.C. & McMenamin, P.G. (2008). Retinal Microglia and Uveal Tract Dendritic Cells and Macrophages Are Not CX3CR1 Dependent in Their Recruitment and Distribution in the Young Mouse Eye. *Investigative Ophthalmology and Visual Science*. 49 (4). 1599–1608.
Khan, J.C., Shahid, H., Thurlby, D.A., Bradley, M., Clayton, D.G., Moore, A.T., Bird, A.C. & Yates, J.R.W. (2006). Age related macular degeneration and sun exposure, iris colour, and skin sensitivity to sunlight. *British Journal of Ophthalmology*. 90 (1). 29–32.
Khandaker, G.M. & Dantzer, R. (2016). Is there a role for immune-to-brain communication in schizophrenia? *Psychopharmacology*. 233 (9). 1559–1573.
Khandhadia, S., Foster, S., Cree, A.J., Griffiths, H., Osmond, C., Goverdhan, S. & Lotery, A. (2012). Chlamydia infection status, genotype, and age-related macular degeneration. *Molecular vision*. 18. 29–37.
Kim, O.Y., Chae, J.S., Paik, J.K., Seo, H.S., Jang, Y., Cavaillon, J.M. & Lee, J.H. (2012). Effects of aging and menopause on serum interleukin-6 levels and peripheral blood mononuclear cell cytokine production in healthy nonobese women. *Age*. 34 (2). 415–425.
Kim, Y., Tarallo, V., Kerur, N., Yasuma, T., Gelfand, B.D., Bastos-Carvalho, A., Hirano, Y., Yasuma, R., Mizutani, T., Fowler, B.J., Li, S., Kaneko, H., Bogdanovich, S., Ambati, B.K., Hinton, D.R., Hauswirth, W.W., Hakem, R., Wright, C. & Ambati, J. (2014). DICER1/ Alu RNA dysmetabolism induces Caspase-8–mediated cell death in age-related macular degeneration. *Proceedings of the National Academy of Sciences*. 111 (45). 16082–16087.
Kimura, K., Isashiki, Y., Sonoda, S., Kakiuchi-Matsumoto, T. & Ohba, N. (2000). Genetic Association of Manganese Superoxide Dismutase With Exudative Age-related Macular Degeneration.

American journal of Ophthalmology. 130 (6). 769–773.

King, T.E., Savici, D. & Campbell, P.A. (1988). Phagocytosis and killing of listeria monocytogenes by alveolar macrophages: Smokers versus nonsmokers. *Journal of Infectious Diseases*. 158 (6). 1309–1316.

Klaver, C.C., Wolfs, R.C.W., Assink, J., van Duijn, C.M., Hofman, A. & de Jong, P.T.V.M. (1998). Genetic Risk of Age-related Maculopathy. *Archives of ophthalmology*. 116. 1646–1651.

Klein, B.E.K. (2001). Risk of Incident Age-related Eye Diseases in People with an Affected Sibling: The Beaver Dam Eye Study. *American Journal of Epidemiology*. 154 (3). 207–211.

Klein, M.L., Ferris, F.L., Armstrong, J., Hwang, T.S., Chew, E.Y., Bressler, S.B. & Chandra, S.R. (2008). Retinal Precursors and the Development of Geographic Atrophy in Age-Related Macular Degeneration. *Ophthalmology*. 115 (6). 1026–1031.

Klein, R., Klein, B.E.K., Knudtson, M.D., Wong, T.Y., Cotch, M.F., Liu, K., Burke, G., Saad, M.F. & Jacobs, D.R. (2006). Prevalence of age-related macular degeneration in 4 racial/ethnic groups in the multi-ethnic study of atherosclerosis. *Ophthalmology*. 113 (3). 373–380.

Klein, R., Klein, B.E.K., Knudtson, M.D., Wong, T.Y., Shankar, A. & Tsai, M.Y. (2005). Systemic markers of inflammation, endothelial dysfunction, and age-related maculopathy. *American Journal of Ophthalmology*. 140 (1). 35–44.

Klein, R., Myers, C.E., Cruickshanks, K.J., Gangnon, R.E., Danforth, L.G., Sivakumaran, T.A., Iyengar, S.K., Tsai, M.Y. & Klein, B.E.K. (2014). Markers of Inflammation, Oxidative Stress and Endothelial Dysfunction and the 20-year Cumulative Incidence of Early Age-Related Macular Degeneration: The Beaver Dam Eye Study. *JAMA Opthalmology*. 132 (4). 446–455.

Kowalski, M.L., Bielecka-Kowalska, A., Oszajca, K., Eusebio, M., Jaworski, P., Bartkowiak, J. & Szemraj, J. (2010). Manganese superoxide dismutase (MnSOD) gene (Ala-9Val, Ile58Thr) polymorphism in patients with age-related macular degeneration (AMD). *Med Sci Monit*. 16 (4). CR190-6.

Kowalski, M.L., Wolska, A., Grzegorczyk, J., Hilt, J., Jarzebska, M., Drobniewski, M., Synder, M. & Kurowski, M. (2008). Increased responsiveness to Toll-like receptor 4 stimulation in peripheral blood mononuclear cells from patients with recent onset rheumatoid arthritis. *Mediators of Inflammation*. 2008. 132732.

Kwak, N., Okamoto, N., Wood, J.M. & Campochiaro, P.A. (2000). VEGF is major stimulator in model of choroidal neovascularization. *Investigative Ophthalmology and Visual Science*. 41 (10). 3158–3164.

Kwok, Y.H., Hutchinson, M.R., Gentgall, M.G. & Rolan, P.E. (2012). Increased Responsiveness of Peripheral Blood Mononuclear Cells to In Vitro TLR 2, 4 and 7 Ligand Stimulation in Chronic Pain Patients. *PLoS ONE*. 7 (8). e44232.

Lad, E.M., Cousins, S.W., Van Arnam, J.S. & Proia, A.D. (2015). Abundance of infiltrating CD163+ cells in the retina of postmortem eyes with dry and neovascular age-related macular degeneration. *Graefe's Archive for Clinical and Experimental Ophthalmology*. 253 (11). 1941–1945.

Lad, E.M., Cousins, S.W. & Proia, A.D. (2016). Identity of pigmented subretinal cells in age-related macular degeneration. *Graefe's Archive for Clinical and Experimental Ophthalmology*. 254 (6). 1239–1241.

Lambert, V., Lecomte, J., Hansen, S., Blacher, S., Gonzalez, M.-L.A., Struman, I., Sounni, N.E., Rozet, E., de Tullio, P., Foidart, J.M., Rakic, J.-M. & Noel, A. (2013). Laser-induced choroidal neovascularization model to study age-related macular degeneration in mice. *Nature protocols*. 8 (11). 2197–211.

Landsman, L., Liat, B.O., Zernecke, A., Kim, K.W., Krauthgamer, R., Shagdarsuren, E., Lira, S.A., Weissman, I.L., Weber, C. & Jung, S. (2009). CX3CR1 is required for monocyte homeostasis and atherogenesis by promoting cell survival. *Blood*. 113 (4). 963–972.

Langmann, T. (2007). Microglia activation in retinal degeneration. *Journal of Leukocyte Biology*. 81 (6). 1345–1351.

Lapaque, N., Walzer, T., Méresse, S., Vivier, E. & Trowsdale, J. (2009). Interactions between human NK cells and macrophages in response to Salmonella infection. *Journal of immunology*. 182 (7). 4339–48.

Latz, E., Xiao, T.S. & Stutz, A. (2013). Activation and regulation of the inflammasomes. *Nature Reviews. Immunology*. 13 (6). 397–411.

Lawson, L.J., Perry, V.H., Dri, P. & Gordon, S. (1990). Heterogeneity in the distribution and morphology of microglia in the normal adult mouse brain. *Neuroscience*. 39 (1). 151–170.

Lechner, J., Chen, M., Hogg, R.E., Toth, L., Silvestri, G., Chakravarthy, U. & Xu, H. (2015). Alterations in Circulating Immune Cells in Neovascular Age-Related Macular Degeneration. *Scientific Reports*. 5:16754.

Lechner, J., Chen, M., Hogg, R.E., Toth, L., Silvestri, G., Chakravarthy, U. & Xu, H. (2017). Peripheral blood mononuclear cells from neovascular age-related macular degeneration patients produce higher levels of chemokines CCL2 (MCP-1) and CXCL8 (IL-8). *Journal of Neuroinflammation*. 14:42.

Lefeber, D.J., Benaissa-Trouw, B., Vliegenthart, J.F.G., Kamerling, J.P., Jansen, W.T.M., Kraaijeveld, K. & Snippe, H. (2003). Th1-Directing Adjuvants Increase the Immunogenicity of Oligosaccharide-Protein Conjugate Vaccines Related to Streptococcus pneumoniae Type 3. *Infection and Immunity*. 71 (12). 6915–6920.

Leung, I. & Snodderly, M. (2006). *Central Retina*. [Online]. 2006. Snodderly Lab Image Gallery. Available from: http://www.sbs.utexas.edu/SnodderlyLab/gallery.html. [Accessed: 1 January 2017].

Li, D., Peng, X. & Sun, H. (2015). Association of CX3CR1 (V249I and T280M) polymorphisms with age-related macular degeneration: A meta-analysis. *Canadian Journal of Ophthalmology*. 50 (6). 451–460.

Li, J., Baud, O., Vartanian, T., Volpe, J.J. & Rosenberg, P.A. (2005). Peroxynitrite generated by inducible nitric oxide synthase and NADPH oxidase mediates microglial toxicity to oligodendrocytes. *Proceedings of the National Academy of Sciences*. 102 (28). 9936–9941.

Liang, K.J., Lee, J.E., Wang, Y.D., Ma, W., Fontainhas, A.M., Fariss, R.N. & Wong, W.T. (2009). Regulation of dynamic behavior of retinal microglia by CX3CR1 signaling. *Investigative Ophthalmology and Visual Science*. 50 (9). 4444–4451.

Liou, L.B. (2003). Different monocyte reaction patterns in newly diagnosed, untreated rheumatoid arthritis and lupus patients probaly confer disparate CRP levels. *Clinical and experimental rheumatology*. 21. 437–444.

Litts, K.M., Wang, X., Clark, M.E., Owsley, C., Freund, K.B., Curcio, C.A. & Zhang, Y. (2017). Exploring Photoreceptor Reflectivity Through Multimodal Imaging of Outer Retinal Tubulation in Advanced Age-Related Macular Degeneration. *Retina*. 37 (5). 978–988.

Liu, B., Wei, L., Meyerle, C., Tuo, J., Sen, H.N., Li, Z., Chakrabarty, S., Agron, E., Chan, C.-C., Klein, M.L., Chew, E.Y., Ferris, F. & Nussenblatt, R.B. (2011a). Complement component C5a promotes expression of IL-22 and IL-17 from human T cells and its implication in age-related macular degeneration. *Journal of translational medicine*. 9. 111.

Liu, J., Jha, P., Lyzogubov, V. V., Tytarenko, R.G., Bora, N.S. & Bora, P.S. (2011b). Relationship between complement membrane attack complex, chemokine (C-C motif) ligand 2 (CCL2) and vascular endothelial growth factor in mouse model of laser-induced choroidal neovascularization. *Journal of Biological Chemistry*. 286 (23). 20991–21001.

Liu, R.T., Gao, J., Cao, S., Sandhu, N., Cui, J.Z., Chou, C.L., Fang, E. & Matsubara, J.A. (2013). Inflammatory Mediators Induced by Amyloid-Beta in the Retina and RPE In Vivo: Implications for Inflammasome Activation in Age-Related Macular Degeneration. *Investigative Ophthalmology and Visual Science visual science*. 54 (3). 2225–37.

Liu, X., Ye, F., Xiong, H., Hu, D., Limb, G.A., Xie, T., Peng, L., Yang, W., Sun, Y., Zhou, M., Song, E. & Zhang, D.Y. (2014). IL-1beta Upregulates IL-8 Production in Human Muller Cells Through Activation of the p38 MAPK and ERK1/2 Signaling Pathways. *Inflammation*. 37 (5). 1486–1495.

Liyanage, S.E., Gardner, P.J., Ribeiro, J., Cristante, E., Sampson, R.D., Luhmann, U.F.O., Ali, R.R. & Bainbridge, J.W.B. (2016). Flow cytometric analysis of inflammatory and resident myeloid populations in mouse ocular inflammatory models. *Experimental Eye Research*. 151. 160–170.

Locati, M., Mantovani, A. & Sica, A. (2013). *Macrophage Activation and Polarization as an*

Adaptive Component of Innate Immunity. Elsevier Inc.

London, A., Cohen, M. & Schwartz, M. (2013). Microglia and monocyte-derived macrophages: functionally distinct populations that act in concert in CNS plasticity and repair. *Frontiers in cellular neuroscience*. 7:34.

Loos, C.M. van der (2008). Multiple Immunoenzyme Staining: Methods and Visualizations for the Observation With Spectral Imaging. *Journal of Histochemistry & Cytochemistry*. 56 (4). 313–328.

Lu, J., Marjon, K.K.D., Mold, C., Du Clos, T.W.T. & Sun, P.P.D. (2012). Pentraxins and Fc receptors. *Immunological Reviews*. 250 (1). 230–238.

Lückoff, A., Scholz, R., Sennlaub, F., Xu, H. & Langmann, T. (2017). Comprehensive analysis of mouse retinal mononuclear phagocytes. *Nature Protocols*. 12 (6). 1136–1150.

Lueck, K., Hennig, M., Lommatzsch, A., Pauleikhoff, D. & Wasmuth, S. (2012). Complement and UV-Irradiated Photoreceptor Outer Segments Increase the Cytokine Secretion by Retinal Pigment Epithelial Cells. *Investigative Ophthalmology and Visual Science*. 53. 1406–1413.

Luger, D., Silver, P.B., Tang, J., Cua, D., Chen, Z., Iwakura, Y., Bowman, E.P., Sgambellone, N.M., Chan, C.-C. & Caspi, R.R. (2008). Either a Th17 or a Th1 effector response can drive autoimmunity: conditions of disease induction affect dominant effector category. *Journal of Experimental Medicine*. 205 (4). 799–810.

Luhmann, U.F.O., Carvalho, L.S., Robbie, S.J., Bainbridge, J.W.B. & Ali, R.R. (2013a). Reply to comment on 'Ccl2, Cx3cr1 and Ccl2/Cx3cr1 chemokine deficiencies are not sufficient to cause age-related retinal degeneration' by Luhmann et al. *Experimental Eye Research*. 111. 136.

Luhmann, U.F.O., Carvalho, L.S., Robbie, S.J., Cowing, J.A., Duran, Y., Munro, P.M.G., Bainbridge, J.W.B. & Ali, R.R. (2013b). Ccl2, Cx3cr1 and Ccl2/Cx3cr1 chemokine deficiencies are not sufficient to cause age-related retinal degeneration. *Experimental Eye Research*. 107. 80–87.

Lumbroso, B. & Rispoli, M. (2012). *Practical Handbook of OCT*. New Delhi, India: Jaypee Brothers Medical Publishers.

Lundvig, D.M.S., Immenschuh, S. & Wagener, F.A.D.T.G. (2012). Heme oxygenase, inflammation, and fibrosis: The good, the bad, and the ugly? *Frontiers in Pharmacology*. 3:81.

Lyzogubov, V. V, Bora, P.S., Wu, X., Horn, L.E., de Roque, R., Rudolf, X. V., Atkinson, J.P. & Bora, N.S. (2016). The Complement Regulatory Protein CD46 Deficient Mouse Spontaneously Develops Dry-Type Age-Related Macular Degeneration–Like Phenotype. *American Journal of Pathology*. 186 (8). 2088–2104.

Lyzogubov, V. V, Wu, X., Jha, P., Tytarenko, R., Triebwasser, M., Kolar, G., Bertram, P., Bora, P.S., Atkinson, J.P. & Bora, N.S. (2014). Complement regulatory protein CD46 protects against choroidal neovascularization in mice. *American Journal of Pathology*. 184 (9). 2537–2548.

Ma, B., Dang, G., Yang, S., Duan, L. & Zhang, Y. (2015). CX3CR1 polymorphisms and the risk of age-related macular degeneration. *International Journal of Clinical and Experimental Pathology*. 8 (8). 9592–9596.

Ma, M.W., Wang, J., Zhang, Q., Wang, R., Dhandapani, K.M., Vadlamudi, R.K. & Brann, D.W. (2017). NADPH oxidase in brain injury and neurodegenerative disorders. *Molecular Neurodegeneration*. 12:7.

Macdonald, R.B., Randlett, O., Oswald, J., Yoshimatsu, T., Franze, K. & Harris, W.A. (2015). Müller glia provide essential tensile strength to the developing retina. *Journal of cell biology*. 210 (7). 1075–1083.

Machalińska, A., Lejkowska, R., Duchnik, M., Kawa, M., Rogińska, D., Wiszniewska, B. & Machaliński, B. (2014). Dose-Dependent Retinal Changes Following Sodium Iodate Administration: Application of Spectral-Domain Optical Coherence Tomography for Monitoring of Retinal Injury and Endogenous Regeneration. *Current Eye Research*. 39 (10). 1033–1041.

Machalińska, A., Lubiński, W., Kłos, P., Kawa, M., Baumert, B., Penkala, K., Grzegrzółka, R., Karczewicz, D., Wiszniewska, B. & MacHaliński, B. (2010). Sodium iodate selectively injuries the posterior pole of the retina in a dose-dependent manner: Morphological and electrophysiological study. *Neurochemical Research*. 35 (11). 1819–1827.

Machalińska, A., Safranow, K., Dziedziejko, V., Mozolewska-Piotrowska, K., Paczkowska, E., Klos, P., Pius, E., Grymula, K., Wiszniewska, B., Karczewicz, D. & Machalinski, B. (2011). Different populations of circulating endothelial cells in patients with age-related macular degeneration: a novel insight into pathogenesis. *Investigative Ophthalmology and Visual Science*. 52 (1). 93–100.

Magdelaine-Beuzelin, C., Pinault, C. & Paintaud, G. (2010). Old is new again. *mAbs*. 2 (2). 176–180.

Maguire, M.G., Shaffer, J., Ying, G., Chakravarthy, U., Berg, K., Bragadóttir, R., Decullier, E., Huot, L., Kodjikian, L., Martin, D.F., Reeves, B.C., Rogers, C.A., Schauwvlieghe, A.-S.M.E. & Schlingemann, R.O. (2017). Serious Adverse Events with Bevacizumab or Ranibizumab for Age-Related Macular Degeneration: Meta-analysis of Individual Patient Data. *Ophthalmology Retina*. doi: 10.1016/j.oret.2016.12.015.

Mahieux, R., Lambert, P.F., Agbottah, E., Halanski, M.A., Deng, L., Kashanchi, F. & Brady, J.N. (2001). Cell cycle regulation of human interleukin-8 gene expression by the human immunodeficiency virus type 1 Tat protein. *Journal of Virology*. 75 (4). 1736–1743.

Maitra, U., Deng, H., Glaros, T., Baker, B., Capelluto, D.G.S., Li, Z. & Li, L. (2012). Molecular Mechanisms Responsible for the Selective and Low-Grade Induction of Proinflammatory Mediators in Murine Macrophages by Lipopolysaccharide. *Journal of Immunology*. 189 (2). 1014–23.

Maneu, V., Noailles, A., Megías, J., Gómez-Vicente, V., Carpena, N., Gil, M.L., Gozalbo, D. & Cuenca, N. (2014). Retinal microglia are activated by systemic fungal infection. *Investigative Ophthalmology and Visual Science*. 55 (6). 3578–85.

Mantovani, A., Biswas, S.K., Galdiero, M.R., Sica, A. & Locati, M. (2013). Macrophage plasticity and polarization in tissue repair and remodelling. *Journal of Pathology*. 229 (2). 176–185.

Marsh, B., Stevens, S.L., Packard, A.E.B., Gopalan, B., Hunter, B., Leung, P.Y., Harrington, C.A. & Stenzel-Poore, M.P. (2010). Systemic LPS protects the brain from ischemic injury by reprogramming the brain's response to stroke: a critical role for IRF3. *Journal of Neuroscience*. 29 (31). 9839–9849.

Martin, R.R. & Warr, G.A. (1977). Cigarette Smoking and Human Pulmonary Macrophages. *Hospital Practice*. 12 (9). 97–104.

Martinet, L. & Smyth, M.J. (2015). Balancing natural killer cell activation through paired receptors. *Nature reviews. Immunology*. 155. 243–254.

Masdottir, B., Jónsson, T., Manfredsdottir, V., Víkingsson, A., Brekkan, A. & Valdimarsson, H. (2000). Smoking, rheumatoid factor isotypes and severity of rheumatoid arthritis. *Rheumatology*. 39 (11). 1202–5.

Mathews, J.D., Hooper, B.M., Whittingham, S. & Mackay, I.R. (1973). Association of Autoantibodies With Smoking, Cardiovascular Morbidity and Death in the Busselton Population. *Lancet*. 2 (7832). 754–758.

McCusker, R.H. & Kelley, K.W. (2013). Immune-neural connections: how the immune system's response to infectious agents influences behavior. *Journal of Experimental Biology*. 216 (1). 84–98.

McGeer, P.L. & Sibley, J. (2005). Sparing of age-related macular degeneration in rheumatoid arthritis. *Neurobiology of aging*. 26 (8). 1199–203.

Mcpherson, S.W., Heuss, N.D., Pierson, M.J. & Gregerson, D.S. (2014). Retinal antigen-specific regulatory T cells protect against spontaneous and induced autoimmunity and require local dendritic cells. *Journal of Neuroinflammation*. 11:205.

McVicar, C.M., Ward, M., Colhoun, L.M., Guduric-Fuchs, J., Bierhaus, A., Fleming, T., Schlotterer, A., Kolibabka, M., Hammes, H.P., Chen, M. & Stitt, A.W. (2015). Role of the receptor for advanced glycation endproducts (RAGE) in retinal vasodegenerative pathology during diabetes in mice. *Diabetologia*. 58 (5). 1129–1137.

Medzhitov, R. (2001). Toll-like receptors and innate immunity. *Nature reviews. Immunology*. 1 (2). 135–145.

Mendes-Jorge, L., Ramosspi-Sup, D., Luppo, M., Llombart, C., Alexandre-Pires, G., Nacher, V., Melgarejo, V., Correia, M., Carretero, A., Tafurospi-Sup, S., Rodriguez-Baeza, A., Esperanca-Pina, J.A., Bosch, F. & Ruberte, J. (2009). Scavenger function of resident autofluorescent

perivascular macrophages and their contribution to the maintenance of the blood-retinal barrier. *Investigative Ophthalmology and Visual Science*. 50 (12). 5997–6005.

Mettu, P.S., Wielgus, A.R., Ong, S.S. & Cousins, S.W. (2012). Retinal pigment epithelium response to oxidant injury in the pathogenesis of early age-related macular degeneration. *Molecular aspects of medicine*. 33 (4). 376–98.

Mevorach, D., Mascarenhas, J.O., Gershov, D. & Elkon, K.B. (1998). Complement-dependent Clearance of Apoptotic Cells by Human Macrophages. *Journal of Experimental Medicine*. 188 (12). 2313–2320.

Michalewski, J., Nawrocki, J., Izdebski, B. & Michalewska, Z. (2014). Morphological changes in spectral domain optical coherence tomography guided bevacizumab injections in wet age-related macular degeneration, 12-months results. *Indian journal of ophthalmology*. 62 (5). 554–560.

Miller, D.M., Espinosa-Heidmann, D.G., Legra, J., Dubovy, S.R., Sũner, I.J., Sedmak, D.D., Dix, R.D. & Cousins, S.W. (2004). The association of prior cytomegalovirus infection with neovascular age-related macular degeneration. *American journal of Ophthalmology*. 138 (3). 323–8.

Mills, C.D., Kincaid, K., Alt, J.M., Heilman, M.J. & Hill, A.M. (2000). M-1/M-2 Macrophages and the Th1/Th2 Paradigm. *Journal of immunology*. 164 (12). 6166–6173.

Min, J.K., Kim, J. & Woo, J.M. (2014). Elevated Plasma Pentraxin3 Levels and Its Association with Neovascular Age-related Macular Degeneration. *Ocular immunology and inflammation*. 23 (3). 205–211.

Mitchell, P. (2011). A systematic review of the efficacy and safety outcomes of anti-VEGF agents used for treating neovascular age-related macular degeneration: comparison of ranibizumab and bevacizumab. *Curr. Med. Res. Opin.* 27 (7). 1465–1475.

Mittrücker, H.W. & Kaufmann, S.H. (2000). Immune response to infection with Salmonella typhimurium in mice. *Journal of leukocyte biology*. 67 (4). 457–463.

Miyashita, N., Fukano, H., Yoshida, K., Niki, Y. & Matsushima, T. (2003). Chlamydia pneumoniae infection in adult patients with persistent cough. *Journal of Medical Microbiology*. 52 (3). 265–269.

Mizutani, M., Gerhardinger, C. & Lorenzi, M. (1998). Müller cell changes in human diabetic retinopathy. *Diabetes*. 47 (3). 445–9.

Morgado, M.G., Cam, P., Gris-Liebe, C., Cazenave, P.A. & Jouvin-Marche, E. (1989). Further evidence that BALB/c and C57BL/6 gamma 2a genes originate from two distinct isotypes. *EMBO*. 8 (11). 3245–51.

Morimura, Y., Okada, A.A., Hayashi, A., Fujioka, S., Hashida, N., Kawahara, S. & Hida, T. (2004). Histological effect and protein expression in subthreshold transpupillary thermotherapy in rabbit eyes. *Archives of ophthalmology*. 122 (10). 1510–1515.

Morohoshi, K., Ohbayashi, M., Patel, N., Chong, V., Bird, A.C. & Ono, S.J. (2012a). Identification of anti-retinal antibodies in patients with age-related macular degeneration. *Experimental and molecular pathology*. 93 (2). 193–9.

Morohoshi, K., Patel, N., Ohbayashi, M., Chong, V., Grossniklaus, H.E., Bird, A.C. & Ono, S.J. (2012b). Serum autoantibody biomarkers for age-related macular degeneration and possible regulators of neovascularization. *Experimental and molecular pathology*. 92 (1). 64–73.

Mosser, D.M. & Edwards, J.P. (2008). Exploring the full spectrum of macrophage activation. *Nature reviews. Immunology*. 8 (12). 958–969.

Mullins, R.F., Russell, S.R., Anderson, D.H. & Hageman, G.S. (2000). Drusen associated with aging and age-related macular degeneration contain proteins common to extracellular deposits associated with atherosclerosis, elastosis, amyloidosis, and dense deposit disease. *FASEB journal*. 14 (7). 835–846.

Murinello, S. (2014). *Fcγ receptors and immune complex-mediated inflammation in age-related macular degeneration*. Centre for Biological Sciences, University of Southampton, UK, PhD Thesis.

Murinello, S., Mullins, R.F., Lotery, A.J., Perry, V.H. & Teeling, J.L. (2014). Fcγ receptor upregulation is associated with immune complex inflammation in the mouse retina and early age-related macular degeneration. *Investigative Ophthalmology and Visual Science*. 55 (1).

247–58.
Murphy, K. & Weaver, C. (2017). *Janeway's Immunobiology*. 9th Ed. New York: Garland Science, Taylor & Francis Group.
Myers, C.L., Wertheimer, S.J., Schembri-King, J., Parks, T. & Wallace, R.W. (1992). Induction of ICAM-1 by TNF-alpha, IL-1 beta, and LPS in human endothelial cells after downregulation of PKC. *American Journal of Physiology*. 263 (23). C767–C772.
Najafi, S. & Mirshafiey, A. (2015). The Effect of Activated Microglia in Progression of Multiple Sclerosis. *International Trends in Immunity*. 3 (4). 96–104.
Nakamura, R., Sene, A., Santeford, A., Gdoura, A., Kubota, S., Zapata, N. & Apte, R.S. (2015). IL10-driven STAT3 signalling in senescent macrophages promotes pathological eye angiogenesis. *Nature communications*. 6:7847.
Nakata, I., Yamashiro, K., Kawaguchi, T., Nakanishi, H., Akagi-Kurashige, Y., Miyake, M., Tsujikawa, A., Yamada, R., Matsuda, F. & Yoshimura, N. (2015). Calcium, ARMS2 genotype, and Chlamydia pneumoniae infection in early age-related macular degeneration: a multivariate analysis from the Nagahama study. *Scientific reports*. 5:9345.
Nasa, P., Juneja, D. & Singh, O. (2012). Severe sepsis and septic shock in the elderly: An overview. *World journal of critical care medicine*. 1 (1). 23–30.
Nassar, K., Grisanti, S., Elfar, E., Lüke, J., Lüke, M. & Grisanti, S. (2015). Serum cytokines as biomarkers for age-related macular degeneration. *Graefe's Archive for Clinical and Experimental Ophthalmology*. 253 (5). 699–704.
Newman, A.M., Gallo, N.B., Hancox, L.S., Miller, N.J., Radeke, C.M., Maloney, M.A., Cooper, J.B., Hageman, G.S., Anderson, D.H., Johnson, L. V & Radeke, M.J. (2012). Systems-level analysis of age-related macular degeneration reveals global biomarkers and phenotype-specific functional networks. *Genome Medicine*. 4:16.
Newman, E.A. (2003). New roles for astrocytes: Regulation of synaptic transmission. *Trends in Neurosciences*. 26 (10). 536–542.
Noda, K., Nakao, S., Zandi, S., Sun, D., Hayes, K.C. & Hafezi-Moghadam, A. (2014). Retinopathy in a novel model of metabolic syndrome and type 2 diabetes: new insight on the inflammatory paradigm. *FASEB journal*. 28 (5). 2038–2046.
Nomellini, V., Faunce, D.E., Gomez, C.R. & Kovacs, E.J. (2008). An age-associated increase in pulmonary inflammation after burn injury is abrogated by CXCR2 inhibition. *Journal of leukocyte biology*. 83 (6). 1493–501.
Norden, D.M. & Godbout, J.P. (2013). Microglia of the Aged Brain: Primed to be Activated and Resistant to Regulation. *Neuropathology and applied neurobiology*. 39 (1). 19–34.
Noris, M., Mescia, F. & Remuzzi, G. (2012). STEC-HUS, atypical HUS and TTP are all diseases of complement activation. *Nature reviews. Nephrology*. 8 (11). 622–33.
Noris, M. & Remuzzi, G. (2013). Overview of complement activation and regulation. *Seminars in Nephrology*. 33 (6). 479–492.
Nork, T.M., Ghobrial, M.W., Peyman, G.A. & Tso, M.O.M. (1986). Massive Retinal Gliosis: A Reactive Proliferation of Muller Cells. *Archives of ophthalmology*. 104. 1383–1389.
O'Koren, E.G., Mathew, R. & Saban, D.R. (2016). Fate mapping reveals that microglia and recruited monocyte-derived macrophages are definitively distinguishable by phenotype in the retina. *Scientific reports*. 6:20636.
Ohta, K., Yamagami, S., Taylor, A.W. & Streilein, J.W. (2000). IL-6 antagonises TNF-beta and abolishes immune privilege in eyes with Endotoxin-Induced Uveitis. *Investigative Ophthalmology and Visual Science*. 41. 2591–99.
Owen, C.G., Jarrar, Z., Wormald, R., Cook, D.G., Fletcher, A.E. & Rudnicka, A.R. (2012). The estimated prevalence and incidence of late stage age related macular degeneration in the UK. *British journal of ophthalmology*. 96 (5). 752–6.
Owen, J.A., Punt, J., Stranford, S.A. & Jones, P.P. (2013). *Kuby's Immunobiology*. 7th Ed. New York: W. H. Freeman and Company.
Panday, A., Sahoo, M.K., Osorio, D. & Batra, S. (2015). NADPH oxidases: an overview from structure to innate immunity-associated pathologies. *Cellular and Molecular Immunology*. 12 (1). 5–23.

Panorgias, A., Zawadzki, R.J., Capps, A.G., Hunter, A.A., Morse, L.S. & Werner, J.S. (2013). Multimodal assessment of microscopic morphology and retinal function in patients with geographic atrophy. *Investigative Ophthalmology and Visual Science*. 54 (6). 4372–4384.

Parker, D.C. (1993). T Cell-dependent B cell activation. *Annu Rev Immunol*. 11. 331–360.

Pashine, A., John, B., Rath, S., George, A. & Bal, V. (1999). Th1 dominance in the immune response to live Salmonella typhimurium requires bacterial invasiveness but not persistence. *International immunology*. 11 (4). 481–9.

Patel, N., Ohbayashi, M., Nugent, A.K., Ramchand, K., Toda, M., Chau, K.-Y., Bunce, C., Webster, A., Bird, A.C., Ono, S.J. & Chong, V. (2005). Circulating anti-retinal antibodies as immune markers in age-related macular degeneration. *Immunology*. 115 (3). 422–30.

Paun, C.C., Ersoy, L., Schick, T., Groenewoud, J.M.M., Lechanteur, Y.T., Fauser, S., Hoyng, C.B., de Jong, E.K. & den Hollander, A.I. (2015). Genetic Variants and Systemic Complement Activation Levels Are Associated With Serum Lipoprotein Levels in Age-Related Macular Degeneration. *Investigative Ophthalmology and Visual Science*. 56 (13). 7766–73.

Penfold, P.L., Killingsworth, M.C. & Sarks, S.H. (1986). Senile Macular Degeneration: The involvement of giant cells in atrophy of the retinal pigment epithelium. *Investigative Ophthalmology and Visual Science*. 27. 364–371.

Penfold, P.L., Liew, S.C., Madigan, M.C. & Provis, J.M. (1997). Modulation of major histocompatibility complex class II expression in retinas with age-related macular degeneration. *Investigative Ophthalmology and Visual Science*. 38 (10). 2125–2133.

Penfold, P.L., Provis, J.M., Furby, J.H., Gatenby, P.A. & Billson, F.A. (1990). Autoantibodies to Retinal Astrocyte Associated with Age-Related Macular Degeneration. *Graefe's Archive for Clinical and Experimental Opthalmology*. 228. 270–274.

Perry, V.H. & Holmes, C. (2014). Microglial priming in neurodegenerative disease. *Nature Reviews. Neurology*. 10 (4). 217–224.

Perry, V.H. & Teeling, J.L. (2013). Microglia and macrophages of the central nervous system: the contribution of microglia priming and systemic inflammation to chronic neurodegeneration. *Seminars in immunopathology*. 35 (5). 601–12.

Petersen, A.M.W. & Pedersen, B.K. (2005). The anti-inflammatory effect of exercise. *Journal of applied physiology*. 98. 1154–1162.

Petrushina, I., Tran, M., Sadzikava, N., Ghochikyan, A., Vasilevko, V., Agadjanyan, M.G. & Cribbs, D.H. (2003). Importance of IgG2c isotype in the immune response to beta-amyloid in amyloid precursor protein/transgenic mice. *Neuroscience letters*. 338 (1). 5–8.

Pilotto, E., Benetti, E., Convento, E., Guidolin, F., Longhin, E., Parrozzani, R. & Midena, E. (2013). Microperimetry, fundus autofluorescence, and retinal layer changes in progressing geographic atrophy. *Canadian Journal of Ophthalmology*. 48 (5). 386–393.

Pinto, L.H., Invergo, B., Shimomura, K., Takahashi, J.S. & Troy, J.B. (2007). Interpretation of the mouse electroretinogram. *Documenta Ophthalmologica*. 115 (3). 127–136.

Poitry-Yamate, C., Poitry, S. & Tsacopoulos, M. (1995). Lactate Released by Muller Glial Cells Is Metabolized Photoreceptors from Mammalian Retina. *Journal of Neuroscience*. 15 (7). 5179–5191.

Poitry, S., Poitry-Yamate, C., Ueberfeld, J., MacLeish, P.R. & Tsacopoulos, M. (2000). Mechanisms of Glutamate Metabolic Signaling in Retinal Glial (Muller) Cells. *Journal of Neuroscience*. 20 (5). 1809–1821.

Poltorak, M.P. & Schraml, B.U. (2015). Fate mapping of dendritic cells. *Frontiers in immunology*. 6:199.

Popp, N.A., Chi, X.K., Shen, D., Tuo, J. & Chan, C. (2013). Evaluating potential therapies in a mouse model of focal retinal degeneration with age-related macular degeneration. *Journal of clinical and experimental ophthalmology*. 4:1000296.

Popp, N.A., Yu, D., Green, B., Chew, E.Y., Ning, B., Chan, C.-C. & Tuo, J. (2016). Functional single nucleotide polymorphism in IL-17A 3' untranslated region is targeted by miR-4480 in vitro and may be associated with Age-Related Macular Degeneration. *Environ Mol Mutagen*. 57 (1). 58–64.

Prinz, M. & Priller, J. (2014). Microglia and brain macrophages in the molecular age: from origin to

neuropsychiatric disease. *Nature reviews. Neuroscience*. 15 (5). 300–12.
Provis, J.M., Diaz, C.M. & Dreher, B. (1998). Ontogeny of the primate fovea: a central issue in retinal development. *Progress in neurobiology*. 54 (5). 549–80.
Püntener, U., Booth, S.G., Perry, V.H. & Teeling, J.L. (2012). Long-term impact of systemic bacterial infection on the cerebral vasculature and microglia. *Journal of Neuroinflammation*. 9:146.
Purves, D., Augustine, G.J., Fitzpatrick, D., Hall, W.C., LaMantia, A.S. & White, L.E. (2011). *Neuroscience*. 5th Ed. Sunderland, Massachusetts: Sinauer Associates.
Qiao, H., Lucas, K. & Stein-Streilein, J. (2009). Retinal laser burn disrupts immune privilege in the eye. *American journal of Ophthalmology*. 174 (2). 414–422.
Qin, S., Rottman, J.B., Myers, P., Kassam, N., Weinblatt, M., Loetscher, M., Koch, A.E., Moser, B. & Mackay, C.R. (1998). The chemokine receptors CXCR3 and CCR5 mark subsets of T cells associated with certain inflammatory reactions. *Journal of Clinical Investigation*. 101 (4). 746–754.
Rakic, P. (2009). Evolution of the neocortex: Perspective from developmental biology. *Current Biology*. 10 (10). 724–735.
Ramirez, J., Ramirez, A., Salazar, J. & Garcia-Sanchez, J. (1994). Immunohistochemical study of human retinal astroglia. *Vision research*. 34 (15). 1935–1946.
Ramkumar, H.L., Zhang, J. & Chan, C.-C. (2010). Retinal Ultrastructure of Murine Models of Dry Age-Related Macular Degeneration (AMD). *Progress in retinal and eye research*. 29 (3). 169–190.
Randlett, O., Norden, C. & Harris, W.A. (2011). The vertebrate retina: A model for neuronal polarization in vivo. *Developmental Neurobiology*. 71 (6). 567–583.
Ransohoff, R.M., Kivisäkk, P. & Kidd, G. (2003). Three or more routes for leukocyte migration into the central nervous system. *Nature reviews. Immunology*. 3 (7). 569–581.
Reichenbach, A. & Bringmann, A. (2013). New functions of muller cells. *Glia*. 61 (5). 651–678.
Reichenbach, A., Fuchs, U., Kasper, M., El-Hifnawi, E. & Ecksteib, A.K. (1995). Hepatic retinopathy: morphological features of retinal glial (Muller) cells accompanying hepatic failure. *Acta Neuropathologica*. 90. 273–281.
Reichenbach, A. & Robinson, S.R. (1995). The involvement of Muller cells in the outer retina. In: M. B. A. Djamgoz, S. N. Archer, & S. Vallerga (eds.). *Neurobiology and Clinical aspects of the outer retina*. Torquay, UK: Springer Science+Business, 395–416.
Remington, L.A. (2012). *Clinical anatomy and physiology of the visual system*. 3rd Ed. St. Louis, Missouri: Elsevier Inc.
Reynolds, R., Hartnett, M.E., Atkinson, J.P., Giclas, P.C., Rosner, B. & Seddon, J.M. (2009). Plasma complement components and activation fragments: Associations with age-related macular degeneration genotypes and phenotypes. *Investigative Ophthalmology and Visual Science*. 50 (12). 5818–5827.
Rezar-Dreindl, S., Sacu, S., Eibenberger, K., Pollreisz, A., Bühl, W., Georgopoulos, M., Krall, C., Weigert, G. & Schmidt-Erfurth, U. (2016). The Intraocular Cytokine Profile and Therapeutic Response in Persistent Neovascular Age-Related Macular Degeneration. *Investigative Ophthalmology and Visual Science*. 57 (10). 4144–50.
Ricci, F., Staurenghi, G., Lepre, T., Missiroli, F., Zampatti, S., Cascella, R., Borgiani, P., Marsella, L.T., Eandi, C.M., Cusumano, A., Novelli, G. & Giardina, E. (2013). Haplotypes in IL-8 Gene Are Associated to Age-Related Macular Degeneration: A Case-Control Study. *PLoS ONE*. 8 (6). e66978.
Ristau, T., Paun, C., Ersoy, L., Hahn, M., Lechanteur, Y., Hoyng, C., De Jong, E.K., Daha, M.R., Kirchhof, B., Den Hollander, A.I. & Fauser, S. (2014). Impact of the common genetic associations of age-related macular degeneration upon systemic complement component C3d levels. *PLoS ONE*. 9 (3). e93459.
Robman, L., Mahdi, O., McCarty, C., Dimitrov, P.N., Tikellis, G., McNeil, J., Byrne, G.I., Taylor, H. & Guymer, R.H. (2005). Exposure to Chlamydia pneumoniae infection and progression of age-related macular degeneration. *American journal of Epidemiology*. 161 (11). 1013–9.
Robman, L., Mahdi, O.S., Wang, J.J., Burlutsky, G., Mitchell, P., Byrne, G.I., Guymer, R.H. & Taylor, H. (2007). Exposure to Chlamydia pneumoniae infection and age-related macular

degeneration: the Blue Mountains Eye Study. *Investigative Ophthalmology and Visual Science*. 48 (9). 4007–11.

Roy, M.-F. & Malo, D. (2002). Genetic regulation of host responses to Salmonella infection in mice. *Genes and Immunity*. 3 (7). 381–393.

Ruby, T., McLaughlin, L., Gopinath, S. & Monack, D. (2012). Salmonella's long-term relationship with its host. *FEMS microbiology reviews*. 36 (3). 600–15.

Rudnicka, A.R., Jarrar, Z., Wormald, R., Cook, D.G., Fletcher, A. & Owen, C.G. (2012). Age and gender variations in age-related macular degeneration prevalence in populations of European ancestry: A meta-analysis. *Ophthalmology*. 119 (3). 571–580.

Saishin, Y., Saishin, Y., Takahashi, K., Silva, R.L.E., Hylton, D., Rudge, J.S., Wiegand, S.J. & Campochiaro, P.A. (2003). VEGF-TRAPR1R2 suppresses choroidal neovascularization and VEGF-induced breakdown of the blood-retinal barrier. *Journal of Cellular Physiology*. 195 (2). 241–248.

Sakurada, Y., Nakamura, Y., Yoneyama, S., Mabuchi, F., Gotoh, T., Tateno, Y., Sugiyama, A., Kubota, T. & Iijima, H. (2015). Aqueous Humor Cytokine Levels in Patients with Polypoidal Choroidal Vasculopathy and Neovascular Age-Related Macular Degeneration. *Ophthalmic Research*. 53 (1). 2–7.

San Giovanni, J.P. & Neuringer, M. (2012). The putative role of lutein and zeaxanthin as protective agents against age-related macular degeneration: Promise of molecular genetics for guiding mechanistic and translational research in the field. *American Journal of Clinical Nutrition*. 96. 1223S–33S.

Sanges, D., Romo, N., Simonte, G., Di Vicino, U., Tahoces, A.D., Fernández, E. & Cosma, M.P. (2013). Wnt/β-catenin signaling triggers neuron reprogramming and regeneration in the mouse retina. *Cell reports*. 4 (2). 271–86.

Sansoni, P., Cossarizza, A., Brianti, V., Fagnoni, F., Snelli, G., Monti, D., Marcato, A., Passeri, G., Ortolani, C. & Forti, E. (1993). Lymphocyte subsets and natural killer cell activity in healthy old people and centenarians. *Blood*. 82 (9). 2767–2773.

Saraswathy, S., Wu, G. & Rao, N.A. (2006). Retinal microglial activation and chemotaxis by docosahexaenoic acid hydroperoxide. *Investigative Ophthalmology and Visual Science*. 47 (8). 3656–63.

Sarks, J.P., Sarks, S.H. & Killingsworth, M.C. (1988). Evolution of geographic atrophy of the retinal pigment epithelium. *Eye*. 2. 552–577.

Sarks, S.H. (1976). Ageing and degeneration in the macular region of the eye. *British journal of ophthalmology*. 60. 324–341.

Schaal, K.B., Freund, K.B., Litts, K.M., Zhang, Y., Messinger, J.D. & Curcio, C.A. (2015). Outer Retinal Tubulation in advanced age-related macular degeneration: Optical coherence Tomographic Findings Correspond to Histology. *Retina*. 35 (7). 1339–50.

Schaumberg, D.A., Rose, L., DeAngelis, M.M., Semba, R.D., Hageman, G.S. & Chasman, D.I. (2014). Prospective study of common variants in CX3CR1 and risk of macular degeneration: pooled analysis from 5 long-term studies. *JAMA ophthalmology*. 132 (1). 84–95.

Schindelin, J., Arganda-Carreras, I., Frise, E., Kaynig, V., Longair, M., Pietzsch, T., Preibisch, S., Rueden, C., Saalfeld, S., Schmid, B., Tinevez, J.-Y.J.-Y., White, D.J., Hartenstein, V., Eliceiri, K., Tomancak, P., Cardona, A., Liceiri, K., Tomancak, P. & A., C. (2012). Fiji: An open source platform for biological image analysis. *Nature Methods*. 9 (7). 676–682.

Schmid, M.K., Bachmann, L.M., Fäs, L., Kessels, A.G., Job, O.M. & Thiel, M.A. (2015). Efficacy and adverse events of aflibercept, ranibizumab and bevacizumab in age-related macular degeneration: a trade-off analysis. *British journal of ophthalmology*. 99. 141–146.

Schmitt, V., Rink, L. & Uciechowski, P. (2013). The Th17/Treg balance is disturbed during aging. *Experimental Gerontology*. 48 (12). 1379–1386.

Schmitz-Valckenberg, S. (2017). The Journey of 'Geographic Atrophy' through Past, Present, and Future. *Ophthalmologica*. 237. 11–20.

Schmitz, Y. & Witkovsky, P. (1997). Dependence of photoreceptor glutamate release on a dihydropyridine-sensitive calcium channel. *Neuroscience*. 78 (4). 1209–16.

Scholl, H.P.N., Issa, P.C., Walier, M., Janzer, S., Pollok-Kopp, B., Börncke, F., Fritsche, L.G., Chong,

N. V., Fimmers, R., Wienker, T., Holz, F.G., Weber, B.H.F. & Oppermann, M. (2008). Systemic complement activation in age-related macular degeneration. *PLoS ONE*. 3 (7). e2593.

Schutt, F., Bergmann, M., Holz, F.G. & Kopitz, J. (2003). Proteins modified by malondialdehyde, 4-hydroxynonenal, or advanced glycation end products in lipofuscin of human retinal pigment epithelium. *Investigative Ophthalmology and Visual Science*. 44 (8). 3663–3668.

Schwartz, M. & Shechter, R. (2010). Protective autoimmunity functions by intracranial immunosurveillance to support the mind: The missing link between health and disease. *Molecular Psychiatry*. 15 (4). 342–354.

Scott, P. (1991). IFN-gamma modulates the early development of Th1 and Th2 responses in a murine model of cutaneous leishmaniasis. *Journal of immunology*. 147 (9). 3149–3155.

Secondi, R., Kong, J., Blonska, A.M., Staurenghi, G. & Sparrow, J.R. (2012). Fundus autofluorescence findings in a mouse model of retinal detachment. *Investigative Ophthalmology and Visual Science*. 53 (9). 5190–5197.

Seddon, J.M., George, S., Rosner, B. & Klein, M.L. (2006). CFH gene variant, Y402H, and smoking, body mass index, environmental associations with advanced age-related macular degeneration. *Human heredity*. 61 (3). 157–65.

Seddon, J.M., George, S., Rosner, B. & Rifai, N. (2005). Progression of Age-Related Macular Degeneration: Prospective Assessment of C-Reactive Protein, Interleukin 6, and Other Cardiovascular Biomarkers. *Archives of ophthalmology*. 123 (6). 774–782.

Seddon, J.M., Reynolds, R. & Rosner, B. (2010). Associations of smoking, body mass index, dietary lutein, and the LIPC gene variant rs10468017 with advanced age-related macular degeneration. *Molecular vision*. 16. 2412–24.

Seo, M.S., Kwak, N., Ozaki, H., Yamada, H., Okamoto, N., Yamada, E., Fabbro, D., Hofmann, F., Wood, J.M. & Campochiaro, P.A. (1999). Dramatic inhibition of retinal and choroidal neovascularization by oral administration of a kinase inhibitor. *American Journal of Pathology*. 154 (6). 1743–53.

Shahid, H., Khan, J.C., Cipriani, V., Sepp, T., Matharu, B.K., Bunce, C., Harding, S.P., Clayton, D.G., Moore, A.T., Yates, J.R.W. & Genetic Factors in AMD Study Group, for the G.F. in A.S. (2012). Age-related macular degeneration: the importance of family history as a risk factor. *British journal of ophthalmology*. 96 (3). 427–31.

Shao, B.Z., Xu, Z.Q., Han, B.Z., Su, D.F. & Liu, C. (2015). NLRP3 inflammasome and its inhibitors: A review. *Frontiers in Pharmacology*. 6:262.

Sharma, N.K., Gupta, A., Prabhakar, S., Singh, R., Bhatt, A.K. & Anand, A. (2013). CC chemokine receptor-3 as new target for age-related macular degeneration. *Gene*. 523 (1). 106–111.

Shechter, R., London, A. & Schwartz, M. (2013). Orchestrated leukocyte recruitment to immune-privileged sites: absolute barriers versus educational gates. *Nature Reviews. Immunology*. 13 (3). 206–218.

Shen, D.F., Buggage, R.R., Eng, H.C. & Chan, C.C. (2000a). Cytokine gene expression in different strains of mice with endotoxin- induced uveitis (EIU). *Ocul Immunol Inflamm*. 8 (4). 221–5.

Shen, D.F., Chang, M.A., Matteson, D.M., Buggage, R., Kozhich, A.T. & Chan, C.C. (2000b). Biphasic ocular inflammatory response to endotoxin-induced uveitis in the mouse. *Archives of ophthalmology*. 118 (4). 521–7.

Shen, D.F., Tuo, J., Patel, M., Herzlich, A.A., Ding, X., Chew, E.Y. & Chan, C. (2009). Chlamydia pneumoniae infection, complement factor H variants and age-related macular degeneration. *British journal of ophthalmology*. 93 (3). 405–408.

Shi, X., Semkova, I., Müther, P.S., Dell, S., Kociok, N. & Joussen, A.M. (2006). Inhibition of TNF-alpha reduces laser-induced choroidal neovascularization. *Experimental eye research*. 83 (6). 1325–34.

Silva, D., Ponte, C.G.G., Hacker, M.A. & Antas, P.R.Z. (2013). A whole blood assay as a simple, broad assessment of cytokines and chemokines to evaluate human immune responses to Mycobacterium tuberculosis antigens. *Acta Tropica*. 127 (2). 75–81.

Silvestri, G., Johnston, P.B. & Hughes, A.E. (1994). Is genetic predisposition an important risk factor in age-related macular degeneration? *Eye*. 8. 564–8.

Singh, A., Faber, C., Falk, M.K., Nissen, M.H., Hviid, T.V.F. & Sorensen, T.L. (2012). Altered

expression of CD46 and CD59 on leukocytes in neovascular age-related macular degeneration. *American Journal of Ophthalmology*. 154 (1). 193–199.

Singh, A., Falk, M.K., Hviid, T.V.F. & Sørensen, T.L. (2013). Increased expression of cd200 on circulating cd11b+ monocytes in patients with neovascular age-related macular degeneration. *Ophthalmology*. 120 (5). 1029–1037.

Singh, T. & Newman, A.B. (2011). Inflammatory markers in population studies of aging. *Ageing Research Reviews*. 10 (3). 319–329.

Smailhodzic, D., Klaver, C.C., Klevering, B.J., Boon, C.J.F., Groenewoud, J.M.M., Kirchhof, B., Daha, M.R., Den Hollander, A.I. & Hoyng, C.B. (2012). Risk alleles in CFH and ARMS2 are independently associated with systemic complement activation in age-related macular degeneration. *Ophthalmology*. 119 (2). 339–346.

De Smedt, T., Pajak, B., Muraille, E., Urbain, J., Leo, O. & Moser, M. (1997). Positive and negative regulation of dendritic cell function by lipopolysaccharide in vivo. *Advanced Experimental Medical Biology*. 417. 535–540.

Snodderly, D.M., Auran, J.D. & Delori, F.C. (1984). The macular pigment. II. Spatial distribution in Primate Retinas. *Investigative Ophthalmology and Visual Science*. 25. 674–685.

Song, H., Vijayasarathy, C., Zeng, Y., Marangoni, D., Bush, R.A., Wu, Z. & Sieving, P.A. (2016). NADPH oxidase contributes to photoreceptor degeneration in constitutively active RAC1 mice. *Investigative Ophthalmology and Visual Science*. 57 (6). 2864–2875.

Sopori, M. (2002). Effects of cigarette smoke on the immune system. *Nature reviews. Immunology*. 2. 372–377.

Sriram, S. & Rodriguez, M. (1997). Indictment of the microglia as the villain in multiple sclerosis. *Neurology*. 48 (2). 464–470.

Sriram, S., Stratton, C.W., Yao, S., Tharp, A., Ding, L., Bannan, J.D. & Mitchell, W.M. (1999). Chlamydia pneumoniae infection of the central nervous system in multiple sclerosis. *Annals of neurology*. 46. 6–14.

Srivastava, B., Błazejewska, P., Heßmann, M., Bruder, D., Geffers, R., Manuel, S., Gruber, A.D. & Schughart, K. (2009). Host genetic background strongly influences the response to influenza A virus infections. *PLoS ONE*. 4 (3). e4857.

Stanton, C.M., Yates, J.R.W., den Hollander, A.I., Seddon, J.M., Swaroop, A., Stambolian, D., Fauser, S., Hoyng, C., Yu, Y., Atsuhiro, K., Branham, K., Othman, M., Chen, W., Kortvely, E., Chalmers, K., Hayward, C., Moore, A.T., Dhillon, B., Ueffing, M. & Wright, A.F. (2011). Complement factor D in age-related macular degeneration. *Investigative ophthalmology & visual science*. 52 (12). 8828–34.

Stein-Streilein, J. (2013). Mechanisms of immune privilege in the posterior eye. *International reviews of immunology*. 32 (1). 42–56.

Stephan, A.H., Madison, D. V, Mateos, M., Fraser, D.A., Lovelett, E.A., Coutellier, L., Kim, L., Tsai, H., Huang, E.J., Rowitch, D.H., Berns, D.S., Tenner, A.J., Shamloo, M. & Barres, B.A. (2013). A Dramatic Increase of C1q Protein in the CNS during Normal Aging. *Journal of Neuroscience*. 33 (33). 13460–13474.

Stewart, P.A. & Tuor, U.I. (1994). Blood-eye barriers in the rat: Correlation of ultrastructure with function. *Journal of Comparative Neurology*. 340 (4). 566–576.

Streilein, J.W. (2003). Ocular immune privilege: therapeutic opportunities from an experiment of nature. *Nature reviews. Immunology*. 3 (11). 879–889.

Suzuki, M., Kamei, M., Itabe, H., Yoneda, K., Bando, H., Kume, N. & Tano, Y. (2007). Oxidized phospholipids in the macula increase with age and in eyes with age-related macular degeneration. *Molecular vision*. 13. 772–8.

Tackenberg, M.A., Tucker, B.A., Swift, J.S., Jiang, C., Redenti, S., Greenberg, K.P., Flannery, J.G., Reichenbach, A. & Young, M.J. (2009). Müller cell activation, proliferation and migration following laser injury. *Molecular vision*. 15. 1886–1896.

Takeda, A., Baffi, J.Z., Kleinman, M.E., Cho, W.G., Yamada, K., Kaneko, H., Albuquerque, R.J.C., Dridi, S., Saito, K., Raisler, B.J., Budd, S.J., Geisen, P., Munitz, A., Ambati, B.K., Green, M.G., Ishibashi, T., Wright, J.D., Alison, A., Gerard, C.J., Ogura, Y., Pan, Y., Smith, J.R., Hartnett, M.E., Rothenberg, M.E. & Ambati, J. (2009). CCR3 is a therapeutic and diagnostic target for

neovascular age- related macular degeneration. *Nature*. 460 (7252). 225–230.

Talbot, S., Tötemeyer, S., Yamamoto, M., Akira, S., Hughes, K., Gray, D., Barr, T., Mastroeni, P., Maskell, D.J. & Bryant, C.E. (2009). Toll-like receptor 4 signalling through MyD88 is essential to control Salmonella enterica serovar Typhimurium infection, but not for the initiation of bacterial clearance. *Immunology*. 128 (4). 472–483.

Tapping, R.I., Akashi, S., Miyake, K., Godowski, P.J. & Tobias, P.S. (2000). Toll-Like Receptor 4, But Not Toll-Like Receptor 2, Is a Signaling Receptor for Escherichia and Salmonella Lipopolysaccharides. *Journal of immunology*. 165 (10). 5780–5787.

Tarallo, V., Hirano, Y., Gelfand, B.D., Dridi, S., Kerur, N., Kim, Y., Cho, W.G., Kaneko, H., Fowler, B.J., Albuquerque, R.J.C., Hauswirth, W.W., Chiodo, V.A., Kugel, J.F., Goodrich, J.A., Ponicsan, S.L., Chaudhuri, G., Murphy, P., Dunaief, J.L., Ambati, B.K., Ogura, Y., Wook, J., Provost, P., Hinton, D.R., Nunez, G., Baffi, J.Z., Kleinman, M. & Ambati, J. (2012). DICER1 loss and Alu RNA Induce Age-Related Macular Degeneration via the NLRP3 Inflammasome and MyD88. *Cell*. 149 (4). 847–859.

Teeling, J.L., Cunningham, C., Newman, T.A. & Perry, V.H. (2010). The effect of non-steroidal anti-inflammatory agents on behavioural changes and cytokine production following systemic inflammation: Implications for a role of COX-1. *Brain, Behavior, and Immunity*. 24 (3). 409–419.

Teeling, J.L., Felton, L.M., Deacon, R.M.J., Cunningham, C., Rawlins, J.N.P. & Perry, V.H. (2007). Sub-pyrogenic systemic inflammation impacts on brain and behavior, independent of cytokines. *Brain, behavior, and immunity*. 21 (6). 836–50.

Thach, D.C., Kimura, T. & Griffin, D.E. (2000). Differences between C57BL/6 and BALB/cBy Mice in Mortality and Virus Replication after Intranasal Infection with Neuroadapted Sindbis Virus. *Journal of Virology*. 74 (13). 6156–6161.

The Angiogenesis Society (2012). *The Science of AMD*. [Online]. 2012. Available from: http://www.scienceofamd.org/learn/.

Tobe, T., Ortega, S., Luna, J.D., Ozaki, H., Okamoto, N., Derevjanik, N.L., Vinores, S.A., Basilico, C. & Campochiaro, P.A. (1998). Targeted disruption of the FGF2 gene does not prevent choroidal neovascularization in a murine model. *American Journal of Pathology*. 153 (5). 1641–1646.

Tolentino, M. (2011). Systemic and Ocular Safety of Intravitreal Anti-VEGF Therapies for Ocular Neovascular Disease. *Survey of Ophthalmology*. 56 (2). 95–113.

Tombran-Tink, J., Shivaram, S.M., Chader, G.J., Johnson, L. V & Bok, D. (1995). Expression, secretion, and age-related downregulation of pigment epithelium-derived factor, a serpin with neurotrophic activity. *Journal of Neuroscience*. 15 (7). 4992–5003.

Tomida, D., Nishiguchi, K.M., Kataoka, K., Yasuma, T.R., Iwata, E., Uetani, R., Kachi, S. & Terasaki, H. (2011). Suppression of choroidal neovascularization and quantitative and qualitative inhibition of VEGF and CCL2 by heparin. *Investigative Ophthalmology and Visual Science*. 52 (6). 3193–3199.

Tosi, M.F. (2005). Innate immune responses to infection. *Journal of Allergy and Clinical Immunology*. 116 (2). 241–249.

Trieschmann, M., van Kuijk, F.J.G.M., Alexander, R., Hermans, P., Luthert, P., Bird, A.C. & Pauleikhoff, D. (2008). Macular pigment in the human retina: histological evaluation of localization and distribution. *Eye*. 22 (1). 132–137.

Trost, A., Lange, S., Schroedl, F., Bruckner, D., Motloch, K.A., Bogner, B., Kaser-Eichberger, A., Strohmaier, C., Runge, C., Aigner, L., Rivera, F.J. & Reitsamer, H.A. (2016). Brain and Retinal Pericytes: Origin, Function and Role. *Frontiers in Cellular Neuroscience*. 10:20.

Tsacopoulos, M. & Magistretti, P.J. (1996). Metabolic coupling between glia and neurons. *Journal of Neuroscience*. 16 (3). 877–85.

Tsai, Y.-Y., Lin, J.-M., Wan, L., Lin, H.-J., Tsai, Y., Lee, C.-C., Tsai, C.-H., Tsai, F.-J. & Tseng, S.-H. (2008). Interleukin gene polymorphisms in age-related macular degeneration. *Investigative Ophthalmology and Visual Science*. 49 (2). 693–8.

Tseng, W.A., Thein, T., Kinnunen, K., Lashkari, K., Gregory, M.S., D'Amore, P.A. & Ksander, B.R. (2013). NLRP3 inflammasome activation in retinal pigment epithelial cells by lysosomal destabilization: implications for age-related macular degeneration. *Investigative*

Ophthalmology and Visual Science. 54 (1). 110–20.

Tuaillon, N., Shen, D.F., Berger, R.B., Lu, B., Rollins, B.J. & Chan, C. (2002). MCP-1 Expression in Endotoxin-Induced Uveitis. *Investigative Ophthalmology and Visual Science*. 43. 1493–1498.

Tuo, J., Bojanowski, C.M., Zhou, M., Shen, D., Ross, R.J., Rosenberg, K.I., Cameron, D.J., Yin, C., Kowalak, J.A., Zhang, K., Chan, C., Zhengping, Z., Zhang, K. & Chan, C. (2007). Murine Ccl2/Cx3cr1 deficiency results in retinal lesions mimicking human age-related macular degeneration. *Investigative Ophthalmology and Visual Science*. 48 (8). 3827–3836.

Tuo, J., Grob, S., Zhang, K. & Chan, C.-C. (2012). Genetics of Immunological and Inflammatory Components in Age-related Macular Degeneration. *Ocular Immunology and Inflammation*. 20 (1). 27–36.

Tuo, J., Smith, B.C., Bojanowski, C.M., Meleth, A.D., Gery, I., Csaky, K.G., Chew, E.Y. & Chan, C.-C. (2004). The involvement of sequence variation and expression of CX3CR1 in the pathogenesis of age-related macular degeneration. *FASEB journal*. 18 (11). 1297–9.

Turgut, B., Uyar, F., Ilhan, F., Demir, T. & Celiker, U. (2010). Mycoplasma pneumoniae and Chlamydia pneumoniae seropositivity in patients with age-related macular degeneration. *Journal of clinical medicine research*. 2 (2). 85–9.

Ufret-Vincenty, R.L., Aredo, B., Liu, X., McMahon, A., Chen, P.W., Sun, H., Niederkorn, J.Y. & Kedzierski, W. (2010). Transgenic mice expressing variants of complement factor H develop AMD-like retinal findings. *Investigative Ophthalmology and Visual Science*. 51 (11). 5878–5887.

Umeda, S., Suzuki, M.T., Okamoto, H., Ono, F., Mizota, A., Terao, K., Yoshikawa, Y., Tanaka, Y. & Iwata, T. (2005). Molecular composition of drusen and possible involvement of anti-retinal autoimmunity in two different forms of macular degeneration in cynomolgus monkey (Macaca fascicularis). *FASEB journal*. 19 (12). 1683–5.

Vallejo, A.N., Mueller, R.G., Hamel Jr, D.L., Way, A., Dvergsten, J.A., Griffin, P. & Newman, A.B. (2011). Expansions of NK-like αβT cells with chronologic aging: Novel lymphocyte effectors that compensate for functional deficits of conventional NK cells and T cells. *Ageing Research Reviews*. 10 (3). 354–361.

Vaure, C. & Liu, Y. (2014). A comparative review of toll-like receptor 4 expression and functionality in different animal species. *Frontiers in Immunology*. 5:316.

Vecino, E., Rodriguez, F.D., Ruzafa, N., Pereiro, X. & Sharma, S.C. (2016). Glia-neuron interactions in the mammalian retina. *Progress in Retinal and Eye Research*. 51. 1–40.

Veleri, S., Lazar, C.H., Chang, B., Sieving, P.A., Banin, E. & Swaroop, A. (2015). Biology and therapy of inherited retinal degenerative disease: insights from mouse models. *Disease Models and Mechanisms*. 8 (2). 109–129.

Ventrice, P., Leporini, C., Aloe, J.F., Greco, E., Leuzzi, G., Marrazzo, G., Scorcia, G., Bruzzichesi, D., Nicola, V. & Scorcia, V. (2013). Anti-vascular endothelial growth factor drugs safety and efficacy in ophthalmic diseases. *Journal of pharmacology & pharmacotherapeutics*. 4. S38-42.

Verderber, L., Johnson, W., Mucke, L. & Sarthy, V. (1995). Differential regulation of a glial fibrillary acidic protein-LacZ transgene in retinal astrocytes and Muller cells. *Investigative Ophthalmology and Visual Science*. 36 (6). 1137–1143.

Vessey, K.A., Greferath, U., Jobling, A.I., Phipps, J.A., Ho, T., Waugh, M. & Fletcher, E.L. (2012). Ccl2/Cx3cr1 knockout mice have inner retinal dysfunction but are not an accelerated model of AMD. *Investigative Ophthalmology and Visual Science*. 53 (12). 7833–7846.

van de Vosse, E. & Ottenhoff, T.H.M. (2006). Human host genetic factors in mycobacterial and Salmonella infection: lessons from single gene disorders in IL-12/IL-23-dependent signaling that affect innate and adaptive immunity. *Microbes and infection / Institut Pasteur*. 8 (4). 1167–73.

Wagley, S., Marra, K. V, Salhi, R.A., Gautam, S., Campo, R., Veale, P., Veale, J. & Arroyo, J.G. (2015). Periodontal Disease and Age-Related Macular Degeneration. *Retina*. 35 (5). 982–988.

Wallace, F.A., Miles, E.A., Evans, C., Stock, T.E., Yaqoob, P. & Calder, P.C. (2001). Dietary fatty acids influence the production of Th1- but not Th2-type cytokines. *Journal of leukocyte biology*. 69 (3). 449–457.

Walter, P., Widder, R., Lüke, C., Königsfeld, P. & Brunner, R. (1999). Electrophysiological abnormalities in age-related macular degeneration. *Graefe's archive for clinical and experimental ophthalmology*. 237 (12). 962–968.

Wang, J.C.C., Cao, S., Wang, A., To, E., Law, G., Gao, J., Zhang, D., Cui, J.Z. & Matsubara, J.A. (2015). CFH Y402H polymorphism is associated with elevated vitreal GM-CSF and choroidal macrophages in the postmortem human eye. *Molecular vision*. 21. 264–72.

Wang, L., Clark, M.E., Crossman, D.K., Kojima, K., Messinger, J.D., Mobley, J.A. & Curcio, C.A. (2010). Abundant lipid and protein components of drusen. *PLoS ONE*. 5 (4). e10329.

Wang, Y., Hanus, J.W., Abu-Asab, M.S., Shen, D., Ogilvy, A., Ou, J., Chu, X.K., Shi, G., Li, W., Wang, S. & Chan, C.-C. (2016). NLRP3 upregulation in retinal pigment epithelium in age-related macular degeneration. *International Journal of Molecular Sciences*. 17:73.

Wang, Y., Wang, V.M. & Chan, C.-C. (2011). The role of anti-inflammatory agents in age-related macular degeneration (AMD) treatment. *Eye*. 25 (2). 127–39.

Wangsa-Wirawan, N.D. & Linsenmeier, R.A. (2003). Retinal Oxygen: Fundamental and Clinical Aspects. *Archives of ophthalmology*. 121. 547–557.

Wei, J., Xu, H., Davies, J.L. & Hemmings, G.P. (1992). Increase of plasma IL-6 concentration with age in healthy subjects. *Life Sciences*. 51 (25). 1953–1956.

Wei, L., Liu, B., Tuo, J., Shen, D., Chen, P., Li, Z., Liu, X., Ni, J., Dagur, P., Sen, H.N., Jawad, S., Ling, D., Park, S., Chakrabarty, S., Meyerle, C., Agron, E., Ferris 3rd, F.L., Chew, E.Y., McCoy, J.P., Blum, E., Francis, P.J., Klein, M.L., Guymer, R.H., Baird, P.N., Chan, C. & Nussenblatt, R.B. (2012). Hypomethylation of IL17RC promoter associates with age-related macular degeneration. *Cell reports*. 2 (5). 1151–1158.

Weinberg, A., Song, L.Y., Wilkening, C., Sevin, A., Blais, B., Louzao, R., Stein, D., Defechereux, P., Durand, D., Riedel, E., Raftery, N., Jesser, R., Brown, B., Keller, M.F., Dickover, R., McFarland, E. & Fenton, T. (2009). Optimization and limitations of use of cryopreserved peripheral blood mononuclear cells for functional and phenotypic T-cell characterization. *Clinical and Vaccine Immunology*. 16 (8). 1176–1186.

Weismann, D., Hartvigsen, K., Lauer, N., Bennett, K.L., Scholl, H.P.N., Charbel Issa, P., Cano, M., Brandstätter, H., Tsimikas, S., Skerka, C., Superti-Furga, G., Handa, J.T., Zipfel, P.F., Witztum, J.L. & Binder, C.J. (2011). Complement factor H binds malondialdehyde epitopes and protects from oxidative stress. *Nature*. 478 (7367). 76–81.

Williams, R.A., Brody, B.L., Thomas, R.G., Kaplan, R.M. & Brown, S. (1998). The psychosocial impact of macular degeneration. *Archives of ophthalmology*. 116 (4). 514–20.

Witmer-Pack, M.D., Crowley, M.T., Inaba, K. & Steinman, R.M. (1993). Macrophages, but not dendritic cells, accumulate colloidal carbon following administration in situ. *Journal of Cell Science*. 105. 965–973.

Wolf-Schnurrbusch, U.E.K., Enzmann, V., Brinkmann, C.K. & Wolf, S. (2008). Morphologic changes in patients with geographic atrophy assessed with a novel spectral OCT-SLO combination. *Investigative Ophthalmology and Visual Science*. 49 (7). 3095–3099.

Wolf-Schnurrbusch, U.E.K., Hess, R., Jordi, F., Stuck, A.K., Sarra, G.-M., Wolf, S. & Enzmann, V. (2013). Detection of Chlamydia and complement factors in neovascular membranes of patients with age-related macular degeneration. *Ocular immunology and inflammation*. 21 (1). 36–43.

Wong, W.L., Su, X., Li, X., Cheung, C.M.G., Klein, R., Cheng, C.Y. & Wong, T.Y. (2014). Global prevalence of age-related macular degeneration and disease burden projection for 2020 and 2040: A systematic review and meta-analysis. *Lancet Global Health*. 2 (2). e106–e116.

Wu, K.H.C., Madigan, M.C., Billson, F.A. & Penfold, P.L. (2003). Differential expression of GFAP in early v late AMD: a quantitative analysis. *British journal of ophthalmology*. 87 (9). 1159–1166.

Wu, Z., Luu, C.D., Ayton, L.N., Goh, J.K., Lucci, L.M., Hubbard, W.C., Hageman, J.L., Hageman, G.S. & Guymer, R.H. (2014). Optical coherence tomography-defined changes preceding the development of drusen-associated atrophy in age-related macular degeneration. *Ophthalmology*. 121 (12). 2415–2422.

Xu, H., Chen, M. & Forrester, J. V (2009). Para-inflammation in the aging retina. *Progress in retinal*

and eye research. 28 (5). 348–68.

Xu, H., Chen, M., Manivannan, A., Lois, N. & Forrester, J. V (2008). Age-dependent accumulation of lipofuscin in perivascular and subretinal microglia in experimental mice. *Aging Cell*. 7. 58–68.

Xu, H., Chen, M., Mayer, E.J., Forrester, J. V & Dick, A.D. (2007a). Turnover of resident retinal microglia in the normal adult mouse. *Glia*. 55. 1189–1198.

Xu, H., Dawson, R., Forrester, J. V. & Liversidge, J. (2007b). Identification of Novel Dendritic Cell Populations in Normal Mouse Retina. *Investigative Ophthalmology and Visual Science*. 48 (4). 1701–1710.

Xu, H., Forrester, J. V, Liversidge, J. & Crane, I.J. (2003). Leukocyte trafficking in experimental autoimmune uveitis: Breakdown of blood-retinal barrier and upregulation of cellular adhesion molecules. *Investigative Ophthalmology and Visual Science*. 44 (1). 226–234.

Yamada, K., Sakurai, E., Itaya, M., Yamasaki, S. & Ogura, Y. (2007). Inhibition of laser-induced choroidal neovascularization by atorvastatin by downregulation of monocyte chemotactic protein-1 synthesis in mice. *Investigative Ophthalmology and Visual Science*. 48 (4). 1839–1843.

Yang, P., Das, P.K. & Kijlstra, A. (2000). Localization and characterization of immunocompetent cells in the human retina. *Ocular immunology and inflammation*. 8 (3). 149–57.

Yang, X., Hu, J., Zhang, J. & Guan, H. (2010). Polymorphisms in CFH, HTRA1 and CX3CR1 confer risk to exudative age-related macular degeneration in Han Chinese. *British journal of ophthalmology*. 94 (9). 1211–4.

Yaspan, B.L., Williams, D.F., Holz, F.G., Regillo, C.D., Li, Z., Dressen, A., Campagne, M.V.L., Le, K.N., Graham, R.R., Beres, T., Bhangale, T.R., Honigberg, L.A., Smith, A., Henry, E.C. & Ho, C. (2017). Targeting factor D of the alternative complement pathway reduces geographic atrophy progression secondary to age-related macular degeneration. *Science Translational Medicine*. 9. eaaf1443.

Yi, J.S., Cox, M.A. & Zajac, A.J. (2010). T-cell exhaustion: Characteristics, causes and conversion. *Immunology*. 129 (4). 474–481.

Yildirim, Z., Ucgun, N.I., Yildirim, F. & Sepici-Dincel, A. (2012). Choroidal neovascular membrane in age-related macular degeneration is associated with increased interleukin-6. *International Journal of Gerontology*. 6 (2). 101–104.

Yu, A.K., Merrill, K.D., Truong, S.N., Forward, K.M., Morse, L.S. & Telander, D.G. (2013). The comparative histologic effects of subthreshold 532- and 810-nm diode micropulse laser on the retina. *Investigative Ophthalmology and Visual Science*. 54 (3). 2216–2224.

Yu, D.-Y. & Cringle, S.J. (2005). Retinal degeneration and local oxygen metabolism. *Experimental eye research*. 80 (6). 745–51.

Yu, Y.R.A., O'Koren, E.G., Hotten, D.F., Kan, M.J., Kopin, D., Nelson, E.R., Que, L. & Gunn, M.D. (2016). A protocol for the comprehensive flow cytometric analysis of immune cells in normal and inflamed murine non-lymphoid tissues. *PLoS ONE*. 11 (3). e150606.

Yuan, X., Gu, X., Crabb, J.S., Yue, X., Shadrach, K., Hollyfield, J.G. & Crabb, J.W. (2010). Quantitative proteomics: comparison of the macular Bruch membrane/choroid complex from age-related macular degeneration and normal eyes. *Molecular & cellular proteomics : MCP*. 9 (6). 1031–46.

Zamiri, P. (2016). Complement C5 inhibition for AMD. In: *Angiogenesis, Exudation and Degeneration*. 2016, Miami.

Zerbib, J., Puche, N., Richard, F., Leveziel, N., Cohen, S., Korobelnik, J.-F., Sahel, J., Munnich, A., Kaplan, J., Rozet, J.-M. & Souied, E.H. (2011). No association between the T280M polymorphism of the CX3CR1 gene and exudative AMD. *Experimental eye research*. 93 (4). 382–6.

Zhang, R., Wang, L.Y., Wang, Y.F., Wu, C.R., Lei, C.L., Wang, M.X. & Ma, L. (2015a). Associations between the T280M and V249I snps in CX3CR1 and the risk of age-related macular degeneration. *Investigative Ophthalmology and Visual Science*. 56 (9). 5590–5598.

Zhang, S., Liu, Y., Lu, S. & Cai, X. (2015b). Genetic Variants of Interleukin 17A Are Functionally Associated with Increased Risk of Age-Related Macular Degeneration. *Inflammation*. 38 (2).

658–663.
Zhao, J., Chen, M. & Xu, H. (2014). Experimental autoimmune uveoretinitis (EAU)-related tissue damage and angiogenesis is reduced in ccl2-/- cx3cr1gfp/gfp mice. *Investigative Ophthalmology and Visual Science*. 55 (11). 7572–7582.
Zhao, J., Kim, H.J. & Sparrow, J.R. (2017). Multimodal fundus imaging of sodium iodate-treated mice informs RPE susceptibility and origins of increased fundus autofluorescence. *Investigative Ophthalmology and Visual Science*. 58 (4). 2152–2159.
Zhou, J.H., Pham, L., Zhang, N., He, S.K., Gamulescu, M.A., Spee, C., Ryan, S.J. & Hinton, D.R. (2005). Neutrophils promote experimental choroidal neovascularization. *Molecular Vision*. 11. 414–424.
Zhou, P., Kannan, R., Spee, C., Sreekumar, P.G., Dou, G. & Hinton, D.R. (2014). Protection of retina by αB crystallin in sodium iodate induced retinal degeneration. *PLoS ONE*. 9 (5). e98275.
Zhu, Y., Liang, L., Qian, D., Yu, H., Yang, P., Lei, B. & Peng, H. (2013a). Increase in peripheral blood mononuclear cell Toll-like receptor 2/3 expression and reactivity to their ligands in a cohort of patients with wet age-related macular degeneration. *Molecular vision*. 19. 1826–33.
Zhu, Z., Yang, Y., Feng, Y., Shi, B., Chen, L., Zheng, Y., Tian, D., Song, Z., Xu, C., Qin, B., Zhang, X., Guan, W., Liu, F., Yang, T., Yang, H., Zeng, D., Zhou, W., Hu, Y. & Zhou, X. (2013b). Infection of inbred BALB/c and C57BL/6 and outbred Institute of Cancer Research mice with the emerging H7N9 avian influenza virus. *Emerging Microbes & Infections*. 2 (8). e50.
Zinkernagel, M.S., Chinnery, H.R., Ong, M.L., Petitjean, C., Voigt, V., McLenachan, S., McMenamin, P.G., Hill, G.R., Forrester, J. V, Wikstrom, M.E. & Degli-Esposti, M.A. (2013). Interferon γ-dependent migration of microglial cells in the retina after systemic cytomegalovirus infection. *American Journal of Pathology*. 182 (3). 875–85.